Ordered Fluids and Liquid Crystals

Publication Date: January 1, 1967 | doi: 10.1021/ba-1967-0063.fw001

In Ordered Fluids and Liquid Crystals; Porter, R., el al.;
Advances in Chemistry; American Chemical Society: Washington, DC, 1967.

Publication Date: January 1, 1967 | doi: 10.1021/ba-1967-0063.fw001

Ordered Fluids and Liquid Crystals

A symposium sponsored by the Division of Colloid and Surface Chemistry at the 150th Meeting of the American Chemical Society, Atlantic City, N. J., Sept. 14-15, 1965.

Roger S. Porter and Julian F. Johnson
Symposium Chairmen

Publication Date: January 1, 1967 | doi: 10.1021/ba-1967-0063.fw001

ADVANCES IN CHEMISTRY SERIES 63

AMERICAN CHEMICAL SOCIETY
WASHINGTON, D.C. 1967

Publication Date: January 1, 1967 | doi: 10.1021/ba-1967-0063.fw001

Library of Congress Catalog Card 67–28847

PRINTED IN THE UNITED STATES OF AMERICA

Advances in Chemistry Series

Robert F. Gould, *Editor*

Advisory Board

AMERICAN CHEMICAL SOCIETY PUBLICATIONS

Publication Date: January 1, 1967 | doi: 10.1021/ba-1967-0063.fw001

In Ordered Fluids and Liquid Crystals; Porter, R., el al.;
Advances in Chemistry; American Chemical Society: Washington, DC, 1967.

Publication Date: January 1, 1967 | doi: 10.1021/ba-1967-0063.fw001

FOREWORD

ADVANCES IN CHEMISTRY SERIES was founded in 1949 by the American Chemical Society as an outlet for symposia and collections of data in special areas of topical interest that could not be accommodated in the Society's journals. It provides a medium for symposia that would otherwise be fragmented, their papers distributed among several journals or not published at all. Papers are refereed critically according to ACS editorial standards and receive the careful attention and processing characteristic of ACS publications. Papers published in ADVANCES IN CHEMISTRY SERIES are original contributions not published elsewhere in whole or major part and include reports of research as well as reviews since symposia may embrace both types of presentation.

PREFACE

We are currently witnessing both a burst of good research and a variety of popular publicity on ordered fluids and liquid crystals. This volume contains papers on ordered fluids and liquid crystals, representing research done in nine countries. Most of the papers were presented at a symposium at the National Meeting of the American Chemical Society, September 1965. The volume also includes comments by several authors who contributed to the international meeting on liquid crystals held at Kent State University, and additional pertinent papers, including a portion of the Garvan Medal Award Address of Gertrude E. Perlmann.

Liquid crystal or mesophase research has gone through tremendous fluctuations. First, there was the burgeoning of research around 1900, soon after Reinetzer's first discovery of liquid crystals in 1888. This was followed by a period of quiescence for a full generation of scientists until the renaissance of research activity in the early 1930's, culminating in the International Meeting on Liquid Crystals in England and the volume devoted to this subject in the *Transactions of the Faraday Society* in 1933. This activity was followed again by another inactive period of about 30 years, which brings us to the present rapid acceleration of research on liquid crystals which has been punctuated by two major meetings on liquid crystals within a single year.

In contrast to previous explosive periods, we have every expectation that research by both physicists and chemists on liquid crystals will continue to accelerate for the foreseeable future for several salient reasons. The first is the variety and importance of systems in which liquid crystals are observed—in biological systems and in items of commerce such as detergents and polymers. The second is the new instrumental techniques to evaluate the intermolecular forces which determine the properties of the unique liquid crystalline state. These techniques include differential thermal analysis and nuclear magnetic resonance. We are now in the eye of this activity and have the happy prospect of a stimulating future in a continuing growth period for studying both ordered fluids and liquid crystals.

Amherst, Mass.
Richmond, Calif.
April 1966

ROGER S. PORTER
JULIAN F. JOHNSON

Publication Date: January 1, 1967 | doi: 10.1021/ba-1967-0063.pr001

The Polymorphism of Tristearin

EDWARD M. BARRALL II and J. C. GUFFY

Chevron Research Co., Richmond, Calif.

Publication Date: January 1, 1967 | doi: 10.1021/ba-1967-0063.ch001

Tristearin, like other simple triglycerides, has been reported to exhibit a complex phase behavior on heating. Earlier publications have indicated that under certain circumstances a transition sequence of solid I → liquid I → solid II → liquid II can occur. This work has established the temperature limits and the transition heats for this sequence using differential thermal analysis and depolarized light intensity measurements. The sample pretreatments required to obtain the various phase sequences have also been studied. The structure of the semiliquid interphase between the two solid phases has been studied by high resolution nuclear magnetic resonance (NMR), and a transformation mechanism has been proposed. For the first time, good photomicrographs have been published of the α_L, β_L interphase and other crystal forms of tristearin.

The polymorphism of the mono-, di-, and triglycerides has been the subject of many studies for over a century. These materials are of particular interest in studies of ordered fluids and liquid crystals because of the peculiar nature of triglyceride polymorphism. A semiliquid phase exists intermediate between two true solid phases as some of these compounds are heated. As long ago as 1849, tristearin was observed to melt at 51–52°C. and then to resolidify and on further heating to melt again at 62–62.5°C. (*14*). A number of times, the triglycerides have been the subject of controversy in the literature concerning the existence of phases and the significance of certain x-ray data.

The subject of triglyceride polymorphism and much of the literature up to 1961 has been reviewed in detail by Chapman (*4*). The triglycerides have been studied by x-ray diffraction (*18*), cooling and heating curves (*15*), microscopy (*16*), dilatometry (*4*), dielectric constant measurement (*9*), infrared spectrophotometry (*6*), broad-line nuclear magnetic resonance (NMR) (*7*), and differential thermal analysis (DTA) (*4*, *13*). The extensive x-ray diffraction literature dealing with triglycerides has been thoroughly reviewed up to 1964 by Gunstone (*12*).

In Ordered Fluids and Liquid Crystals; Porter, R., el al.;
Advances in Chemistry; American Chemical Society: Washington, DC, 1967.

The most detailed x-ray structure study of these materials to date is of trilaurin in the β_L form by Vand (*18*). This study was instrumental in clarifying the confused picture of the molecular arrangement of the triglycerides in the crystal lattice. Chapman's review (*4*) made a special effort towards clarifying the complex phase nomenclature which had surrounded the triglycerides with confusion and previously made it all but impossible to compare English and American work in the field. Chapman's phase designations are followed as closely as possible in this work.

Tristearin, the triglyceride of octadecanoic acid, has received some attention from a number of workers. To date only one precise calorimetric investigation of the phase transformations has been carried out (*8*). The previous differential thermograms (*4*, *13*), although showing good detail, were apparently made in such a way that quantitative heat determinations were impossible. Only broad-line NMR spectra have been taken (*7*). These NMR spectra were made to aid in interpreting the glass phase, from 20°K. to room temperature, and not in the region of the higher temperature transitions where high resolution NMR is possible. Although the microscope has been one of the favorite tools in studying triglyceride polymorphism (*4*), no charts of depolarized light intensity (DLI) as a function of temperature have been published. Experiments were carried out in this laboratory to supply the calorimetric, DTA, NMR, and DLI data which are not available in the literature on tristearin.

Publication Date: January 1, 1967 | doi: 10.1021/ba-1967-0063.ch001

Experimental

A sample of zone-refined tristearin was obtained from the Hormel Institute, 801 N.E. 16th Ave., Austin, Minn. This material had a purity of > 99% by thin layer chromatography. A sample of stearic acid was obtained from Matheson, Coleman and Bell, Cincinnati, Ohio. After recrystallization from alcohol, a purity of 99% (determined by titration and thin-layer chromatography) was obtained.

Since preliminary survey work had indicated that the crystal forms of tristearin were extremely sensitive to impurity and previous thermal history, several samples were prepared: acetone-recrystallized tristearin, annealed melt (cooled at 0.5°C./minute to 10°C.) tristearin, and 97% (mole %) tristearin–3% stearic acid treated in all of the above fashions.

DTA Instrumentation. The differential thermograph used in this study has been described in detail (*1*, *2*, *3*). The microcalorimeter cell which used ~0.005 gram of sample was used. The thermograms were recorded on an x–y recorder with the differential temperature, ΔT, on the y-axis and the sample temperature, T, on the x-axis. The sample temperature was measured with the same thermocouple as the ΔT. This produces thermograms with peak locations independent of heating rate. The heating rate was 4°C./minute. The calorimeter was calibrated with zone-purified dotriacontane, $\Delta H_r + \Delta H_f = 51.7$ cal./gram.

Microscope and DLI Apparatus. The apparatus is shown in Figure 1 in block form. A Zeiss Ultraphot II photomicroscope equipped with a polarizer and analyzer, Polaroid filters, and strain-free optics was used to obtain all photographs discussed here. This microscope was modified for

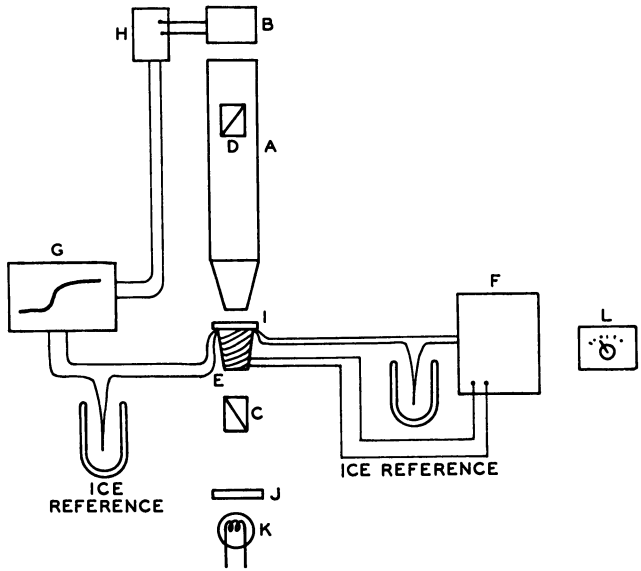

Figure 1. Depolarized light intensity apparatus

A. Microscope optics
B. Photocell, cadmium telluride
C. Polarizer
D. Analyzer
E. Hot stage
F. Temperature regulator
G. Recorder
H. Photocell amplifier
I. Sample
J. Filter
K. Light source
L. Premelter

DLI measurement by introducing a cadmium telluride photoconductive cell at the movie camera focus. The light-dependent resistance changes of the photoconductive cell were measured and amplified in the usual manner and recorded on the y-axis of a 1 mv. per inch Moseley x–y recorder. The photometer was arranged so that a 7-mv. signal at the recorder corresponded to complete transmission through the polarizing filters oriented parallel to one another. The recorder zero was adjusted to correspond to the light throughput when the polarizers were crossed. DLI measurements were carried out with the polarizers crossed.

Samples were heated on a Zeiss hot stage, modified by replacing the platinum sample temperature thermocouple by a more sensitive copper-constantan couple, located as close as possible beneath the sample cover slip. A second temperature program thermocouple was placed in contact with the ceramic heater frame of the hot stage. The stage was programmed at 2°C. per minute with a slope-proportional band controller. Temperature was controlled to ±0.05°C. Ice reference junctions were used on both samples and program thermocouples. The output of the sample–ice junction thermocouple was recorded on the 0.5 mv. per inch x-axis of the Moseley x–y recorder.

Publication Date: January 1, 1967 | doi: 10.1021/ba-1967-0063.ch001

NMR Apparatus. NMR spectra were obtained on a Varian A-60 equipped with a Varian V-6040 variable temperature controller and probe. Scans were made at 7-second intervals. Care was taken to avoid radio-frequency saturation of the proton resonance. The temperatures at the beginning and end of the runs were determined in the standard manner from the chemical shift of the two ethylene glycol peaks. Calibration of the heating characteristics of the apparatus as a function of time, heater current, and temperature was carried out prior to the triglyceride spectra determinations with the ethylene glycol peaks. Knowing heater current and time elapsed from the onset of heating permitted temperatures to be determined to ±1°C. in 10 trial runs.

Results

Differential Thermal Analysis. Acetone-recrystallized tristearin has a very complex differential thermogram. Figure 2 shows a trace which is representative of three separate determinations. This curve resembles those published by Chapman (*6*) in gross features. Three endotherms and one exotherm are evident. The temperatures of transition are given in Table I.

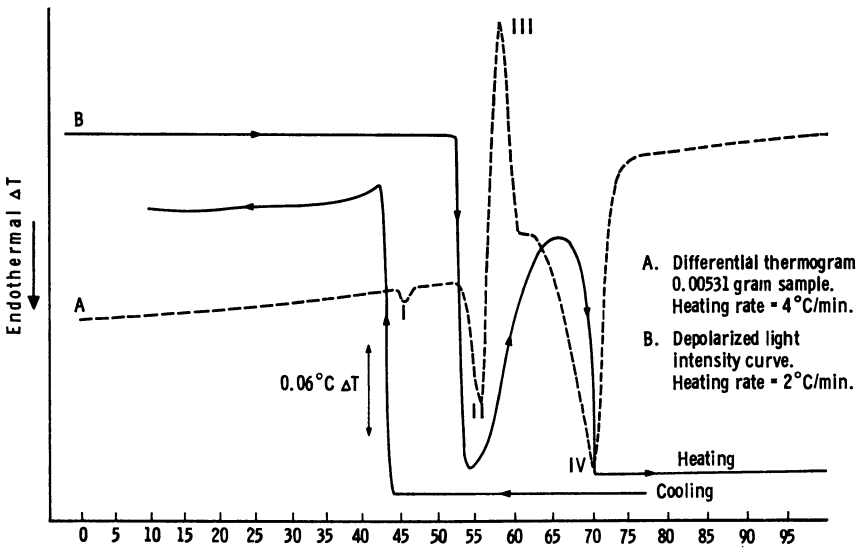

Figure 2. Tristearin

The agreement between the two sets of data on tristearin is good when the probable differences in instrumentation are considered. Only the temperatures of the endothermal minima, T_m, should be considered since the beginning of the endotherm depends greatly on the sensitivity and sample shape used in some instruments. The location of the exotherm depends on heating rate to some extent. Heating rate data were not given with Chap-

Publication Date: January 1, 1967 | doi: 10.1021/ba-1967-0063.ch001

Table I. Temperatures of Transition for Tristearin and Stearic Acid

		Thermograph Features[a] °C.			
Compound	*Reference*	T_b	T_m	T_e	*Process*
Tristearin	This work	44.5	47.1	51.5	Endotherm
		54.5	57.5	58.9	Endotherm
		58.9	60.3	63.4	Exotherm
		64.8	70.3	76.8	Endotherm
	Chapman (*6*)	—	—	—	Not noted
		51	56	57	Endotherm
		57	58	63	Exotherm
		66	73	76	Endotherm
	Melting point, capillary (*6*)		54		α_L[b]
			64		β'_L
			73.1		β_L
Stearic acid	This work	57.5	68.6	71.4	Endotherm
	Vold (*19*)	Not given	69.0	Not given	Endotherm

[a] T_b. Temperature at beginning of endotherm or exotherm.
T_m. Temperature at endothermal or exothermal inflex.
T_e. Temperature at end of endotherm or exotherm.
[b] Phase nomenclature is that suggested by Chapman (*4*).

man's curves (*4*). The initial endotherm seen in this work and not noted in Chapman's curves could be caused by the close pack orthorhombic → open hexagonal (α_L) transition. Chapman's infrared studies have indicated the presence of these phases (*5*). For the remaining transitions close agreement between literature melting points and DTA data cannot be expected. The literature melting points given for the monoacid triglycerides were determined by plunging capillaries containing the esters into preheated baths and noting the presence or absence of a change. Timmermans (*17*) has described this method in detail and given precise instructions for its application to triglycerides. Dynamic heating data would show corresponding effects at lower temperatures, as do the DTA data shown in Table I. This effect is generally observed when the transitions measured are broad—i.e., not isothermal.

Table II. Heats of Transition of Tristearin and Stearic Acid

Fig. 2 Peak No.	*Substance*	*Transition*	ΔH, *Cal./G.* *This work*	*Lit.*
I	Tristearin	Orthorhombic → hexagonal (*4*) α_L	2.0	—
II		Hexagonal α_L → triclinic (*4*) β_L	6.4	
III			—12.4	—13.7 (*14*)
IV		Triclinic β_L → liquid	31.1	54.5 (*19*)
	Stearic acid	Solid → liquid	47.6	47.6 (*11*)
				49.2 (*19*)

Publication Date: January 1, 1967 | doi: 10.1021/ba-1967-0063.ch001

The heats involved in the various DTA endotherms and exotherms shown in Figure 2 are given in Table II. The data are compared with the literature where possible. The previous studies of tristearin have employed conventional calorimetric techniques. Close agreement is noted between the work of Charbonnet and Singleton (*8*) and our DTA for the exothermal portion of the $\alpha_L \rightarrow \beta_L$ transition. The endothermal portion of this transition appears to have been overlooked in the classical calorimetric treatment. However, these same writers give large values for the $\alpha_L \rightarrow$ liquid transition (38.9 cal. per gram) and the $\beta_L \rightarrow$ liquid transition (54.5 cal. per gram). From theoretical considerations and general similarity of structure, the heat of fusion of the β_L form should be comparable to that of stearic acid. Two previous values for stearic acid are given: 47.6 cal. per gram (*15*) and 49.2 cal. per gram (*16*) by calorimetry and DTA, respectively. A value of 47.6 cal. per gram using *n*-dotriacontane as calibration standard was obtained in the present work. These data indicate that the DTA method is capable of giving excellent calorimetric results on a system similar to tristearin. If peak IV, Figure 2, is the fusion of the pure $\beta_L$form, the heat of fusion is 31.1 and not 54.5 cal. per gram as previously given (*8*). From the DTA results it is possible to calculate an approximate heat of fusion for the pure α_L form, $\alpha_L \rightarrow$ liquid: 31.1 + 6.4 − 12.4 or 26.1 cal. per gram. Charbonnet and Singleton obtained 38.9 cal. per gram (*8*) using an analogous method of calculation. Both heats of fusion neglect heat capacity effects involved in the calculation. We are unable to account for the differences between earlier heat of transition and fusion data and the present DTA results.

The pure tristearin sample which was annealed slowly formed only the β_L phase. Naturally, no exotherms were observed. Only a single peak owing to the fusion of the β_L form was observed at 70.3°C. The heat of fusion of the β_L form measured from this sample was 31.9 cal. per gram.

The liquid nitrogen–quenched sample of pure tristearin did not show the orthorhombic → hexagonal transition. All other thermographic characteristics were identical to the acetone-recrystallized material.

The tristearin sample containing 3 mole % of stearic acid gave only the α_L form, which melted directly to the liquid irrespective of the sample pretreatment. The presence of impurities appears to inhibit the formation of the β_L form even on slow annealing from the melt. The heat of fusion of the α_L form was 29 cal. per gram, with the 3% stearic acid being taken into account in the calculation.

Depolarized Light Study. The samples used for DLI were melted between cover slips and rapidly quenched. The cover slips were held 0.01 mm. apart with a glass spacer. This treatment should result in the hexagonal, α_L, phase as the room temperature solid.

The depolarized light intensity curve, Figure 2, shows a sharp loss in intensity beginning at 57°C. and approaches extinction at 58°C. This in-

dicates a loss of anisotropic structure which would normally accompany a phase transition from solid to liquid. On further heating the intensity increases to form a shoulder at 64.8°C. approximately one-half as intense as the initial solid-phase rotation. A new peak rotation, one-half of the original intensity, is reached at 76°C. This corresponds to the final melting of the compound. The conclusions regarding these transitions are in substantial agreement with those drawn on the basis of the differential thermograms. The first transition into a disordered state is the onset of melting of the α_L phase. The re-formation of the rotation of light is the exothermal conversion of α_L into the β'_L phase. The increase in depolarization above 64.8°C. is probably caused by the formation of the β_L phase from β'_L. The final extinction at 76°C. corresponds to the melting of the solid. The molecular arrangement of the β'_L phase is not known with certainty.

Since transition through an optically isotropic phase, cubic, is excluded by x-ray data (*12*), the 57°C. extinction of rotation indicates the formation of a phase with disorder normally associated with a melt. This indicates that the chain separation and dislocation during the transition from the perpendicularly oriented α_L hexagonal structure to the obliquely oriented β_L triclinic structure, Figure 2, are larger than has previously been described or implied.

Microscopic Examination. Seven crystal types have been described from optical microscope examination. All of these phases were seen in this work. Figures 3 and 4 show some examples. A new α_L form, α_L-spherulite, crystallized on slow cooling of the melt (1°C. per minute or less).

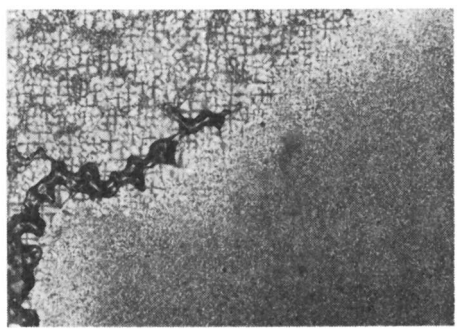

Figure 3. Interpenetration of α-spherulite and mosaic forms of tristearin

At faster rates, the previously reported α_L-mosaic formed. Figure 3 shows a field with both forms cocrystallized. The α_L-mosaic and α_L-spherulite were identical in DTA and DLI behavior to the solvent-recrystallized crystals. Figure 4 shows the transformation of α_L-spherulites into dull β'_L-spherulites. On further heating, the β_L phase forms and the crystals brighten somewhat. The extinctions of these crystals correspond to those

Publication Date: January 1, 1967 | doi: 10.1021/ba-1967-0063.ch001

previously given in the literature (*16*) and permit the assignment of probable phases.

Rapid cooling DLI curves show the reformation of the solid α_L phase in one step. The β_L or β'_L phases do not reform from the melt. This further confirms the irreversibility of these transformations.

Nuclear Magnetic Resonance. Previous NMR studies have been concerned with broad band spectra at subambient temperatures (*7*). These data indicated a large amount of free rotation in the low temperature orthorhombic phase. Figure 5 shows a series of rapid high resolution scans

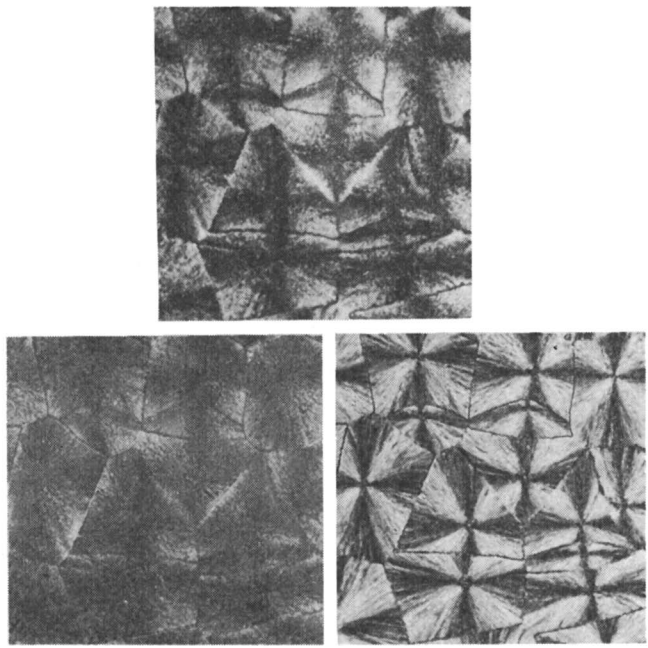

Figure 4. Crystal forms of tristearin
Upper. β 69°C.
Left. β interphase 62°C.
Right. α 55°C.

made from 55° to 73°C. using a sample made by rapidly freezing a liquid melt. Three points are significant in these curves: the appearance of CH_2 proton resonance from 55.4° to 60°C., the disappearance of this resonance from 60.3° to 64.6°C., and the ratio of the resonance maximum at 59.0°C. to that at 72.3°C.

The appearance of a high resolution proton resonance immediately indicates the formation of an open, nonrestrictive structure. The temperature range over which this signal is seen corresponds to endotherm II on the differential thermogram and the first extinction of the DLI curve. The transition between α_L and β'_L forms consists of a disordered state.

Publication Date: January 1, 1967 | doi: 10.1021/ba-1967-0063.ch001

Publication Date: January 1, 1967 | doi: 10.1021/ba-1967-0063.ch001

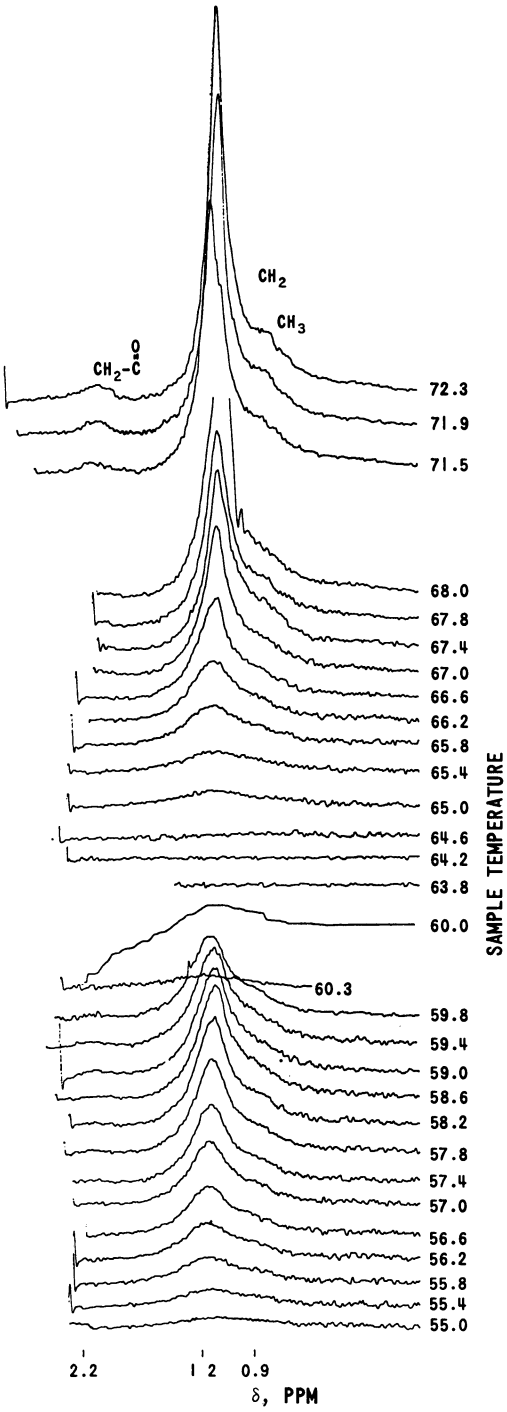

Figure 5. High resolution NMR spectra of tristearin at 55°–72.3° C. 3.5°C. per minute heating rate

The disappearance of the proton signal from 60.3° to 64.6°C. indicates the formation of a new restricted or solid phase, β_L or β'_L phase. This range corresponds to the exotherm of recrystallization on the differential thermogram and the second DLI maximum.

The ratio of the proton signal maximum at 59°C. to the proton signal from the isotropic liquid phase at 72.3°C. is 42%. This indicates that somewhat less than half of the total protons are free to resonate. This condition can be most easily explained by postulating a separation of the intrachain crystalline zones. The lack of

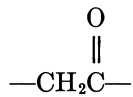

signal at 59°C. indicates that the separation does not extend up to the carbon before the ester group. The terminal CH_3 protons are smeared into the principal chain CH_2 peak because of poor resolution at 59°C. This mode of transition, although not previously suggested, does not disagree with any previous evidence. Figure 6 shows the percent free protons as a function of temperature. The curve is derived from the areas shown in Figure 5. The shape and temperature of the inflexes correspond directly to DTA and DLI features.

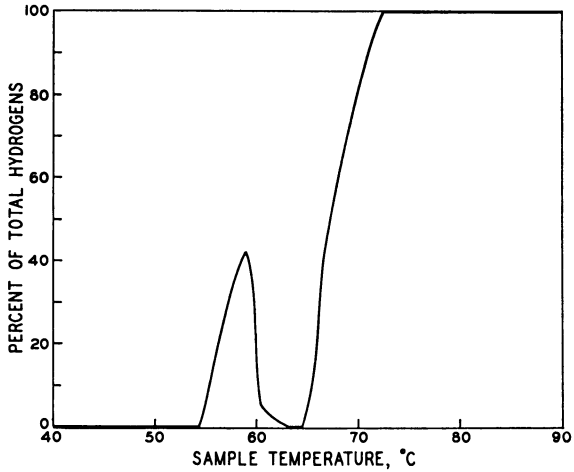

Figure 6. Percent of rotatable hydrogen as a function of temperature for tristearin

Conclusions

DTA indicates that after some initial absorption of heat, the $\alpha_L$form in the hexagonal base plane perpendicular arrangement translates to the 62° inclined triclinic β_L form (Figure 7) with an emission of heat. The β_L

Publication Date: January 1, 1967 | doi: 10.1021/ba-1967-0063.ch001

form then melts at 73°C. to give the liquid phase. Such a model is in substantial agreement with the literature (*4*, *10*, *12*) and the observed thermal phenomena.

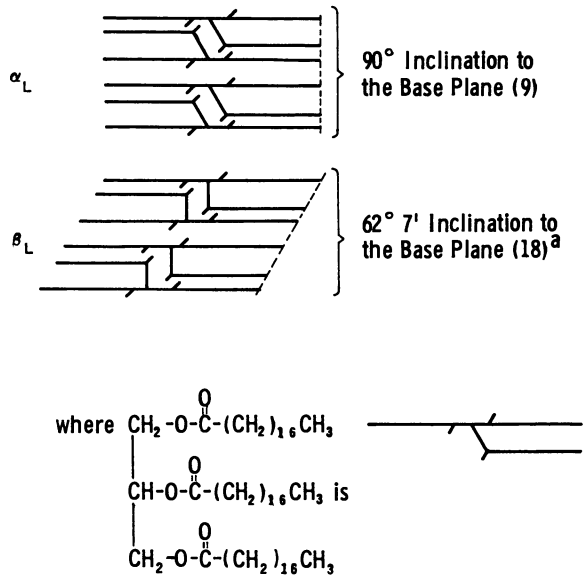

Figure 7. Chain arrangements in tristearin crystals

[a] Assuming that the structure of the β_L phase is the same as that of trilaurin, the only triglyceride for which single-crystal data are available

On the basis of DTA, DLI, and NMR studies, the interphase between the α_L and β_L or β'_L phases of tristearin appears to be a semiliquid. The heat of crystallization into the β_L phase is large enough to cause this effect. The direct assumption that this interphase is simply melted α_L phase is ruled out by the absence of proton signals other than the chain CH_2 and CH_3. The open interphase structure also explains previously observed infrared doublets (*6*).

The thermal history of tristearin as well as the purity is important in determining the type of crystal phase formed on cooling the melt or on recrystallization. Acetone recrystallization produces the form stable at lowest temperature, the orthorhombic. Rapid quenching of the melt produces the next most stable phase, the hexagonal or α_L phase. Slow cooling permits the β_L phase to form, which does not revert to the α_L form at room temperature but remains metastable until the normal melting point is reached on reheating. Small amounts of impurity cause the α_L form to appear irrespective of thermal treatment. The impure α_L crystals melt directly without changing into the β_L form. This last effect is probably caused by the lowering of the free energy of the crystal structure.

Publication Date: January 1, 1967 | doi: 10.1021/ba-1967-0063.ch001

Acknowledgment

The authors thank John Q. Adams for obtaining the NMR spectra and structure assignments.

Literature Cited

(1) Barrall, E. M., II, Gernet, J. F., *Anal. Chem.* **35**, 1837 (1963).
(2) Barrall, E. M., II, Porter, R. S., Johnson, J. F., *Anal. Chem.* **36**, 2172 (1964).
(3) Barrall, E. M., II, Porter, R. S., Johnson, J. F., *J. Phys. Chem.* **68**, 2810 (1964).
(4) Chapman, D., *Chem. Revs.* **62**, 433 (1962).
(5) Chapman, D., *J. Chem. Soc.* **1957**, 4489.
(6) Chapman, D., *Nature* **176**, 216 (1955).
(7) Chapman, D., Richards, R. E., Yorke, R. W., *J. Chem. Soc.*, **1960**, 436.
(8) Charbonnet, G. H., Singleton, W. S., *J. Am. Oil Chemists' Soc.* **24**, 140 (1947).
(9) Crowe, R. W., Smyth, C. P., *J. Am. Chem. Soc.* **72**, 4427 (1950).
(10) Fox, D., Labes, M. M., Weissberger, A., eds., "Physics and Chemistry of the Organic Solid State," Vol. I, p. 135, Interscience, New York, 1963.
(11) Garner, W. D., Madden, F. C., Rushbrooke, J. E., *J. Chem. Soc.* **1926**, 2941.
(12) Gunstone, F. D., *Chem. Ind. (London)* **1964**, 84.
(13) Haighton, A. J., Hannewijk, J., *J. Am. Oil Chemists' Soc.* **35**, 344 (1958).
(14) Heintz, W., *Jahresber.* **2**, 342 (1849).
(15) Malkin, T., "Progress in Chemistry of Fats and Other Lipids," Vol. II, Pergamon Press, London, 1954.
(16) Quimby, O. T., *J. Am. Chem. Soc.* **72**, 5063 (1950).
(17) Timmermans, J., "Chemical Species," Chemical Publishing Co., New York, 1940.
(18) Vand, V., Bell, I. P., *Acta Cryst.* **4**, 104 (1951).
(19) Vold, M. J., *Anal. Chem.* **21**, 683 (1949).

RECEIVED April 18, 1966.

Effect of Thermal History and Impurities on Phase Transitions in Long-Chain Fatty Acid Systems

T. J. R. CYR, W. R. JANZEN, and B. A. DUNELL

The University of British Columbia, Vancouver 8, Canada

Publication Date: January 1, 1967 | doi: 10.1021/ba-1967-0063.ch002

Broad-line nuclear magnetic resonance has been used to study melting in stearic acid and a mesomorphic (crystalline to waxy) phase transition in lithium stearate. Extensive motion, liquid-like, though less extensive than that in an isotropic free-flowing liquid, takes place within the system below the melting point of stearic acid or the crystalline to waxy phase transition of lithium stearate. The amount of liquid-like character, as measured by the intensity of a narrow component in the NMR spectrum relative to the total intensity of the whole spectrum, depends on the presence of impurities in the system and even more significantly on whether and how many times the sample has been melted.

Broad line nuclear magnetic resonance (NMR) investigation of stearic acid (*9*) and other long chain fatty acids (*3*) has indicated that a significant fraction of the protons in these substances is in rapid motion—almost liquid-like—several or even tens of degrees below the accepted melting points of the acid. This motion is made evident by a narrow component, between 0.1 and 0.01 gauss wide, which appears in the normal broad-line spectrum well below the melting point, and which, without apparent change in width, grows in intensity at the expense of the intensity of the broad-line component (which remains of constant width) until the melting point is reached.

The fatty acids used in these experiments were carefully purified, so that it can be asserted confidently that the protons in liquid-like motion, which contribute to the narrow line, are not mainly in impurity molecules. We have, however, suggested (*3*, *9*) that the liquid-like motion in the fatty acids centers about, and with increasing temperature grows out from, impurity centers or lattice defect centers in the crystal. An attempt has been made in the work reported here to obtain evidence that this liquid-like

In Ordered Fluids and Liquid Crystals; Porter, R., el al.;
Advances in Chemistry; American Chemical Society: Washington, DC, 1967.

behavior originates, in part at least, around impurity centers by adding definite amounts of known impurities to carefully purified stearic acid. During this work it became apparent that defect centers must play an equally or more important part than impurity centers in promoting the existence of liquid-like regions in the crystal. A study of lithium stearate has also been reported in detail (*7*); in this paper we note the influence of the thermal history of the sample on one of the phase changes in lithium stearate and consider it as evidence for the importance of lattice defects in promoting phase transition at temperatures below that at which the transition is macroscopically evident.

Experimental

Materials. Two different lots of stearic acid were used in the experiments reported here, one purified sample being used for the stearic acid experiments, the other for making lithium stearate. The initial source for both was Eastman Kodak White Label grade, further purified by recrystallization according to the method of Brown and Kolb (*6*) from freshly distilled reagent grade acetone at −20°C.

The batch used to prepare lithium stearate had a freezing point, after two recrystallizations, of 69.5°C.; a thermometer calibrated at the ice and steam points was used and corrected (+0.48°C.) for stem exposure. A hot, 50% by volume water-ethanol mixture was saturated with reagent grade lithium hydroxide and titrated into a hot ethanol solution of the purified stearic acid to a phenolphthalein end point, and a few drops of excess base were added. The precipitated soap was filtered on a Büchner funnel after it had cooled and was dried in a vacuum desiccator over phosphorus pentoxide overnight and then in an oven at 110°C. for 4 hours. This sample was then heated gently in a 200-ml. flask, fitted with a stopcock, until the soap had melted and flowed freely for a few minutes. The stopcock was closed and the sample allowed to cool to room temperature. The resulting glassy material was ground up in a mortar and kept in a vacuum desiccator for 10 days. After the sample had been loaded into an NMR sample tube, it was heated for 3 hours at 125°C. under vacuum, and the glass sample tube was sealed off while still evacuated. A second lithium stearate sample was precipitated by titration as above but was at no time fused during its preparation. Water and other solvents were removed by sucking air through the precipitated soap on the Büchner funnel for 1 1/2 hours, then drying in an oven at 120°C. for 12 hours, and cooling and keeping in a vacuum desiccator over P_2O_5 for 5 days. This sample was also heated at 120°C. under vacuum for 4 hours after it had been powdered and transferred to its NMR sample tube, and the tube was sealed off while still under vacuum.

The other sample of stearic acid was purified by an initial distillation of the acid at reduced pressure and by subsequent recrystallizations, by the method of Brown and Kolb (*6*), of the middle fraction of the distillate. After three recrystallizations the freezing point, as observed from a time-temperature cooling curve on 5 grams of the sample, was 69.5°C. (with thermometer stem exposure correction of 0.48°C.), and the plateau in the cooling curve at 69.5°C. continued at that temperature until the substance was completely solidified. Although this freezing point is lower than that

Publication Date: January 1, 1967 | doi: 10.1021/ba-1967-0063.ch002

In Ordered Fluids and Liquid Crystals; Porter, R., el al.;
Advances in Chemistry; American Chemical Society: Washington, DC, 1967.

of Guy and Smith, 69.60°C. (*11*), it is higher than that of Francis and his co-workers, 69.32°C. (*8*). A purity check on this sample by gas chromatography of the methyl and ethyl esters on a Carbowax 20 M column showed that the middle fraction of distillate contained 1% palmitic acid and 2% linolenic acid and that after one recrystallization from acetone no impurity was detectable.

The substances added to the stearic acid as controlled impurities were themselves carefully purified. The palmitic acid was Eastman Kodak White Label grade, further purified by repeated crystallization. The oleic and elaidic acids were obtained from the Hormel Institute as better than 99% pure and were used without further treatment. The water was distilled, outgassed, and added to the stearic acid as water vapor through a vacuum system. For all samples it was important to prevent contamination with water or addition of more than the purposely added quantity of water. The purified stearic acid was packed into glass sample tubes that had been cleaned and baked out. If impurities other than water were to be added, these were weighed into the sample tubes at this point, and the tubes were sealed into a vacuum system. The sample was held in a water bath at 70°–71°C. for about 1 hour under vacuum and then at 68°C. (just below the freezing point) under vacuum for 6 or 8 days, after which the sample tube was sealed off while the system was still under vacuum, and the sample was not exposed to the atmosphere during any subsequent experiment. In the case where water was the added impurity, a sample tube of pure stearic acid, previously prepared as above, was opened and immediately sealed into the vacuum system. Water vapor was transferred through the vacuum system to the sample, and the sample tube was resealed at liquid nitrogen temperature. The sealed-off sample was then melted and held at 70°–71°C. for a short time and annealed at 68°C. for several days. All samples were allowed to cool to room temperature standing in a polystyrene foam sample support and were then ready for NMR examination. In addition to the samples prepared according to the above description, two samples of stearic acid, mentioned below, were prepared without being melted.

Procedure. All spectra were obtained from a Varian magnet and DP60 spectrometer at 60 Mc. per sec. Temperature control was achieved by flowing heated air past the sample, which was placed in a Dewar vessel within the probe insert of the spectrometer. The temperature of the sample was monitored by two thermocouples, one upstream and one downstream from the sample. The temperature gradient between these thermocouples depends on the temperature sought, and the uncertainty of temperature is estimated to be ±0.5°C. at 50°C., ±2°C. at 150°C., and ±3°C., at 210°C.

One hour was allowed for the sample to come to thermal equilibrium before a spectrum was run at a new temperature. At the end of 45 minutes–1 hour, the time required to run a wide-line spectrum, a repeat run was made at the same temperature and was found in all cases to agree with the first spectrum. Limitation of machine time did not permit extension of equilibration times. No evidence of hysteresis was found if temperatures were approached from above or below, unless the sample had been fused in the interval between observations.

Publication Date: January 1, 1967 | doi: 10.1021/ba-1967-0063.ch002

In Ordered Fluids and Liquid Crystals; Porter, R., el al.;
Advances in Chemistry; American Chemical Society: Washington, DC, 1967.

Second moments were calculated using the correction of Andrew (*1*) for modulation amplitude, namely, subtraction of $H_m^2/4$ from the value calculated from the experimental derivative curve. The fraction of protons in the sample in rapid, liquid-like motion was estimated by taking this fraction to be the ratio of the area under the narrow component of the absorption curve to the area under the whole absorption curve. This supposes that the same saturation factor applies to both components. This condition was checked by running spectra at different r.f. power inputs but otherwise having the same operating conditions and same state of the sample. Within the range of r.f. power input used in these experiments the ratio of the height of the narrow derivative peak to the height of the broad derivative peak was independent of r.f. power input for the stearic acid. For lithium stearate, preliminary spectra were run over a wide range of r.f. power, and an r.f. level well below the saturation level was chosen for the running of all reported spectra. For convenience, a calibration curve was constructed for a specific modulation amplitude, circuit response time, recorder rate, and rate of scan through resonance, this calibration being of the ratio, height of narrow derivative peak to height of broad derivative peak, against fraction of integrated absorption intensity lying under the narrow component—i.e., fraction of protons in liquid-like motion. All the stearic acid curves were then run under the specific conditions for which the curve was constructed, and the ratio of derivative peak heights was taken as a direct measure of the fraction of the system which was in liquid-like motion. For a case in which a spectrum was repeated at a different scan rate, the ratio of peak heights was the same for both scan rates. It was thus confirmed that the circuit and recorder response times were short compared with the scan rate through resonance.

Results and Discussion

Stearic Acid. The growth of narrow component and the quality of the stearic acid spectra are shown in Figure 1 by a series of typical spectra taken at various temperatures. A more detailed study of the spectrum

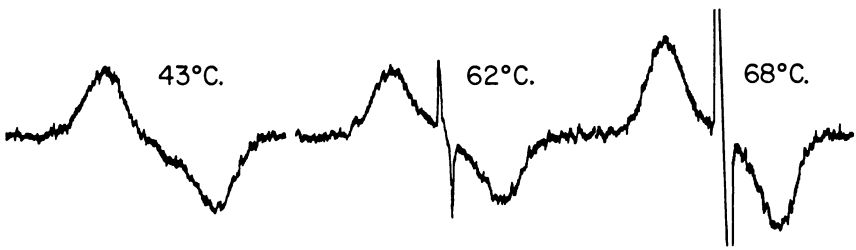

Figure 1. Growth of narrow component in a pure stearic acid sample with increasing temperature

Ratio of derivative peak heights, narrow to broad component: 43°C., no narrow component observable; 62°, 1.5 to 1; 68°, 23.6 to 1

just below the melting point using a high resolution spectrometer (Varian A-60) with a temperature-controlled probe showed a line width at half height of approximately 5 milligauss or some 20 to 25 c.p.s. The temperature in the probe was measured as 66°C. by observing the chemical shift of pure ethylene glycol and knowing its dependence on temperature. Since the width of a normal liquid line is a fraction of a cycle per second, one concludes that the narrow component corresponds to a highly viscous liquid or to a state in which diffusional motion is seriously restricted. The results of initial experiments in which increasing amounts of palmitic acid were added as an impurity to stearic acid are shown in Figure 2, together with the curve for the fraction of protons in liquid-like motion in a stearic

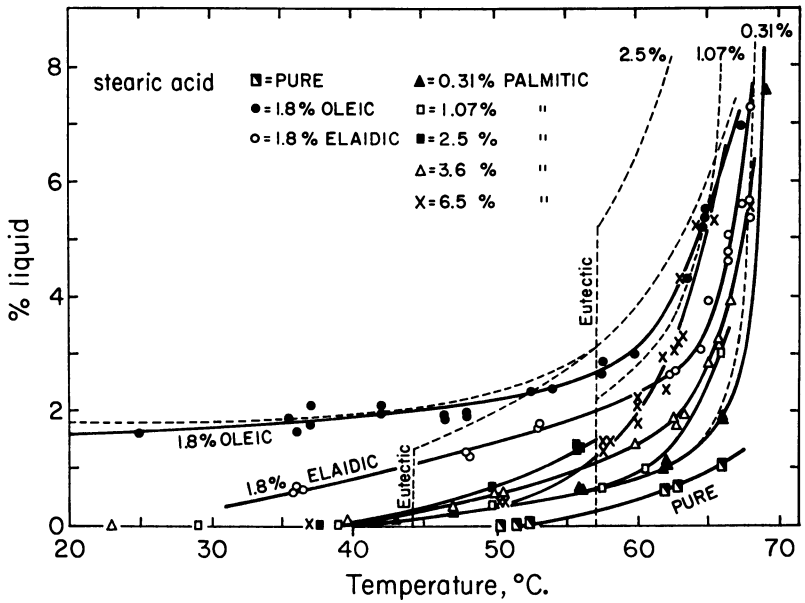

Figure 2. Percent of protons in liquid-like motion as a function of temperature for pure and impure stearic acid samples

– – – Equilibrium amounts of liquid predicted from assumed phase diagram

acid sample to which no impurity had been added. Also shown in this figure is the effect of adding two 18-carbon unsaturated acids—oleic and elaidic. The fraction of protons involved in liquid-like motion is found to be an order of magnitude smaller in the results reported here than in the results first obtained in this laboratory and reported in 1960 (*9*). We have no explanation for this difference. The observed freezing point of the stearic acid used in the 1960 work indicated that if the impurity were palmitic acid (a most probable impurity), the quantity of impurity in the stearic acid was much less than 1%. It is possible that the broad-line component in the previous studies was being saturated whereas the narrow

Publication Date: January 1, 1967 | doi: 10.1021/ba-1967-0063.ch002

component was not. No other evidence was found, however, to indicate any degree of saturation in the system. As we discuss below, thermal history is important with respect to the intensity of liquid-like line seen in the spectra of these substances, and although it seems to tax the applicability of this effect to explain so large a discrepancy, it is possible that the earlier results can be attributed to the effect of repeated fusion of the sample without subsequent annealing.

The work of Francis, Collins, and Piper on melting and freezing points of stearic and palmitic acid mixtures (*8*) indicates that a eutectic is formed at about 55°C., but it is not clear whether the systems forming the eutectic are the two pure acids or solid solutions. If they are the pure acids, then the amounts of liquid-like motion as given by the narrow components of the spectra above the eutectic temperature lie approximately within the limit of the amount of liquid one should expect to be in equilibrium with pure stearic acid for simple eutectic formation and the melting points given by Francis. These percentages of liquid can be calculated by simple application of the "lever law" to a simple eutectic phase diagram constructed on the basis of Francis' melting or freezing points. In the cases where the liquid fraction observed by NMR is smaller than the liquid fraction predicted from the phase diagram, one can assume that thermal equilibrium was not achieved in the NMR sample. The equilibrium mole fraction of liquid to be expected at any temperature for a particular mole % of palmitic acid impurity in stearic acid, as determined from the supposed simple eutectic phase diagram, is shown by dashed lines in Figure 2. The irregularity in the order of the curves for palmitic acid impurity is not understood.

Although one may be able to attribute the liquid-like motion appearing in the NMR spectra to expected equilibrium amounts of liquid present in a two-component system above a eutectic temperature, this does not account for the 0–1% liquid character present at temperatures below 54° or 56°C., the eutectic temperature. We believe that this must be attributed to liquid-like motion of a few molecules centered about impurity and structural defects in the crystal lattice, or alternatively (*12*) to motion of molecules in defects on the surface of the crystals.

The more extensive liquid character found in samples containing the 18-carbon unsaturated acids as impurity appears also to be simply explainable in terms of a phase diagram involving eutectic formation between the two pure components. We assume that the freezing point curves of Smith (*14*) for mixtures of stearic and oleic or elaidic acids can be combined with simple eutectic formation involving the two pure components. The equilibrium mole percentages of liquid that can be calculated for such phase equilibria are shown as dashed curves in Figure 2. Again one must attribute residual liquid-like motion below the 43°C.-eutectic of elaidic and stearic acid to disorientation at lattice defects. The eutectic for oleic and stearic acids lies at about 13°C.

Publication Date: January 1, 1967 | doi: 10.1021/ba-1967-0063.ch002

The importance of the sample's thermal history is illustrated by observations made on some pure stearic acid sample—i.e., purified acid to which no impurity was added—and shown in Figure 3. Two stearic acid samples were prepared without being fused after recrystallization from acetone, but they were thoroughly dried in a vacuum. The stearic acid

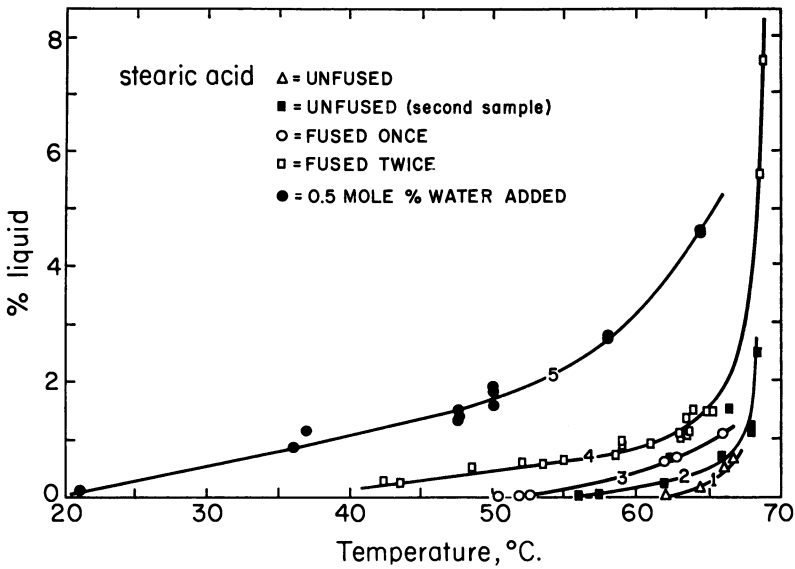

Figure 3. Percent of protons in liquid-like motion as a function of temperature

1. *Pure unfused stearic acid*
2. *Pure unfused stearic acid (different sample)*
3. *Pure stearic acid, fused once*
4. *Pure stearic acid, fused twice*
5. *Stearic acid containing 0.5 mole % water*

was first dried in a vacuum desiccator over P_2O_5, then put into sample tubes which had been baked out, and the tubes were then sealed into a vacuum system and left under vacuum at about 65°C. for a few days. The percentage of the protons in liquid-like motion, shown in curves 1 and 2, is lower for these samples than for any other stearic acid samples observed.

A third sample, which was fused during preparation, as described above, showed more liquid-like motion, as illustrated by curve 3. This sample was melted a second time after the points on curve 3 were obtained. It was taken to 70°–71°C. for 1 hour ± 15 minutes and then cooled over a period of some 16 hours to room temperature. A large hysteresis effect was observed in the curve for percent liquid character *vs.* temperature, the points for descending temperature lying above both sets for ascending temperature—namely, curves 3 and 4. The sample was then again observed with increasing temperature beginning 4 hours later, and as curve 4 shows, the extent of liquid-like motion was greater than that observed on

Publication Date: January 1, 1967 | doi: 10.1021/ba-1967-0063.ch002

initial heating (curve 3). Thermal history has in this example as much effect as adding 0.3 mole % palmitic acid impurity. Variation in the rate of cooling of a sample from the melt would no doubt influence the number and nature of lattice defects and impurity centers, and the length of time for which a sample is held at an elevated temperature should affect the annealing out of these defects and the possible consolidation of impurity centers by diffusion.

Water produces a more profound effect than any of the impurities tried, except possibly oleic acid (curve 5, Figure 3). Although one may again be able to explain this result as the straightforward prediction of a phase equilibrium study, we are not aware of the possible nature of the stearic acid–water phase diagram. An alternative explanation seems readily available, however, in that hydrogen bonding of water with stearic acid should occur and disturb the regularity of the polar carboxyl layers in the stearic acid crystal and thus produce many defects about which extensive molecular motion may center.

Further evidence of the importance of thermal history in determining the extent to which some molecules are involved in rapid and extensive motion before the bulk of a sample is involved in such motion is offered by a study of lithium stearate.

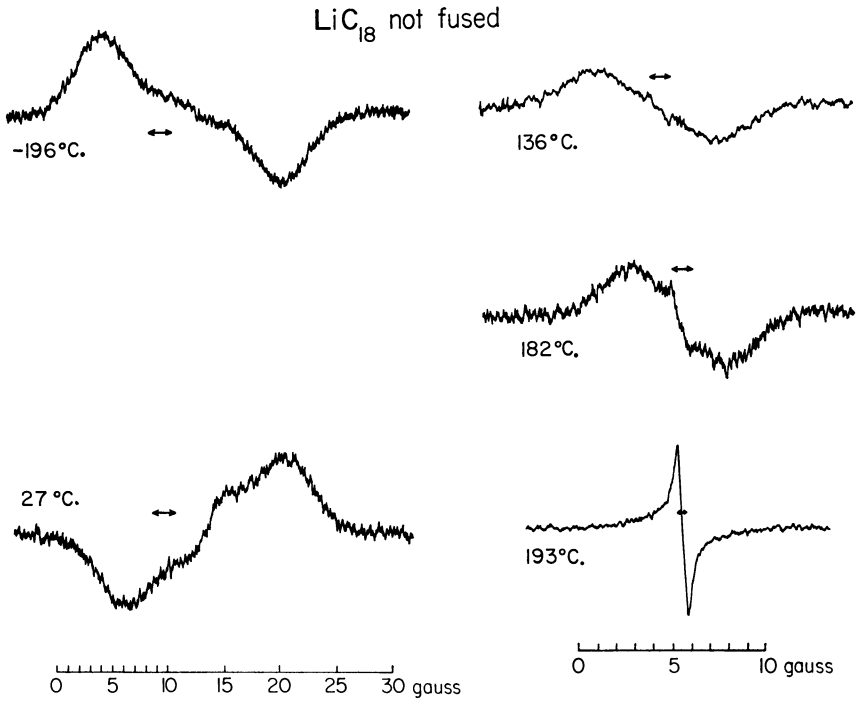

Figure 4. Typical spectra of unfused lithium stearate sample at various temperatures

Publication Date: January 1, 1967 | doi: 10.1021/ba-1967-0063.ch002

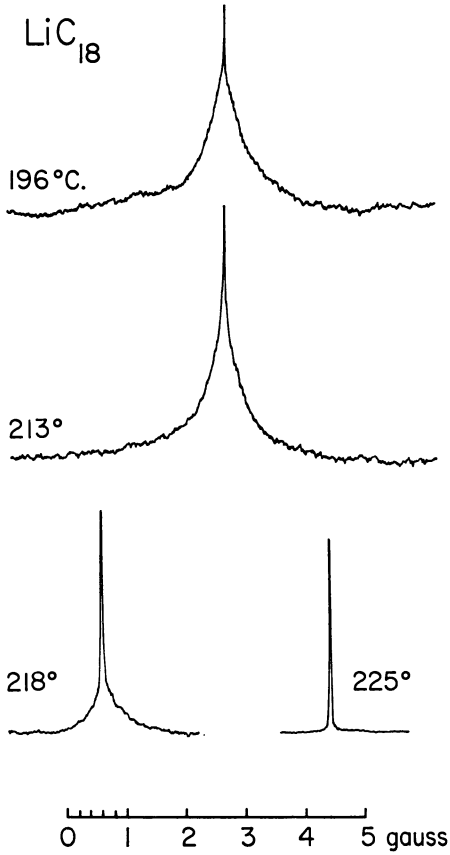

Figure 5. Absorption spectra of fused lithium stearate obtained from a high resolution spectrometer

Lithium Stearate. Differential thermal analysis (*16*) and dilatometric (*5*) studies of lithium stearate have shown that phase transitions occur at 114° ± 1°C. and 180° ± 5°C. Its melting point is near 229°C. (*4*, *5*, *16*). The first of these transitions is regarded as a change from one crystalline form to another, the corresponding change in lithium palmitate at 103°C. having been verified by microscopy as a change in crystal form (*17*). An NMR study (*7*) places the first transition at 114°C. and indicates that the second transition, which depends on thermal history, occurs at about 187° ± 5°C. and has the character of a change from a crystal form to a waxy condition. Figure 4 shows typical line shapes at several temperatures for a lithium stearate sample which had never been fused. The broad line of the second (or high temperature) crystalline form disappears between 184° and 191°C., and the narrow line with significant intensity in the wings, which replaces the broad line, is characteristic of waxy phases of the soaps,

Publication Date: January 1, 1967 | doi: 10.1021/ba-1967-0063.ch002

corresponding to the NMR signal of sodium stearate above 114°C. (*2*), and of potassium, rubidium, and cesium stearates above 170°, 143°, and 100°C., respectively (*10, 13*). We do not imply that the transition from crystalline to waxy is not sharp but only that we did not attempt to specify the transition temperature more precisely, in part because of uncertainty of sample temperature (*ca.* ±2°) in this range.

The absorption signal for the waxy phase of lithium stearate, as obtained from the high resolution spectrometer, is shown in Figure 5 for four temperatures from 196° to 225°C., at which point the spectrum appears to be indistinguishable from that of an isotropic liquid. The second moment of the waxy phase is of the order of 1 gauss² up to 215°C., above which it decreases rapidly to a value of the order of 10^{-4} gauss² at 225°C. This behavior corresponds to the view that the waxy phases in the soaps involve an ordered arrangement of the polar ends of the molecules with the hydrocarbon chains restricted in extent of motion only by the comparative immobility of the polar parts. Diffusion at a rate sufficiently great further to decrease line width and second moment becomes important above 215°C.

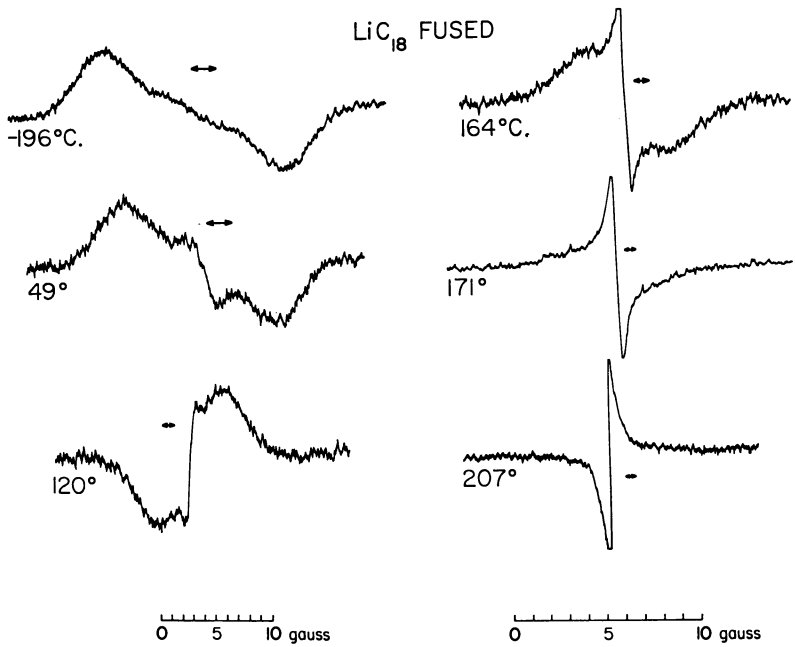

Figure 6. Typical spectra of fused lithium stearate sample at various temperatures

One should also examine spectra for a sample which had been melted during preparation. These are shown in Figure 6, from which one can see that a narrow component "anticipates" the phase change to the waxy state

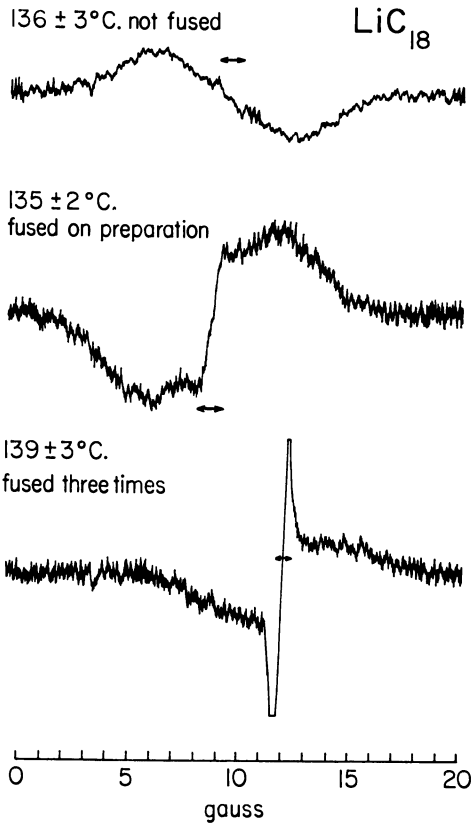

Figure 7. Growth of narrow component with repeated fusion in lithium stearate

many degrees below 187°C., at which temperature we have placed the transition from spectra for the unfused sample. Here, however, the intensity of the narrow component increases so greatly that the broad component becomes lost at as low a temperature as 171°C. Finally, Figure 7 shows the growth of narrow component, attributed to the growth of waxy regions in the lithium stearate crystal phase, with increase in the number of times the sample was fused. At about 136°C. there is no clear evidence of waxy regions in an unfused sample, a small but finite amount of waxy region in a once-fused sample, and a significantly large amount in a thrice-fused sample. It seems reasonable to suggest that in resolidification after melting the sample develops lattice defects about which "waxy" disorder and motion of the hydrocarbon chains can occur at rather low temperatures.

The question arises as to what the behavior is if the lithium stearate is heated only through the crystalline to waxy phase transition and then

Publication Date: January 1, 1967 | doi: 10.1021/ba-1967-0063.ch002

cooled. The spectra in Figure 8 were obtained from the sample which had never been melted but had been heated to 193°C. The 137°C. spectrum in this figure was run 45 minutes after the 193°C. spectrum of Figure 4. Of the 45 minutes, 10 minutes was cooling time and 35 minutes equilibration time. The 184°C. spectrum in Figure 8 was run after 2 hours at this temperature and in a series of spectra taken at progressively increasing temperature beginning at 137°C. (the first spectrum in this figure). The third spectrum in Figure 8 (191°C.) shows the completion of the second passage of this lithium stearate sample through the mesomorphic phase transition, which is shown to be a reproducible transition. Both the 137°

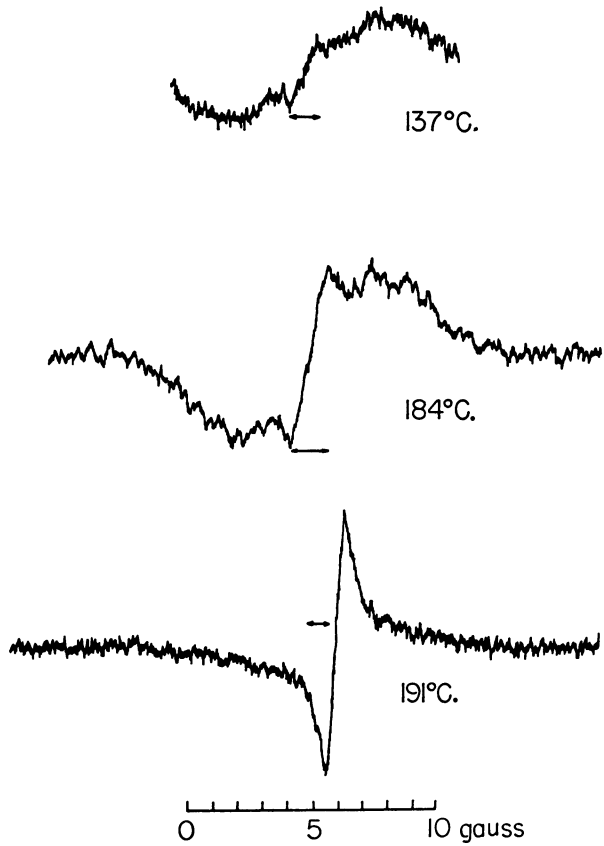

Figure 8. Spectra for unfused lithium stearate sample taken through mesomorphic phase transition, cooled to 137°C., and heated again

and 184°C. spectra show somewhat but not greatly more pronounced evidence of narrow component than corresponding spectra from the sample which had been neither fused nor taken through the mesomorphic transi-

Publication Date: January 1, 1967 | doi: 10.1021/ba-1967-0063.ch002

tion. Because the equilibration time for the 137°C. spectrum was short and 184°C. does not correspond exactly to the 182°C. spectrum of Figure 4, we only say that passage through the crystalline to waxy phase transition has little effect in producing lattice defects about which liquid-like motion can occur compared with the effect of melting, and indeed, it may have no effect at all. This would agree with the work of Vold and Hattiangdi (*15*), who raised the temperature of a sample of lithium stearate to 200°C. and then cooled it slowly to room temperature, taking x-ray diffraction patterns. Correspondence of x-ray patterns before and after heating indicated that the lithium salt is well crystallized and that the phase transitions are reversible.

Acknowledgment

We are grateful to the National Research Council of Canada for the financial assistance of a grant-in-aid of this research.

Literature Cited

(1) Andrew, E. R., *Phys. Rev.* **91**, 425 (1953).
(2) Barr, M. R., Dunell, B. A., *Can. J. Chem.* **42**, 1098 (1964).
(3) Barr, M. R., Dunnell, B. A., Grant, R. F., *Can. J. Chem.* **41**, 1188 (1963).
(4) Benton, D. P., Howe, P. G., Puddington, I. E., *Can. J. Chem.* **33**, 1384 (1955).
(5) Benton, D. P., Howe, P. G., Farnand, R., Puddington, I. E., *Can. J. Chem.* **33**, 1798 (1955).
(6) Brown, J. B., Kolb, D. K., "Progress in the Chemistry of Fats and Other Lipids," Vol. 3, p. 58, Pergamon Press, London, 1955.
(7) Dunell, B. A., Janzen, W. R., *Wiss. Z. Friedrich-Schiller Univ., Jena* **14**, 191 (1965).
(8) Francis, F., Collins, F. J. E., Piper, S. H., *Proc. Roy. Soc. (London)* **A158**, 691 (1937).
(9) Grant, R. F., Dunell, B. A., *Can. J. Chem.* **38**, 359 (1960).
(10) *Ibid.*, p. 1951.
(11) Guy, J. B., Smith, J. C., *J. Chem. Soc.* **1939**, 615.
(12) Krynicki, K., Powles, J. G., *Proc. Phys. Soc.* **83**, 983 (1964).
(13) Shaw, D. J., Dunell, B. A., *Trans. Faraday Soc.* **58**, 132 (1962).
(14) Smith, J. C., *J. Chem. Soc.* **1939**, 974.
(15) Vold, R. D., Hattiangdi, G. S., *Ind. Eng. Chem.* **41**, 2311 (1959).
(16) Vold, R. D., Vold, M. J., *J. Am. Oil Chemists Soc.* **26**, 520 (1949).
(17) Vold, R. D., Vold, M. J., *J. Phys. Chem.* **49**, 32 (1945).

RECEIVED February 11, 1966.

3

Characterization of Mesomorphic Phases by Nuclear Magnetic Resonance Spectroscopy

T. J. FLAUTT and K. D. LAWSON

Miami Valley Laboratories, The Procter & Gamble Co., Cincinnati, Ohio

Publication Date: January 1, 1967 | doi: 10.1021/ba-1967-0063.ch003

The potential of nuclear magnetic resonance spectroscopy for studying liquid crystalline systems is discussed. Typical spectra of nematic, smectic, and cholesteric mesophases were obtained under high resolution conditions. The observed line shape in the cholesteric phase agrees with that proposed on the basis of the preferred orientation of this phase in the magnetic field. The line shapes observed in lyotropic smectic phases appear to be the result of a distribution of correlation times in the hydrocarbon portions of the surfactant molecules. Thermotropic and lyotropic phase transitions are easily detected by NMR and agree well with those reported by other methods. The NMR parameters of the neat and middle lyotropic phases allow these phases to be distinguished and are consistent with their proposed structures.

Mesomorphic phases [or as originally named by Lehmann (*18*), liquid crystals] have been traditionally investigated by optical means, principally with the polarizing microscope. The most important physical method other than the microscope has been x-ray diffraction. This paper shows how nuclear magnetic resonance spectroscopy (NMR) may be used to characterize these phases and discusses the kinds of information which are available from a close analysis of NMR spectra.

NMR investigations of mesomorphic materials were initiated by Spence, Moses, and Jain, who observed that the NMR signal from the nematic phase of *p*-azoxyanisole (PAA) had a line width intermediate between that of a solid and a liquid (*32*). In later papers (*13*, *31*) they discuss the structure found in the NMR spectrum of this compound and the deuterated methoxy analog, ascribing the structure to dipole-dipole interactions. In the last of these papers (*13*) they discuss the temperature dependence of the separation of the triplet structure in PAA. The investigation of the nematic state of PAA and higher homologs was next taken up

In Ordered Fluids and Liquid Crystals; Porter, R., el al.;
Advances in Chemistry; American Chemical Society: Washington, DC, 1967.

by Lippmann and Weber (*20*), who recorded the line shapes and temperature dependence of the second moments of the azoxyphenol di-*n*-alkyl ethers in which the alkyl chains varied from C_1 to C_7. The origin of the structure in the NMR spectra of PAA and its homologs was the subject of further papers by Lippmann (*19*) and Weber (*38*, *39*).

Until the recent work of Saupe and Englert (*5*, *27*) the nematic mesomorphic state had not been observed under high resolution conditions. They found that the NMR signal from the nematic state of PAA is much more complex than had been previously reported. They give a complete analysis of the spin Hamiltonian of the liquid crystal state, including the dipole-dipole interactions, chemical shifts, and spin coupling constants. Although the PAA spectra were too complicated to analyze completely, they were able to apply the theory to molecules dissolved in a nematic phase and to deduce, in favorable cases, ratios of intermolecular distances, anisotropies of chemical shifts, and absolute signs of the spin coupling constants of the dissolved species (*27*, *28*).

Smectic and cholesteric phases have been somewhat less extensively investigated until recently, probably because of the lack of gross structure in the NMR signals from these phases. Dunell and his co-workers (*1*, *9*, *10*, *15*, *29*) have published extensively on the temperature dependence of the NMR signal from various alkali soaps. Their work, however, has been principally concerned with the definition of the crystal-mesomorphic transitions by NMR. Recently Lawson and Flautt (*16*, *17*) have studied the NMR signals of the mesomorphic states of several surfactant and surfactant-water phases under high resolution conditions.

Nematic Phases

The term "nematic," derived from the Greek, *nematos* (threadlike), was given to this mesomorphic phase by Friedel (*7*) because microscopic threadlike structures are usually observable in these systems. At present there are two schools of thought on the over-all molecular structure of the nematic state. One hypothesis is that the molecules are arranged in "swarms" (*2*, *24*, *25*), randomly arranged with respect to one another but with the long molecular axes of the individual molecules approximately parallel to one another in each swarm. The molecules are not, however, separated into layers in the swarms. The size of the swarms depends to some extent upon the temperature. Estimations by several methods place the mean diameter at 10^{-5}–10^{-6} cm. (*3*, *11*). The second hypothesis was proposed by Zocher (*40*). The three basic assumptions of Zocher's hypothesis, commonly called the distortion hypothesis, are: (1) the entire nematic structure is such that the molecular axial directions are everywhere the same; (2) any force disturbing this condition is met by a restoring force of an elastic nature which balances the applied force; (3) the molecular positions originally adopted when the nematic phase is formed in contact

Publication Date: January 1, 1967 | doi: 10.1021/ba-1967-0063.ch003

with a solid surface are almost unchangeable by an external force. Gray (*11*) points out that a compromise between the two hypotheses may be nearer the truth in the light of all the experimental evidence which has been collected on the nematic state. In this respect, Furth and Sitte (*8*) sought to show that the two hypotheses are not incompatible. The nematic phase can be oriented by either an electric or a magnetic field and the effects of these fields on various properties of nematic substances have been extensively studied (*3*, *11*).

Figure 1 shows the absorption spectrum of the nematic phase of PAA obtained under high resolution conditions, at several temperatures. These spectra were obtained under "first side band modulation conditions" discussed by Lawson and Flautt (*17*). These modulation conditions produce base line stability while minimizing the influence of the amplitude and frequency of the modulating field.

Publication Date: January 1, 1967 | doi: 10.1021/ba-1967-0063.ch003

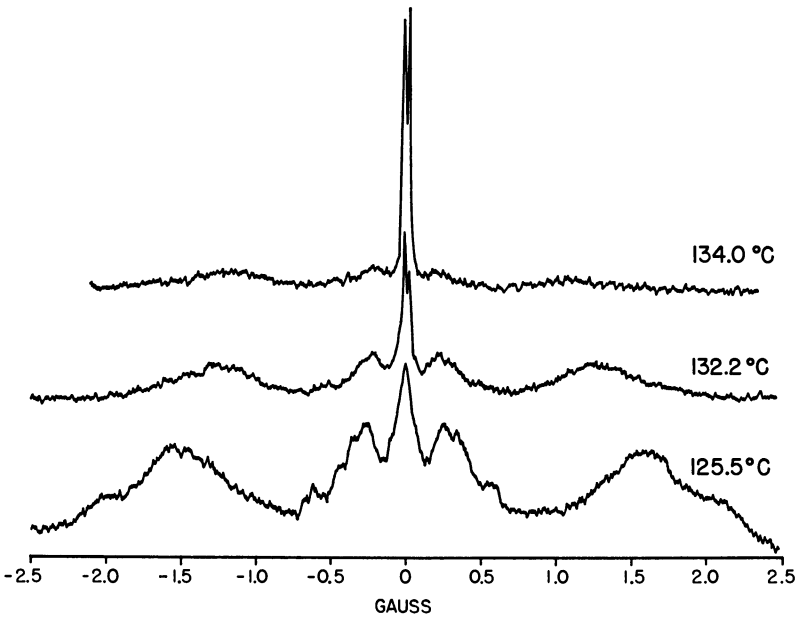

Figure 1. 40-MHz Spectrum of the nematic phase of PAA as function of temperature

The pattern obtained at 125.5°C. has the gross triplet structure observed by Spence and co-workers. However, there is considerably more structure in the signal, particularly in the center feature, as suggested by Saupe and Englert (*5*, *27*). It has been shown by deuterating the methoxy groups (*13*) that the center feature is caused by these groups. The two bands at about ±1.5 gauss are thought to be from the dipole-dipole splittings of the ortho aromatic protons (*19*). The additional structure is undoubtedly caused by other dipole-dipole interactions—for example, the

methoxy group should interact to some extent with all the protons on the aromatic ring, while the cross-ring coupling of the aromatic protons would give additional structure. The center feature is not exactly midway between the side features. It is displaced upfield by 0.3–0.4 gauss, the chemical shift difference between aromatic and alkoxy protons at 40 MHz. The remaining spectra in Figure 1 demonstrate the effect of heating the nematic phase through the nematic-isotropic boundary. As the temperature increases, the outer wings move closer together as the molecular motion of the nematic clusters increases.

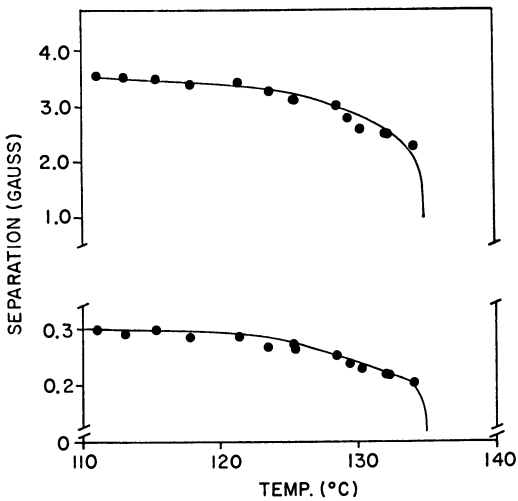

Figure 2. Temperature dependence of separation of the outer features (top) and structure in the inner feature (bottom) of the spectrum of PAA

Figure 2 shows a plot of the separation of the two outer features (upper curve) and the two major components flanking the center component of the center feature (lower curve) as a function of temperature. Both separations decrease continuously throughout the nematic region. The fact that both separations show the same temperature dependence indicates that they are related to the over-all ordering of the nematic phase and that one portion of the molecule probably does not significantly change its motion relative to the other portion over the temperature range characteristic of the nematic phase. Jain, Lee, and Spence (*13*) have related the separation of the outer features to the ordering parameter $\Theta = \langle 3\cos^2\beta - 1\rangle_{av.}$ (here β is the angle between the ortho proton-proton vector and the applied magnetic field). They find a linear relation between the separation and the values of Θ measured by Tsvetkov (*34*) for PAA. This relation is reproduced in Figure 3.

Publication Date: January 1, 1967 | doi: 10.1021/ba-1967-0063.ch003

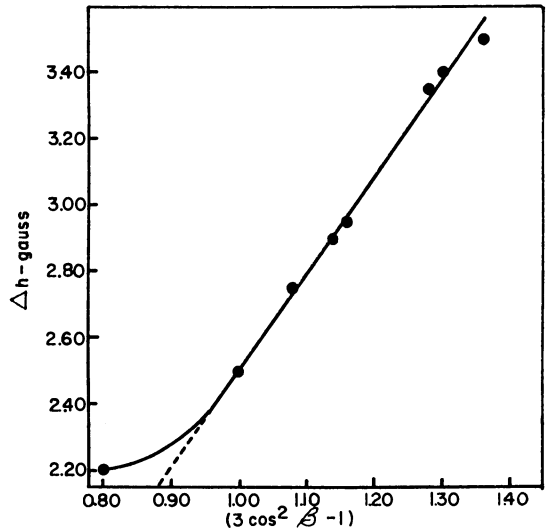

Figure 3. Separation of outer features of PAA (vs.) $\langle 3\cos^2\beta - 1\rangle_{av}$ (13)

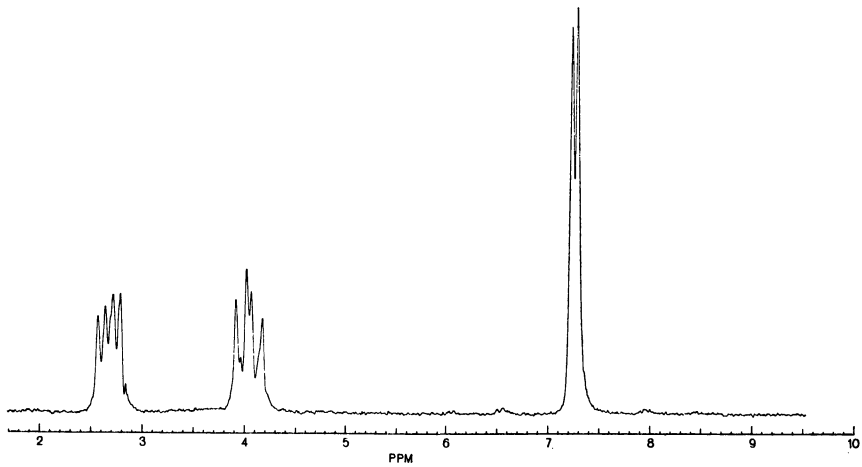

Figure 4. 60-HMz Spectrum of isotropic phase of PAA Obtained at 135°C. on a Varian A-60 spectrometer and calibrated with respect to external TMS

Several degrees below the transition temperature, as defined by optical microscopy, there appear two sharp peaks at the center of the central feature. These peaks may be assigned to the isotropic liquid. Their intensity grows as the nematic pattern diminishes when the temperature is raised through the transition temperature. Above the transition temperature one sees an ordinary high resolution spectrum as shown in Figure 4.

Publication Date: January 1, 1967 | doi: 10.1021/ba-1967-0063.ch003

The low-field multiplet arises from the aromatic protons, and the high-field doublet arises from the methoxy protons.

Smectic Phases

Friedel (*7*) chose the name smectic, from the Greek, *smectos* (soaplike), because these phases have certain properties reminiscent of those found in many soaps. In the smectic phase the molecules are arranged side by side in a series of layers. In some cases the molecules within the individual layers are arranged in rows, but in other materials they are randomly distributed. In either case, however, the long axes of all the molecules in a given layer are approximately parallel and are perpendicular or almost perpendicular to the plane of the layers. The layers may in some cases be two molecules thick, in other cases only one molecule thick (*11*).

The spectrum of a smectic phase, the superwaxy phase of anhydrous sodium stearate (NaS), is shown in Figure 5. There is considerably less structure than in the spectra of nematic mesophases. Hence, the smectic

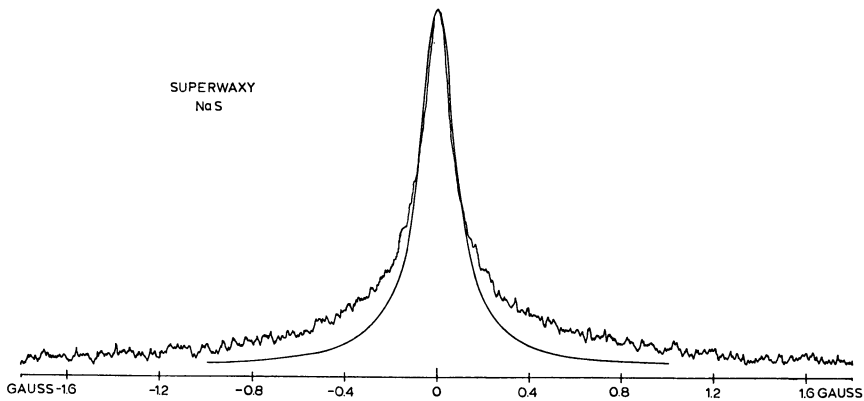

Figure 5. 40-MHz Spectrum of superwaxy phase of NaS at 160°C.
——Lorentzian line

phase is probably not ordered by the magnetic field. The line shapes of the smectic phases are unique. They are broader in the wings than one would expect from the width at half height. Generally one would expect the line shape of NMR signals, in the limit of rapid molecular motion, to lie somewhere between the Gaussian and the Lorentzian shape. These lines fall off more slowly than a Lorentzian line of the same width, as shown in Figure 5. The smooth curve represents a Lorentzian curve having the same intensity and half width as the experimental curve. Hence it has been proposed that these smectic phase NMR line shapes be termed "super-Lorentzian" (*16*, *17*). A suggested origin of the shape has been given (*16*, *17*) in terms of a distribution of correlation times in the hydrocarbon portion of the surfactant molecules.

Publication Date: January 1, 1967 | doi: 10.1021/ba-1967-0063.ch003

Cholesteric Phases

The name of the cholesteric phase was also suggested by Friedel (*7*). It was chosen because the majority of compounds exhibiting this type of mesophase are derivatives of cholesterol or some other sterol system. The molecules in a cholesteric mesophase are similar to those in a smectic phase in the sense that they are arranged in layers. However, within the layers the molecules have a parallel alignment reminiscent of the nematic arrangement. The layers in the cholesteric phase are thin and, because of the molecular geometry, the long axes of the molecules in each sheet or layer are slightly displaced from those in the neighboring layers. Through successive layers the over-all displacement of the molecular axes traces out a helix.

When placed in a magnetic field it is believed that the cholesteric phase orients so that the axis of the helix, which is the optical axis, is perpendicular to the field (*27*). In this orientation the planes of the individual molecules are parallel to the field, and the long axes of the molecules, which lie in these planes, are oriented at all angles with respect to the field. On the basis of this orientation Saupe (*27*) has suggested that the NMR line from the cholesteric phase should be broad at the base (roughly as wide as the separations noted in nematic phases) but taper to a relatively sharp spike in the center. No specific structure is expected to be present in the lines.

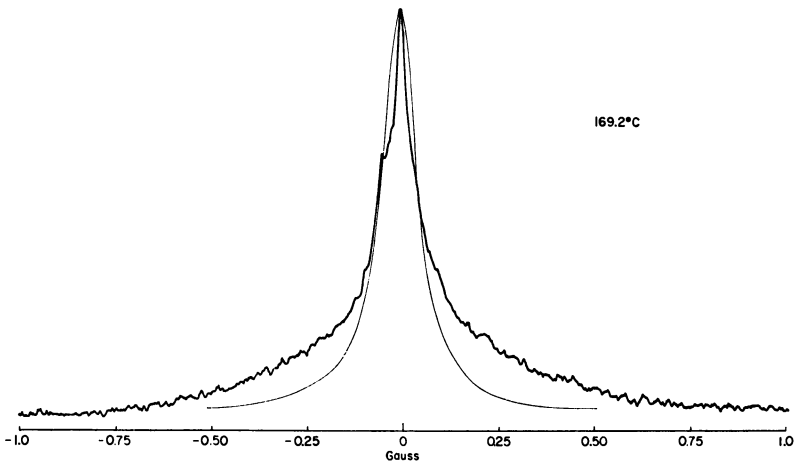

Figure 6. 40-MHz Spectrum of cholesteric phase of ChBz at 169.2°C. ——Lorentzian line

This kind of shape is expected, Saupe points out, because the line-broadening mechanism, mainly dipole-dipole interactions, obeys a $(3\cos^2\alpha - 1)$ relation where α is the angle between the field and the proton-proton vectors. Some of the sheets of molecules will be oriented so that α will be 0°,

thus producing a wide line; others will be arranged so that the angle is about 55°, which reduces the broadening function to zero. The lines from these sheets will be sharp. The observed shape is then a superposition of the lines from the various molecular sheets, which should lead to the shape described above.

In Figure 6 the spectrum of the cholesteric phase of cholesteryl benzoate (ChBz) is reproduced. Also shown, by the smooth curve, is a calculated Lorentzian line having the same intensity and width at half height as the experimental curve. The line shape is just as Saupe predicted (*27*), broad at the base and sharp in the center. No structure is seen except the small shoulder on the low-field side which arises from the aromatic protons in the benzoate group. A completely structureless line has been reported for ChBz (*14*), but that line was not obtained with as much resolution as the one in Figure 6.

The cholesteric phase line shape is similar to those found in smectic phases and could also be called "super-Lorentzian." It is not believed, however, that the origins of the line shapes in the two kinds of phases are the same since the smectic phase has never been shown to have any preferred orientation in a magnetic field (*27*). It is shown below that the smectic line shape can be changed significantly by changing the molecular structure and that it appears to have its origin in the molecules rather than in the over-all orientation of the phase.

Publication Date: January 1, 1967 | doi: 10.1021/ba-1967-0063.ch003

Phase Transitions

One-Component Systems. Since the line widths of the mesomorphic states are all intermediate between those displayed by a solid and those displayed by a liquid, it is possible to use the line width to construct phase diagrams.

For a one-component system, such as cholesteryl benzoate, the change in most physical properties (such as optical activity) is sufficiently large so that NMR need not be used. Nevertheless, Figure 7 shows that the changes in line width from the crystalline phase to the mesomorphic phase and from the mesomorphic phase to the isotropic phase are large enough and abrupt enough to enable the phase transitions to be detected easily. The transition temperatures determined from the line width changes agree well with those found by other techniques (*3*, *11*). As in the case of PAA, ChBz shows a normal high resolution spectrum above the cholesteric-isotropic transition.

In Figure 8 the line widths of the crystalline, nematic, and isotropic phases of PAA are shown as a function of temperature. As in ChBz, the changes are abrupt enough and of such magnitudes that the phase transitions are easily detected. The two widths indicated in the nematic phase are of the center feature and of the members of the outer feature (*see* Figure

In Ordered Fluids and Liquid Crystals; Porter, R., el al.;
Advances in Chemistry; American Chemical Society: Washington, DC, 1967.

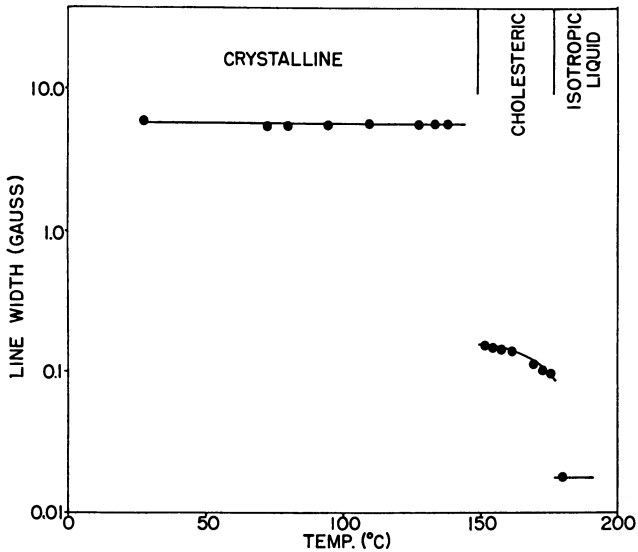

Figure 7. Line width of ChBz as a function of temperature

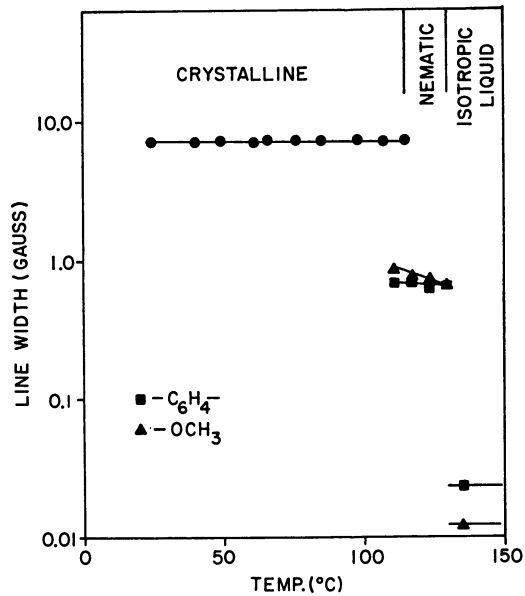

Figure 8. Line widths of PAA as a function of temperature

1). Here again the transition temperatures agree well with those determined by other methods (*3*, *11*).

When there are several mesomorphic phases, NMR can detect the phase changes by small but abrupt changes in the line width. For ex-

Publication Date: January 1, 1967 | doi: 10.1021/ba-1967-0063.ch003

ample, studying several anhydrous sodium soaps has shown that all the phase changes can be detected by NMR (*17*). Figure 9 shows the NMR line widths of the high-temperature mesophases in anhydrous sodium stearate (NaS), sodium palmitate (NaP), sodium myristate (NaM), and sodium laurate (NaL) as a function of temperature. The line widths were

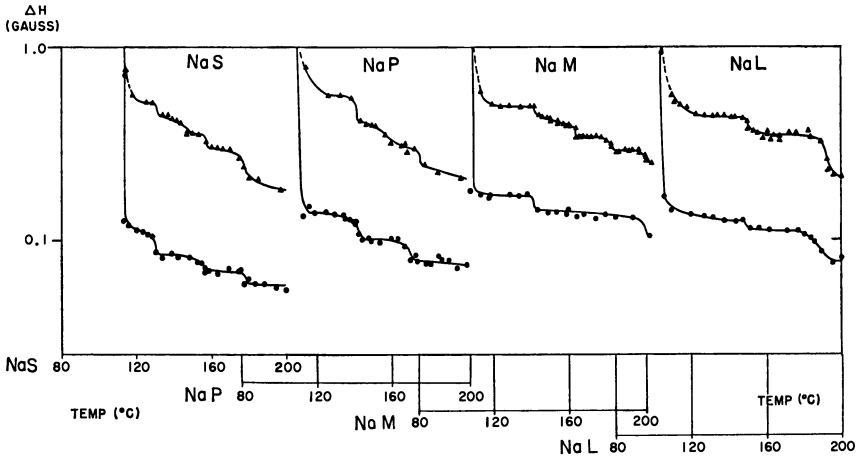

Figure 9. Line widths of waxy phases of anhydrous NaS, NaP, NaM, and NaL as function of temperature (16)

Table I. Phase Transitions in High Temperature Mesophases of Anhydrous Sodium Soaps

	Transition Temperature, °C.							
	NaS		*NaP*		*NaM*		*NaL*	
Transition	*NMR*	*Other*	*NMR*	*Other*	*NMR*	*Other*	*NMR*	*Other*
Crystalline → subwaxy	114	108–18	113	114–25	108	98–113	104	98–100
Subwaxy → waxy	131	129–34	143	134–40	141	133–42	148	130–42
Waxy → superwaxy	158	165–80	174	172–76	182	175–82	191	182–87
Superwaxy → subneat	180	188–210	>200	195–200	203	204–18	>200	200–20

measured in two ways. The triangles represent the widths as measured at one-half the maximum intensity of the absorption curves. The circles represent the widths as measured between the maxima and minima points of the derivatives of the absorption curves. The ratio between the widths measured in the two positions is 1.73 for a Lorentzian line and 1.18 for a Gaussian shape. The mesophase lines shown in Figure 9 have ratios from 5 to about 3, indicating the large deviation from a Lorentzian shape, as was shown in Figure 5.

The transitions among the various phases are indicated by the abrupt changes in the line widths. In most cases the changes are observed by both methods of measuring, but it appears that the half-height measure-

ment is the most sensitive to small changes. This is reasonable, since this measurement is made farther down on the curves, and the changes in width are larger here. The transition temperatures taken from the line width changes are tabulated in Table I and are compared with values reported by other methods. A specific listing of the sources is given by Lawson and Flautt (*17*). The accuracy of the NMR data is about ±2°C. In some cases the line width changes occur over a 4–5°C. range, making it difficult to select a single value for the transition temperature. In these cases the temperature listed in Table I is the temperature in the center of the range. In general the agreement between the NMR values and the values reported by other methods (optical microscopy, x-ray diffraction, calorimetry, dilatometry) is good. In addition to the transitions listed in Table I, according to the NMR line width, there is apparently an additional transition in NaM at 162°C.

Publication Date: January 1, 1967 | doi: 10.1021/ba-1967-0063.ch003

The mesomorphic phases occurring at high temperatures in anhydrous or nearly anhydrous sodium soaps have been grouped into two distinct families by Skoulios and Luzzati (*30*) on the basis of information obtained from x-ray studies. The family which occurs at the lowest temperatures is made up of the subwaxy, waxy, superwaxy, and subneat phases. The other family contains only one member, the neat phase. Since there is no NMR information on this high-temperature phase, the structure will not be discussed. In the low-temperature family the polar ends of the soap molecules are arranged in double layers. This layering of the polar groups produces layers of molecules which are two molecular lengths thick. The molecular layers have finite widths but may extend indefinitely, having a "ribbon-like" appearance. The polar groups are believed to be well ordered in the layers, but the hydrocarbon chains are disordered and exist more or less as they would in a liquid, except that they do not have translational freedom.

Table II. Experimental Second Moments of High Temperature Mesophases in Anhydrous Sodium Soaps

	Second Moment, Gauss[2]			
System	*Subwaxy phase*	*Waxy phase*	*Superwaxy phase*	*Subneat phase*
Sodium stearate	0.84 (126°C.)	0.36 (140°C.)	0.24 (170°C.)	0.11 (197°C.)
Sodium palmitate	0.29 (134°)	0.25 (157°)	0.13 (185°)	....
Sodium myristate	0.92 (133°)	0.60 (150°)	0.24 (190°)	0.16 (200°)
		0.39 (170°)		
Sodium laurate	0.37 (130°)	0.21 (155°)	0.18 (195°)	....

When a transition occurs between two of the waxy type phases, the average width of the polar ribbons is believed to change. Decreases in the widths of the polar layers should allow the hydrocarbon chains to have

more freedom of movement and should lead to a decrease in the width of the NMR line.

The order of the line widths of the waxy phases deserves some comment. There is some correlation between the line widths and the lengths of the hydrocarbon portion of the molecules. With perhaps the exception of NaL, the line widths increase as the chains become shorter. At most temperatures the order of the line widths is NaM > NaL > NaP > NaS. It is expected that a longer chain will be more mobile and thus have a sharper line. The order of the line widths in a given soap is without exception subwaxy > waxy > superwaxy > subneat; the neat phase is not found in the temperature range covered in this study. As expected, the line widths decrease with increasing temperature.

In Table II representative second moments of the various waxy phases are tabulated (*17*) along with the temperatures at which they were determined. In most cases the determinations were made in the center of the range of existence of the particular phase. Second moments were not determined at every temperature at which a line width measurement was made. The second moments are in the same order as the line widths within a given soap, but there appears to be little correlation between the chain lengths and the magnitude of the moments. For the most part it appears that the values of the second moments depend upon the temperature.

Multicomponent Systems. There are many mesomorphic systems in which at least two components are present. The most common variety is called a lyotropic mesophase; it consists of a molecule with a hydrophilic and a hydrophobic portion dissolved in water. Since at least two components are present, there can be a coexistence of more than one phase. The classical method of investigating such systems consisted of mixing the two components together, centrifuging until the two phases were separate, and analyzing each phase. By NMR it is possible to make a qualitative analysis of each phase without separation in many cases. The sodium palmitate (NaP)–deuterium oxide (D_2O) system shows the sort of information which can come from such an analysis. The NaP–D_2O system exists in several different mesomorphic phases in addition to the isotropic liquid and crystalline phases (*6*, *23*, *36*, *37*). The mesophases are mainly of the smectic type although the lyotropic mesophase normally called middle does not have all the characteristics of a true smectic phase.

The NMR line widths of the hydrocarbon chain protons of NaP in D_2O are shown in Figure 10 as a function of temperature and concentration. The line widths are represented on the vertical axis. Figure 10 shows clearly the relationships among the line widths of crystalline, mesomorphic, and liquid phases which were pointed out in the one-component systems discussed previously. The widest lines (10 to 12 gauss) arise from the crystalline phase, which in this system is identified as the beta phase (*33*) by x-ray diffraction. The intermediate line widths (in the areas enclosed

Publication Date: January 1, 1967 | doi: 10.1021/ba-1967-0063.ch003

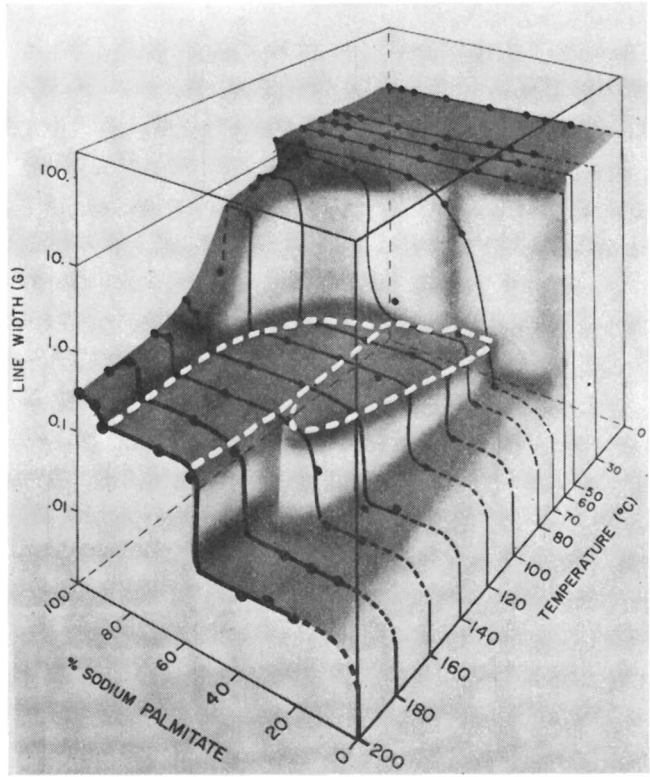

Figure 10. Line widths of NaP-D_2O system as a function of temperature and concentration (16)

by the light dashed lines) are from the neat and middle mesomorphic phases (*26*). The line widths intermediate between those from the neat and middle phases and those from the crystalline phase represent the waxy family of mesophases (*33*, *37*) described previously. The sharpest lines (the level around 10 milligauss) arise from the fluid isotropic phase. The lines from this phase are nearly the same in width as those one would find in any normal liquid. With the exception of the crystalline lines, all the widths were measured at one-half height on the absorption curves (*17*). The crystalline line widths were measured from derivatives of the absorption curves.

It is obvious that the differences in line widths can be used to determine the temperatures of the various phase transitions in this system in the same way in which they were used in the simpler one-component systems. Several transition temperatures determined from the NMR line widths are tabulated in Table III along with values taken from other sources (*23*). The NMR values and the literature values, which were taken from a constructed phase diagram, are both probably no more accurate than ±2°C.

The literature values were determined from x-ray and vapor pressure measurements. For the most part the agreement between the two sets of data is good. The substitution of D_2O for H_2O is expected to have little effect on the phase diagram (*4*), making it possible to compare the two sets of data directly.

The second moments of the crystalline phase range from about 12 to about 18 gauss^2 at room temperature, the change being produced by changing concentration of NaP. The moments decrease with temperature in roughly the same manner as the line widths. The second moments of the waxy type phases in anhydrous NaP range from about 0.1 to about 0.3 gauss^2 as shown in Table II and are in the order subwaxy > waxy > superwaxy. These three waxy phases are the only ones encountered in this system in the temperature range covered. The second moments of the isotropic liquid phase were not determined, but, as with most liquids, they should be of the order of 10^{-4}–10^{-6} gauss^2.

Table III. Phase Transitions in Sodium Palmitate-Deuterium Oxide System

Transition[a]	*Concentration of Sodium Palmitate*	*Transition Temperature, °C.*	
		NMR	*Lit. (23)*
Omega + neat → subwaxy + neat	95	115	124[b]
Subwaxy + neat → waxy + neat	95	150	140[b]
Waxy + neat → superwaxy + neat	95	190	184[b]
Omega + neat → neat	90	125	122[b]
Beta + neat → neat	70	87	82
			87[b]
Beta + liquid → beta + middle	70	70	70
	55	70	70
	40	70	70
Beta + neat → middle + neat	55	81	81
Beta + middle → middle	40	75	78
Middle → liquid	40	165	169
Beta + liquid → middle + liquid	30	70	70
Middle + liquid → liquid	30	135	130
Beta + liquid → liquid	20	67	69

[a] Crystal phase identification by F. B. Rosevear.
[b] Transition determined by F. B. Rosevear.

Of all the lines encountered in this system only those from the isotropic liquid phase show any structure. The shapes of the lines from the lyotropic mesophases are similar to that of superwaxy NaS shown in Figure 5. These shapes are discussed in more detail below. There are also small but definite differences between the line widths from the neat and middle phases which are not visible on the scale used in Figure 10.

While not illustrated in Figure 10, NMR can detect one phase in the presence of another when the line widths of the two phases are sufficiently

Publication Date: January 1, 1967 | doi: 10.1021/ba-1967-0063.ch003

different. Crystalline phase lines and mesophase or liquid phase lines are different enough to allow this, and in many sections of the NaP–D_2O system two-component lines are observed. In fact, in most of the crystalline region the presence of the liquid phase or one of the mesomorphic phases can be observed.

Phase Identification

Structures. The three types of mesomorphic phases are usually identified by using the polarizing microscope (*11*). The different types of lyotropic smectic mesophases can also be distinguished through their microscopic textures (*26*) by careful and detailed study. Using the microscope for such identifications is sometimes made more difficult by the tendency of the mesophases to orient when placed in contact with a surface. This orientation, of course, changes the microscopic textures. A mesophase in the presence of a crystalline phase may also be difficult to identify by microscopy. NMR can provide distinguishing characteristics which are unique for several mesophases. The use of the NMR characteristics for phase

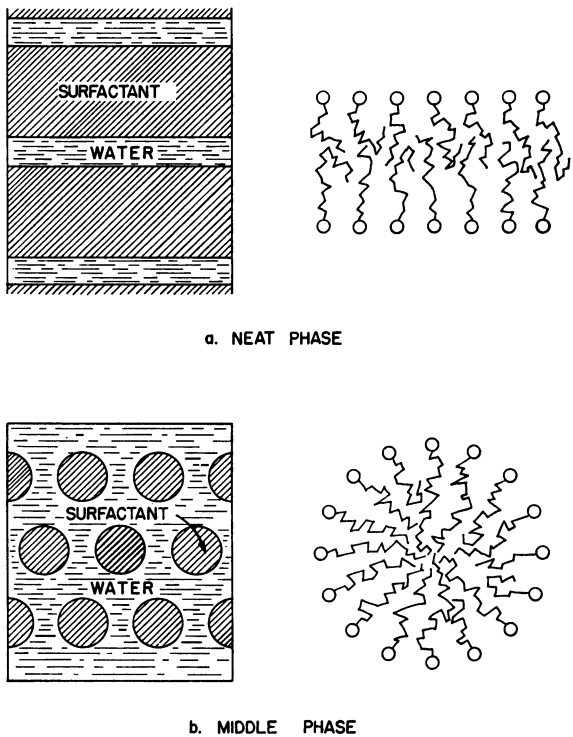

Figure 11. Schematic structures of neat and middle phases (22)

identification has proved most useful in the lyotropic smectic mesophases and in cases where the mesophase is in equilibrium with another phase.

The two most common lyotropic mesophases are designated "neat" and "middle" (*26*). Both are members of the family of mesomorphic structures derived by Hermann (*12*). The neat phase structure is generally accepted as being made up of parallel, equidistant sheets of double molecules separated by solvent (*4*, *21*, *22*). Neat phase is optically anisotropic and flows easily. Figure 11 indicates the structure (*22*) and a cross-sectional view of one of the layers.

The structure proposed for middle phase is made up of either cylindrical units arranged in a hexagonal array (*22*) or rodlike units made up of linearly aggregated spherical micelles (*4*) also arranged in a hexagonal array. The latter arrangement has the appearance of a rigid "string of beads." A sketch of the middle phase structure is also shown in Figure 11 along with a cross-sectional view of the cylindrical or "beaded" units. In either of the middle structures the units of surfactant molecules are separated from each other by the solvent. Normally the hydrophilic groups of the surfactant molecules lie on the surfaces of the units, as shown in Figure 11, and the hydrocarbon chains fill the interiors in a random arrangement. Middle phase is optically anisotropic, plastic-like, and in most systems, transparent.

A third lyotropic mesophase which occurs frequently in surfactant-water systems is normally designated "viscous isotropic." This phase is very viscous, sometimes brittle, but unlike neat and middle it is not birefringent. The structure of the viscous isotropic phase is still not known with certainty. In some systems x-ray studies have indicated that the structure consists of spherical units packed in a face-centered arrangement (*4*, *22*). It has been proposed that the polar groups of the molecules cover the outside surfaces of the spherical units and that the hydrocarbon chains are essentially liquid in their arrangement inside the units. In this respect the structure is similar to one of the proposed middle phase structures (*4*). As in the other lyotropic phases, the solvent probably fills the voids among the spherical units of surfactant.

Spectra of Neat and Middle Phases. Typical spectra of the neat and middle phases are shown in Figures 12 and 13. These spectra were obtained at 100°C. from systems of 70% surfactant (neat phase) and 40% surfactant (middle phase) in D_2O. The small peak, or shoulder, visible on the low-field side of the spectra arises from the residual HDO in the solvent. Shown also in the figures, by means of dots, are calculated Lorentzian lines having the same heights and widths as the experimental lines. The experimental lines have the "super-Lorentzian" shapes discussed above.

The line widths of several neat and middle phases, all measured at 100°C., are included in Table IV. The widths were all determined at half height on the absorption curves. In all systems the middle phase line width is less than the neat phase line width. Evidently in the neat phase,

Publication Date: January 1, 1967 | doi: 10.1021/ba-1967-0063.ch003

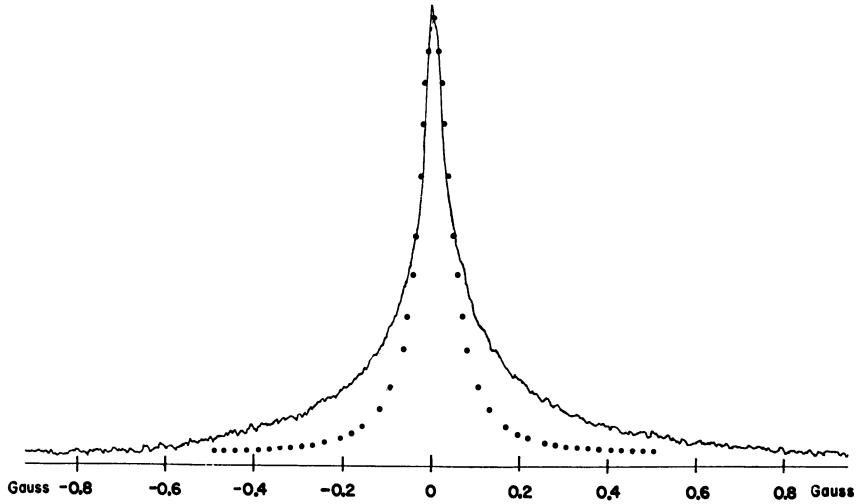

Figure 12. 40-MHz Spectrum of neat phase NaP at 100°C. (16)
. . . . Lorentzian line

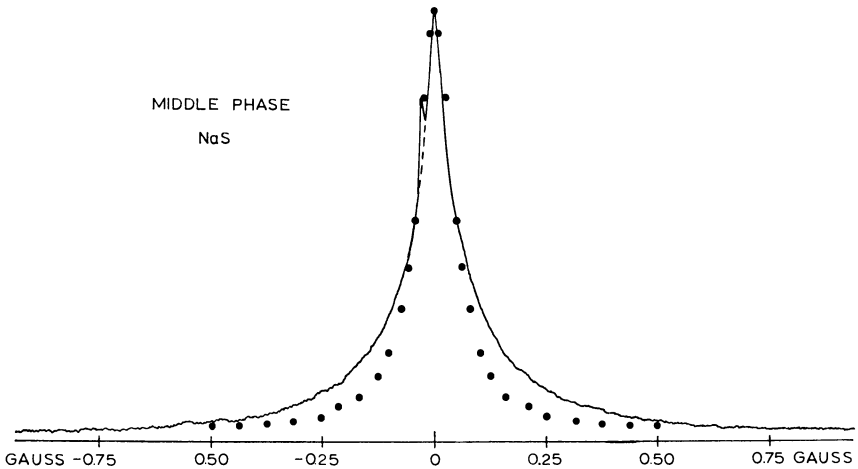

Figure 13. 40-MHz Spectrum of middle phase NaS at 100°C.
. . . Lorentzian line

where the amount of solvent is less, the surfactant molecules are packed closer and are more ordered. Both factors would tend to broaden the line. In general, the difference between the line widths of the two phases, in the same system, is about 20 to 30 milligauss.

For the most part the relation between the neat and middle phase line widths noted at 100°C. holds at all temperatures. The neat phase widths remain larger than the middle phase widths in all the systems listed in

Table IV except in the dimethyldodecylamine oxide ($DC_{12}AO$) system. The line widths of this system are shown in Figure 14. Around 60°C. the middle phase width becomes greater than the neat phase width. The abrupt changes in the two widths occur at the mesomorphic-isotropic tran-

Table IV. Line Widths of Neat and Middle Phases in Surfactant-Deuterium Oxide Systems at 100°C.

	Line Width, Milligauss		
System	*Neat phase (70% in D_2O)*	*Middle phase (40% in D_2O)*	*No. of Carbon Atoms in Hydrocarbon Chain*
Dimethyldodecylamine oxide	134[a]	120[b]	12
Sodium laurate	197	128	12
Potassium laurate	157	118	12
Sodium myristate	165	117	14
Potassium myristate	151	125	14
Sodium palmitate	162	112	16
Potassium palmitate	152	95	16
Sodium stearate	139	105	18
Potassium stearate	115	95	18
Sodium oleate	183	105	18 (cis)
Potassium oleate	130	89	18 (cis)
Sodium elaidate	140	106	18 (trans)

[a] 75% in D_2O.
[b] 45% in D_2O.

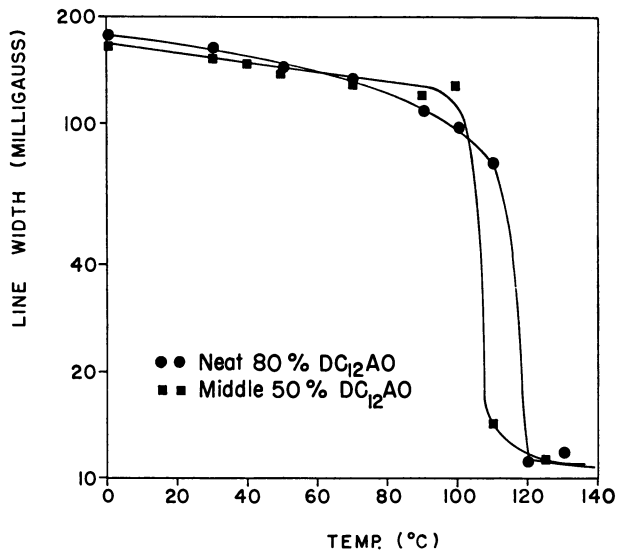

Figure 14. Line widths of neat and middle phases of $DC_{12}AO$ as a function of temperature

Table V. Second Moments of Neat and Middle Mesomorphic Phases in Surfactant-Deuterium Oxide Systems

System	*Temp., °C.*	*Second Moment, Gauss²*	
		Middle phase[a]	*Neat phase*[b]
Sodium palmitate	75.0	3.43×10^{-2}	...
	80.0	...	1.05×10^{-1}
	100.0	2.91×10^{-2}	1.41×10^{-1}
	120.0	2.48×10^{-2}	1.47×10^{-1}
	150.0	1.87×10^{-2}	1.07×10^{-1}
	185.0	...	0.80×10^{-1}
Sodium myristate	60.0	3.70×10^{-2}	...
	85.0	3.93×10^{-2}	1.71×10^{-1}
	100.0	2.71×10^{-2}	1.47×10^{-1}
	120.0	2.37×10^{-2}	...
	140.0	2.38×10^{-2}	...
Sodium oleate	40.0	2.91×10^{-2}	...
	45.5	...	1.35×10^{-1}
	50.0	...	2.11×10^{-1}
	55.0	2.57×10^{-2}	...
	60.6	...	1.12×10^{-1}
	80.0	...	0.97×10^{-1}
	85.0	2.05×10^{-2}	...
	100.0	2.00×10^{-2}	0.84×10^{-1}
	120.0	2.06×10^{-2}	...
	124.5	...	0.93×10^{-1}
	140.0	2.15×10^{-2}	0.82×10^{-1}
Dimethyldodecylamine oxide	28.0	5.00×10^{-2}	1.61×10^{-1}[c]

[a] 40% surfactant in D_2O.
[b] 70% surfactant in D_2O.
[c] 75% amine oxide in D_2O.

sitions. Although the neat and middle phase line widths are slightly different, the difference is generally not great enough to allow the widths to be used as a reliable means of distinguishing the two phases. The order of the line widths appears to be consistent with the structural pictures of the two phases; however, the details of the middle phase structure cannot be determined from the NMR data.

In Table V some experimental second moments from several neat and middle phases are shown. Although the accuracy of the second moment measurements is not great, mainly because the wide "wings" in the curves make it difficult to determine where to truncate, it is obvious that the moments from the neat phases are larger than those from the middle phases. This again is reasonable since the molecules in the neat phase are expected to be more closely packed and to enjoy less freedom of movement. The moments from the neat phases are nearly the same in magnitude as the moments from the waxy phases (Table II). This is consistent with their structural similarity.

Publication Date: January 1, 1967 | doi: 10.1021/ba-1967-0063.ch003

Another parameter which illustrates the differences between the lines from the two kinds of phases, as well as the deviation of the line shapes from a Lorentzian shape, is illustrated in Figures 15 through 17. This parameter, designated $R(8/2)$, is the ratio of the line width at eighth-height to the line width at half-height. In all systems studied, $R(8/2)$ is always larger for the lines from the neat phase than from the middle phase, regard-

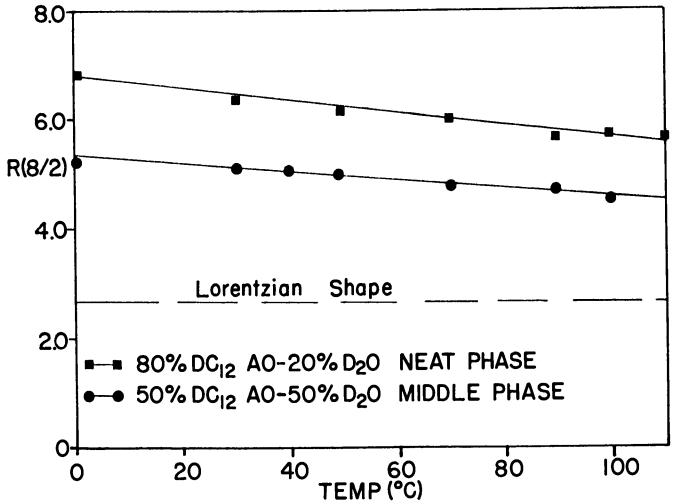

Figure 15. Line width ratios from neat and middle phases of $DC_{12}AO$ as a function of temperature

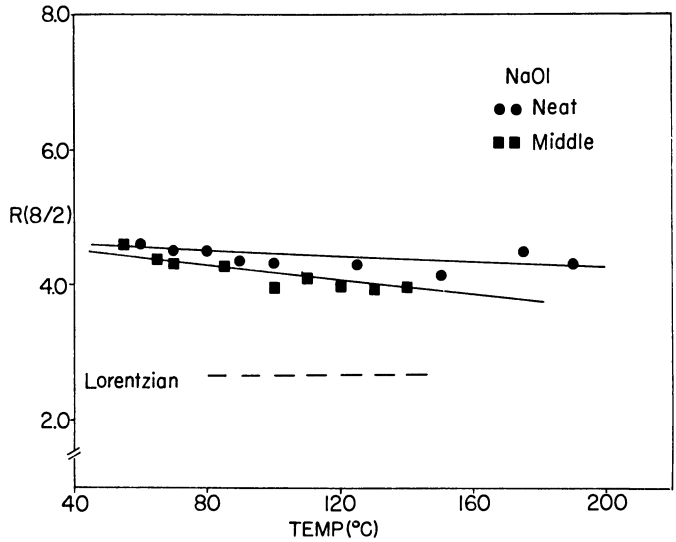

Figure 16. Line width ratios from neat and middle phases of NaOl as a function of temperature

less of the order of the line widths—for example, the line widths in the $DC_{12}AO$ system (Figure 15) actually reverse order as the temperature is raised, but the $R(8/2)$'s for the same lines (Figure 15) remain in the same order.

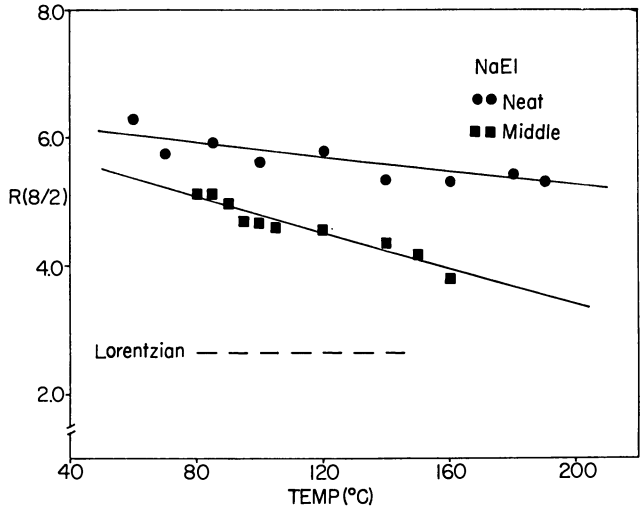

Figure 17. Line width ratios from neat and middle phases of NaEl as a function of temperature

Of the three parameters, line width, second moment, and $R(8/2)$, the $R(8/2)$'s appear to be most useful in offering a clear distinction between the neat and middle phases. The second moments appear to be consistently different in the two phases, but reliable values of this parameter are difficult to obtain from these lines.

Spectra of Viscous Isotropic Phase. The viscous isotropic phase has been found in several systems (*4*, *22*). The structure which has been proposed for this phase, mainly on the basis of x-ray diffraction studies, has been described. The viscous isotropic phase has been studied in two different systems by NMR. In Figure 18 the spectrum of the viscous isotropic phase in the $DC_{12}AO$ system (67.5% $DC_{12}AO$ in H_2O) is shown. This spectrum was obtained at 32°C. Except for a slight broadening of the individual lines, it is almost identical to that found in the dilute fluid micellar phase. In Figure 19 the spectrum of the viscous isotropic phase in 3-(dodecyldiethylammonio)-propane-1-sulfonate, $[C_{12}H_{25}N^+(C_2H_5)_2(CH_2)_3 SO_3^-]$ ($DEC_{12}APS$), is shown. The spectrum was also obtained at 32°C. from a 60% solution in D_2O and is similar to that of a normal low viscosity isotropic liquid.

Positive statements relating the structure of the viscous isotropic phase to the high resolution spectra are difficult to make. It is evident, because of the large differences between the spectra of this phase and the middle

Publication Date: January 1, 1967 | doi: 10.1021/ba-1967-0063.ch003

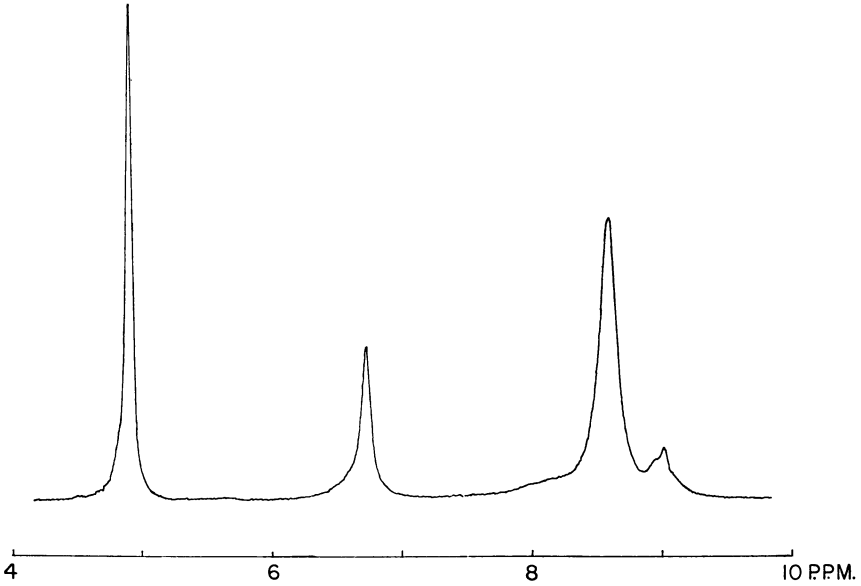

Figure 18. The 60-MHz spectrum of viscous isotropic phase of $DC_{12}AO$ Obtained at 32°C. on a Varian A-60 spectrometer and calibrated with respect to external TMS

phase, that the structures of the two must be considerably different. According to the proposal of Clunie, Corkill, and Goodman (*4*), the middle and the viscous isotropic phases possess similar structures, in the former a hexagonal arrangement of spherical units and in the latter a cubic arrangement. This proposal is difficult to reconcile with the enormous differences in the NMR spectra.

Obviously the viscous isotropic phase is easily distinguished from the neat and middle phases by means of its NMR characteristics.

Line Shapes and Structure of Lyotropic Mesophases

The unique "super-Lorentzian" line shapes found in the lyotropic neat and middle phases can be explained in terms of a distribution of correlation times of the surfactant chain protons similar to the conditions in the waxy phases (*17*). This explanation can be related to the structures proposed by Luzzati (*22*) for these phases, shown in Figure 11, if it is assumed that the chain protons near the hydrophilic groups are more restricted in their motion than those near the ends of the hydrocarbon chains. Several lines of evidence support this hypothesis.

The $R(8/2)$ parameter may be considered as a measure of the departure from a single correlation time; in the neat and middle phases $R(8/2)$ is always larger than that expected from the Lorentzian line shape characteristic of a single correlation time. The deviation of the $R(8/2)$'s from the

Publication Date: January 1, 1967 | doi: 10.1021/ba-1967-0063.ch003

Lorentzian value (2.64) is shown in Figures 15, 16, and 17. $R(8/2)$ is always larger for the neat phase than for the middle phase at a given temperature. Because the middle phase is a less compact structure than the neat phase, there should be more over-all motion and therefore less of a distribution of relaxation times in middle phase. The line widths tabulated in Table IV indicate that the middle phase is more mobile. The temperature dependences of $R(8/2)$, pictured in Figures 15, 16, and 17, show that this parameter decreases with increasing temperatures. This would be expected, because there would be a greater over-all motion at higher temperature and therefore less of a distribution. The fact that the greatest temperature dependence is found in the material with the longest chain (NaS) (not shown) bears this out.

Publication Date: January 1, 1967 | doi: 10.1021/ba-1967-0063.ch003

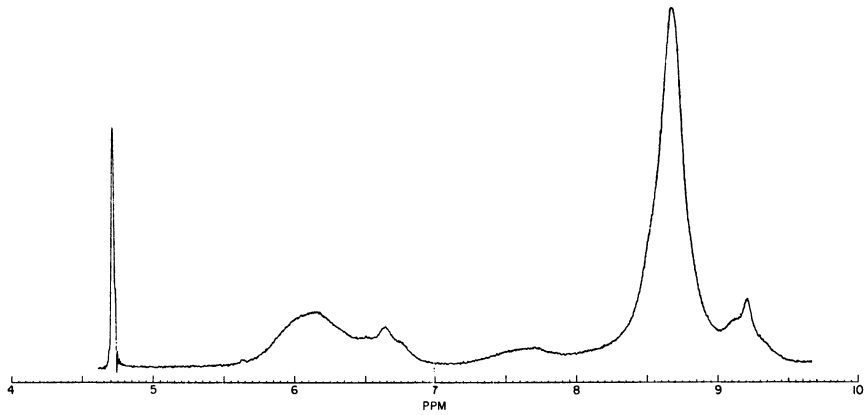

Figure 19. The 60-MHz spectrum of viscous isotropic phase of $DEC_{12}APS$ Obtained at 32°C. on a Varian A-60 spectrometer and calibrated with respect to external TMS

Finally, there is an interesting correlation between the values of $R(8/2)$ and molecular structure. For $DC_{12}AO$ the values of $R(8/2)$ are much greater than the Lorentzian value: At 100° they are 5.5 for the neat phase and 4.5 for the middle phase. Sodium oleate (NaOl), which has a cis double bond in the middle of the chain, has considerably lower values of $R(8/2)$ for both middle (3.9) and neat (4.3) phases. The differences between the NaOl values and values found for saturated soaps are even greater. The lower values of $R(8/2)$ for NaOl indicate that the distribution of motions along the NaOl chain is more uniform. The double bond appears to act as another "end," in effect making the chains much shorter. This is supported by the line width of NaOl (Table IV) which in the neat phase is roughly what one finds in a $C_{12} — C_{14}$ chain. The double bond in the chain should have little effect in the middle phase. This appears to be borne out by both the $R(8/2)$ and line width data. The $R(8/2)$ for sodium elaidate

(NaEl) (Figure 17) also supports the above hypothesis. The $R(8/2)$ values are 5.6 at 100°C. for the neat phase and 4.6 for the middle phase, similar to the $DC_{12}AO$ values. The trans double bond apparently does not produce a marked structural discontinuity. Molecular models indicate the similar chain geometry. The temperature dependence of the $R(8/2)$'s is consistent with the above hypothesis. Both $DC_{12}AO$ and NaEl have a more pronounced temperature dependence over the neat and middle ranges than does NaOl. The smaller temperature dependence of NaOl is consistent with a more complete averaging (uniformity) of the motions.

Conclusions

NMR spectroscopy can be a valuable tool for studying liquid crystalline systems. The three basic types of mesomorphic phases—nematic, smectic, and cholesteric—have distinctive spectra which agree with the proposed structures of these phases. The spectra of the nematic phase consist of highly structured bands because of the ordering in the magnetic field along the molecular axis. Both smectic and cholesteric phases show a unique line shape, designated "super-Lorentzian." In the lyotropic smectic phase it is believed that the line shape is a result of a distribution of correlation times in the hydrocarbon chains of the surfactant molecules. In the cholesteric phase it is believed that the line shape is a result of the particular orientations of the planes of the molecules in the magnetic field.

The NMR line widths can be used to determine phase transitions in both one- and multicomponent mesomorphic systems. Transition temperatures and phase boundaries determined by NMR are usually in good agreement with those determined by other methods. The NMR data can therefore be used to construct reliable phase diagrams. They are most useful in systems where separation of the mesophase from other phases is difficult or impossible.

By careful measurement of line widths, second moments, and the $R(8/2)$ parameter (the ratio of the line width at eighth-height to that at half-height) the neat and middle lyotropic mesophases can be distinguished from each other. The $R(8/2)$ parameter is shown to be sensitive to changes in both phase structure and molecular structure. The NMR parameters of the neat and middle phases are consistent with the structural pictures proposed for these phases (*4*, *22*) but do not define the details of the middle structure. The NMR spectra observed in viscous isotropic mesophases are surprising since they are essentially the same as those obtained from dilute, micellar solutions. This type of spectrum does not appear to be consistent with the proposed structure of this phase.

The NMR data illustrate, as do many other kinds of experiments, that liquid crystals are intermediate between solids and liquids with respect to molecular motion. Finally, a considerable amount of further experimental

Publication Date: January 1, 1967 | doi: 10.1021/ba-1967-0063.ch003

In Ordered Fluids and Liquid Crystals; Porter, R., el al.;
Advances in Chemistry; American Chemical Society: Washington, DC, 1967.

and theoretical work is required before the structure and properties of mesophases are well understood.

Acknowledgment

We thank M. C. Beisner for obtaining many of the spectra. We appreciate many stimulating discussions with our colleagues, particularly A. J. Mabis, F. B. Rosevear, and W. L. Courchene.

Literature Cited

(1) Barr, M. R., Dunell, B. A., *Can. J. Chem.* **42**, 1098 (1964).
(2) Bose, E., *Physik. Z.* **10**, 32, 230 (1909).
(3) Brown, G. H., Shaw, W. G., *Chem. Revs.* **57**, 1049 (1957).
(4) Clunie, J. S., Corkill, J. M., Goodman, J. F., *Proc. Roy. Soc.* (*London*) **A285**, 520 (1965).
(5) Englert, G., Saupe, A., *Z. Naturforsch.* **19a**, 172 (1964).
(6) Ferguson, R. H., Rosevear, F. B., Stillman, R. C., *Ind. Eng. Chem.* **35**, 1005 (1943).
(7) Friedel, G., *Ann. Phys.* **18**, 273 (1922).
(8) Furth, R., Sitte, K., *Ann. Physik.* **30** (5), 388 (1937).
(9) Grant, R. F., Dunell, B. A., *Can. J. Chem.* **38**, 1951 (1960).
(10) *Ibid.*, p. 2395.
(11) Gray, G. W., "Molecular Structure and the Properties of Liquid Crystals," Academic Press, London, 1962.
(12) Hermann, C., *Z. Krist.* **79**, 186, 337 (1931).
(13) Jain, P. L., Lee, J. C., Spence, R. D., *J. Chem. Phys.* **23**, 878 (1955).
(14) Jain, P. L., Moses, H. A., Lee, J. C., Spence, R. D., *Phys. Rev.* **92**, 844 (1953).
(15) Janzen, W. R., Dunell, B. A., *Trans. Faraday Soc.* **59**, 1260 (1963).
(16) Lawson, K. D., Flautt, T. J., *Mol. Crystals* **1**, 241 (1966).
(17) Lawson, K. D., Flautt, T. J., *J. Phys. Chem.* **69**, 4256 (1965).
(18) Lehmann, O., *Z. Krist.* **18**, 464 (1890); *Ann. Physik* **25** (4), 852 (1908); **27** (4), 1099 (1908); *Ber.* **41**, 3774 (1908).
(19) Lippmann, H., *Ann. Physik* **2** (7), 287 (1958).
(20) Lippmann, H., Weber, K. H., *Ann. Physik.* **20** (6), 265 (1957).
(21) Luzzati, V., Husson, F., *J. Cell. Biol.* **12**, 207 (1962).
(22) Luzzati, V., Mustacchi, H., Skoulios, A., *Nature* **180**, 600 (1957); *Discussions Faraday Soc.* **25**, 43 (1958).
(23) McBain, J. W., Lee, W. W., *Oil and Soap* **20**, 17 (1943).
(24) Ornstein, L. S., Kast, W., *Trans. Faraday Soc.* **29**, 931 (1933).
(25) Oseen, C. W., *Z. Krist.* **79**, 10 (1931); *Trans. Faraday Soc.* **29**, 883 (1933).
(26) Rosevear, F. B., *J. Am. Oil Chemists' Soc.* **31**, 628 (1954).
(27) Saupe, A., *Z. Naturforsch.* **19a**, 161 (1964).
(28) Saupe, A., Englert, G., *Phys. Rev. Letters* **11**, 462 (1963).
(29) Shaw, D. J., Dunell, B. A., *Trans. Faraday Soc.* **58**, 132 (1962).
(30) Skoulios, A. E., Luzzati, V., *Acta Cryst.* **14**, 278 (1961).
(31) Spence, R. D., Gutowsky, H. S., Holm, C. H., *J. Chem. Phys.* **21**, 1891 (1953).
(32) Spence, R. D., Moses, H. A., Jain, P. L., *J. Chem. Phys.* **21**, 380 (1953).
(33) Thiessen, P. A., Stauff, J., *Z. Physik. Chem.* (*Leipzig*) **A176**, 397 (1936).
(34) Tsvetkov, V. N., *Acta Physicochim. URSS* **16**, 132 (1942).
(35) Vold, M. J., Macomber, M., Vold, R. J., *J. Am. Chem. Soc.* **63**, 168 (1941).
(36) Vold, R. D., Rosevear, F. B., Ferguson, R. H., *Oil and Soap* **16**, 48 (1939).
(37) Vold, R. D., Vold, M. J., *J. Am. Chem. Soc.* **61**, 808 (1939).
(38) Weber, K. H., *Ann. Physik.* **3** (7), 1 (1959).
(39) *Ibid.*, p. 125.
(40) Zocher, H., *Physik. Z.* **28**, 790 (1927); *Trans. Faraday Soc.* **29**, 931, 945 (1933).

RECEIVED March 10, 1966.

Determination of Bond Angle of CH_3 Groups by Proton Magnetic Resonance in Nematic Liquid Crystalline Solutions

ALFRED SAUPE, GERHARD ENGLERT, and ANNA POVH

Physical Institute, University of Freiburg, Freiburg, Germany, and Physical Department, F. Hoffmann–La Roche & Co., Ltd., Basel, Switzerland

Publication Date: January 1, 1967 | doi: 10.1021/ba-1967-0063.ch004

The theory of NMR spectra of molecules dissolved in nematic liquids is briefly reviewed, with emphasis on the determination of H-C-H bond angles of CH_3 groups. Measurements have been carried out with carbon-13—labeled acetonitrile and methyl iodide in 4,4'-di-n-hexyloxyazoxybenzene and with acetonitrile and methanol in 4-n-octyloxybenzoic acid. The H-C-H bond angles obtained are in good agreement with previous microwave data. In the two solvents, the H-C-H angle of acetonitrile is slightly different (6'), probably because of a partial protonation in the acidic solvent. With acetonitrile, the positive sign of the indirect scalar coupling J_{CH} was confirmed. Methanol showed an abnormal temperature and concentration dependence of the orientation, which may be explained by a varying degree of association.

Nematic liquid crystals provide an anisotropic liquid solvent in which highly resolved nuclear magnetic resonance (NMR) spectra of partially oriented solute molecules have been observed (*2–4, 10–14, 16*). The following properties of nematic liquid crystals are important in this respect:

Nematic liquids differ from normal isotropic liquids only by the more or less complete spontaneous parallel orientation of the elongated molecules. This means that different orientations of the molecular axes occur with different statistical weights. The diffusion and rotary motion of the molecules, however, are as fast as in many isotropic liquids.

Nematic liquids can be homogeneously ordered in thick layers by a magnetic field of only a few thousand gauss. Homogeneously ordered samples behave optically like uniaxial crystals. The optical axis coincides with the preferred orientation of the long molecular axis. It turns parallel to the magnetic field direction.

In Ordered Fluids and Liquid Crystals; Porter, R., el al.;
Advances in Chemistry; American Chemical Society: Washington, DC, 1967.

As the molecules retain their high mobility, the intermolecular magnetic dipole interactions are averaged to zero. The molecules can therefore be treated as isolated spin systems. As a consequence of the second property, the homogeneous orientation of the nematic sample is achieved by the magnetic field, H_o, which in the NMR experiment is needed to introduce the Zeeman splitting of the nuclear spin levels. In such homogeneously ordered samples the intramolecular dipole interactions are reduced to sharp average values.

A considerable disadvantage arises because of the fact that no sample spinning around an axis perpendicular to the H_o field is possible since this would destroy the molecular orientation. Therefore the minimum line width obtained for proton signals is appreciably larger than that obtainable in isotropic solutions.

The parallel orientation of the molecules in the nematic phase is usually characterized by the degree of order or S value of the long molecular axis defined by the expectation value (*1*, *7*, *8*, *15*, *19*, *20*):

$$S = (1/2)\langle 3 \cos^2\theta - 1\rangle \tag{1}$$

Here θ is the angle between the long molecular axis and the optical axis of the liquid. In the same way we can define a degree of order of any molecular axis, whether we consider a molecule of the pure nematic liquid or a molecule dissolved in a nematic solvent. By definition the S values range between 1 and $-1/2$. $S = 1$ means that the corresponding axis is always parallel to the optical axis; $S = -1/2$ means that it is always perpendicular to it; $S = 0$ corresponds to a random orientation as in isotropic liquids. The S value of the long molecular axis in pure nematic liquids usually lies between 0.4 and 0.7 (*1*, *6*, *7*, *8*, *15*, *19*, *20*).

The S values of different molecular axes are not independent of each other. In general, the average orientation of a rigid molecule can be completely described by a matrix (*12*) that contains only five (in certain limits) independent parameters. We denote by ξ, η, and ζ the axes of a cartesian coordinate system fixed to the molecule (or a rigid part of the molecule) and by θ_ξ, θ_η, and θ_ζ the angles of these axes toward the optical axis. The matrix elements are then given by the average values:

$$S_{ij} = (1/2)\langle 3 \cos\theta_i \cos\theta_j - \delta_{ij}\rangle; \quad i,j = \xi,\eta,\zeta \tag{2}$$

$\delta_{ij} = 1$ for $i = j$; otherwise $\delta_{ij} = 0$. The matrix is symmetric, and its trace disappears. Between the S value of an arbitrary axis, a, with the angles $\alpha_\xi{}^a$, $\alpha_\eta{}^a$, and $\alpha_\zeta{}^a$ toward the coordinate axes, and the matrix elements, S_{ij}, the following relation holds:

$$S_a = \sum_{ij} \cos\alpha_i{}^a \cos\alpha_j{}^a S_{ij} \tag{3}$$

Publication Date: January 1, 1967 | doi: 10.1021/ba-1967-0063.ch004

This equation may be used to determine the degree of order of any axis if the S matrix is completely known or to determine the matrix elements, S_{ij}, if sufficient S_a values are known.

By a suitable choice of the molecular coordinate system the S matrix may be transformed into a diagonal form (*12*) with two independent elements. In sufficiently symmetrical molecules these principal axes are determined by symmetry. If, in special cases, we can choose, for instance, the ζ-axis parallel to an axis of threefold or higher symmetry, the off-diagonal elements are zero and we obtain:

$$S_{\xi\xi} = S_{\eta\eta} = -(1/2)S_{\zeta\zeta} \tag{4}$$

Relation 3 reduces now to

$$S_a = (1/2)(3\cos^2\alpha_\zeta^a - 1)S_{\zeta\zeta} \tag{3'}$$

Relations 4 and 3′ also apply for a rigid part of a molecule, provided that there exists a rotary motion around its three- or more-fold symmetry axis with respect to the rest of the molecule. This always occurs in the case of CH_3 groups, in the spectra of which we are especially interested here.

Spin-Hamiltonian in Nematic Liquids

In this paper we consider diamagnetic molecules only and denote by x, y, and z the axes of a Cartesian coordinate system fixed in space. The z axis is directed parallel to the strong magnetic field, H_o. We assume that the screening of a nucleus p can be described by a screening tensor (σ_{lk}^p) $(l,k = x,y,z)$ and that the spin-spin interaction can be described by a coupling tensor (A_{lk}^{pq}) [interaction energy terms $hI^p(A_{lk}^{pq})I^q$]. We further assume that the motion of the molecules is so fast that intermolecular interactions can be neglected and that intramolecular interactions are reduced to average values. For nuclei with spin 1/2, the effective Hamiltonian (*12*) is then given by

$$\begin{aligned}\mathbf{H} = &-\frac{h}{2\pi}H_o\sum_p \gamma_p(1-\langle\sigma_{zz}^p\rangle)I_z^p \\ &+ h\sum_{p>q}\left\{\frac{1}{2}\langle A_{xx}^{pq} + A_{yy}^{pq}\rangle(I_+^pI_-^q + I_-^pI_+^q)\right. \\ &\left. + 2\langle A_{zz}^{pq}\rangle I_z^pI_z^q\right\}\end{aligned} \tag{5}$$

Here the sums have to be taken over the interacting nuclei p and q. γ_p is the gyromagnetic ratio, I_z^p is the z component of $\mathbf{I}^p$, the spin operator of nucleus p, and $I_\pm^p = I_x^p \pm iI_y^p$. The brackets $\langle\ \rangle$ indicate that average values over the molecular motion have to be taken.

Publication Date: January 1, 1967 | doi: 10.1021/ba-1967-0063.ch004

The Hamiltonian can also be written in the following form:

$$\mathbf{H} = -\frac{h}{2\pi} H_0 \sum_p \gamma_p(1 - \sigma_p - \delta_p) I_z^p + h \sum_{p>q} J_{pq} \mathbf{I}_p \mathbf{I}_q + h \sum_{p>q} B_{pq}(3 I_z^p I_z^q - \mathbf{I}_p \mathbf{I}_q) \quad (6)$$

Here we use the following abreviations:

$$\begin{aligned} \sigma_p &= \tfrac{1}{3} \langle \sigma_{xx}{}^p + \sigma_{yy}{}^p + \sigma_{zz}{}^p \rangle \\ J_{pq} &= \tfrac{2}{3} \langle A_{xx}{}^{pq} + A_{yy}{}^{pq} + A_{zz}{}^{pq} \rangle \\ \delta_p &= \tfrac{1}{3} \langle 2\sigma_{zz}{}^p - \sigma_{xx}{}^p - \sigma_{yy}{}^p \rangle \\ B_{pq} &= \tfrac{1}{3} \langle 2A_{zz}{}^{pq} - A_{xx}{}^{pq} - A_{yy}{}^{pq} \rangle \end{aligned} \quad (7)$$

σ_p and J_{pq} correspond to the familiar scalar screening constant and spin-spin coupling constant, respectively, observable in normal liquids. δ_p and B_{pq} are additional constants that appear because of nonvanishing S values.

In cases where the regarded molecular properties—e.g., the internuclear distances—do not change with the orientation of the molecule against the optical axis of the nematic solvent, we can express the effective constants in the Hamiltonian by the matrix elements that are related to the molecular coordinate system:

$$\begin{aligned} \sigma_p &= \tfrac{1}{3} (\sigma_{\xi\xi}{}^p + \sigma_{\eta\eta}{}^p + \sigma_{\zeta\zeta}{}^p) \\ J_{pq} &= \tfrac{2}{3} (A_{\xi\xi}{}^{pq} + A_{\eta\eta}{}^{pq} + A_{\zeta\zeta}{}^{pq}) \\ \delta_p &= \tfrac{2}{3} \sum_{i,j} S_{ij} \sigma_{ij}{}^{pq} \qquad (i,j = \xi,\eta,\zeta) \\ B_{pq} &= \tfrac{2}{3} \sum_{i,j} S_{ij} A_{ij}{}^{pq} \end{aligned} \quad (8)$$

The spin-spin coupling constants, B_{pq}, contain the anisotropic part of the indirect (electron-coupled) spin-spin interaction and the direct dipole-dipole interaction between the magnetic dipole moments of the nuclei. The latter part is always given by

$$B_{pq}{}^{\mathrm{dir}} = -\frac{h}{4\pi^2} \gamma_p \gamma_q \frac{1}{2} \left\langle \frac{3\cos^2 \theta_{pq} - 1}{r_{pq}{}^3} \right\rangle \quad (9)$$

Here θ_{pq} is the angle between the axis through p and q and the optical axis and r_{pq} is the distance between p and q. If p and q belong to the same rigid part of the molecule, we can write

$$B_{pq}{}^{\mathrm{dir}} = -\frac{h}{4\pi^2} \gamma_p \gamma_q S_{pq} \frac{1}{r_{pq}{}^3} \quad (10)$$

S_{pq} is the degree of order of the axis through p and q. Here r_{pq} means an

Publication Date: January 1, 1967 | doi: 10.1021/ba-1967-0063.ch004

average distance. It is equal to the equilibrium distance between nuclei p and q if we neglect the influence of vibrational motions.

The anisotropic part of the indirect spin-spin interaction will in general be much smaller than the direct coupling. However, its existence has been proved by Snyder and Anderson (*16*) with hexafluorobenzene in a nematic liquid solution. In the case of benzene, on the other hand, no anisotropic contribution of the indirect spin-spin coupling has been observed (*13*, *16*). Its influence seems not to be noticeable with proton-proton spin couplings. If, therefore, the indirect contribution is neglected, the experimental values of B_{pq} may be used to calculate S_{pq} with the aid of Equation 10. In this way it is possible to determine experimentally the complete S matrix provided the internuclear distances are known.

With a $^{13}CH_3$ group we can observe two anisotropic coupling constants —one between the protons (B_{HH}) and one between carbon-13 and the protons (B_{CH}). For the calculation of B_{HH} and B_{CH} we neglect all anisotropic contributions of the indirect spin-spin interactions as well as the influence of vibrational motions. We use Equations 3′, 10,

and

$$S_{HH} = -(1/2)S_{C_3}$$
$$S_{CH} = (1/2)(3\cos^2\beta - 1)S_{C_3}$$

Here S_{C_3} denotes the degree of order of the symmetry axis, S_{HH} that of an axis connecting two protons, and S_{CH} that of the CH-bond axis. β is the angle between the latter bond axis and the symmetry axis. We find:

$$B_{HH} = \frac{1}{8\pi^2}\gamma_p^2 S_{C_3}\frac{1}{r_{HH}^3}$$
$$B_{CH} = -\frac{1}{4\pi^2}\gamma_p\gamma_c\frac{1}{2}(3\cos^2\beta - 1)S_{C_3}\frac{1}{r_{CH}^3} \qquad (11)$$

From the symmetry of the CH_3 group it follows that $r_{HH} = 2\sin(\alpha/2)r_{CH}$ and $(3\cos^2\beta - 1)/2 = 1 - 2\sin^2(\alpha/2)$. With this we finally obtain:

$$\frac{B_{CH}}{B_{HH}} = 16\frac{\gamma_c}{\gamma_p}\sin^3(\alpha/2)(2\sin^2(\alpha/2) - 1) \qquad (12)$$

γ_p and γ_c are the known gyromagnetic ratios of the proton and of the carbon-13 nucleus. Equation 12 can therefore be used to determine the H-C-H bond angle, α.

Experimental Results

Measurements have been made with methanol (CH_3OH) and acetonitrile (CH_3CN) in nematic liquid 4-*n*-octyloxybenzoic acid (II; *see* Table I) and with acetonitrile and methyl iodide (CH_3I) in nematic liquid

Publication Date: January 1, 1967 | doi: 10.1021/ba-1967-0063.ch004

4,4′-di-*n*-hexyloxyazoxybenzene (I). Part of the results are mentioned by Englert and Saupe (*2*).

The CH_3 groups of the solute molecules can be treated as isolated spin systems: the effective couplings of the CH_3 protons with the ^{14}N nucleus in acetonitrile and with ^{127}I in methyl iodide average to zero, for these

Table I. Scalar Coupling Constant J_{CH} and Bond Angles of CH_3-Groups

			PMR Data	*Microwave Data (r_o Structure)*	
Compound	*Solvent*	J_{CH}, *CPS.*	∢ *HCH*	∢ *HCH*	*Ref.*
$N \equiv C\text{–}CH_3$	I	136	109°2′ ± 2′	109°16′	(*17*)
	II	136	108°56′ ± 2′		
CH_3OH	II	141	110°3′ ± 8′	109°2′ ± 45′	(*18*)
CH_3I	I	151	111°42′ ± 2′	111°25′	(*9*)

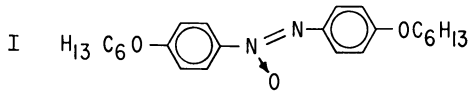

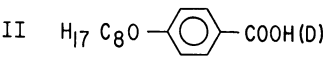

nuclei possess a quadrupole moment which is coupled with the electrostatic field of the electrons. With methanol in 4-*n*-octyloxybenzoic acid as solvent the protons of the OH groups exchange very rapidly with the acidic protons, and their couplings to the CH_3 group also average to zero.

An isolated $^{12}CH_3$ group in a nematic solution gives rise to a symmetrical spectrum of three lines with relative intensities of 1:2:1 (*3*, *4*). The separation between the lines is given by:

$$\nu_{HH} = 3|B_{HH}| \tag{13}$$

When the three protons are bound to carbon-13 which possesses spin 1/2 like the protons, we have a system of four interacting spins. The interaction between carbon-13 and the protons has to be taken into account in a first-order calculation only. A spectrum is thus obtained consisting of two of the described symmetrical triplets. The triplets have a frequency shift with respect to each other of

$$\nu_{CH} = |2B_{CH} + J_{CH}| \tag{14}$$

Relations 13 and 14 can be used to calculate B_{HH} and B_{CH} from the observed splittings. For the calculation of B_{CH} the value of J_{CH} and its relative sign to B_{CH} must be known.

Figure 1 shows as an example the 60-Mc. per sec. (Mc.p.s.) PMR spectrum of methanol in nematic liquid 4-*n*-octyloxybenzoic acid. The very stong line belongs to the acidic protons and the OH protons of methanol. The solvent was partially deuterated to suppress this line somewhat. All other lines can be assigned to the protons of the $^{12}CH_3$ and the $^{13}CH_3$ groups.

Publication Date: January 1, 1967 | doi: 10.1021/ba-1967-0063.ch004

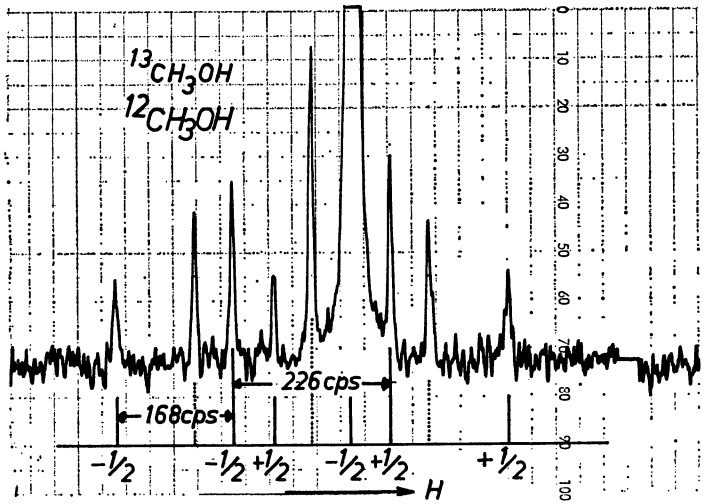

Figure 1. PMR spectrum (60 Mc.p.s.) of $^{12}CH_3OH$ and $^{13}CH_3OH$ in 4-n-octyloxybenzoic acid at 70°C.

Concentration ca. 15 mole %
Very strong line assigned to rapidly exchanging protons of OH and COOH groups. At theoretical spectrum of $^{13}CH_3OH$ the corresponding spin orientation of the carbon-13 nucleus is indicated.
. . . . Signals of $^{12}CH_3OH$

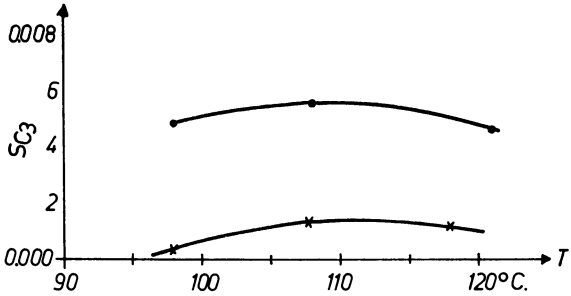

Figure 2. Degree of order, S_{C_3}, of C_3 axis of CH_3OH dissolved in 4-n-octyloxybenzoic acid

Concentration
● *ca. 15 mole %*
× *30 mole %*

The signals of the aliphatic and aromatic protons of the solvent disappear in the background.

Figure 2 presents the dependence of the S_{C_3} values of methanol on the temperature measured for two different concentrations. The S_{C_3} values obtained are below 0.006. There is also no steady increase of S_{C_3} with decreasing temperature, but the curves pass through a maximum. For the higher concentration the sign of S_{C_3} is uncertain; for the lower concentration it was determined with ^{13}C-labeled methanol.

Publication Date: January 1, 1967 | doi: 10.1021/ba-1967-0063.ch004

This unusual orientation behavior of methanol is probably caused by an association which varies with the concentration and the temperature. In the nematic phase of solvent I no interpretable spectrum of methanol has been obtained.

With acetonitrile much larger splittings have been observed [*see* the 100 Mc.p.s. spectrum, Figure 4 of (*2*)]. The splittings are of comparable magnitude in both solvents. ν_{HH} ranged between 2400 and 3100 c.p.s.; ν_{CH} between 1200 and 1600 c.p.s. The corresponding S_{C_3} values were between 0.08 and 0.10. They increased steadily with decreasing temperature.

A mixture of methyl iodide and acetonitrile has been investigated in solvent I. With the former compound the ν_{HH} value and hence the S_{C_3} values were considerably smaller. For instance, at 75°C. we obtained for methyl iodide:

$$\nu_{HH} = 1206 \text{ c.p.s.}$$
$$\nu_{CH} = 826 \text{ c.p.s.}$$
$$S_{C_3} = 0.042$$

and for acetonitrile:

$$\nu_{HH} = 2752 \text{ c.p.s.}$$
$$\nu_{CH} = 1426 \text{ c.p.s.}$$
$$S_{C_3} = 0.089$$

The S_{C_3} value of acetonitrile indicates that this more elongated molecule is considerably better oriented than methyl iodide. The S_{C_3} values of the latter compound also steadily increased with decreasing temperature from 0.03 at 85°C. to 0.05 at 68°C.

Discussion

The H-C-H angles calculated from Equation 12 are summarized in Table I. The errors given are the root mean square deviations of our results. Systematical errors are not included. The J_{CH} values were determined with the same samples used for the determination of ν_{HH} and ν_{CH}. The same sign for J_{CH} and B_{CH} was used in the calculations. This leads to reasonable values for the bond angles without a noticeable temperature dependence. The assumption of opposite signs can be discarded: with acetonitrile opposite signs lead to a temperature dependence of the bond angle—e.g., in solvent I, $\alpha = 111°38'$ at 77°C.; $\alpha = 112°20'$ at 95°C. —and with methanol and methyl iodide values of α higher than 120° would result. With J_{CH} and B_{CH} also J_{CH} and S_{C_3} have the same sign. J_{CH} is known to be positive (*5*), and therefore S_{C_3} is positive, too.

For an elongated molecule such as acetonitrile one can assume with certainty that in a nematic solution the long molecular axis will be oriented preferably parallel to the optical axis, and therefore S_{C_3} is positive. The

Publication Date: January 1, 1967 | doi: 10.1021/ba-1967-0063.ch004

same preferred orientation has been experimentally confirmed with compounds of similar structure—e.g., propyne—by measurement of the anisotropy of the chemical shift (*2*). Our results for acetonitrile can therefore be regarded as a direct experimental confirmation of the positive sign of J_{CH}.

The bond angles obtained by microwave measurements (*see* Table I) in the gas phase agree satisfactorily with our results obtained by PMR spectroscopy. The small differences may be partly caused by the influence of vibrational motions. There may also be a small difference be tween the molecular geometry in the gas phase and in the liquid solution. As there is no systematic deviation between the microwave and PMR values, we can conclude that neglecting the anisotropic part of the electron-coupled spin-spin interaction is justified.

These results indicate that by PMR measurements in nematic solutions the bond angle of CH_3 groups may be determined in a simple and fairly precise manner. Even very small changes of the bond angle can be detected. This might be useful for investigating the influence of substituents on the bond angle in CH_3X molecules and for studying correlations between the magnitude of J_{CH} and the bond angle.

The difference of 6′ observed with acetonitrile in solvent II against solvent I is probably caused by a small change in molecular geometry. In both solvents measurements were made in the same temperature range, and the observed line splittings have the same magnitude. We conclude that neglecting the vibrational motions has no influence on the difference.

A small change of the bond angle was in fact to be expected, because acetonitrile in solvent II will be at least partially protonized. The CH bonds carry in general a permanent electrical dipole moment. There is then an electrostatic interaction between these dipole moments and the attached proton. A simple calculation with an assumed bond moment of 0.4 debye shows that these electrostatic interactions may change the H-C-H angle, α, by about 20′. If the electrostatic interactions are really dominant, the decrease of α in the acidic solvent shows that in the CH_3 group of acetonitrile the H atoms carry the positive charge.

Acknowledgment

We are grateful to R. Mecke, Freiburg, Germany, for support of this investigation. H. Spiesecke, Ispra, Italy, kindly provided a sample of carbon-13–enriched acetonitrile and methyl iodide.

Literature Cited

(1) Chatelain, P., *Bull. Soc. Franc. Mineral. Crist.* **78**, 262 (1955).
(2) Englert, G., Saupe, A., *Molecular Crystals* **1**, 503 (1966).
(3) Englert, G., Saupe, A., *Z. Naturforsch.* **19a**, 172 (1964).
(4) *Ibid.*, **20a**, 1401 (1965).
(5) Karplus, M., *J. Am. Chem. Soc.* **84**, 2458 (1962).
(6) Lippmann, H., *Ann. Phys. (Leipzig)* **2**, 287 (1958).
(7) Maier, W., Englert, G., *Z. Elektrochem.* **64**, 689 (1960).

(8) Maier, W., Saupe, A., *Z. Naturforsch.* **13a**, 564 (1958); **14a**, 882 (1959); **15a**, 287 (1960).
(9) Miller, S. L., Aamodt, L. C., Dousmanis, G., Townes, C. H., Kraitchman, J., *J. Chem. Phys.* **20**, 1112 (1952).
(10) Phillips, W. D., Rowell, J. C., Melby, C., *J. Chem. Phys.* **41**, 2551 (1964).
(11) Saupe, A., Proceedings of XIIIth Colloque Ampère, p. 321, North Holland Publishing Co., Amsterdam, 1964.
(12) Saupe, A., *Z. Naturforsch.* **19a**, 161 (1964).
(13) *Ibid.*, **20a**, 572 (1965).
(14) Saupe, A., Englert, G., *Phys. Rev. Letters* **11**, 462 (1963).
(15) Saupe, A., Maier, W., *Z. Naturforsch.* **16a**, 816 (1961).
(16) Snyder, L. C., Anderson, E. W., *J. Chem. Phys.* **42**, 3336 (1965); *J. Am. Chem. Soc.* **86**, 5023 (1964).
(17) Thomas, L. F., Sherrard, E. I. S., Sheridan, J., *Trans. Faraday Soc.* **51**, 619 (1955).
(18) Venkatesvarlu, P., Gordy, W., *J. Chem. Phys.* **23**, 1200 (1955).
(19) Weber, K. H., *Ann. Phys. (Leipzig)* **3**, 1 (1959); *Discussions Faraday Soc.* **25**, 74 (1958).
(20) Zwetkoff, V., *Acta Physicochim. URSS* **16**, 132 (1942).

RECEIVED March 11, 1966. Investigation sponsored in part by the Deutsche Forchungsgemeinschaft.

Interfaces in Nematic Liquids

RICHARD WILLIAMS

RCA Laboratories, Princeton, N. J.

Publication Date: January 1, 1967 | doi: 10.1021/ba-1967-0063.ch005

Since the physical properties of nematic liquids are highly anisotropic, the differences between regions of a nematic liquid which are differently oriented become comparable to those between different phases or different compounds in a system of ordinary liquids. This can give rise to interfaces in a single-phase nematic liquid system at the boundaries of differently oriented regions. When an electric field is applied to a suitable specimen of a nematic liquid, a domain structure appears. This is believed to indicate the underlying preferred orientation of molecules in the liquid. From observations of the domains, two kinds of interfaces have been found in nematic liquids. These are illustrated by photographs of the corresponding domain structure.

Nematic liquids are formed by certain organic compounds which have long rodlike molecules. The essential and characteristic feature of the nematic phase (*3*) is the ordering of molecules; all are oriented so that their long axes are approximately parallel. This relative mutual orientation is preserved over distances always large compared with the size of molecules and sometimes over macroscopic dimensions. While there is long-range order with respect to the orientation of molecules, there is none with respect to the positions of their centers of mass. In fact, translation of molecules takes place as in an ordinary liquid. An important result of this combination of rigidity with respect to rotation and fluidity with respect to translation is that the liquid takes on the properties of a uniaxial crystal having a unique susceptibility to orientation by external electric and magnetic fields (*3*, *9*, *10*, *11*, *12*). A further ordering effect is produced by the walls of the container. The orientation of the common axis of the molecules in a nematic liquid may be determined by the wall out to macroscopic distances from the wall. Combined orienting effects of the container wall and an external electric field give rise to a domain structure. This permits the observation of certain interfaces within nematic liquids, discussed below.

In Ordered Fluids and Liquid Crystals; Porter, R., el al.;
Advances in Chemistry; American Chemical Society: Washington, DC, 1967.

The arrangement of molecules in nematic liquids imposes a high degree of anisotropy on the bulk properties, such as dielectric constant, magnetic susceptibility, optical absorption, and viscosity (*8*, *9*). Therefore, the differences between regions of a nematic liquid which are differently oriented become comparable to those between different phases or different chemical compounds in a system of ordinary liquids—for example, in the nematic liquid, *p*-azoxyanisole, at 117°C. the refractive index (*1*) for the ordinary ray is 1.561 and that for the extraordinary ray is 1.849. The difference between these is greater than between the refractive indices of water and benzene, which is about as great as that between any two common laboratory solvents. We may expect, then, that regions of differing orientation or molecular arrangement will be sensitively detected by optical observations and that interfaces between differently oriented regions will have some of the properties of ordinary interfaces in systems of two phases. These include interfacial tension and possibly electrical properties. In what follows, optical observations of nematic liquids in electric fields are used to demonstrate the existence of such interfaces and to show some of their properties.

When a thin layer of a nematic liquid is in an electric field, a domain structure appears which is readily visible under a microscope or even to the unaided eye (*2*, *5*, *6*, *7*, *8*). An example of this structure in *p*-azoxyanisole

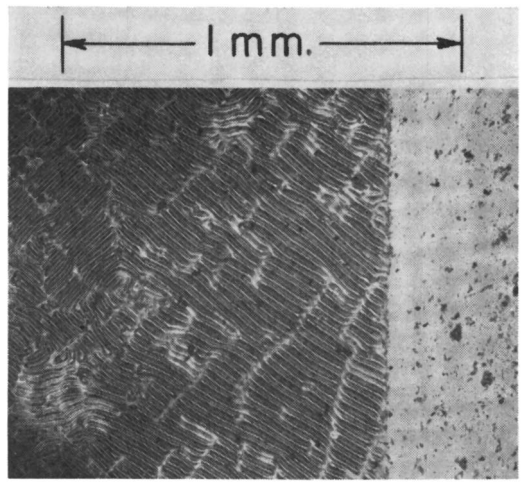

Figure 1. Domains in p-azoxyanisole liquid crystal

Vertical line about ¼ of the way in from the right border is the edge of a strip of transparent conductive coating on the glass plates between which the liquid is contained. To the right of this there is no field. To the left there is a 1-kc. a.c. field of 2500 volts/cm. directed perpendicular to the plane of the page. When the field is removed, the domain pattern disappears in 10 or 20 milliseconds. Speciman thickness 50 microns. Temperature, 125°C. Viewed in unpolarized light

Publication Date: January 1, 1967 | doi: 10.1021/ba-1967-0063.ch005

is shown in Figure 1. The characteristic feature is a periodic macroscopic structure which appears when an electric field is applied across the liquid. The time constants for the appearance and disappearance of the domains as the field is applied and removed are on the order of milliseconds. The reason for the formation of the domains is not yet known with certainty. If the field is removed and then applied again, the orientation of the domains is the same at a given point. This and the sharp changes of domain orientation which coincide with visible boundaries within the liquid lead to the hypothesis that the domain orientation is related in some way to the underlying orientation of the molecules and serves as an indicator of this. A possible ordering mechanism was discussed by Williams (*10*, *11*, *12*). If these are, indeed, the result of molecular ordering, the walls between adjacent domains are interfaces in the sense defined above. In addition, an abrupt change in the orientation of the domains such as that seen in the upper left corner of Figure 1 indicates a change in the orientation of the liquid on a larger scale than that of the domains themselves. We attribute this to abrupt changes in the orientation of the nematic axis. All these effects are sensitive to the surface properties of the conducting glass plates between which the liquid is contained but appear to be primarily properties of the nematic liquid.

Publication Date: January 1, 1967 | doi: 10.1021/ba-1967-0063.ch005

Crystal Boundaries in p-Azoxyanisole

If we accept the orientations of the domains as indicators of the local orientation of the nematic axis (*9*), then regions where the domains are all parallel correspond to individual single crystals of the nematic liquid. Williams (*10*, *11*, *12*) suggested that the nematic axis coincides with the long axes of the domain figures. For this discussion it is only necessary that the domains be oriented at some constant angle with respect to the nematic axis. Figure 2 shows what is believed to be a polycrystalline specimen of nematic *p*-azoxyanisole. Such a specimen is readily obtained by heating above the nematic-isotropic transition temperature and quickly cooling. The specimen first appears to be criss-crossed by many fine dark lines, the "threads" from which the name "nematic" derives. They are present before the field is applied and are unchanged by application of the field. When the electric field is applied, the domains become visible. It can be seen from Figure 2 that these all lie parallel within a given area enclosed by a thread. On crossing the thread into the adjacent area, the domains are again all parallel, but there is an abrupt change in their orientation, usually by about 90°. We interpret the threads as crystal boundaries of individual liquid crystallites which have nucleated at different places and grown until they touch. The orientations of the individual liquid crystallites are indicated by the domain orientations. Over a period of several minutes the small liquid crystallites merge and grow larger until there is often only one within the field of view. This is similar to the be-

havior of ordinary solids, where the individual crystallites of a polycrystalline mass merge and grow into larger crystallites if the material is held near the melting point.

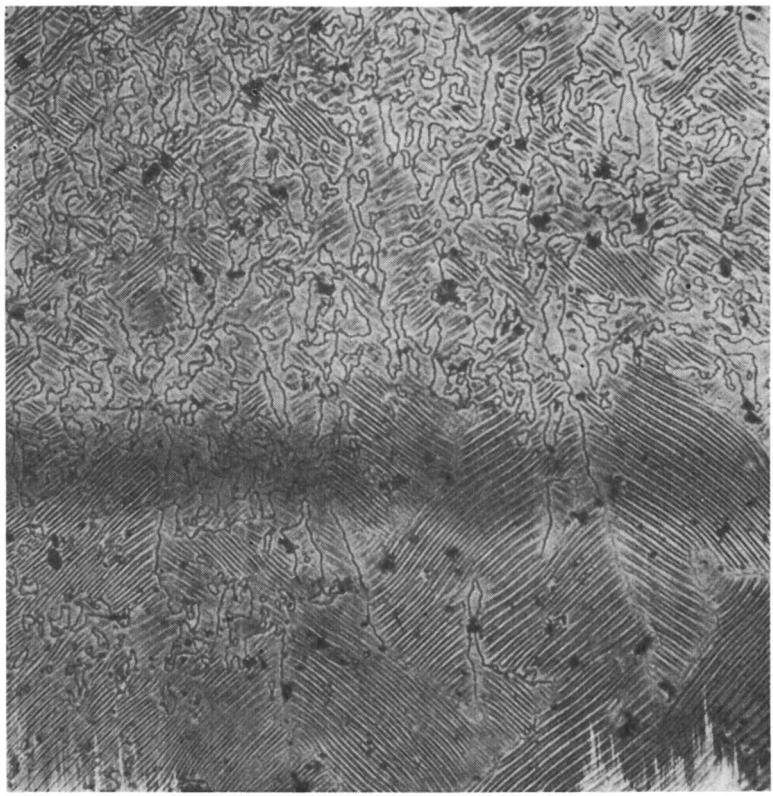

Figure 2. Domain pattern in a specimen of p-azoxyanisole formed by cooling from the isotropic phase

Complicated "thread" structure is present both with and without the electric field and appears to be the boundaries of individual liquid crystallites. Domain pattern appears only in an electric field and serves as an indicator of the orientation of the nematic axes of the crystallites. Unpolarized light

Publication Date: January 1, 1967 | doi: 10.1021/ba-1967-0063.ch005

Experimental

The *p*-azoxyanisole and *p*-methoxycinnamic acid were obtained from the K and K Chemical Co. They were used without further purification and after recrystallization. Results were the same in both cases. The materials were melted between 1 × 3 cm. pieces of glass, with transparent conductive coatings of tin oxide on their inner faces. This glass is obtainable from the Corning Glass Co. Electrical connections to the conductive coatings are made through conducting silver paste to strips of aluminum foil cemented to the glass. A transparent heating stage for microscopic observation was made from a 5 × 8 cm. piece of glass, having a transparent

conductive coating. This was connected to a Variac power supply. The arrangement of the glass pieces containing the melted liquid is illustrated in another article (*9*). The glass pieces are cleaned in toluene and alcohol before using. Surface tension prevents the melted material from running out from between the plates. Domain figures may be obtained with any a.c. voltage source giving 10 volts or more. The pictures shown were obtained using a Hewlett-Packard 202-C oscillator at a frequency of 1.0 kc. The specimen on the heated stage is observed by transmitted light, which may be either polarized or unpolarized. Domain patterns appear at any temperature within the nematic range of the liquids.

Interface between Domains in p-Methoxycinnamic Acid

In five nematic liquids investigated, the domain structure is similar to that shown in Figure 1. This structure persists indefinitely as long as the field is applied. The behavior of nematic *p*-methoxycinnamic acid (*3*) is different and illustrates some interesting features of the interface or wall between domains.

When an electric field of several thousand volts/cm. is applied to a thin specimen of the nematic liquid contained between glass plates having transparent conductive coatings, a domain pattern forms. At the instant the field is applied this pattern is similar to that in Figure 1, as shown in Figure 3. Within a few seconds this pattern evolves to that shown in

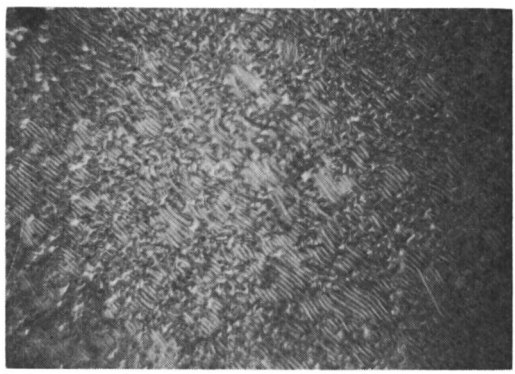

Figure 3. Domain structure in nematic p-methoxycinnamic acid at instant the field is applied

Material nematic from 173.5° to 190°C. Initial pattern similar to typical pattern shown in Figure 1. Picture taken with specimen between crossed polarizers. Magnification same as Figure 1. 1-kc. a.c. field

Figure 4 and after about 12 seconds to that in Figure 5. Ultimately the pattern disappears entirely, even though the field remains on. This appears to be the action of an interfacial tension contracting the domain walls to minimize their length. The optical properties indicate that the nematic axis in *p*-methoxycinnamic acid is parallel to the glass. There is some

Publication Date: January 1, 1967 | doi: 10.1021/ba-1967-0063.ch005

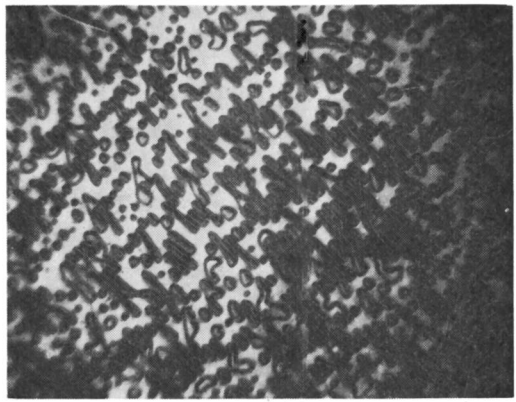

Figure 4. Domain structure of same specimen as in Figure 3
Picture taken 4 seconds after electric field was applied

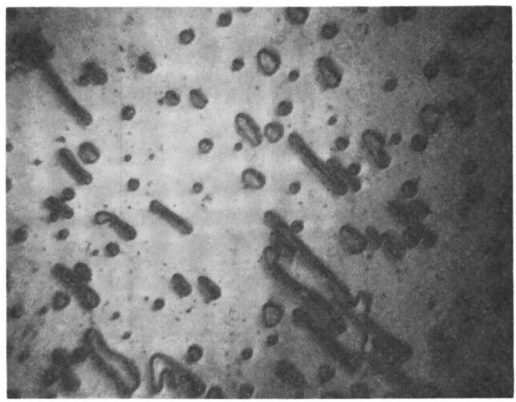

Figure 5. Domain structure of same specimen as in Figure 3
Picture taken 12 seconds after electric field was applied

Publication Date: January 1, 1967 | doi: 10.1021/ba-1967-0063.ch005

macroscopic periodic molecular ordering which gives the domain structure. With this structure the interfacial or domain wall energy gives a stable structure with long thin domains. When the field is applied, there is reorientation of the liquid. With this orientation the driving force producing the domain structure is undoubtedly different from that with the original orientation. Apparently the interfacial energy is too high to preserve the original geometry, and the transition to a circular interface takes place. Finally even these disappear.

The changes which are produced here by reorientation of molecules in a single-phase system are of a kind usually produced by the addition to a system or the removal from it of chemically different molecules. For ex-

ample, consider a system consisting of a large number of bubbles in contact made by aerating a water solution of a surface active material. Such an arrangement might be stable for a long time. If the surface-active material could be somehow gradually removed from the bubbles, the structure would change shape and finally collapse since a large number of bubbles is an unstable configuration for pure water. In nematic liquids the differences in physical properties owing to reorientation of molecules within a one-component system are comparable to those produced in ordinary systems by introduction of new chemical species.

Conclusions

Optical examination of the effects of applied electric fields provides a sensitive technique for investigating the structure of nematic liquids. Two distinct kinds of interfaces exist in pure nematic liquids. One corresponds to the crystallite boundaries in ordinary polycrystalline solids. The other is the interface between domains which shows effects of interfacial tension in *p*-methoxycinnamic acid. In other nematic liquids this effect is not found.

Acknowledgment

The author is indebted to A. Willis for assistance with some of the experiments.

Literature Cited

(1) Chatelaine, P., Pellet, O., *Bull. Soc. Franç. Mineral. Crist.* **73**, 154 (1950).
(2) Elliott, G., Gibson, J. G., *Nature* **205**, 995 (1965).
(3) Gray, G. W., "Molecular Structure and Properties of Liquid Crystals," Chap. 2, 4, Academic Press, London, 1962.
(4) Gray, G. W., Jones, B., *J. Chem. Soc.* **1954**, 1467.
(5) Heilmeier, G., *J. Chem. Phys.*, in press.
(6) Kapustin, A. P., Dmitriev, L. M., *Kristallografiya* **7**, 332 (1962).
(7) Kapustin, A. P., Vistin, L. K., *Kristallografiya* **10**, 118 (1965).
(8) Porter, R. S., Johnson, R., *J. Phys. Chem.* **66**, 1826 (1962).
(9) Saupe, A., Maier, W., *Z. Naturforsch.* **16a**, 816 (1961).
(10) Williams, R., *J. Chem. Phys.* **39**, 384 (1963).
(11) Williams, R., *Nature* **199**, 273 (1963).
(12) Williams, R., Heilmeier, G., *J. Chem. Phys.*, in press.

RECEIVED March 10, 1966.

6

Some Cooperative Effects in Butyl *p*-Anisylidene-*p'*-Aminocinnamate

GEORGE H. HEILMEIER

RCA Laboratories, Princeton, N. J.

Publication Date: January 1, 1967 | doi: 10.1021/ba-1967-0063.ch006

Observations between crossed polarizers of the effects of electric fields on the optical properties of butyl p-anisylidene-p'-aminocinnamate (BAAC) have demonstrated the existence of a domain pattern which, in contrast to the cigar-shaped patterns of p-azoxyanisole, is circular. These circular domains have their optic axis parallel to the applied field, while in p-azoxyanisole the optic axis is essentially perpendicular to the field. Measurement of the polarization as a function of applied field in nematic BAAC has yielded hysteresis loops similar to those found in ferroelectric crystals. This evidence for a spontaneous polarization indicates that in a material such as BAAC with a dipole moment essentially along the molecular axis the molecules are predominantly oriented in one direction within the domains.

The behavior of liquid crystals in applied electric fields has been the object of several recent studies (*1*, *3*, *4*). The materials primarily used here were those in which the dipole moment of the molecule was not in the same direction as the molecular axis. When an electric field is applied to such a system by transparent electrodes, the characteristic cigar-shaped domains shown in Figure 1 for *p*-azoxyanisole are readily observed, using relatively low magnification with or without polarized light. The optical behavior of such domains between crossed polarizers indicates that their optic axis is essentially parallel to the electrode surface and essentially perpendicular to the direction of the applied field.

This communication reports a new type of domain pattern which we have recently observed in butyl-*p*-anisylidene-*p'*-aminocinnamate (*2*) (BAAC). This material, in contrast to *p*-azoxyanisole, has a dipole moment which is essentially parallel to the molecular axis (Figure 2). When a d.c. electric field of approximately 3 kv./cm. is applied to the 25×10^{-4} cm. thick sample by means of transparent electrodes and the sample is viewed between crossed polarizers, the pattern shown in Figure 2 is found.

In Ordered Fluids and Liquid Crystals; Porter, R., el al.;
Advances in Chemistry; American Chemical Society: Washington, DC, 1967.

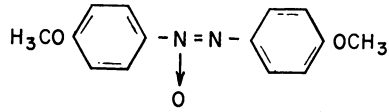

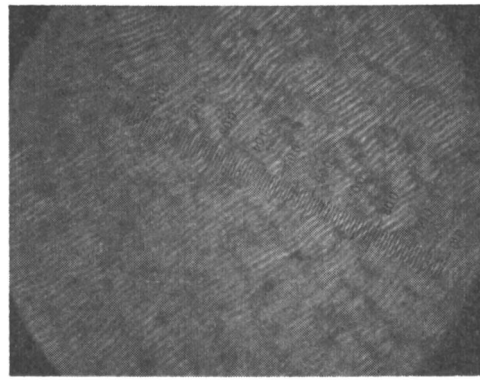

Figure 1. Structure and domain pattern of p-azoxyanisole in applied field of several hundred volts per cm.
E = 1 kv. per cm. × *120*

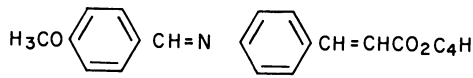

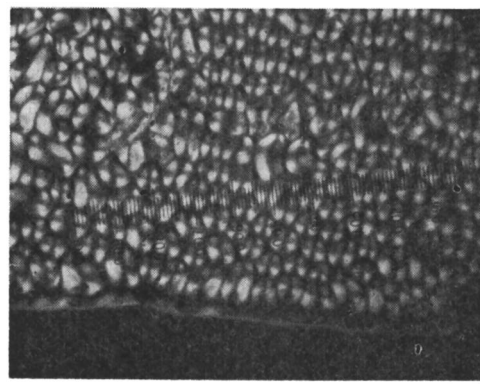

Figure 2. Structure and domain pattern of butyl-p-anisylidene-p'-aminocinnamate between crossed polarizers with approximately 3 kv. per cm. applied. × *120*

In this case the individual domains have almost circular symmetry about the field direction with a diameter of 30 to 60 microns. In addition, each domain possesses the isogyres characteristic of a uniaxial crystal viewed along its optic axis in poorly collimated light. The isogyres appear along

Publication Date: January 1, 1967 | doi: 10.1021/ba-1967-0063.ch006

the directions of polarization of the polarizer and analyzer. Since light off the optic axis is split into two component rays (ordinary and extraordinary), polarized perpendicular and parallel, respectively, to the plane of incidence, that portion in the polarization direction of the polarizer or analyzer is not transmitted. When the sample was excited using a low frequency (1 to 10 c.p.s.) a.c. field, the isogyres were observed to fold and reappear on each half cycle of the field. This indicates that the observed orientation is probably primarily caused by the interaction of the permanent moment with the applied field rather than by the molecular polarizability.

The observation of optical properties in an applied electric field, which are similar to those of a collection of oriented uniaxial crystallites, suggests that within each domain the molecules are cooperatively oriented. It remains to be determined whether or not the observed domains present a net spontaneous polarization. Previous experiments with nematic *p*-azoxyanisole indicated that dielectric peculiarities did accompany the formation of domains which appear when thin samples of this material are subjected to an electric field (*4*).

The Sawyer-Tower circuit, which is the standard method for observing polarization as a function of applied field in solid ferroelectrics, was modified slightly as shown in Figure 3 to adapt it better to the properties

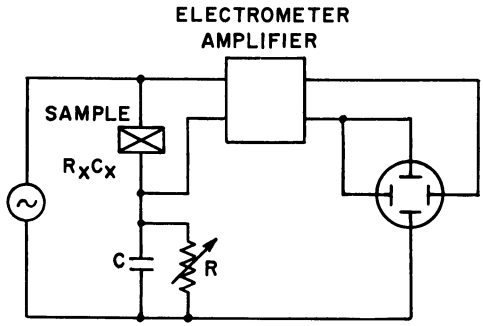

Figure 3. Modified Sawyer-Tower circuit for hysteresis loop measurement.

of the liquid crystal (*4*). With nematic butyl *p*-anisylidene-*p'*-aminocinnamate hysteresis loops which show all the general features of those found with ferroelectric crystals were observed, as seen in Figure 4. In particular, the loops show a coercive field and a saturation polarization and seem to be independent of electrode material. No substantial deviation from linear behavior in the current-voltage characteristic is observed over a range of fields far in excess of those normally used in obtaining the polarization data. In practically all aspects the behavior is similar to that which we previously reported for *p*-azoxyanisole. In that material, dispersion

Publication Date: January 1, 1967 | doi: 10.1021/ba-1967-0063.ch006

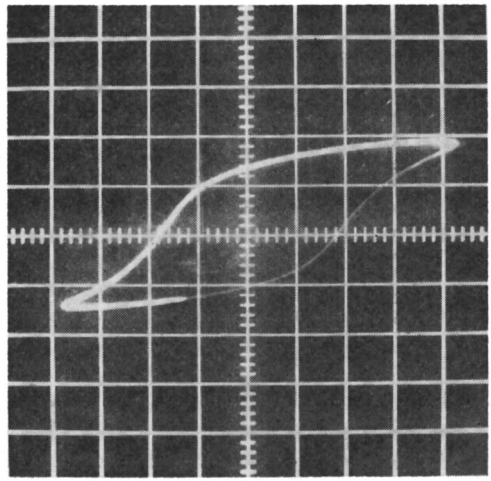

Figure 4. Typical hysteresis loop for nematic butyl-p-anisylidene-p'-aminocinnamate
Vertical scale ~0.02 μcoul./sq. cm./div.
Horizontal scale ~2 × 10³ volts/cm./div.

data and switching transients strongly substantiated the existence of a spontaneous polarization.

Butyl *p*-anisylidene-*p'*-aminocinnamate exhibits a saturation polarization, P_s, which is roughly inversely proportional to the sample thickness. This indicates the importance of surface effects in the alignment process. The saturation polarization was a strong function of the substrate cleaning procedure. The maximum polarization which we have observed is roughly 0.9 μcoul. per sq. cm., which corresponds to approximately 80% alignment for a molecular dipole moment of roughly one Debye.

Acknowledgment

I thank Joel Goldmacher for preparing the materials used in these experiments and Louis Zanoni for his assistance.

Literature Cited

(1) Heilmeier, G. H., *J. Chem. Phys.* **44**, 644 (1966).
(2) Vorlander, O., *Ber.* **41**, 2033 (1908).
(3) Williams, R., *J. Chem. Phys.* **39**, 384 (1963).
(4) Williams, R., Heilmeier, G. H., *Ibid.*, **44**, 638 (1966).

RECEIVED March 10, 1966.

7

Field Dependence of the Magnetic Susceptibility of the Liquid Crystal Phase of *p*-Azoxyanisole

C. H. MASSEN and J. A. POULIS

Technological University of Eindhoven, Eindhoven, The Netherlands

R. D. SPENCE

Michigan State University, East Lansing, Mich.

Publication Date: January 1, 1967 | doi: 10.1021/ba-1967-0063.ch007

We have studied the field- and temperature-dependence of the susceptibility of the liquid crystal phase of p-azoxyanisole for fields from 201 to 2550 gauss. The results at the highest fields agree with those of Föex at 8000 gauss, but at lower fields the susceptibility becomes field-dependent. The experimental results may be adequately represented by a simple theoretical expression obtained from statistical considerations. The only adjustable parameter in the theoretical formula is an effective mass which arises from interactions between the molecules and amounts to $\sim 2 \times 10^{-11}$ *gram.*

The relation of the magnetic susceptibility of the liquid crystal phase to that of the solid phase is a complicated, many-body problem. The energy of the system depends not only on the orientation of the molecules with respect to the magnetic field but also on their orientation with respect to each other. To obviate this difficulty, one introduces a set of noninteracting quasi particles (swarms) of mass M (*3*). The energy is then

$$E = -\frac{M}{2} \sum_i (\chi_\perp \sin^2 \theta_i + \chi_{||} \cos \theta_i) H^2 \qquad (1)$$

where the sum extends over quasi-particles. Here $\chi_\perp$ and $\chi_{||}$ are the diamagnetic susceptibilities perpendicular and parallel to the axis of the molecules, and θ_i is the angle between the magnetic field, H, and the axis of the molecules in the ith quasi-particle. Using the standard procedures of

In Ordered Fluids and Liquid Crystals; Porter, R., el al.;
Advances in Chemistry; American Chemical Society: Washington, DC, 1967.

statistical mechanics (*4*), one finds for the susceptibility of the liquid crystal phase,

$$\bar{\chi} = \chi_\perp + (\chi_\parallel - \chi_\perp) \frac{\partial}{\partial \xi} \left(\log \int_{-1}^{+1} e^{\xi \mu^2} d\mu \right) \tag{2}$$

where

$$\xi = \frac{H^2 M}{2kT} (\chi_\parallel - \chi_\perp)$$

and $\mu = \cos \theta_i$

Equations 1 and 2 contain a single adjustable parameter, M, which in principle can be obtained by measuring $\bar{\chi}$ at one temperature, T, and one field, H. However, it is important to attempt to check the validity of Equation 1. Since the absolute temperature varies little throughout the liquid crystal phase, the only practical method for examining the general correctness of the previous expressions is to vary field H. The small value of $\bar{\chi}$ implies that a balance of considerable sensitivity is needed for small fields. Complications of two different kinds arise. The swarms may be embedded in normal liquid, which does not contribute to the variation of the observed susceptibility with the applied field, implying a reduction of the effective volume of the swarms. One further complication arises from the fact that the walls of the container exert an orienting force on the molecules which cannot be overcome even by the application of large (10^4 oersteds) magnetic fields. This again reduces the effective volume of material which may be oriented by the field. If one assumes that the molecules in the layer of material on the walls have an orientation that varies randomly from place to place over the surface of the vessel, the susceptibility of the surface layer is then just that of the liquid phase. The effective volume of the sample may then be determined by measuring the $\bar{\chi}$ in a large magnetic field and comparing the value so obtained with the value of $\chi_\parallel$ which would be the susceptibility if the material were completely and uniformly aligned.

Experimental Method and Results

Although for *p*-azoxyanisole (PAA) a number of measurements in electric fields have been reported (*1*, *5*), only Föex (*2*) reported measurements in a high magnetic field. In this paper we report the results of magnetic susceptibility measurements on PAA, which have been obtained by using the Faraday method with a sensitive balance described by Poulis *et al.* (*6*). The sample consisted of 0.2841 gram of PAA held in an evacuated spherical quartz container. Measurements were made at fields of 2550, 1050, 275, and 200 oersteds at a number of temperatures in the liquid crystal and liquid phase. The absolute accuracy of the susceptibility measurements was about 3%, determined by the irreproducibility in the adjustment of

Publication Date: January 1, 1967 | doi: 10.1021/ba-1967-0063.ch007

the sample to the place where the calibration is taken and by the correction for the quartz container in which the PAA was stored.

The temperature dependence of the susceptibility for the field strengths used is shown in Figure 1, where the curves are drawn to fit best to the measured points. The susceptibility at 2550 oersteds is in good agreement

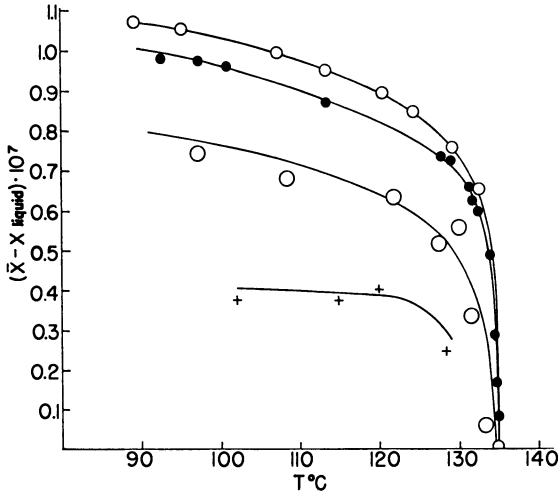

Figure 1. Field dependence of $\bar{\chi} - \chi_{liquid}$ *of p-azoxyanisole*

\+ *200 oersteds*
O *275 oersteds*
• *1050 oersteds*
o *2550 oersteds*

with that observed by Föex (*2*) at 8000 oersteds and may therefore be considered characteristic of the completely oriented liquid crystal phase. According to Föex (*2*) the principal susceptibilities of crystalline PAA are

$$\chi_x = -0.655 \times 10^{-6}, \quad \chi_y = -0.634 \times 10^{-6}, \quad \chi_z = -0.408 \times 10^{-6} \text{ c.g.s.}$$

The z direction lies along the long axis of the molecule, and therefore

$$\chi_\perp = \tfrac{1}{2}(\chi_x + \chi_y)$$
$$\chi_\parallel = \chi_z$$

In Figure 2 we have plotted the quantity $(\bar{\chi} - \chi_{liquid})/(\chi_\parallel - \chi_\perp)$ calculated from Equation 2, as a function of $\xi^{\frac{1}{2}}$. The three experimental points have been fitted to the theoretical curve by assuming that a field of 2550 oersteds produces essentially complete alignment of the molecules (represented by the point plotted at the upper right of Figure 2) and using a value of 2×10^{-11} grams for the quasi-particle mass, M.

The agreement between the theory and observations is qualitatively satisfactory but not sufficiently good that one may regard the theory as

Publication Date: January 1, 1967 | doi: 10.1021/ba-1967-0063.ch007

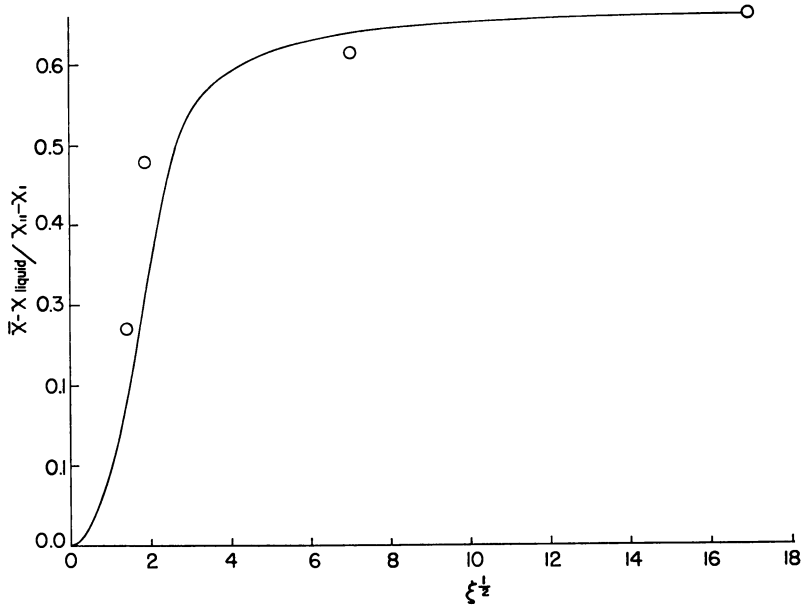

Figure 2. Predicted and observed values of $\frac{\bar{x} - x_{liquid}}{x_{\parallel} - x_{\perp}}$

more than a rough picture of a rather complicated situation. The value of M derived from these measurements is larger than that derived from other methods (*3*), but at present there appears to be no ready explanation of this fact.

Acknowledgment

We express our gratitude to the Eindhoven Hogeschool Fonds for financial aid in this work.

Literature Cited

(1) Carr, E. F., Spence, R. D., *J. Chem. Phys.* **22**, 1481 (1954).
(2) Föex, G., *Trans. Faraday Soc.* **29**, 958 (1933).
(3) Gray, G. W., "Molecular Structure and Properties of Liquid Crystals," Academic Press, London, 1962.
(4) Landau, L. D., Lifshitz, E. M., "Course of Theoretical Physics," Vol. 5, "Statistical Physics," Pergamon Press, London-Paris, 1958.
(5) Maier, W., Barth, G., Wiehl, H. E., *Z. Elektrochem.* **58**, 674 (1954).
(6) Poulis, J. A., Massen, C. H., van der Leeden, P., *Appl. Sci. Res.* **B9**, 133 (1961).

RECEIVED February 11, 1966.

8

Ordering in Liquid Crystals Owing to Electric and Magnetic Fields

EDWARD F. CARR

Physics Department, University of Maine, Orono, Maine

Publication Date: January 1, 1967 | doi: 10.1021/ba-1967-0063.ch008

*A great deal of work has been carried out using electric fields to align molecules in the anisotropic liquid phase, and the results have often been conflicting. Results are shown for anisal-*p*-aminoazobenzene, which exhibits positive dielectric anisotropy, and for* p*-azoxyanisole, which exhibits negative dielectric anisotropy. The molecular alignment was investigated in the presence of external electric and magnetic fields acting individually and also simultaneously. Measurements of the dielectric loss at a microwave frequency were used to indicate the extent of the ordering. The results indicate the existence of a process causing molecular alignment which depends on the electric or magnetic field but is not associated with either the anisotropy in the dielectric constant or the permeability.*

The effect of an externally applied electric field on the alignment of molecules in liquid crystals has been studied by many investigators, and the results have frequently been conflicting. The literature regarding the effect owing to electric fields has been reviewed recently by Gray (*8*).

This paper is concerned with the liquid crystals, *p*-azoxyanisole and anisal-*p*-aminoazobenzene. The structural formulas are:

COMPOUND	STRUCTURE
Anisal - p - aminoazobenzene	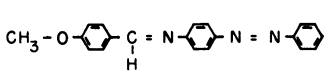
p - Azoxyanisole	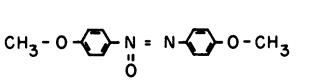

In the presence of external magnetic fields both substances show a molecular alignment, with the long axes of the molecules preferring a direction

In Ordered Fluids and Liquid Crystals; Porter, R., el al.;
Advances in Chemistry; American Chemical Society: Washington, DC, 1967.

parallel to the field. Measurements by Zwetkoff and Marinin (*26*) involving the Kerr effect indicated that in anisal-*p*-aminoazobenzene an alignment should exist, with the long axes of the molecules preferring a direction parallel to an externally applied electric field. Measurements (*3*) which involve microwave dielectric techniques agree with their work as to the direction of the molecular axes relative to an external electric field. The results for *p*-azoxyanisole in a static electric field have been conflicting. Since the low frequency dielectric constant (*15*) is greatest perpendicular to the long axes of the molecules, one would expect an alignment perpendicular to the electric field. Some observers agreed with this prediction, but Kast (*14*) and later other investigators reported alignments with the long molecular axes preferring a direction parallel to the field. It is generally agreed that for frequencies of approximately 0.5 Mc. the orientation of the long molecular axes will be perpendicular to the field.

Publication Date: January 1, 1967 | doi: 10.1021/ba-1967-0063.ch008

Experimental

Except for a few details, the experimental techniques used for the work discussed have been described (*1*, *4*, *5*), so only a few comments are made here.

The cell is a section of *K*-band wave guide as illustrated in Figure 1 *A*. Figure 1, *B* and *C*, shows end views of the cell with a center plate electrically insulated from the guide. The cell is divided into two sections, each containing the same amount of sample. As the microwave beam enters the

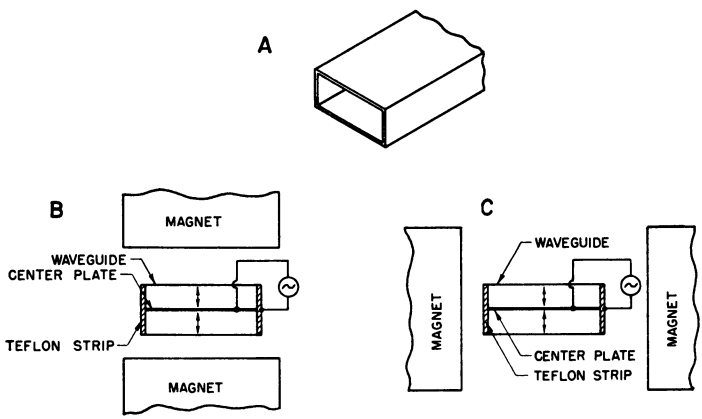

Figure 1. Diagram of cell

A. Wave guide for sample cell
B. Magnetic field parallel to polarized microwave electric field
C. Magnetic field perpendicular to polarized microwave electric field

cell, it divides in such a way that we have a polarized wave with the microwave electric field perpendicular to the wide side of the guide in each section. An external a.c. electric field, applied between the center plate and the wave guide, produces an external electric field parallel to the microwave

electric field. The arrangement shown in Figure 1, *B*, provides for an external magnetic field parallel to the external electric field while Figure 1, *C*, shows the arrangement for a magnetic field perpendicular to the electric field. The center plate and Teflon insulating strips will produce some mismatch in the guide, but this is not serious since only relative measurements of the transmitted power at a frequency of 24 kMc. were recorded with this arrangement.

For measurements in anisal-*p*-aminoazobenzene the magnetic field was varied from 500 to 3000 gauss, and for *p*-azoxyanisole only values of 500 and 1000 gauss were used. Although magnetic fields above 500 gauss may produce a molecular alignment which is slightly more complete than a field of 500 gauss, the change did not appear to affect the results discussed in this article appreciably.

The samples of anisal-*p*-aminoazobenzene were obtained commercially and were purified by dissolving in hot methanol, followed by filtration and recrystallization. The clearing point was 185°C. The samples of *p*-azoxyanisole were also obtained commercially and purified by recrystallization.

Anisal-p-aminoazobenzene

Dielectric Loss in the Presence of an External Magnetic Field. Figure 2 shows the temperature dependence of the dielectric loss at a microwave frequency of 24 kMc. (*3*). The upper curve represents the loss in a field of 2800 gauss perpendicular to the microwave electric field, hence a molecular

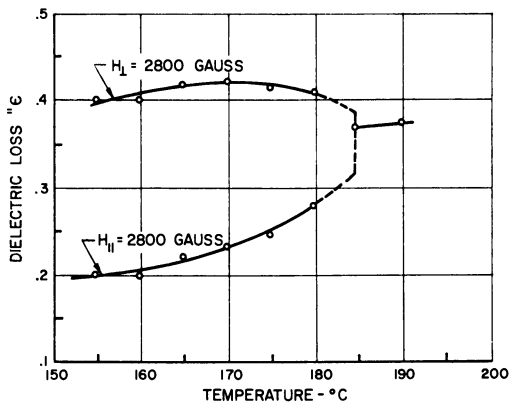

Figure 2. Temperature dependence of dielectric loss for anisal-p-aminoazobenzene at a frequency of 24 kMc.

External magnetic field of 2800 gauss applied parallel and perpendicular to microwave electric field

alignment with the long axes of the molecules preferring a direction perpendicular to the electric field. The lower curve shows the loss with the external field parallel to the microwave electric field, hence a molecular alignment parallel to the electric field. Increasing the magnetic field to values greater than 2800 gauss did not produce a noticeable change in the dielec-

tric loss. Above 185°C. (clearing point) the effect of the magnetic field was negligible. Measurements of the dielectric loss in the region between the two curves will provide some information about the molecular alignment inside the cell.

Molecular Alignment for Electric and Magnetic Fields Parallel to Each Other. In Figure 1, *B*, both the electric and magnetic fields produce alignments of the molecules with the long axes parallel to the microwave electric field. When a 370-kc. electric field of 1100 volts per cm. was replaced by a d.c. magnetic field of 3000 gauss, no change in the dielectric loss was detectable. A change in the dielectric loss of approximately 0.5% of the difference for the parallel and perpendicular orientations relative to the microwave electric field should be detectable with this arrangement. For electric fields of frequencies 60 c.p.s. and 1.7 Mc. the molecular alignment was not as complete as in the presence of a magnetic field. This work indicates that the degree of molecular alignment which can be obtained with magnetic fields is the same as with electric fields if the proper frequency is chosen. If one assumes that the alignment is primarily caused by the anisotropy in the low-frequency dielectric constant and the permeability, this work also shows that the direction for the maximum value of the low frequency dielectric constant is parallel to the direction for which the absolute value of the diamagnetic suseptability is a minimum in an ordered sample.

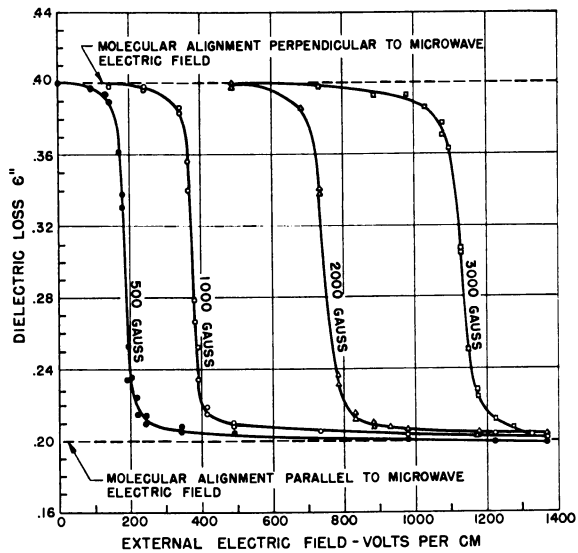

Figure 3. Dielectric loss in anisal-p-aminoazobenzene at a microwave frequency of 24 kMc., as a function of externally applied 370-kc. electric field

Individual curves are for various values of a static magnetic field applied perpendicular to the external electric field. Temperature, 155°C.

Publication Date: January 1, 1967 | doi: 10.1021/ba-1967-0063.ch008

Molecular Alignment in Magnetic and Electric Fields at Right Angles to Each Other. Figure 3 (*4*) is a plot of the dielectric loss, ϵ'', as a function of the externally applied electric fields for various constant values of the steady magnetic field. The frequency of the external electric field was 370 kc., and the temperature of the sample was 155°C. The maximum value of $\epsilon'' = 0.40$ (upper dashed line) for each of the magnetic fields at low electric fields represents an alignment of the molecules perpendicular to the microwave electric field and hence parallel to the magnetic field. For sufficiently large externally applied electric fields, the minimum value of $\epsilon'' = 0.2$ (lowest dashed line) is approached, indicating an alignment parallel to the microwave electric field and therefore parallel to the externally applied electric field.

Figure 3 (*4*) shows that for certain values of the external electric field small changes in the electric field will produce marked changes in the alignment of the molecules. Electric and magnetic fields were compared, for producing molecular alignment, at a dielectric loss of $\epsilon'' = 0.30$. This corresponds to a random orientation of the molecules in the plane of E and H. Table I shows the ratios of the electric field to the magnetic field for different values of the magnetic field. This ratio does not allow for any effect

Table I. Ratio of Electric Field to Magnetic Field for Random Orientation of Molecules in Plane of E and H with a 370-Kc. Electric Field

$T = 155$°C.		$T = 175$°C.	
H, gauss	$\frac{E}{H}$, $\frac{V}{cm.\ gauss}$	H, gauss	$\frac{E}{H}$, $\frac{V}{cm.\ gauss}$
500	0.374	500	0.374
1000	0.377	1000	0.380
2000	0.374	2000	0.382
3000	0.377	3000	0.382

owing to walls, temperature gradients, or other aligning processes that might be present which do not involve the electric or magnetic field. E/H for $T = 155$°C. is constant within the limits of the experimental error. E/H for $T = 175$°C. appears to be slightly lower than for 155°C., but this difference could be caused by experimental error.

Measurements similar to those illustrated in Figure 3 were also made with a 60-c.p.s. external electric field. These results were similar to those in Figure 3, and the ratios of E/H agreed with those given in Table I within the limits of experimental error.

After the sample had been used approximately 10 hours at 155°C. and 2 hours at 175°C., it was heated to approximately 180°C. and left for about 15 hours. Figure 4 (*4*) illustrates the molecular alignment in the presence of a 370-kc./second and a 60-c.p.s. electric field.

Table II shows the ratios of E/H for $\epsilon'' = 0.30$. These ratios for the 370 kc./second field are consistent with those shown in Table I, but those

Publication Date: January 1, 1967 | doi: 10.1021/ba-1967-0063.ch008

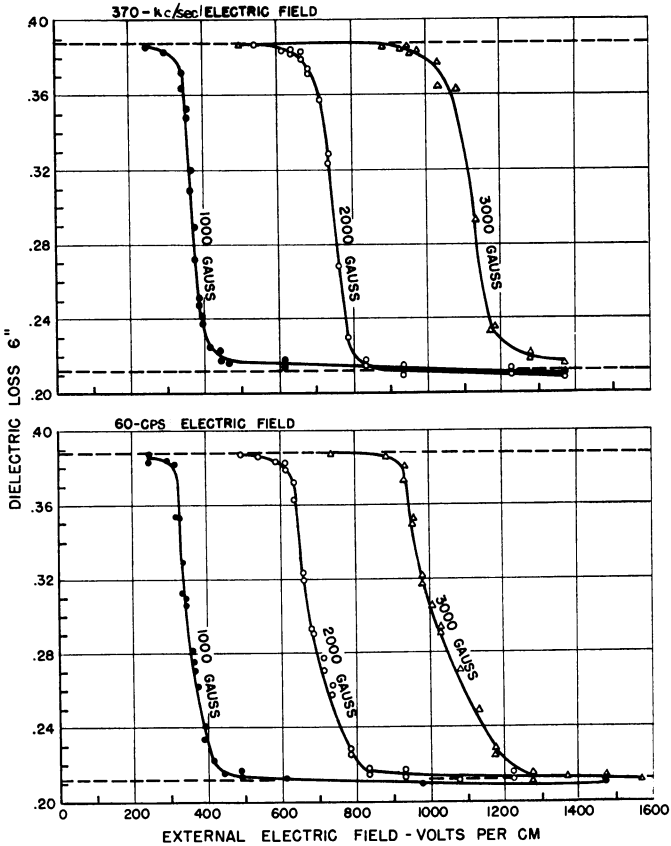

Figure 4. Dielectric loss in a decomposed sample of anisal-p-amino-azobenzene at a microwave frequency of 24 kMc. as a function of an externally applied a.c. electric field

Upper. Frequency of electric field 370 kc.
Lower. Frequency 60 c.p.s.
Individual curves are for different values of magnetic field applied perpendicular to external electric field
Temperature 155°C.

Table II. Ratio of Electric Field to Magnetic Field for Random Orientation of Molecules in Plane of *E* and *H* at 155°C.

370 Kc.		*60 C.p.s.*	
	$\frac{E}{H}$, *cm. gauss*		$\frac{E}{H}$, *cm. gauss*
H, gauss	*V*	*H, gauss*	*V*
1000	0.373	1000	0.349
2000	0.373	2000	0.338
3000	0.375	3000	0.338

Publication Date: January 1, 1967 | doi: 10.1021/ba-1967-0063.ch008

for the 60-c.p.s. field are noticeably lower. Since the sample is appreciably decomposed, the results do not have much significance except to illustrate the effect of decomposition. The lower values for the 60-c.p.s. field imply that fields of this frequency are more effective in producing a molecular alignment than fields of much higher frequencies. This seems to be consistent with some of the results on liquid crystals with a negative dielectric anisotropy, in that low frequencies seem to be more effective in producing an alignment with the long axes of the molecules preferring a direction parallel to the field. The change in the molecular alignment is not as sharp for the 60-c.p.s. field as for the 370 kc./second field, which indicates the presence of other disturbances in the sample.

If it is assumed that the alignment of the molecules is caused only by the anisotropies in the low-frequency dielectric constant and the permeability, the following relation should hold:

$$(\epsilon_{||}' - \epsilon_{\perp}')E^2 = (\mu_{||} - \mu_{\perp})H^2 \quad (1)$$

where $\epsilon_{||}'$ and $\mu_{||}$ are the dielectric constant and permeability, respectively, parallel to the axis of symmetry when the maximum molecular alignment has been attained. $\epsilon_{\perp}'$ and $\mu_{\perp}$ are the dielectric constant and permeability perpendicular to the axis of symmetry. Using the value of $(\mu_{||} - \mu_{\perp})$ at 155°C. given by Zwetkoff and Sosnovsky (*27*) and density measurements by Porter and Johnson (*19*), one obtains the value of 1.09 for $(\epsilon_{||}' - \epsilon_{\perp}')$. $(\epsilon_{||}' - \epsilon_{\perp}')$ at 6 kMc. is 0.48 and decreasing with frequency, which implies that the anisotropy in the dielectric constant is not sufficient to explain the ratios of E/H obtained in this work. However, a crude check on the low-frequency dielectric constant has indicated that $(\epsilon_{||}' - \epsilon_{\perp}')$ is greater than 0.48. Since there appear to be no accurate measurements of the low-frequency dielectric constant for this material, and the ratio of E/H appears to be constant, one can write as a first approximation

$$[c + (\epsilon_{||}' - \epsilon_{\perp}')]E^2 = [\mu_{||} - \mu_{\perp}]H^2 \quad (2)$$

where c is a constant that possibly might be associated with the anisotropy in the conductivity. The value of c may be a very small number or even zero for a very pure compound, but would be something other than zero for a decomposed sample. Recent measurements with techniques identical to those mentioned in this article have been made by Twitchell and Carr (*23*) in *p*-azoxyanisole with a 500-c.p.s. external electric field. Equation 2 describes the behavior well for high fields, and the value of c was found to be much larger than the difference in the low-frequency dielectric constants.

p-Azoxyanisole

Molecular Alignment in A.C. Electric and Static Magnetic Fields Parallel to Each Other. Freedericksz and Zwetkoff (*7*) have investigated the ordering in the anisotropic liquid phase of *p*-azoxyanisole using optical

Publication Date: January 1, 1967 | doi: 10.1021/ba-1967-0063.ch008

techniques and compared the effectiveness of electric and magnetic fields. Their investigation was carried out with static magnetic fields and electric fields with frequencies greater than 300 kc./second. For given values of the magnetic field they obtained values of the electric field intensity which would be equivalent to the magnetic fields for producing molecular alignment. These results indicated that the ratio of the electric field to the magnetic field was independent of the magnetic field but did vary with temperature.

Figure 5 is a plot of the dielectric loss, ϵ'', as a function of the externally applied electric field for various constant values of the steady magnetic field. The frequency of the external field was 370 kc./second, and the temperature of the sample was 132°C. The experimental arrangement for these

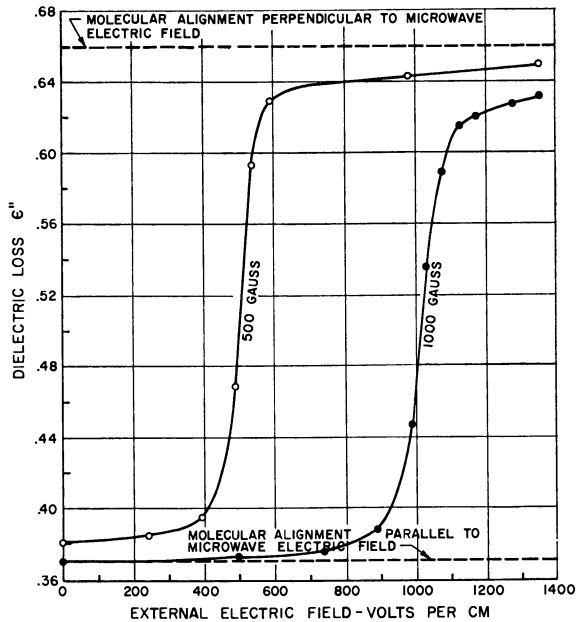

Figure 5. Dielectric loss in p-azoxyanisol at a microwave frequency of 24 kMc. as a function of an externally applied 370-kc. electric field

Individual curves are for various values of a static magnetic field applied parallel to external electric field Temperature, 132°C.

results is shown in Figure 1, *B*. The maximum value of $\epsilon'' = 0.66$ (upper dashed line in Figure 5) represents an alignment of the molecules perpendicular to the microwave electric field, hence perpendicular to the external electric field for sufficiently large values of the electric field. For sufficiently large values of the magnetic field the minimum value of $\epsilon'' = 0.37$ (lowest

dashed line) indicates an alignment parallel to the microwave electric field and therefore parallel to the magnetic field.

The effectiveness of electric and magnetic fields were compared for a value of the dielectric loss $\epsilon'' = 0.515$. The ratio of E/H for a magnetic field of 500 gauss was 1.01 and for a field of 1000 gauss was 1.02. This is in agreement with Freedericksz and Zwetkoff, in that E/H appears to be independent of the magnetic field. The value they reported was 1.08, which is appreciably higher. It is felt that this difference is not caused by experimental error.

Although a detailed study was not carried out for temperatures below 132°C., a few preliminary measurements were made at 120°C. These measurements agreed with those of Freedericksz and Zwetkoff, in that they showed a decrease in E/H as the temperature was lowered. Some preliminary measurements were also made in the presence of an external electric field at a frequency of 1.7 Mc., and the ratios of E/H appeared to be the same as those for a frequency of 370 kc.

Since E/H appears to be independent of the magnetic field strength, an equation similar to Equation 2 should hold. With $\epsilon_\perp'$ greater than $\epsilon_{||}'$ for liquid crystals exhibiting negative dielectric anisotropy, this equation becomes

$$[-c + (\epsilon_\perp' - \epsilon_{||}')]E^2 = [\mu_{||} - \mu_\perp]H^2 \qquad (3)$$

Using the value $(\mu_{||} - \mu_\perp)$ given by Zwetkoff and Sosnovsky (*27*) and $(\epsilon_\perp' - \epsilon_{||}')$ given by Maier and Meier (*15*), in Equation 2, $c = 0.01$ for the results shown in Figure 4. The work of Freedericksz and Zwetkoff (*7*) gives $c = 0.03$. Alignment of molecules owing to wall effects might account for this difference since the thickness of the samples used by Freedericksz and Zwetkoff was less than that used by the author. Also different samples could give different values for c.

Molecular Alignment in a D. C. Electric Field. Figure 6 (*2*) shows the temperature dependence of the dielectric loss at a microwave frequency of 6 kMc. This shows larger loss than similar measurements at 24 kMc., which were used to illustrate the effects in Figure 5. The upper curve shows the loss in the presence of a field of 2500 gauss perpendicular to the microwave electric field, and the lower curve gives the loss with a magnetic field parallel to the microwave electric field. The curve representing the results in the presence of an external electric field shows the dielectric loss using a coaxial cell which produces a radial rather than a homogenous field. A potential of 300 volts was applied between the center and outer conductors. Increasing the potential difference did not appreciably change the dielectric loss. These results imply that in a d.c. electric field a molecular alignment is obtained with the long axes of the molecules preferring a direction parallel to the externally applied electric field. Although the alignment is parallel to the field, it is not as complete as the alignment which can be obtained with

Publication Date: January 1, 1967 | doi: 10.1021/ba-1967-0063.ch008

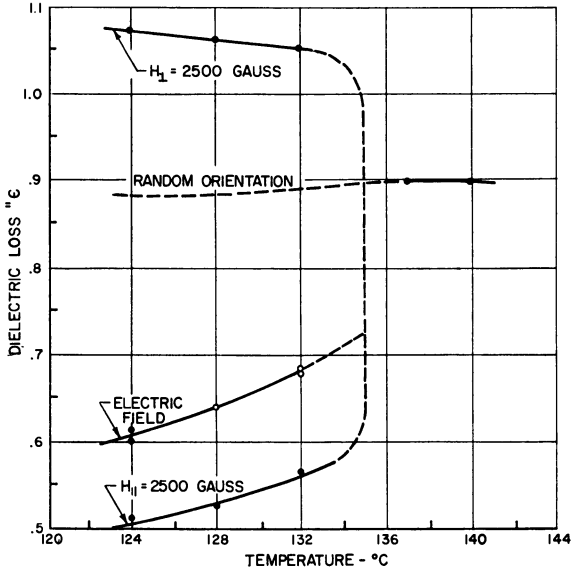

Figure 6. Temperature dependence of dielectric loss of p-azoxyanisole at a frequency of 6 kMc.

For measurements with rectangular wave guide an external magnetic field of 2500 gauss was applied parallel and perpendicular to the microwave electric field. For measurements with a coaxial line the dielectric loss was measured with a potential difference between inner and outer conductors in absence of any external magnetic field

a magnetic field. Although many investigators (*8*) have reported results similar to those given here for d.c. fields, it is the opinion of the author (*2*) that the direction in which the molecules tend to align themselves may depend on the purity of the sample.

Anisaldazine, which also exhibits negative dielectric anisotropy, was also investigated (*1*) using microwave dielectric techniques. The results in the presence of a d.c. electric field are very similar to those shown for *p*-azoxyanisole.

Recent Work with Other Techniques

Rowell, Phillips, Melby, and Panar (*20*) have investigated the molecular alignment for *p*-azoxyanisole and *p*-azoxyphenetole in the presence of an external electric field using NMR techniques. Their work agrees with the work of the author, in that the molecular alignment is parallel to the electric field for low frequencies. The agreement as to the degree of alignment owing to electric fields as compared with magnetic fields is somewhat uncertain. Results with microwave dielectric techniques (*2*) indicate that the molecular alignment in a magnetic field is more nearly complete than in a low frequency electric field. If one considers only the separation of the

Publication Date: January 1, 1967 | doi: 10.1021/ba-1967-0063.ch008

outer peaks of their doublet, results with NMR techniques seem to indicate that the alignment owing to an electric field is comparable with that of a magnetic field, but a detailed study of the signal might reveal a difference. Their work involved liquid crystals with hydrogen replaced by deuterium in the end groups of the molecules. Earlier work (*11*) had shown that the molecular alignment was less complete when hydrogen was replaced by deuterium, so any comparison between the work of Rowell, Phillips, Melby, and Panar and the author should not be taken too seriously. Since the alignment in an electric field seems to have some dependence on the sample used, it might be worthwhile to have all samples as nearly alike as possible for measurements with various techniques. This is now being attempted by the author and collaborators using NMR and microwave dielectric techniques.

Slovak and Biscoe (*21*) recently obtained results with x-ray techniques indicating an alignment of the molecules with their long axes parallel to the externally applied electric field. This agrees with the work of Kast (*14*) and of the author. Their work also agreed with that of the author in that the alignment in the presence of an external magnetic field was more nearly complete than in an electric field.

Optical techniques have been used recently to investigate liquid crystals in the presence of external electric fields. Williams (*24*) reported the formation of a regular domain pattern when an electric field is applied. He has suggested the possibility of ferroelectric domains to explain his results. He reported an upper frequency limit for the applied voltage, above which the domains did not form. Since this limit was usually around 20 kc./second, it might correspond to the critical frequency reported by the author (*2*). For frequencies above 20 kc./second an alignment with the molecular axes parallel to the external field was seldom obtained using microwave dielectric techniques. A number of other liquid crystals have been studied with optical techniques by Elliott and Gibson (*6*), Kapustin and Larionova (*12*), and Kapustin and Vistin (*13*), whose techniques were similar to those used by Williams.

Kapustin and Vistin (*13*) have reported a dielectric anomaly resembling a ferroelectric hysteresis loop for *p*-azoxyphenetole. They interpreted this as a ferroelectric effect. Williams and Heilmeier (*25*) have reported ferroelectric hysteresis loops in *p*-azoxyanisole for frequencies below 10 c.p.s. They also investigated other electrical properties of liquid crystals which characterize ferroelectric crystals. Transient behavior of domains in liquid crystals has been studied by Heilmeier (*10*) using electric fields. Neff, Gulrich, and Brown (*18*) have investigated the molecular alignment in thin films of nematic liquid crystals from infrared dichroic measurements in a homogeneous electric field. They indicated that the degree of orientation obtained for *p*-methoxybenzylidene-*p*-cyanoaniline is somewhat lower than that obtained by others on *p*-azoxyanisole with different techniques. They

Publication Date: January 1, 1967 | doi: 10.1021/ba-1967-0063.ch008

used electric fields to produce the alignment, whereas most alignment studies in *p*-azoxyanisole have been carried out in the presence of external magnetic fields. Since results with microwave dielectric techniques (*1*, *2*) have indicated that the degree of orientation in the presence of low frequency electric fields is lower than in magnetic fields, the use of an electric field instead of a magnetic field is a possible explanation.

Electric field effects have been studied in cholesteric liquid crystals by Muller (*17*) and Harper (*9*). Since the structure for this phase is different from the nematic phase, their work and the work discussed in this article cannot be compared at this time.

Conclusions

Electric fields can be used to replace magnetic fields in some experiments where molecular alignment is essential. In experiments involving such techniques as magnetic resonance, where the spatial alignment of the molecules is determined by the magnetic field which must be present, electric fields can be used to reorient the molecules. Attempts are being made to investigate liquid crystals using NMR techniques where the sample is aligned with a strong electric field which is not parallel to the magnetic field.

The author believes that ionizable impurity may be associated with some of the processes which are responsible for molecular alignment. If this is the case, the effect of an aligning process which might involve ionizable impurity would depend on the type and amount of impurity and the frequency of the applied electric field. Svedberg (*22*) measured the conductivity in some liquid crystals of the nematic type which were rendered conducting by the addition of traces of other substances. When the samples were aligned with a magnetic field, he found that the conductivity was greatest in a direction parallel to the long axes of the molecules. This was also the case for the samples used to obtain the results discussed in this article, where the conductivity depended to a certain extent on the impurities present. If one assumes that the anisotropic liquid is made up of regions where the molecules prefer a direction parallel to each other within a region but are not parallel to the molecules of an adjacent region, the conductivity in a given direction will change. This might give rise to an accumulation of charge at the boundary between the regions, which could result in a dipole moment associated with a region which would interact with the external electric field.

Although accurate measurements could not be made with the equipment available for a.c. electric fields above 10 Mc., a few observations were made with anisal-*p*-aminoazobenzene at approximately 14 and 21 Mc./second. The degree of molecular alignment decreased with an increase in frequency. When a 21-Mc. field was turned on parallel to an existing magnetic field, the molecular alignment produced by the magnetic field was almost completely destroyed. This indicates anisotropic dielectric dispersion

Publication Date: January 1, 1967 | doi: 10.1021/ba-1967-0063.ch008

in anisal-*p*-aminoazobenzene comparable to that reported by Maier and Meier (*16*) for other liquid crystals. Plans are now being made to extend this work to frequencies above 10 Mc.

Acknowledgment

The author is indebted to the Air Force Office of Scientific Research for financial assistance for much of the work described in this paper.

Literature Cited

(1) Carr, E. F., *J. Chem. Phys.* **38**, 1536 (1963).
(2) *Ibid.*, **39**, 1979 (1963).
(3) *Ibid.*, **42**, 738 (1965).
(4) *Ibid.*, **43**, 3905 (1965).
(5) Carr, E. F., Spence, R. D., *J. Chem. Phys.* **22**, 1481 (1954).
(6) Elliott, G., Gibson, J. G., *Nature* **205**, 995 (1965).
(7) Freedericksz, V., Zwetkoff, V., *Acta Physiochim. URSS* **3**, 895 (1935).
(8) Gray, G. W., "Molecular Structure and Properties of Liquid Crystals," Academic Press, New York, 1962.
(9) Harper, W. J., *Mol. Crystals* **1**, 235 (1966).
(10) Heilmeier, George, *J. Chem. Phys.* **44**, 644 (1965).
(11) Jain, P. L., Lee, J. C., Spence, R. D., *J. Chem. Phys.* **23**, 878 (1955).
(12) Kapustin, A. P., Lurionova, L. S., *Soviet Phys. Cryst.* **9**, 235 (1964) (English translation).
(13) Kapustin, A. P., Vistin, L. K., *Soviet Phys. Cryst.* **10**, 95 (1965).
(14) Kast, W., *Z. Physik* **71**, 39 (1931).
(15) Maier, W., Meier, G., *Z. Naturforsch.* **16a**, 470 (1961).
(16) *Ibid.*, p. 1200.
(17) Muller, J. H., *Z. Naturforsch.* **20a**, 849 (1965).
(18) Neff, V. D., Gulrich, L. W., Brown, G. H., *Mol. Crystals* **1**, 225 (1966).
(19) Porter, R. S., Johnson, F. F., *J. Appl. Phys.* **34**, 51 (1963).
(20) Rowell, J. C., Phillips, W. D., Melby, L. R., Panar, M., *J. Chem. Phys.* **43**, 3442 (1965).
(21) Slovak, J. P., Biscoe, J., unpublished results.
(22) Svedberg, T., *Ann. Physik* **44**, 1121 (1914).
(23) Twitchell, R. P., Carr, E. F., unpublished work.
(24) Williams, Richard, *J. Chem. Phys.* **39**, 384 (1963).
(25) Williams, Richard, Heilmeier, George, *J. Chem. Phys.* **44**, 638 (1965).
(26) Zwetkoff, V., Marinin, V., *Zh. Eksperimen. i. Teor. Fiz.* **18**, 841 (1948).
(27) Zwetkoff, V., Sosnovsky, A., *Acta Physicochim. URSS* **18**, 358 (1943).

RECEIVED February 11, 1966.

Occurrence of Different Mesomorphous Phases in Ternary Systems of Amphiphilic Substances and Water

LEO MANDELL, KRISTER FONTELL, and PER EKWALL

Laboratory for Surface Chemistry, Royal Swedish Academy of Engineering Sciences, Stockholm, Sweden

Publication Date: January 1, 1967 | doi: 10.1021/ba-1967-0063.ch009

A thorough study has been made of the system sodium caprylate–decanol–water at 20°C. Various mesophases in the heterogeneous regions can be separated by centrifugation under suitable conditions. The mesomorphous substance has different internal structures in different concentration regions, and these structures do not change continuously into one another but represent separate mesophases. The regions of existence of the various mesophases are separated by two- and three-phase regions, where two or three phases occur side by side in accordance with the requirements of the phase rule. Similar conditions have been shown in a large number of other ternary systems. A systematic study of the dependence of phase equilibrium on molecular structure in such ternary systems has so far disclosed five main types of phase diagram.

In addition to the order on the molecular level, which is characteristic of systems with thermotropic mesomorphism, the lyotropic mesomorphous systems are also distinguished by the arrangement of aggregates in a superlattice. These systems exhibit not only the joining and directing forces between individual molecules but also the interaction between larger molecular aggregates—for instance, micelle-like aggregates—and account must be taken of their internal arrangement. This would appear to explain the variety of the inner structure of the lyotropic mesomorphous systems.

Liquid crystalline products are formed in aqueous soap systems at high concentrations. The existence of different mesophases in such systems was observed by McBain (*17*, *18*). Toward the end of the 1950's Luzzati *et al.* (*11*, *14*, *15*, *16*) discovered by x-ray diffraction various mesomorphous structures in these two-component systems and regarded this as a proof that they contained different mesophases, which, however, they did not separate.

In Ordered Fluids and Liquid Crystals; Porter, R., el al.;
Advances in Chemistry; American Chemical Society: Washington, DC, 1967.

The presence in systems of soap and soaplike substances of a third component with amphiphilic and predominantly lipophilic properties strongly promotes the formation of aqueous mesomorphous phases. In such ternary systems an extensive, continuous concentration region containing mesomorphous substances often forms, from fairly low concentrations upward. The view commonly held during the 1950's and later that there is only one mesomorphous phase in this region (*1*, *2*, *3*, *12*, *13*, *22*) would seem to be incorrect; our x-ray diffraction studies have disclosed that the region contains areas of different inner structure of the mesomorphous matter and that distinct mesomorphous phases, each with its own inner structure, properties, and area of existence, can be separated by centrifugation. Between these areas are two- and three-phase regions, where, in conformity with the phase rule, the phases occur side by side (*4–8*, *10*, *19*, *20*, *21*).

Previous Investigations of Sodium Caprylate-Decanol-Water System

We first consider a model system of sodium caprylate, decanol, and water. In Figure 1 all the concentration areas in which any mesomorphous substance at all has been observed are included in one extensive region referred to as "liquid crystal." Regions L_1 and L_2 consist of homogeneous,

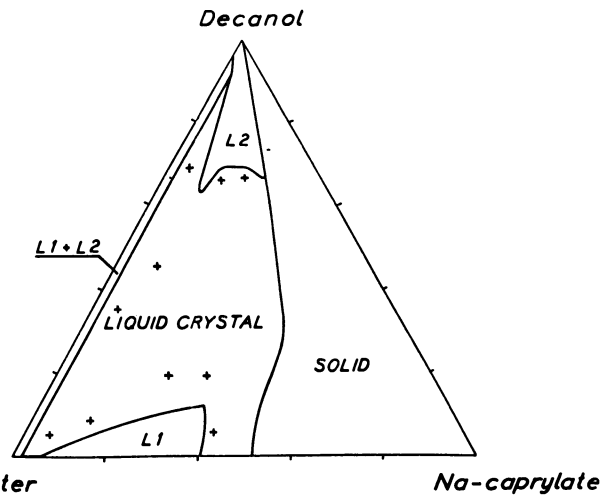

Figure 1. Triangular diagram of three-component system sodium caprylate–decanol–water at 20°C.

L_1. Homogeneous, isotropic solutions in water
L_2. Homogeneous, isotropic solutions in decanol
$L_1 + L_2$. Two-phase region consisting of L_1 and L_2
"Liquid crystal" area comprises all regions where mesomorphous matter exists. Areas denoted by + contain mesomorphous matter and homogeneous isotropic solutions in equilibrium

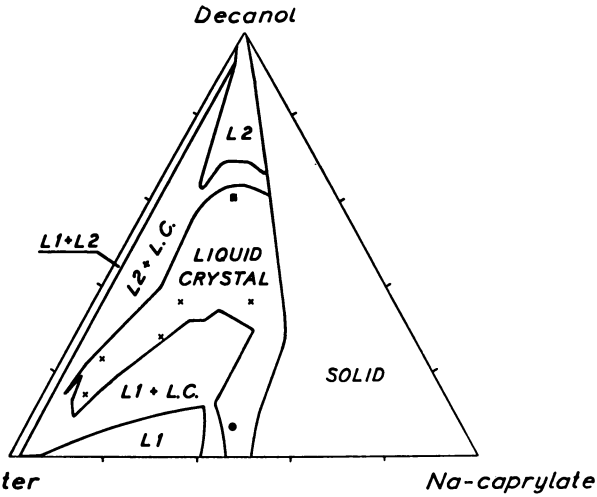

Figure 2. Triangular diagram of three-component system sodium caprylate–decanol–water at 20°C.

L_1. *Homogeneous, isotropic solutions in water*
L_2. *Homogeneous, isotropic solutions in decanol*
$L_1 + L_2$. *Two-phase region consisting of L_1 and L_2*
$L_1 + L.C.$ *Two-phase region consisting of L_1 and mesomorphous matter*
$L_2 + L.C.$ *Two-phase region consisting of L_2 and mesomorphous matter*
Liquid crystal area comprises all regions where only mesomorphous matter exists.

isotropic solutions; in L_1 water is the solvent, in L_2, decanol. L_1 extends to the water corner (as a narrow region close to the base line, just discernable on the scale of the figure.). The region $L_1 + L_2$ on the extreme left is a two-phase region where solutions L_1 and L_2 are in equilibrium. Within the large liquid crystal region there are areas with an isotropic solution L_1 or L_2, as well as the mesomorphous matter. The sites of such areas are indicated by a plus sign. In some cases the solution will ultimately separate more or less completely from the mesomorphous substance; complete separation can be effected by centrifugation. When these regions containing solution and mesomorphous matter are marked in the diagram, Figure 2 is obtained. Here, the liquid crystal area contains only concentration regions where there is mesomorphous substance but no solutions.

X-ray diffraction has shown that the inner structure of the mesomorphous matter varies from one part of the liquid crystal area to another (*5*, *6*, *10*). The over-all picture of the x-ray diffraction pinhole patterns provided by the substance in this area is the following (*10*): all the patterns show a diffuse, weak, water reflection with a value of 1/3.2 A.$^{-1}$ for S and another reflection with a value of 1/4.5 A.$^{-1}$. The fact that the latter reflection is identical in position and shape to that for liquid paraffin chain

Publication Date: January 1, 1967 | doi: 10.1021/ba-1967-0063.ch009

hydrocarbons indicates that the paraffin chains of the amphiphilic compounds in the mesomorphous substance are in a more or less liquid state. In addition to these reflections there is in the "low angle" region—that is, at angles below 10°—a series of sharp lines, which are as distinct as if they were given by a truly crystalline substance. These low angle patterns, however, differ from one part of the liquid crystal region to another.

Around position ● x-ray diffraction patterns designated as type E are obtained (*10*) (Figure 3). Analysis of the photograms gives the ratio between the Bragg spacings as 1: $1/\sqrt{3}$: $1/\sqrt{4}$—that is, they satisfy the

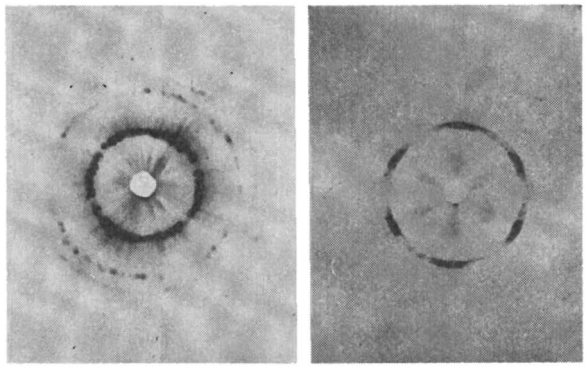

Figure 3. Low-angle x-ray diffraction patterns of a mesomorphous substance with type E hexagonal structure

Bragg spacing ratio $1:1/\sqrt{3}:1/\sqrt{4}$

criterion for a two-dimensional hexagonal arrangement. The diffraction diagram has a spotty appearance even when the sample is rotated. The spots are often arranged in a definite hexagonal pattern, and occasionally photograms were obtained with three concentric six-rings with a relative displacement of 30°. This suggests a system of hexagonally arranged parallel cylinders. The cylinders themselves are composed of amphiphilic matter—caprylate and decanol—and their core consists of hydrocarbon chains in a liquid or semiliquid state; the hydrophilic end groups are anchored to the surface of the cylinders and are in contact with the water separating the cylinders. The unit cell parameter of this hexagonal network is 30 to 35 A.

The same type of x-ray diffraction pattern is obtained in the parts of the system around position ■ (*10*) (Figure 4); this indicates that here, too, is a similar two-dimensional hexagonal arrangement. The unit cell parameter for the hexagonal network, however, is up to 47 A., a value that is inconsistent with the above model since the proportion of water is too low in relation to the amount of amphiphilic substance. It is therefore necessary to assume what may be referred to as an inverse hexagonal structure,

Publication Date: January 1, 1967 | doi: 10.1021/ba-1967-0063.ch009

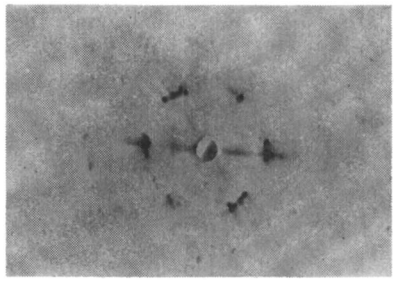

Figure 4. Low-angle x-ray diffraction pattern of a mesomorphous substance with type F hexagonal structure

Bragg spacing ratio $1:1/\sqrt{3}:1/\sqrt{4}$

with long parallel water cylinders in hexagonal arrangement, separated by a liquid or semiliquid hydrocarbon environment consisting of molecules of the amphiphiles with the hydrophilic groups facing the water. We call this structure type F.

In the middle of the system, around points × in Figure 2, a mesomorphic structure was encountered that gave x-ray diffraction patterns of a completely different kind (*10*) (Figure 5). These show up to three distinct reflections, whose Bragg spacings are in the ratio 1 : 1/2 : 1/3. Here, then, is an arrangement with linear symmetry consisting of layers of amphiphilic substance alternating with layers of water molecules. The former are obviously composed of double layers of amphiphilic molecules, arranged with the hydrophilic groups facing outward toward the water and

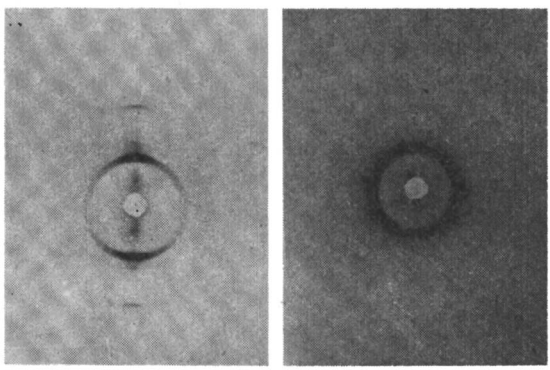

Figure 5. Low-angle x-ray diffraction patterns of mesomorphous substances with lamellar structures types D (left) and C (right)

Bragg spacing ratio $1:\frac{1}{2}:\frac{1}{3}$

Publication Date: January 1, 1967 | doi: 10.1021/ba-1967-0063.ch009

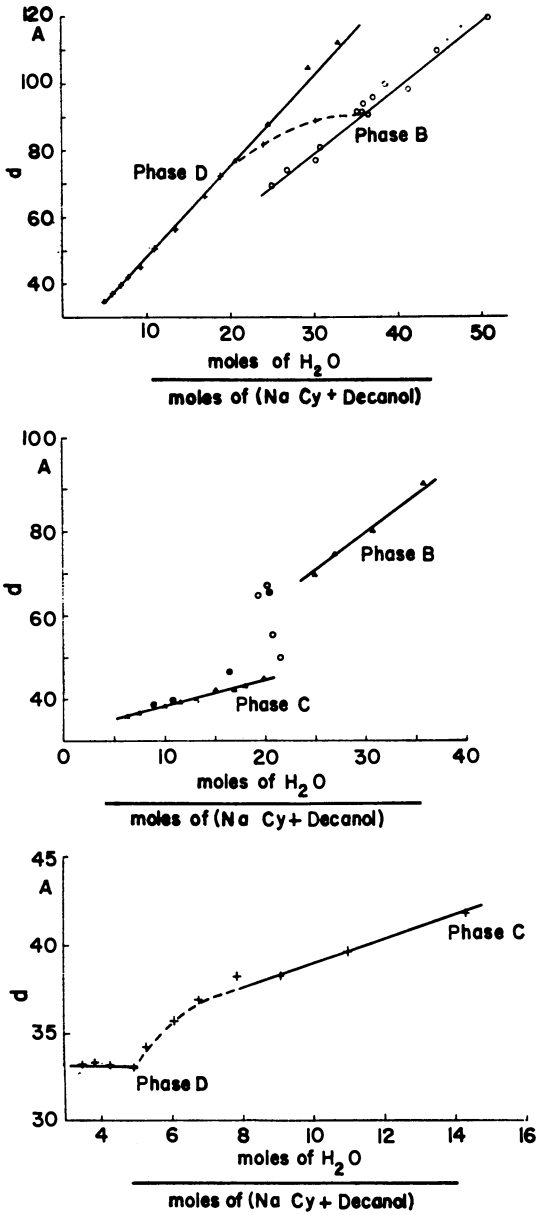

Figure 6. Dependence of Bragg spacing on water content of mesomorphous substance, sodium caprylate–decanol–water, at 20°C.

Upper. Transition from mesophase D to mesophase B. Molar ratio for decanol–sodium caprylate. Mesophase D = 2.4, mesophase B = 1.4 to 1.9

Center. Transition from mesophase C to mesophase B. Molar ratio for decanol–sodium caprylate × 1.56

Lower. Transition from mesophase D to mesophase C. Molar ratio for decanol–sodium caprylate × 1.56

the more or less parallel hydrocarbon chains inward, forming a liquid or semiliquid hydrocarbon region within the double layer. We have, however, found three distinct subtypes with linear symmetry, which differ in that their Bragg spacings vary differently with the water content of the mesomorphous substance (Figure 6) (*5*). These we call types D, C, and B. The most extensive is type D.

If all the mesomorphous matter of the liquid crystal area belonged to one phase, there would be a continuous change of the different inner structures into another. However, this was not the case, for each structure represents a distinct phase, and the areas containing homogeneous mesophases are separated from one another by two- and three-phase zones, within which the two or three phases, respectively, exist in equilibrium (*4*, *5*, *6*, *10*).

Publication Date: January 1, 1967 | doi: 10.1021/ba-1967-0063.ch009

Is There a True Equilibrium State?

To examine the phase equilibria in the system mentioned, mixtures of sodium caprylate, decanol, and water were prepared in different ways. The time to reach equilibrium was shortened by mixing, vigorous shaking, and prolonged warming. In some experiments finely powdered sodium caprylate and decanol were mixed thoroughly and allowed to stand at various temperatures before water was added, either in small portions at different intervals or all at once. The mixture was subsequently treated at different temperatures. In other experiments sodium caprylate and water were mixed and heated until a homogeneous solution was obtained or until there was no further change; decanol was then added, either in small portions at different intervals or as a single volume. In the other experiments all three components were mixed, and the reaction was promoted by thorough mixing and agitation for different periods and at a range of fairly high temperatures (100° to 180°C.). All the mixtures were mixed in glass ampoules, which were then sealed. Irrespective of the method of treatment, all the samples were cooled to room temperature with constant agitation. The period of storage was never less than 24 hours, even if equilibrium had been obtained in a shorter time, and some were stored for as long as 13 weeks. Whatever the method of preparation, the state of equilibrium obtained for each mixture was always the same (*5*, *6*).

That the systems were in true equilibrium is evident from the findings given in the following tables for samples with the same composition but different treatment.

Irrespective of the method of treatment, samples having the same composition gave the same x-ray diffraction patterns with the same Bragg spacing. They also displayed the same microscopic texture and other external properties. In the examples presented in Table I centrifugation did not result in separation into layers, nor did it disclose any difference in x-ray pattern or external properties; we therefore concluded that the samples were homogeneous from the standpoint of phase.

All the preparations in Tables II and III separated in two layers, which differed in composition, x-ray diffraction pattern, and microscopic texture.

In Ordered Fluids and Liquid Crystals; Porter, R., el al.;
Advances in Chemistry; American Chemical Society: Washington, DC, 1967.

Table I. Samples from

Sample	Initial Composition, % NaCy	H_2O	Dec.	Treatment	Storage Time at 20°C., Days
E 1	41.0	48.0	11.0	Heating to homogeneous solution (130°C.). Cooling to 20° in air by agitation (*ca.* 5°/minute)	23
E 2	41.0	48.0	11.0	Heating to homogeneous solution (130°). Cooling in stages to 20° over 5 days	81
E 3	41.0	48.0	11.0	Heating to homogeneous solution (130°). Rapid cooling in ice bath. Warming in stages to 20°, over 5 days	22
D 1	30.0	31.0	39.0	Heating to homogeneous solution (130°). Cooling to 20° in air by agitation (*ca.* 5°/minute)	21
D 2	30.0	31.0	39.0	Heating to homogeneous solution (130°). Cooling in stages to 20°, over 5 days	81
D 3	30.0	31.0	39.0	Heating to homogeneous solution (130°). Rapid cooling in ice bath. Warming in stages to 20°, over 5 days	22

Table II. Preparations

Samples with the Same Composition

	Initial Composition, %			Storage Time at 20°C.,	Centrifuge Data			Approximate % Distribution by Volume		Top Layer Composition, %		
Sample	NaCy	H_2O	Dec.	Days	Field, g	Time, hrs.	No. of layers	Top layer	Bottom layer	NaCy	H_2O	Dec.
1[a]	39.5	39.5	21.0	9	100,000	17	2	58.0	42.0	39.0	32.9	28.1
2[b]	39.5	39.5	21.0	7	100,000	16	2	57.0	43.0	38.8	32.8	28.4
3[c]	39.5	39.5	21.0	30	100,000	15	2	56.0	44.0	38.8	32.9	28.3
4[d]	39.5	39.5	21.0	6	100,000	16	2	56.0	44.0	38.9	33.0	28.1
5[e]	39.5	39.5	21.0	6	100,000	16	2	56.0	44.0	39.0	33.1	27.9

Treatment

[a] Heating to 100°C. Nonhomogeneous solution. Cooling in air by agitation (*ca.* 5°/minute)
[b] Heating to homogeneous solution (*ca.* 160°). Cooling to 20° in air by agitation (*ca.* 5°/mniute)
[c] As preparation 2

One-Phase Regions

X-Ray Diffraction Data		*Microscopic Texture*	*Centrifuge Data*		
Bragg spacing, A.	*Structure*		*Field, g*	*Time, hr.*	*Result*
32.0, 18.4, 15.9	Hexagonal type E	Type E	130,000	3	
31.5, 18.2, 15.8	Hexagonal type E	Type E	130,000	4	No separation. No change in properties
31.6, 18.5, 15.9	Hexagonal type E	Type E	130,000	3	
31.8, 16.0, 10.6	Linear type D	Type D	130,000	5	
31.8, 16.0	Linear type D	Type D	130,000	4	No separation. No change in properties
32.2, 16.0	Linear type D	Type D	130,000	6	

from a Two-Phase Region

but Different Treatment, E + D

Top Layer			*Bottom Layer*					
Microscopic texture	*X-Ray Diffraction Data*		*Composition, %*			*Microscopic texture*	*X-Ray Diffraction Data*	
	Structure	*Bragg spacing, A.*	*NaCy*	*H_2O*	*Dec.*		*Structure*	*Bragg spacing, A.*
Type D	Linear, type D	30.2, 15.0	40.7	48.0	11.3	Type E	Hexagonal, type E	32.0, 18.3, 16.0
Type D	Linear, type D		40.7	48.1	11.2	Type E	Hexagonal, type E	
Type D	Linear, type D		40.6	48.2	11.2	Type E	Hexagonal, type E	
Type D	Linear, type D		40.6	48.2	11.2	Type E	Hexagonal, type E	
Type D	Linear, type D		40.8	48.4	10.8	Type E	Hexagonal, type E	

[d] Heating to homogeneous solution (*ca.* 160°). Rapid cooling in ice bath. Warming in stages to 20° over 3 days

[e] Heating to homogeneous solution (160°). Cooling in stages to 20° over 5 days

Table III. Preparations
Samples with Same Composition

Sample	Initial Composition, % NaCy	H_2O	Dec.	Storage Time at 20°C., Days	Centrifuge Data: Field, g	Time, hr.	No. of layers	Approximate % Distribution by Volume: Top layer	Bottom layer	Top Layer Composition, %: NaCy	H_2O	Dec.
1[a]	21.0	25.0	54.0	10	20,000	17	2	49	51	17.3	20.4	62.3
2[b]	21.0	25.0	54.0	30	20,000	19	2	50	50	17.3	20.2	62.5
3[c]	21.0	25.0	54.0	40	20,000	16	2	52	48	17.3	20.4	62.3
4[d]	21.0	25.0	54.0	6	20,000	17	2	51	49	17.4	20.1	62.5
5[e]	21.0	25.0	54.0	6	20,000	17	2	51	49	17.4	20.2	62.4
6[f]	21.0	25.0	54.0	3	20,000	16	2	51	49	17.3	20.4	62.3

Treatment

[a] Heating to homogeneous solution. Cooling to 20°C. in air by agitation (*ca.* 5°/minute)
[b] As in preparation 1
[c] As in preparation 1

Table IV. Preparation
Samples with the Same Composition

Sample	Initial Composition, % NaCy	H_2O	Dec.	Storage Time at 20°C., Days	Centrifuge Data: Field g	Time, hr.	No. of layers	Top Layer Composition, %: NaCy	H_2O	Dec.	Microscopic texture
1[a]	36.0	47.2	16.8	5	100,000	17	3	36.2	34.3	29.5	Type D
2[b]	36.0	47.2	16.8	28	70,000	16	3	36.4	33.5	30.1	Type D
3[c]	36.0	47.2	16.8	6	100,000	16	3	36.1	34.2	29.7	Type D
4[d]	36.0	47.2	16.8	5	100,000	17	3	36.2	34.3	29.5	Type D

Treatment

[a] Heating to 100°C. Not homogeneous soluion. Cooling in air. by agitation (*ca.* 5°/minute)
[b] As in preparation 1

Both the top and bottom layers in a particular series had, however, the same composition, x-ray diffraction pattern, inner structure, and texture.

All the preparations in Tables IV and V separated into three layers of different composition, inner structure, and microscopic texture. The top layers of each series had the same composition and properties as the middle and bottom layers.

Publication Date: January 1, 1967 | doi: 10.1021/ba-1967-0063.ch009

from a Two-phase Region
but Different Treatment, F + D

Top Layer			*Bottom Layer*					
	X-Ray Diffraction Data						*X-Ray Diffraction Data*	
Microscopic texture	*Structure*	*Bragg spacing, A.*	*Composition, % NaCy*	*H_2O*	*Dec.*	*Microscopic texture*	*Structure*	*Bragg spacing, A.*
Type F	Hexagonal type F	30.1, 17.4, 15.1	25.1	29.4	45.5	Type D	Linear, type D	32.5, 16.3, 10.8
Type F	Hexagonal, type F		25.3	29.4	45.3	Type D	Linear, type D	
Type F	Hexagonal, type F		25.4	29.2	45.4	Type D	Linear, type D	
Type F	Hexagonal, type F		25.5	29.5	45.0	Type D	Linear, type D	
Type F	Hexagonal, type F		25.4	29.4	45.2	Type D	Linear, type D	
Type F	Hexagonal, type F		25.3	29.7	45.0	Type D	Linear, type D	

[d] Heating to homogeneous solution. Rapid cooling to 20°
[e] Heating to homogeneous solution. Rapid cooling in ice bath. Warming in stages to 20° over 3 days
[f] Heating to homogeneous solution. Cooling in stages to 20° over 3 days

from a Three-Phase Region
but Different Treatment, D + E + L1

Middle Layer					*Bottom Layer*					
X-Ray Diffraction Data						*X-Ray Diffraction Data*				
Structure	*Bragg spacing, A.*	*Composition, % NaCy*	*H_2O*	*Dec.*	*Microscopic texture*	*Structure*	*Bragg spacing, A.*	*Composition, % NaCy*	*H_2O*	*Dec.*	*Appearance*
Linear, type D	30.9, 15.5	—	51.2	—	Type E	Hexagonal, type E	33.4, 19.5, 16.7	35.5	53.2	11.3	Isotropic solution *L1*
Linear, type D		37.0	50.1	12.9	Type E	Hexagonal, type E		35.5	52.7	11.8	
Linear, type D		36.9	51.6	11.5	Type E	Hexagonal, type E		35.7	53.0	11.3	
Linear, type D		37.6	50.9	11.5	Type E	Hexagonal, type E		35.5	53.0	11.5	

[c] Heating to homogeneous solution. Rapid cooling in ice bath. Warming in stages to 20° over 3 days
[d] Heating to homogeneous solution. Cooling in stages to bath. Warming in stages to 20° over 3 days

The results, thus, seem to prove that irrespective of the mode of treatment the equilibria in the preparations are in fact true states of heterogeneous equilibrium.

The findings in Tables II to V indicate that these heterogeneous equilibria were not affected by centrifugation under the prevailing conditions.

Publication Date: January 1, 1967 | doi: 10.1021/ba-1967-0063.ch009

Table V. Preparation
Samples with the Same Composition

Sample	Initial Composition, % NaCy	H_2O	Dec.	Storage Time at 20°C., Days	Centrifuge Data: Field, g	Time, hrs.	No. of layers	Top Layer: Composition, % NaCy	H_2O	Dec.	Appearance
1[a]	10.6	32.4	57.0	28	20,000	16	3	9.5	27.1	63.4	Isotropic solution
2[b]	10.6	32.4	57.0	5	20,000	17	3	9.5	27.5	63.0	Isotropic solution
3[c]	10.6	32.4	57.0	26	20,000	16	3	9.5	27.6	62.9	Isotropic solution
4[d]	10.6	32.4	57.0	26	20,000	16	3	9.4	27.1	63.5	Isotropic solution

Treatment

[a] Heating to homogeneous solution (100°C.). Cooling to 20° in air by agitation (*ca.* 5°/minute)
[b] As in preparation 1

Table VI. Preparation from
Preparation Was Divided in
Layers Were Mixed

Initial Composition, % NaCy	H_2O	Dec.	Sample No.	Centrifuge Data[c]: No. of runs	Time, hrs.	No. of layers	% Distribution by Volume: Top layer	Bottom layer	Composition, % NaCy	H_2O	Dec.
39.5	39.5	21.0	I	1	16	2	57.9	42.1	39.0	32.7	28.3
			II	2	16 + 16	2	56.7	43.3	38.9	32.7	28.4
			III	3	16 + 16 +16	2	56.4	43.6	38.9	32.9	28.2

[a] Substance in top layer centrifuged again, no separation occurred.
[b] Substance in bottom layer centrifuged again, no separation occurred.

For further confirmation of this the layers were again mixed after centrifugation and recentrifuged. The results were identical (Table VI).

Since recentrifugation of the individual substances in the various layers did not result in further separation or change, these layers may be taken to represent homogeneous phases.

Thus, the various treatments of the samples resulted in true equilibrium in them, which was not disturbed by the centrifugation. (However, in some parts of the system the equilibria were influenced by the centrifugation under extreme conditions.) Separation into two or three layers by centrifugation must therefore be regarded as proof that the samples are in a state of heterogeneous equilibrium. The composition and properties of the layers give the composition and properties of the respective phases which are in equilibrium.

Publication Date: January 1, 1967 | doi: 10.1021/ba-1967-0063.ch009

from a Three-Phase Region
but Different Treatment, L2 — F — D

Middle Layer						*Bottom Layer*					
Composition, %			*Micro-scopic texture*	*X-Ray Diffraction Data*		*Composition, %*			*Micro-scopic texture*	*X-Ray Diffraction Data*	
NaCy	*H_2O*	*Dec.*		*Structure*	*Bragg spacing, A.*	*NaCy*	*H_2O*	*Dec.*		*Structure*	*Bragg spacing, A.*
11.0	31.4	57.6	Type F	Hexagonal, type F	40.3, 23.8, 19.8	12.7	45.9	41.4	Type D	Linear, type D	43.1, 21.4
10.9	31.4	57.7	Type F	Hexagonal, type F		12.6	45.8	41.6	Type D	Linear type D	
11.1	31.8	57.1	Type F	Hexagonal, type F		12.5	46.1	41.4	Type D	Linear, type D	
11.0 solution	31.9	57.1	Type F	Hexagonal, type F		12.7	46.3	41.0	Type D	Linear, type D	

[c] Heating to homogeneous solution (100°). Rapid cooling in ice bath. Warming in stages to 20° over 3 days
[d] Heating to homogeneous solution (100°). Cooling in stages to 20° over 3 days

a Two-Phase Region (D + E)
Three Parts, Samples I, II, and III.
and Centrifuged Again.

Top Layer[a]			*Bottom Layer*[b]				
Micro-scopic texture	*X-Ray Diffraction Data*		*Composition, %*			*Micro-scopic texture*	*X-Ray Diffraction Data*
	Structure	*Bragg spacing, A.*	*NaCy*	*H_2O*	*Dec.*		*Structure*	*Bragg spacing, A.*
Type D	Linear, type D	30.2, 15.0	40.7	48.0	11.3	Type E	Hexagonal, type E	32.0, 18.3, 16.0
Type D	Linear, type D		40.7	48.3	11.0	Type E	Hexagonal, type E	
Type D	Linear, type D		40.9	48.2	10.9	Type E	Hexagonal, type E	

[c] Field = 100,000 gauss.

Examples of Separation of Phases by Centrifugation

Two series of figures are presented to illustrate the separation of two and three phases by centrifuging the samples within the regions with heterogeneous equilibrium. The samples were taken from parts of the liquid crystal region. After complete separation by centrifugation, the centrifuge cells were photographed to illustrate the division into layers; the substance in the various layers were examined by x-ray diffraction and under the microscope.

The first series comprises samples denoted by ×, △, +, and ▽ in Figure 7.

The first sample, ×, lies in a two-phase area between solution L_1 and a region consisting of mesomorphous substance. Here, as Figure 8 shows, a division into two layers is obtained; the lower one is an isotropic solu-

Publication Date: January 1, 1967 | doi: 10.1021/ba-1967-0063.ch009

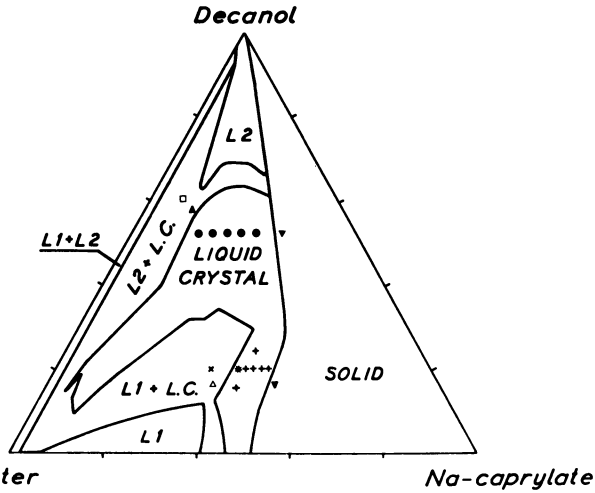

Figure 7. Triangular diagram of three-component system sodium caprylate–decanol–water at 20°C.

L_1. *Homogeneous, isotropic solutions in water*
L_2. *Homogeneous, isotropic solutions in decanol*
$L_1 + L_2$. *Two-phase region consisting of* L_1 *and* L_2
L_1 + *L.C. Two-phase region consisting of* L_1 *and mesomorphous matter*
L_2 + *L.C. Two-phase region consisting of* L_2 *and mesomorphous matter*
Liquid crystal. Area comprising all regions where only mesomorphous substances exist
×, △, ∗, +, ▽, □, ▲, ●, ▼. *Samples from two- and three-phase regions*

tion giving an x-ray diffraction pattern consisting of the diffuse band characteristic of the micellar solutions (Figure 8, b_{L_1}). The upper layer consists of a gel-like substance, with pattern indicating a type D linear structure (Figure 8, b_D).

A little to the right in Figure 7, near the border of the liquid crystal region, there is a narrow region that by centrifugation gives three layers. Within this lies sample △. In this case, too, the bottom layer consists of solution L_1, but above it (Figure 9, *a*) there are two layers with different mesomorphous substances; the upper layer gives the type D pattern (Figure 9, b_D) while the middle layer shows type E hexagonal symmetry (Figure 9, b_E). The distinct difference in microscopic texture of the substances in those layers is portrayed in Figure 9, c_D and c_E.

Slightly further to the right, within the border of the liquid crystal region a new two-phase region is entered, but here two mesophases are in equilibrium. Figure 10 relates to one of the samples, ✳. Both layers in the cell consist of a gel-like mesomorphous substance, the lower one having the type E hexagonal structure, as Figure 10, b_E, shows; the upper layer is linear, of type D (Figure 10, b_D). Their microscopic textures differ

Publication Date: January 1, 1967 | doi: 10.1021/ba-1967-0063.ch009

(Figure 10, c_E and c_D) and are of the types encountered in Figures 9, c_E and c_D. All samples denoted by + in Figure 7 gave similar separations.

Still further to the right the boundary with the two-phase region is reached, followed by a three-phase region. The sample denoted by ▽ separates into three layers, the top one of which has the type D linear structure, and the bottom the type E hexagonal structure whereas the middle layer is a fibrous substance, which is extremely difficult to separate com-

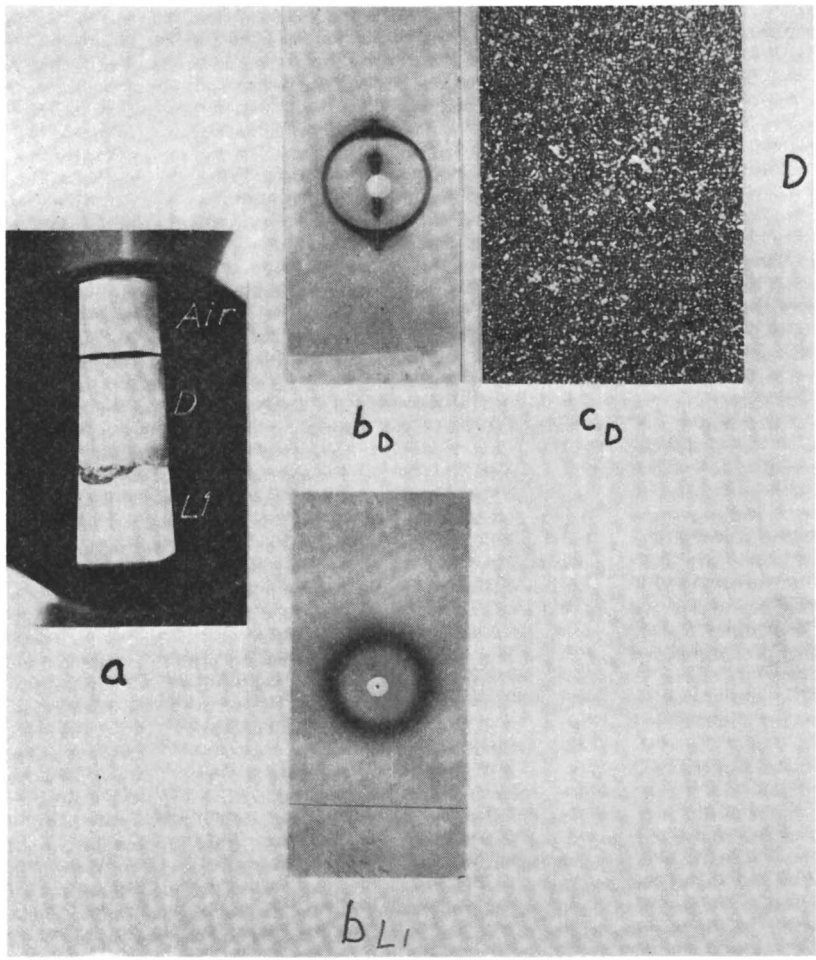

Figure 8. Separation of sample (× in Figure 7) in ultracentrifuge

a. Cell after centrifugation. Top, mesophase D; bottom, solution L_1

b. Low-angle diffraction patterns of substances comprising two layers

c. Microscopic texture of mesomorphous substance comprising upper layer

Publication Date: January 1, 1967 | doi: 10.1021/ba-1967-0063.ch009

pletely from the mesophase E. The microscopic texture of the fibrous substance is shown in Figure 11.

The above-mentioned two-phase area within the liquid crystal region is fairly large and bordered on both sides by three-phase regions, and above

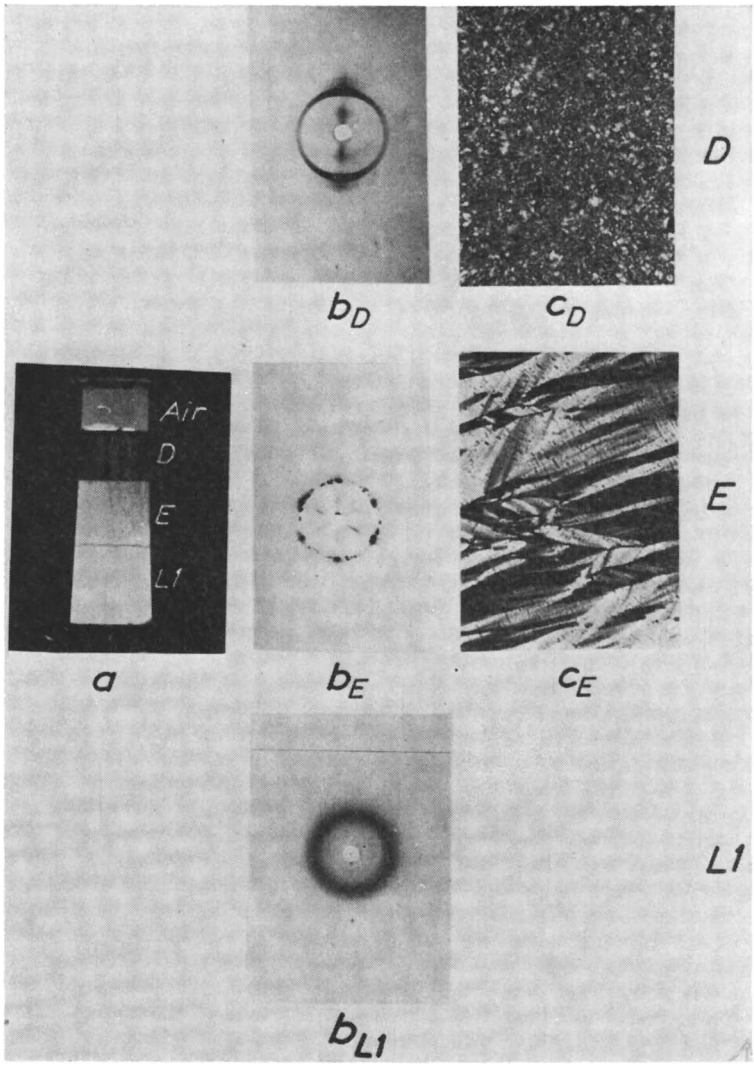

Figure 9. Separation of sample (△ in Figure 7) in ultracentrifuge

a. Cell after centrifugation. Top, mesophase D; middle, mesophase E; bottom, solution L_1
b. Low-angle diffraction patterns of substances comprising three layers
c. Microscopic texture of mesomorphous substances in middle and upper layers

Publication Date: January 1, 1967 | doi: 10.1021/ba-1967-0063.ch009

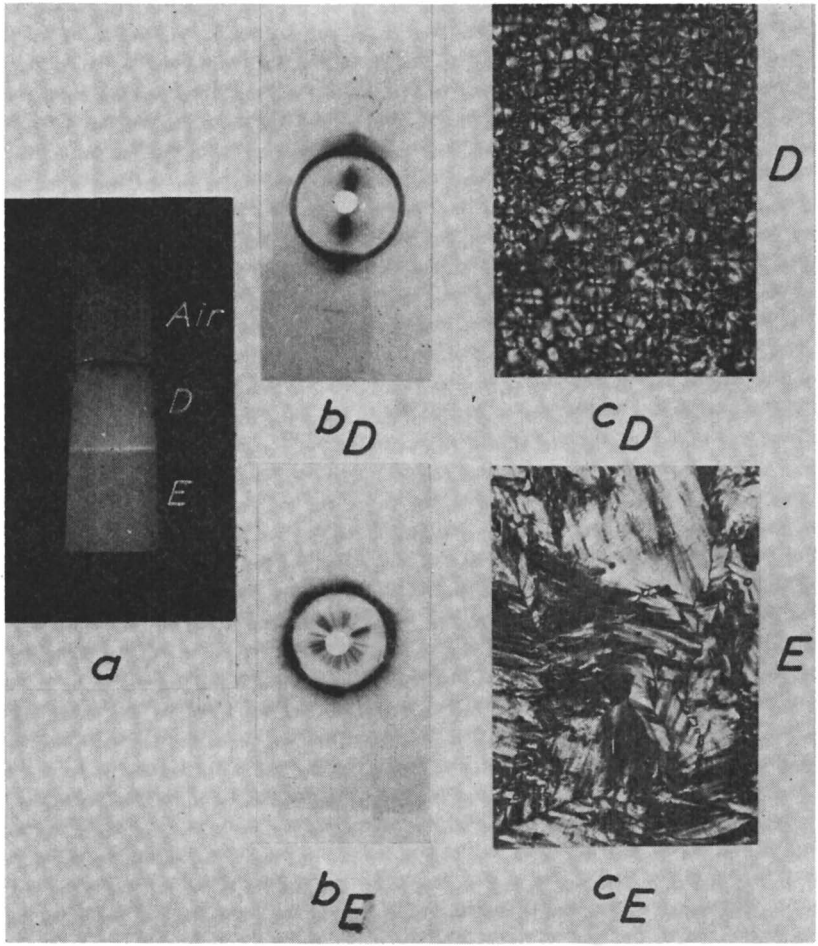

Figure 10. Separation of sample (✳ in Figure 7) in ultracentrifuge
a. Cell after centrifugation. Top, mesophase D; middle, mesophase E
b. Low-angle diffraction pattern of substances comprising two layers
c. Microscopic texture of mesomorphous substances in two layers

and below by regions where no separation is achieved by centrifugation; the upper is the homogeneous mesophase with the type D layered structure, the lower is a homogeneous mesophase having the type E hexagonal structure.

In the second series the samples are denoted by □, ▲, ●, and ▼ (Figure 7).

Sample □ separates into two layers, the upper consisting of a homogeneous solution, L_2, and the lower of mesomorphous substance with the type D layered structure (Figure 12, *a*, b_{L_2}, b_D, and c_D).

Publication Date: January 1, 1967 | doi: 10.1021/ba-1967-0063.ch009

In Ordered Fluids and Liquid Crystals; Porter, R., el al.;
Advances in Chemistry; American Chemical Society: Washington, DC, 1967.

Sample ▲ separates into three layers (Figure 13, *a*), the top one consisting of solution L_2 (Figure 13, b_{L_2}), and the two others of a mesomorphous substance, the bottom layer having a layered D structure (Figure 13, b_D, c_D) and the middle layer the type F hexagonal structure (Figure 13, b_F and c_F).

Figure 11. Microscopic texture of fibrous substance in middle layer (▽ in Figure 7)

Samples ● separate into two layers, both consisting of mesomorphous substance (Figure 14, *a*); that of the bottom one has the type D layered structure (Figure 14, b_D and c_D), and the upper one is the type F hexagonal structure (Figures 14, b_F and c_F).

This two-phase area is bordered on the right by a three-phase region where centrifugation causes separation into three layers (Sample ▼): the top one, type F hexagonal (Figure 15, c_F), and bottom one, type D linear (Figure 15, c_D) while the middle layer consists of a fibrous substance (Figure 15, c_G). The two-phase area within the liquid crystal region is thus situated between two homogeneous mesophase regions; below it there is a region with the type D layered mesophase and above, a region with type F hexagonal structure.

Phase Equilibria in Sodium Caprylate-Decanol-Water System

By centrifugation, in which the composition of the separated layers was analyzed, the boundaries were determined for the concentration areas where there was no separation, which must therefore be considered as homogeneous one-phase regions. The results of these experiments have been summarized in a triangular diagram for the sodium caprylate–decanol–water system at 20°C. (Figure 16) (*5*, *6*). The black areas denote homogeneous mesophase areas. Five such areas were found, denoted by B to F, according to the structure of the substance of which they are composed. These regions do not pass continuously into each other but are separated

Publication Date: January 1, 1967 | doi: 10.1021/ba-1967-0063.ch009

by heterogeneous areas where two or three phases, each with its own structure, exist side by side in equilibrium.

The positions of the two- and three-phase areas in the diagram comply with the phase rule. From the data in Table VII it is evident that the distribution of the substance of a two-phase region between two layers obeys the phase rule quantitatively. The three samples with different composition considered in Table VII lie on the same tie line in the two-phase area between mesophases D and E. According to the phase rule centrifugation of such samples should distinguish two layers: all the upper and lower ones, respectively, having the same composition; the ratio be-

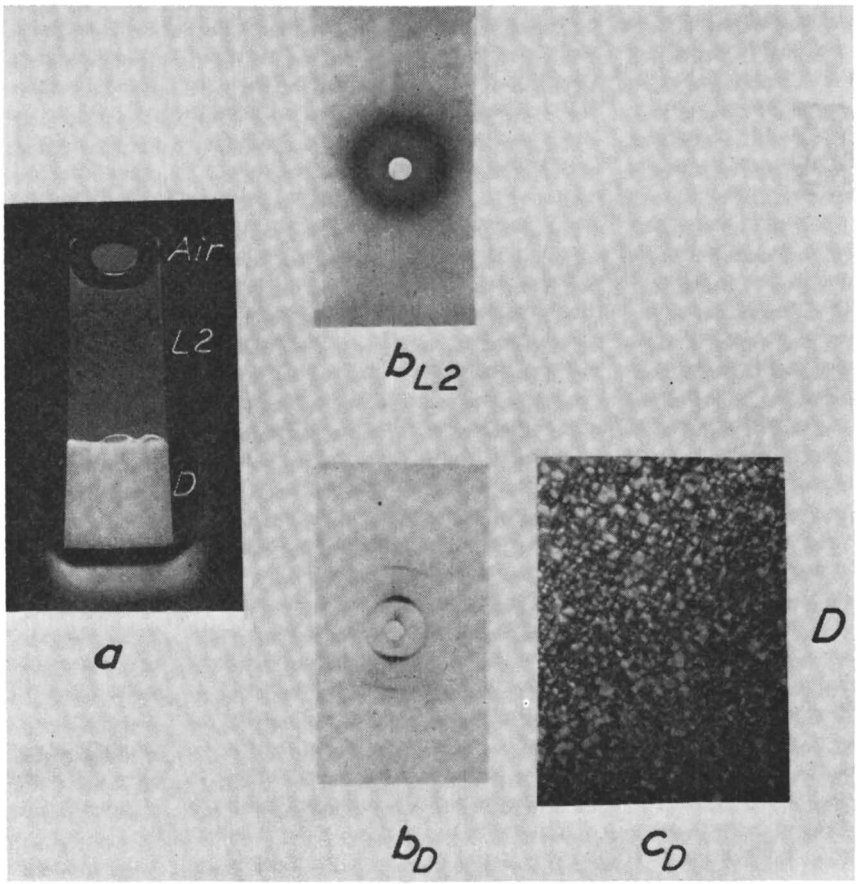

Figure 12. Separation of sample (□ in Figure 7) in ultracentrifuge

a. Cell after centrifuging. Top, solution L_2; bottom, mesophase D
b. Low-angle x-ray diffraction patterns of substance comprising two layers
c. Microscopic texture of mesomorphous substance comprising bottom layer

Publication Date: January 1, 1967 | doi: 10.1021/ba-1967-0063.ch009

Publication Date: January 1, 1967 | doi: 10.1021/ba-1967-0063.ch009

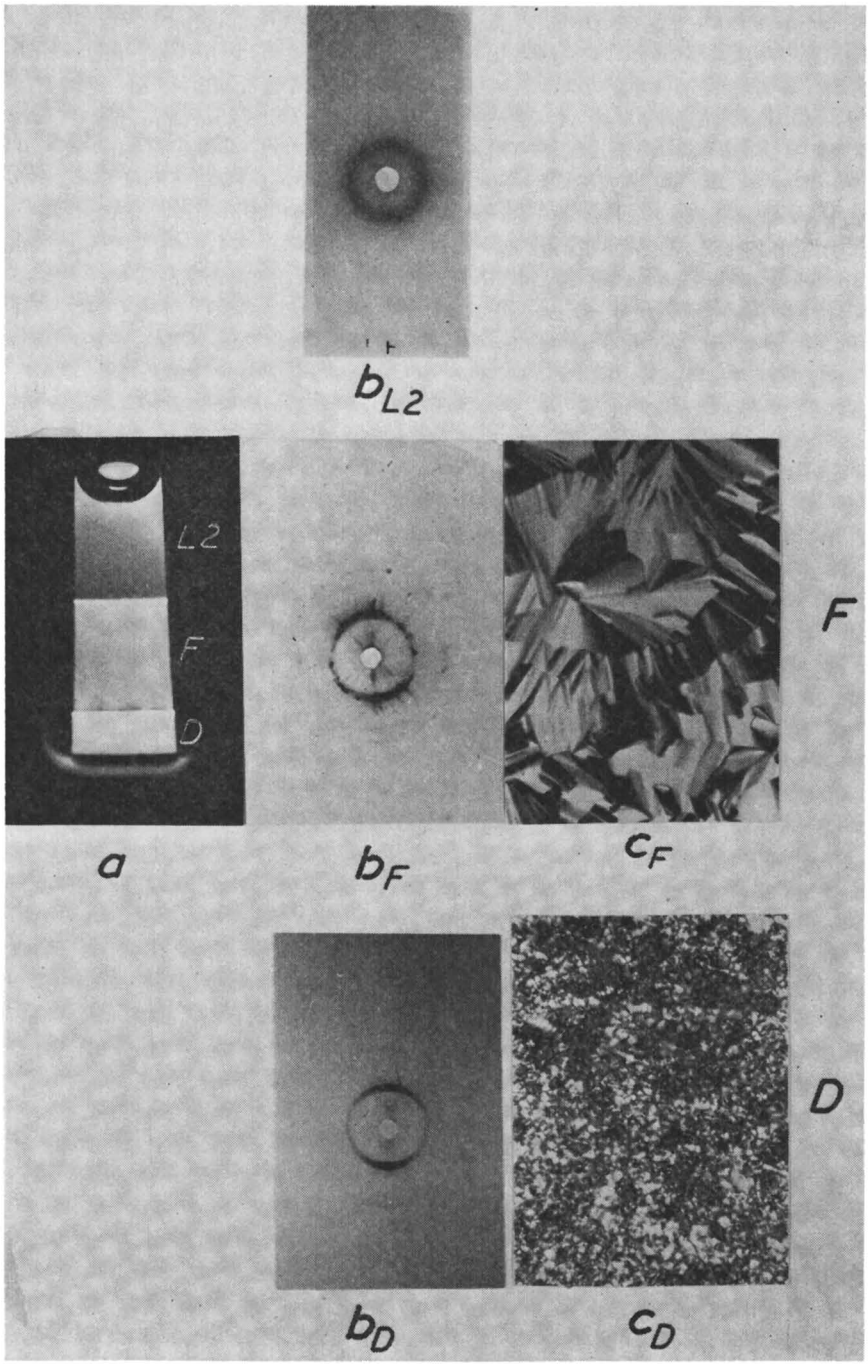

In Ordered Fluids and Liquid Crystals; Porter, R., el al.;
Advances in Chemistry; American Chemical Society: Washington, DC, 1967.

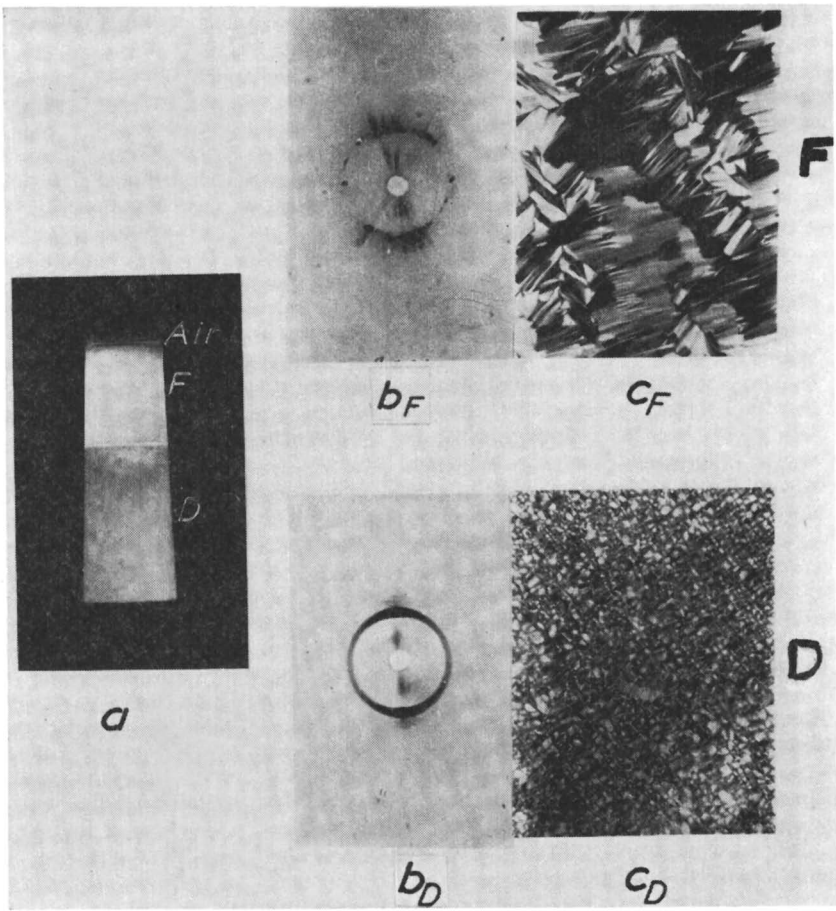

Figure 14. Separation of samples (● in Figure 7) in ultracentrifuge

a. Cell after centrifuging. Top, mesophase F; bottom, mesophase D
b. Low-angle x-ray diffraction patterns of substances comprising two layers
c. Microscopic texture of mesomorphous substances comprising two layers

---

← *Figure 13. Separation of sample (▲ in Figure 7) in ultracentrifuge*

a. Cell after centrifuging. Top, solution L_2; middle, mesophase F; bottom, mesophase D
b. Low-angle x-ray diffraction patterns of substances comprising three layers
c. Microscopic texture of mesomorphous substance comprising middle and bottom layers

Publication Date: January 1, 1967 | doi: 10.1021/ba-1967-0063.ch009

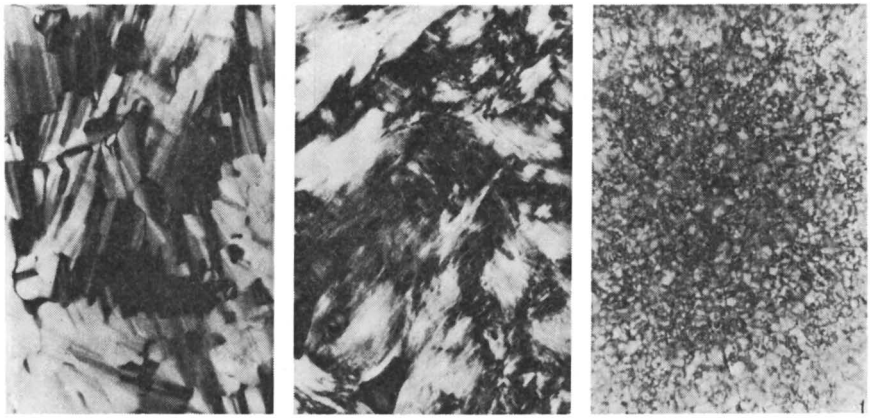

Figure 15. Separation of sample (▼ in Figure 7)
Microscopic texture of mesomorphous substances comprising three layers
Left. C_F Center. C_G Right. C_D

tween the amounts of the layers, however, should vary according to the composition of the samples and their position on the tie line.

The distribution in the three cases is shown in Figure 17.

The composition of the respective layers was the same in the three cases within ±1%, and the distribution was in agreement with the calculated values within ±2%.

Characteristic Findings on Structure of Mesophases

Thorough examination of the substance in the various homogeneous mesophase regions revealed that the inner structure of the substance within a given region is the same throughout the region but varies from one area to another. Figure 18 represents diagrammatically the structure of mesophases D, E, and F, and shows their location in the system (*4*, *20*, *21*).

Although throughout the region of existence of a phase the structure remains unchanged, there is a large variation in the interplanar distance and other characteristic quantities (outlined below). The following notation is used:

d , Bragg spacing
d_a , thickness of the amphiphilic layer
d_o , apparent thickness of the amphiphilic layer for the two- or three-dimensional swelling
d_w, thickness of the water layer
d_p , the unit cell parameter of the hexagonal array
d_c , diameter of the cylinders filled with amphiphilic matter or water
d_r , the shortest distance between the surfaces of the cylinders
S , area per hydrophilic group in the layer of hydrophilic groups

The variation in the regions of the two hexagonal mesophases is shown in Figure 19.

In phase E the side length of the hexagonal network, d_p, is constant in the decanol-free phase, but in the presence of decanol it increases steadily from 30 to about 35 A. with the concentration of amphiphilic substance. The same applies to the diameter of the amphiphilic cylinders, d_c, which increased from 21 to 27 A. The area per hydrophilic group in the cylinder surface, S, diminishes slowly from 49 to about 40 A. The shortest distance between the cylinder surfaces, d_r—that is, the thickness of the water layer between them—was almost constant at 8 to 10 A.

In phase F, the side length of the hexagonal network, d_p, shortens from 47 to 31 A. as the water content decreases. In the same way the diameter

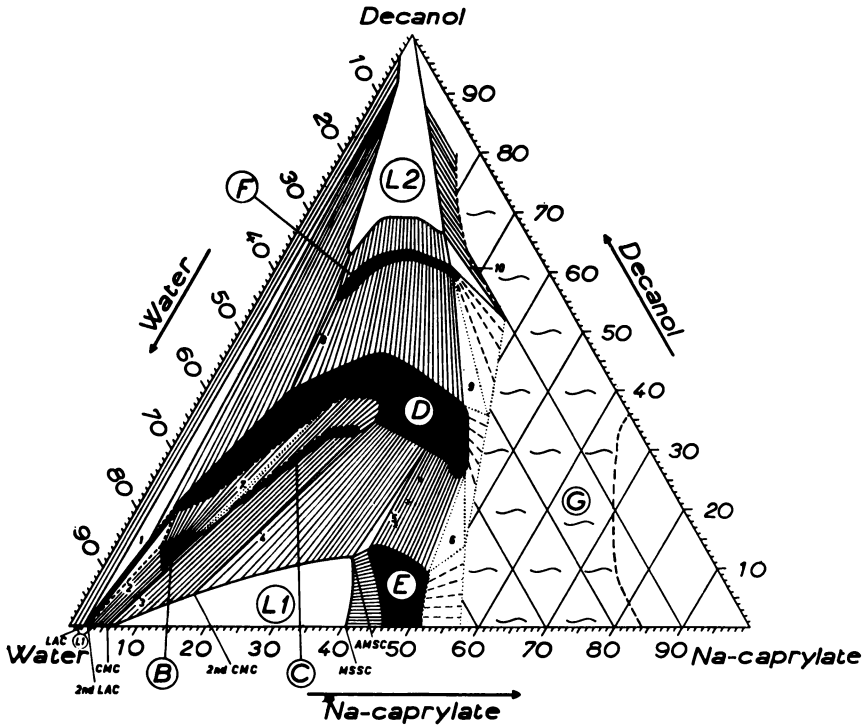

Figure 16. Phase equilibria in three-component system sodium caprylate–decanol–water at 20°C.

Concentrations expressed as percentage by weight (5, 6)
L_1. Homogeneous, isotropic solutions in water
L_2. Homogeneous, isotropic solutions in decanol
B to F. Homogeneous, mesomorphous phases
1 to 10. Three-phase triangles
Tie lines of two-phase regions represented by straight lines.
Area G consists of solid crystalline sodium caprylate and a hydrated substance. Three points marked X in two-phase region between areas with mesophases E and D show positions of samples reported in Table VII and Figure 17.

Table VII. Distribution of Same Tie Line in the

Initial Composition, %			Separation in Preparative Rotor								
			Centrifuge Data			Composition, %					
						Top Layer (Type D)			Bottom Layer (Type E)		
NaCy	H_2O	Dec.	Field, g.	Time, hrs.	No. of layers	NaCy	H_2O	Dec.	NaCy	H_2O	Dec.
38.7	36.0	25.3	100,000	25	2	38.4	32.5	29.1	40.7	47.7	11.6
38.8	39.8	21.4	100,000	25	2	38.2	32.6	29.2	40.0	47.6	12.4
39.4	43.3	17.3	100,000	25	2	38.9	32.5	28.6	40.7	47.6	11.7
					Mean	38.5	32.5	29.0	40.5	47.6	11.9

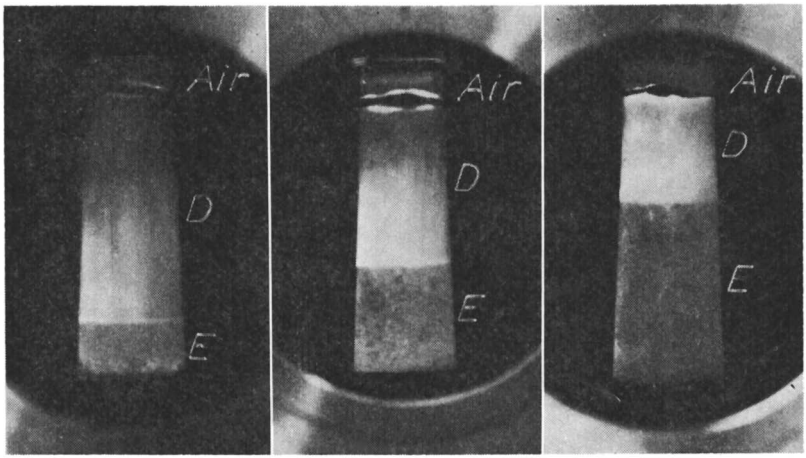

Figure 17. Distribution of phases in three two-phase preparations on same tie line

See Table VII and Figure 16

of the water cylinders, d_c, decreases from 28 to 12 A. while the area per hydrophilic group, S, if all groups are supposed to lie in the surface of the water cylinder, is between 19 and 14 A. The shortest distance between adjacent water cylinders, d_r, the thickness of the interjacent amphiphilic layer, is constant, at about 19 A.

Particular importance should be given to the great difference in packing density in the layers of hydrophilic groups of the two hexagonal mesophases—i.e., the area per hydrophilic group—namely, 40 to 50 A.^{2} for phase E and only about 18 A.^{2} for phase F.

In spite of the extremely wide variation in composition of lamellar mesophase D, a curve could be drawn through all the values of the various characteristic quantities (Figure 20). The change in the interplanar distance with volume fraction of amphiphilic substance, V_{amph}, varied in phase D in a way consistent with a "one-dimensional swelling," where the water is inserted between coherent double layers of amphiphilic substance. The variation in the thickness of the amphiphilic layer, d_a, is small; it increases slowly with the decanol content from 22 to 24 A. The area per hydro-

Publication Date: January 1, 1967 | doi: 10.1021/ba-1967-0063.ch009

Different Phases in Samples Situated on Two-Phase Region D — E

Centrifuge Data			*Separation in Analytical Rotor Percentage Distribution*			
			Found		*Calculated*	
Field, g.	*Time, hrs.*	*No. of layers*	*Top layer*	*Bottom layer*	*Top layer*	*Bottom layer*
130,000	19	2	81.1	18.9	79.2	20.8
130,000	16	2	56.5	43.5	56.0	44.0
130,000	23	2	31.7	68.3	32.3	67.7

philic group in the surface of the double layer, S, is also almost constant, diminishing slowly from about 25 to 24 A.[2] The thickness of the layers of water molecules, d_w, between the amphiphilic double layers varies widely, however, from 7 A. for the parts of the mesophase with the lowest water content to about 80 A. for the parts with most water. So long as the molar ratio between the decanol and sodium caprylate is low, the thickness of the water layer increases extremely slowly, but as the ratio rises, the thickness increases more rapidly. To be independent of the changes in the molar volume of the amphiphilic substance, the values for the thickness of the water layer were plotted against the volume ratio of water to amphiphilic substance. The values of d_w then collect about a curve that for low water

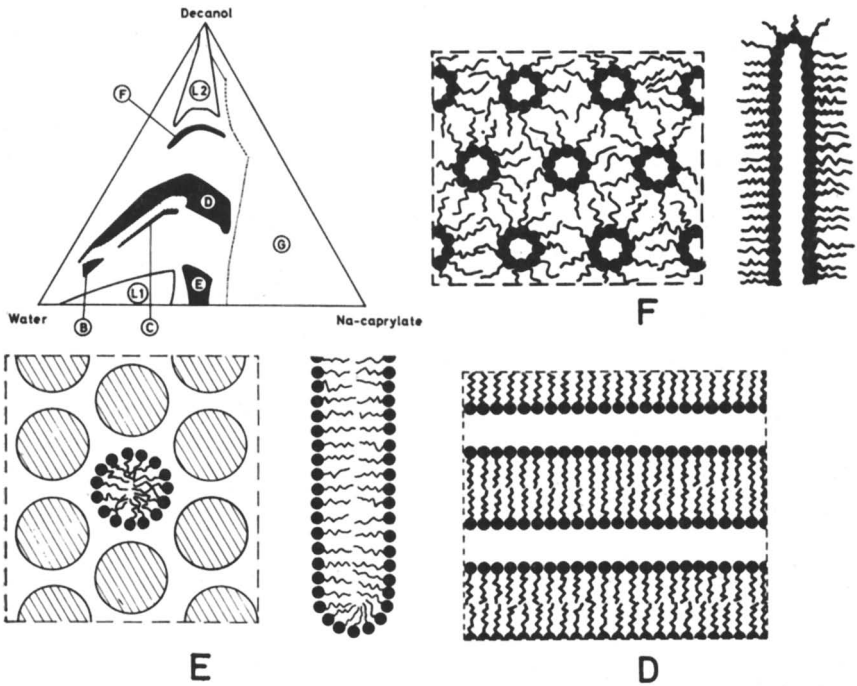

Figure 18. Schematic picture of mesomorphous structures in phases E, D, and F in three-component system sodium caprylate–decanol–water (4, 20, 21)

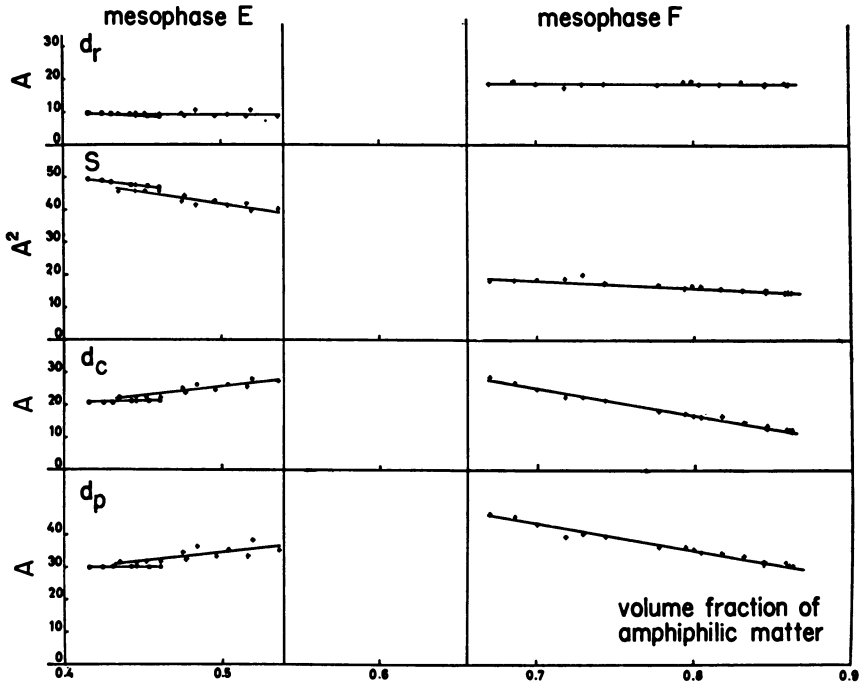

Figure 19. Quantities characteristic of structure of hexagonal mesophases E and F

○. *Decanol-free mesophase*
+. *Mesophase containing decanol*
System NaCy–decanol–H_2O

content is almost linear but slowly turns upwards from a volume ratio of unity between water and amphiphilic substance.

In the uppermost curve of Figure 20 an attempt was made to illustrate the remarkable capacity of mesophase D in one part of the region of its existence for taking up large amounts of water without destroying the structure. The curve was drawn for the maximum water content that the phase could incorporate against the area per carboxylate group in the surfaces of the double layers—i.e., against the density of the ionizable groups in these surfaces. The capacity for taking up water remains low until this area exceeds about 75 A.^{2} per ionizable group, at which point the total water content is low; as far as the sudden rise of the curve there are still only 6 molecules of water per hydrophilic group—i.e., the maximum number that can be bound on the assumption that each alcohol group does not bind more than 3 and each sodium carboxylate group not more than 11. Up to this point all the water is thus probably firmly bound to the amphiphilic substance; above this point free water must be obtained. This change in the water binding and in the maximum uptake of water occurs when the decanol content of the amphiphilic layer exceeds about 2 moles

Publication Date: January 1, 1967 | doi: 10.1021/ba-1967-0063.ch009

of decanol per mole of sodium caprylate. It is obviously this weaker binding of the water that is manifested in the slightly more rapid increase per water molecule in the Bragg spacing and the thickness of the water layer at higher water contents.

Throughout its region of existence mesophase B has a high water content between 72 and 82%. For this mesophase, too, the x-ray examination disclosed a layered structure. The interplanar distance increases slightly more slowly than in phase D, but it is still rapid enough to justify the assumption of a coherent amphiphilic layer. The thickness of this layer is 20 to 22 A. (Figure 21, d_a), and the area per hydrophilic group, S, lies between 29 and 26 A.^{2}. The thickness of the water layer, d_w, increases

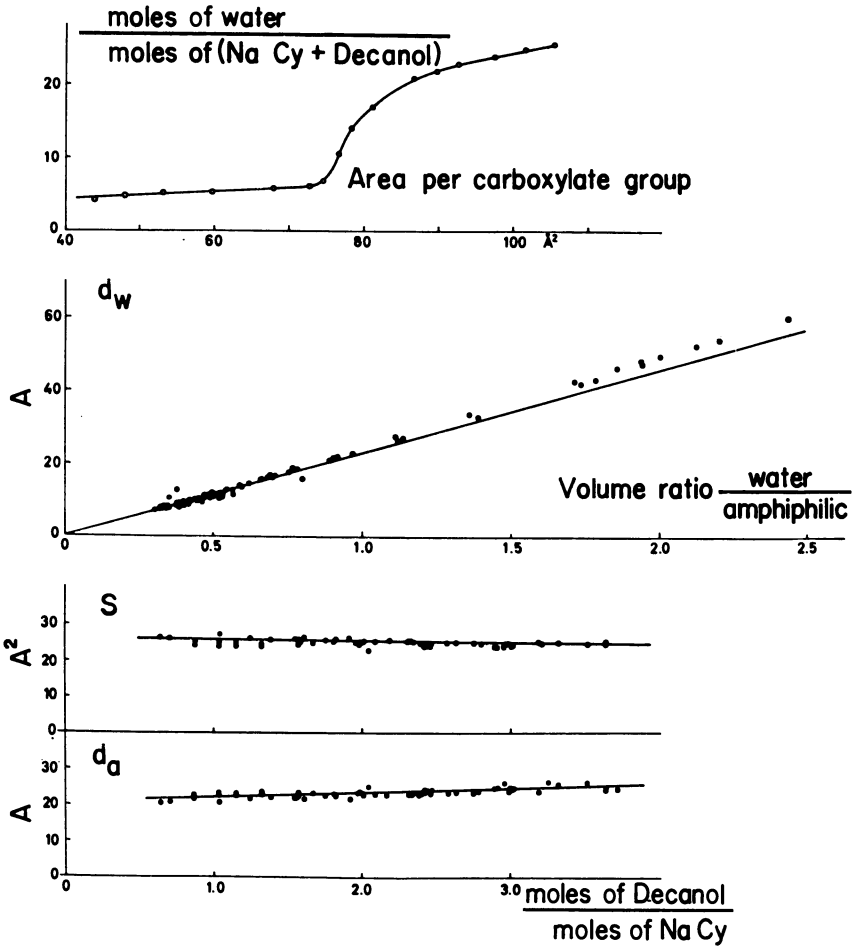

Figure 20. Quantities characteristic of structure of linear mesophase D
System NaCy–decanol–H_2O

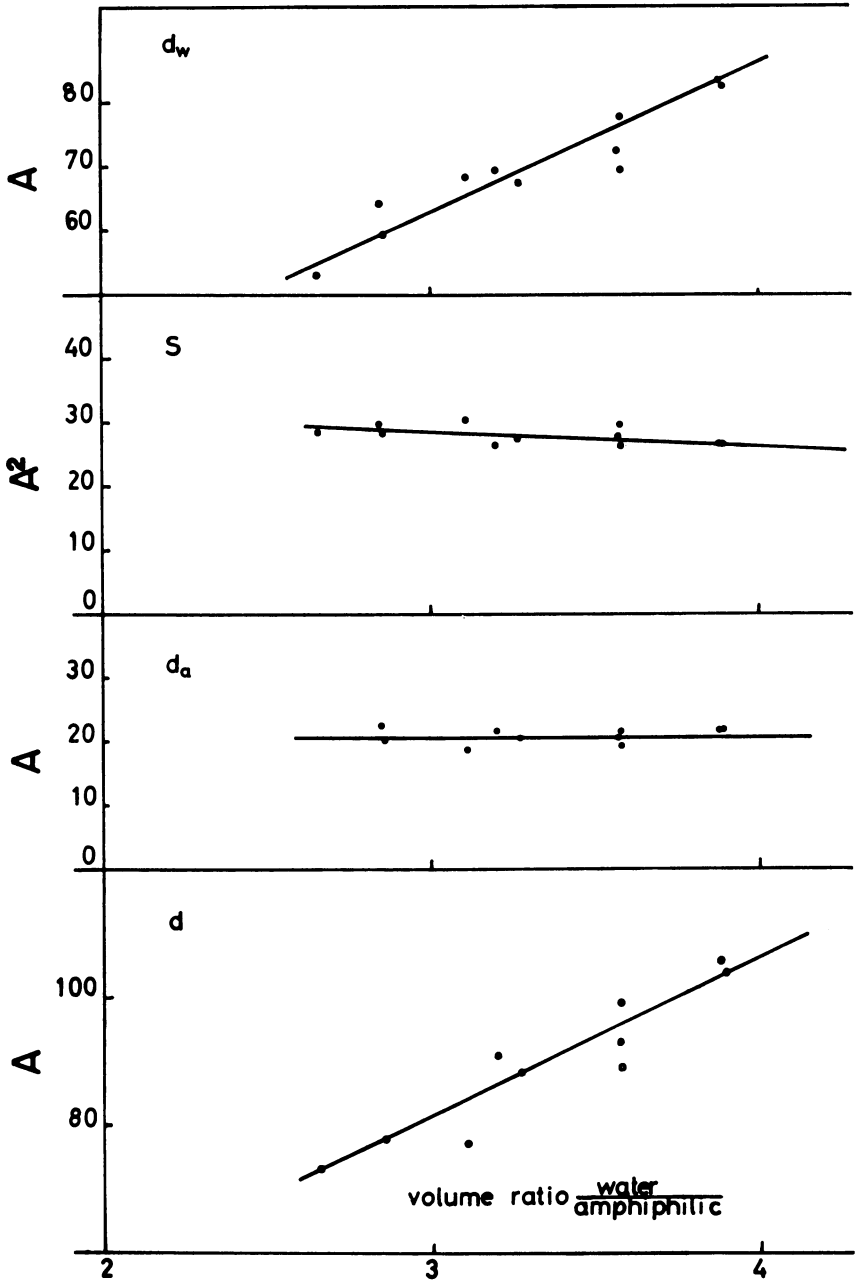

Figure 21. Quantities characteristic of structure of the linear mesophase B

System NaCy–decanol–H_2O

with the water content from about 53 to 84 A. This mesophase differs from the other mesophases by virtue of its sparser packing and thinner layer of amphiphilic substance.

In mesophase C with its linear symmetry the conditions are to some extent similar to those in phase D, but they present well defined differences. If it is assumed that, as in the two other linear phases, there is a coherent double layer of amphiphilic molecules, this will result in a decrease in the layer thickness and in a rapid increase in the area per hydrophilic group when the water content of the phase rises. In addition, the interplanar distance increases with the water content only one half as rapidly as in the D phase. This indicates a difference in the arrangement of

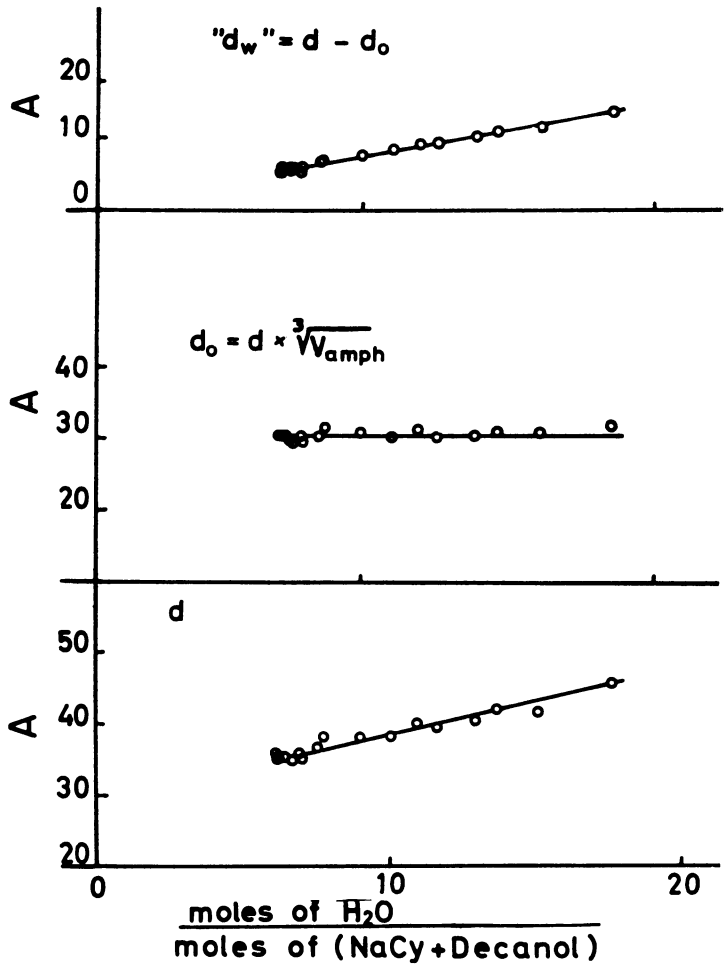

Figure 22. Quantities characteristic of structure of linear mesophase C NaCy–decanol–H_2O System

the water between double layers in mesophases C and D. An analysis of the conditions shows that the increase in the interplanar distance fits an expression of the type $d = d_o/(V_{amph})^{\frac{1}{3}}$ or $d = d_o/(V_{amph})^{\frac{1}{2}}$. In other words, in phase C there is a two- or three-dimensional swelling. In this phase the amphiphilic double layer is presumably divided into lamellae or particles arranged as a layered structure. As Figure 22 shows, there is an increase in interplanar distance with water content from 35.5 to about 45 A. The product of the interplanar distance and $(V_{amph})^{\frac{1}{3}}$ gives a constant value of d_o = 30 A. The value for the apparent thickness of the water layer, d_w, rises from about 5 to 15. (In the two-dimensional case the corresponding product is about 27 A., and d_w rises from 8 to 18 A.) It is notable that the mesophase C has an extremely limited region of existence linked with an extremely small variation in the molar ratio between decanol and sodium caprylate (about 1.55).

Existence of Different Mesophases in Other Ternary Systems

Similar conditions, with two or more different mesophases, were encountered in several other ternary systems. Special attention was devoted to ascertaining whether there was coexistence between hexagonal mesophase type E, linear type D, and their interjacent two-phase region.

In the sodium caprylate–alcohol–water system the length of the alcohol chain was systematically varied from decanol down to ethanol, and in all the systems mesophases D and E with an intervening two-phase area were found (*21*). The same applies to the systems with potassium soaps; it was notably the case also for the system potassium caprate–octanol–water (Figure 23), which has been described as containing only a single mesophase (*1*, *2*, *3*).

Hexagonal mesophase F has hitherto been found in the decanol and nonanol systems (*21*). Linear mesophases C and B appear to occur as far down as the hexanol system (*21*).

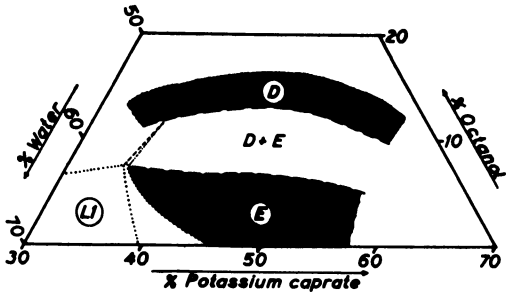

Figure 23. Part of triangular diagram of system potassium caprate–octanol–water at 20°C. showing existence of mesophases E with hexagonal structure and mesophase D with linear structure, separated by two-phase region

Mesophases E and D, separated by a two-phase region, were found also in the cetyl trimethylammonium bromide–hexanol–water system (Figure 24), where there is considered to be a continuous transition throughout the liquid crystal region with no intervening phase boundaries and two-phase areas (*13*). The mesophases mentioned also appear in the sodium caprylate–caprylic aldehyde–water, sodium caprylate–caprylic acid methyl ester–water, and sodium caprylate–caprylic acid–water systems (*19*, *20*, *21*). In the last of these, mesophases F, C, and B were also found.

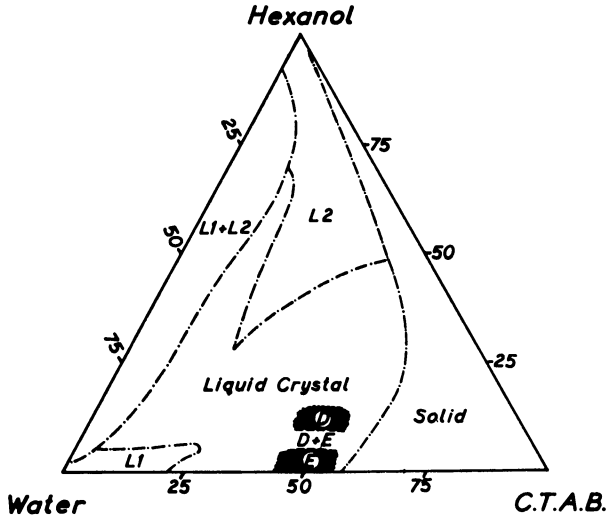

Figure 24. Triangular diagram of system cetyl trimethylammonium bromide–hexanol–water at 25°C.

Boundaries marked ____ . ____ . ____ between L_1, L_2, $L_1 + L_2$ and liquid crystal regions drawn in accordance with determinations by Lawrence at 27.5°C. (13). In our experience the last region contains mesophase E with hexagonal structure and mesophase D with linear structure separated by a two-phase region.

In ternary systems, too, where the anion- and cation-active association colloids are replaced by a non-ion-active colloid of the polyoxyethylene type, similar conditions were found, with different mesophases separated by two-phase and three-phase regions. For instance, in the alkylpolyoxyethylene–oleic acid–water system all five of known mesophases E, D, F, C, and B, are found as well as two extremely stiff, completely transparent gels, which are optically isotropic (*19*, *21*). Their x-ray patterns, which are similar but differ from the other phases on essential points, have so far resisted satisfactory interpretation. These mesophases, I_1 and I_2, occur in different parts of the system; it is obvious that one structure is the reverse of the other—thus parallel to E and F. The structure would possibly be one of spheres with the densest cubical packing.

Publication Date: January 1, 1967 | doi: 10.1021/ba-1967-0063.ch009

Mesophase I_1 occurs also, together with mesophase E, in soap systems containing hydrocarbons, such as sodium caprylate–octane–water and sodium caprylate–xylene–water (*20*).

Finally, in the sodium caprylate–cholesterol–water system mesophases E and D were accompanied by another with a distinctive character, possibly with a layered structure and separated from the others by two- and three-phase regions (*7*).

Thus, the occurrence of two or more mesophases in the ternary systems is a common phenomenon. There is a great variety in the structures of the mesophases; the number of lyotropic mesophases is large, and may be caused by variations in the superlattice formed by the molecular aggregates.

Types of Phase Diagrams

From the results of this investigation five main types of phase diagrams were constructed for ternary systems of the type described above. These are presented below in a schematic form.

Figure 25 shows the equilibria in sodium caprylate–hydrocarbon–water systems (the hydrocarbon can be octane or xylene). Here there is the one-phase system, L_1, with homogeneous aqueous solutions and mesophases E and I_1. The hydrocarbon is solubilized in the micellar aqueous L_1 solution, but the sodium caprylate is not dissolved in the hydrocarbon.

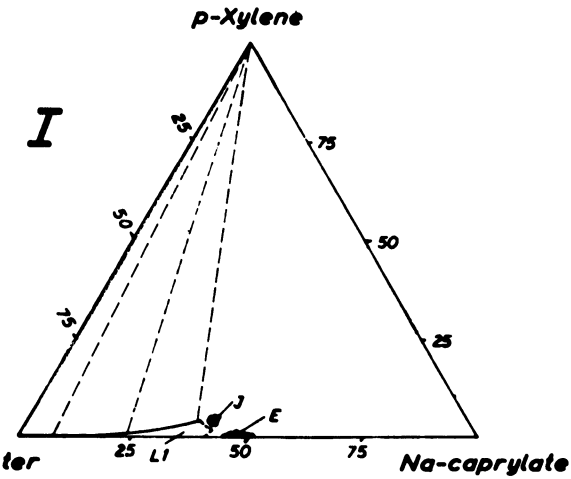

Figure 25. Triangular diagram of system sodium caprylate–p-xylene–water, 20°C.

If the hydrocarbon in such a system is replaced by a compound in whose hydrocarbon chain is substituted a group with weak hydrophilic properties, such as an aldehyde or ester group, we obtain equilibrium diagrams of a slightly different type. Figure 26 shows the phase diagram

Publication Date: January 1, 1967 | doi: 10.1021/ba-1967-0063.ch009

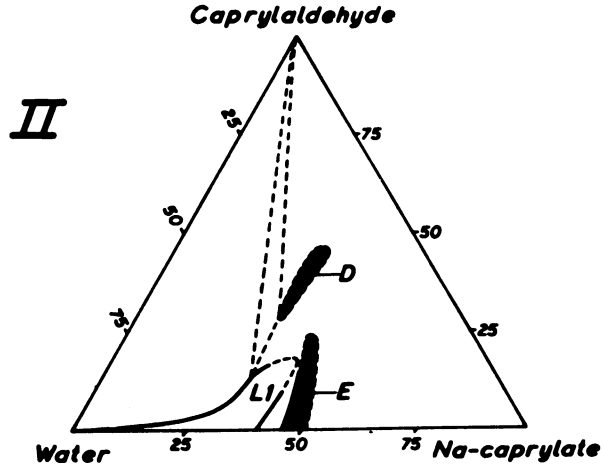

Figure 26. Triangular diagram of system sodium caprylate–caprylaldehyde–water, 20°C.

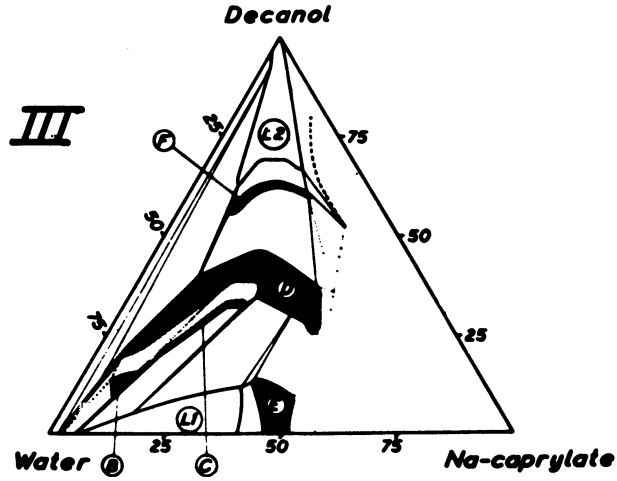

Figure 27. Triangular diagram of system sodium caprylate–decanol–water, 20°C.

for the sodium caprylate–caprylic aldehyde–water system. Here, again, are the one-phase regions, L_1, with homogeneous aqueous solutions, and E, with the hexagonal mesophase E, but toward the center of the diagram there is now also a region D with a layered structure. The lipophilic third component is solubilized to a large extent in the micellar aqueous solutions, L_1, but here too the caprylate is insoluble in the third component.

When the aldehyde group is replaced with the more hydrophilic alcohol group, we obtain the type of phase equilibrium familiar from the sodium caprylate–alcohol–water systems (Figure 27). Here the number of different mesophases can be large; according to our experience their presence

Publication Date: January 1, 1967 | doi: 10.1021/ba-1967-0063.ch009

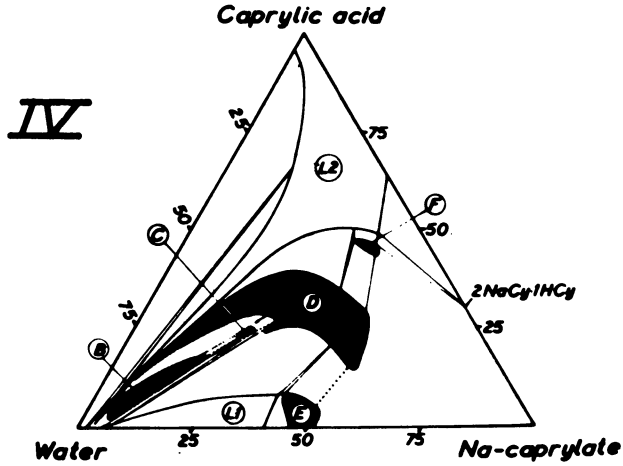

Figure 28. Triangular diagram of system sodium caprylate–caprylic acid–water, 20°C.

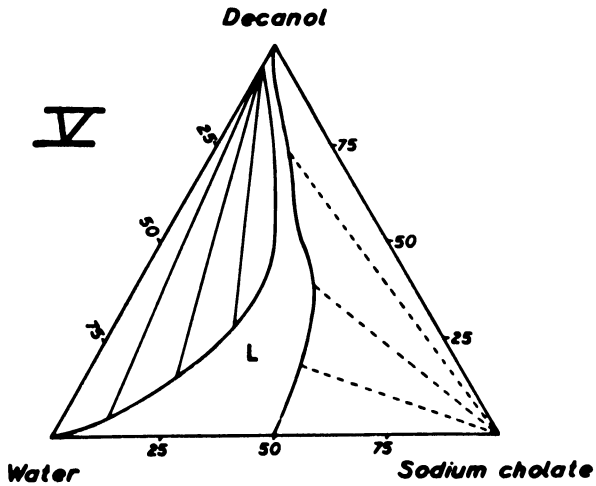

Figure 29. Triangular diagram of system sodium cholate–decanol–water, 20°C.

depends on the length of the hydrocarbon chain in the amphiphilic substance and on temperature. The most important differences, however, are that the alcohols and soaps are to some extent mutually soluble but only in the presence of a certain minimum of water; this is the case for region L_2 with homogeneous solutions, where alcohol is the solvent. The minimum amount of water required to form this solution varies with the nature of the alkali ion of the soap and seems to depend on its hydration number. The same applies to the limits for the regions of mesophases F and D in these systems.

If the alcohol in the ternary soap system is replaced by a fatty acid, yet another type is obtained. Here, as in the previous main type, there are the five mesophases B, C, D, E, and F and the two regions, L_1, and L_2, with homogeneous solutions. In this case, however, no water is needed to make soap and fatty acid mutually soluble. This is illustrated in Figure 28, which shows the phase equilibrium in the sodium caprylate–caprylic acid–water system. Here L_2 extends to the caprylate–caprylic acid axis, and in the other direction far into the water corner. This is obviously caused by the ability of the soap and fatty acid to form molecular compounds with one another—the familiar acid soaps, which can also exist in the solid crystalline form.

The fifth main type occurs in systems in which the soap component is not an association colloid of the paraffin chain type but a salt of a bile acid, with its condensed four-ring skeleton with two or three hydroxyl groups and with one carboxyl group at the end of a branched hydrocarbon chain. Figure 29 shows the phase diagram for the sodium cholate–decanol–water system (*9*). There is no mesomorphous phase but one extensive continuous area with homogeneous isotropic solutions. The cholate and decanol are mutually soluble in the presence of water, as in the case of the soap and the alcohol in the soap-alcohol systems, but here we have the remarkable phenomenon that water and decanol, which are practically insoluble in one another, become mutually soluble in all proportions in the presence of a certain quantity of a bile acid salt.

It may be confidently predicted that further research will lead to the discovery of more new types of phase equilibria in the ternary systems and will show the conditions under which these types approach and are transformed into one another.

Publication Date: January 1, 1967 | doi: 10.1021/ba-1967-0063.ch009

Literature Cited

(1) Dervichian, D. G., Proceedings of Second International Congress on Surface Activity, London, 1957, Vol. I, p. 326.
(2) Dervichian, D. G., *Discussions, Faraday Soc.* **25**, 58 (1958).
(3) Dervichian, D. G., *Kolloid-Z.* **169**, 107 (1960).
(4) Ekwall, P., *Finska Kemistsamfundets Medd.* **72**, 49 (1963).
(5) Ekwall, P., Danielsson, I., Mandell, L., *Kolloid-Z.* **169**, 113 (1960).
(6) Ekwall, P., Danielsson, I., Mandell, L., Proceedings of Third International Congress on Surface Activity, Cologne, 1960, Vol. I, p. 193.
(7) Ekwall, P., Mandell, L., *Acta Chem. Scand.* **15**, 1403 (1961).
(8) Fontell, K., *Finska Kemistsamfundets Medd.* **72**, 99 (1963).
(9) Fontell, K., "Surface Chemistry," Second Scandinavian Symposium on Surface Activity, Stockholm, 1965, p. 252, Munksgaard, Copenhagen.
(10) Fontell, K., Ekwall, P., Mandell, L., Danielsson, I., *Acta Chem. Scand.* **16**, 2294 (1962).
(11) Husson, F., Mustacchi, H., Luzzati, V., *Acta Cryst.* **13**, 668 (1960).
(12) Lawrence, A. S. C., *Discussions Faraday Soc.* **25**, 50, 64, 65, 69, 70 (1958).
(13) Lawrence, A. S. C., Pearson, J. T., Fourth International Congress on Surface Active Substances, Brussels, 1964, Preprint **B IV 132.**
(14) Luzzati, V., Mustacchi, H., Skoulios, A., *Discussions Faraday Soc.* **25**, 43 (1958).

(15) Luzzati, V., Mustacchi, H., Skoulios, A., *Nature* **180**, 600 (1957).
(16) Luzzati, V., Mustacchi, H., Skoulios, A., Husson, F., *Acta Cryst.* **13**, 660 (1960).
(17) McBain, J. W., Field, M. C., *J. Am. Chem. Soc.* **55**, 4776 (1933).
(18) McBain, J. W., Sierichs, W. C., *J. Am. Chem. Soc.* **25**, 221 (1948).
(19) Mandell, L., *Finska Kemistsamfundets Medd.* **72**, 49 (1963).
(20) Mandell, L., "Surface Chemistry," Second Scandinavian Symposium on Surface Activity, Stockholm, 1965, p. 185, Munksgaard, Copenhagen.
(21) Mandell, L., Ekwall, P., Fourth International Congress on Surface Active Substances, Brussels, 1964; Preprint **B IV/6.**
(22) Winsor, P. A., "Solvent Properties of Amphiphilic Compounds," Butterworths, London, 1954.

RECEIVED February 11, 1966.

Molecular Association in Mono- and Dihydric Alcohol and Alcohol-Water Systems

M. P. McDONALD

Sheffield College of Technology, Sheffield, England

Publication Date: January 1, 1967 | doi: 10.1021/ba-1967-0063.ch010

The results of nuclear magnetic resonance, infrared, dielectric, and viscosity measurements on pure mono- and dihydric alcohols and alcohol-water systems are discussed in terms of the information they provide on the nature and extent of molecular association in these systems. This association leads to the formation of dimeric and multimeric species in the pure liquid alcohols, an unexpectedly high solubility of water in the long-chain alcohols, and the occurrence of a liquid crystalline phase in 1,2-diol–water systems.

In the absence of other more specific interactions, hydrogen bonding leads to an aggregation of water into clusters and in liquid alcohols and diols to the formation of associated species, which are thought to include dimers, trimers, and higher multimers.

The interaction of water, the simplest hydrogen-bonding material, with some alcohols and 1,2-diols leads to the formation of solid hydrates (pentamethylethanol, pinacol) while longer chain 1,2-diols and monoglycerides form a liquid crystalline (l.c.) phase at higher temperatures. The factors governing the appearance and structure of the l.c. phase in nonionic systems are not yet fully understood, and work is going on in this laboratory on the systems themselves and their simple liquid and solid analogs in an attempt to determine these factors.

This paper discusses some of the results of nuclear magnetic resonance (NMR), infrared, dielectric, and viscosity measurements on the liquid phases of mono- and dihydric alcohols alone and with water. Finally, the monolaurin-water phase diagram is briefly described.

Liquid Alcohol Systems

Infrared measurements have been made on most simple alcohols in dilute solution in carbon tetrachloride, and it is agreed that the three prin-

In Ordered Fluids and Liquid Crystals; Porter, R., el al.;
Advances in Chemistry; American Chemical Society: Washington, DC, 1967.

cipal bands in the OH stretching frequency region denote the existence of simple monomers, dimers, and a number of more highly associated species.

Controversy has arisen over the years as to the exact interpretation of the infrared spectra in terms of the type of dimer formed. Van Thiel, Becker, and Pimentel (*29*) have shown that a cyclic dimer occurs in the solid state of methanol at low temperatures. Quantitative infrared (*18*) and NMR (*2*) measurements in dilute solutions have enabled the enthalpy of dimer formation to be calculated if certain assumptions are made. The high value of the enthalpy—9.2 kcal. per mole in the case of methanol—again suggests that cyclic dimers are formed since this is a rather high value for a single hydrogen bond.

The values of the enthalpy obtained do not depend on the model chosen for the dimer, as shown by Lussan (*19*) in a comprehensive summary of the possible theoretical treatments of the NMR data. Lussan demonstrates the form of the equilibrium constant calculation in the case of (1) monomer-dimer (open or cyclic), (2) monomer-cyclic trimer, and (3) monomer-higher acyclic multimers in the two cases of (3a) all K's equal and (3b) k_1 for monomer-dimer equilibrium unique, k's for higher multimers all equal. He then takes the experimental curves for a number of alcohols in carbon tetrachloride and achieves a reasonable fit to the data up to 0.6 mole fraction by using one or the other of the theoretical relationships. In some cases two sets of theoretical points are plotted on the same graph as the experimental data; both are a good fit in the low concentration region, up to 0.1 mole fraction. Above this concentration one or the other of the theoretical curves is much closer to the experimental curve. Lussan implies that hypothesis 3b may be a more accurate fit to the data in the more concentrated solutions. Methanol, ethanol, 2-methyl-2-propanol (*tert*-butyl alcohol) and 2,2,4-trimethyl-3-pentanol follow the curve for equilibrium 3a, while 2,2,4,4-tetramethyl-3-pentanol fits the monomer-dimer data. Lussan points out that the behavior of the latter alcohol fits in with that of two similar heavily substituted tertiary alcohols which have been found by infrared methods to form only dimers.

These theoretical treatments show, as Lussan points out, that the shape of the curves of chemical shift *vs.* concentration will not be affected by the model chosen for the dimer.

An interesting attempt to distinguish between the occurrence of open or cyclic dimers has been made by Josien *et al.* (*5*), who have carried out infrared and cryoscopic measurements at the same temperature on the same dilute solutions of a number of alcohols in Freon 112 (1,1,2,2-tetrachloro-1,2-difluoroethane). From the cryoscopic data a "mean degree of association," χ, is defined as $\chi = x/x_p$, where x is the mole fraction of the dissolved alcohol and x_p is the mole fraction of particles (monomer and multimer) indicated by the freezing point depression. The quantity χ is compared with β, where $1/\beta$ is the fraction of free OH groups from the infrared spectra,

Publication Date: January 1, 1967 | doi: 10.1021/ba-1967-0063.ch010

and Josien shows that when only open dimers are formed, the curves of χ and β *vs.* concentration should be superposable since each species then contains one free OH group.

For 2-methyl-2-propanol, 3-ethyl-3-pentanol, 3-ethyl-2,4-dimethyl-3-pentanol, and 2,2,4,4-tetramethyl-3-pentanol, the curves are superposable while for 3-methyl-3-pentanol, 2,2,4-trimethyl-3-pentanol, and 1-butanol there is an appreciable separation between the curves. As Josien points out, the formation of open dimers in 2-methyl-2-propanol is in agreement with the low enthalpy of dimer formation, 4.8 kcal., obtained by Liddel and Becker (*18*).

In 2,2,4,4-tetramethyl-3-pentanol dimers are formed exclusively according to Lussan, and they are open dimers according to Josien. On the other hand, 2,2,4-trimethyl-3-pentanol, which Lussan finds to form higher multimers, is probably beginning to form these in the dilute solutions of Josien. We feel that this higher association could be another cause of the divergence of the two curves in her case rather than the exclusive formation of closed dimers as Josien implies.

Dunken and Fritzsche (*6*) have summarized all the equilibrium constant calculations from infrared data used by earlier workers. They have shown that within the limits of accuracy in measurement, agreement can be reached between the results of two methods of calculation which contradict each other in their assumptions. By making infrared measurements at different temperatures, they also show that these chance agreements can come about at one temperature and not at another. Dunken and Fritzsche consider that simplified treatments of the type enumerated by Lussan are only approximations to the truth, and one should always employ a general model of association in which all the associated species (up to a certain maximum size) are present. The authors discuss the evidence for the cyclic dimer form but do not refer specifically to it in their calculations nor do they suggest that any of the higher multimers are cyclic.

Infrared results are presented for 2-propanol, 2-methyl-2-propanol, and 2-methyl-2-butanol in carbon tetrachloride and by a method of successive approximations equilibrium constants for the formation of each multimer are worked out from an equation based on the general model of association. Resultant graphs of percentage multimer *vs.* concentration show a greater percentage of pentamers and higher multimers in 1*M* 2-methyl-2-propanol than in the same concentration of 2-methyl-2-butanol. It is suggested that the formation of higher aggregates in the latter case is prejudiced by steric hindrance.

A number of workers have made dielectric measurements on alcohols and found that curves of polarization *vs.* concentration for several alcohols exhibit maxima or minima which have been ascribed to the formation of associated species of greater or less polarity as the concentration is progressively increased.

Publication Date: January 1, 1967 | doi: 10.1021/ba-1967-0063.ch010

Ibbitson and Moore (*13*) conclude that the maximum in the curve of polarization *vs.* concentration for ethanol in carbon tetrachloride is caused by linear multimers, and the subsequent fall in polarization is caused by an increasing amount of cyclic multimer (Figure 1). The concentration at which the maximum occurs coincides with that at which the 3350-cm.$^{-1}$ band first appears in the infrared spectrum, so they have suggested that this band arises from cyclic multimers. They have fitted their data to a system containing linear dimer and trimer and cyclic tetramer only and have evaluated association constants for these species.

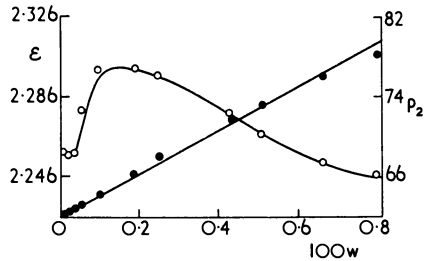

Figure 1. Variation of dielectric constant (ε, ●) *and solute polarization* (P_2, ○) *with weight fraction, w, for ethanol in carbon tetrachloride*

The model proposed by Zachariasen (*31*) to explain the x-ray diffraction peaks of liquid alcohols was that of long hydrogen-bonded chains in which the hydrogen bonds are linear, the oxygen atom of each alcohol molecule being linked by hydrogen bonds to that of two neighbors, the alkyl groups of the molecules falling consecutively on opposite sides of the chain. Oster and Kirkwood (*21*) made the further stipulation that there were no hydrogen bonds between the chains. Harris *et al.* (*8*), using the Oster and Kirkwood theory, deduced from values of the dielectric constant of 2-methyl-2-propanol at room temperature that these chains have an average length of 3.55 units, decreasing to 1.77 at 50°C.

Huyskens *et al.* (*10*, *12*) have measured the dielectric constants of the butyl alcohols in different solvents between 25° and 55°C. and have calculated dipole moments, μ, using a slightly modified form of the Onsager equation. The plots of μ^2 *vs.* concentration show minima which Huyskens ascribes to cyclic multimers of low resultant moment. The curves then rise again with increasing concentration and in the primary alcohols appear to reach a maximum value at which they flatten off at about 0.9 mole fraction. He notes that the minimum value of μ^2 occurs at lower concentrations for the more associated alcohols and becomes less pronounced as the temperature rises, vanishing altogether at 55°C. for 1-butanol.

Later work by Huyskens *et al.* (*11*) on a range of normal alcohols up to octanol showed results in each case rather similar to those on 1-butanol.

Publication Date: January 1, 1967 | doi: 10.1021/ba-1967-0063.ch010

Assuming that the minimum in the curve of μ^2 *vs.* concentration is caused by the presence of cyclic multimers, Huyskens calculated the relative numbers of molecules, r, involved in the cyclic structures from the dipole moment curves. He then obtained values of the monomer concentrations, c_1, from infrared data and compared qualitatively the variation with concentration of r and appropriate functions of c_1 for the case of two-, three-, and four-membered cyclic multimers. Best agreement was obtained with the cyclic trimer curve in most cases although the importance of bigger rings seemed to increase with the chain length of the alcohol.

At a mole fraction of about 0.3 in all the primary alcohols up to octanol, μ^2 is independent of temperature. Below this concentration μ^2 increases with temperature, which is presumably caused by the breaking up of cyclic multimers of low dipole moment, and above 0.3 mole fraction it decreases with temperature, presumably because of the breaking up of linear multimers of high dipole moment. In 2-methyl-2-propanol the point at which μ^2 is independent of temperature occurs at 0.6 mole fraction, and the maximum value of μ^2 is only 6.4 Debye^2 compared with 8.75 Debye^2 for 1-butanol and 8.52 Debye^2 for 2-butanol. These facts seem to confirm Harris's deduction that 2-methyl-2-propanol forms only short chains and also indicate a greater stability for the cyclic multimer in this alcohol. Huyskens' results also show that the effect of increasing temperature on the values of μ^2 for the pure alcohols increases markedly with the chain length of the alcohol. In view of this behavior it would probably be more realistic to compare the tendencies to form cyclic multimers at corresponding temperatures for the various alcohols rather than at the fixed value of 25°C.

The field dependence of the dielectric constant is known as the dielectric saturation effect (DSE), and in an unassociated medium $\Delta\epsilon/E^2$ increases linearly with concentration. Malecki (*20*) has found that in alcohol solutions considerable nonlinearities occur—positive saturation is obtained at low concentrations and negative at high concentrations. This behavior is interpreted according to the theory of Piekara (*22*), and for 1-hexanol in hexane Malecki shows that the degree of association increases with increasing concentration.

The large positive saturation in dilute solutions is caused by the high concentration of dimers, in which the dielectric saturation is shown by Piekara to lead to the largest increase in dipole moment. From curves which show the variation in mole fraction of each multimer with concentration it appears that in 1-hexanol there are 65 mole % pentamers, 25 mole % tetramers, and 10 mole % trimers approximately in the pure liquid. Malecki has also calculated that 60% of dimers and 37% of trimers are cyclic, the tetramers and pentamers revealing no cyclic structures. The forms of the curves showing variations in concentration of monomer and the various multimers with total concentration of hexanol are similar to

Publication Date: January 1, 1967 | doi: 10.1021/ba-1967-0063.ch010

those obtained by Dunken and Fritzsche for 2-propanol, 2-methyl-2-propanol, and 2-methyl-2-butanol. Malecki has compared the values of r from these results with those of Huyskens for 1-hexanol and shows that there is a good measure of agreement.

The influence of structure on molecular association in the alcohols was shown by Smyth (*24*), who determined the dielectric constant and molar polarization of 22 isomeric octanols in the pure state. Only general conclusions can be drawn from these results. As Smyth says, associations in which the dipoles reinforce each other, giving high P and ϵ, seem to occur when the OH group is at the end of a long C chain and remote from a branch in the chain—i.e., when linear multimer formation is most favored. When the OH group is in the middle of the chain and there is also branching at that point as in 4-methyl-4-heptanol, P is approximately half the value for 1-octanol, as would be expected if cyclic multimers predominate.

Thomas (*25*, *26*) studied the effects of association in alcohols on their viscosities and vapor pressures. Using a combination of empirical relationships, he obtained values of hydrogen bond enthalpies and average degrees of association, γ, for a large number of alcohols. He finds γ is constant

Table I. Summary of Data

Ref.	*Methods*	*Conclusions Reached*
Lussan (*19*)	NMR	Range of acyclic multimers, no distinction possible between cyclic and acyclic dimer structures
Josien (*5*)	Infrared–colligative property	Acyclic dimers only in some cases, acyclic + cyclic in others
Dunken and Fritzsche (*6*)	Infrared	Cyclic dimers discussed, higher multimers formed but all assumed acyclic
Ibbitson and Moore (*13*)	Infrared–dielectric measurements	Linear dimers and trimers, cyclic tetramers
Huyskens (*10*, *11*, *12*)	Infrared–dielectric measurements	Some cyclic multimers, predominantly trimers
Malecki (*20*)	Dielectric measurements	Calculated percentages of cyclic and acyclic dimers and trimers, all tetramers and pentamers acyclic
Thomas (*25*, *26*)	Viscosity measurements	Cyclic dimer in *n*-alkanols, higher cyclic multimers in branched-chain alkanols

around the value 2 for normal straight-chain alcohols up to octanol—i.e., the preponderant associated species is the dimer—while values of γ up to 5 are obtained for branched-chain alcohols.

On the basis of these results Thomas suggests that the normal alcohols associate in double-length rod-shaped molecules by forming two bonds between the two hydroxyl groups—the cyclic dimer. It is proposed that the

Publication Date: January 1, 1967 | doi: 10.1021/ba-1967-0063.ch010

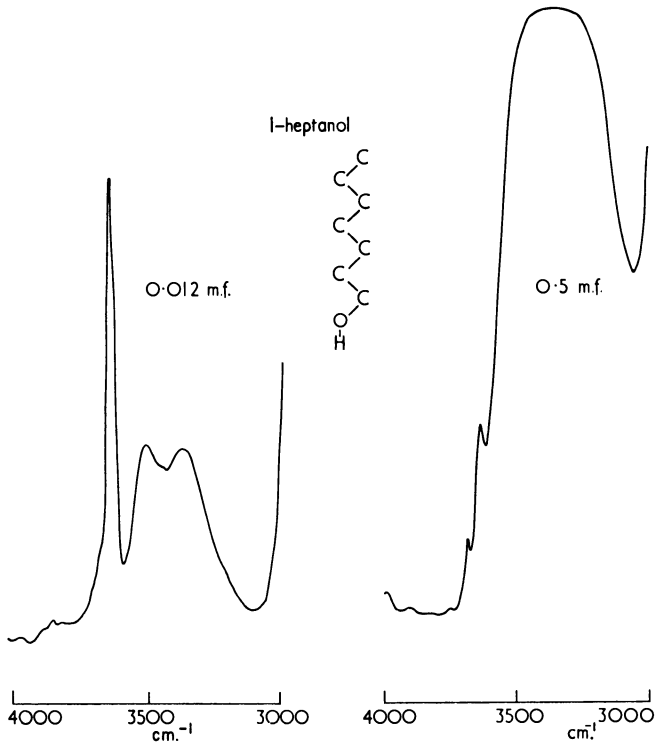

Figure 2. OH stretching vibrations in solutions of 1-heptanol in CCl_4

branched chain alcohols will have less reason to form dimers in this way, principally because of the smaller London forces between their hydrocarbon portions.

Direct conclusions have been drawn from the viscosities of alcohols in different solvents by Huyskens (*9*), who infers from the greater viscosity of 2-methyl-2-propanol at 25°C. than the other butanols that cyclic multimers having a greater resistance to flow than linear multimers are present in greater proportions in the tertiary alcohol.

Our own work on 1-heptanol and a number of its isomers has involved infrared and NMR measurements on the pure liquids and their solutions in carbon tetrachloride. Infrared measurements have been made on a Unicam SP100 spectrophotometer and NMR measurements on a Varian A-60 spectrometer.

The OH stretching region of the infrared spectrum has been compared for dilute solutions of five heptanols in carbon tetrachloride; the spectrum at 0.1 molarity and 25°C. gives a good indication of the association behavior of the alcohol. The picture for the two extreme types of behavior, as exemplified by 1-heptanol and pentamethylethanol, is shown in Figures 2 and 3. The three OH stretching bands occur in 1-heptanol at 3630,

Publication Date: January 1, 1967 | doi: 10.1021/ba-1967-0063.ch010

3500, and 3350 cm.$^{-1}$ and have been assigned by most workers to monomer, dimer, and multimer OH groups, respectively.

Since the multimer band is the furthest shifted from the monomer band, we can assume that the hydrogen bonds formed in this association are of higher energy than in the dimer. We therefore presume that this

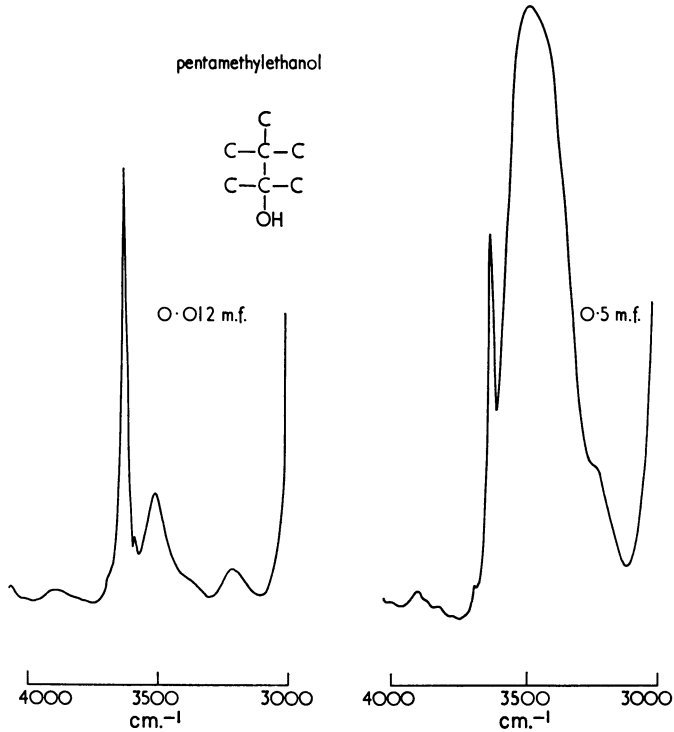

Figure 3. OH stretching vibrations in solutions of pentamethylethanol in CCl_4

band arises from hydrogen bonds in either the long-chain multimers described by Zachariasen, or three- and four-membered cyclic multimers, or possibly in all these species. Since the linear chains may well curl up into helices of low resultant dipole moment by internal rotation of the hydrogen bonds (*17*, *21*), their formation is not incompatible with the polarization data of Ibbitson.

In pentamethylethanol the multimer band never appears, but the dimer band becomes broader as the concentration increases. In 2,4-dimethyl-3-pentanol the multimer band is only just perceptible at 0.1*M* and develops much more slowly with increasing concentration than in the case of 1-heptanol. 4-Heptanol shows slightly more evidence of multimers at 0.1*M*, and the cycloheptanol spectrum is practically indistinguishable from that of 1-heptanol.

Publication Date: January 1, 1967 | doi: 10.1021/ba-1967-0063.ch010

It seems that multimer formation occurs with increasing ease in the series pentamethylethanol, 2,4-dimethyl-3-pentanol, 4-heptanol, cycloheptanol, 1-heptanol. Since we have detected the above differences between alcohols, three of which are secondary isomers, the process of association does not seem to depend on the class of alcohol.

Space models of these alcohols shows immediately how important must be the steric influences on the association processes. One can see how difficult it is for molecules such as pentamethylethanol to form linear hydrogen-bonded chains of the Zachariasen type. The alkyl groups of alternate molecules can be seen to be close together if no bending occurs in the hydrogen bond chain, and when alkyl substitution occurs in the α position, there is certain to be some hindrance to free rotation around the —C—O— bond. Accordingly, from the lack of a multimer band in the infrared spectrum and the linearity of the curve of NMR chemical shift *vs.* concentration out to $0.35M$ we can presume that only dimers are formed initially in pentamethylethanol, with possibly cyclic multimers at higher concentrations.

Because of this behavior we have been able to obtain values for the enthalpy of dimerization from infrared data by the method of Liddel and Becker (*18*) and from NMR data by the method of Davis, Pitzer, and Rao (*2*) without having to resort to such low concentrations as usual. Extrapolated values of the infrared molar extinction coefficients, ϵ_m, of the monomer OH band at zero concentration were obtained from curves of ϵ_m *vs.* concentration at 25° and 50°C., and from these a value of 5.4 kcal. per mole was obtained for the enthalpy of dimerization. The limiting slopes of the curves of NMR chemical shift *vs.* concentration at 0° and 35°C. gave a value of 6.1 kcal. per mole. These values are in reasonable agreement with each other and significantly lower than the values of 8 kcal. for 1-heptanol and 7.9 kcal. for 2,4-dimethyl-3-pentanol, obtained from NMR data only.

Although the association of the latter alcohol is hindered by substitution in the 2 and 4 positions, one can see that linear multimers are possible, and this is even more true of 4-heptanol because of the greater freedom of movement of the unsubstituted methylene groups. In cycloheptanol we feel that complete rotation of the molecule may be hindered in the linear multimer, but there is still room for appreciable torsional movement.

Josien's results indicate a difference in the type of dimer formed in 3-methyl-3-pentanol and 3-ethyl-3-pentanol, and we would prefer to explain this behavior by the formation of linear multimers at low concentrations in the former but not in the latter case. Again space models show that an ethyl group on the α-carbon atom in 3-pentanol will be a considerably greater hindrance to linear multimer formation than a methyl group.

Steric factors will affect the formation of cyclic as well as linear multimers, and in the case of pentamethylethanol it is thought that only in

Publication Date: January 1, 1967 | doi: 10.1021/ba-1967-0063.ch010

cyclic trimer will there be sufficient "elbow room" for free rotation of the bulky alkyl radicals.

The NMR chemical shifts of the hydroxyl proton line in the pure alcohols measured at 30°C. bear out the general conclusions obtained from the infrared spectra since the greater association shifts occur in the alcohols showing the greater tendencies toward multimer formation in every case.

There is still no certain information obtainable from infrared and NMR measurements on cyclic dimers or multimers. The dimer band may arise from a cyclic species involving nonlinear hydrogen bonds, and one might expect that if a cyclic trimer exists, the OH stretching frequency would be similar to and slightly lower than that of a cyclic dimer. This would account for the broadening of the dimer band in pentamethylethanol at high concentrations.

The higher values of enthalpy for dimer formation in the normal alcohols, possibly representing the formation of two hydrogen bonds, could mean that they form a cyclic dimer at low concentrations more readily than the heavily substituted alcohols, again for steric reasons.

The infrared, NMR, and dielectric results are thus in general agreement on the nature of the association processes in liquid alcohols although there are many differences in detail. Obviously steric considerations are of prime importance in these systems. More specific and certain conclusions may follow from an extension of the dielectric methods of Ibbitson, Huyskens, and Malecki to some of the isomeric alcohols studied by the infrared workers.

Publication Date: January 1, 1967 | doi: 10.1021/ba-1967-0063.ch010

Diols

Information on intermolecular hydrogen bonding in aliphatic 1,2-diols is hard to find. The OH stretching vibration of intermolecular bonds was observed by Kuhn (*14*) in a number of aromatic and aliphatic diols. The band occurs between 3400 and 3500 cm^{-1}. in all cases, but Kuhn does not discuss the intermolecular association processes. He did, however, investigate the influence of structure on the intramolecular hydrogen bond and found that when bulky alkyl groups are attached to the glycol residue in meso 1,2-disubstituted glycols, they can prevent the formation of the intramolecular hydrogen bond by forcing the two OH groups to occupy trans positions. By using different substituent alkyl groups he proved fairly conclusively that this effect is of steric rather than polar origin. It would be interesting to know the effect of these changes on the nature and degree of intermolecular bonding.

Recently Thomas (*27*) measured γ values for a number of aliphatic and aromatic diols. He finds again, as in the alcohols, that the degree of association is low for the straight-chain diols and high for the highly substituted ones ($\gamma = 2.1$ for ethylene glycol, $\gamma = 3.7$ for tetramethylethylene

glycol) and therefore concludes that the association is not hindered by steric factors.

Because γ for these diols is only slightly higher than for the corresponding monohydric alcohols, it is suggested that multimers are chiefly formed through only one of the OH groups, a conclusion which is supported by the values of a function q/m derived from enthalpy considerations. Thomas concludes that cyclic tetramers are formed in the highly associated diols involving only one OH group from each molecule. In less associated diols the values of q/m suggest that both OH groups are involved in the association, and polydentate structures involving two and three molecules of diol are suggested and shown to be geometrically feasible.

Debye *et al.* (*3*, *4*) published two papers containing infrared measurements on monoglycerides. They assigned overlapping bands (at 3584 and 3460 cm^{-1}. in the first paper and 3676 and 3572 in the second) to "free" and "bonded" OH groups, respectively, and found the ratio of the estimated optical densities of these bands; OH free/OH bound decreased linearly with concentration in carbon tetrachloride solution because of increasing molecular association. In chloroform and benzene, however, the ratio remained almost constant, indicating that association was taking place between

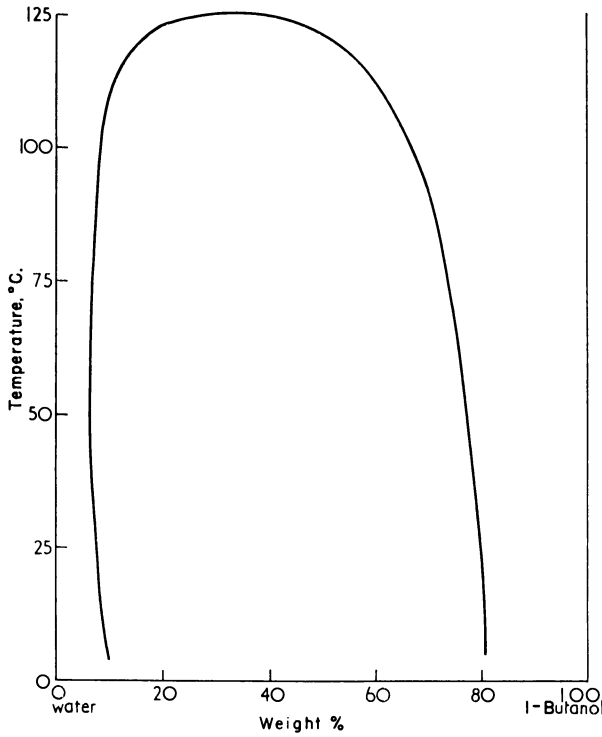

Figure 4. Binary liquid-phase diagram for 1-butanol–water

Publication Date: January 1, 1967 | doi: 10.1021/ba-1967-0063.ch010

glyceride and solvent molecules. Unfortunately, Debye does not distinguish between intra- and intermolecular hydrogen bonding.

We have observed the OH stretching vibrations for a pure sample of monocaprin in carbon tetrachloride and at 0.008*M* have found a monomer or "free" OH band at 3620 cm.$^{-1}$ and a band which we think is caused by the intramolecular hydrogen bond at 3540 cm^{-1}. At 0.04*M* the OH band is much broader, with a maximum at 3460 cm^{-1}., presumably owing to extensive intermolecular association. It seems therefore that this type of association sets in at similar OH group concentrations in the diols and the monohydric alcohols, as can also be seen in Kuhn's spectrum of tetramethylethylene glycol, in which the intermolecular band in 0.05*M* solution has approximately the same intensity as in 0.1*M* solutions of the normal alkanols.

Liquid Alcohols Plus Water

The lower aliphatic alcohols are completely miscible with water; higher homologs have a partial miscibility as shown by a typical conjugate solution diagram (Figure 4), and from hexanol upward they are virtually insoluble in water.

The solubility of water in the alkanols does not fall off so drastically, and Figure 5 shows a plot of solubility *vs.* chain length. Furthermore, the water-in-alcohol portion of Figure 4 shows the small change in solubility over a wide range of temperature; in fact, this curve (for the 1-butanol–water system) is binodal. This behavior reflects the delicate balance between the association and the ideal mixing tendencies in alcohol–water mixtures.

Ginnings and Hauser (*7*) determined some mutual solubilities in a number of isomeric heptanol–water systems over a limited temperature range. The temperature coefficients for the solubility of water in alcohol are positive in some cases and negative in others, and there is a perceptible grouping of the actual solubility values. In the heptanols chosen all the tertiary isomers take up approximately 6% water at 20°C., while the secondary isomers dissolve approximately 3% water. The solubilities of the heptanols in water decrease with temperature in all cases.

NMR spectra have been observed in this laboratory of samples of heptanol, octanol, and dodecanol saturated with water. With pure specimens of octanol and dodecanol we have obtained a picture at low temperatures similar to that of Weinberg and Zimmerman (*30*), the alcohol and water OH groups giving separate resonances. As the temperature was increased in these samples, the lines coalesced to give a single very broad peak. When the lines are distinct, the alcohol OH resonance remains at the same value of chemical shift, δ, as in the anhydrous material, whereas for the water line, δ decreases by approximately 0.4 p.p.m. in each alcohol from the value in pure water. One deduces that the hydrogen bonding

Publication Date: January 1, 1967 | doi: 10.1021/ba-1967-0063.ch010

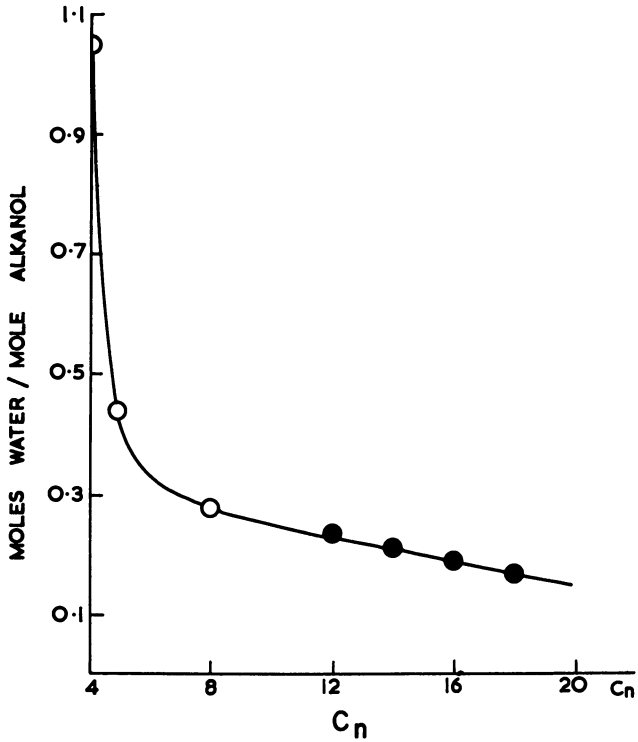

Figure 5. Solubilities of water in normal alkanols
○ *25°C.*
● *60°C.*

within the alcohol is not affected by the addition of water, but the amount of bonding between the water molecules is decreased in the alcohol solution.

The rate of change of δ_{OH} with temperature has also been measured in the pure alcohols and alcohol–water systems; here it is evident that the combined OH line varies with temperature in the same way as the mean value of the separate alcohol and water OH lines. Again this indicates that there is no major change in the nature of the hydrogen bonding when water is added to alcohols in these amounts.

From the infrared and NMR results showing different degrees of association among the different alcohols, it is tempting to try to correlate this association with the amount of water taken up at corresponding temperatures. One might conclude from the figures of Ginnings and Hauser that the tertiary alcohols take up more water because they probably contain more of the small nonlinear multimers which more readily associate with individual water molecules.

Measurements of dielectric constant in the 2-methyl-2-propanol–water system by Brown and Ives (*1*) are explicable in terms of a water-centered

Publication Date: January 1, 1967 | doi: 10.1021/ba-1967-0063.ch010

association, and the authors assemble other evidence in favor of this hypothesis. Dielectric measurements on a number of structurally isomeric alkanols with water would probably help to elucidate the nature of this association.

In the solid state, however, the normal long-chain aliphatic alcohols take up almost exactly the same amount of water as in the liquid (*15*), and Trapeznikov (*28*) has suggested that specific hydrates are formed, as in the well known case of pentamethylethanol. Since the structure of solid alcohols certainly contains linear chains of hydrogen bonds, it seems unnecessary to evoke the specific association of small clusters of alcohol molecules with individual water molecules in the liquid state.

Diols Plus Water

Complete miscibility of aliphatic diols with water occurs up to higher chain lengths than in the alcohol series, and hexane-1,2-diol is described as miscible with water. As the chain length increases further, adding water

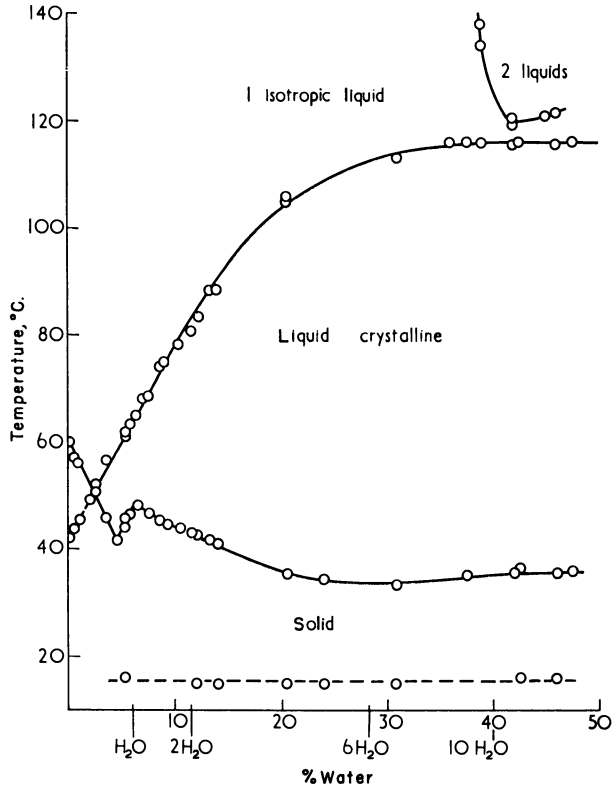

Figure 6. Monolaurin-water phase diagram
Lower dotted line refers to transition between a metastable solid phase and an l.c. phase

leads to the formation of a smectic l.c. phase which has been observed in a number of monoglycerides and in hexadecane-1,2-diol (*15*) over limited ranges of temperature.

At higher temperatures in the presence of large amounts of water, only a brief region of liquid miscibility occurs before the system separates into two liquids. A similar behavior is seen in some of the longer chain amines in the presence of water (*23*). The monolaurin-water system, which has been fully described elsewhere (*16*), is shown in Figure 6. A feature of these systems is the large amount of water taken up by the l.c. phase. In octylamine a maximum stability of this phase occurs at a ratio of 6 molecules of water to 1 of octylamine, but in monolaurin the stability is still at a maximum when the system reaches the point at which it can take up no more water. The conjugate solution curve at the top of the diagram is steep, showing that monolaurin can contain up to 10 molecules of water per molecule in the liquid or l.c. phase without breaking down at any temperature. One of the conditions for the formation of the l.c. phase is the same as in the well characterized soap-water systems—the chain must be at least six carbon atoms long, by which time the London forces between chains are sufficient to maintain the structure of the smectic phase.

Further work in this field will involve the study of some of the intermediate chain length 1,2-diol–water, monoglyceride-water, and amine–water systems. We would like to establish all the conditions necessary for formation of the l.c. phase in these systems and to determine the factors governing its stability and final instability as the percentage of water in the system increases.

Publication Date: January 1, 1967 | doi: 10.1021/ba-1967-0063.ch010

Acknowledgment

The author thanks G. Porter for the use of NMR and infrared facilities at the Department of Chemistry, Sheffield University, and A. S. C. Lawrence for many helpful discussions.

Literature Cited

(1) Brown, A. C., Ives, D. J. G., *J. Chem. Soc.* **1962**, 1608.
(2) Davis, J. C., Pitzer, K. S., Rao, C. N. R., *J. Phys. Chem.* **64**, 1744 (1960).
(3) Debye, P., Prins, W., *J. Colloid Sci.* **13**, 86 (1958).
(4) Debye, P., Coll, H., *J. Colloid Sci.* **17**, 220 (1962).
(5) Dos Santos, J., Pineau, P., Josien, M.-L., *J. Chim. Phys.* **1965**, 628
(6) Dunken, H., Fritzsche, H., *Spectrochim. Acta* **20**, 785 (1964).
(7) Ginnings, P. M., Hauser, M., *J. Am. Chem. Soc.* **60**, 2581 (1938).
(8) Harris, F. E., Haycock, E. W., Alder, B. J., *J. Chem. Phys.* **21**, 1943 (1953).
(9) Huyskens, P., *J. Chim. Phys.* **62**, 158 (1965).
(10) Huyskens, P., Cracco, F., *Bull. Soc. Chim. Belg.* **69**, 422 (1960).
(11) Huyskens, P., Gillerot, G., Zeegers-Huyskens, Th., *Bull. Soc. Chim. Belg.* **72**, 666 (1963).
(12) Huyskens, P., Henry, R., Gillerot, G., *Bull. Soc. Chim. France.* **1962**, 720.
(13) Ibbitson, D. A., Moore, L. F., *Chem. Commun.* **1965**, 339.
(14) Kuhn, L., *J. Am. Chem. Soc.* **74**, 2492 (1952); **80**, 5950 (1958).

(15) Lawrence, A. S. C., Capper, B., Hume, K., *J. Phys. Chem.* **68**, 3470 (1964).
(16) Lawrence, A. S. C., McDonald, M. P., *Molecular Crystals* **1**, 205 (1966).
(17) Le Fèvre, R. J. W., Williams, A. J., *J. Chem. Soc.* **1960**, 108.
(18) Liddel, U., Becker, E. D., *Spectrochim. Acta* **10**, 70 (1957).
(19) Lussan, C., *J. Chim. Phys.* **1963**, 1100.
(20) Malecki, J., *J. Chem. Phys.* **43**, 1351 (1965).
(21) Oster, G., Kirkwood, J. G., *J. Chem. Phys.* **11**, 175 (1943).
(22) Piekara, A., *J. Chem. Phys.* **36**, 2145 (1962).
(23) Ralston, A. W., Hoerr, C. W., Hoffman, E. J., *J. Am. Chem. Soc.* **64**, 1516 (1942).
(24) Smyth, C. P., *Chem. Revs.* **6**, 549 (1929).
(25) Thomas, L. H., *J. Chem. Soc.* **1963**, 1995.
(26) Thomas, L. H., Meatyard, R., *J. Chem. Soc.* **1963**, 1986.
(27) *Ibid.*, **1966**, A92.
(28) Trapeznikov, A. A., "Proceedings of 2nd International Congress of Surface Activity," Vol. 1, p. 109, Butterworth & Co., London, 1957.
(29) Van Thiel, M., Becker, E. D., Pimentel, G. C., *J. Chem. Phys.* **27**, 95 (1957).
(30) Weinberg, I., Zimmerman, J. R., *J. Chem. Phys.* **23**, 748 (1955).
(31) Zachariasen, W. H., *J. Chem. Phys.* **3**, 158 (1935).

RECEIVED January 27, 1966.

Liquid Crystals as Ordered Components of Living Substance

G. T. STEWART

Departments of Epidemiology and Pathology, University of North Carolina, Chapel Hill, N. C.

Publication Date: January 1, 1967 | doi: 10.1021/ba-1967-0063.ch011

The complex integral lipids and lipoproteins of many living cells and tissues exist as lyotropic mesophases within the thermal range 4°–42°C. In this form, these substances have a combined structural and functional role in situations where interfacial activity and limited flow are essential, as in membranes, subcellular particles, and certain systematically layered tissues. The molecular structure, orientation, and dimensions of these mesophases appear, in general, to be complex elaborations of patterns set by experimental models with binary and ternary systems of solute, amphiphile, and solvents. It is postulated that the lyotropic mesophase represents a vital physicochemical element in the organization of certain components in protoplasm from organic precursors. Disorders of regulation of the lipoprotein mesophase in man and some animals contribute to aging.

Structures with the appearance or properties of mesophases and liquid crystals have been observed in extracts of animal tissue since the end of the 19th century. There is, however, a difference between matter extracted from tissue—usually dead or dying—and matter integrally present in living tissue. Matter in the first category is easily obtainable but liable to be deceptive in appearance for the tissue is altered or killed by the process of extraction. Matter in the second category is extremely difficult, sometimes impossible, to visualize by methods appropriate to identifying ordered systems, but there are now some observations which establish the importance of mesoforms as components of cells and tissue.

The first biological observations were made on preparation of the yolks of amphibian eggs and of cephalopod spermatozoa by Schmidt (*33*) and of molluscan eggs by Pfeiffer (*29*) though almost a century before Virchow (*42*) had described polarization crosses in fresh and preserved specimens of myelin. Nageotte (*26*) studied these structures and myelinic figures in

In Ordered Fluids and Liquid Crystals; Porter, R., el al.;
Advances in Chemistry; American Chemical Society: Washington, DC, 1967.

detail though he was not able to reach any conclusion about how they entered into the structure of intact myelin. The work of Finean (*12*) and his colleagues threw some light on this by disclosing the concentrically multilayered structure of the myelin sheath, composed of three lipids (phosphatide, cerebroside, and sterol) in a fixed ratio.

The possibility that these and other observations meant that paracrystalline states were widespread in biological material was reviewed by Needham (*27*), who drew an analogy between the development of a mesophase and the growth of limb buds and other organs in amphibia (*16*). Substances with paracrystalline or birefringent properties had also been noted in muscle, collagen, reticulin, adrenal cells, ovary, and other tissues, as well as in plant viruses (*4*). A leading crystallographer (*3*) had already predicted that liquid crystals possessed properties essential for the organization of protoplasm.

From these and many other studies there was by 1950 plenty of evidence pointing to the possible importance of liquid crystals in tissue. Since then the subject has been explored by direct and experimental methods. My purpose is to examine the chemical forms in which liquid crystals occur and to identify more closely their precise structure and integration into protoplasm and biological fluids. This is often a matter of great difficulty for obvious technical reasons. My own work in this respect has been concerned mainly with lipids and lipoproteins, so I shall refer mainly to these though several other important classes of substances, especially certain proteins and polynucleotides, can exist in the liquid crystalline state and may be present as such in living tissue.

Lipoid and Lipoprotein Mesoforms in Tissue

Simple spherulites with polarization crosses can readily be found in intact cells from the corpus luteum of the ovary, in the adrenal cortex, and in certain abnormal lipoid deposits (*39*). The lipoid nature of these spherulites is confirmed by their dissolution in organic solvents though not necessarily by conventional histo- or cytochemical tests since integral lipoid usually fails to develop a color with oil-soluble dyes. In these situations, the liquid crystal is present as a relatively particulate component of a phase system containing various lipids or lipoproteins. In the cells of the corpus luteum and adrenal, steroids are present in the complex, probably as intermediates or end product in hormone synthesis since steroid dehydrogenase and other enzymes appropriate for this are present in the identical cells.

The mesophase in these entirely normal cells of the adrenal cortex and ovary has interesting properties. It has a yellow pigment and a relatively high cholesterol content though this varies according to the intensity of hormonal synthesis and, in the ovary, cyclically (*17*). The lipid is fairly evenly distributed throughout the cell and is an integral part of the cytoplasm (*1*), not a dispersed phase or micellar solution as in some other fat-

Publication Date: January 1, 1967 | doi: 10.1021/ba-1967-0063.ch011

containing cells. In these two organs, therefore, it seems highly probable that the mesophase is vital functionally as well as structurally.

Lipoprotein Mesophase in Plasma

The normal ovarian and adrenal lipid is intracellular, but there is another important situation in which a lipoid mesophase may be present more or less normally, entirely outside cells. This is in the plasma (*39*), in the low density β-lipoprotein fraction (S_f 12 to 20). In health, this fraction is low or absent until adult life. It begins to increase in males from about the age of 20 onward; in females, it remains low until the menopause, after which it increases rapidly as in males. It can be produced experimentally in rabbits, dogs, fowls, and some other animals by feeding cholesterol. Analogous to this is the pathological increase seen in humans with certain renal and metabolic disorders, especially in diabetes mellitus and in hereditary or essential hyperlipemia, where there is an increase in several fatty components in the blood, with abnormal deposition of fat in various tissues.

In healthy individuals, the low density lipoprotein can be isolated in the natural state only by ultracentrifugation. In experimental animals or in the hyperlipemic diseases the larger amounts present can be recovered conveniently and rapidly from fresh plasma by immediate centrifugal flotation at 37°C. The layer of lowest density yields particulate chylomicrons in micellar form. The next layer with a hydrated density of <1.04 grams/ml. is composed of a lipoprotein mesophase which is turbid and shows many myelinate structures with positive optical signs. The mesothermal range is limited: warming to 42°C. produces an isotropic melt; cooling to 25° through 4°C. produces uniform spherulites. Sudden cooling to subzero temperatures disrupts the spherulitic pattern irreversibly although irregular myelinate figures may thereafter develop. If the patient or experimental animal is injected immediately beforehand with macromolecular polysaccharide in the form of heparin or dextran sulfate, there is an alteration in the lipoprotein equilibrium in the plasma (*35*) which provokes a striking increase in the turbid mesophase, sometimes to the extent of allowing it to separate from the plasma colloid as a semisolid film. Under polarized light, this appears at 37°C. as a continuous sheet of myelinate structures, all optically positive (Figure 1).

To understand the significance of this occurrence, it is necessary to follow the pharmacodynamic action of macromolecular polysaccharide, which is complex. The essential point is that heparin and its analogs normally produce a clearing effect in lipemic plasma, probably attributable to activation of a lipase which hydrolyzes triglycerides (*15*). In the presence of an excess of low density lipoprotein, this clearing mechanism is imperfect, and there is reason to believe that the low density component actually inhibits the process. If, as seems likely, the heparin-clearing effect bears

Publication Date: January 1, 1967 | doi: 10.1021/ba-1967-0063.ch011

some relationship to physiological lipolysis (*32*), it follows that removal of fat from the plasma decreases as the lipoprotein increases; furthermore, when an abnormal excess of this lipoprotein component is present, as in cases of untreated diabetes mellitus, essential hyperlipemia, or nephrosis, activation of the physiological lipase can conceivably increase the proportion of lipoprotein in mesophase. Whether or not this change provokes deposition is uncertain, but it clearly increases the amount of lipoid mesoform in circulation. More study is needed to trace the disposal of this load of presumably useless fat.

Relationship between Plasma and Tissue Mesophase

The plasma mesophase consists mainly if not entirely of a fraction which increases only with aging or metabolic disease. This fraction is of low density (1.00–1.04 grams/ml. hydrated) for it contains 95% lipid in

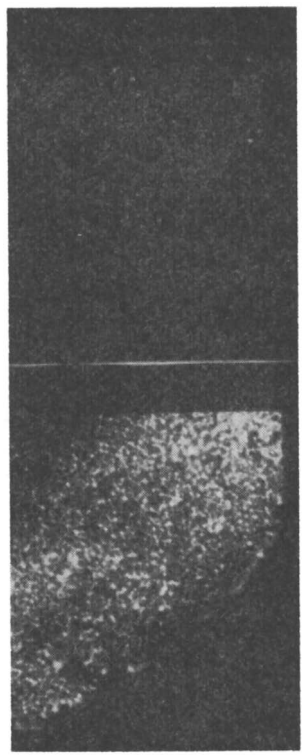

Figure 1. Low-density lipoprotein in hyperlipemic plasma

Before (A) and 5 minutes after (B) injection of heparin intravenously. Marked increase in birefringence in B is caused by aggregation of lipoprotein in mesophase.

Polarized light × 80

Publication Date: January 1, 1967 | doi: 10.1021/ba-1967-0063.ch011

the form of roughly equal proportions of cholesterol (50% esterified) and phosphatide, and a more variable proportion of triglyceride. In terms of density and chemical composition, this fraction differs only in degree from the continuous ultracentrifugal gradient of the other lipoprotein fractions

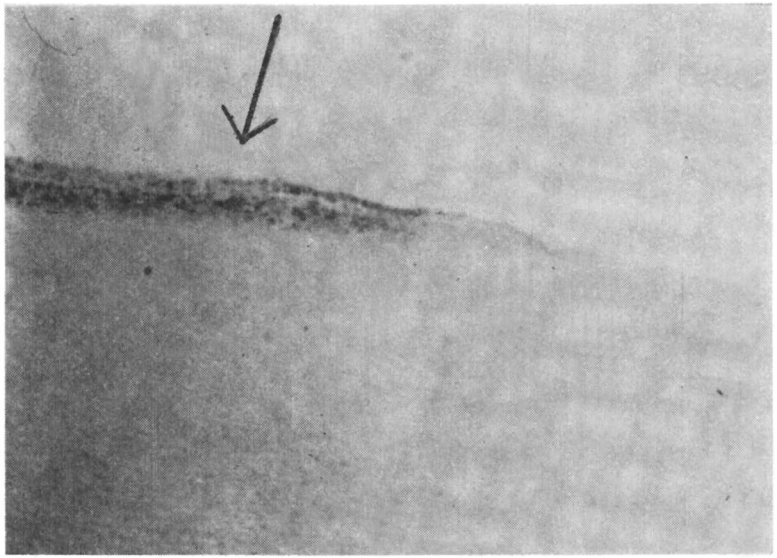

Figure 2. Section of intimia of human artery showing early atheromatous deposit partly soluble in Sudan black

× 400

(*43*), or from the chylomicrons which circulate after a fatty meal in any individual. The essential difference is that the low density fractions exist wholly or partly in the liquid crystalline form whereas the other lipoprotein fractions are in colloid solution while the chylomicrous are particulate or micellar. The physical difference is important, structurally and functionally. The early lipid deposition (Figure 2) which initiates the process of atherosclerosis in arteries is in this same form (Figure 3), which can be produced experimentally by pulsating the low density component into healthy vessels (*36*); other forms of lipid or lipoprotein do not produce these atheromatous deposits of liquid crystals (*37*). In their appearance, main properties, and degradation products, the liquid crystals of early atherosclerosis, whether natural or experimental, are strikingly similar to those seen in the lipoprotein mesophase of the plasma. Other factors undoubtedly contribute materially to the pathogenesis of atherosclerosis, which is the most obvious chemical lesion of aging, in man as well as in some other mammals when metabolism slows down; but the presence of a macromolecular lipoprotein mesoform is an essential prelude (*40*).

Publication Date: January 1, 1967 | doi: 10.1021/ba-1967-0063.ch011

In Ordered Fluids and Liquid Crystals; Porter, R., el al.;
Advances in Chemistry; American Chemical Society: Washington, DC, 1967.

The progesterone-secreting corpus luteum cells of the ovary also contain a mesophase similar in form, properties, and composition to that of the lowest density lipoprotein of plasma, and of the early atheroma deposits. Superficially, it might seem that women keep the mesophase in the cyclically forming corpora lutea while men let it circulate and thence deposit itself in arteries; women begin to do this only when they reach the menopause and no longer form corpora lutea. This may simply be a localized expression of the fact that fat distribution is fundamentally different

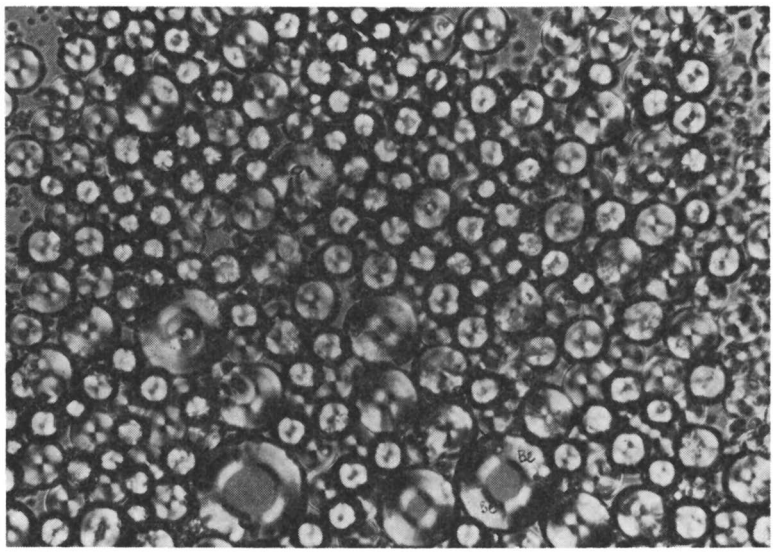

Figure 3. Atheromatous deposit from human artery (Figure 2) showing smectic mesophase with spherulitic structure

Polarized light × 1000 with quarter-wave plate
Radial direction ↖↘s

in male and female, under hormonal regulation. It is plausible, therefore, to suppose that there is in the ovarian hormonal complex a lipoprotein-regulating factor which controls the amount and distribution of the low density, high lipid fractions in plasma and in certain tissues from puberty until the menopause. The administration of estrogens causes partial reversal of the lipoprotein imbalance in males (*28*) but only at the cost of feminization, which few would regard as a fair bargain. Estrogens alone are unlikely to be adequate for treatment since the essential regulating mechanism would seem to depend upon the development of the lipoid mesoform in the progestin-secreting corpus luteum following ovulation. There is proof of this in the fact that pregnancy, with persistence and growth of mesoform substance in the corpus luteum, is often associated with a considerable rise in cholesterol and phosphatide in the plasma, but

Publication Date: January 1, 1967 | doi: 10.1021/ba-1967-0063.ch011

In Ordered Fluids and Liquid Crystals; Porter, R., el al.;
Advances in Chemistry; American Chemical Society: Washington, DC, 1967.

not in the low-density β-lipoprotein fraction and therefore without atheromatous deposition.

The atherogenic propensity resides less in the amount of circulating lipid than in its physicochemical form,—i.e., the presence of lipoprotein in mesophase. Given this initiation, however, there is evidence (*38*) that triglyceride lipemia can aggravate atherogenesis by forming secondary lipoid complexes with the primary mesophase and by other less direct mechanisms, which include the formation of calcium soaps, accumulation of fibrin, attraction of phagocytes, and interference with the firm structure of the subintimal elastic layers of the artery. Atherosclerosis is, in the early stages, a misnomer since the essential chemical and histological lesion is a soft, infiltrative lipoidosis. Sclerosis comes later, when the liberated fatty acids form calcium salts and when free calcium is deposited in the inert tissue.

Publication Date: January 1, 1967 | doi: 10.1021/ba-1967-0063.ch011

Experimental Studies of Phase Equilibria

The simplest lyotropic system is exemplified by the behavior of a fatty acid salt in water; thus, using potassium palmitate, McBain and Marsden (*24*) identified three phases: an isotropic micellar solution, a turbid, viscous coagel, and an intermediate region. These phases exist because of the amphiphilic property of the fatty acid salt which has a hydrophilic polar group and a water-insoluble hydrocarbon chain; any substance of similar structure can behave as an amphiphile. If water is used as the solvent, a considerable number of substances capable of forming equilibrated phases can thus be identified predictably from their molecular structure: salts of fatty acids, ionic and nonionic detergents, phosphatides, and many others.

The structure, symmetry, and dimension of each mesophase have a unique character determined by the molecular configuration of the amphiphile and its degree of solvation. Working with various lipid amphiphiles and water, Luzzati and his colleagues (*22*, *23*) have shown by x-ray crystallography and polarization microscopy that the essential feature common to all phases is a disordered liquid-like configuration of the hydrocarbon chain of the lipid. In binary systems, the unit of structure is usually assumed to be a micelle with a liquid core. In the isotropic phase, the micelles are spherical, arranged in a cubic lattice; in the middle phase, they are uniformly elongated into cylinders of uniform diameter, arranged hexagonally; in the neat phase, the micelles are arranged in parallel sheets with solvent between. Electron micrographs (*41*) of thin sections, dehydrated and osmium-fixed, provide confirmation of this general structure which finds expression in the theory that the various phases represent different ways of packing micellar units in the solvent system. Recent work (*8*) with a semipolar surfactant-solvent system at low solvent concentrations suggests that the middle phase may consist of linear aggregates of spherical micelles, but this may be at variance with the structure formed when solvation is

more complete, as when lecithim swells into water to form myelin tubes which are obviously cylindrical (Figure 4). Lawrence (*19*, *20*, *21*) and Dervichian (*10*) consider that the structure here is a smectic lattice with free water between holding the layers of opposed hydrophilic polar groups of the phospholipid. In ternary systems, the introduction of a third organic component—e.g., a long-chain alcohol—allows closer packing by reducing the repulsive force between the ionized head groups of the surfactant (*5*). The development of mesophases, their structure, and stability

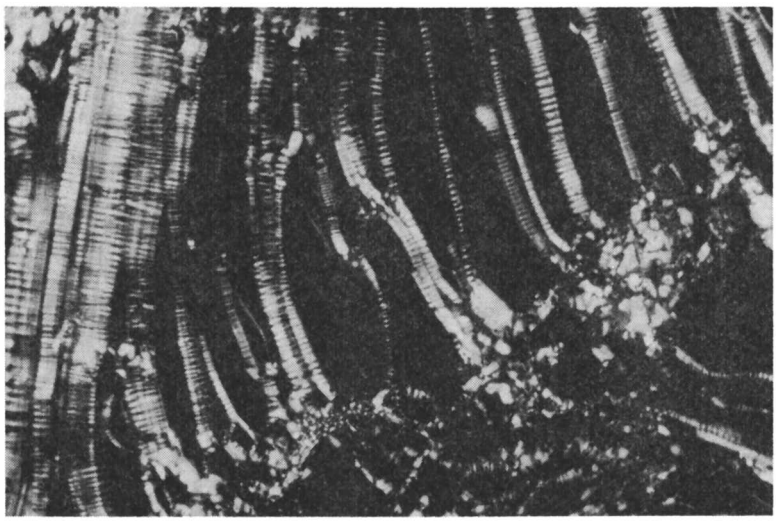

Figure 4. Experimental smectic mesophase with cylinders at phospholipid-water interface
Polarized light × 100

would appear therefore to depend primarily upon solvent concentration, polar solubility, and intermolecular forces while secondarily, innumerable variations in phase transition and structure can be ascribed to the ionic or nonionic nature of the amphiphile, hydrocarbon chain length, and temperature.

Thus far, we have been considering relatively simple binary and ternary systems in which the main components are known. Lyotropic systems in living cells and body fluids are much more complex insofar as steroids, compound lipids, protein, and electrolytes among other substances are usually present, often as polymers or macromolecules. The precise composition of most biologic mesoforms awaits definition, but the elementary structure is illustrated by introducing cholesterol into a ternary system with water and a surfactant such as the long chain polyoxyethylene esters of the Tween series. A solid crystal of cholesterol is thereby brought into a mesophase with a highly characteristic optical pattern (Figure 5) which closely resembles the mesoforms seen—for example, in atheroma and

Publication Date: January 1, 1967 | doi: 10.1021/ba-1967-0063.ch011

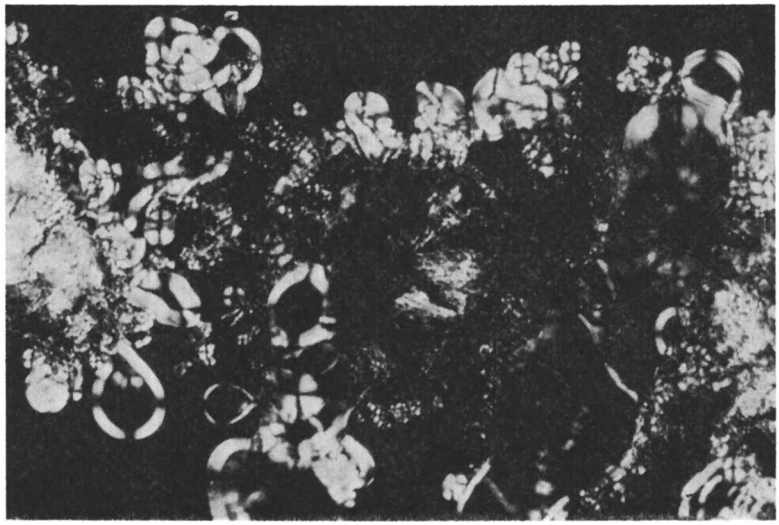

Figure 5. Solid crystal of cholesterol forming spherulitic mesophase with a polyoxyethylene ester (Tween 40) in water
Polarized light × 100

ovarian lipid (Figure 3). This experiment can also be performed with various fatty acid esters, in which case the minimum concentration required to effect conversion to mesophase decreases as the chain length of the parent fatty acid increases (*11*). If oleates are used, the required concentration is relatively low, of the order of 10^{-4} M, which is within physiological limits. If phospholipid is also present (Figure 5), the spherulitic cholesterol mesophase is compounded with cylindrical micelles caused by the more rapid solvation of the polar groups of the phospholipid. The presence of protein does not impede this process and may in fact at low concentrations lead to the formation of tubular structures similar to those seen in myelin from nervous tissue. An important feature of complex mesoforms, according to Brown and Shaw (*6*), is their ability to incorporate a variety of unrelated as well as related molecules. This may explain the incorporation of protein and the formation of lipoprotein macromolecules. Finean's studies showed that three lipid components are present in the concentric layers of neural myelin but that protein is required for the formation of tubes.

It seems likely that newer techniques will be required to elucidate the structure of these complex mesoforms. From the work of Chapman (*7*) and others (*25*) it seems possible that infrared spectroscopy and proton magnetic resonance may divulge details of fine structure between, for example, saturated and unsaturated phospholipids which serve as likely prototypes for many biologic mesoforms. In its simplest form, a membrane is a molecular monolayer between two liquid phases. The polar solubility of phospholipids produces momentarily an elementary membrane at an

Publication Date: January 1, 1967 | doi: 10.1021/ba-1967-0063.ch011

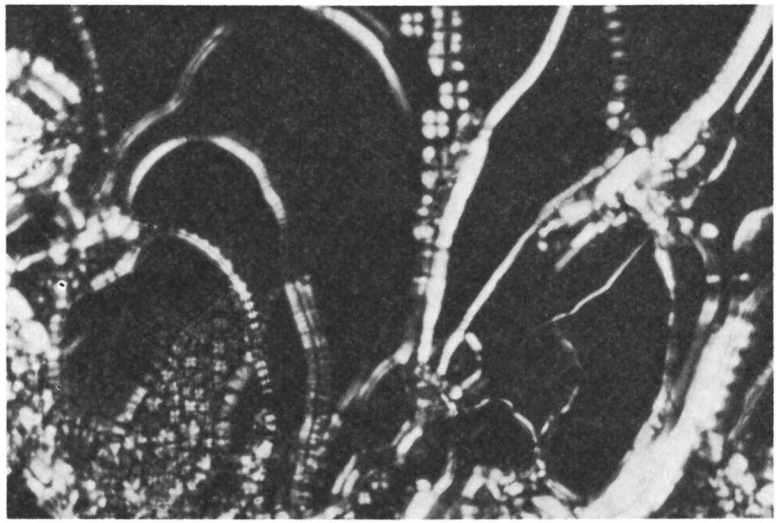

Figure 6. Complex lyotropic mesophase at interface of cholesterol (solid phase), phospholipid (amphiphile), and water (solvent)
Polarized light × 100

Publication Date: January 1, 1967 | doi: 10.1021/ba-1967-0063.ch011

aqueous interface, which can be stabilized if an oil phase is also present to attract the hydrocarbon chain. No chemical change and no activation energy are required for the formation of such systems; yet they represent a transition, in the case of the liquid phase, from a random to an ordered system with a natural limitation upon growth governed by the conditions of phase equilibria.

Nature of Biologic Mesoforms

If the physicochemical models described above are valid, the formation of small ordered micellar structures, such as lysosomes and mitochondria (*1*) within cells, and of the cell membrane itself is more easily understood, for it has long been known that phospholipids are integral components of these structures. The lipoproteins of plasma (*43*) contain, in addition, relatively large amounts of free and esterified cholesterol, together with triglyceride in the lower density fractions. There is a reciprocal relationship between the protein (globulin) and the lipid components: Increase in the former raises the density and gives a colloid solution; increase in the latter lowers the density and produces either a mesophase, with excess cholesterol and phospholipid, or a micellar suspension (chylomicrons) when triglycerides are the predominant lipids. In the mesophase of atheroma, cholesterol, phospholipid, triglycerides, protein, electrolytes, and water are all present (*38*) and form spherulitic structures which, in a limited mesothermal range of about 4°–42°C., grow into complex secondary structures (Figure 6) with a central homeotropic mesophase, a rising order of circum-

ferential colors, and a positive optical sign (Figures 7 and 8). This structure has considerable stability to physical and chemical stresses (Table I) but is irreversibly destroyed by sudden cooling or exposure to organic solvents. To form these structures and understand their origin, the best experimental model is the living animal. If microcrystalline cholesterol is injected intraperitoneally into a mouse, it appears an hour or two later as liquid crystalline spherulites within the living leucocytes of the peritoneal exudate and also in the regional lymph glands, or if cholesterol is fed to a rabbit, there is at first a rise in the low-density lipoprotein mesophase of the plasma and then deposition of atheroma lipid in a similar mesoform.

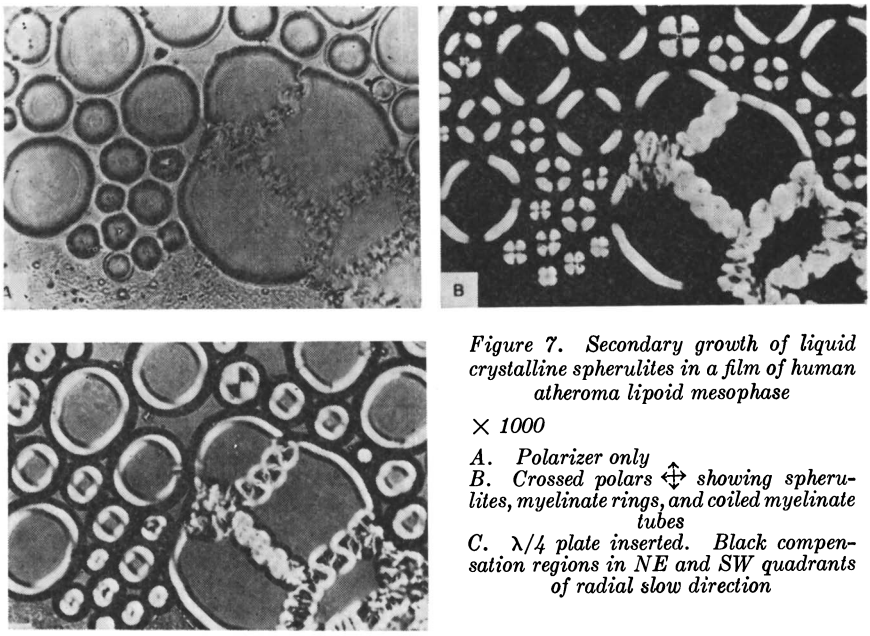

Figure 7. Secondary growth of liquid crystalline spherulites in a film of human atheroma lipoid mesophase

× 1000

A. Polarizer only
B. Crossed polars ⇳ showing spherulites, myelinate rings, and coiled myelinate tubes
C. λ/4 plate inserted. Black compensation regions in NE and SW quadrants of radial slow direction

Cholesterol and phospholipid are present in many tissues, and it is possible, though unproved, that they exist outside the systems mentioned in liquid crystalline form. One interesting possibility is the eye. Pirie (*30*) has shown that cholesterol and its esters are present in the tapetum lucidum, backing the retina, of the opossum. Some years ago, Pirie kindly showed me her preparations of this tissue, and there was no doubt that cholesterol was present in liquid crystalline form, but since the tissue had been excised, one could not exclude an artifact. Since then, Fergason (*14*) has demonstrated iridescence in mixtures of cholesterol esters, and it is known that unpolarized light is split by thin layers of these substances into a transmitted beam (clockwise) and a reflected beam (anticlockwise). The need for a mirror backing to the retina has already been stated by Pirie, and

Publication Date: January 1, 1967 | doi: 10.1021/ba-1967-0063.ch011

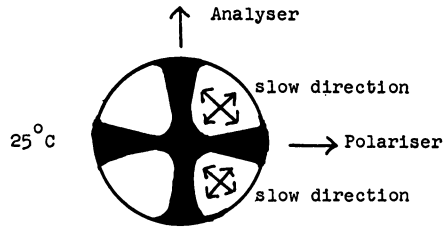

Primary structure: spherulite with polarisation color first order white.

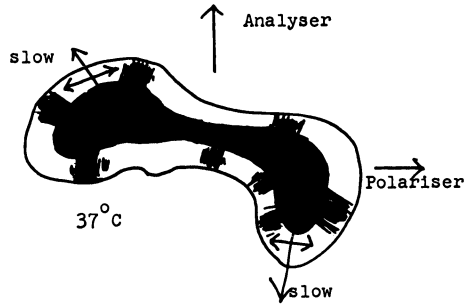

Myelinate figure produced by compression or heating within mesothermal range.

Figure 8. Diagrammatic analysis of spherulite from atheroma mesophase
Primary structure

it is tempting to speculate that, in the opossum at least, this property of cholesterol is connected with vision. Fergason's experiments show also that cholesterol esters in thin layers change in iridescence and therefore, presumably, in orientation when exposed to strain, to certain vapors, and to small changes in temperature; it seems possible, therefore, that the liquid crystalline structure of this substance and of its esters might have a functional role in other organs.

In this paper, I have dealt mainly with lipid and lipoprotein mesoforms which are familiar to me, but for completeness it is necessary to mention briefly some proteins, polypeptides, and polynucleotides, which can also assume liquid crystalline form. The outstanding example is poly-γ-benzyl-L-glutamate, which Robinson (*31*) has shown to exist as a liquid crystalline α-helix in organic solvents. Paracrystalline forms of nucleoprotein have been recognized in vitro since 1955 (*13*, *18*), but more recently Wilkins and his colleagues (*34*) have shown that transfer RNA of cellular origin also has a twisted liquid crystalline structure. Among the proteins, it is well known that myosin exhibits changes in birefringence during contraction (*2*),

Publication Date: January 1, 1967 | doi: 10.1021/ba-1967-0063.ch011

and this would seem to be an ideal elongated protein for direct observation of a functional mesophase.

Conclusions

The presence of lipid, protein, and other substances in various forms of lyotropic mesophases explains many of the properties which distinguish protoplasm from inanimate colloid or even,in more general terms, some of the essential differences between the physical structure of living and nonliving matter. In the living cell or tissue, the essential components invariably have a functional as well as a structural role, even if they are relatively rigid. Most biochemical reactions proceed, normally, in liquid phases and, intravitally, are mediated by cell membranes, tissue interfaces, and subcellular particles or organelles such as lysosomes and mitochondria. The existence of the mesophase in these structures offers on explanation of how structure and position can be maintained in the liquid state and, more important, how a preferred orientation of reactive or structurally vital molecules can be maintained in the liquid state. The preservation of orientation while flow develops is the primary characteristic of any mesophase, but, in the lyotropic mesophases, an additional provision for mobility and reactivity is introduced by the solvent and amphiphile. In the simplest case, a polar substance like phospholipid or soap forms a reactive interface with water; if protein in aqueous or electrolytic solution is introduced, a

Table I. Properties of Lipoprotein Mesophase of Atheromatous Tissue

Physical	
Mesothermal range	0°–42°C.
−20°C. (30 min.)	99% disintegration
−185°C. (2 min.)	100% disintegration
Ultrasonic vibration (2 min.)	No change
Ultrasonic vibration (10 min.-ice-cooled)	100% disintegration
Dehydration	Unstable
Ultracentrifugation	Stable at 70,000 g
γ-Radiation	Stable to 5 Mrads
Linear accelerator	Stable to 4 m.e.v.
Optical sign	Positive
Chemical	
Triglyceride lipase	Stable
Lipoprotein lipase (clearing factor)	Stable
Esterase	Stable
Surfactants	Relatively stable
Mineral acids	Relatively stable
Water	Secondary growth
Electrolytic solution	Secondary growth
Glycerol	Equilibrium
Organic solvents	Unstable
Benzpyrene	Stable (fluorescence)
Sudan dyes	Minimal solubility

In Ordered Fluids and Liquid Crystals; Porter, R., el al.;
Advances in Chemistry; American Chemical Society: Washington, DC, 1967.

lipoprotein with ionic linkage is formed, behaving at the interface like an elementary cell membrane or, in dispersion, as a micelle capable of incorporating other related molecules and even some unrelated ones. This is probably the essential structure of a lysosome, which has been described (*9*) as a "lipoprotein bag of hydrolytic enzymes." Experimental models of biologic mesoforms are optimally stable within a limited thermal range of 4°–42°C., and it seems no accident that this same range represents the usual limits of metabolism and growth in all forms of life.

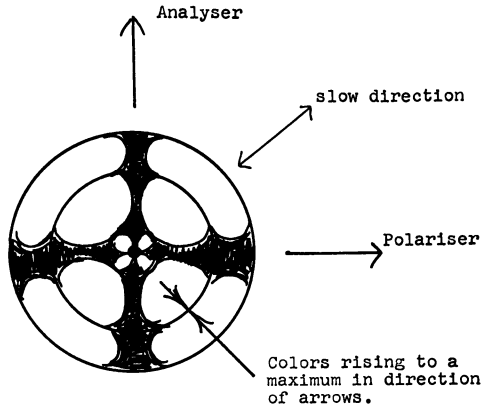

Figure 9. Diagrammatic analysis of spherulite from atheroma mesophase

Secondary structure

The properties of a stable yet dynamic mesophase are therefore consistent with physicochemical conditions appropriate to living cells, tissue, and body fluids, involving a variety of organic molecular and macromolecular aggregates, and playing a part in physiological and pathophysiological processes. There may, however, be a more fundamental role for the lyotropic mesophase. The essential condition for the development of a mesophase is the contiguity of aggregates of more than one amphiphilic molecules with more than one solvent molecule. Given this approximation, the mesophase will develop if the thermal range is appropriate but apparently without further external activation. Even a small aggregate will develop into a complex structure which will reach an equilibrium governed mainly by random factors of concentration and temperature. The structure is maintained, as in a thermotropic mesophase, by simple linkages and van der Waals forces (*3*); chemically, the molecules are unchanged, but physically they are aggregated, orientated, stable yet mobile. When the process of orderly aggregation starts, it replicates the molecular pattern and sequence faithfully until equilibrium conditions are reached. If it is assumed that in warm primeval liquids, simple lipids and elementary peptides ex-

Publication Date: January 1, 1967 | doi: 10.1021/ba-1967-0063.ch011

isted, it can equally be assumed that some of these molecules would come into contact with each other by chance. In this event, orderly aggregation in mesophase would occur sooner or later. In so far as it is a vital element when detected in living matter, the lyotropic mesophase might therefore also be a key biodynamic factor in the transformation of certain organic molecules with salts and water into living matter.

Literature Cited

(1) Ambrose, E. J., "Progress in Biophysics and Biophysical Chemistry," Pergamon Press, New York, 1958.
(2) Apsley, T., Gurnes, E. F., "Tissue Elasticity," J. W. Remington, ed., American Physiological Society, Washington, D. C., 1957.
(3) Bernal, J. D., Faraday Society Symposium, p. 1082 (1933).
(4) Bernal, J. D., Faukuchen, I., *Nature* **139**, 923 (1937).
(5) Boffey, B. J., Collison, R., Lawrence, A. S. C., *Trans. Faraday Soc.* **55**, 650 (1959).
(6) Brown, G. H., Shaw, W. G., *Chem. Rev.* **57**, 1049 (1957).
(7) Chapman, D., *J. Am. Oil Chemists' Soc.* **42**, 353 (1965).
(8) Clunie, J. S., Corkill, J. M., Goodman, J. F., *Proc. Roy. Soc. (London)* **A285**, 520 (1965).
(9) de Duve, C., *Symp. Soc. Exptl. Biol.* **10**, 50 (1957).
(10) Dervichian, D. G., *Trans. Faraday Soc.* **42 B**, 180 (1946).
(11) Ekwall, P., Baltscheffsly, H., Maudell, L., *Acta. Chem. Scand.* **15**, 1195 (1961).
(12) Engstrom, A., Finean, J. B., "Biological Ultrastructure," Academic Press, New York, 1958.
(13) Fenghelman, M., *et al.*, *Nature* **175**, 834 (1955).
(14) Fergason, J. L., *Sci. American* **211**, 76 (1964).
(15) French, J. E., Robinson, D. S., Florey, H. W., *Quart. J. Exptl. Physiol.* **38**, 101 (1953).
(16) Harrison, R. G., *J. Exptl. Zool.* **32**, 1 (1921).
(17) Jacoby, F., "The Ovary," S. Zuckerman, ed., Academic Press, New York, 1962.
(18) Kacser, H., *Science* **124**, 151 (1956).
(19) Lawrence, A. S. C., *Discussions Faraday Soc.* **25**, 51 (1958).
(20) Lawrence, A. S. C., *J. Roy. Microscop. Soc.* **58**, 30 (1938).
(21) Lawrence, A. S. C., *Trans. Faraday Soc.* **29**, 1008 (1933).
(22) Luzzati, V., Husson, F., *J. Cell Biol.* **12**, 207 (1962).
(23) Luzzati, V., Mustacchi, H., Skoulios, A., Husson, F., *Acta Cryst.* **13**, 660, 668 (1960).
(24) McBain, J. W., Marsden, S. S., *Acta Cryst.* **1**, 270 (1948).
(25) *Molecular Crystals* **1**, 205 *ff.* (1966).
(26) Nageotte, J., "Actualités Scientifiques et Industrielles," No. 9, pp. 431–4: Hermann et Cie., Paris 1936.
(27) Needham, J., "Biochemistry and Morphogenesis," Cambridge University Press, 1950.
(28) Oliver, M. F., Boyd, G., *Lancet* **2**, 499 (1961).
(29) Pfeiffer, H. H., *Nature* **138**, 1054 (1936).
(30) Pirie, Antoinette, *Ibid.*, **191**, 708 (1961).
(31) Robinson, C., *Trans. Faraday Soc.* **52**, 571 (1955).
(32) Robinson, D. S., Harris, P. M., *Quart. J. Exptl. Physiol.* **44**, 80 (1954).
(33) Schmidt, W. J., "Die Bausteine des Tierkorpers in Polarisierten Lichte," Cohen, Bonn, 1924.
(34) Spencer, M., Fuller, W., Wilkins, H. H., Brown, G. L., *Nature* **194**, 1014 (1962).
(35) Stewart, G. T., *Brit. J. Exptl. Pathol.* **39**, 109 (1958).
(36) *Ibid.*, **41**, 389 (1960).
(37) *Ibid.*, **43**, 345 (1962).
(38) Stewart, G. T., *J. Pathol. Bacteriol.* **81**, 385 (1961).

Publication Date: January 1, 1967 | doi: 10.1021/ba-1967-0063.ch011

In Ordered Fluids and Liquid Crystals; Porter, R., el al.;
Advances in Chemistry; American Chemical Society: Washington, DC, 1967.

(39) Stewart, G. T., *Nature* **183**, 873 (1959).
(40) *Ibid.*, **192**, 624 (1961).
(41) Stoeckenius, W., *J. Cell Biol.* **12**, 221 (1962).
(42) Virchow, R., *Virchows Arch.* **6**, 562 (1954).
(43) Washington, D. C.: Symposium on Lipoproteins and Ultracentrifugal Technique, Technical Group and Committee on Atherosclerosis, U. S. Public Health Service, 1952.

RECEIVED February 11, 1966.

12

Liquid Crystalline Nature of Phospholipids

DENNIS CHAPMAN

Molecular Biophysics Unit, Unilever Research Laboratory, The Frythe, Welwyn, Herts, England

Publication Date: January 1, 1967 | doi: 10.1021/ba-1967-0063.ch012

Phospholipids are important components of biological membranes. Various classes of phospholipid occur, and within each class, a distribution of fatty acid residues is found. A variety of physical techniques have shown that a number of pure phospholipids undergo a transition from a crystalline to a liquid crystalline form at a temperature dependent upon the presence and type of unsaturation in the fatty acid residues. The implications of these results to the dispersibility of phospholipids in water, the formation of myelin tubes, the production of model membranes, and to the natural biological systems, are discussed.

Phospholipids were first observed as long ago as 1811 in material extracted from brain, but it is only in recent years that interest has sharpened in their properties and functions because these molecules are important constituents of biological membranes. In particular, nervous tissue in animals is rich in phospholipid, and 25 to 30% of the dry weight of the adult brain contains these molecules. The present interest in the properties of phospholipids springs from a number of directions, including considerations of the architecture of biological membranes, the diseases of atherosclerosis and coronary thrombosis, the nature of the nerve impulse and the ion pump, the structure of the fatty sheath, called myelin, surrounding nerve fibers, and the effects of demyelination. The organization in chloroplasts and mitochondria, of chlorophyll and enzyme systems respectively, may also be dependent upon phospholipids.

Various types of phospholipids occur in biological membranes, the most important of which are phosphatidylethanolamines, phosphatidylcholines (lecithins), phosphatidylserines, and sphingomyelins (Figure 1). Mixtures of these classes occur in the biological membranes, and the proportions of these classes vary from one animal to another (*17*). The fatty acid residues associated with a given type of phospholipid in biological membranes usually show a distribution in chain length and in degree of unsaturation.

In Ordered Fluids and Liquid Crystals; Porter, R., el al.;
Advances in Chemistry; American Chemical Society: Washington, DC, 1967.

Analysis of natural phospholipids shows that, in general, there is a saturated fatty acid in the 3-position and an unsaturated fatty acid in the 2-position of the phospholipids (*11*) (*see* Figure 1). Stearic, palmitic, and myristic acids are common among the saturated fatty acids present, and oleic acid is common among the unsaturated fatty acids. The reasons for this distribution of fatty acid residues associated with a given phospholipid in biological tissues are not understood, nor is it clear why, corresponding to the occurrence of certain diseases, these characteristic fatty acid patterns are sometimes altered. Our present studies should throw some light on these questions.

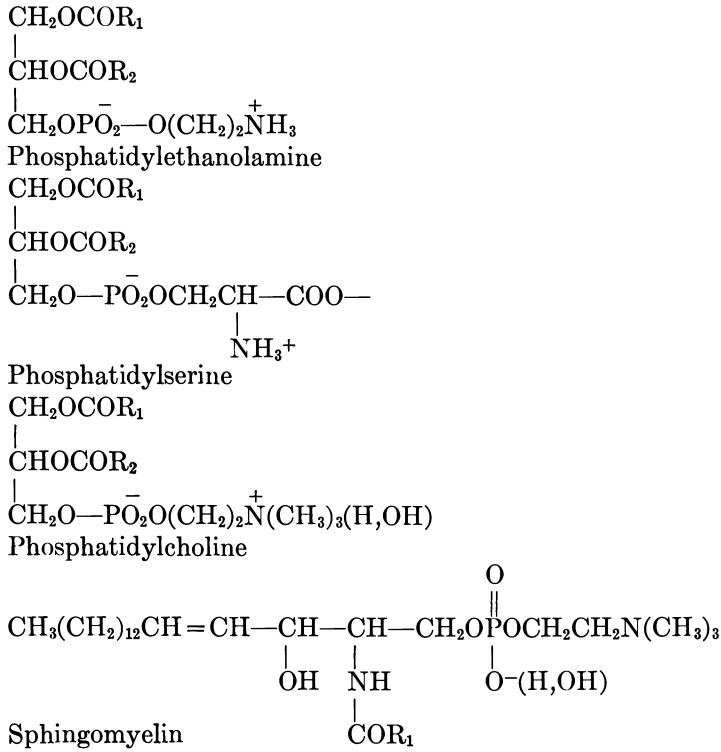

Figure 1. Molecular structure of types of phospholipid in biological membranes

Recently it was shown (*2*) that when a fully saturated phospholipid is heated, a marked change takes place in the appearance of the infrared spectrum, corresponding to a transition from a crystalline to a liquid crystalline phase, many tens of degrees below the reported capillary melting point. Phospholipids therefore exhibit thermotropic mesomorphism. In this paper we discuss the results obtained by other techniques which we have been using in our laboratory for the study of phospholipids.

Publication Date: January 1, 1967 | doi: 10.1021/ba-1967-0063.ch012

Experimental Studies

Differential Thermal Analysis Studies. Recent studies of pure anhydrous phospholipids (*7*) using differential thermal analysis (DTA) have revealed the existence of more than one thermal transition when a phospholipid is heated. Thus, 2,3-dimyristoyl-DL-phosphatidylethanolamine shows on heating a marked endothermic transition at about 120°C. and a smaller endothermic transition at about 135°C. (Figure 2). The major thermal transition is not immediately reversible with the phosphatidylethanolamines, and even holding at room temperature for some days does not produce complete reversion to the original form. The transition with the phosphatidylcholines, in contrast, is lower for the same fatty acid residues and is reversible in character. When one of the chains is unsaturated with a cis group, as occurs with a phospholipid such as 3-stearoyl-2-oleoylphosphatidylethanolamine, the main endothermic transition occurs at a lower temperature, about 70°C. The transition temperatures for

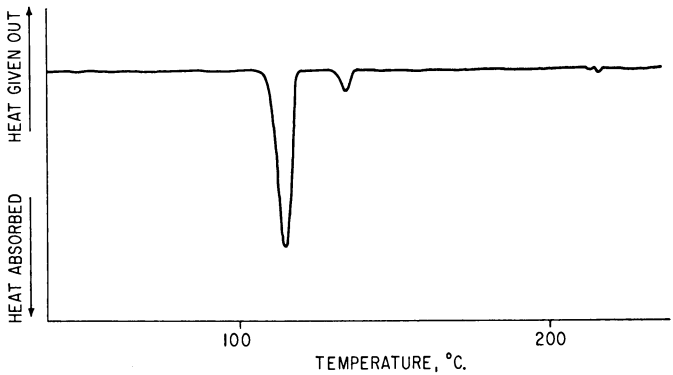

Figure 2. Differential thermal analysis heating curve of 2,3-dimyristoyl-DL-1-phosphatidylethanolamine

phospholipids containing trans groups are at higher temperatures. Little heat change is observed at the temperature corresponding to the capillary melting point of the phospholipids, and it is presumed that this temperature corresponds to the breakdown of the ionic sheets of the molecule. Other phospholipids, such as sphingomyelins, phosphatidylserines, and natural lipid molecules, also show similar marked endothermic transitions many degrees below the capillary melting point. Egg yolk phosphatidylcholine, which has been the subject of many investigations, shows a marked endothermic transition at about 20°C. A number of DTA curves of phospholipids are shown in Figure 3. In the presence of water, the endothermic transitions occur at lower temperatures than in the anhydrous condition.

X-Ray Studies. Single-crystal x-ray studies of phospholipids are in progress in our laboratory but are not yet complete. Several studies using

x-ray powder methods have been carried out (*6*, *12*, *13*). With long-chain crystals the spacings on the x-ray powder photographs fall into two types, called long and short spacings. This division into two types of spacing arises from the considerable difference which exists between the length of the molecules and their width. For a particular polymorphic form the x-ray short spacings are similar from one homolog to another and with the phospholipids are found to be similar to those which occur with other long-chain crystals, such as fatty acids, esters, and glycerides. The long spacings are known to vary with the length of the molecule, and the molecules

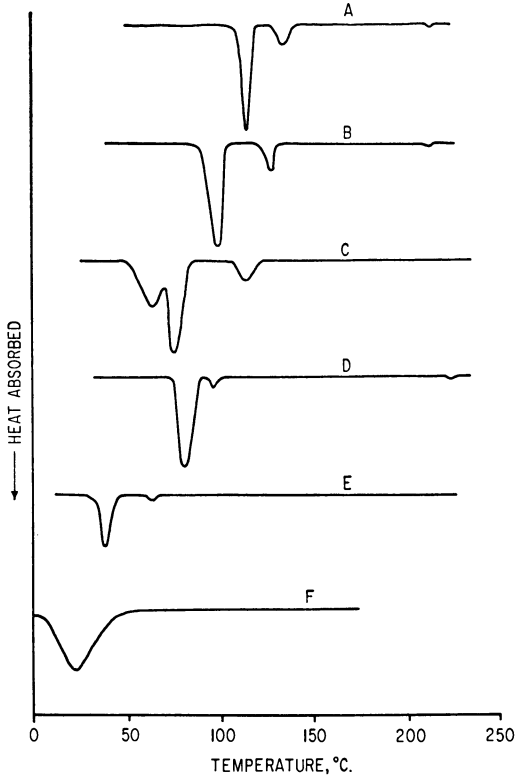

Figure 3. Series of differential thermal analysis heating curves of various phospholipids (6)

A. 2,3-Dimyristoyl-DL-1-phosphatidylethanolamine
B. 2,3-Dielaidoyl-DL-1-phosphatidylethanolamine
C. 2-Oleoyl-3-stearoyl-DL-1-phosphatidylethanolamine
D. 2,3-Distearoyl-DL-1-phosphatidylcholine
E. 2-Oleoyl-3-stearoyl-DL-1-phosphatidylcholine
F. Egg yolk lecithin

Publication Date: January 1, 1967 | doi: 10.1021/ba-1967-0063.ch012

can be at different angles to the crystallographic planes. By plotting the long spacings as a function of chain length of a number of homologs, it is possible to deduce approximately the angle of tilt of the molecules in the unit cell. The effect of heat on the phospholipids, such as the 2,3-dimyristoyl-DL-phosphatidylethanolamines, is to produce at the crystalline-to-liquid crystalline transition, at 120°C., a sudden considerable reduction in the long spacing. Further heating to about 140°C. produces a further, but smaller, reduction in the long spacing. This reduction in long spacing occurs at lower temperatures with phospholipids containing unsaturated chains and, significantly, at temperatures corresponding to those determined by differential thermal analysis. By plotting the reduced long spacings as a function of carbon number for a number of homologs, it has been possible to show that the space taken up by the polar grouping portion of the phospholipid remains unchanged in length while the transitions occur, so that the reduction in long spacing is related to phenomena associated with the hydrocarbon chains. At the temperature at which the considerable reduction in long spacing occurs, the short spacings also show a marked change. In general, the new short spacing is a diffuse line at about 4.6 A. (similar to the spacing observed with liquid long-chain hydrocarbons). The x-ray powder diagrams of unsaturated phospholipids show this diffuse short spacing at 4.6 A. at room temperature.

Infrared Spectroscopic Studies. The infrared absorption bands of a molecule in solution arise from vibrations of the whole molecule but are often associated predominantly with vibrations of functional groups such as OH and C=O groupings. With a molecule in a crystal, additional bands can arise from interactions between the vibrations of molecules in the unit cell so that different crystallographic forms can show marked differences in their associated infrared spectra (*3*). An additional effect is shown by long-chain molecules because of the possibility of rotational isomerism in the liquid state or in solution as a result of the CH_2 groups of the chain twisting and flexing. This gives rise to broad smeared-out bands in certain regions of the spectrum. In the solid state usually only one isomer occurs, and the chains lie in the all-planar trans configuration. The spectrum of a crystalline long-chain compound shows considerable fine structure, and often a regular series of bands occur in the 1250-cm.$^{-1}$ region, the number of bands being related directly to the hydrocarbon chain length.

When we examine the infrared absorption spectra of a fully saturated phospholipid, such as 2,3-dilauroyl-DL-phosphatidylethanolamine at room temperature, we note the considerable fine structure associated with the absorption bands usually observed with a molecule present in a crystalline condition. Cooling the phospholipid to liquid nitrogen temperatures shows an increase in the fine structure in the spectra, and many bands, which are single in appearance at room temperature, are observed to be split into doublets at the lower temperature. This shows that the phospholipid, al-

Publication Date: January 1, 1967 | doi: 10.1021/ba-1967-0063.ch012

though crystalline at room temperature, has some degree of mobility, probably associated with the hydrocarbon chain portion of the molecule. The absorption band associated with the CH_2 rocking mode at 720 cm.$^{-1}$, apparently single at room temperature, shows considerable splitting, and a doublet occurs at the low temperature. This doublet may indicate that the hydrocarbon chains have the orthorhombic O⊥ type packing. When

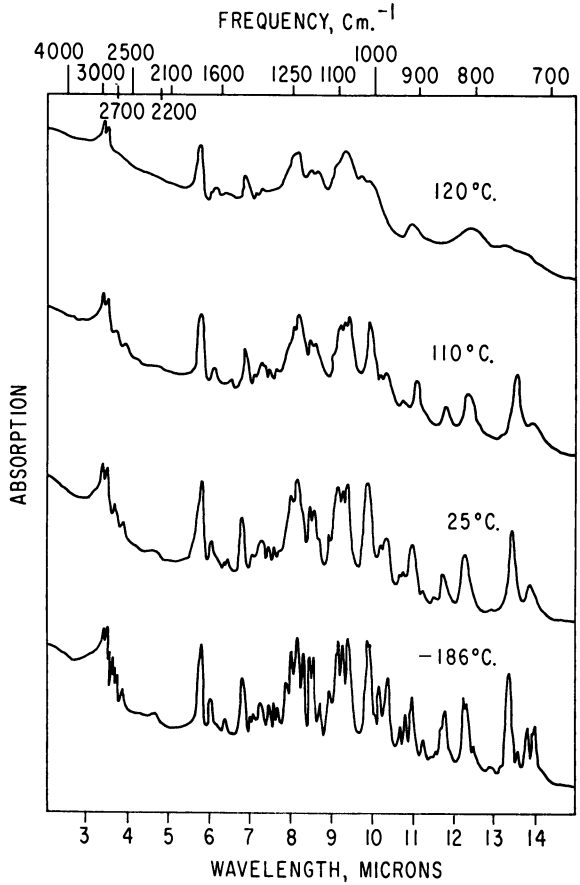

Figure 4. Infrared spectra of 2,3-dilauroyl-DL-phosphatidylethanolamine at different temperatures (6)

the phospholipid is heated and particularly when the temperature exceeds 120°C., all the fine structure in the spectrum is replaced by broad diffuse bands—i.e., the spectrum becomes similar to that normally observed with a long-chain molecule in the liquid condition, and it is clear that the hydrocarbon chain part of the phospholipids is undergoing considerable molecular motion. This is some 80° below the published capillary melting point of

Publication Date: January 1, 1967 | doi: 10.1021/ba-1967-0063.ch012

the phospholipid (Figure 4). A similar effect was observed with anhydrous sodium soaps some years ago (*4*).

The infrared absorption spectra of unsaturated phospholipids, such as 2,3-dioleoyl-DL-phosphatidylethanolamines, at room temperature are similar to those observed with a liquid. Cooling unsaturated phospholipids, such as 2-oleoyl-3-stearoylphosphatidylcholine (lecithin), to lower temperatures enables a crystalline-type spectra to be obtained. This is in agreement with the DTA results, which show that the transition temperature for crystalline to liquid crystalline is lower with the unsaturated than with the saturated phospholipids. When this particular phospholipid is heated to about 40°C., the spectrum is replaced by one in which all the fine structure vanishes, and the spectrum is again typical of that observed with a liquid (*5*).

Nuclear Resonance Studies. The technique of nuclear magnetic resonance spectroscopy has also been applied to the study of pure phospholipids in our laboratory. With a solid, because of magnetic dipole interactions between the magnetic nuclei, the nuclear magnetic resonance usually occurs over a broad region of magnetic field and, therefore, a broad absorption band is observed. As molecular motion increases, the magnetic interactions between the magnetic nuclei become averaged out, and if the frequency of the motion exceeds a certain value, the resulting absorption band is narrowed. From the narrowing of the line it is therefore possible to deduce the degree of molecular motion concerned.

The studies of the proton resonance spectrum of pure anhydrous phospholipids show that with a fully saturated phospholipid, such as 2,3-dimyristoyl-DL-phosphatidylethanolamine (Figure 5), the line width at liquid nitrogen temperature is about 15 gauss and decreases with increasing temperature, showing that some molecular motion is occurring. As the temperature approaches 120°C., the line width falls at a considerably increased rate, giving rise to a very narrow line ~0.09 gauss wide (*10*). This line is sufficiently narrow to be observed with high resolution nuclear resonance techniques (*6*). As the resonance spectrum is being produced by the hydrogen nuclei in the phospholipid molecule, this indicates the very high degree of molecular motion which occurs with the hydrocarbon chains of the phospholipid. In agreement with the results obtained with other physical techniques, the liquid crystalline transitions of the unsaturated phospholipids occur at lower temperatures.

Electron Microscope Studies. Electron microscope studies of phospholipids have been made by many investigators, but in general the material used has been natural phospholipid and particularly egg yolk phosphatidylcholine. Recently we have studied some pure phosphatidylethanolamines (*8*). Fully saturated phospholipids are crystalline at room temperature and show no interaction with the material commonly used for staining purposes—i.e., osmium tetroxide. If these phospholipids are

Publication Date: January 1, 1967 | doi: 10.1021/ba-1967-0063.ch012

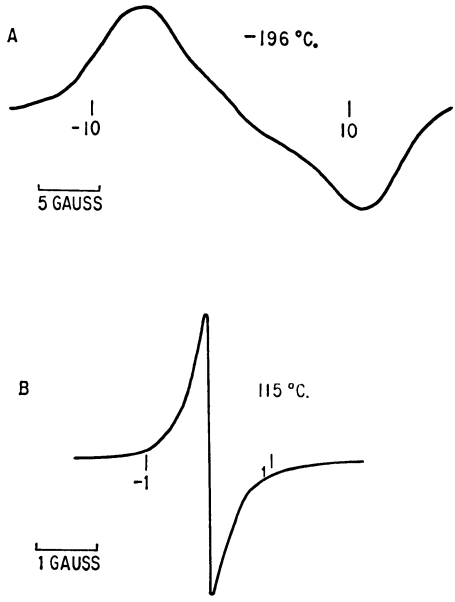

Figure 5. Proton resonance spectra of 2,3-dimyristoyl-DL-phosphatidylethanolamine
A. −196°C.
B. 115°C.

heated in the presence of water, because of the interaction of the water with the phospholipid, the endothermic transition temperature is reduced from 120° to 80°C. At this temperature myelin tubes are formed, and it is possible to stain these with osmium tetroxide. Negative staining techniques have also been used. The lines in the electron micrograph are similar to those observed with biological tissues fixed at room temperature.

Monolayer Studies. Monolayer studies of phospholipids have been carried out for a number of years, in general, with natural phospholipid mixtures and, in the vast majority of cases, with egg yolk phosphatidylcholine. In recent years a few studies have been made with pure synthetic phospholipids (*1*, *18*). These show that the fully saturated phospholipids exhibit at room temperature monolayers which are more condensed than the unsaturated phospholipids containing cis hydrocarbon chains. The monolayers obtained with phosphatidylcholines are much more expanded than the corresponding phosphatidylethanolamines. These results can be compared with the DTA results discussed above. A high transition temperature for liquid crystal formation is, in general, correlated with a condensed-type monolayer and a low transition temperature with an expanded film. The DTA transition temperatures are higher for the phosphatidylethanolamines than the corresponding phosphatidylcholines. Phospholipids containing trans unsaturated chains have high transition tempera-

Publication Date: January 1, 1967 | doi: 10.1021/ba-1967-0063.ch012

tures and give condensed monolayers similar to those observed with fully saturated phospholipids (*9*).

Conclusions

Pure phospholipids all undergo a transition from crystalline to the liquid crystalline phase many degrees below the capillary melting point. In the liquid crystalline phase the hydrocarbon chains are in a fluid condition. In the presence of water this transition temperature is lowered. At this temperature myelin tubes are formed, and the phospholipids can be more easily dispersed. The temperature for lyotropic transitions from lamellar to hexagonal phases is also related to this temperature.

A number of implications arise from these studies:

The ability to disperse phospholipids in water is related to the melting transition temperature of the hydrocarbon chains. (An analogous situation is observed with soaps, where the ability to disperse occurs only above a temperature which is nearly constant over a wide range of concentrations and varies with the chain length.) At room temperature the fully saturated phospholipids cannot readily be dispersed in water. On the other hand, the natural unsaturated phospholipids disperse readily (*16*). Raising the temperature increases the dispersibility of the fully saturated phosphatidylethanolamines.

The swelling of phospholipids in water, with the formation of myelin tubes, is also related to this transition temperature. With highly unsaturated phospholipids, such as egg yolk lecithin, myelin tube formation occurs readily at room temperature, but with the fully saturated phospholipids it occurs at higher temperatures.

Brain phospholipid can exist in the presence of water in two different phases (*15*), the usual so-called lamellar phase and a hexagonal phase dependent upon temperature and concentration. The temperature at which a particular phase of this type can exist for a given phospholipid will also depend upon the transition temperature for melting of the hydrocarbon chains.

Model phospholipid membranes of bilayer dimensions have been made with egg yolk phosphatidylcholine, but the formation of membranes becomes impossible as the temperature of preparation is lowered from 36° to 20°C. (*14*). This is probably related to the degree of fluidity of the hydrocarbon chains of the lipid at the temperature of the experiment, and the DTA results on egg yolk phosphatidylcholine are of interest in this respect.

We can envisage that the distribution of fatty acid residues observed with the phospholipids in biological tissues provides the correct fluidity at a particular environmental temperature to match the required diffusion or rate of metabolic processes required for the tissue. Thus in membranes where metabolic and diffusion processes must be rapid, such as in the mito-

Publication Date: January 1, 1967 | doi: 10.1021/ba-1967-0063.ch012

In Ordered Fluids and Liquid Crystals; Porter, R., el al.;
Advances in Chemistry; American Chemical Society: Washington, DC, 1967.

chondria, the average transition temperature of the phospholipids present will probably be low compared with the biological environmental temperature, while in membranes where these processes are slow—e.g., in myelin of the central nervous system—the average transition temperature will be higher and may be close to that of the biological environmental temperature.

Literature Cited

(1) Anderson, P. J., Pethica, B. A., "Biochemical Problems of Lipids," Butterworth and Co., London, 1956.
(2) Byrne, P., Chapman, D., *Nature* **202**, 987 (1964).
(3) Chapman, D., *J. Am. Oil Chemists Soc.* **42**, 353 (1965).
(4) Chapman, D., *J. Chem. Soc.* **1958**, 784.
(5) Chapman, D., "Structure of Lipids," Methuen, London, 1965.
(6) Chapman, D., Byrne, P., Shipley, G. G., *Proc. Roy. Soc.* **A290**, 115 (1966).
(7) Chapman, D., Collin, D. T., *Nature* **206**, 189 (1965).
(8) Chapman, D., Fluck, D. J., *J. Cell. Biol.* **30**, 1 (1966).
(9) Chapman, D., Owens, N. F., Walker, D. A., *Biochem. Biophys. Acta* **120**, 148 (1966).
(10) Chapman, D., Salsbury, N. J., *Trans. Faraday Soc.* **62**, 2607 (1966).
(11) de Haas, G. H., van Deenen, L. L. M., *Rec. Trav. Chim. Pays Bas* **80**, 951 (1961).
(12) Finean, J. B., *Biochim. Biophys. Acta* **10**, 371 (1953).
(13) Finean, J. B., Millington, P. F., *Trans. Faraday Soc.* **51**, 1008 (1955).
(14) Huang, C., Wheeldon, L., Thompson, T. E., *J. Mol. Biol.* **8**, 148 (1964).
(15) Luzzati, V., Husson, F., *J. Cell. Biol.* **12**, 207 (1962).
(16) Saunders, L., *J. Pharm. Pharmacol.* **G.B. 9**, 834 (1957).
(17) van Deenen, L. L. M., "Progress in the Chemistry of Fats and Other Lipids," Vol. 8, Part I, "Phospholipids and Biomembranes," 1965.
(18) van Deenen, L. L. M., Houtsmuller, U. M. T., de Haas, G. H., Mulder, E., *J. Pharm. Pharmacol.* **14**, 429 (1962).

RECEIVED February 11, 1966.

13

Paramyosin, a Model α-Helical Protein

LYNN M. RIDDIFORD

Biological Laboratories, Harvard University, Cambridge, Mass. 02138

Paramyosin is proposed as a model protein helix upon which to base optical rotatory dispersion estimates of protein helical content. It is suggested that this rigid two-chain coiled coil is one chain with the proline residues comprising the hairpin turn. ORD studies from 600 to 190 mμ for the native helix and to 205 mμ for the 7M guanidine-denatured molecule were performed and analyzed. In both the 600- to 300-mμ and the 315- to 240-mμ regions, the Moffitt parameters are shown to be colinear with $[m']_{232}$ *but not with* λ_c*, over the entire three-step helix-coil transition. An estimate of helical content for myoglobin based on the paramyosin parameters (using* b_0 *as the most reliable index) agrees well with the x-ray crystallographic analysis.*

Optical rotatory dispersion (ORD) is one of the common methods of investigating protein conformation. Most native globular proteins show simple dispersion in the visible spectrum (*63*), and thus, the data can be described by the one-term Drude equation,

$$[m']_\lambda = \frac{k}{\lambda^2 - \lambda_c^2} \tag{1}$$

where $[m']_\lambda$ is the reduced mean residue rotation. By contrast, the soluble fibrous proteins and helical synthetic polypeptides show complex dispersion (*12*, *63*). In 1956, Moffitt (*39*) proposed a theory to explain the complex dispersion of the α-helical polypeptides, from which arose the following phenomenological equation (*40*):

$$[m']_\lambda = \frac{a_0\lambda_0^2}{\lambda^2 - \lambda_0^2} + \frac{b_0\lambda_0^4}{(\lambda^2 - \lambda_0^2)^2}$$

where b_0 and λ_0 are mainly functions of the helical backbone and are relatively insensitive to environmental factors, and a_0 is a function of both intrinsic residue rotations and interactions within the helix and thus may vary with the environment. Although the theoretical basis of this equa-

In Ordered Fluids and Liquid Crystals; Porter, R., el al.;
Advances in Chemistry; American Chemical Society: Washington, DC, 1967.

tion is incomplete, its empirical use for the estimation of helical content remains valid (*54*, *63*, *66*).

ORD measurements are commonly extended into the far-ultraviolet region where the Cotton effects characteristic of the α-helix (a trough at 233 mμ and a maximum near 200 mμ) (*8*, *56*) are found. By analyzing the circular dichroic spectra of α-helical polypeptides, Holzwarth and Doty (*24*) have shown that three rotatory bands (the $n_1 - \pi^-$ transition at 222 mμ, the parallel-polarized $\pi^\circ - \pi^-$ exciton transition at 206 mμ, and the perpendicularly polarized $\pi^\circ - \pi^-$ exciton transition at 190 mμ) can account for these Cotton effects. When the polypeptide chain becomes disordered, only a single Cotton effect with a trough at 204 mμ is seen (*8*).

Previously, all the estimates of helical content of proteins have been based on the polypeptide models. Independent evidence is available for the existence of these polypeptides as α-helical rigid rods or as random coils in aqueous solution, depending upon pH [for reviews, *see 27*, *63*]. Recently, Yang and McCabe (*68*) and McDiarmid (*37*) have shown that the magnitudes of the helical Cotton effects for the fully helical polyglutamic acid (PGA) vary with pH and ionic strength; this phenomenon may be correlated with the aggregation of helical chains which apparently affects only the specific rotation and a_0 but not b_0 (*55*). In any case, PGA seems to be an inadequate model helix. Not all helical polypeptides, especially those of the aromatic amino acids, exhibit normal ORD behavior, even in the visible range (*27*). In the ultraviolet range helical aromatic polypeptides show Cotton effects in the 260- to 300 mμ region as well as anomalous Cotton effects in the far-ultraviolet region (*6*, *7*, *17*, *18*). Helical polypeptides composed of two or three amino acids, such as copoly-L-tyrosine-L-glutamic acid (5% tyrosine) (PTGA) (*17*, *61*) and copoly-L-alanine-L-lysine-L-glutamic acid (PALGA) (*19*, *62*) give somewhat different values for the Moffitt parameters than the single polyamino acids. Presumably the different values arise from the effects of the increasing number of side-chain interactions possible in these copolymers. Yet, with only two or three amino acids, the many varied types of side-chain interactions found in proteins are still not implicitly accounted for in the ORD of either the helical or the random conformation or of any mixtures of the two conformations. Consequently, a better model is a protein which is natively an α-helical rigid rod from evidence independent of ORD and which can be transformed readily and reversibly into a random coil. Also, it should contain all the common amino acids except proline, which disrupts the α-helical structure, and possibly cystine.

As originally pointed out by Cohen and Szent-Györgyi (*12*), the soluble fibrous proteins which possess the α-type wide-angle x-ray diffraction diagram, with the exception of fibrinogen, show complex rotatory dispersion similar to that of the synthetic polypeptides. Light meromyosin Fraction I (LMM Fr. I), tropomyosin, and paramyosin all have over 90% helix (*12*)

Publication Date: January 1, 1967 | doi: 10.1021/ba-1967-0063.ch013

In Ordered Fluids and Liquid Crystals; Porter, R., el al.;
Advances in Chemistry; American Chemical Society: Washington, DC, 1967.

which is correlated with their low proline content (*58*). These proteins show a 5.1-A. meridional reflection instead of the 5.4-A. pitch reflection, characteristic of the α-helical polypeptides, which both Crick (*15*) and Pauling and Corey (*44*) have attributed to the presence of a coiled coil. The two-chain coiled coil model is the best fit for the wide-angle x-ray pattern of the paramyosin-rich (over 50% of the structural protein) anterior byssus retractor muscle of the mussel *Mytilus edulis* (*10*). The physicochemical data for paramyosin, LMM Fr. I, and tropomyosin agree with the proposed two-chain structure (*34–36*, *65*). Their crystalline patterns as seen by the electron microscope are different but have some inherent similarities—namely, a repeated occurrence of the 70-A. and 140-A. spacings (*11*, *23*, *60*). The only native protein which appears to be a single α-helical chain is *Pinna nobilis* tropomyosin A (similar in amino acid composition to *Venus* paramyosin) (*28*, *29*); some controversy has arisen over existence of this protein as a single chain [for the criticism and its rebuttal, *see* (*36* and *30*)]. Certainly, *Pinna* tropomyosin is more unstable than *Venus* paramyosin since it is completely (and not entirely reversibly) denatured in 8*M* urea (*29*). *Venus* paramyosin is about two-thirds denatured in 9.5*M* urea (*12*) or in 5*M* guanidine–1.2*M* urea (*48*), and completely (and reversibly) denatured only in 7*M* guanidine-HCl (G-HCl) (*42*, *43*, *46*).

The coiled coil configuration of these proteins apparently does not alter their rotatory behavior, at least in the visible wavelength range as indicated by b_0 (*12*). This relative insensitivity is not surprising since the major helix of the coiled coil requires a tilt angle relative to the minor helix of only 10° and a twist per residue of 2.86° as compared with the twist per residue in the minor helix of 100° (*14*). Therefore, one of these three fibrous muscle proteins would be a good protein model since they are all readily available.

Paramyosin as a Model Helix

Of these three α-helical proteins, paramyosin is a suitable model helix for the following reasons:

Paramyosin is the only one for which there is experimental evidence of the existence of the two-chain coiled coil *in situ* (*10*) as well as in the dried fiber (*4*, *5*) and in solution (*36*).

Paramyosin behaves as an extremely asymmetric α-helical rigid rod in solution, as shown by its hydrodynamic and light-scattering properties (*22*, *36*), its dynamic viscoelastic behavior (*1*, *2*), the hypochromicity of its far-ultraviolet absorption spectrum (*50*), and its optical rotatory properties (*12*, *56*).

Paramyosin is reversibly denatured by 7*M* G-HCl (*42*, *43*, *46*) whereas LMM Fr. I is irreversibly dissociated into the protomyosins by 5*M* urea (*59*), and the 3.5*M* G-HCl denaturation of tropomyosin is only 80% reversible (*42*, *43*). All three proteins are insensitive to pH denaturation, except that above pH 10 tropomyosin begins to unfold partially (*34*).

Publication Date: January 1, 1967 | doi: 10.1021/ba-1967-0063.ch013

In Ordered Fluids and Liquid Crystals; Porter, R., el al.;
Advances in Chemistry; American Chemical Society: Washington, DC, 1967.

Paramyosin has, at most, 2 to 3 prolines per 220,000 molecular weight (*32*, *47*), a weight % similar to that found for LMM Fr. I. and lower than that for tropomyosin (*58*).

Paramyosin has no cystine residues and a low number of cysteine residues (*11*, *46*, *47*), whereas LMM Fr. I (*35*) has half-cystines and shows no trace of free sulfhydryl groups by the *p*-chloromercuribenzoate titration. Tropomyosin also has at least one disulfide bond (*11*) which may link the two chains of the coiled coil (*65*).

Paramyosin has 37% highly hydrophobic residues and 36% charged amino acids (*34*, *46*), and lacks only tryptophan of the common amino acids (*47*).

One uncertainty as to paramyosin structure remains: whether the coiled coil consists of two separate α-helical chains (each about 1400 A. long) or merely two parts of one 2800-A. α-helical chain with a hairpin turn near its center. From the intrinsic viscosity of the completely denatured molecule (6*M* G-HCl, 43°), Noelken (*42*) calculated a radius of gyration which agrees fairly well with that expected for a single-chain random coil with a molecular weight of 225,000. However, he also showed that two randomly coiled chains of molecular weight near 110,000 can give equally good agreement. Hydrodynamic and light-scattering studies in 7*M* G-HCl, in which the molecule exists in its random conformation at room temperature (*42*, *46*), are needed to resolve the question.

Since the molecule always refolds to its native conformation upon removal of the guanidine (*see* Table I), even after prolonged heating at 50°C. in this solvent (*46*) and since there are no disulfide bonds or other known covalent cross-links (*11*, *47*), I favor the one-chain hypothesis. It seems

Table I. Optical Rotatory Dispersion

Solvent	a_o	b_o
		Wavelength Range 600–240
0.6*M* KCl, pH 7.2	−17° ± 5°	−440° ± 3°
		Wavelength Range 600–300
0.3*M* KCl, pH 7.4[c]	−1° ± 5.4°	−574° ± 10°
0.6*M* KCl, pH 7.2[d]	+14° ± 1.4°	−600° ± 3°
7*M* guanidine + 0.6*M* KCl, pH 7.2[d]	−543° ± 5°	+20° ± 7°
		Wavelength Range 315–240
0.6*M* KCl, pH 7.2 or 0.6*M* NaF or KF, pH 7.2	−109° ± 9°	−343° ± 4°
7*M* guanidine + 0.6*M* KCl, pH 7.2	−476° ± 9°	+20° ± 4°
0.6*M* KCl, pH 7.2 after 7*M* guanidine	−106° ± 10°	−343° ± 4°

[a] All values are averages for at least 6 different preparations. Errors indicated for a_o, b_o, k_{Drude}, and λ_c are standard deviations for individual values. Errors indicated for [*m'*] values are limits of values averaged.
[b] Data from only two experiments calculated in this manner.

Publication Date: January 1, 1967 | doi: 10.1021/ba-1967-0063.ch013

unlikely that pairs of completely separated chains could reassemble in the fairly dilute solutions (about 20 μM). Also, although Ramakrishnan and Ramachandran (*45*) have recently shown that an α-helical chain can incorporate an L-proline residue towards an end with a minimum 35° angle between the two helical portions if there is a slight distortion of the planarity of the peptide group, the location of the two prolines in paramyosin at a hairpin turn would both account for the turn and least disrupt the α-helical structure of the two single chains of the coiled coil.

In the fully denatured molecule (7M G-HCl at 50°), where there is about 10% residual helix as compared with polypeptides (*46*), these proline residues might restrict complete randomness by allowing interactions between amino acids to remain in a localized region (a minimum of eight residues involved) on either side of them. Brant and Flory (*9*) have shown that only electrostatic interactions between amide groups and not specific side-chain or solvent interactions influence the configuration of random polypeptide chains if the polypeptide chain is entirely in the trans conformation. Yet, the proline peptide linkage can be either the trans or the cis conformation, and the existence of the cis conformation indicates the presence of favorable intramolecular interactions which counteract the higher energy of this conformation (*54*). In paramyosin the existence of such interactions in the random conformation cannot be ruled out. Hydrophobic interactions certainly are important in stabilizing the native coiled coil structure (*10, 34, 47, 48*) and are implicated in the denatured state (*46, 48*). These hydrophobic interactions may exist between side chains in other portions of the unfolded molecule as well as in the region of the hair-

Parameters for Paramyosin[a]

		$k_{Drude} \times 10^6$	λ_e ($m\mu$)
$m\mu$ (λ_o = *218* $m\mu$)[b]			
		Nonlinear	Nonlinear
$m\mu$ (λ_o = *212* $m\mu$)			
		Nonlinear	Nonlinear
		Nonlinear	Nonlinear
		−24.6 ± 0.2	208.2 ± 0.8
$m\mu$ (λ_o = *220* $m\mu$)[d]			
$[m']_{232}$	$[m']_{198.5}$		
−15,400° ± 150°	+70,200° ± 500°	(−23.0 ± 1.5)[e]	(236.7 ± 0.7)[e]
−2090° ± 20°	....	−23.2 ± 0.2	214.2 ± 0.4
−15,000° ± 200°	....	(−22.5 ± 1.4)[e]	(236.7 ± 0.7)[e]

[c] Recalculated from Riddiford and Scheraga (*48*), using Lorentz correction for dispersion of refractive index of water.
[d] From Table III (*46*).
[e] Parentheses indicate that these values based on assumption of a linear Drude plot are not strictly valid since larger standard deviations indicate nonlinearity.

Publication Date: January 1, 1967 | doi: 10.1021/ba-1967-0063.ch013

pin turn. A possible method for testing this hypothesis is now available. In a preliminary note, Wilchek *et al.* (*64*) report the use of sodium in liquid ammonia for the specific cleavage of *N*-proline peptides including poly-L-proline (molecular weight 1500). If this method is specific for proline linkages in proteins, then this type of reductive cleavage of denatured paramyosin should give two chains of approximately equal length and molecular weight 110,000, on the assumption that the proline residues are involved in the hairpin turn.

ORD Studies of Paramyosin

Experimental. All the ORD studies were made with paramyosin prepared from the white portion of the adductor muscle of the clam *Venus mercenaria*, as outlined by Riddiford and Scheraga (*47*). The experimental procedure has been given in detail (*46*). All ORD measurements were made on the Cary model 60 recording spectropolarimeter at 23° ± 2°C., except as otherwise noted.

The computations of the Moffitt parameters (*see* Equation 2), utilizing the statistical procedures with error analyses developed by Sogami, Leonard, and Foster (*57*) to determine the best λ_0 values, and of the Drude parameters {*see* Equation 1; a modified Drude plot of $[m']$ *vs.* $[m']\lambda^2$ (*67*) was used} with error analyses were performed with the IBM 7094 computer. Correction for the dispersion of refractive index of the solvent was made as outlined (*46*).

As shown in Figure 1, the Moffitt plot of the ORD data from 600 to 300 mμ does not differ significantly with KCl concentration. The data in

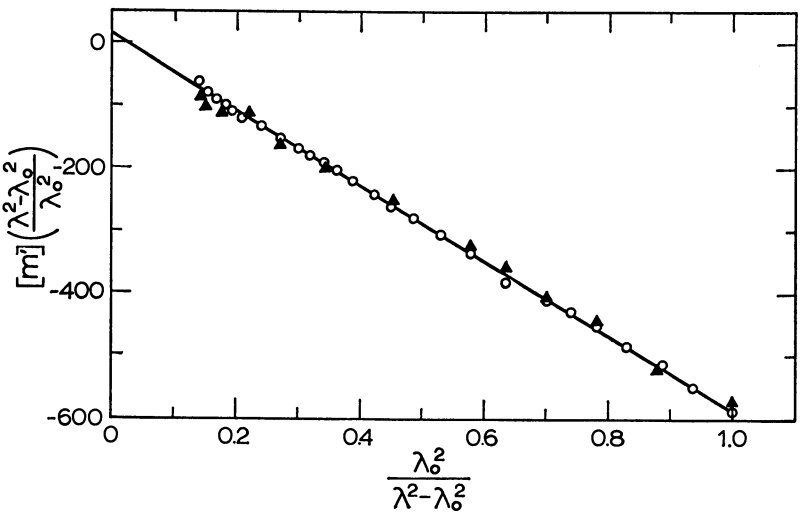

Figure 1. Moffitt plot of optical rotatory dispersion of paramyosin from 600 to 300 mμ at 24° and 20°C., respectively

○ 0.6M KCl, 0.01M phosphate buffer, pH 7.2
▲ 0.3M KCl, 0.01M phosphate buffer, pH 7.4
λ_0 = 212 mμ

Publication Date: January 1, 1967 | doi: 10.1021/ba-1967-0063.ch013

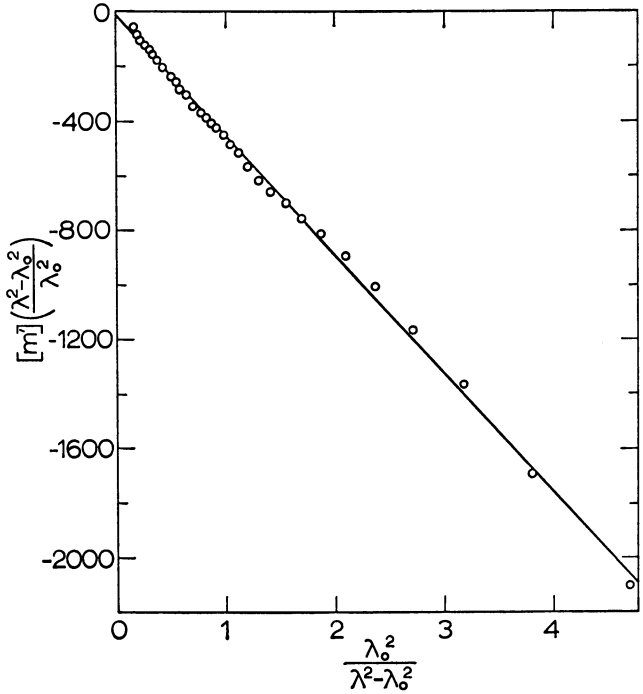

Figure 2. Moffitt plot of optical rotatory dispersion of paramyosin in 0.6M KCl, 0.01M phosphate buffer, pH 7.2, from 600 to 240 mμ at 24°C.

λ_o = *218 mμ*

0.3*M* KCl were obtained on a Rudolph model 200 polarimeter as described by Riddiford and Scheraga (*48*) and are the same as shown in Figure 2 of that paper; they have been recalculated to incorporate the correction for the dispersion of refractive index of water (*16*). The best λ_o for these data in 0.3*M* KCl is 215 mμ, but the points on the figure are those calculated with λ_o as 212 mμ since that is the best value for the more accurate Cary data in 0.6*M* KCl (the circles) for which the line shown is computed.

When the data from 300 to 240 mμ are added, the typical Moffitt plot for the native protein in 0.6*M* KCl is seen in Figure 2. The best λ_o is now found to be 218 mμ, but the deviations from the plotted line (negative above 275 mμ and positive below) are greater than seen in plots for the two separated regions (Figures 1 and 3).

Figure 3 shows typical Moffitt plots for the native and the 7*M* G-HCl denatured protein in the 240- to 315-mμ region where λ_o is 220 mμ. In this wavelength range the Drude plot for the native protein appears linear although the statistical analysis indicates much larger standard deviations for the slope and the intercept, especially the latter [nearly ten times as great as for the random form of the protein (*46*)]. Also, λ_c and the Drude

Publication Date: January 1, 1967 | doi: 10.1021/ba-1967-0063.ch013

constant obtained from a Lowry plot of the same data for the native protein do not agree. λ_c is only about 8 mμ larger, but the Drude constant is about 25% less. Table I gives the pertinent Moffitt and Drude parameters and their standard deviations for these three ranges as well as the values of $[m']_{232}$ and $[m']_{198.5}$ (the trough and the maximum of the helical Cotton effect, respectively).

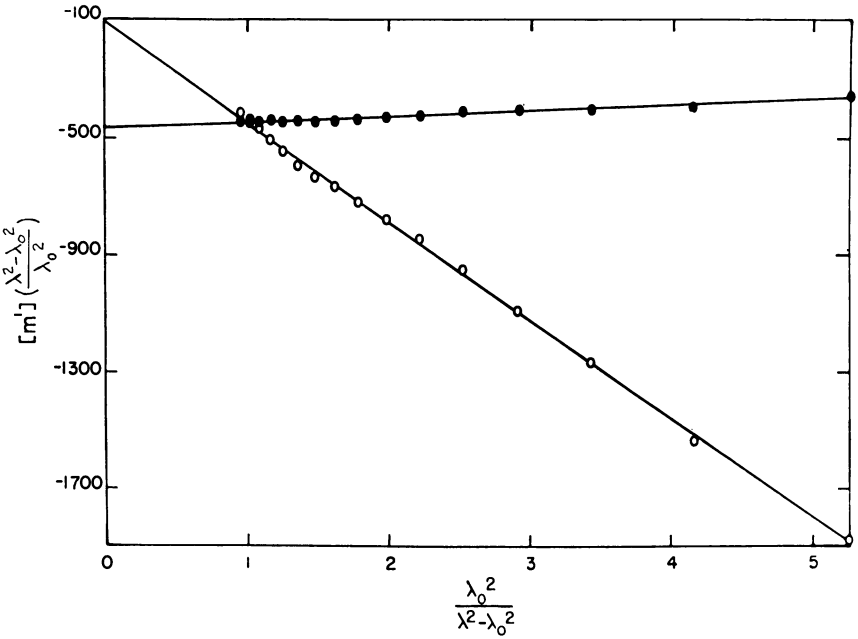

Figure 3. Moffitt plots of optical rotatory dispersion of paramyosin from 315 to 240 mμ at at 22°C. (46)

○ 0.6M KCl, 0.01M phosphate buffer, pH 7.3
● 7M guanidine–HCl (prepared with 0.6M KCl, 0.01M phosphate buffer, pH 7.3)
λ_o = 220 mμ

The helix-coil transition of paramyosin as a function of G-HCl concentration occurs in three distinct steps as measured by $[m']_{232}$ or b_o or a_o (for either wavelength region) (*46*). Figure 4 shows these transitions of $[m']_{232}$ (open symbols, solid curve) as a function of G-HCl concentration and also shows that the Drude parameter λ_c (for the 240- to 315-mμ range) (closed symbols, dashed curve) is not as sensitive to these changes. No distinct transition in λ_c coincides with the first transition in $[m']_{232}$, and only a small transition in λ_c is evident in the second step. The sharper transition in λ_c coincides with the third and final transition indicated by $[m']_{232}$ and occurs as the molecule becomes less than 30% helical and the rigorous statistical definition of the best λ_o (*57*) ceases to hold.

Publication Date: January 1, 1967 | doi: 10.1021/ba-1967-0063.ch013

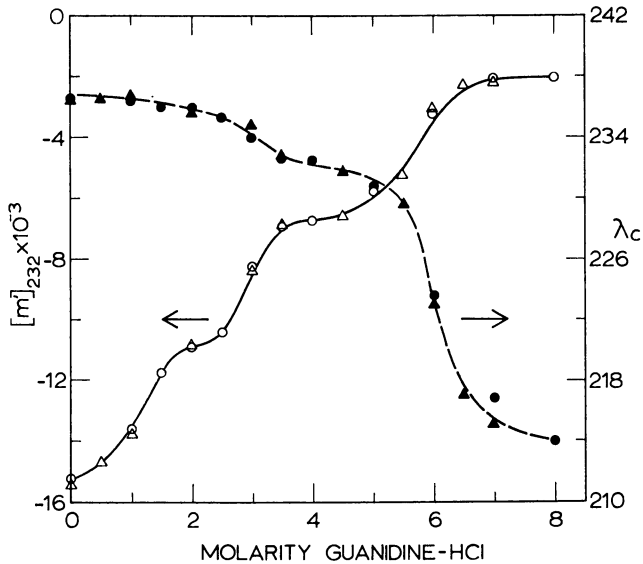

Figure 4. Reduced mean residue rotation and λ_c as a function of guanidine–HCl concentration at 25°C.

Open symbols and left-hand ordinate. 232-mμ minimum of helical Cotton effect (46)
Solid symbols and right-hand ordinate. λ_c of one-term Drude equation for 315- to 240-mμ range
Triangles and circles indicate two different stock solutions

Discussion

Mizukami (*38*) has shown that paramyosin is a mixture of monomers and dimers (monomeric molecular weight 206,000) at $\Gamma/2 = 0.25$, pH 7.8, and of monomers, dimers, and trimers at $\Gamma/2 = 0.4$, pH 7.2, but is solely in its monomeric condition at $\Gamma/2 = 0.6$, pH 7.2, as also found by Lowey, Kucera, and Holtzer (*36*). Therefore, the molecular weight of 330,000 obtained by Riddiford and Scheraga (*47*) at $\Gamma/2 = 0.3$, pH 7.4, is presumably indicative of a mixture of monomers and dimers. Yet, there is no significant difference in the values of the Moffitt parameters in the visible wavelength range (*see* Figure 1 and Table I) for these two states of aggregation. Schuster (*55*) has recently found for helical PGA that b_o is relatively insensitive to the state of aggregation whereas a_o changes. Perhaps the aggregation is more extended in his case.

Although aggregation is not the same as supercoiling, the relative insensitivity of the Moffitt parameter, b_o, to aggregation of helices leads one to suspect that supercoiling of two helices as occurs in native paramyosin also will have little effect on this parameter. Supercoiling may have an effect upon the specific rotation at one wavelength, particularly the rotation at the trough of the helical Cotton effect at 233 mμ. For paramyosin, the difference in $[m']_{232}$ between the helical and random conformations is

Publication Date: January 1, 1967 | doi: 10.1021/ba-1967-0063.ch013

$-13{,}300°$ (*46*), which is slightly less than the values for PGA of $-14{,}000°$ to $-14{,}500°$ found by various workers (*25*, *26*, *51*, *68*). Whether this decrease is caused by supercoiling or by specific side chains and/or their interactions within the molecule is not known. Optically active transitions of the aromatic chromophores of phenylalanine, tyrosine, tryptophan, and histidine occur in the 210- to 230-mμ region as well as in the 250- to 300-mμ region (*6*, *7*, *17*, *18*, *49*). The random incorporation of as little as 5% tyrosine or phenylalanine into PGA decreases the absolute magnitude of $[m']_{233}$ (*17*, *51*), apparently a result of such aromatic transitions. Rosenberg (*49*) suggests that these aromatic effects will generally be accommodated in the Moffitt parameter a_o unless very large, in which case they will drastically change λ_o, as is observed in native carbonic anhydrase (*3*, *49*), where aromatic Cotton effects which are observable in the 260- to 300-mμ region (*3*, *13*, *41*, *49*) apparently dominate the far-ultraviolet ORD (*49*).

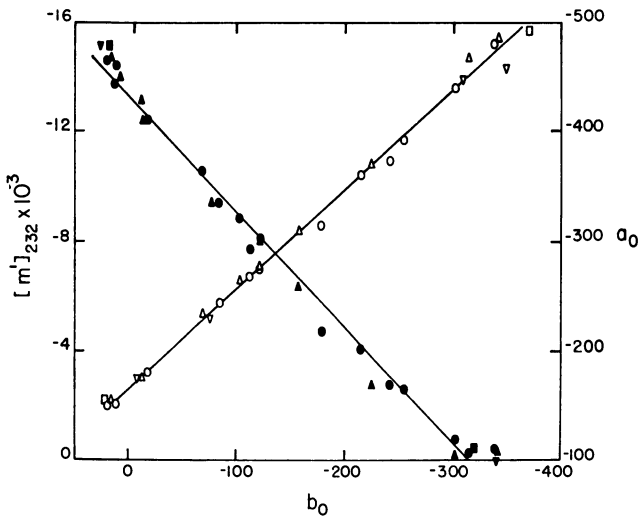

Figure 5. Reduced mean rotation and a_o as a function of the Moffitt parameter, b_o, for the entire helix-coil transition of paramyosin in guanidine–HCl at 25°C. (46)
Open symbols and left-hand ordinate. 232-mμ minimum of helical Cotton effect
Solid symbols and right-hand ordinate. Moffitt parameter a_o
Moffitt parameters calculated from optical rotatory dispersion data from 315 to 240 mμ using λ_o = 220 mμ

For paramyosin $[m']_{232}$ and the Moffitt parameters a_o and b_o are colinear for the entire helix-coil transition (*see* Figure 5), but since b_o represents an averaging of rotatory contributions at many wavelengths and is relatively insensitive to the environment, it is the preferable parameter for the estimation of helix content.

As seen for the helical polypeptides (*33*, *61*, *62*), the extension of the Moffitt plot to 240 mμ for paramyosin changes the best value of λ_o to 218

Publication Date: January 1, 1967 | doi: 10.1021/ba-1967-0063.ch013

mμ [(*20*, *46*), *see also* Table I]. Yet this value of λ_o does not give perfectly linear plots [Figure 2, (*61*, *62*)] which are found if the wavelength range is split into two separate regions (600 to 300 mμ and 315 to 240 mμ) (*62*) (*see* Figures 1 and 3). Since the helical peptide transitions dominate the dispersion below 300 mμ [native paramyosin becomes more levorotatory than the unfolded protein about 310 mμ (*see* Figure 3)], a question has been raised about the validity of using the Moffitt equation in this region (*53*, *57*). Schecter and Blout (*52*) proposed the two-term Drude equation as a better method for analyzing ORD data from 700 to 275 mμ. This two-term Drude approach gives nearly the same estimates of helix content for the various polypeptides and for paramyosin (*52*, *53*) as does the Moffitt treatment. The small magnitude of F_Q at the maximum of F for the 315- to 240-mμ range (*46*) shows that the Moffitt equation is adequate to fit the ORD data for a fully helical protein molecule from 300 to 240 mμ (in the absence of any observable Cotton effects in this region), as Urnes (*61*, *62*) has previously found for the polypeptides PGA, PTGA, and PALGA.

The statistical criteria for the best λ_o (a maximum in F and a minimum in F_Q at the same wavelength) fail when paramyosin becomes less than 30% helical (*46*)—i.e., above 5.5*M* G-HCl—which as expected (*57*) is precisely the point at which the one-term Drude equation becomes sufficient to describe the data. The value of λ_c begins to decrease rapidly (Figure 4), and the standard deviations in the slope and intercept of the Drude plot decrease to those characteristic of a rigorously linear plot (equal to those found for the random coil). The apparent linearity of the Drude plot for the native helical protein in the 315- to 240-mμ range can be misleading. As seen in Figure 4, λ_c shows only two steps of the three-step helix-coil transition indicated by $[m']_{232}$ (or by a_o or b_o, Figure 5). Furthermore, if λ_c is used to estimate helix content (*67*), there is a great discrepancy with estimates based on either $[m']_{232}$ or b_o. For example, at 4*M* G-HCl, the λ_c estimate gives 80% helix whereas either $[m']_{232}$ or b_o estimates give about 35% helix. This discrepancy is consistent with the statistical indication of nonlinearity of the Drude plot since λ_c has no meaning if the plot is not linear.

The Moffitt treatment remains valid where the one-term Drude equation is sufficient if λ_o is kept constant (*63*). Therefore, in the case of the denatured helical protein or of the native globular protein with low helix content, λ_o should be maintained at the value found for the helical polypeptides and for paramyosin—λ_o = 220 mμ in the 240- to 315- mμ range (*46*, *61*, *62*) and λ_o = 212 mμ in the 300- to 600-mμ range (*46*, *63*). Hence, b_o can readily be used as a measure of helical content according to Equation 3.

$$f_H = \frac{b_0 \text{ (native protein)} - b_0 \text{ (unfolded protein)}}{b_0 (\alpha\text{-helix}) \qquad - b_0 \text{ (random coil)}} \tag{3}$$

Publication Date: January 1, 1967 | doi: 10.1021/ba-1967-0063.ch013

As seen in Table I, b_o in the lower wavelength range is $-343°$ for the native protein and $+20°$ for the denatured protein. Therefore, using myoglobin as an example, the value of $-250°$ obtained by Harrison and Blout (*21*) gives 74% helix, and the value of $-266°$, corrected for the Soret Cotton effect, obtained by Urnes (*61*, *62*) gives 79% helix. These two values agree well with the 77% amide bonds in helical array from the x-ray analysis of the myoglobin crystal (*31*) and also with the values of 73% and 77% helix, respectively, based on the polypeptide models (an average of the values for PGA, PTGA, and PALGA) (*61*, *62*). Thus, in spite of the apparent lack of complete randomness and the possible effects of supercoiling on optical activity, paramyosin seems to be a satisfactory model upon which to base estimates of helical contents of proteins.

Acknowledgment

I thank Judy Campbell for her technical assistance, Peter Urnes for many enlightening discussions and his criticisms of this manuscript, and John Edsall for his critical appraisal of the manuscript.

For use of the Cary 60 spectropolarimeter I thank Paul Doty and the Harvard Chemistry Department.

Literature Cited

(1) Allis, J., Ferry, J., *J. Am. Chem. Soc.* **87**, 4681 (1965).
(2) Allis, J., Ferry, J., *Proc. Natl. Acad. Sci. U. S.* **54**, 369 (1965).
(3) Armstrong, J., Myers, D. V., Verpoorte, J. A., Edsall, J. T., *J. Biol. Chem.* **241**, 5137 (1966).
(4) Bear, R. S., *J. Am. Chem. Soc.* **66**, 2043 (1944).
(5) Bear, R. S., Selby, C., *J. Biophys. Biochem. Cytol.* **2**, 55 (1956).
(6) Beychok, S., Fasman, G., *Biochemistry* **3**, 1675 (1964).
(7) Beychok, S., Pflumm, M. N., Lehman, J. E., *J. Am. Chem. Soc.* **87**, 3990 (1965).
(8) Blout, E. R., Schmier, I., Simmons, N. S., *J. Am. Chem. Soc.* **84**, 3193 (1962).
(9) Brant, D. A., Flory, P. J., *J. Am. Chem. Soc.* **87**, 2788, 2791 (1965).
(10) Cohen, C., Holmes, K. C., *J. Mol. Biol.* **6**, 423 (1963).
(11) Cohen, C., Szent-Györgyi, A. G., "Fourth International Congress of Biochemistry," Vol. 8, "Proteins," p. 108, Pergamon Press, London, 1960.
(12) Cohen, C., Szent-Györgyi, A. G., *J. Am. Chem. Soc.* **79**, 248 (1957).
(13) Coleman, J. E., *Biochemistry* **4**, 2644 (1965).
(14) Crick, F. C., *Acta Cryst.* **6**, 639 (1953).
(15) Crick, F. C., *Nature* **170**, 882 (1952).
(16) Fasman, G., "Methods in Enzymology," Vol. 6, p. 928, Academic Press, New York, 1963.
(17) Fasman, G., Bodenheimer, E., Lindblow, C., *Biochemistry* **3**, 1665 (1964).
(18) Fasman, G., Landsberg, M., Buchwald, M., *Can. J. Chem.* **43**, 1588 (1965).
(19) Friedman, E., Gill, T. J., Doty, P., *J. Am. Chem. Soc.* **84**, 3485 (1962).
(20) Harrap, B. S., private communication, 1960.
(21) Harrison, S. C., Blout, E. R., *J. Biol. Chem.* **240**, 299 (1965).
(22) Hodge, A., *Proc. Natl. Acad. Sci. U. S.* **38**, 850 (1952).
(23) Hodge, A. J., *Rev. Mod. Phys.* **34**, 409 (1959).
(24) Holzwarth, G., Doty, P., *J. Am. Chem. Soc.* **87**, 218 (1965).
(25) Iizuka, E., Yang, J. T., *Biochemistry* **4**, 1249 (1965).
(26) Jirgensons, B., *J. Biol. Chem.* **240**, 1064 (1965).

(27) Katchalski, E., Sela, M., Silman, H. I., Berger, A., "The Proteins," 2nd ed., Vol. 2, p. 405, Academic Press, New York, 1964.
(28) Kay, C. M., *Biochim. Biophys. Acta* **27**, 469 (1958).
(29) Kay, C. M., Bailey, K., *Biochim. Biophys. Acta.* **31**, 20 (1959).
(30) Kay, C. M., Smillie, L. B., "Biochemistry of Muscle Contraction," p. 379, Little Brown, Boston, 1964.
(31) Kendrew, J. C., Watson, H. C., Strandberg, B. E., Dickerson, R. E., Phillips, B. C., Shore, V. C., *Nature* **190**, 666 (1961).
(32) Kominz, D. R., Saad, F., Laki, K., "Proceedings of Conference on Chemistry of Muscular Contraction," p. 66, Igaku Shoin, Osaka, Japan, 1957.
(33) Leonard, W. J., Jr., Foster, J. F., *J. Mol. Biol.* **7**, 590 (1963).
(34) Lowey, S., *J. Biol. Chem.* **240**, 2421 (1965).
(35) Lowey, S., Cohen, C., *J. Mol. Biol.* **4**, 293 (1962).
(36) Lowey, S., Kucera, J., Holtzer, A., *J. Mol. Biol.* **7**, 234 (1963).
(37) McDiarmid, R. S., Ph.D. thesis, Harvard University, Cambridge, 1965.
(38) Mizukami, H., Ph.D. thesis, University of Illinois, Urbana, 1963.
(39) Moffitt, W., *J. Chem. Phys.* **25**, 467 (1956).
(40) Moffitt, W., Yang, J. T., *Proc. Natl. Acad. Sci. U. S.* **42**, 597 (1956).
(41) Myers, D. V., Edsall, J. T., *Proc. Natl. Acad. Sci. U. S.* **53**, 169 (1965).
(42) Noelken, M., Ph. D. thesis, Washington University, St. Louis, 1962.
(43) Noelken, M., Holtzer, A., "Biochemistry of Muscle Contraction," p. 374, Little, Brown, Boston, 1964.
(44) Pauling, L., Corey, R. J., *Nature* **171**, 59 (1953).
(45) Ramakrishnan, C., Ramachandran, G. N., *Biophys. J.* **5**, 909 (1965).
(46) Riddiford, L. M., *J. Biol. Chem.* **241**, 2792 (1966).
(47) Riddiford, L. M., Scheraga, H. A., *Biochemistry* **1**, 95 (1962).
(48) *Ibid.*, p. 108.
(49) Rosenberg, A., *J. Biol. Chem.* **241**, 5119, 5126 (1966).
(50) Rosenheck, K., Doty, P., *Proc. Natl. Acad. Sci. U. S.* **47**, 1775 (1961).
(51) Sage, H. J., Fasman, G., *Biochemistry* **5**, 286 (1966).
(52) Schechter, E., Blout, E. R., *Proc. Natl. Acad. Sci. U. S.* **51**, 695 (1964).
(53) Schechter, E., Carver, J. P., Blout, E. R., *Proc. Natl. Acad. Sci. U. S.* **51**, 1029 (1964).
(54) Schellman, J. A., Schellman, C. G., "The Proteins," 2nd ed., Vol. 2, p. 1, Academic Press, New York, 1964.
(55) Schuster, T. M., *Biopolymers* **3**, 681 (1965).
(56) Simmons, N. S., Cohen, C., Szent-Györgyi, A. G., Wetlaufer, D. B., Blout, E. R., *J. Am. Chem. Soc.* **83**, 4766 (1961).
(57) Sogami, M., Leonard, W. J., Jr., Foster, J. F., *Arch. Biochem. Biophys.* **100**, 260 (1963).
(58) Szent-Györgyi, A. G., Cohen, C., *Science* **126**, 697 (1957).
(59) Szent-Györgyi, A. G., Cohen, C., Philpott, D. E., *J. Mol. Biol.* **2**, 133 (1960).
(60) Tsao, T., Kung, T., Peng, C., Chang, Y., Tsou, Y., *Sci. Sinica* **14**, 91 (1965).
(61) Urnes, P., *J. Gen. Physiol.* **49**, 75 (1965).
(62) Urnes, P., Ph.D. thesis, Harvard University, Cambridge, 1963.
(63) Urnes, P., Doty, P., *Advan. Protein Chem.* **16**, 401 (1961).
(64) Wilchek, M., Said, S., Patchornik, B., *Biochim. Biophys. Acta* **104**, 616 (1965).
(65) Woods, E. F., *Nature* **207**, 82 (1965).
(66) Yang, J. T., *Proc. Natl. Acad. Sci. U. S.* **53**, 438 (1965).
(67) Yang, J. T., Doty, P., *J. Am. Chem. Soc.* **79**, 761 (1957).
(68) Yang, J. T., McCabe, W., *Biopolymers* **3**, 109 (1965).

RECEIVED March 1, 1966. Supported by National Science Foundation Grant GB-3748

14

Helix-Coil Transition in Deuterated Poly-γ-Benzyl-L-Glutamate

F. E. KARASZ and J. M. O'REILLY

General Electric Research and Development Center, Schenectady, N. Y.

Publication Date: January 1, 1967 | doi: 10.1021/ba-1967-0063.ch014

Our present knowledge of the helix-coil transition in synthetic polypeptides, with particular reference to the poly-γ-benzyl-L-glutamate–dichloroacetic acid–1,2-dichloroethane system, is briefly reviewed. Recent results concerning the effect of solvent composition and of polypeptide and solvent deuteration on the thermodynamic properties of the transition show that both the thermodynamics and presumably the molecular mechanism of the transition are generally more complicated than had been previously supposed.

Certain synthetic polypeptides in dilute solution can undergo a reversible cooperative transition from a helical to a randomly coiled configuration (*16*). For polypeptides in organic solvents the transition can be induced by changing the temperature of the solution or the composition of the solvent. Of the several systems that have been investigated, the most thoroughly studied have been solutions of poly-γ-benzyl-L-glutamate (PBG) in mixtures of dichloroacetic acid (DCA) and either 1,2-dichloroethane (DCE) or chloroform (*17*). The work presented here deals with the PBG-DCA-DCE system.

The transition can perhaps most conveniently be followed polarimetrically. Figure 1 shows the change in specific optical rotation of a 3% PBG solution (solvent, 70 volume % DCA–30 volume % DCE) as the temperature is varied through the transition range. From optical rotatory dispersion measurements one may obtain the Moffitt parameter, b_o, and from this it has been shown that for PBG the high temperature form (with positive $[\alpha]_D$) corresponds to the helical conformation of the polypeptide (*12*).

In Ordered Fluids and Liquid Crystals; Porter, R., el al.;
Advances in Chemistry; American Chemical Society: Washington, DC, 1967.

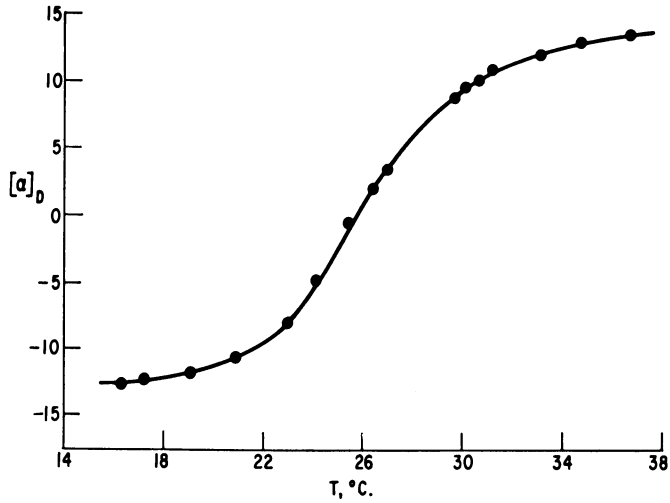

Figure 1. Specific optical rotation of a 3% PBG solution as a function of temperature

The changes which occur in solution around the transition temperature, T_c, can be written schematically and only to a first approximation, as follows:

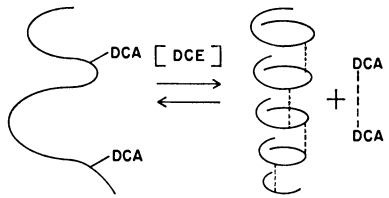

(1)

As the temperature is raised, the DCA bound to the coil is released and dimerizes, permitting the polypeptide α-helix to form, the equilibrium thus moving to the right. It is important to realize that in this approximation the total number of hydrogen bonds in the system remains unchanged; therefore it is clearly the relatively small differences in the enthalpies and entropies of the bonds that are pertinent in any quantitative discussion. As such differences are not calculable with any confidence, it is not possible to decide *a priori* whether, for example, the helical or the randomly coiled configuration is stable at high temperatures in any given system.

From polarimetric data, such as are shown in Figure 1, the fractional helical content, f_H, of the polypeptide may be calculated as a function of temperature, and by the formal application of the van't Hoff equation, an apparent heat of transition, ΔH, is derived. Figure 2 shows such a plot [slightly modified by using f_H values instead of log (equilibrium constants) in the ordinate) (*2*)] for the data shown in Figure 1. For PBG under these

Publication Date: January 1, 1967 | doi: 10.1021/ba-1967-0063.ch014

conditions, the van't Hoff heat, $\Delta H = 80$ kcal./mole. An obvious question is: to what physical process does this relatively large enthalpy value relate, or, equivalently, what is the significance, in this context, of a mole?

It is the differences in hydrogen bond strengths that are relevant. These might be of the order of a few hundred calories per mole or less; thus 80 kcal. is equivalent to upwards of 10^2 or 10^3 of such bonds. As shown quantitatively below, ΔH is related to the statistical number of neighboring polypeptide residues which cooperatively change their conformational state in the course of the transition.

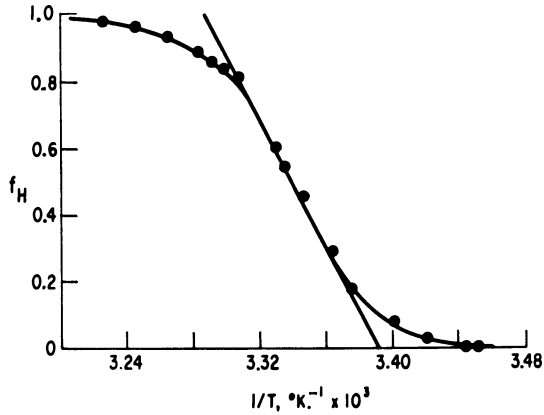

Figure 2. Fractional helical content, f_H, of PBG as a function of reciprocal absolute temperature

Polarimetric (or indeed, any optical) data alone can yield only two thermodynamic parameters describing the thermal transition, T_c and ΔH. To proceed further, it becomes desirable to use one of the statistical mechanical treatments of one-dimensional cooperative transitions which have been recently formulated to treat this and more generalized problems (*8*, *15*). In the present work we use the theory of Zimm and Bragg (*18*, *19*) and extensions of this by Applequist (*2*). The theory predicts all the major features of the transition found experimentally in terms of a parameter, σ, which in our nomenclature is given by

$$\sigma = \left(\frac{\Delta H_o}{\Delta H}\right)^2 \tag{2}$$

in which ΔH_o is the calorimetric heat associated with the transfer of a mole of amino acid residues from the random coil conformation to the end of existing helical sequences. Superficially, therefore, it is analogous to the heat of fusion of a one-component system and as such can be obtained calorimetrically by measuring the heat capacity of the appropriate polypeptide solution as a function of temperature. The result of such a meas-

Publication Date: January 1, 1967 | doi: 10.1021/ba-1967-0063.ch014

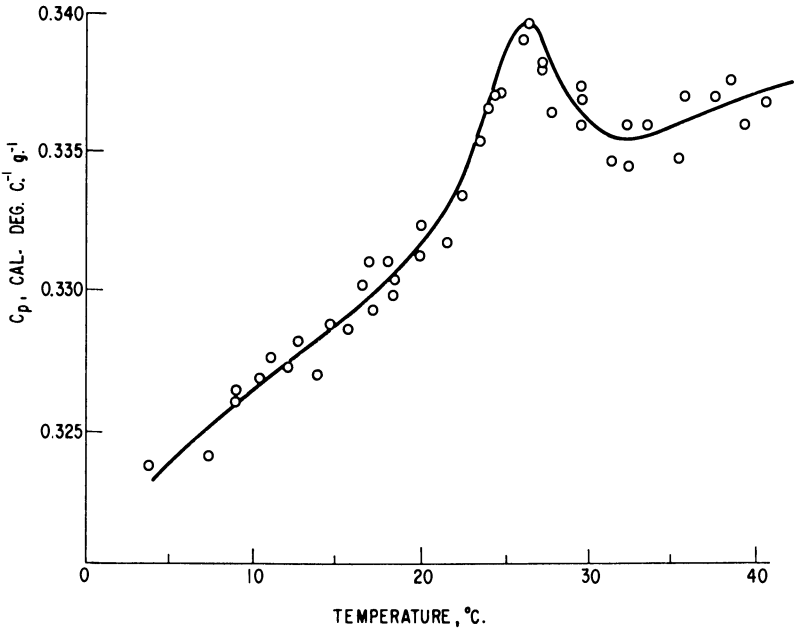

Figure 3. Heat capacity of PBG solution
1 gram of solution contains 0.02002 gram of PBG (7)

urement is shown in Figure 3; ΔH_o is directly proportional to the area under the peak. For PBG, ΔH_o is of the order of 500 cal. per mole of residue (*11*); therefore σ lies between 10^{-4} and 10^{-5}.

σ can be interpreted physically in several essentially equivalent ways. It is fundamentally a measure of the cooperativeness of the transition. In particular, at T_c (i.e., at $f_H = 1/2$), $\sigma^{-1/2}$ is equal to the average number of residues in a helical sequence; a low value of σ indicates a high degree of cooperation. Thus σ may also be regarded an an equilibrium constant for the formation of an interruption in a helical sequence (*2*). Other interpretations of σ are brought out below.

We have been interested in the behavior of σ as a function of a number of variables.

Structure of Polypeptides. It had originally been suggested that σ might be relatively unaffected by changes in the chemical nature of the amino acid side groups or in the solvent system. This was based on the belief that as σ was related to the relative difficulty of interposing a randomly coiled sequence in an existing helical sequence in a polypeptide chain, it should be determined by interactions along the polyglycine-type basic structure of the chain. This has now been shown to be too drastic an assumption; in chemically rather similar polypeptides, σ changed by a factor of $\sim$5 (*10*). In dissimilar systems (PBG compared with polyglutamic acid

Publication Date: January 1, 1967 | doi: 10.1021/ba-1967-0063.ch014

in aqueous solution) orders of magnitude differences have been observed (*13*).

Temperature Variation of σ. If σ were in fact largely determined by the conformational restrictions imposed on adjacent residues in forming a random coil sequence, as was in effect postulated above, then it might be expected to be entirely entropic, in which case it could be written as:

$$\sigma = e^{\Delta S_i/R} \tag{3}$$

The large negative value of ΔS_i (~ -19 e.u. per mole of interruptions for PBG) implied by this relationship has been fairly well accounted for by calculating the reduction in the number of accessible configurations (*19*). The temperature independence of σ, also implied in Equation 3, had not up to now been directly verified for any system, though both theoretical (*18*, *19*) and some rather indirect experimental evidence (*13*) had suggested that any temperature dependence might be small. Recently it has been suggested, however, that dipole interactions along the polypeptide chain might be important in both the random-coil and helical configurations. If this is the case, it would result in a significant enthalpic term in σ (*4*).

Deuteration of Polypeptide and Solvent. Although it had been previously shown that σ was somewhat affected by variations in side group interactions, it might be postulated that σ would be invariant to the substitution of deuterons for the labile hydrogen-bonding protons in the polypeptide and the DCA. In such an exchange side group interactions would be minimally affected; furthermore one would similarly predict rather small entropic (as distinct from enthalpic) perturbations of the over-all reaction. The test of this hypothesis formed the original basis of the work described below.

Other Variables. The effect of the polypeptide molecular weight upon σ has not yet been conclusively established for any polypeptide–organic solvent system. Recent extensive studies of the charge-induced transition of polyglutamic acid in aqueous solution have shown an increase in σ with a reduction in molecular weight (*15*). Similarly the influence of polypeptide solute concentration is not yet clear, though Ackermann and Rüterjans (*1*) have demonstrated a remarkably large effect of this variable upon ΔH_o in PBG. Neither of these points is discussed further in the present paper.

Deuterated PBG

Calvin, Hermans, and Scheraga (*5*) have shown polarimetrically, for PBG in a solvent of constant composition (80 volume % DCA–20 volume % DCE), that in the deuterated system T_c decreased from 40° to 29°C., and the corresponding ΔH's rose from 65 (protonated PBG) to 83 kcal./mole (deuterated PBG). Therefore if σ were to display no isotope effect (*see* above), then according to Equation 2, ΔH_o would have to undergo a concomitant change.

Publication Date: January 1, 1967 | doi: 10.1021/ba-1967-0063.ch014

In the course of this work it developed, however, that this change in ΔH was more directly related to the change in T_c in the deuterated, as compared with the protonated, system, and a study of ΔH *vs.* T_c for both systems was undertaken. T_c was varied over the range 5°-50°C. by varying the composition of the solvent from about 62 to 84 volume % DCA (the other component being DCE). Experimental details are given elsewhere (*9*). The results are shown in Figure 4. In both cases T_c rises with DCA concentration; this agrees with the schematic reaction mechanism (Equation 1), which shows that the presence of DCA favors the coiled or low temperature form. Therefore by application of Le Chatelier's principle, a higher temperature is needed to induce the endothermic reaction. Figure 4

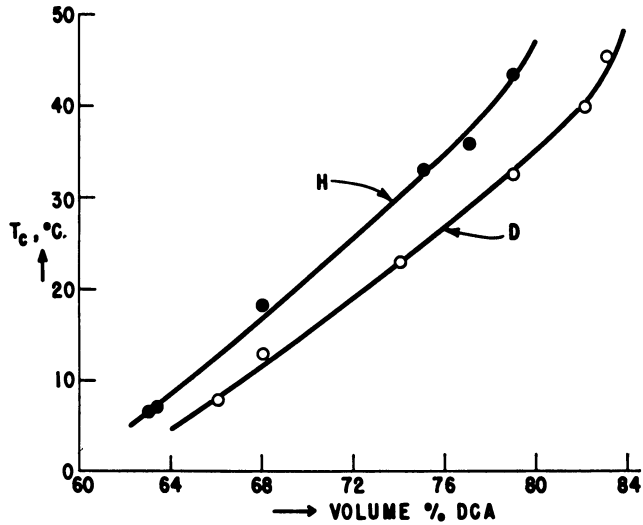

Figure 4. T_c as a function of solvent composition for PBG(H) and PBG(D) solutions

also confirms the fact that deuteration lowers T_c, for a given solvent composition, by from 5° to 10°C. These results are in good quantitative agreement with those of Calvin, Hermans, and Scheraga (*5*).

Figure 5 shows the ΔH's calculated from polarimetric data for the various solutions, as a function of T_c. Within the rather sizable experimental errors the data for both the protonated and deuterated solutions can be represented by a single curve. The implication is therefore that differences in ΔH for PBG(H) and PBG(D) solutions with identical solvent compositions are reflections of changes in T_c rather than a result of deuteration per se.

The calorimetric heats, ΔH_o, for two deuterated solutions with T_c's of 40° and 8.5°C. are given, together with the corresponding ΔH's, in Table I. While both ΔH_o and ΔH decrease with increasing T_c, the rates are not

Publication Date: January 1, 1967 | doi: 10.1021/ba-1967-0063.ch014

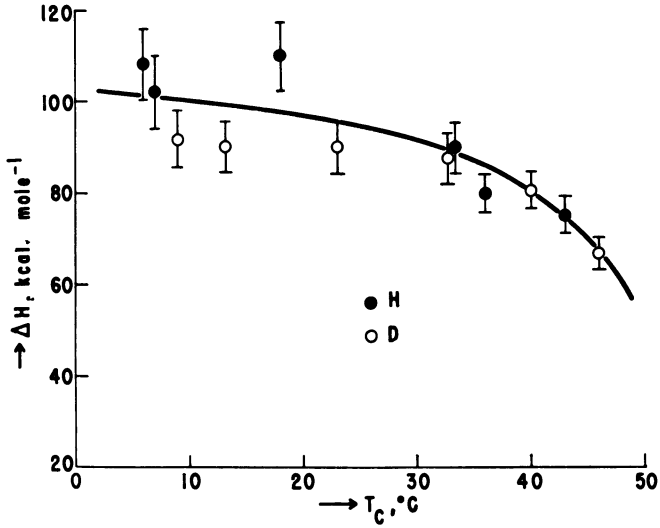

Figure 5. ΔH as a function of T_c for PBG(H) and PBG(D) solutions

equal. Because of the experimental errors arising in both ΔH_o and ΔH, the accuracy with which σ can be determined at present is rather low. Nevertheless, the calculated σ's (last column in Table I) show a significant variation. This is the first direct indication that, contrary to earlier supposition, σ is substantially temperature-dependent, at least in PBG. If we write σ in the expanded form,

$$\sigma = \exp -\left(\frac{\Delta H_i}{RT} - \frac{\Delta S_i}{R}\right) \tag{4}$$

we find $\Delta H_i = -3700$ cal. and $\Delta S_i = -33.1$ e.u., both per mole of interruptions. In addition, by comparing the values of σ for the deuterated solutions with a previously obtained result for a proton-containing PBG solution of intermediate T_c (26°C.) (*11*), it is found that within experimental error all three results fall on the same line when plotted as a function of T_c. This fact appears to confirm our original hypothesis that deuteration in itself does not affect σ. It does have an indirect effect because of the resultant change in T_c, and the temperature dependence of σ.

Table I. Data on Deuterated Solutions

	T_c, °C.	ΔH_0, Cal./ Mole Residues	ΔH, Kcal./Mole	$\sigma \times 10^5$
PBG(D)	8.5	670 ± 50	100 ± 15	4.5 ± 2.0
	40.0	380 ± 50	80 ± 10	2.3 ± 1.1
PBG(H)	26.0	525 ± 80	95 ± 12	3.1 ± 1.4

Publication Date: January 1, 1967 | doi: 10.1021/ba-1967-0063.ch014

Discussion

A number of implications of these results are discussed in greater detail elsewhere (*9*). However, we touch briefly on some points below. First, the ΔH_o results indicate that at least formally a large ΔC_p term is involved in the transition. From the temperature dependence of ΔH_o we calculate that the heat capacity of the random coil conformation exceeds that of the helical conformation by ~9 cal./deg./mole of PBG residues, or approximately 0.04 cal./deg./gram of PBG. This is the order of magnitude change found in crystal-liquid transitions in many organic solids and might thus be accounted for on this basis. A ΔC_p of similar magnitude was also found in the equivalent change in ribonuclease A (*3*). Two reservations must be attached to these considerations, however. First, the whole system has to be taken into account. Therefore an unknown fraction of the ΔC_p observed must be caused by changes in the solvent during the transition. Second, the fact that the ΔH_o measurements refer to solutions of different solvent composition suggests that it may be necessary to consider whether the change in ΔH_o with T_c is an inherent solvent effect (and not caused by the existence of a finite ΔC_p).

The appearance of a large enthalpy term in σ is unexpected from the basis of the Zimm-Bragg theory. In physical terms the implication is that the interposition of a random coil sequence in a helical sequence, as well as involving significant entropic restraints on the adjacent residues, also involves comparatively large energetic changes. The magnitude of the latter is such as to make the suggestion that they stem exclusively from changes in hydrogen bonding doubtful. Furthermore, whereas it was possible to explain an entropy term in σ of ~ -19 e.u. per mole of interruptions [a net of two additional residues is involved per interruption (*19*)], a value as high as 33 e.u. suggests that further ordering within the system accompanies the change. In this connection, therefore, it is pertinent to consider the recent results of Hanlon and Klotz (*7*) and Hanlon (*6*), who found, in PBG and other polypeptides, that the transition involved changes in protonated as well as hydrogen-bonded species. Such changes may be expected to involve enthalpies closer to the magnitude of those found here. Another possible enthalpic contribution stems from the dipole interaction between peptide units (*4*), while a third is the changes in noncovalent bonding between the amino acid side groups as a result of changes in configuration (*14*).

Conclusions

The present results demonstrate on a thermodynamic basis that the helix-coil transition in PBG is generally more complicated than previously supposed. In particular, the large temperature dependencies of both ΔH and ΔH_o carry new implications. Experimentally it would seem highly de-

sirable to reconcile all the thermodynamic parameters involved with the molecular changes that occur in solution during the transition.

Literature Cited

(1) Ackermann, T., Rüterjans, H., *Z. Physik. Chem.* **41**, 116 (1964).
(2) Applequist, J., *J. Chem. Phys.* **38**, 934 (1963).
(3) Beck, K., Gill, S. J., Downing, M., *J. Am. Chem. Soc.* **87**, 901 (1965).
(4) Brant, D. A., Flory, P. J., *J. Am. Chem. Soc.* **87**, 663 (1965).
(5) Calvin, M., Hermans, J., Jr., Scheraga, H. A., *J. Am. Chem. Soc.* **81**, 5048 (1959).
(6) Hanlon, S., "Abstracts of Papers," 150th Meeting, ACS, September 1965, 105C.
(7) Hanlon, S., Klotz, I. M., *Biochemistry* **4**, 37 (1965).
(8) Hill, T. L., *J. Chem. Phys.* **30**, 383 (1959).
(9) Karasz, F. E., O'Reilly, J. M., *Biopolymers*, in press.
(10) Karasz, F. E., O'Reilly, J. M., Bair, H. E., *Biopolymers* **3**, 241 (1965).
(11) Karasz, F. E., O'Reilly, J. M., Bair, H. E., *Nature* **202**, 693 (1964).
(12) Moffitt, W., Yang, J. T., *Proc. Natl. Acad. Sci. U. S.* **42**, 596 (1956).
(13) Rifkind, J., Applequist, J., *J. Am. Chem. Soc.* **86**, 4207 (1964).
(14) Scheraga, H. A., "The Proteins," 2nd ed., H. Neurath, ed., Vol. 1, Academic Press, New York, 1963.
(15) Snipp, R. L., Miller, W. G., Nylund, R. E., *J. Am. Chem. Soc.* **87**, 3547 (1965).
(16) Urnes, P., Doty, P., *Advan. Protein Chem.* **16**, 401 (1961).
(17) *Ibid.*, **16**, 434, 474 (1961).
(18) Zimm, B. H., Bragg, J. K., *J. Chem. Phys.* **31**, 526 (1959).
(19) Zimm, B. H., Doty, P., Iso, K., *Proc. Natl. Acad. Sci. U. S.* **45**, 1601 (1959).

RECEIVED February 11, 1966.

Studies on the Structure of Synthetic Polypeptides in Solution by Polarization of Fluorescence Techniques

THOMAS J. GILL III and GILBERT S. OMENN

Laboratory of Chemical Pathology, Department of Pathology, Harvard Medical School, Boston, Mass.

Publication Date: January 1, 1967 | doi: 10.1021/ba-1967-0063.ch015

The investigations presented focus on interpretation of polarization of fluorescence measurements and use of these measurements to study the structure of a representative spectrum of linear synthetic polypeptides, a vinyl polymer, and an intramolecularly cross-linked synthetic polypeptide. The methodological studies investigate the validity of the transition temperature as a structural parameter, the interaction of the fluorescent dye and the polymer to which it is conjugated, and the influence of the dye-polymer interaction on the measurements of various molecular parameters. The structural studies focus on the structure of the random coil, the helix-coil transition, the α-helix to β-conformation transition in polylysine, and the stability of the spatial structure in intramolecularly cross-linked synthetic polypeptides.

The polarization of fluorescence technique employing dye-macromolecule conjugates is a sensitive hydrodynamic method for studying the structure and interactions of proteins (*19*, *20*, *41*, *54*, *65*) and synthetic polypeptides (*26*, *30*, *31*, *49*). The relationship describing the dependence of polarization of fluorescence upon the Brownian rotational diffusion of the macromolecule was developed by Perrin (*50*) and extended by Weber (*65*) in the form of the equations (for excitation with natural light):

$$(1/p + 1/3) = (1/p_o + 1/3)(1 + RT\tau/V\eta) \quad (1)$$

$$RT/V\eta = 3/\rho_h \quad (2)$$

where p = polarization of fluorescence at absolute temperature T
p_o = limiting degree of polarization in absence of Brownian motion
R = gas constant
η = solvent viscosity
τ = lifetime of excited state
V = molar volume

In Ordered Fluids and Liquid Crystals; Porter, R., el al.;
Advances in Chemistry; American Chemical Society: Washington, DC, 1967.

The derivation of these relationships, which were developed for rigid spheres or ellipsoids, contains five assumptions: (1) The equipartition of energy pertains, (2) the solvent is a continuum—i.e., the microviscosity of the solution is equivalent to the measured viscosity—(3) the fluorescent oscillators are randomly oriented on the molecule, (4) there is no internal rotation in the macromolecule, and (5) changes in the orientation of the oscillators can yield all possible directions. If τ and V are constant, the Perrin law of isotropic depolarization by Brownian motion predicts a linear relationship between $(1/p + 1/3)$ and T/η. According to the theory, equivalent changes in T/η can be produced by a change in either temperature or viscosity and the effect on the polarization, p, would be the same. However, departure of this relationship from linearity at high values of T/η has been noted for several proteins (*66*, *68*) and synthetic polypeptides (*26*, *31*). The point at which this departure occurs, the transition temperature, represents the onset of accelerated internal rotation in the polypeptide chain (*65*), and it is related to the stability of the internal structure of the molecule (*26*). Thus at this point the crucial assumption that there is no internal rotation breaks down. In order for the transition temperature to reflect the activation energy that is needed to disrupt the internal structure of the macromolecule, the transition must depend only upon temperature over a wide range of viscosities.

The usefulness of polarization of fluorescence for studying the tertiary structure of polymers and proteins is unique in that it provides a hydrodynamic method for detecting small changes in internal structure and in over-all rigidity (*26*). The transition temperature provides a measurement of the stability of the intramolecular structure whose subtlety falls between that of the usual hydrodynamic methods of intrinsic viscosity, sedimentation, and diffusion, which indicate the over-all size and shape of a molecule, and that of the spectroscopic and optical rotatory dispersion techniques, which provide intimate details about the structure of the polypeptide chain. The changes in rotational relaxation time give a quantitative measurement of the over-all rigidity of the macromolecule. Thus the technique of polarization of fluorescence has special applicability to studies of the organized spatial structure of macromolecules and is particularly fruitful when used in conjunction with intramolecularly cross-linked synthetic polypeptides as models for the tertiary structure of proteins.

The studies reported here present first a validation of the transition temperature as a structural parameter and then a study of the relationship between the fluorescent dye and the polypeptide to which it is conjugated. With this material as a background, the structures of poly $Glu^{97}Lys^{3}$, poly Lys (No. 2), polyvinylamine, and poly $Glu^{63}Lys^{37}$ (No. 3) are presented as a systematic study of linear synthetic polypeptides, which vary from completely negatively charged to completely positively charged. [The nomenclature is defined systematically by Gill (*25*). Superscripts refer to molar

Publication Date: January 1, 1967 | doi: 10.1021/ba-1967-0063.ch015

percentages of each amino acid, and number in parenthesis refers to the number of the preparation.] Then the investigation progresses to a study of the internal structure of molecules by examining the cross-linked derivatives of poly $Glu^{52}Lys^{33}Tyr^{15}$ (No. 3). Finally, the helix-coil transition in the linear synthetic polypeptides is investigated in detail and compared with the same transitions measured by optical rotatory dispersion and the results of the hydrodynamic and conformational studies are evaluated.

These studies begin to provide a systematic basis for the detailed interpretation of polarization of fluorescence measurements in structural terms as well as hydrodynamic data about a wide range of linear and cross-linked synthetic polypeptides. The further development of such studies will provide a firm basis for applying polarization of fluorescence techniques to the study of the structure of native proteins in solution.

Publication Date: January 1, 1967 | doi: 10.1021/ba-1967-0063.ch015

Synthetic Polypeptides

The polypeptides were synthesized by polymerization of the *N*-carboxyanhydrides of the amino acids at a concentration of 1% in benzene with sodium methoxide as the initiator and an anhydride-initiator ratio of 400 (*23*). The amino acid composition was determined by amino acid analysis, and the molecular weights were determined either from the previously established relationship between the degree of polymerization and intrinsic viscosity or by the approach-to-equilibrium technique in the ultracentrifuge. The partial specific volumes for the polymers were calculated from the data of Cohn and Edsall (*8*).

Fluorescent dye-polypeptide conjugates were prepared by labeling with either fluorescein isothiocyanate adsorbed onto Celite (*51*) or with 1-dimethylaminonaphthalene sulfonyl chloride (DNS) dissolved in ethanol (*65*). The degree of labeling was determined from the amount of dye on the polypeptide estimated by fluorescent intensity or ultraviolet absorption measurements and from the concentration of the polypeptide determined by Kjeldahl nitrogen. There were generally two to four dye residues per polypeptide molecule.

Fluorescent Measurements

Fluorescent intensity was measured in a modified Brice-Phoenix light-scattering photometer Model 2000 equipped with an AH3 mercury lamp and modified to have a manually controlled, rotating polarizer in front of the phototube (*26*). DNS was excited by unpolarized light at 365 mμ, and the intensity of the fluorescent radiation was measured at 90° from the direction of the exciting light after passing through a 460-mμ cutoff filter. In the case of fluorescein the excitation filter was 436 mμ, and the cutoff filter was 520 mμ. A glass water bath equipped with a coil was mounted on a hollow base plate through which fluid could be circulated. The temperature was measured by a calibrated thermistor immersed in the sample solution; the thermistor was attached to a Wheatstone bridge, and a galvanometer was used as a null point indicator. The lifetimes of the excited state,

In Ordered Fluids and Liquid Crystals; Porter, R., el al.;
Advances in Chemistry; American Chemical Society: Washington, DC, 1967.

τ, of DNS, and of fluorescein were taken as 1.2×10^{-8} and 0.48×10^{-8} second, respectively (*60*). Experimental measurements were made at small temperature intervals in order to locate the structural transitions in each polypeptide accurately. The degree of polarization of fluorescence was calculated according to the equation:

$$p = (I_V - I_H)/(I_V + I_H) \tag{3}$$

The limiting polarization, p_o, was measured in an 83.5% (w./w.) glycerol solution at 4°C. The values of p_o determined by direct measurement and by extrapolating the straightline segment of the experimental curve coincide in every case.

The polarization of fluorescence data below the transition temperature were analyzed according to Equation 1, and the rotational relaxation time, ρ_h[5], and the equivalent volume of the rotating segment, V_e[5], were calculated at 5°C. from the equations:

$$\rho_h = 3\tau\{(1/p_o + 1/3)/[(1/p + 1/3) - (1/p_o + 1/3)]\} \tag{4}$$

$$V_e = (R/3)(T/\eta)\rho_h \tag{5}$$

The transition temperature, T_T, was determined empirically from the graph of $(1/p + 1/3)$ against T/η as the point at which the experimental relationship deviated from linearity to follow the exponential curve. The slope, S, was calculated from the straight-line portion of the curve.

The standard deviation in the measurement of p was $\pm 5\%$, of ρ_h, $\pm 10\%$, and of S, $\pm 10\%$; changes in any of these parameters greater than 20% were significant. Below 15°, T_T has a standard deviation of $\pm 10\%$, and changes greater than 20% were significant. Above 15° the standard deviation in T_T was $\pm 5\%$, and changes greater than 10% were significant (*26*, *32*).

The data of the curved portion of the graph for poly $Glu^{63}Lys^{37}$ (No. 3) labeled with DNS or fluorescein were analyzed by the least squares method using an IBM 1620 computer. The function which describes these points is the exponential relationship:

$$(1/p + 1/3) = K \exp(aT/\eta) \tag{6}$$

The values of parameters K and a were optimized, and the correlation coefficient for the closeness of fit of the data was 0.998. The value of K is constant within experimental variation while the value of a varies markedly as the initial viscosity of the solution changes; this variation reflects the rate of change of the exponential portion of the curve. The data for the straight line portion of the curve cannot be fitted into this exponential function; hence, they truly represent a separate and distinct portion of the experimental curve.

Publication Date: January 1, 1967 | doi: 10.1021/ba-1967-0063.ch015

In Ordered Fluids and Liquid Crystals; Porter, R., el al.;
Advances in Chemistry; American Chemical Society: Washington, DC, 1967.

The experimental parameters were compared with those of the theoretical rigid sphere, the model upon which the theory of polarization of fluorescence is based, which were calculated from the following equations:

$$\rho_o = 3(V_o/R)(\eta/T) \tag{7}$$

$$V_o = \bar{v}M \tag{8}$$

No transition temperature would be expected for a rigid sphere because there would be no deviation from Equation 1.

Transition Temperature

Experiments to establish the transition temperature as a valid structural parameter were carried out with poly $Glu^{63}Lys^{37}$ (No. 3) (*48*). This polymer was chosen because it contains only two different amino acids, both of which are common in proteins, and because its net charge at neutra-pH is similar to that of many serum proteins. The polarization of fluoresl cence at pH 7.2 as a function of temperature in aqueous-glycerol solutions of different viscosities shows that in solutions up to 50% glycerol (9 cp. at 10°C.) the plot of $(1/p + 1/3)$ against T/η gives rise to a characteristic curve upon heating: at low temperatures and small values of T/η, $(1/p + 1/3)$ varies linearly with T/η, but at higher temperatures departure from linearity occurs, and the relationship becomes exponential. Representative graphs for the polypeptide labeled with DNS and fluorescein are shown in Figure 1, and the data derived from them are summarized in Table I. The most striking feature of the data is the constancy of the transition temperature—i.e., the point of onset of accelerated depolarization. For the solutions containing 0 to 50% glycerol, the transition temperature remains at 10° to 11°C. even though the corresponding values for T/η decrease from 2.2×10^4 to 0.3×10^4 degrees per poise. No transition can be detected in the 83.5% (200 cp. at 10°C.) glycerol solution. The effects of the heating and cooling studies with both dyes were reversible in all cases.

The transition temperature is the same for the polymers labeled with fluorescein and with DNS, but the rotational relaxation times in aqueous solution are different. $\rho_h{}^5$ measured with DNS is 1.8×10^{-8} second, while that measured with fluorescein is 0.9×10^{-8} second. This twofold difference is reproducible in a number of different measurements on the polypeptide-dye conjugates and is seen also in studies of polylysine and lysozyme (*32*). The discrepancy may reflect different degrees of interaction between each dye and the polypeptide. This is discussed further below.

Since the transition temperature is constant over a wide range of viscosities, it is apparent that changes in temperature and viscosity do not produce the same effect. In the experiments where temperature is varied in a given solution, the viscosity is an implicit function of the temperature; hence the variable T/η is a function of temperature. Thus the presence of

Publication Date: January 1, 1967 | doi: 10.1021/ba-1967-0063.ch015

a constant transition temperature suggests that a certain activation energy is required to overcome the barriers to segmental rotation, such as side-chain interactions and steric effects. An increase in temperature can supply the activation energy in a way that changing viscosity to equivalent values of T/η cannot.

The accelerated depolarization seen in Figure 1 reflects the presence of smaller rotational kinetic units in the polypeptide chain and not the ro-

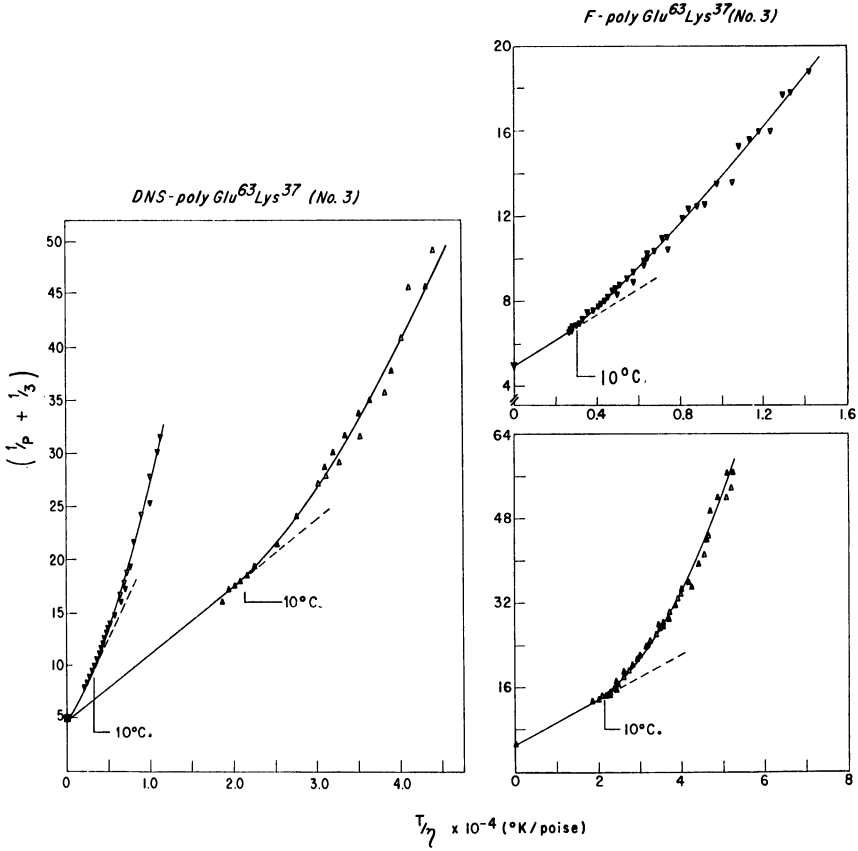

Figure 1. Effect of variation in temperature on polarization of fluorescence of poly Glu^{63}Lys^{37} (No. 3) conjugated with DNS or fluorescein (48)

Viscosity of solution altered by adding glycerol (w./w.) to a solution of polypeptide in 0.2M NaCl + 0.1M phosphate buffer, pH 7.2. Temperature was increased gradually to 60° to 70°C. and then decreased slowly to 5° to 10°C. Polymers contain 2 moles of dye per mole of polymer and concentration of polymers is 0.1 to 0.3 mg./ml.

▲, △. *Data for polymer dissolved in 0.2M NaCl + 0.1M phosphate buffer*
▼, ▽. *Data for 50% (w./w.) glycerol solution*
Solid symbols. Heating phase
Open symbols. Cooling phase

Transition temperatures indicated on graphs. Measured and extrapolated values of $(1/p_o + 1/3)$ coincide

Table I. Effect of Variation in Viscosity on Molecular Parameters Calculated from Polarization of Fluorescence Measurements in Aqueous Glycerol Solutions of Poly Glu^{63}Lys^{37} (No. 3) (*48*)[f]

% Glycerol (W/W)	p^5[a]	$S \times 10^4$[b]	T_T, °C.[c]	$\rho_h^5 \times 10^8$, Sec.	ρ_h^5/ρ_o^5	$V_e^5 \times 10^{-3}$, Cc./Mole[d]	K[e]	a[e]
Labeled with 1-Dimethylaminonaphthalene Sulfonyl Chloride (2 Molecules/Molecule Polypeptide)								
0	0.071	6.3	10	1.8	0.09	9	1.95	0.44
23.8	0.086	9.1	10	2.2	0.05	5	1.81	0.80
38.4	0.108	11.8	11	2.8	0.04	4	1.67	1.30
50.0	0.124	15.8	10	4.4	0.03	3	1.80	1.52
83.5	0.211	50.2	None	46	0.01	1	1.64	5.91
Labeled with Fluorescein Isothiocyanate (2 Molecules/Molecule Polypeptide)								
0	0.079	4.3	10	0.9	0.05	5	1.72	0.45
23.8	0.116	4.4	10	2.0	0.05	5	1.68	0.59
38.4	0.135	6.1	10	2.6	0.03	3	1.71	0.76
50.0	0.161	6.2	10	4.7	0.03	3	1.69	0.94
67.0	0.192	7.7	16	13	0.03	3	1.60	1.62
83.5	0.211	19.8	None	55	0.01	1	1.61	2.79

[a] For a rigid sphere limiting degree of polarization $p_o = -0.143$ to 0.333.
[b] S is slope of initial straight-line segment of experimental curve.
[c] T_T is transition temperature; none would be expected for a rigid sphere.
[d] $V_o \times 10^{-3} = 100$ for a rigid sphere calculated using $\bar{v} = 0.66$ and $M = 152{,}000$. $V_o \times 10^{-3}$ for dye + lysine side chain are: DNS 0.25 and fluorescein 0.34. $V_e^5/V_o = \rho_h^5/\rho_o^5$.
[e] K and a are constants in exponential function that describes experimental curve after transition temperature.
[f] Experimental conditions described in caption of Figure 1.

tation of the dye because the equivalent volumes, V_e^5, of the rotational kinetic units are many times larger (Table I) than the molar volumes of the fluorescent dye plus the lysine side chain (DNS 0.25 $\times$ 10^3 cc. per mole and fluorescein 0.34 $\times$ 10^3 cc. per mole) (*31*). Thus, the assumption that the equivalent volume of the rotational kinetic units does not change, one of the assumptions upon which the Perrin equation is based, is not valid above the transition temperature. In addition, V_e^5 decreases as the viscosity increases because of the constraints imposed upon the Brownian motion of the polypeptide chain by the increased viscosity.

The degree of polarization at 5°, p^5, is less for the DNS-labeled polymer because of the longer lifetime of DNS, which allows a greater degree of depolarization in a given time than does fluorescein. The two constants S and a reflect the rate of depolarization before and after the transition temperature, respectively. These constants are affected by the rate of change in structure of the polypeptide, the lifetime of the dye, and the interaction between the dye and the polypeptide chain. DNS interacts less strongly with the polypeptide chain than does fluorescein; consequently, its be-

Publication Date: January 1, 1967 | doi: 10.1021/ba-1967-0063.ch015

havior is affected independently from that of the polypeptide chain. The rates of depolarization both before and after the transition temperature, S and a, respectively, will be increased because of the increased rotation and the longer lifetime of the DNS. Thus, using the two constants S and a to assess structural changes in the polypeptide chain can be hazardous unless the polymers are labeled with the same fluorescent dye and the degree of interaction between the fluorescent dye and the polymer is the same in each case.

Relationship between Fluorescent Dye and Polypeptide Chain

The changes in polarization of fluorescence with isothermal changes in viscosity at a series of constant temperatures display separate effects owing to the dye moiety and the polypeptide chain (*48*). In the case of DNS-poly $Glu^{63}Lys^{37}$ (No. 3) there are two distinct relaxation times shown in the plot of $(1/p + 1/3)$ against $1/\eta$ (Figure 2). [The variable $1/\eta$ at constant temperature is, obviously, equivalent to parameter T/η and differs from it only by a constant which is the temperature, T. $1/\eta$ is more convenient to use in experiments where the viscosity is varied and the temperature is held constant.] The segment of the curve reflecting the effect of viscosity on the DNS is seen at high viscosities, and its slope increases with increasing temperature. The segment reflecting changes in the polypeptide itself occurs at lower viscosities, and its slope at each temperature is the same. In contrast to these findings, the fluorescein-labeled polymer displays a series of straight lines, each of which has a different slope and a slight deviation concave to the $1/\eta$ axis at high viscosities (Figure 2). The different slopes reflect a composite effect owing both to the dye and to the polypeptide; the effects caused by the changes in the dye are small. In this type of experiment, where viscosity is varied at a series of constant temperatures, the variable T/η (or $1/\eta$ for each isotherm) is a function of viscosity. Thus, it is basically a different type of experiment from the one in which T/η is a function of the temperature.

The departure of the Perrin equation from linearity may be considered more generally. A curvature convex to the T/η axis may result from the complete kinetic dissociation of rigid units or from increased rotational freedom within the polypeptide chain (*26*, *32*, *65*, *66*, *68*). A curvature concave to the T/η axis may occur whenever more than one rotational relaxation time is present and may be detected when the two rotational relaxation times differ by more than fivefold (*65*). The initial slope, for small values of T/η, depends upon the harmonic mean of the relaxation times involved and is determined practically by the shorter one. Such curvature has been reported in studies with DNS-labeled polyvinylamine and poly-*p*-aminostyrene (*22*, *33*, *64*). By applying a theory which deals with the case of an emitting group which has only one degree of rotational freedom, Gottlieb and Wahl (*33*) concluded that the rotations activated by temperature in

Publication Date: January 1, 1967 | doi: 10.1021/ba-1967-0063.ch015

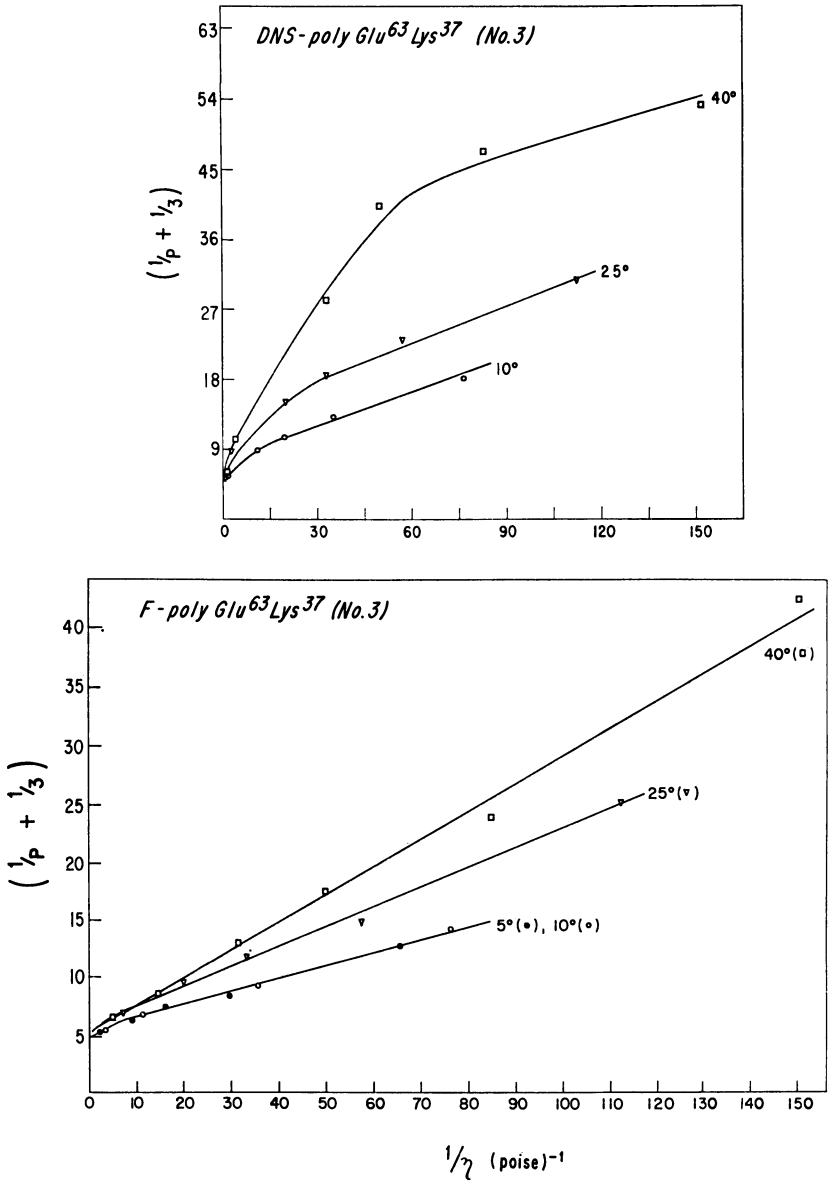

Figure 2. Effect of variation in viscosity on polarization of fluorescence of poly Glu^{63} *Lys*^{37} *(No. 3) conjugated with DNS or fluorescein (48)*
Conditions same as in Figure 1

DNS–poly-*p*-aminostyrene are those of a volume equal to the dye or only a little larger. The data with DNS–poly Glu^{63}Lys^{37} (No. 3) show that the depolarizations which are constrained only at high viscosities are caused by the rotation of the dye moiety itself, as in the case described by Gottlieb

and Wahl. [The linear portion of the curve, at higher values of $1/\eta$, corresponds to the arithmetic mean of the relaxation times and is, therefore, determined by the longest of them (*66*). Thus, this portion of the curve reflects the behavior of the polypeptide chain itself.]

The concave deviations in the plot of $(1/p + 1/3)$ against T/η at high viscosities are apparently at variance with the general observation that the measured p_o values in solutions of high viscosity agree well with the p_o values obtained by extrapolating the plot of $(1/p + 1/3)$ against T/η to $T/\eta = 0$. However, this apparent discrepancy is caused by the different molecular events observed when T/η approaches 0 under different experimental conditions. The value of p_o should be the same regardless of the preceding events since it depends upon molecular properties that manifest themselves only when all Brownian motion has effectively ceased. In the case where the temperature is varied in a solution of given initial viscosity (T/η is a function of temperature), a linear extrapolation to p_o would be expected since temperature and viscosity changes are equivalent for such experiments in the same solution. When the viscosity is changed at constant temperature (T/η is a function of viscosity), $(1/p + 1/3)$ would not show the same dependence upon T/η as in the preceding case, but the extrapolation to $1/\eta = 0$ at each temperature leads to the same p_o.

There are three different lines of evidence which indicate that fluorescein interacts more strongly with the polypeptide than does DNS. First, there is only one rotational relaxation time for the fluorescein-labeled polymer in the plot of $(1/p + 1/3)$ against $1/\eta$ whereas there are two for the DNS-labeled polymer above 15°C. (Figure 2). Secondly, fluorescent intensity studies indicate that there is a rapid decrease in intensity for the DNS-labeled polymer as a function of increasing temperature in aqueous-glycerol solutions, but there is relatively little change in the intensity of fluorescein (*48*). These changes can be explained by thermal quenching of the loosely bound DNS which does not occur with the more tightly bound fluorescein. Finally, a variety of spectral studies indicate that the absorption characteristics (shape of the spectral curves, position and number of absorption maxima, and absorption intensity) of fluorescein-labeled polypeptides are less susceptible to changes in pH, ionic strength, and organic solvents than those of DNS-labeled polypeptides (*29*). These findings indicate that the more tightly bound fluorescein is less susceptible to solvent perturbation than DNS.

The differences in dye-polypeptide interaction may explain the difference in measurements of the rotational relaxation time of poly $Glu^{63}Lys^{37}$ (No. 3) with the DNS and the fluorescein conjugates. The loosely bound DNS may less accurately reflect the true behavior of the rotational kinetic unit of the polypeptide chain in aqueous solution because it could interact with a portion of the chain remote from the point of attachment of the dye and give a spuriously long rotational relaxation time; the tightly bound

Publication Date: January 1, 1967 | doi: 10.1021/ba-1967-0063.ch015

fluorescein would not be capable of such long-range interaction. Adding glycerol to the solution lowers its dielectric constant and would diminish the long-range interactions of the DNS: in this case the dye could interact only with the segment of the polypeptide chain adjacent to its point of attachment.

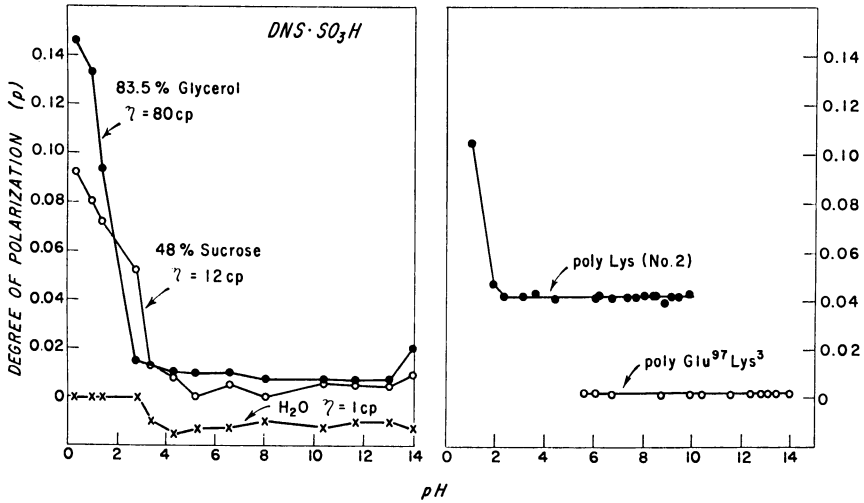

Figure 3. Changes in polarization of fluorescence of DNS caused by solutions of different viscosities and by conjugating the dye to poly Lys (No. 2) and poly Glu^{97} Lys^{3}

Studied over pH range where there are no structural transitions in polymers (29). Dyes and polymers dissolved in 0.2M NaCl + 0.1M buffer (citrate, phosphate, or carbonate). Viscosity of dye solutions changed by adding sucrose or glycerol to solution. Same patterns seen with polymers dissolved in water or in 3.0M NaCl + 0.1M buffer

The utility of DNS and fluorescein for studies of pH-dependent alterations in polypeptide structure—e.g., a study of the helix-coil transition—depends upon the spectral characteristics of the dyes, especially their absorbance, as a function of pH: in order for a dye to be useful, its spectral characteristics must not vary within the pH range where it is to be used (*29*). The polarization of fluorescence of DNS and of fluorescein was studied as a function of pH in solvents of different viscosity and compared with the results obtained when they were attached to polymers whose structural characteristics did not change over the pH range studied. This study was undertaken on the hypothesis that when the dye is attached to a polypeptide chain, its rotation is constrained and its behavior in solutions of increased viscosity will mimic its behavior when attached to the polypeptide. The results of these studies are shown in Figure 3 for DNS and in Figure 4 for fluorescein. There is no change in the degree of polarization of DNS between pH 2.5 and 14 as the viscosity of the solution increases. In

Publication Date: January 1, 1967 | doi: 10.1021/ba-1967-0063.ch015

like manner, when DNS is attached to poly Lys (No. 2), there is no change in the degree of polarization between pH 2.5 and the beginning of the helix-coil transition at pH 9.8. When the DNS is attached to poly $Glu^{97}Lys^{3}$, there is no change in the degree of polarization between pH 5.7 and 14. Hence DNS is useful for studying the effect of pH on polypeptide structure over the pH range 2.5 to 14. A similar conclusion was reached by Weber,

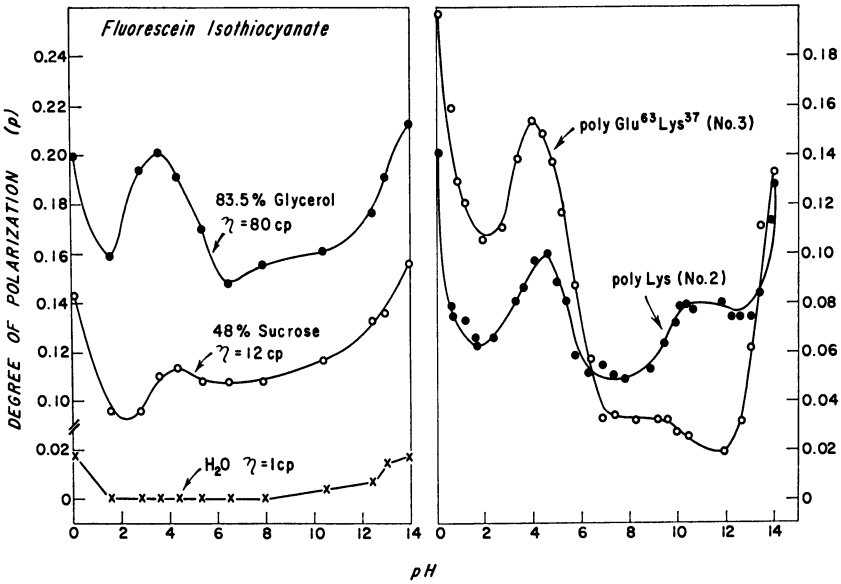

Figure 4. Changes in polarization of fluorescence of fluorescein caused by solutions of different viscosities and by conjugating dye to poly Lys (No. 2) and poly $Glu^{63}Lys^{37}$ (No. 3) Studied over entire pH range (29). Solvents and conditions same as in Figure 3. Helix-coil transition in each polymer is shifted and distorted by effects of dye on polarization of fluorescence. Same patterns seen with polymers dissolved in water or in 3.0M NaCl + 0.1M buffer

who reported that the lifetime of DNS was constant from pH 1.6 to 14 (*65*). When the same study is carried out with fluorescein, the degree of polarization of the dye is found to vary markedly in solutions of different viscosities. Likewise, when the fluorescein is attached to either poly Lys (No. 2) or poly $Glu^{63}Lys^{37}$ (No. 3), the degree of polarization varies in the same fashion as when fluorescein is placed in solutions of increased viscosity. Thus the behavior of the fluorescein-polypeptide conjugate reflects to a large extent the spectral characteristics of fluorescein as a function of pH and any changes owing to the changes in polypeptide structure are superimposed upon it and thus obscured. For example, the mid point of the helix-coil transition measured in 0.2*M* NaCl + 0.1*M* buffer with fluorescein–poly Lys (No. 2) would occur at pH 9.6 instead of the correct pH of 10.3 as measured with the DNS-conjugate. From our studies then, the useful

Publication Date: January 1, 1967 | doi: 10.1021/ba-1967-0063.ch015

range of fluorescein for studying pH-dependent phenomena is approximately pH 6 to 8. Steiner and McAlister reported that the lifetime of fluorescein is constant from pH 4.5 to 10 (*60*), but it is apparent from our studies that the dye is not useful over this entire range.

Intensity Measurements

Fluorescent intensity measurements (total intensity or I_v) do not reflect the structural alterations measured by the transition temperature or by changes in the rotational relaxation time; these changes are detected only by polarization of fluorescence measurements (*26*, *48*). The fluorescent intensity measurements of all the polypeptides studied show small, gradual changes with temperature, but no abrupt transitions. These changes are greater for DNS-labeled polypeptides than for fluorescein-labeled polypeptides.

Poly $Glu^{97}Lys^{3}$

This polymer was used as a model for polyglutamic acid since a few lysine residues were needed for conjugation with the fluorescent dyes; there are too few lysine residues to alter the behavior of the glutamic acid residues. The coil form has a high degree of Brownian motion in solution and therefore little rigidity [$p^{22}(F) = 0.015$]. [$p^{22}(F)$ is the polarization of fluorescence at 22°C. measured with a fluorescein-polypeptide conjugate. These measurements were made in 0.2*M* NaCl + 0.1*M* phosphate buffer, pH 7, except in the case of PVA, in which the solvent was 0.3*M* NaCl adjusted to pH 7.] There is little internal organization of the polypeptide

Table II. Polarization of Fluorescence Parameters and Intrinsic Viscosity of Poly $Glu^{97}Lys^{3}$[a,b]

pH	*Transition Temp.*, (T_T), °C.	$\rho_h^5 \times 10^8$, *Sec.*	$V_e^5 \times 10^{-3}$, *Cc./Mole*	[η], *Dl./G.*[c]
3.3	21	5.2	26	gel
4.4				1.03
5.4	12	0.8	4	1.20
9.6	<0			1.53
Rigid sphere	None	14	71	0.014

[a] MW = 125,000; pK° of poly Glu = 4.45 (*46*, *63*); conjugated with fluorescein.
[b] Solvent is 0.2*M* NaCl + 0.1*M* buffer (citrate, phosphate, or carbonate).
[c] Changes in intrinsic viscosity as a function of pH are reversible.

chain since the transition temperature at pH 9.6 is less than 0°. In acid solution the polymer undergoes transition to the helical conformation: The transition temperature, the rotational relaxation time, and the equivalent volume of the rotational kinetic unit increase, which indicates the transition to a more rigid structure. The intrinsic viscosity decreases in the pH range where helices and coils coexist and becomes high, ultimately forming

Publication Date: January 1, 1967 | doi: 10.1021/ba-1967-0063.ch015

a gel, as all the residues go into the helical conformation. This sequence of changes is the same as that previously reported for the intrinsic viscosity of polyglutamic acid as a function of pH (*3*, *12*). The data are summarized in Table II.

Poly Lys (No. 2)

The coil form of polylysine is more rigid [$p^{22}(F) = 0.050$] than that of polyglutamic acid and has more internal organization since the transition temperature at pH 7.2 is 13°C. in 0.2*M* NaCl + 0.1*M* buffer (low salt). In 3.0*M* NaCl + 0.1*M* buffer (high salt), however, the coil has less internal organization, and its transition temperature is 6°C.

In alkaline solutions poly Lys (No. 2) undergoes a helix-coil transition which is manifested by an increase in transition temperature, rotational relaxation time, equivalent volume, and by gel formation in viscosity measurements. In high salt the transition temperatures of the partially helical and the completely helical forms are higher than in low salt. This indicates a stronger internal structure for the helix and would be expected since the uncharged helical residues would interact more strongly in the high dielectric solvent. The shorter rotational relaxation times and the smaller equivalent volumes in high salt could reflect either a greater number of breaks in the helix or helical segments containing the same number of residues as in low salt but packed more tightly. The latter interpretation seems more reasonable because the uncharged helical residues will interact more strongly and could thus form a more compact helix in high salt. The

Table III. Polarization of Fluorescence Parameters and Intrinsic Viscosity of Poly Lys (No. 2)[a]

	Transition Temperature (T_T), °C.		*$\rho_h^5 \times 10^8$, Sec.*		*$V_e^5 \times 10^{-3}$, Cc./Mole*		*$[\eta]$, Dl./G.*[c]	
pH	*0.2M NaCl, 0.1M buffer*[b]	*3.0M NaCl, 0.1M buffer*	*0.2M NaCl, 0.1M buffer*	*3.0M NaCl, 0.1M buffer*	*0.2M NaCl, 0.1M buffer*	*3.0M NaCl, 0.1M buffer*	*0.2M NaCl, 0.1M buffer*	*3.0M NaCl, 0.1M buffer*
2.6	31	59	2.6	1.6	13	6	1.55	1.00
4.1	40	40	2.0	1.8	10	7	1.30	0.72
6.3	14		0.7		3		1.00	0.92
7.2	13	6	0.7	0.8	4	3	0.70	0.90
9.1	17		1.0		5		0.68	0.76
10.0	30	37	1.2	1.3	6	5	0.62	0.71
11.4		59		1.9		7	0.58	Gel
12.6	54		2.9		15		Gel	Gel
Rigid sphere	None	None	16	22	83	83	0.020	0.020

[a] MW = 105,000; pK° = 10.44 (*40*); conjugated with fluorescein.
[b] Buffer citrate, phosphate, or carbonate.
[c] Changes in intrinsic viscosity as a function of pH are reversible.

intrinsic viscosity of the polymer in high salt is comparable to that in low salt, except that gel formation occurs at a lower pH (Table III). This would be expected, because the uncharged or partially charged helix would be less soluble at high salt concentration; therefore, gelation would occur earlier.

In acid solution (below pH 6.3) and low salt concentration the polylysine coil expands, becomes more rigid, and has a greater degree of internal organization. These changes are reflected in higher intrinsic viscosities, longer rotational relaxation times, and higher transition temperatures (Table III). The same phenomenon occurs at high salt concentration, and in addition, the polymer has a more stable internal structure (higher T_T) and a smaller equivalent volume at pH 2.6. The increase in intrinsic viscosity is largely suppressed by the high salt concentration; therefore, its basis is electrostatic. One hypothesis to explain the experimental findings in acid solution postulates the adsorption of hydrogen ion by the amide groups of the polypeptide backbone: the increased electrostatic repulsion

Table IV. Effect of Aging in Solid State on High and Low Molecular Weight Poly Lys·HCl, Poly $Glu^{97}Lys^{3}$, and Poly Glu^{6} Lys^{37} (No. 3)

	Intrinsic Viscosity			
Time, Weeks	*Poly Lys (No. 2)*[a]	*Poly Lys (No. 3)*[a]	*Poly* $Glu^{97}Lys^{3}$[b]	*Poly* $Glu^{63}Lys^{37}$ *(No. 3)*[b]
0	0.35	2.08	1.69	0.98
30	1.16	2.30		
65	1.31	2.15	1.75	0.92

[a] Solvent 0.3*M* NaCl, pH 7.2; stored at 25°C.
[b] Solvent 0.11*M* NaCl + 0.04*M* phosphate, pH 7.6; stored at 25°C.

would cause an expansion and increased rigidity of the coil. Adding salt would stabilize the adsorbed hydrogen ions; therefore the internal structure of the molecule would become more rigid as the pH is lowered. In addition, the increased salt concentration would shield some of the long-range effects of the adsorbed hydrogen ions and thus decrease the expansion of the coil.

When poly Lys (No. 2) in solution at pH 10.03 is heated, it shows a melting out of rigid structure and then a transition to a more rigid structure; on cooling there is a transition to a less rigid structure and then a return to the original structure (*30*, *31*, *32*). In water these transitions occur at 36° ± 1°, 55° ± 3°, 43° ± 3°, and 29° ± 11°C., respectively, and in 0.2*M* NaCl + 0.1*M* carbonate buffer they occur at 31° ± 1°, 52° ± 1°, 33° ± 3°, and 15° ± 5°C., respectively. These changes in rigidity are reversible, and they correspond to the α-helix to β-conformation transition observed in solid films (*4*) and in solutions (*1*). The reversibility is probably caused, at least in part, by using dilute solutions (0.03 mg. per ml.). In 3.0*M*

Publication Date: January 1, 1967 | doi: 10.1021/ba-1967-0063.ch015

In Ordered Fluids and Liquid Crystals; Porter, R., el al.;
Advances in Chemistry; American Chemical Society: Washington, DC, 1967.

NaCl + 0.1*M* carbonate buffer only one transition occurs, at 41° ± 6°, and shortly thereafter the polymer precipitates; the nature of this transition is not understood at present.

Poly Lys (No. 2) displays an increase in viscosity on standing in the solid state; this occurs within the first several months after preparation. In contrast, a higher molecular weight sample of polylysine, poly Lys (No. 3), does not show a change in viscosity with aging. Neither poly $Glu^{97}Lys^{3}$ nor poly $Glu^{63}Lys^{37}$ (No. 3) shows any significant evidence of change on standing in the solid state for a comparable amount of time (Table IV). In contrast to its behavior in the solid state, poly Lys (No. 2) in solution in 0.2*M* NaCl + 0.1*M* phosphate buffer, pH 7.2, maintains a constant viscosity at 2°C. for at least 3 months. Thus, the change that occurs in the solid state does not take place in solution. The reason for the change in viscosity of low molecular weight polylysine in the solid state is not understood.

Polyvinylamine (PVA)

This polycation was used as a model for polylysine, especially to study its behavior in acid solution. Since it has a vinyl and not a polyamide backbone, it should not adsorb hydrogen ions in acid solution and thus should not show any changes in intrinsic viscosity, transition temperature, or rotational relaxation time in acid solution. The pK° is 9.4, but because of nearest neighbor interactions, the molecule is not completely charged until pH 4 to 5 in 0.1 to 1.0*M* NaCl (*39*, *40*). The data in Table V show

Table V. Polarization of Fluorescence Parameters and Intrinsic Viscosity of Polyvinylamine[a,b]

pH	*Transition Temp.* (T_T), °C.	$\rho_h^5 \times 10^8$, *Sec.*	$V_e^5 \times 10^{-3}$, *Cc/Mole*	[η], *Dl./G.*[c]
2.5	53	0.6	3	3.5
3.6	59	0.7	4	3.6
4.8	62	0.8	4	3.6
7.8	18	0.8	4	3.0
12.6	15	1.2	6	2.0
Rigid sphere	None	7.9	40	0.020

[a] MW = 51,000; pK° = 9.4 (*39*); conjugated with fluorescein.
[b] Solvent 0.3*M* NaCl adjusted to pH 7.2.
[c] Changes in intrinsic viscosity as a function of pH are reversible.

that the behavior of the molecule at pH 4.8 and below is essentially the same so that once the molecule is completely charged, its behavior does not change with the addition of more hydrogen ions. These findings add support to the hypothesis that the change in behavior of polylysine in acid solution is caused by hydrogen ion adsorption by the polypeptide backbone.

In alkaline solution the molecular domain shrinks rapidly as the ammonium groups are titrated, and the internal organization of the molecule,

Publication Date: January 1, 1967 | doi: 10.1021/ba-1967-0063.ch015

reflected in the lower transition temperatures, decreases. The rigidity of the uncharged molecule (at pH 12.6) is greater than that of any of the charged species since its rotational relaxation time is approximately 70 to 100% longer.

Poly Glu^{63}Lys^{37} (No. 3)

The rigidity of the coil form at neutral pH [$p^{22}(F) = 0.037$] and the stability of the internal structure ($T_T = 10°$) are approximately the same as those of poly Lys (No. 2) and considerably greater than those of poly Glu^{97}Lys^{3}.

In acid solution, the polymer undergoes a helix-coil transition with an increase in transition temperature, rotational relaxation time, equivalent volume, and intrinsic viscosity as the molecule goes into the helical conformation (Table VI). At pH 3.3 the rotational relaxation time decreases,

Table VI. Polarization of Fluorescence Parameters and Intrinsic Viscosity of Poly Glu^{63}Lys^{37} (No. 3)[a,b]

pH	*Transition Temp.* (T_T), °C.	$\rho_h^5 \times 10^8$, *Sec.*	$V_e^5 \times 10^{-3}$, *Cc./Mole*	[η], *Dl./G.*[c]
3.3	None	4.5	23	2.20
4.7	32	7.5	38	1.30
5.9	14	1.2	6	1.28
7.2	10	0.9	5	1.14
9.7	7	0.6	3	1.48
Rigid sphere	None	20	100	0.016

[a] MW = 152,000; $pK_A° = 4.62$, $pK_B° = 10.05$ (*34*); conjugated with fluorescein.
[b] Solvent 0.2*M* NaCl + 0.1*M* buffer (citrate, phosphate, or carbonate).
[c] Changes in intrinsic viscosity as a function of pH are reversible.

and there is no transition temperature, but the intrinsic viscosity continues to increase. These findings indicate the existence of a polypeptide chain with a very stable structure but with decreased rigidity. Likewise, changes in the degree of polarization and in optical rotation show a decrease between pH 4 and 5, at which point all of the residues are theoretically in the helical conformation. These data suggest that there is a transformation of the α-helix into a more stable, but less rigid, structure as the pH decreases. The increase in intrinsic viscosity at pH 3.3 can be explained by increased repulsions among the charged lysine residues when the glutamic acid residues are completely titrated.

In the alkaline region the intrinsic viscosity increases because of expansion of the coil by the increasingly potent repulsion among the charged glutamic acid residues as the lysine residues are titrated.

Helix-Coil Transition

The helix-coil transition is an important structural transition in polypeptides, and it has been extensively studied by a variety of methods.

Publication Date: January 1, 1967 | doi: 10.1021/ba-1967-0063.ch015

Polarization of fluorescence measurements were made with poly $Glu^{97}Lys^{3}$, poly Lys (No. 2), and poly $Glu^{63}Lys^{37}$ (No. 3) in order to investigate the rigidity and stability of the glutamic acid helix, the lysine helix, and the helix in the copolymer containing both glutamic acid and lysine (*31*). The helix-coil transition determined by hydrodynamic measurements—i.e., polarization of fluorescence—was compared with that detected by optical rotation and by titration. In addition, the effects of changes in ionic strength on the helix-coil transition were studied.

The helices of poly $Glu^{97}Lys^{3}$ and poly $Glu^{63}Lys^{37}$ (No. 3) show a higher degree of polarization and a longer rotational relaxation time than the helix of poly Lys (No. 2), and the equivalent volumes of the glutamic acid helices are larger (Table VII). The modest increases in ρ_h^5, ρ_h^5/ρ_o^5, and V_e^5 in going from the coil to helical form in poly Lys (No. 2) reflect a helical structure that is less rigid than that of poly $Glu^{97}Lys^{3}$ or poly $Glu^{63}Lys^{37}$ (No. 3).

The helix-coil transition in the copolymer clearly shows that the glutamic acid residues form the dominant helix (Table VII). There is no helix formation at alkaline pH owing to the lysine residues either by polarization of fluorescence or by optical rotation measurements; in fact, both p and $[\alpha]_D$ decrease. The degree of polarization at pH 4 can be 85% reduced by $9M$ urea in both poly $Glu^{97}Lys^{3}$ and poly $Glu^{63}Lys^{37}$ (No. 3); this reflects destruction of the glutamic acid helix.

The pH's of the midpoint and of the point of completion of the helix-coil transition at different salt concentrations, as measured by polarization of fluorescence, are given in Table VIII. The transition in poly Lys (No. 2) is shifted to higher pH by an increased salt concentration. This shift is caused by stabilization of the charged coil form by the increasing salt con-

Table VII. Summary of Data for Helix-Coil Transition in Synthetic Polypeptides Measured by Polarization of Fluorescence Methods (*31*)[d]

Polymer	*pH*	p[a]	T_T, °C.	$\rho_h^5 \times 10^8$, *Sec.*[b]	ρ_h^5/ρ_o^5	$V_e^5 \times 10^{-3}$[c], *Cc./Mole*
Poly $Glu^{97}Lys^{3}$	3.27	0.185	21	5.2	0.37	26
	5.35	0.022	12	0.8	0.06	4
	9.58	0.010	<0			
Poly Lys (No. 2)	7.20	0.053	13	0.7	0.04	4
	9.13	0.053	17	1.0	0.06	5
	10.03	0.061	30	1.2	0.08	6
	11.00	0.087				
Poly $Glu^{63}Lys^{37}$ (No. 3)	4.67	0.088	32	7.5	0.38	38
	7.20	0.049	10	0.9	0.05	5
	9.72	0.049	7	0.6	0.03	3
	11.00	0.044				

[a] Measured with DNS-labeled polypeptides at 22°C.
[b] Measured with fluorescein-labeled polypeptides.
[c] $\rho_h^5/\rho_o^5 = V_e^5/V_o$.
[d] Solvent is $0.2M$ NaCl + $0.1M$ buffer (citrate, phosphate, or carbonate).

Table VIII. pH of Helix-Coil Transition as a Function of Salt Concentration Measured by Polarization of Fluorescence Methods[a]

	Mid-Point of Transition			*Completed Transition*		
Solvent	*Poly $Glu^{97}Lys^{3}$*	*Poly Lys (No. 2)*	*Poly $Glu^{63}Lys^{37}$ (No. 3)*	*Poly $Glu^{97}Lys^{3}$*	*Poly Lys (No. 2)*	*Poly $Glu^{63}Lys^{37}$ (No. 3)*
Water		9.6	6.1		10.7	5.0
0.2*M* NaCl, 0.1*M* buffer[b]	4.5	10.3	5.1	3.5	11.2	4.2
3.0*M* NaCl, 0.1*M* buffer[b]		10.7	4.6		12.4	3.6

[a] Measured with DNS-labeled polypeptides at 22°C.
[b] Buffer citrate, phosphate, or carbonate.

centration, which, in turn, causes the pH of the transition to be shifted to higher values. In poly $Glu^{63}Lys^{37}$ (No. 3) the pH of the transition decreases as the salt concentration increases. This change is also caused by stabilization of the charged coil by the increased salt concentration so that lower pH's must be attained to effect the helix-coil transition. The same conclusions are apparent from the pH's of the completed helix-coil transitions.

The midpoint of the helix-coil transition in poly $Glu^{97}Lys^{3}$ (pH 4.5 in 0.2*M* NaCl + 0.1*M* buffer) is lower than that obtained from titration(pH 5.1 in 0.2*M* NaCl) (*46*, *63*) and from optical rotation (pH 5.1 in 0.2*M* NaCl) (*12*, *17*, *37*, *63*). This suggests that the glutamic acid residues assume the helical conformation before the helix reaches its maximal rigidity. The midpoint of the transition in poly Lys (No. 2) (pH 9.6 in water) is approximately the same as that obtained by titration (pH 9.4 in water) (*1*) but lower than that obtained from optical rotation (pH 10.0 in water) (*1*). This indicates that the helical form reaches its maximal rigidity before all the residues have gone into the helical conformation. The discrepancy between the hydrodynamic and conformational measurements could be explained by the presence of breaks in the polylysine helix. Several such breaks would profoundly affect the hydrodynamics of the helix, but the small number of residues not in the helical conformation at the sites of the breaks would not be detected by optical rotation measurements. The midpoint of the transition for poly $Glu^{63}Lys^{37}$ (No. 3) (pH 5.1 in 0.2*M* NaCl + 0.1*M* buffer) is higher than that obtained by titration (pH 4.42 in 0.15*M* KCl) (*34*) but the same as that from optical rotation in polypeptides of comparable composition (pH 5.2 in 0.2*M* NaCl) (*3*, *12*). Thus the changes in rigidity and conformation occur at the same time in this polymer.

The same conclusions concerning the relationship between changes in rigidity and helical content can be substantiated by comparing the pH values at which the maximal rigidity (polarization of fluorescence) and the maximal helical content (optical rotation) occur. The pH values of max-

In Ordered Fluids and Liquid Crystals; Porter, R., el al.;
Advances in Chemistry; American Chemical Society: Washington, DC, 1967.

imal polarization, complete titration, and maximal optical rotation, under the same conditions where the mid-points were measured are, respectively, 3.5, 2.8, and 4.5 for poly $Glu^{97}Lys^{3}$; 10.7, 11.0, and 11.8 for poly Lys (No. 2); and 4.2, 3.0, and 4.0 for poly $Glu^{63}Lys^{37}$ (No. 3). [The references for the data on the end points of the helix-coil transition are the same as for the data on the mid-points. Similar data on DNS-polylysine are given by Edelhoch and Steiner (*16*).]

Cross-linked Synthetic Polypeptides

Polymers with intramolecular cross-links have organized spatial structures, and are good models for the tertiary structure of proteins (*26*, *27*, *42*). In the studies discussed here poly $Glu^{52}Lys^{33}Tyr^{15}$ (No. 3) was internally cross-linked with Woodward's reagent K or ionic carbodiimide and fractionated on Sephadex G-100. The number of cross-links in each fraction was determined by amino acid analysis. In addition, the parent polymer was fractionated in the same way to provide standards for comparison with the cross-linked polypeptides.

The presence of intramolecular cross-links introduces organized spatial structure into the molecules, as indicated by the increased transition temperatures but does not endow them with a greater degree of rigidity until the derivative contains six intramolecular cross-links. The transition temperature, hence the stability of the internal structure, increases as the number of cross-links in the molecules increases. Typical examples of the effect of introducing increasing numbers of cross-links into the molecule are shown in Figure 5, and all of the data are summarized in Table IX. Halving the molecular weight of poly $Glu^{52}Lys^{33}Tyr^{15}$ (No. 3) does not affect its rigidity

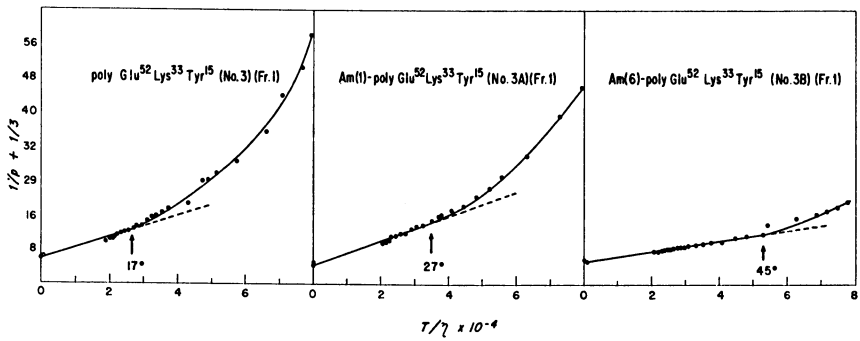

Courtesy Biopolymers

Figure 5. Changes in polarization of fluorescence with temperature for two cross-linked polymers and their parent polymer

Measurements made in 0.2M NaCl + 0.1M phosphate buffer, pH 7.2, at concentration of 0.1 to 0.2 mg./ml. (26). Transition temperatures indicated on graph

Publication Date: January 1, 1967 | doi: 10.1021/ba-1967-0063.ch015

(ρ_h^5) but does decrease the internal organization of the polypeptide chain (T_T).

In contrast to the graded effect on the polarization measurements of introducing one, four, or six cross-links into the molecule, the effect on the intrinsic viscosity does not vary with the number of cross-links. Thus the presence of one cross-link decreases the over-all hydrodynamic domain of the molecule approximately as much as four or six cross-links.

Table IX. Polarization of Fluorescence Parameters and Intrinsic Viscosities of Cross-linked Synthetic Polypeptides and Their Parent Polymers (*26*)[a]

Polypeptide	*Transition Temp.* (T_T), °C.	$\rho_h^5 \times 10^8$, *Sec.*	ρ_h^5/ρ_o^5	$V_e^5 \times 10^{-3}$, *Cc./Mole*	[η], *Dl./G.*
Poly Glu[52]Lys[33]Tyr[15] (No. 3)[b]	22	0.9	0.13	5	0.30
Poly Glu[52]Lys[33]Tyr[15] (No. 3) (alkali-degraded)[c]	12	1.1	0.16	6	0.18
Poly Glu[52]Lys[33]Tyr[15] (No. 3) (Fr. 1)	17	1.3	0.19	7	0.40
Am(1)-poly Glu[52]Lys[33]Tyr[15] (No. 3A) (Fr. 1)	27	1.2	0.18	6	0.26
Am(6)-poly Glu[52]Lys[33]Tyr[15] (No. 3B) (Fr. 1)	45	4.7	0.69	24	0.28
Poly Glu[52]Lys[33]Tyr[15] (No. 3) (Fr. 2)	12	1.2	0.18	6	0.34
Am(1)-poly Glu[52]Lys[33]Tyr[15] (No. 3A) (Fr. 2)	15	0.9	0.13	5	0.12
Am(4)-poly Glu[52]Lys[33]Tyr[15] (No. 3B) (Fr. 2)	33	1.5	0.22	8	0.13
Rigid sphere	None	6.8	1.00	34	0.016

[a] Measured at pH 7.2 (0.2*M* NaCl + 0.1*M* phosphate); conjugated with fluorescein.
[b] MW = 50,000.
[c] MW = 25,000.

The internal structure of the cross-linked synthetic polypeptides is maintained by heat-stable, covalent bonding between the cross-linked amino acid side chains and by heat-labile, noncovalent side chain interactions between glutamic acid and lysine residues (electrostatic) and between tyrosine residues (nonpolar). The stability of the spatial structure of a polymer depends upon the relative proportion of covalent and noncovalent bonding that it contains and increases as the number of cross-links increases. According to the current theories of protein structure, the charged amino acid residues would be arrayed on the surface of the molecule, and the tyrosine residues would be internally placed and thus interact to give a hypochromic effect. Am(6)-poly Glu[52]Lys[33]Tyr[15] (No. 3B) (Fr. 1) displays such an effect, and the molar extinction coefficient of the cross-linked derivative is 25% lower than that of the parent polymer. This hypo-

Publication Date: January 1, 1967 | doi: 10.1021/ba-1967-0063.ch015

chromic effect occurs at 280 mμ in water and 0.2*M* NaF but not at 190 mμ in either of these solvents. The latter finding indicates that the polypeptide chain is not arrayed in such a fashion that the peptide bond chromophores interact. Further evidence for the existence of an organized internal structure in cross-linked synthetic polypeptides is the existence of a hysteresis effect in the heating studies: when the polymer is cooled following heating to 60° to 70°C., the polarization measurements do not coincide with those of the heating cycle. The increased values of $(1/p + 1/3)$ on cooling indicate a more rapid depolarization owing to loss of the constraints of the internal structure. A second heating and cooling cycle indicates that the loss of internal structure is irreversible.

Stability in Solution

The five polypeptides investigated were studied for their stability in solution at 25°, 2°, and −20°C. by measuring the polarization of fluorescence periodically for up to 6 months. The results are shown in Figure 6. Poly $Glu^{63}Lys^{37}$ (No. 3) and PVA are very stable in solution and poly Lys (No. 2) is moderately stable. On the other hand, poly $Glu^{97}Lys^{3}$ and Am(6)-poly $Glu^{52}Lys^{33}Tyr^{15}$ (No. 3B) (Fr. 1) are unstable in solution; hence these two polymers must be studied within several days after they are dissolved.

Proteins

The broad aim of studying synthetic polypeptide model systems is to interpret better data obtained from studies of proteins and to design better experiments to gain new information about proteins. Protein studies using the polarization of fluorescence method have been reviewed recently by Weber (*65*), Steiner and Edelhoch (*54*) and Edelhoch and Steiner (*16*).

Rotational relaxation times have been calculated for proteins ranging in molecular weight from insulin (6000) (*59*) to thyroglobulin (670,000) (*55*). The molecular dimensions computed from polarization of fluorescence data are generally consistent with those expected from results of other approaches. Perhaps the most important generalization from these studies is that with two exceptions, the reported values of ρ_h/ρ_o are equal to, or greater than, unity (*16*). The implications are that internal degrees of rotational freedom are largely absent and that the molecular organization of these globular proteins endows them with a great deal of structural rigidity. The two exceptions are legumin (*38*) and γ-globulin (*56*), both of which have ρ_h/ρ_o values less than unity, implying that these proteins possess some degree of internal flexibility. In both of these proteins, this finding may reflect the flexibility of the attachments between the structural units (*18*, *47*).

The native state of most globular proteins appears to consist of highly compact, rigid, and nearly symmetrical particles, suggesting that a maximal

Publication Date: January 1, 1967 | doi: 10.1021/ba-1967-0063.ch015

In Ordered Fluids and Liquid Crystals; Porter, R., el al.;
Advances in Chemistry; American Chemical Society: Washington, DC, 1967.

number of intramolecular interactions are present. The degree of modification of the native structure produced by thermal stress, denaturing solvents, or extremes of pH may be studied by the polarization of fluorescence. The loss of native structure generally produces a new molecular state characterized by enhanced flexibility of the polypeptide chains. The ratio of the observed rotational relaxation time to that of a rigid model furnishes a measure of the disruption of internal structure (*16*). For example, thyroglobulin shows a particularly sensitive and graded response to the action of various denaturants (*55*); at pH's greater than 11 or at low concentrations of urea or detergent a partial dissociation into half-molecules occurs, and exposure to more drastic conditions produces a further fragmentation into smaller subunits. This fragmentation is accompanied by an extensive loss of internal structure which is reflected by a decrease in ρ_h/ρ_o to values ranging down to 0.11. The effect of urea or detergents

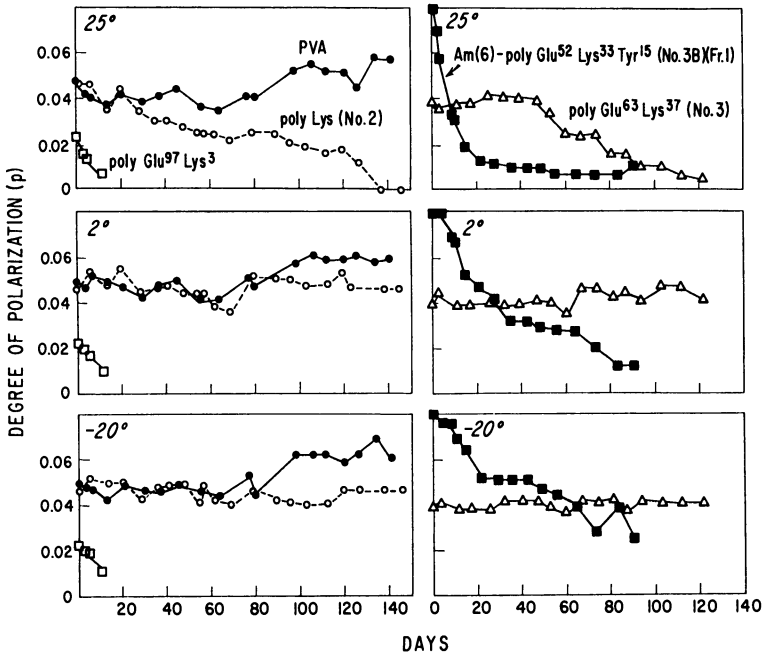

Figure 6. Effect of aging in solution at three temperatures on polarization of fluorescence of four synthetic polypeptides and a vinyl polymer

Synthetic polypeptides dissolved in 0.2M NaCl + 0.1M phosphate buffer, pH 7.2, and polyvinylamine dissolved in 0.3M NaCl adjusted to pH 7.2. Symbols for different polymers are same throughout.

was much more drastic than exposure to heat or alkali. The limiting degree of molecular disorganization was not attained even in 9*M* urea at neutral pH since a further drop in relaxation time occurred under more

alkaline conditions. Thus the denaturation of proteins produces increased segmental rotation in a manner analogous to the disruption of internal structure of the synthetic polypeptide model systems. By applying the sensitive polarization of fluorescence method to model systems and proteins, subtle changes of structure may be associated with important alteration in biological activity (*28*). Such variation in activity may be more significant than drastic structural changes, which lead only to total loss of function.

Other proteins similarly studied are bovine serum albumin (*5*, *6*, *36*, *65*, *67*) and ovalbumin (*65*); actin (*61*); fumarase (*43*); α-chymotrypsin (*44*); lysozyme (*59*, *64*); arachin (*5*); β-lactoglobulin and κ-casein (*45*); γ-globulin (*56*); ribonuclease (*24*, *35*, *68*); glutamic dehydrogenase (*7*); soybean trypsin inhibitor (*15*, *57*); and pepsinogen (*14*, *21*, *58*).

Fluorescence polarization is particularly suited to studying the interaction of two proteins, only one of which is labeled with a fluorescent dye. In the absence of free rotation between the components of the complex, the observed increase in relaxation time will reflect the behavior of the entire complex. This approach has been applied to the determination of association constants and free energy characterizing the electrostatic interaction of lysozyme with serum albumin and with DNA (*52*), to the stoichiometric interaction of trypsin and the soybean trypsin inhibitor (*53*), to the self-association of α-chymotrypsin with chymotrypsinogen (*44*), and to the binding of reduced coenzyme to dehydrogenases (*62*). The effects of solvent composition, pH, and ionic strength upon the multiple equilibria of insulin were studied by Steiner and McAlister (*59*). Finally, this technique has been employed to study the direct molecular combination of labeled protein antigens with their antibodies (*2*, *9*, *10*, *11*, *35*). The sensitivity of this method permits direct study of the antibody-antigen interaction without resorting to secondary phenomena of the immunological reaction, such as precipitation or complement fixation.

Publication Date: January 1, 1967 | doi: 10.1021/ba-1967-0063.ch015

Discussion

The investigations presented in this study focus on the interpretation of polarization of fluorescence measurements and the use of these measurements to study the structure of a representative spectrum of linear synthetic polypeptides, of polyvinylamine, and of a cross-linked synthetic polypeptide.

The first methodological study validated the use of the transition temperature as a measure of the stability of the internal structure of a synthetic polypeptide. The constancy of the transition temperature over a wide range of viscosities indicates that it reflects the activation energy needed to disrupt the internal structure of the polypeptide and that this energy cannot be provided by changes in viscosity alone. Since the equivalent volume of the rotational kinetic unit, V_e, decreases above the transition

temperature, the Perrin equation (Equation 1) must be modified if it is to be applicable above the transition temperature. This may be done by using a more general description of the volume, such as an empirical function of the form:

$$V_e = V_o - \int_{T_T}^{T} \frac{dV_s(T)}{d(T/\eta)}\, dT \tag{9}$$

where V_o is the constant equivalent volume of the rotational kinetic unit below the transition temperature, and $V_s(T)$ is a function describing the dependence of the equivalent volume on temperature above the transition temperature.

The second aspect of the methodological studies demonstrates the importance of understanding the relationship between the fluorescent dye and the polypeptide to which it is conjugated. This is especially important for determining rotational relaxation times, ρ_h, and for studying the variation in polypeptide structure as a function of pH. The properties of the fluorescent dyes can give adventitious results in both of these experiments if their independent effects on the polarization of fluorescence are not understood and a suitable dye is not selected for use. The first major problem involves independent solvent effects on the dye causing changes which do not reflect changes in the polypeptide chain. DNS is bound less tightly to the adjacent polypeptide chain, and the rotational relaxation time of the polymer-dye conjugate is adventitiously long because the dye does not accurately follow the rotational behavior of the polypeptide in solution. Fluorescein is bound more strongly; hence it is a better dye for following the rotational behavior of the polypeptide chain. The second major source of error is the change in spectral properties of the dye when it conjugated to the polypeptide. Many of the latter difficulties arise because in essence, the dye conjugated to a polymer is in a medium of high viscosity and any changes in the polarization behavior of the dye owing to this constraint can seriously bias the results of the measurements. The properties of DNS in solutions of high viscosity or conjugated to a synthetic polypeptide are little affected by pH's above 2.5; hence, this dye is useful for studying the variation of the polypeptide structure as a function of pH. On the other hand, the polarization properties of fluorescein are profoundly affected in solutions of high viscosity and when conjugated to a polypeptide. Thus, fluorescein is not generally useful for studying the effect of pH on the structure of polypeptides.

The studies of the molecular structure of representative classes of synthetic polypeptides in solution focus on four areas: (1) the structure of the random coil, (2) the helix-coil transition, (3) the α-helix to β-conformation transition in polylysine, and (4) the stability of the internal structure of intramolecularly cross-linked synthetic polypeptides. The "random coil" is not truly random in solution, and its structure depends upon its

Publication Date: January 1, 1967 | doi: 10.1021/ba-1967-0063.ch015

amino acid composition and a variety of intramolecular interactions. The structure can be altered by changes in ionic strength, the addition of organic solvents, and ion adsorption. The coil forms of polypeptides composed of different amino acids display different degrees of rigidity, ρ_h, and internal organizations of different stability, T_T. The over-all hydrodynamic domain of the polypeptide (intrinsic viscosity) reflects the expansile properties of the entire polypeptide chain, and it can vary independently of the changes in internal organization and rigidity of the polypeptide.

The helix-coil transition can be demonstrated by polarization of fluorescence techniques, and the results may be compared with spectroscopic measurements to correlate the change in the hydrodynamic properties of the molecule with the change of its conformational structure. It is clear that the hydrodynamic and conformational changes do not necessarily parallel one another. Ion adsorption, breaks in the helix, and changes in helical type can occur without being reflected in the optical rotation parameters.

The α-helix to β-conformation transition can be measured hydrodynamically, and the results agree well with the same transition demonstrated by infrared spectroscopy in solid films. Recent studies (*32*) of this transition by far-ultraviolet and infrared spectroscopy in solution confirm the nature of the conformational changes.

Introducing intramolecular amide bonds into synthetic polypeptides produces organized spatial structure which makes these polymers good models for the tertiary structure of proteins. The transition temperature, which measures the organized internal structure of the molecule, increases as the number of cross-links increases. The amount of internal structure has little effect on the over-all rigidity of the molecule until six cross-links have been introduced into the polymer. On the other hand, the over-all hydrodynamic domain of the molecule decreases to the same extent whether one, four, or six intramolecular cross-links are present.

The usefulness of polarization of fluorescence measurements for studying the secondary and tertiary structure of polymers is unique, in that it provides a sensitive hydrodynamic method for detecting rather small changes in the stability of the internal structure and in the rigidity of the molecule. The criterion of transition temperature provides a measurement of the stability of the internal structure whose subtlety falls between that of the usual hydrodynamic methods of intrinsic viscosity, sedimentation, and diffusion, which indicate the over-all size and shape of the molecule, and that of the spectroscopic and optical rotatory dispersion techniques, which provide intimate details about the structure of the polypeptide chain. The changes in the rotational relaxation time give a quantitative estimate of the over-all rigidity of the molecule. Thus the technique of polarization of fluorescence has unique applicability to the studies of the organized spatial structure of macromolecules and is especially useful in studies corre-

Publication Date: January 1, 1967 | doi: 10.1021/ba-1967-0063.ch015

In Ordered Fluids and Liquid Crystals; Porter, R., el al.;
Advances in Chemistry; American Chemical Society: Washington, DC, 1967.

lating changes in the hydrodynamic properties of molecules with the changes in their conformational properties.

Acknowledgment

The authors thank Elaine M. McLaughlin for her excellent technical assistance throughout the course of these studies and Edie West for her help in preparing the manuscript.

Literature Cited

(1) Applequist, J., Doty, P., "Polyamino Acids, Polypeptides and Proteins," M. A. Stahmann, ed., p. 161, University of Wisconsin Press, Madison, 1962.
(2) Bennett, J. C., Haber, E., *J. Biol. Chem.* **238**, 1362 (1963).
(3) Blout, E. R., Idelson, M., *J. Am. Chem. Soc.* **80**, 4909 (1958).
(4) Blout, E. R., Lenormant, H., *Nature* **179**, 960 (1957).
(5) Chadwick, C. S., Johnson, P., *Biochim. Biophys. Acta* **53**, 482 (1961).
(6) Churchich, J. E., *Arch. Biochem. Biophys.* **97**, 574 (1962).
(7) Churchich, J. E., Wold, F., *Biochemistry* **2**, 781 (1963).
(8) Cohn, E. J., Edsall, J. T., "Proteins, Amino Acids and Peptides," p. 375, Reinhold, New York, 1943.
(9) Dandliker, W. B., Feigen, G. A., *Biochem. Biophys. Res. Commun.* **5**, 299 (1961).
(10) Dandliker, W. B., Halbert, S. P., Florin, M. C., Alonso, R., Schapiro, H. C., *J. Expt. Med.* **122**, 1029 (1965).
(11) Dandliker, W. B., Schapiro, H. C., Meduski, J. W., Alonso, R., Feigen, G. A., Hamrick, J. R., Jr., *Immunochem.* **1**, 165 (1964).
(12) Doty, P., Imahori, K., Klemperer, E., *Proc. Natl. Acad. Sci. U.S.* **44**, 424 (1958).
(13) Edelhoch, H., Steiner, R. F., *Biochem. Biophys.* Acta **60**, 365 (1962).
(14) Edelhoch, H., Frattali, V., Steiner, R. F., *J. Biol. Chem.* **240**, 112 (1965).
(15) Edelhoch, H., Steiner, R. F., *J. Biol. Chem.* **238**, 931 (1963).
(16) Edelhoch, M., Steiner, R. F., "Electronic Aspects of Biochemistry," p. 7, Academic Press, New York, 1964.
(17) Fasman, G., Lindblow, C., Bodenheimer, E., *Biochemistry* **3**, 155 (1964).
(18) Feinstein, A., Rowe, A. J., *Nature* **205**, 147 (1965).
(19) Feofilov, P. P., "Physical Basis of Polarized Emission," Consultants Bureau, New York, 1961.
(20) Forster, T., "Fluöreszenz der Organischer Verbindungen," Vandenhoeck and Ruprecht, Göttingen, 1951.
(21) Frattali, V., Steiner, R. F., Edelhoch, H., *J. Biol. Chem.* **240**, 112 (1965).
(22) Frey, M., Wahl, Ph., Benoit, H., *J. Chim. Phys.* **61**, 1005 (1964).
(23) Friedman, E., Gill, T. J., III, Doty, P., *J. Am. Chem. Soc.* **83**, 4050 (1961).
(24) Gally, J. A., Edelman, G. M., *Biochim. Biophys. Acta* **60**, 499 (1962).
(25) Gill, T. J., III, *Biopolymers* **2**, 283 (1964).
(26) *Ibid.*, **3**, 43 (1965).
(27) Gill, T. J., III, Kunz, H. W., Marfey, P. S., *Biopolymers* **2**, 395 (1964).
(28) Gill, T. J., III, Kunz, H. W., Marfey, P. S., *J. Biol. Chem.* **240**, PC3227 (1965).
(29) Gill, T. J., III, McLaughlin, E. M., Omenn, G. S., *Biopolymers*, in press.
(30) Gill, T. J., III, Omenn, G. S., "Abstracts of Papers," 150th Meeting, ACS, September 1965, C230.
(31) Gill, T. J., III, Omenn, G. S., *J. Am. Chem. Soc.* **87**, 4188 (1965).
(32) Gill, T. J., III, Omenn, G. S., unpublished observations.
(33) Gottlieb, Y. Y., Wahl, Ph., *J. Chim. Phys.* **60**, 849 (1963).
(34) Gould, H. J., Gill, T. J., III, Doty, P., *J. Biol. Chem.* **239**, 3071 (1964).
(35) Haber, E., Bennett, J. C., *Proc. Natl. Acad. Sci. U.S.* **48**, 1935 (1962).
(36) Harrington, W. F., Johnson, P., Ottewill, R. H., *Biochem. J.* **62**, 569 (1956).
(37) Idelson, M., Blout, E. R., *J. Am. Chem. Soc.* **80**, 4631 (1958).

(38) Johnson, P., Richards, E. G., *Arch. Biochem. Biophys.* **97**, 260 (1962).
(39) Katchalsky, A., Mazur, J., Spitnik, P., *J. Polymer Sci.* **23**, 513 (1957).
(40) Katchalsky, A., Shavit, N., Eisenberg, H., *J. Polymer Sci.* **13**, 69 (1954).
(41) Laurence, D. J. R., in "Methods of Enzymology," Vol. IV, S. P. Colowick and N. O. Kaplan, eds., p. 174, Academic Press, New York, 1957.
(42) Marfey, P. S., Gill, T. J., III, Kunz, H. W., *Biopolymers* **3**, 27 (1965).
(43) Massey, V., quoted in (*65*).
(44) Massey, V., Harrington, W. F., Hartley, B. S., *Discussions Faraday Soc.* **20**, 24 (1955).
(45) Morr, C. V., van Winkle, Q., Gould, I. A., *J. Dairy Sci.* **45**, 811, 817, 823 (1962).
(46) Nagasawa, M., Holtzer, A., *J. Am. Chem. Soc.* **86**, 538 (1964).
(47) Noelken, M. E., Nelson, C. A., Buckley, C. E., III, Tanford, C., *J. Biol. Chem.* **240**, 218 (1965).
(48) Omenn, G. S., Gill, T. J., III, *J. Biol. Chem.* **241**, 4899 (1966).
(49) Oster, G., Nishijima, Y., in "Newer Methods of Polymer Characterization," B. Ke, ed., p. 207, Interscience, Wiley, New York, 1964.
(50) Perrin, F., *J. Phys.* Ser. VI, **7**, 390 (1926); Ser. VII, **5**, 497 (1934); Ser. VII, **7**, 1 (1936); *Acta Phys. Polon.* **5**, 335 (1936); *Ann. Phys.* Ser. X, **12**, 169 (1929).
(51) Rinderknecht, H., *Nature* **193**, 167 (1962).
(52) Steiner, R. F., *Arch. Biochem. Biophys.* **46**, 291 (1953).
(53) *Ibid.*, **49**, 71 (1954).
(54) Steiner, R. F., Edelhoch, H., *Chem. Revs.* **62**, 457 (1962).
(55) Steiner, R. F., Edelhoch, H., *J. Am. Chem. Soc.* **83**, 1435 (1961).
(56) *Ibid.*, **84**, 2139 (1962).
(57) Steiner, R. F., Edelhoch, H., *J. Biol. Chem.* **238**, 925 (1963).
(58) Steiner, R. F., Frattali, V., Edelhoch, H., *J. Biol. Chem.* **240**, 128 (1965).
(59) Steiner, R. F., McAlister, A. J., *J. Colloid Sci.* **12**, 80 (1957).
(60) Steiner, R. F., McAlister, A. J., *J. Polymer Sci.* **24**, 105 (1957).
(61) Tsao, T. C., *Biochim. Biophys. Acta* **11**, 227, 236 (1953).
(62) Velick, S. F., *J. Biol. Chem.* **233**, 1455 (1958).
(63) Wada, A., *Mol. Phys.* **3**, 409 (1960).
(64) Wahl, Ph., Ph.D., thesis, University of Strasbourg, 1962; *J. Chim. Phys.* **63**, 68 (1966).
(65) Weber, G., *Biochem. J.* **51**, 145, 155 (1952); *Advan. Protein Chem.* **8**, 415 (1953).
(66) Weber, G., Teale, F. W. J., in "The Proteins," H. Neurath, ed., Vol. III, p. 445, Academic Press, New York, 1965.
(67) Weber, G., Young, L. B., *J. Biol. Chem.* **239**, 1415, 1424 (1964).
(68) Young, D. M., Potts, J. T., Jr., *J. Biol. Chem.* **238**, 1995 (1963).

RECEIVED January 28, 1966. Studies supported by grants from the National Science Foundation (GB-940 and GB-3603) and the National Institutes of Health (H-1771). T. J. G. was the recipient of a Lederle Medical Faculty Award (1962–1965) and is currently the recipient of a Research Career Development Award from the U. S. Public Health Service (1-K3-AM-5242). G.S.O. received a Student Research Fellowship from the U. S. Public Health Service.

16

Electrical Ordering in Polypeptide Solutions

Molecular Aggregation Studied by the Kerr Effect

JOHN C. POWERS, JR. and WARNER L. PETICOLAS

IBM Research Laboratory, San Jose, Calif.

Publication Date: January 1, 1967 | doi: 10.1021/ba-1967-0063.ch016

Polypeptides possess large dipole moments when in a helical conformation and can be easily ordered in solution by an electric field. Such ordering results in the material's becoming doubly refractive (the Kerr effect). We have investigated the mode of aggregation of poly-γ-benzyl-L-glutamate dissolved in benzene, dioxane, and ethylene dichloride by measuring the Kerr constant as a function of concentration. From a consideration of this dependence on concentration, the calculated dipole moments of the polymers in these solvents, and the measured intrinsic viscosities, two different modes of aggregation are proposed—a linear association for high dielectric solvents (ethylene dichloride) and a lateral (antiparallel) association for low dielectric solvents (benzene, dioxane).

The ordering of solutions of helical polymers may be brought about in a number of ways. If the polymer has a sufficiently high molecular weight, the solution will become ordered spontaneously if the concentration is increased beyond a certain critical concentration. The solution is then said to be in the liquid crystalline state, and it exhibits birefringence because of the anisotropic nature of the solution. If the polymers possess a sufficiently large dipole moment or polarizability, they may be ordered by applying an electric field. This phenomenon is known as the Kerr effect (linear electric birefringence) and may be thought of as the electrical analog of streaming birefringence, the orienting force being an applied electrostatic field instead of forced laminar flow. The external field causes an orientation of the molecules in solution in a direction parallel to the electric field, and this orientation is manifested in an anisotropy of the indices of refraction of the solution in the directions parallel and perpendicular to the applied field—i.e., the solution becomes doubly refracting. This anisotropy produces a phase change in an incident, linearly polarized light beam and can be detected either by a suitable compensator or by photoelectric means.

In Ordered Fluids and Liquid Crystals; Porter, R., el al.;
Advances in Chemistry; American Chemical Society: Washington, DC, 1967.

Although the Kerr effect is common to all matter, it has been particularly valuable in studying solutions of high molecular weight polymers since the degree of ordering of a given solute molecule depends on the size of the interaction of its permanent and/or induced dipole moments with the applied field while the time required for the ordering to be relaxed gives some information as to the size and/or shape of the molecule. Furthermore, if the molecules tend to aggregate, then by measuring the ordering effects in the electric field as a function of concentration, one can learn a great deal about the nature of the aggregates—their size and dipolar characteristics. Thus the main purpose of the work reported here has been to study aggregates of polypeptides in various solvents of low polarity by means of the Kerr effect.

The general theory of the Kerr effect has been well summarized by Le Fèvre and Le Fèvre (*8*, *9*). Kerr's equation for the Kerr constant, B, of a material is given by the relation

$$B = \frac{\delta}{2\pi \times l \times E^2} = \frac{\Delta n}{E^2 \lambda} \tag{1}$$

where δ is the phase change induced by an incident linearly polarized light beam of wavelength λ, l is the length of the cell, E is the applied field in statvolts [1 statvolt (e.s.u.) = 300 volts (c.g.s.)], and Δn is the difference in indices of refraction in the material parallel and perpendicular to the direction of the field; the field is applied at right angles to the direction of propagation of the light. In general for solutes a specific Kerr constant, B/C, is employed; C is in units of grams of solute per unit volume.

An expression for the Kerr constant of a solute has been derived by O'Konski (*14*) by assuming a rigid molecule with the same symmetry axis for electric, optic, and hydrodynamic properties. This derivation has proved useful in the study of rigid macromolecules since it allows a clean separation of the electrical factors responsible for the orientation of the molecule.

The fundamental equation for the birefringence of a dilute solution of axially symmetric particles is that of Peterlin and Stuart (*15*)

$$\frac{1}{\theta_v} \frac{\Delta n}{n} = \frac{2\pi}{n^2} (g_1 - g_2) \int_0^{\pi} f(\theta) \times \frac{3 \cos^2 \theta - 1}{2} \times 2\pi \sin \theta d\theta \tag{2}$$

where θ_v is the volume fraction of particles, Δn is the birefringence, n is the index of refraction of the solution, $(g_1 - g_2)$ is the optical anisotropy factor (subscripts 1 and 2 refer to the major and minor axes, respectively, of the particle), $f(\theta)$ is an orientation distribution function, and θ is the angle between the symmetry axis of the particle and the axis of anisotropy (the direction of the applied field). The interaction energy, U, of the particle with the external field is

$$U = -\mu E B_1 \cos \theta - \tfrac{1}{2} (\alpha_1 - \alpha_2) E^2 \cos^2 \theta \tag{3}$$

Publication Date: January 1, 1967 | doi: 10.1021/ba-1967-0063.ch016

B_1 is an internal field function (equal to 1 for long rods), and α_1 and α_2 are the excess polarizabilities of the particle. The orientation distribution function, $f(\theta)$, becomes

$$f(\theta) = e^{-U/kT} \Big/ \int_0^{\pi} e^{-U/kT} 2\pi \sin\theta d\theta \tag{4}$$

The integral in Equation 2 can be defined as $\Phi(\beta, \gamma)$, a function of a dipole term, $\beta = \mu E B_1/kT$, and a polarizability term, $\gamma = (\alpha_1 - \alpha_2)E^2/2kT$, and is an expression of the degree of orientation. From Equation 2 one obtains,

$$\frac{1}{\theta_v}\frac{\Delta n}{n} = \frac{2\pi}{n^2}(g_1 - g_2)\Phi(\beta,\gamma) \tag{5}$$

and the Kerr constant is given as the product of an optical factor and an orientation factor. Since $\Phi(\beta, \gamma) \to 1$ as $E \to \infty$—i.e., saturation occurs—we have the relation

$$\frac{\Delta n}{\Delta n_s} = \Phi(\beta,\gamma) \tag{6}$$

where Δn_s is the value of the birefringence at saturation. The limiting form of $\Phi(\beta, \gamma)$ for low fields was shown to be

$$\lim_{E\to 0} \Phi(\beta,\gamma) = \beta^2/15 + 2\gamma/15 \tag{7}$$

and for high fields Equations 8 and 9 were obtained.

$$\Phi(\beta,0) = \Phi_\beta = 1 - 3/\beta + 3/\beta^2 \tag{8}$$

$$\Phi(0,\gamma) = \Phi_\gamma = 1 - 3/(2\gamma - 1) \tag{9}$$

The specific Kerr constant defined by Peterlin and Stuart is,

$$K_{sp} = \frac{1}{\theta_v n}\left(\frac{\Delta n}{E^2}\right)_{E\to 0} \tag{10}$$

and from the definitions of β and γ and Equations 5 and 7 it is possible to obtain

$$K_{sp} = \frac{2\pi(g_1 - g_2)}{15n^2}\left(\frac{\mu^2}{k^2T^2} + \frac{\alpha_1 - \alpha_2}{kT}\right) \tag{11}$$

From Equation 1 the experimentally determined specific Kerr constant, B/C, becomes

$$B/C = \frac{2\pi}{15n\rho\lambda}(g_1 - g_2)\left(\frac{\mu^2}{k^2T^2} + \frac{\alpha_1 - \alpha_2}{kT}\right) \tag{12}$$

ρ being the density of the solute. Shah (*19*) has extended this treatment to a disk model, in which the axes of permanent dipole moment and maximum polarizability lie at right angles, and a completely general calcula-

Publication Date: January 1, 1967 | doi: 10.1021/ba-1967-0063.ch016

In Ordered Fluids and Liquid Crystals; Porter, R., el al.;
Advances in Chemistry; American Chemical Society: Washington, DC, 1967.

tion, with no assumptions concerning common axes, has been made by Tinoco (*7*). His result is the same as that obtained from the Langevin-Born orientation theory as given by Le Fèvre and Le Fèvre.

Benoit (*1*) performed a calculation similar to that of O'Konski at a somewhat earlier date and included equations for the rise and decay of the birefringence under the action of a rectangular voltage pulse. Since the rise time depends on both permanent and induced dipole moments, it is a complex function involving more than one time constant and rather difficult to deal with experimentally. The decay time of birefringence, however, depends only on the molecular dimensions and for a rigid rod Benoit obtained the simple formula

$$\Delta n = \Delta n_0 e^{-6\theta\tau} = \Delta n_0 e^{-1/\tau} \tag{13}$$

where Δn_0 is the birefringence at time zero, τ is the exponential time constant, and $\theta_r = 1/6\tau$ is the rotatory diffusion constant. This expression has been used widely to estimate particle dimensions.

Much of the published work using electric birefringence to study macromolecules has been concentrated on substances that could be considered to have a rigid, axially symmetric conformation. Unfortunately, the occurrence of such materials is less widespread than originally supposed. Tobacco mosaic virus (TMV) has been shown by electron microscopy and by light scattering to be a large helical rod. The dimensions of the material obtained by the measurement of decay of birefringence (*12*) in aqueous solution are in agreement with those obtained by light scattering. From the dependence of the Kerr constant on the frequency of the applied field, and the saturation of birefringence (*14*), the orientation of TMV with the field was shown to be caused almost entirely by the induced dipole moment (*13*). Fibrinogen, which initially seemed to have axial symmetry (*24*), was shown on re-examination to have an axis of maximum polarizability at right angles to the axis of permanent dipole moment (*6*). The assumption of an axially symmetric molecule is, however, correct for the case of helical polypeptides.

Poly-γ-benzyl-L-glutumate (PBLG) has been the substance most widely studied, probably because of its solubility in organic solvents. It forms a rigid helix (presumably the Pauling α-helix) in many organic solvents including dimethyl formamide (DMF), *m*-cresol, dioxane, ethylene dichloride, and chloroform-formamide as evidenced by its optical rotatory dispersion spectrum (ORD) (*5*, *29*) and by light scattering and viscosity measurements (*4*). The Kerr constants and the time constants for decay of birefringence were measured by Tinoco (*25*) for two different molecular weight samples of PBLG at low concentrations in ethylene dichloride. He obtained reasonable agreement with the particle sizes as determined by the above light-scattering measurements. By measuring the saturation of

Publication Date: January 1, 1967 | doi: 10.1021/ba-1967-0063.ch016

birefringence O'Konski *et al.* (*14*) showed that the orientation of PBLG in ethylene dichloride is predominantly caused by the permanent dipole interaction with the field. Nearly complete saturation was obtained for a polymer of molecular weight 195,000 at fields of 3×10^4 volts/cm. Watanabe, Yoshioka, and Wada (*27*) examined the change in Kerr constant of PBLG produced by adding dichloroacetic acid to a solution of the polymer in ethylene dichloride. At least two transitions were observed, the second occurring at 75% dichloroacetic acid content being the helix-coil transition. This experiment establishes the utility of birefringence measurements in determining changes in molecular conformation.

An extensive but unfortunately, as yet, unpublished study by Yamaoka (*28*) was concerned with the mode of orientation of several polypeptides in varied solvents under the influence of a rectangular voltage pulse. While measurements could be made in most organic solvents, he was unable to obtain steady-state values for the birefringence of PBLG dissolved in benzene and dioxane, except at low concentrations in dioxane. Extremely long rise times were observed in these solvents, and the 1.4-millisecond limit on his pulse width prevented establishment of equilibrium. Yamaoka showed by means of optical rotatory dispersion that PBLG assumes a helical conformation in benzene.

All of the above experiments were performed on dilute solutions of the polymers in order to reduce molecular interactions to a minimum. We have recently become interested in concentrated polypeptide solutions and their behavior when subjected to an ordering field. Solutions of PBLG in benzene and dioxane were originally reported to be extremely viscous (*4*) and presumably highly aggregated in an end-to-end manner.

Luzzati and co-workers (*10*, *11*) examined the structure of concentrated solutions of PBLG in DMF, pyridine, and *m*-cresol by the method of small-angle x-ray scattering. Their results indicated that in dilute solutions the polymer exists as the 3_{10} helix while several other phases are possible at higher concentrations. In the highest concentrations in DMF and pyridine a complex multistranded helix was formed. Takashima (*22*) using electron microscopy was unable to find evidence for the multistranded structure in dioxane. While the idea of the multistranded helix has not been universally accepted, Luzzati's work has pointed out the complexities present in these polymeric systems. It is unfortunate that the short pulse times available to Yamaoka did not permit him to make birefringence measurements on solutions of PBLG in dioxane and benzene.

By using a substantially longer pulse time (10 milliseconds), we have been able to examine solutions of PBLG in benzene, dioxane, and ethylene dichloride at concentrations much higher than those ordinarily employed and to determine concentration dependent Kerr constants. Since the birefringence depends approximately on the square of the dipole moment in the polymer, an association which increases or decreases the dipole moment of

Publication Date: January 1, 1967 | doi: 10.1021/ba-1967-0063.ch016

the aggregate relative to the unassociated particle would give rise to increased or decreased values respectively of the specific Kerr constant.

The only other pertinent study on the aggregation of polypeptides is that of Wada (*26*), who examined the dielectric properties of solutions of PBLG in dioxane and dioxane-DMF mixtures. (Adding DMF to solutions of the polymer in dioxane decreases the viscosity and presumably reduces the aggregation.) By measuring the specific polarization and the critical frequency, he was able to formulate a theory involving two separate types of association, a head-to-tail, occurring in mixtures of dioxane-DMF and dependent on polymer concentration, and a random or side-by-side, inversely dependent on the amount of DMF in the solvent. Although not explicitly stated, he apparently found no evidence for head-to-tail association in pure dioxane, and the behavior of the polymer in the absence of DMF is markedly different from that in the mixed solvent. Our own studies have led us to prepare models for the types of aggregation which occur in different pure solvents.

Publication Date: January 1, 1967 | doi: 10.1021/ba-1967-0063.ch016

Experimental

Materials. Three samples of poly-γ-benzyl-L-glutamate were studied. Polymer I was obtained by polymerizing γ-benzyl *N*-carboxy-L-glutamate anhydride by sodium methoxide in DMF and polymer II by a similar polymerization using *n*-hexylamine as initiator. Both were purified by reprecipitation. The molecular weights determined from the viscosity–molecular weight ratio of Doty *et al.* (*4*) were 67,000 for polymer I and 21,000 for polymer II. Polymer III was a commercial sample (Pilot Chemical Co.) of molecular weight 275,000. All solvents were purified by standard laboratory procedures.

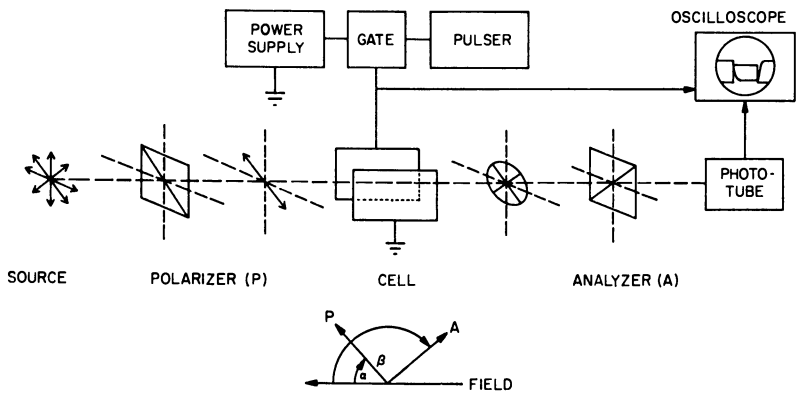

Figure 1. Schematic diagram of birefringence apparatus

Apparatus and Experimental Procedures. A diagram illustrating the experimental setup is shown in Figure 1. Pulsed fields of 10-millisecond duration were used for polymers I and II, and a static field was used for

polymer III. The maximum pulsed field was 3500 volts/cm., considerably below saturation. The phase change occurring at any particular voltage was determined by using Equation 14,

$$I = I_0[\cos^2(\alpha - \beta) - \sin 2\alpha \sin 2\beta \sin^2 \delta/2] \quad (14)$$

where I is the measured intensity of light, I_0 is the incident intensity of light, and α and β are the angles between the applied field direction and the optic axis of the polarizer and analyzer, respectively (*21*). The Kerr constant is obtained from Equation 1.

Experiments were all carried out at 35.52°C. at a wavelength of 5000 A. Viscosities were measured with Ubbelohde viscometers at 35°C. Complete experimental details and the actual data will be published elsewhere.

Results

The specific Kerr constants for polymers I and II in the three solvents are plotted against the log of the concentration in Figures 2 and 3, and the

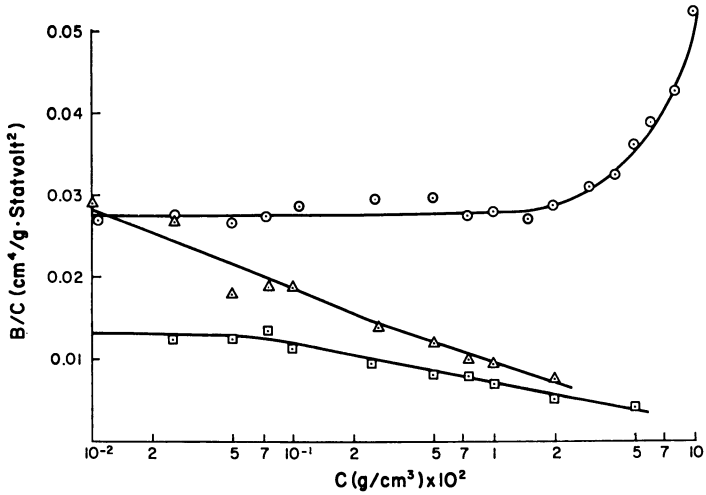

Figure 2. Specific Kerr constant (B/C) vs. log C for PBLG-I
Mol. wt. 67,000
○ *Ethylene dichloride*
□ *Dioxane*
△ *Benzene*

available data for polymer III are given in Figure 4, again plotted against the log of the polymer concentration. The difference in behavior is striking. The specific Kerr constants in ethylene dichloride, in both pulsed and static field experiments, are independent of concentration at low concentrations and then show a rise. In the low dielectric solvents the constants show a decrease with increasing polymer concentration. The values of the intrinsic Kerr constants, $[B/C]$, are listed in Table I along with the values for the intrinsic viscosities of the polymers in the various solvents. The dipole moments in the table are calculated from Equation 12, assuming

Publication Date: January 1, 1967 | doi: 10.1021/ba-1967-0063.ch016

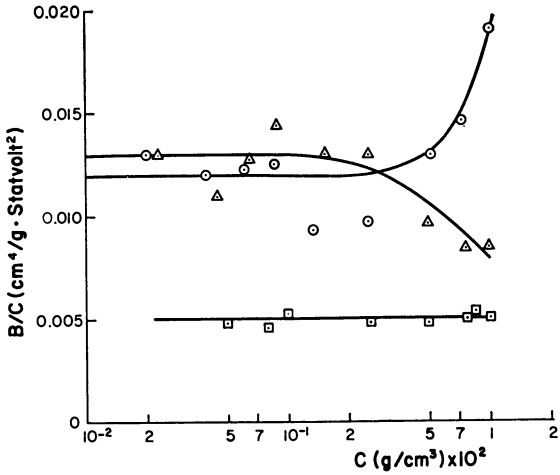

Figure 3. Specific Kerr constant (B/C) vs. log C for PBLG-II

Mol. wt. 21,000
○ *Ethylene dichloride*
□ *Dioxane*
△ *Benzene*

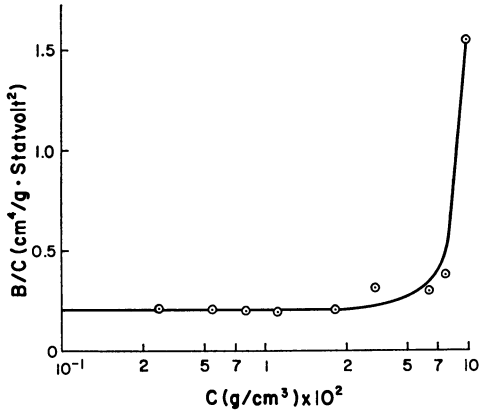

Figure 4. Specific Kerr constant (B/C) vs. log C for PBLG-III in ethylene dichloride

Mol. wt. 275,000

only permanent dipole orientation and using values for $(g_1 - g_2)$ as follows: 4.1×10^{-3} in ethylene dichloride (*3, 14, 25, 28*), 2.8×10^{-3} in dioxane (*28*), and 3×10^{-2} in benzene [estimated from the preceding values, the known solvent indices of refraction and the definition of $(g_1 - g_2)$ (*18*)]. [This assumption is probably somewhat optimistic, as the specific Kerr constants ought to vary directly with the molecular weight if only permanent dipole

Publication Date: January 1, 1967 | doi: 10.1021/ba-1967-0063.ch016

interactions were responsible. Although there is probably some contribution from induced dipole interactions (*28*), the relative magnitudes of dipole moments in the various solvents certainly lie in the indicated order. Saturation experiments (impossible with our pulser) would clarify the situation.]

In Table II are listed some values for the decay times obtained by measuring the decay of birefringence in these solutions. Because of the limitations of the instrumental time constant (30 μ sec.) and low signal to noise ratio, the decay times could not be obtained for dilute solutions of polymer I and for almost all solutions of Polymer II.

Discussion

Before discussing the Kerr measurements on the solutions, we briefly outline how the size of the polymers was obtained from viscosity and relaxation data. Two well-known expressions which are useful in interpreting these data are the Simha and Burgers equations. The Simha equation (*20*) relates the intrinsic viscosity of a solution of elongated ellipsoids

Table I. Summary of Data for Poly-γ-benzyl-L-glutamate

Polymer	*Solvent*	$[B/C]$(*Cm.⁴/Gram Statvolt²*)	$[\eta]$(*Cc./Gram*)	μ, *Debye*
I	Ethylene dichloride	0.029	39	1670
	Dioxane	0.0125	150	1330
	Benzene	0.028	400	625
II	Ethylene dichloride	0.012	9	1090
	Dioxane	0.005	50	840
	Benzene	0.013	120	430

of revolution to the molecular dimensions of the particles. A useful modification of this equation for our purposes is that of Doty *et al.* (*4*).

$$[\eta] = 6.85 \times 10^{-4}\left[\frac{(Mb^{-3})^2}{15[\ln (0.602Mb^{-3}) - 1.5]} + \frac{(Mb^{-3})^2}{5[\ln (0.602Mb^{-3}) - 0.5]} + 0.84\right] \quad (15)$$

in which $[\eta]$ is given in units of 100 cc. per gram, M is the molecular weight of the particle, and b is the semiminor axis of the ellipsoid. The diameter, $2b'$, of the equivalent cylindrical rod is given by $2b' = (2/3)^{\frac{1}{2}}\ 2b$. (*4*). Burgers equation (*2*, *12*) relates the observed rotatory diffusion constant to the length, $2a$, and the diameter, $2b'$, of the rod; η is the viscosity of the medium;

$$\theta = 3kT\frac{[-0.80 + \ln (2a/b')]}{8\pi\eta a^3} \quad (16)$$

Publication Date: January 1, 1967 | doi: 10.1021/ba-1967-0063.ch016

The behavior of PBLG in ethylene dichloride shows little suggestion of intermolecular association at low polymer concentration. The specific Kerr constant is independent of concentration except at the highest polymer concentrations. The intrinsic viscosities obtained for polymers I and II are close to those determined for polymers of similar molecular weight in DMF by Doty and co-workers (*4*). By using Equation 15 the diameters of the rods are calculated to be almost 15A, near the diameter of the corresponding Pauling α-helix (*23*). However, the length of polymer I in concentrated solution ($\sim$8%) can be estimated from the data in Table II and

Table II. Decay Times of Solutions of Poly-γ-benzyl-L-glutatmate

Polymer	*Solvent*	*Concn., (Grams/Cc.)* $\times$ 10^2	τ, μsec.
I	Ethylene dichloride	7.9	50
		10.0	60
I	Dioxane	1.0	80
		2.0	125
I	Benzene	0.50	165
		0.70	500
I	Benzene	1.02	880
		2.00	2000
II	Ethylene dichloride	0.50	100
		0.76	140

Equation 16 and turns out to be about 600A. The length of the molecule can be estimated to be around 450A. The estimated decay time for a molecule of this length is less than 30 μsec., the instrumental time constant. This increase in apparent length, together with the dependence of the specific Kerr constant on concentration in this region, strongly suggests intermolecular association. The extent of this phenomenon seems to be more pronounced the lower the molecular weight. The static field experiments with polymer of molecular weight 275,000 show only a slight trend until a critical concentration (about 10%) is reached, and then the Kerr constant rises abruptly. Gelation takes place beyond this point, and a permanent birefringence sets in.

The sudden increase in the specific Kerr constants and the relaxation times of these polymers at certain critical concentrations is in agreement with the theory of Peticolas (*16*, *17*) for the order-disorder transitions of linear molecular aggregates. This theory has two parameters, σ and ξ, which enter into the theory in terms of the interaction energies between like and unlike species in a one-dimensional two-component, lattice solution. The parameter σ gives the decrease in statistical weight of a specific configuration of the system owing to the formation of the ends of an aggregate, which are in an unfavorable energetic situation because of the imbalance between the forces on each side of the molecules at these ends. For

Publication Date: January 1, 1967 | doi: 10.1021/ba-1967-0063.ch016

the helix-coil transition in polypeptides, this end effect means that a single hydrogen bond or single turn is highly improbable since it is both the first and the last of a sequence (*30*). The same is not true of associative helical colloids. The colloidal particle really does not start to grow until at least two molecules come together. Consequently, parameter ξ is specific for the isolated solute molecule and accounts for the fact that an unassociated molecule is much more probable than it would be if it really were the beginning and end of a colloidal aggregate; this term is related to the configurational partition function of the monomer in the potential-energy well of the solvent. It also accounts for the fact that the unassociated molecule has more degrees of freedom than associated molecules.

The theory relates parameters σ and ξ to directly measurable physical quantities. The product, $\sigma^2\xi$, is the volume fraction of solute at which aggregation occurs while σ^2 is a measure of the sharpness of the transition. For a given value of the product, $\sigma^2\xi$, the transition will become more or less sharp as the value of σ^2 is decreased or increased. Thus, the important fact to observe is that one can obtain measurable physical properties in terms of the potential energies of interaction and partition functions of the individual molecules. However, the precise definitions of these parameters are in terms of a rather crude lattice model. Consequently, errors in this model will be taken up by corresponding errors in the experimental assignment of values of these parameters.

From the theory, one can calculate three different concentrations: θ_1, the number of lattice sites occupied by solute molecules divided by N, the total number of sites (the volume fraction of solute molecules); θ_2, the number of contiguously occupied sites, divided by N (the moles of aggregate per unit volume), and θ_3, the number of lattice sites filled with isolated molecules but surrounded by solvent divided by N (the moles of unassociated molecules per unit volume). These concentrations are calculated from the partition function, Ξ, by the equations,

$$\theta_1 = N^{-1}(\partial \ln \Xi/\partial \ln s)$$
$$\theta_2 = N^{-1}(\partial \ln \Xi/\partial \ln \sigma^2)$$
$$\theta_3 = N^{-1}(\partial \ln \Xi/\partial \ln \xi)$$

where $s = a_1/a_o$, and a_1 and a_o are the Lewis thermodynamic activities of the isolated molecule and solvent, respectively, relative to their standard states which are the quasi-infinitely long colloid molecule, and pure solvent, respectively.

The partition function, Ξ, is the Nth power of the largest root of the cubic equation,

$$\lambda(1 - \lambda)(s - \lambda) + \sigma^2 s\xi(s - \lambda) - \sigma^2 s^2 = 0$$

that is,

$$\Xi = (\lambda_{max})^N$$

Publication Date: January 1, 1967 | doi: 10.1021/ba-1967-0063.ch016

In Ordered Fluids and Liquid Crystals; Porter, R., el al.;
Advances in Chemistry; American Chemical Society: Washington, DC, 1967.

From these relations, it is possible using combinatorial methods described earlier (*16*), to obtain all of the various degrees of association as a function of θ_1. Thus,

$$Z_n = \theta_2/\theta_1$$
$$Z_w = 1 + [2(\theta_1 - \theta_2)^2/\theta_1(\theta_2 - \theta_3)]$$
$$\langle Z^2\rangle_w = 1 + [6(\theta_1 - \theta_2)^3/\theta_1(\theta_2 - \theta_3)^2]$$

where Z_n is the number average degree of aggregation, Z_w is the weight average, and $\langle Z^2\rangle_w$ is the weight average of the square of the degree of aggregation.

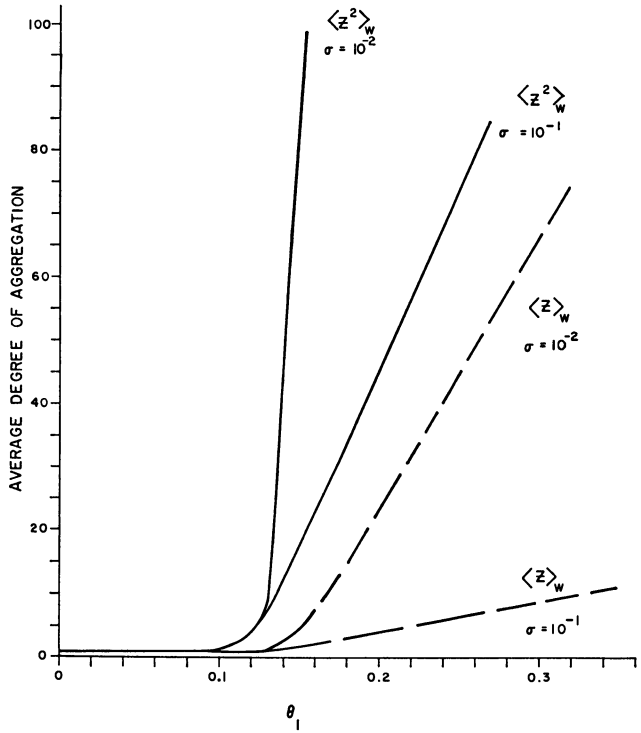

Figure 5. Averages $\langle Z^2\rangle_w$ and Z_w when product $\sigma^2\xi$ = 0.2 for different values of σ

Transition becomes more abrupt with decreasing σ

One of the interesting predictions of the theory is that the abruptness of the transition above the critical concentration depends on which property is being measured. This point is illustrated in Figure 5, where $\langle Z\rangle_w$ and $\langle Z^2\rangle_w$ are plotted against θ_1 (volume fraction of solute molecule) for various values of σ. Quantities which depend upon $\langle Z^2\rangle_w$ will show a much more abrupt change above the transition point.

Publication Date: January 1, 1967 | doi: 10.1021/ba-1967-0063.ch016

Since the Kerr effect depends upon the weight average square length of the macromolecules, it should show an abrupt increase above the critical concentration. In fact, the comparison of Figures 4 and 5 shows that the aggregation of PBLG in dichloroethane is nearly described by the Peticolas theory with $\sigma = 10^{-2}$ and $\sigma^2\xi \sim 0.1$. This latter value indicates that aggregation should occur at approximately 10% by volume. For PBLG in ethylene dichloride, the critical concentration increases with increasing molecular weight. The lowered threshold for appearance of this concentration effect in solutions of low molecular weight polymer may be caused by an increased number of polymer "ends" present per unit volume. At low concentrations it is safe to say that the polymers behave as individual unassociated particles.

In benzene and dioxane a different situation exists. The remarkably high viscosities of solutions of PBLG in these two solvents are suggestive of the formation of some sort of large aggregates. These aggregates must be present at low concentrations since the plot of reduced specific viscosity *vs.* concentration (used to determine $[\eta]$) does not fall off significantly and one can obtain an apparent intrinsic viscosity for the aggregate by extrapolation. These intrinsic viscosities are so high that they cannot be easily fitted to the Simha equation (*20*). If a standard diameter, 15 A., of the rod is assumed, the length of the aggregate is at least three times the length of the discrete particle and in the case of polymer II in benzene, even much longer. The rotatory diffusion constants for polymer I are strongly concentration dependent and Equation 16 indicates that the lengths of the rods must be much greater than 1000 A. in a 1% solution. There is a very pronounced inverse dependence of the specific Kerr constant on polymer concentration. The dipole moments are all substantially below those found in ethylene dichloride and generally parallel the order of the intrinsic viscosities.

Clearly, the behavior of the polymers differs greatly in ethylene dichloride from that in benzene and dioxane. Three types of molecular association can be considered: (1) head-to-tail, (2) head to-head, and (3) side-by-side or antiparallel.

Type 1 association is probably occurring in concentrated solutions in ethylene dichloride. It would result in an increased dipole moment for the aggregate and the large rods would increase both the viscosity and decay time. Of the three solvents ethylene dichloride with the highest dielectric constant (10.25) would be the best for stabilizing a large dipole moment and reducing the free energy of charging the dipole.

Associations of type 2 and/or type 3 are necessary to explain the observations on solutions of the polymers in benzene and dioxane. Head-to-head association would result in a reduced dipole moment in the aggregate owing to internal cancellation of the opposing moments. However, the nature of the interaction holding two molecules head-to-head is not clear

Publication Date: January 1, 1967 | doi: 10.1021/ba-1967-0063.ch016

In Ordered Fluids and Liquid Crystals; Porter, R., el al.;
Advances in Chemistry; American Chemical Society: Washington, DC, 1967.

and must be especially strong to overcome the repulsive force of two like charges. The assumption of rigid trimers to explain the magnitudes of the intrinsic viscosities and decay constants is also somewhat unreasonable. Lateral or antiparallel association would, on the other hand, explain the experimental facts without much difficulty. A two-dimensional sheet would have a reduced dipole moment and a much larger intrinsic viscosity than a rod of equivalent length. Such an association could arise from molecular dipole interactions, as suggested by Wada (*26*). The differences noted in solutions in benzene and dioxane are probably caused by the small dipole moment of dioxane, making it a slightly better solvating agent for the large dipole. The enormous differences in behavior of PBLG as a function of solvent are somewhat unexpected. Even more unusual is the observation that the antiparallel association in low dielectric solvents is so strong that it persists at low concentrations.

Publication Date: January 1, 1967 | doi: 10.1021/ba-1967-0063.ch016

Acknowledgment

The authors thank I. Tinoco for helpful discussions and for the loan of K. Yamaoka's thesis.

Literature Cited

(1) Benoit, H., *Ann. Phys.* **6** (ser. 12), 561 (1951).
(2) Burgers, J. M., *Verhandel. Koninkl. Ned. Acad. Wetenschap. Afdel. Natuurk.*, Sec. 1, Dell XVI, No. 4, 113 (1938).
(3) Doty, P., unpublished result quoted in (25).
(4) Doty, P., Bradbury, J. H., Holtzer, A. M., *J. Am. Chem. Soc.* **78**, 947 (1956).
(5) Doty, P., Yang, J. T., *J. Am. Chem. Soc.* **78**, 498 (1956).
(6) Haschemeyer, A., Tinoco, I., *Biochem.* **1**, 996 (1962).
(7) Holcomb, D. N., Tinoco, I., *J. Phys. Chem.* **67**, 2691 (1963).
(8) Le Fèvre, C. G., Le Fèvre, R. J. W., in "Physical Methods," A. Weissberger, "Technique of Organic Chemistry," Vol. I, Part 3, 3rd ed., p. 2459, Interscience, New York, 1960.
(9) Le Fèvre, C. G., Le Fèvre, R. J. W., *Revs. Pure Appl. Chem.* (*Australia*) **5**, 261 (1955).
(10) Luzzati, V., Cesari, M., Spach, G., Masson, F., Vincent, J. M., *J. Mol. Biol.* **3**, 566 (1961).
(11) Luzzati, V., Cesari, M., Spach, G., Masson, F., Vincent, J. M., in "Polyamino Acids, Polypeptides, and Proteins," M. A. Stahmann, ed., p. 121, University of Wisconsin Press, Madison, 1962.
(12) O'Konski, C. T., Haltner, A. J., *J. Am. Chem. Soc.* **78**, 3604 (1956).
(13) *Ibid.*, **79**, 5634 (1957).
(14) O'Konski, C. T., Yoshioka, K., Orttung, W. H., *J. Phys. Chem.* **63**, 1558 (1959).
(15) Peterlin, A., Stuart, H. A., *Z. Physik* **112**, 129 (1939).
(16) Peticolas, W. L., *J. Chem. Phys.* **37**, 2323 (1962).
(17) *Ibid.*, **40**, 1463 (1964).
(18) Scheraga, H. A., Signer, R., in "Physical Methods," A. Weissberger, "Technique of Organic Chemistry, Vol. I, part 3, 3rd ed., p. 2414, Interscience, New York, 1960.
(19) Shah, M. J., *J. Phys. Chem.* **67**, 2215 (1963).
(20) Simha, R., *J. Phys. Chem.* **44**, 25 (1940).
(21) Stevenson, E. C., Beams, J. W., *Phys. Rev.* **38**, 133 (1931).
(22) Takashima, S., *Biopolymers* **2**, 287 (1964).

(23) Tanford, C., "Physical Chemistry of Macromolecules," p. 408. Wiley, New York, 1961.
(24) Tinoco, I., *J. Am. Chem. Soc.* **77**, 3476 (1955).
(25) *Ibid.*, **79**, 4336 (1957).
(26) Wada, A., *J. Polymer Sci.* **45**, 145 (1960).
(27) Watanabe, H., Yoshioka, K., Wada, A., *Biopolymers* **2**, 91 (1964).
(28)Yamaoka, K., thesis, University of California, Berkeley, 1962.
(29) Yang, J. T., Doty, P., *J. Am. Chem. Soc.* **79**, 761 (1957).
(30) Zimm, B. H., Bragg, J. H., *J. Chem. Phys.* **31**, 526 (1959).

RECEIVED March 1, 1966.

17

Mechanism of Dielectric Relaxation of Deoxyribonucleic Acid

SHIRO TAKASHIMA

Electromedical Division, Moore School of Electrical Engineering, University of Pennsylvania, Philadelphia, Pa.

Publication Date: January 1, 1967 | doi: 10.1021/ba-1967-0063.ch017

The dielectric dispersion of DNA solutions was measured with various samples. The dielectric increment and the relaxation time of helical DNA are proportional to the square of the length of the molecule, but values for coil DNA are distinctly smaller than for helical DNA. The rotary diffusion constant is measured simultaneously with the dielectric measurement. The agreement of both relaxation times is fair in a region of low molecular weight, but the disparity becomes pronounced when DNA is larger. Theories on the mechanism of ionic electric polarization are reviewed. Currently, counter ion polarization for a cylindrical model seems to account most reasonably for the dielectric relaxation of DNA.

The dielectric constant of deoxyribonucleic acid (DNA) solution was first measured by Allgen (*1*) and Jungner, Jungner and Allgen (*9*), who reported that DNA exhibited an anomalous dispersion in the 100-kc. region with a large dielectric increment. They calculated the dipole moment and the dielectric relaxation time and observed a dipole moment of approximately 10^3 to 10^4 Debye units and a relaxation time of about 10^{-7} second. They attempted to account for the dielectric relaxation of DNA in terms of the Debye theory.

However, the relaxation time they observed was widely different from the relaxation time of rotary diffusion (τ_{ro}) of about 10^{-3} second observed by Edsall (*4*). If dielectric polarization is caused by the orientation of a permanent dipole, the relaxation time must be similar to that for rotary diffusion. The rotary diffusion of elongated particles usually represents the rotary motion of the whole body around the short axis. If DNA has a permanent dipole in the transverse direction, the whole molecule would rotate around the major axis and the dielectric relaxation time would not necessarily be the same as that of rotary diffusion. Thus they concluded that the difference between the rotary and dielectric relaxation times ob-

In Ordered Fluids and Liquid Crystals; Porter, R., el al.;
Advances in Chemistry; American Chemical Society: Washington, DC, 1967.

served was caused by the fact that DNA had a permanent dipole across the major axis.

Later, Jerrard and Simmons (*8*) measured the dielectric dispersion of DNA and also observed a dispersion in the 30-kc. region. The frequency region used by Allgen *et al.* and Jerrard *et al.* was restricted to high frequencies. Moreover, the DNA samples used by Allgen *et al.* seem to have low molecular weight. The dielectric properties depend rather strongly on the degree of polymerization, and the results obtained with a DNA of low molecular weight cannot be generalized.

Recently, Takashima (*27*) measured the dielectric dispersion of DNA in the low frequency region with DNA samples of varying molecular weights. He extended the measurements down to 50 c.p.s. and observed a dielectric dispersion of DNA in a much lower frequency region than those observed by previous workers and a dielectric increment much larger than the values previously obtained. Furthermore, he observed that the dielectric increment and the relaxation time depend strongly on molecular weight —i.e., degree of polymerization in this case. He suggested on the basis of these observations that DNA had a longitudinal instead of a transverse moment as concluded by Allgen *et al.*, and indicated the possibility that the major axis of DNA is oriented to some extent in the direction of the electric field after the creation of an induced dipole. This conclusion was criticized by Pollack (*18*), who concluded on the basis of his theory that the dielectric relaxation of DNA may be explained in terms of a simple Maxwell-Wagner theory (*11*, *29*).

In this work, the size dependence of the dielectric increment and the relaxation time is reinvestigated (*28*). The hydrodynamic length, which is estimated from the rotary diffusion constant, is used instead of molecular weight since the latter by no means represents the actual length in the solution. Also a careful comparison of dielectric relaxation time and rotary relaxation time is attempted. Actually, the comparison is meaningless unless it is made on the same DNA sample because both relaxation times, particularly the rotary relaxation time, are strongly dependent on the size of the molecule. Therefore, the attempt by Allgen *et al.* to compare the value of dielectric relaxation time they obtained with the value of rotary relaxation time obtained by Edsall with a different DNA sample is not particularly significant.

Finally, attempts are made on a theoretical basis to explain the unusually large dielectric increments and relaxation times of DNA. The discussion is limited to ionic-type polarizations in this report. The available theories, such as the Maxwell-Wagner theory (*29*) and the surface conductivity treatment, are reviewed and analyzed. These theories do not explain the dielectric relaxation of DNA satisfactorily. Finally, the counter ion polarization theory is described, and it is demonstrated that it explains most reasonably the dielectric relaxation of DNA.

Publication Date: January 1, 1967 | doi: 10.1021/ba-1967-0063.ch017

In Ordered Fluids and Liquid Crystals; Porter, R., el al.;
Advances in Chemistry; American Chemical Society: Washington, DC, 1967.

Experiments

A Wheatstone bridge designed by Schwan (*21*) was used for dielectric measurements, which were carried out between 50 c.p.s. (cycles per second) and 200 kc. The bridge was designed for measurement with conductive materials and is suitable for a DNA solution. The conductance of a dilute DNA solution is usually 20 to 50 μmhos at a concentration of 0.01 to 0.03%. The magnitude of the experimental error in lossy solutions has been discussed in detail by Schwan (*21*). The major source of experimental error with conductive solutions is electrode polarization. Two methods are used to eliminate this effect. In the first, the platinum electrodes are very carefully plated with platinum black according to the method of Maczuk and Schwan (*21*). The measured capacity of the solution can be expressed by Equation 1 (*21*), where C_s is the true capacity of the solution, C_p is the electrode polarization capacitance, ω is the angular frequency, and R is the measured resistance. To make the second term of Equation 1 small,

$$C = C_s + 1/[C_p^2 R\omega^2] \quad (1)$$

either R or C_p must be made large. An increase in electrode capacity is the easier method for decreasing the second term. The effect of electrode polarization can still be considerable with conductive solutions, even with a good plating. This gives rise to a difficulty in determining the low frequency dielectric constant. The dispersion of DNA depends largely on the length of the molecule. The effect of electrode polarization is not serious for small DNA molecules because the dielectric dispersion is in a relatively high frequency region. For large molecules, however, further correction is essential. A dielectric cell was constructed in which the distance between the electrodes was variable. Measurements were repeated twice at two

Table I. Experimental Error of Measurement of Capacity and Conductivity at Low Frequencies

Frequency, C.p.s.	*Capacity* (ΔC), $\mu\mu f$.	*Conductivity* (ΔG), μmho	*Dielectric Const.*
200	±0.2	±0.0015	± 4.28
100	±0.3	±0.003	± 6.24
70	±0.8	±0.003	± 8.58
50	±2.0	±0.003	±21.42

electrode distances, say 10 and 1 cm. Electrode polarization is independent of the electrode distance and can be eliminated by using Equation 2 (*21*). C_s is the true capacity at 10 cm., and C_1 and C_2 are the capacities and R_1 and R_2 are the resistances at electrode distances of 10 and 1 cm., respectively.

$$C_s = \left[C_1 - C_2 \left(\frac{R^2}{R_1}\right)^2_{5kc}\right] \Big/ \left[1 - \left(\frac{R_2}{R_1}\right)_{5kc}\right] \quad (2)$$

The capacity and conductivity of the solution can be measured down to 100 c.p.s. with reasonable accuracy (Table I). High molecular weight DNA, however, has an anomalous dispersion in a low frequency region. The low frequency plateau of the dielectric dispersion of these samples seems to appear even below 100 c.p.s. The capacity of a DNA solution

In Ordered Fluids and Liquid Crystals; Porter, R., el al.;
Advances in Chemistry; American Chemical Society: Washington, DC, 1967.

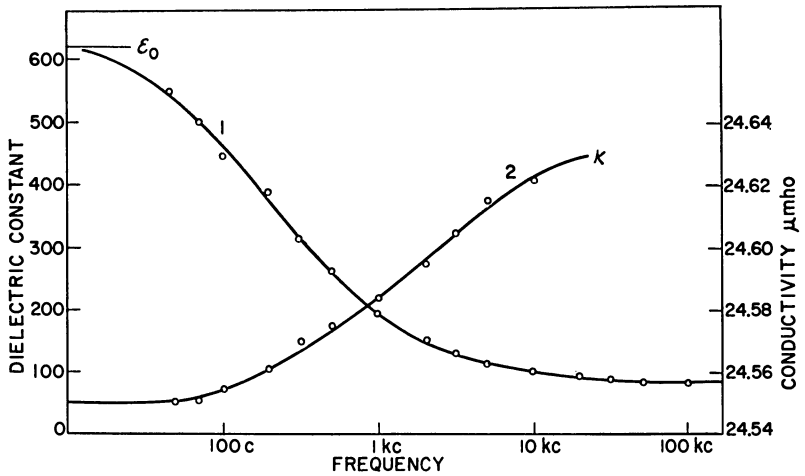

Figure 1. Dielectric dispersion of salmon sperm DNA

1. Dielectric constant
2. Conductivity
Concentration. 0.01%
Horizontal line, ϵ_0, indicates low frequency dielectric constant obtained from Cole-Cole's plot

becomes much more difficult to measure below 100 c.p.s. One cannot obtain the low frequency plateau by extrapolating the dispersion curve without considerable arbitrariness. In a case like this, the use of a Cole-Cole plot (*3*) is helpful. As shown in Figure 2, the Cole-Cole plot of DNA is symmetrical. Thus we can estimate the low frequency dielectric constant from the intersection of the circle with the abscissa. The value of the low frequency dielectric constant obtained by this method is much more reliable. In the present experiment, the low frequency dielectric constant is always obtained by this method.

The imaginary part of the dielectric constant (dielectric loss ϵ'') is calculated from the formula

$$\epsilon'' = (\kappa - \kappa_0)/2\pi f\epsilon_r \qquad (3)$$

where κ_0 is the low frequency conductivity in micromhos, and ϵ_r is the absolute value of the dielectric constant of free space. The dispersion of conductivity is shown in Figure 1. It is evident from Equation 3 that a small error in the conductivity measurement can cause a considerable error in the dielectric loss at low frequencies. Conductivity is measured with an error of ± 0.001 μmho. Although the temperature of the solution is controlled by circulating thermostated water, the fluctuation of conductivity cannot be prevented. The correction method for the drift of conductivity has been given (*10, 27*). The random error of the conductivity reading is sufficiently small for determining the dielectric loss.

The experimental errors in the capacity and conductivity readings in the low frequency region are summarized in Table I. In the last column, the magnitude of the error in the dielectric constant is shown. The error of ± 21.42 at 50 c.p.s. in the dielectric constant seems large; however, the total dielectric increment is so large that this error is not really serious.

Publication Date: January 1, 1967 | doi: 10.1021/ba-1967-0063.ch017

The flow birefringence and the extinction angle of DNA solution are measured with a Rao birefringence apparatus Model-B-22. The extinction angle, χ, is related to a parameter, α, in the equation of Boeder (*2*) and that of Peterlin and Stuart (*17*);

$$\chi = \frac{1}{2} \tan^{-1} \frac{6}{\alpha} = \frac{\pi}{4} - \frac{\alpha}{12} [1 - f(\alpha,a,b)] \quad (4)$$

(Parameter α should not be confused with the Cole-Cole parameter.) The value of α is tabulated by Edsall *et al.* (*19*) for various axial ratios. The rotary diffusion constant is related to α by the following formula,

$$\alpha = \beta/\theta \quad (5)$$

where β is the velocity gradient. The rotary relaxation time is calculated from the rotary diffusion constant by the formula

$$\tau = \theta/2 \quad (6)$$

The length of DNA is calculated by using the Perrin equation (*16*),

$$\theta_b = \frac{3kT}{16\pi\eta a^3} \left(\ln \frac{a}{b} - 1 \right) \quad (7)$$

where θ_b is the rotary diffusion constant around the minor axis, η is the viscosity of the solvent in poises, and a and b are the semimajor and minor axes in centimeters. Axis a is not necessarily the fully stretched length of DNA, and b is not necessarily the radius of the double helix. Since the Perrin equation could not be solved analytically, an IBM 1710 computer was used to obtain the solution for the length of the DNA molecule.

Calf thymus and salmon sperm DNA were used in this experiment. The length of calf thymus ranges from 10,500 to 1500 A. and that of salmon sperm DNA from 7400 to 1300 A. A 20-kc. sonic oscillation is applied to produce smaller DNA samples. Viscosity is measured with a Rao couette-type viscometer with varying shearing stress. It is obtained by extrapolating the consistency curve to zero shear.

DNA is dissolved in freshly deionized water. The pH of the water is examined each time since distilled water becomes acidic on storage. Since DNA is unstable at low ionic strength, the pH of the water must be maintained close to neutral to avoid denaturation. If DNA is dissolved in acidic water, it does not exhibit flow birefringence nor large dielectric increment. This indicates denaturation, probably strand separation. Calf thymus DNA is more stable than salmon sperm DNA. The concentration of DNA is 0.01% unless otherwise stated.

Results

Native DNA. The dielectric dispersion of salmon testes DNA is shown in Figure 1. It is obvious that the dielectric constant of a DNA solution rises far above the dielectric constant of water and is still increasing at 50 c.p.s. Unless we have an entirely different measurement technique, we cannot hope to extend the frequency toward the lower frequency region. Thus at present it is not possible to obtain the complete dispersion curve to estimate the low frequency dielectric constant.

Publication Date: January 1, 1967 | doi: 10.1021/ba-1967-0063.ch017

In Ordered Fluids and Liquid Crystals; Porter, R., el al.;
Advances in Chemistry; American Chemical Society: Washington, DC, 1967.

The use of the Cole-Cole plot is often helpful for obtaining the low and high frequency dielectric constant. A typical example of the Cole-Cole plot of a DNA solution is shown in Figure 2. The intersections between the arc and the abscissa give values of 620 and 70, respectively. The horizontal line designated ϵ_o in Figure 1 is the value obtained by this

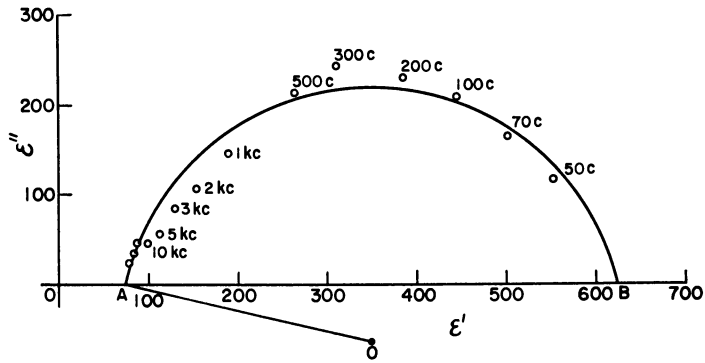

Figure 2. Cole-Cole plot of salmon sperm DNA
Ordinate. Imaginary part
Abscissa. Real part of dielectric constant
Numbers in figure are frequencies
A,B. High and low frequency dielectric constant

method, and seems to be in reasonable agreement with the possible value which would have been obtained by the extrapolation of the dispersion curve. The dielectric measurements are carried out with DNA solutions with widely different molecular dimensions. The dielectric increment as well as the relaxation time decreases with the decrease of the length. The decrease in the dielectric increment is particularly pronounced. Curve 1 in Figure 3 shows the relationship between the dielectric increment and the length of the molecule. The following empirical relationship between the length and the dielectric increment is obtained:

$$\Delta\epsilon = 0.29 \times 10^{-5} \times L^2 = AL^2 \tag{8}$$

The relaxation time is calculated by using the equation

$$\tau = 1/2\pi f_c \tag{9}$$

where τ is the relaxation time, and f_c is the critical frequency. The relationship between relaxation time and length is shown by curve 2 in Figure 3, and is expressed by the following empirical formula,

$$\tau = 1.6 \times 10^{-5} \times L^2 = BL^2 \tag{10}$$

Comparison between Rotary and Dielectric Relaxation Time. The conclusion drawn by Allgen *et al.* (*1*) was based on the fact that the dielectric relaxation time they observed was widely different from the rotary relaxa-

Publication Date: January 1, 1967 | doi: 10.1021/ba-1967-0063.ch017

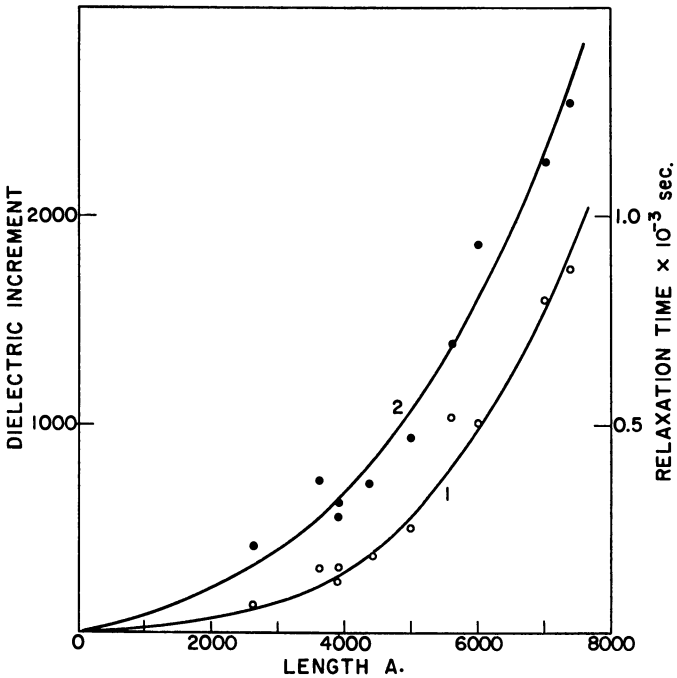

Figure 3. Dependency of dielectric increment and dielectric relaxation time of DNA on length in solution

Ordinate (left). Dielectric increment
Ordinate (right). Relaxation time
Abscissa. Length obtained from Equation 7, expressed in A.
○ *(curve 1). Dielectric increment (scale left ordinate)*
● *(curve 2). Relaxation time (scale right ordinate)*

tion time. The dielectric relaxation time observed in this experiment is considerably larger than those observed by Allgen *et al.* Moreover, the dielectric and rotary relaxation times were previously obtained independently with different DNA samples. It is now evident that the comparison is almost meaningless unless it is made on the same DNA sample since both relaxation times depend on the size of DNA. In this experiment, dielectric dispersion and rotary diffusion constant were measured simultaneously with the same DNA sample (Figure 4). The relaxation times are plotted with the ordinate on a logarithmic scale. The difference between the two relaxation times is approximately twofold when the DNA molecule is small—i.e., in the range of 2000 to 3000 A. Considering the error involved in the determination of relaxation times, the similarity is much closer than expected. However, the disparity becomes more and more pronounced as the DNA molecule gets larger. The rotary relaxation time is about 20 times larger than the dielectric relaxation time with the largest DNA used in this experiment (length about 10,000 A.). This result is as expected

Publication Date: January 1, 1967 | doi: 10.1021/ba-1967-0063.ch017

since the rotary relaxation time is proportional to the cube of the length and the dielectric relaxation time is proportional to the square of the length, according to Equation 9. Therefore, rotary relaxation time increases much faster than dielectric relaxation time.

Although the difference between the two relaxation times is substantial, the disparity is much smaller than that observed by Allgen *et al.*: a 1000-fold difference with a DNA of molecular weight of about 10^6. Undoubtedly the discrepancy between the results of Allgen *et al.* and the present results is greater than the experimental error and not merely owing to the difference in the size of DNA. Recently, O'Konski *et al.* (*25*) reported that DNA had two dielectric dispersions, one in the megacycle region and the other in the few-kilocycle region. Obviously, Allgen *et al.* based their conclusion

Publication Date: January 1, 1967 | doi: 10.1021/ba-1967-0063.ch017

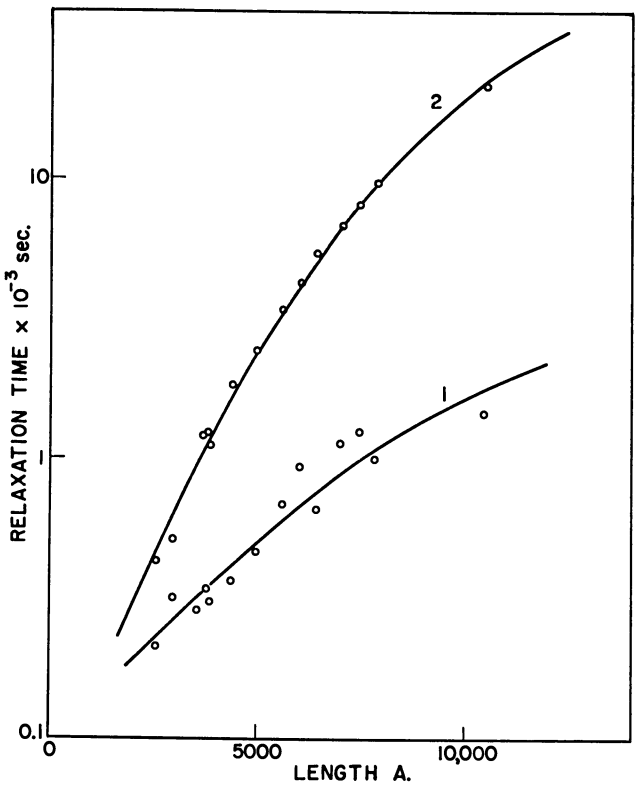

Figure 4. Dielectric relaxation time and rotary relaxation time of DNA against length of DNA molecule

1. Dielectric relaxation time
2. Rotary relaxation time
○ Calf thymus DNA
Ordinate on logarithmic scale

on the high frequency dispersion and Takashima observed only the low frequency dispersion.

Denatured DNA. Figure 5 illustrates the dielectric dispersion of heat-denatured DNA. DNA undergoes a transition from a double helical configuration to a single-strand random coil configuration, caused by heating or by acid or alkali. The dispersion curve shown here represents a dielectric dispersion of heat-denatured coil DNA. The denaturation is confirmed by the decrease of viscosity and the disappearance of flow birefringence.

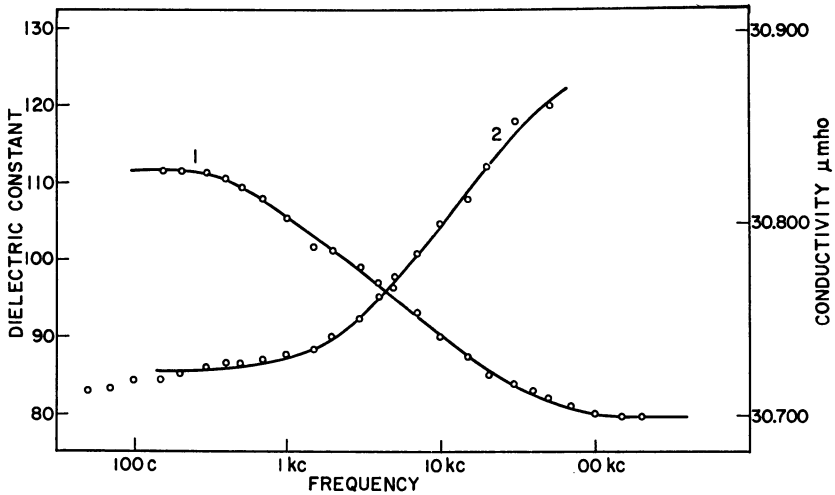

Figure 5. Dielectric dispersion of heat-denatured DNA

1. Dielectric constant
2. Conductivity in μmhos
Concentration 0.03%

Although the magnitude of dielectric increment is much smaller than that of helical DNA (the scale of the ordinate is greatly enlarged), one can still observe considerable increment and distinct dispersion in the 5-kc. region. Undoubtedly the dispersion of denatured DNA is different from that of native helical DNA. Figure 6 shows the change in the dielectric increment as a function of the temperature of heating.

The measurements were carried out at 25°C. after quick cooling. The changes in the magnitude of birefringence and specific viscosity are also plotted in Figure 6. The parallelism among these three quantities is remarkable. This clearly indicates that the dipole moment is associated with the major axis of DNA and hence it disappears with the loss of secondary structure on denaturation.

Discussion

The above results strongly indicate that DNA has a longitudinal dipole moment. Since there is a substantial difference between the dielectric and

Publication Date: January 1, 1967 | doi: 10.1021/ba-1967-0063.ch017

rotary relaxation times, we can hardly explain the dielectric polarization of DNA with a permanent dipole model. DNA may have a transverse permanent dipole which arises mainly from the group moment of base pairs. However, it does not seem to give rise to a large net moment because of partial cancellation of these moments with each other as a result of the spiral structure.

Since DNA is a highly charged macromolecule surrounded by a layer of counter ions, it is more probable that the dielectric polarization of DNA arises from the polarization of the ion atmosphere. Various mechanisms of ionic polarization have been proposed. The theories of ionic polarization for a spherical particle suspension were reviewed and carefully discussed by Schwan (*20*, *21*). Since DNA is a thin elongated molecule, those theories must be modified substantially. Various theories for ellipsoids are briefly reviewed here.

Publication Date: January 1, 1967 | doi: 10.1021/ba-1967-0063.ch017

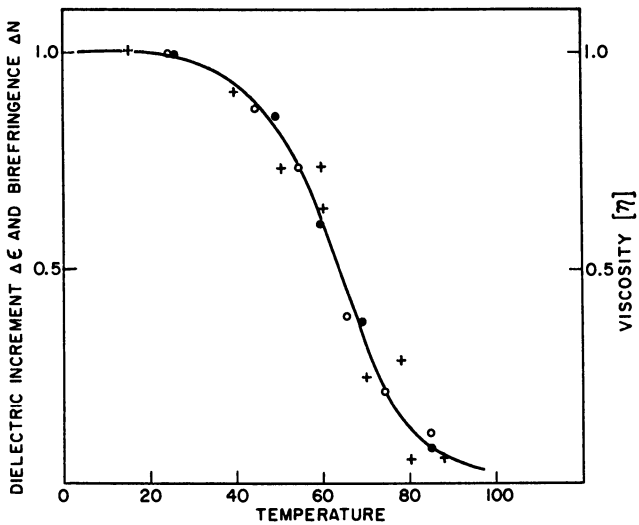

Figure 6. Change of dielectric increment, $\Delta\epsilon$, flow birefringence, Δn, and intrinsic viscosity $[\eta]$ as function of temperature of heating

Ordinate. Normalized scale.
All measurements at 25°C.

Maxwell-Wagner Type Theory. If a sphere with a dielectric constant ϵ_2 and conductivity k_2 is suspended in a medium with a dielectric constant ϵ_1 and a conductivity k_1, the dielectric constant of the suspension may be expressed by the Maxwell equation (*11*),

$$\frac{\epsilon_1^* - \epsilon}{2\epsilon_1^* + \epsilon} = q\frac{\epsilon_1^* - \epsilon_2^*}{2\epsilon_1^* + \epsilon_2^*} \tag{11}$$

where q is the volume fraction of spherical particles. If we insert the fol-

lowing relations for the complex dielectric constants and rearrange the equation,

$$\epsilon_1^* = \epsilon_1 - \frac{4\pi k_1}{\omega} i$$
$$\epsilon_2^* = \epsilon_2 - \frac{4\pi k_2}{\omega} i \tag{12}$$

The dielectric constant of the spherical suspension becomes

$$\epsilon^* = \epsilon_\infty + \frac{\Delta\epsilon}{1 + i\omega\tau} \tag{13}$$

$$\Delta\epsilon = 9q \frac{(\epsilon_1 k_2 - \epsilon_2 k_1)^2}{\epsilon_1(2\epsilon_1 + \epsilon_2)(2k_1 + k_2)^2} \tag{14}$$

The high frequency dielectric constant is

$$\epsilon_\infty = \epsilon_1 \left[1 + 3q \frac{(\epsilon_2 - \epsilon_1)}{2\epsilon_1 + \epsilon_2} \right] \tag{15}$$

The relaxation time is

$$\tau = \frac{2\epsilon_1 + \epsilon_2}{4\pi(2k_1 + k_2)} \tag{16}$$

This is the well known Maxwell-Wagner theory of spherical suspensions (*29*). According to this theory, the dielectric increment of a spherical suspension is determined solely by the dielectric constant and the conductivities of the particle and the solvent.

This theory was extended to an ellipsoid in a parallel field by Sillars (*24*) and Fricke (*6*) independently. Their results are exactly the same. Only Fricke's equation is reviewed here. Instead of Equation 11, Fricke obtained the following equation of the dielectric constant of ellipsoidal suspension,

$$\epsilon = \epsilon_1^* + q \frac{\epsilon_1^*(\epsilon_2^* - \epsilon_1^*)}{\epsilon_2^* + n(\epsilon_2^* - \epsilon_1^*)} \tag{17}$$

where the symbols have the same meaning as before. n represents a parameter which contains the elliptic integral,

$$n = abc \int_0^\infty \frac{ds}{(a^2 + s)^{3/2}(b^2 + s)^{1/2}(c^2 + s)^{1/2}} \tag{18}$$

where a, b, and c represent the axes of the ellipsoid. Introducing again Relations 2 and 3 and assuming $k_1 = 0$ and $b = c$, one obtains the following equations,

$$\epsilon = \epsilon_\infty + \frac{\Delta\epsilon}{\perp + i\omega\tau} \tag{19}$$

Publication Date: January 1, 1967 | doi: 10.1021/ba-1967-0063.ch017

where

$$\epsilon_\infty = \epsilon_1 + q\frac{\epsilon_1(\epsilon_2 - \epsilon_1)}{\epsilon_1(1 - n) + n\epsilon_2} \tag{20}$$

$$\Delta\epsilon = \frac{(1/n)^2\epsilon_1^2 q}{\epsilon_1(1/n - 1) + \epsilon_2} \tag{21}$$

$$\tau = \frac{(1/n - 1)\epsilon_1 + \epsilon_2}{4\pi\kappa_2} \tag{22}$$

Again, ϵ_∞ and τ are the high frequency dielectric constant and relaxation time. In contrast to the spherical suspension, the dielectric increment and the relaxation time depend on the shape and dimensions of the molecule because of the presence of parameter n in the numerator of Equations 21 and 22. According to Equation 18, $1/n$ becomes very large, as the molecule is elongated. Accordingly, both dielectric increment and relaxation time can be large for elongated molecules. This theory appears promising in explaining the unusually large dielectric increment and the relaxation time of DNA.

If we assume that the axial ratio of DNA is 200, n becomes about 0.00013. Let us assume that ϵ_1 and ϵ_2 are 80 and 5, respectively. Also if we assume 10^{-4} to 10^{-6} μmho for k_2, Equation 22 gives a value of 4.3×10^{-4} to 4.3×10^{-2} second. These values are comparable with the observed values. However, Equation 21 gives a value for the dielectric increment of about 10.8 for the volume fraction 0.0001, which is the concentration divided by the specific gravity. This is far too small compared with the observed value. The difference between the theoretical and experimental values is so great that no improvement of this theory is expected. Moreover, the assumption $k = 0$ used here is evidently unrealistic for aqueous suspensions. For the present case, Equations 21 and 22 must be derived by assuming a finite value for the conductivity of the solvent. The derivation of these equations with a finite value for k_1 is not straight-forward, and the form such as Equation 19 cannot be reached without an assumption which is not generally acceptable. In addition, electrolyte molecules are surrounded by a counter ion layer which has a conductivity and a dielectric constant different from those of the solute or medium. Thus they form a shell surrounding the molecule. Therefore, the simple model used above is not appropriate for polyelectrolytes.

Recently, Pollack derived, by adapting a simple procedure, a Maxwell-Wagner type of equation for a highly elongated ellipsoid of revolution (*18*). Although his procedure is considerably different from those of Fricke and Sillars, the final form is essentially the same. He derived the following equations for the relaxation time:

$$\tau_l = 2a^2\epsilon/Cb^2k_l \tag{23}$$

$$\tau_t = 2\epsilon/k_t \tag{24}$$

Publication Date: January 1, 1967 | doi: 10.1021/ba-1967-0063.ch017

where τ_l is the relaxation time in the longitudinal direction and τ_t that in the transverse direction. k_l and k_t are the longitudinal and transverse conductivities, a and b are the major and minor axes, and $C = 2 + \ln(4a^2 + b^2)$. The resemblance between Equations 22 and 23 and 24 is rather obvious. Equation 23 gives a value for relaxation time which is comparable with the observed one. However, Pollack did not derive an equation for dielectric increment, and the test of his theory cannot be complete. Moreover, the model he used is the same as that of Fricke and is not appropriate for electrolyte molecules. In conclusion, the Maxwell-Wagner type theories for elongated molecule do not seem to account for the dielectric properties of DNA satisfactorily.

Shell Model. The case of a sphere surrounded by a layer of a shell with a complex dielectric constant,

$$\epsilon_3^* = \epsilon_3 - \frac{4\pi k_3}{\omega} i \tag{25}$$

is treated by Miles and Robertson (*12*). They arrived at an expression for relaxation time as follows:

$$\tau = \frac{2\epsilon_1 + \bar{\epsilon}_2}{4\pi(2k_1 + \bar{k}_2)} \tag{26}$$

where

$$\bar{\epsilon}_2 = \epsilon_2 + 2d/a\epsilon_3 \tag{27}$$

$$\bar{k}_2 = k_2 + 2d/ak_3 \tag{28}$$

where subscripts 1, 2, and 3 refer to the medium, the particle, and the shell, respectively. The presence of the shell increases ϵ_2 and k_2 in the Maxwell-Wagner equation by the amounts of $2(d/a)\epsilon_3$ and $2(d/a)k_3$, but does not change the form of the equation. The shell model, including the calculation of dielectric increment, was treated more completely by Pauly and Schwan (*14*).

This model is pertinent for polyelectrolytes which have a counter ion layer surrounding the molecules. However, the mathematical difficulties are considerable for the ellipsoidal shape with a shell. Fricke (*5*) derived an equation for an ellipsoid with a nonconducting shell. Since polyelectrolytes are surrounded by a conducting counter ion atmosphere, his treatment may not be relevant to the present case.

Surface Conductivity. The basic difference between the previous treatments and this treatment is that a fluctuation of counter ions is considered in this case. A particle with a pure conducting shell (with k_3, $\epsilon_3 = 0$) is treated by O'Konski (*13*) for spherical and ellipsoidal particles. O'Konski assumed the existence of a frequency-independent surface con-

Publication Date: January 1, 1967 | doi: 10.1021/ba-1967-0063.ch017

ductance, k_3, around the particle which a complex dielectric constant,

$$\epsilon_2^* = \epsilon_2 - \frac{4\pi k_2}{\omega} i$$

in a continuous medium with a complex dielectric constant,

$$\epsilon_1^* = \epsilon_1 - \frac{4\pi k_1}{\omega} i$$

He also assumed that the surface charge density undergoes a tangential as well as a vertical variation when an electric field is applied. By solving the continuity equation with appropriate boundary conditions, he obtained an equation for an ellipsoid which has the same form as Fricke's Equation 17 except for the magnitude of the excess conductivity.

$$\epsilon - \epsilon_1^* = q(\epsilon_j^* - \epsilon_1^*)/[1 + n(\epsilon_j^* - \epsilon_1^*)/\epsilon_1^*] \tag{29}$$

where n is given by Equation 18. The complex dielectric constants, ϵ_1^* and ϵ_j^*, are now given by

$$\epsilon_1^* = \epsilon_1 - \frac{4\pi k_1}{\omega} i \tag{30}$$

$$\epsilon_j^* = \epsilon_j - \frac{4\pi(k_j + 2k_3/J)}{\omega} \tag{31}$$

whereas ϵ_j^* is given by $\epsilon_j^* = \epsilon_j - 4\pi k_j i/\omega$. in Fricke's original equation. J represents axes a, b, and c, depending on the direction of field. It is obvious that the presence of surface conductivity, k_3, merely increases the conductivity, k_2, by the amount of $2k_3/J$.

The dielectric increment at low frequencies is given by the following expression;

$$\Delta\epsilon_1 = \frac{q}{3} \epsilon_1 \sum_{abc} \frac{\epsilon_j/\epsilon_1 - 1 + (k_j/k_1 - 1)^2 n_j}{1 + (k_j/k_1 - 1)n_j} \tag{32}$$

n_j is again a parameter given by Equation 18; j refers to the direction of the electric field. Likewise relaxation time is given by

$$\tau = \frac{1}{4\pi} \frac{\epsilon_j + \epsilon_1(1/n_j - 1)}{k_j + k_1(1/n_j - 1)} \tag{33}$$

The numerical values of dielectric increment were calculated by O'Konski on the basis of Equation 32, for various axial ratios and surface conductivities. The length of the largest DNA sample used in this experiment is approximately 1×10^4 A. If we assume the radius of the cylinder which contains the DNA molecule is about 50 A., the axial ratio would be about 100. Equation 32 gives a value for specific dielectric increment ($\Delta\epsilon/q$) of about 8200 for a parallel field for this axial ratio with the surface

Publication Date: January 1, 1967 | doi: 10.1021/ba-1967-0063.ch017

conductivity 100 times greater than the conductivity of the medium. This value is too small compared with the observed value of 1500 at a concentration of 0.01% (this will give 0.375 volume % on the basis of the above dimension and the specific dielectric increment of 40×10^4).

In the above calculation, the volume fraction is estimated without the counter ion layer. If we include the counter ion layer (with the Debye-Hückel radius approximately 200 A. at the ionic strength used for measurements), the volume fraction will be larger than that used above by a factor of 15 to 20. Therefore, the volume fraction of the solution used for the measurement is 6.0 instead of 0.375%. Thus the observed specific dielectric increment would be 2.5×10^4, which is still considerably larger than the theoretical value. As we have seen, there are great uncertainties concerning the estimation of the volume fraction of polyelectrolytes. Under these conditions, it may be better to discuss the problem on a qualitative basis and not take the numerical agreement as conclusive.

From Figure 4 and Table VIII of Ref. *13*, O'Konski's theory predicts that the increment increases with the increase of axial ratio with a slope of less than 1 and that the dielectric increment reaches a maximum value at the axial ratio of 30 and decreases again with the further increase of axial ratio. These predictions contradict the experimental observations.

Relaxation time can be calculated from Equation 33. When the molecule is highly elongated, $1/n_a$ has a value of $(0.000133)^{-1}$ for an axial ratio of 200. Therefore, the value in the brackets is represented only by the term $1/n_j$. Usually the dielectric constant of the particle is taken to be much smaller than that of water, and the numerator is represented by ϵ_1/n_a. Therefore,

$$\tau_j = \frac{1}{4\pi} \times \frac{\epsilon_1/n_a}{k_j + k_1/n_a} \tag{34}$$

Since $k_j \ll 2k_3/a$, $(k_j + 2k_3/a)$ would be practically equal to $2k_3/a$. We assume that if $2k_3/a = 4.0 \times 10^{-3}$ mho cm.$^{-1}$ and $k_1 = 10^{-6}$ mho cm.$^{-1}$, the relaxation time would be about 0.5×10^{-5} second, about one one-hundredth of the value obtained by measurement. Although the agreement may be improved somewhat by choosing different values for various parameters, it does not seem possible to reach satisfactory agreement.

Counter Ion Polarization. Schwan (*20*) attempted to explain the dielectric dispersion of a spherical particle suspension in terms of counter ion polarization, and Schwarz carried out the mathematical formulation (*23*), and found that the displacement of the counter ion in the double layer is equivalent to the existence of complex surface conductivity,

$$k_s = \frac{i\omega\tau}{1 + i\omega\tau} k_{so} \tag{35}$$

where k_{so} ($eu\sigma$) is the frequency-independent surface conductivity defined by O'Konski. Schwarz found that the presence of this complex surface

Publication Date: January 1, 1967 | doi: 10.1021/ba-1967-0063.ch017

conductivity gives rise to a surface capacitance which rises far above the capacitance of water. He derived equations for the dielectric increment and relaxation time,

$$\Delta\epsilon = \frac{9}{4} \frac{P}{(1 + P/2)^2} \frac{e^2 R\sigma}{kT} \tag{36}$$

$$\tau = \frac{R^2}{2ukT} \tag{37}$$

where P is the volume fraction, e is the electronic charge, R is the radius of the particle, σ is the surface charge density, and u is the mobility of the counter ion.

This theory is extended to an ellipsoidal particle by Takashima by using ellipsoidal coordinates. The procedure is described in detail in the following discussion. [Pennock (*15*) treated this problem by using spheroidal ordinates and reached the same conclusion.]

GENERAL ELLIPSOID. If one suspends an ellipsoid with complex dielectric constant,

$$\epsilon_1^* = \epsilon_1 - \frac{4\pi k_1 i}{\omega}$$

in a medium with complex dielectric constant,

$$\epsilon_2^* = \epsilon_2 - \frac{4\pi k_2 i}{\omega}$$

and applies a parallel electric field along the major axis, the field causes a flux of counter ions

$$J_E = -eu\sigma\nabla\psi_s \tag{38}$$

where u is the mobility of counter ion, and ψ_s is the surface potential. The flux is opposed by a diffusion-controlled flux of counter ions of magnitude,

$$J_D = -ukT\nabla\sigma \tag{39}$$

Therefore, the equation of continuity is given by

$$\frac{\alpha\sigma}{\alpha t} = eu\sigma\nabla^2\psi_s + ukT\nabla^2\sigma \tag{40}$$

The Laplacian $\nabla^2\psi_s$ in ellipsoidal coordinates is

$$\nabla^2\psi_s = \frac{4}{(\zeta - \xi)(\xi - \eta)(\eta - \zeta)} \times \left[(\zeta - \xi)R_\eta \frac{\alpha}{\alpha\eta}\left(R_\eta \frac{\alpha\psi_s}{\alpha\eta}\right) + (\xi - \eta)R_\zeta \frac{\alpha}{\alpha\zeta}\left(R_\zeta \frac{\alpha\psi_s}{\alpha\zeta}\right) + (\eta - \zeta)R_\xi \frac{\alpha}{\alpha\xi}\left(R_\xi \frac{\alpha\psi_s}{\alpha\xi}\right)\right] \tag{41}$$

where ξ, η, and ζ are three coordinate axes, and

$$\begin{aligned} R_\xi &= [(\xi + a^2)(\xi + b^2)(\xi + c^2)]^{\frac{1}{2}} \\ R\eta &= [(\eta + a^2)(\eta + b^2)(\eta + c^2)]^{\frac{1}{2}} \\ R_\zeta &= [(\zeta + a^2)(\zeta + b^2)(\zeta + c^2)]^{\frac{1}{2}} \end{aligned} \tag{42}$$

Since ψ_s is independent of ξ on the surface of an ellipsoid, the form of ψ_s would be

$$\psi_s = \beta F_2(\eta) F_3(\zeta) \tag{43}$$

where β is a constant and

$$\begin{aligned} F_2(\eta) &= (\eta + a^2)^{\frac{1}{2}} \\ F_3(\zeta) &= (\zeta + b^2)^{\frac{1}{2}} \end{aligned} \tag{44}$$

Likewise,

$$\sigma = \alpha F_2(\eta) F_3(\zeta) \tag{45}$$

Replacing $\alpha\sigma/\alpha t$ by $i\omega\bar{\sigma}$ ($\bar{\sigma} = \sigma - \sigma_o$ where σ_o is the counter ion density without a field and σ is an instantaneous density in the field) assuming $\bar{\sigma} \ll \sigma$, one obtains a relation between α and β:

$$\alpha = -\frac{1}{1 + i\omega\tau}\beta \tag{46}$$

where τ is the relaxation time given by

$$\tau = \frac{(\xi - \eta)(\xi - \zeta)}{u(b^2 + c^2 + 2\xi)kT} \tag{47}$$

Since $\xi = 0$ on the surface of an ellipsoid, the relaxation time reduces to

$$\tau = \frac{\eta\zeta}{u(b^2 + c^2)kT} \tag{48}$$

Since η and ζ are the coordinate axes, the value of τ cannot be specified explicitly. However, we can obtain an explicit expression for the limiting cases, discussed below.

The surface current density is given by

$$i_s = e(J_E + J_D) = \frac{i\omega\tau}{1 + i\omega\tau} k_{so} E_s \tag{49}$$

by using the relation $i_s = k_{so} \times E_s$

$$k_s = \frac{i\omega\tau}{1 + i\omega\tau} k_{so} \tag{50}$$

Publication Date: January 1, 1967 | doi: 10.1021/ba-1967-0063.ch017

In Ordered Fluids and Liquid Crystals; Porter, R., el al.;
Advances in Chemistry; American Chemical Society: Washington, DC, 1967.

Accordingly the relation between surface dielectric constant and k_{so} is

$$\epsilon_s^* = \frac{4\pi\tau k_{so}}{1 + i\omega\tau} \tag{51}$$

The potential inside and outside the ellipsoid with a parallel field is obtained by solving the two Laplace equations (*25*).

$$\Delta\psi_1 = 0 \tag{52}$$

$$\Delta\psi_2 = 0 \tag{53}$$

Here it is assumed that the double layer is infinitely thin, and there is no charge outside the double layer. This assumption can hardly be justified, but this simplifies the mathematics greatly. ψ_1 is the potential inside the particle and ψ_2 is the potential outside the particle. The boundary conditions are:

$$\psi_1 = \psi_2 = \psi_s \text{ for } \xi \to 0 \tag{54}$$

$$\psi_2 = \psi_0 = -E_0 X \text{ for } \xi \to \infty \tag{55}$$

$$\epsilon_1\left[\frac{1}{h_1}\frac{\alpha\psi_1}{\alpha\xi}\right]_{\xi=0} - \epsilon_2\left[\frac{1}{h_1}\frac{\alpha\psi_2}{\alpha\xi}\right]_{\xi=0} = -e\sigma \tag{56}$$

where

$$x = \left[\frac{(\xi + a^2)(\eta + a^2)(\zeta + a^2)}{(b^2 - a^2)(c^2 - a^2)}\right]^{\frac{1}{2}} \tag{57}$$

$$h_1 = \frac{1}{2}\left[\frac{(\xi - \eta)(\xi - \zeta)}{(\xi + a^2)(\xi + b^2)(\xi + c^2)}\right]^{\frac{1}{2}} \tag{58}$$

With these boundary conditions, the potentials outside and inside the ellipsoid become

$$\psi_1 = -\frac{E_{0x}X}{1 + \frac{abc}{2\epsilon}(\epsilon_1 - \epsilon_2)A_1} \tag{59}$$

$$\psi_2 = \psi_0 \frac{1 + \frac{abc}{2}\frac{\epsilon_1 - \epsilon_2}{k_1}A_2}{1 + \frac{abc}{2}\frac{\epsilon_1 - \epsilon_2}{\epsilon_2}A_1} \tag{60}$$

where

$$A_1 = \int_0^\infty \frac{d\xi}{(\xi + a^2)R_\xi} \tag{61}$$

$$A_2 = \int_0^\xi \frac{d\xi}{(\xi + a^2)R_\xi} \tag{62}$$

In Ordered Fluids and Liquid Crystals; Porter, R., el al.;
Advances in Chemistry; American Chemical Society: Washington, DC, 1967.

And also

$$\bar{\epsilon}_1 = \epsilon_1 + \frac{e^2a^2}{1 + i\omega\tau} \frac{\sigma}{kT} \frac{(\eta\zeta)^{1/2}}{2abc} \tag{63}$$

The presence of a frequency-dependent surface conductance results in an increase of dielectric constant of the suspension by an amount of

$$\Delta\epsilon = \frac{e^2a^2}{1 + i\omega\tau} \frac{\sigma}{kT} \frac{(\eta\zeta)^{1/2}}{2abc} \tag{64}$$

Again the second term on the right-hand side of Equation 62 remains unspecified except for limiting cases.

Limiting Case I, Cylinder. We cannot express the dielectric increment and relaxation time in terms of the molecular dimension for a general ellipsoid explicitly. However, DNA can be approximated by a highly elongated cylinder. On the surface of the ellipsoid, the following relation is obtained since $\xi = 0$,

$$\frac{x^2}{a^2} + \frac{y^2}{b^2} + \frac{z^2}{c^2} = \frac{\eta\zeta}{a^2b^2c^2} \tag{65}$$

where x, y, and z are the coordinate axes in rectangular coordinates. If we use cylindrical coordinates for x, y, and z, assuming x is in the direction of the major axis of the cylinder, Equation 64 reduces to

$$\eta\zeta = b^2(a^2 + b^2) \tag{66}$$

If we insert this relation in Equations 48 and 63, they reduce to the following expressions:

$$\tau = \frac{a^2 + b^2}{2ukT} \tag{67}$$

$$\bar{\epsilon}_1 = \epsilon_1 + \frac{1}{1 + i\omega\tau} \frac{a^2}{2b} \frac{e^2\sigma}{kT} \tag{68}$$

The Maxwell equation of a cylinder can be expressed by the following equation with simplifying assumptions,

$$\epsilon - \epsilon_\infty = \frac{9}{4} \frac{P}{(1 + P)^2} (\bar{\epsilon}_1 - \epsilon_1) \tag{69}$$

Hence,

$$\epsilon = \epsilon_\infty + \frac{9}{4} \frac{P}{(1 + P)^2} \frac{1}{1 + i\omega\tau} \frac{a^2}{2b} \frac{e^2\sigma}{kT} \tag{70}$$

Finally we obtain

$$\Delta\epsilon_0 = \frac{9}{8} \frac{P}{(1 + P)^2} \frac{e^2\sigma}{kT} \frac{a^2}{b} \tag{71}$$

Publication Date: January 1, 1967 | doi: 10.1021/ba-1967-0063.ch017

LIMITING CASE II, SPHERE. Another limiting case is a sphere where $a = b = c$; then Equation 65 reduces to $a^2 = (\eta\zeta)^{1/2}$ where a is the radius of the sphere. Hence the expressions for dielectric increment and the relaxation time would be

$$\tau = \frac{a^2}{2ukT} \tag{72}$$

$$\Delta\epsilon = \frac{1}{1 + i\omega\tau} \frac{e^2 a\sigma}{kT} \tag{73}$$

These are essentially the expressions obtained by Schwarz (*see* Equations 36 and 37.)

According to Equation 71, the dielectric increment is proportional to a^2/b. Since we can safely assume that b is practically constant, $\Delta\epsilon$ is actually proportional to a^2. This relation agrees with the experimental observation (*see* Experimental). Moreover, if we insert appropriate values into Equation 71, $a = 10^{-4}$ cm., $b = 400 \times 10^{-8}$ cm. (including the counter ion layer assuming the Debye-Hückel radius to be 200×10^{-8} cm.), $P = 0.06$, $\sigma = 2.5 \times 10^{12}$ cm.$^{-2}$, and $e = 4.8 \times 10^{-10}$ e.s.u., the value for the dielectric increment is approximately 5050, which is about three times larger than the observed value of 1500. However, the above treatment is carried out with an assumption that DNA molecules are aligned completely in the direction of the electric field. Actually the DNA molecules are almost randomly distributed. Therefore, Equation 70 must be rewritten as

$$\epsilon^* = \epsilon_\infty + \frac{1}{3}\left[\frac{\Delta\epsilon_a}{1 + i\omega\tau_a} + \frac{2\Delta\epsilon_b}{1 + i\omega\tau_b}\right] \tag{74}$$

where

$$\Delta\epsilon_a = \frac{9}{8} \frac{P}{(1 + P)^2} \frac{e^2\sigma}{kT} \frac{a^2}{b} \tag{75}$$

representing the longitudinal dielectric increment. The second term in brackets represents the transverse increment. The dielectric increment of a cylinder with a transverse electric field is treated by Ishiwatari and Schwan (*7*). The transverse dielectric increment is given by

$$\Delta\epsilon_b = \frac{P}{(1 + P)^2} \frac{e^2 b\sigma}{kT} \tag{76}$$

The dielectric increment in the transverse direction is much smaller than that of the longitudinal direction and the total increment is practically one third of the longitudinal increment. Thus, the total dielectric increment turns out to be about 1580, which is in an excellent agreement with the experimental result. However, there are uncertainties in estimating the volume fraction and the charge density. The numerical agreement should not be taken as conclusive. However, the formula (Equation 74)

Publication Date: January 1, 1967 | doi: 10.1021/ba-1967-0063.ch017

predicts a large dielectric increment and a size dependence in agreement with the experimental observation. The experimental verification of the relaxation time is even more difficult because no data concerning the mobility of counter ions at the interface are available. However, Equation 67 indicates that the relaxation time of the cylinder in a parallel field would be proportional to $(a^2 + b^2)$. However, b is much smaller than a; therefore, the relaxation time is practically proportional to a_2. This is qualitatively in agreement with the experimental results.

Although we made some assumptions which may not be justified for the rigorous discussion, the counter ion polarization mechanism described above seems to give a reasonable explanation of the dielectric behavior of DNA solutions.

Acknowledgment

The author is indebted to H. P. Schwan and B. E. Pennock for valuable discussions.

Literature Cited

(1) Allgen, L. G., *Acta Physiol. Scand.* **22**, Suppl., 76 (1950).
(2) Boeder, P., *Z. Physik* **75**, 273 (1932).
(3) Cole, K. S., Cole, R. H., *J. Chem. Phys.* **9**, 341 (1941).
(4) Edsall, J. T., "Proteins, Amino Acids and Peptides," E. J. Cohn and J. T. Edsall eds., p. 450, Reinhold, New York, 1943.
(5) Fricke, H., *J. Appl. Phys.* **24**, 644 (1953).
(6) Fricke, H., *J. Phys. Chem.* **57**, 934 (1953).
(7) Ishiwatari, H., Schwan, H. P., unpublished calculation.
(8) Jerrard, H. G., Simmons, B. A. W., *Nature* **184**, 1715 (1959).
(9) Jungner, G., Jungner, I., Allgen, L. G., *Nature* **63**, 849 (1949).
(10) Maczuk, J., Intramural report, University of Pennsylvania, 1957.
(11) Maxwell, J. C., "Treatise on Electricity and Magnetism," Vol. 1, p. 451, Oxford, 1892.
(12) Miles, J. B., Robertson, H. P., *Phys. Rev.* **40**, 583 (1932).
(13) O'Konski, C. T., *J. Phys. Chem.* **64**, 605 (1960).
(14) Pauly, H., Schwan, H. P., *Z. Naturforsch.* **14,b**, 125 (1959).
(15) Pennock, B. E., University of Pennsylvania, unpublished manuscript.
(16) Perrin, F., *J. Phys. Rad.* **7**, (5), 497 (1934).
(17) Peterlin, A., Stuart, H. A., *Z. Physik.*, **112**, 129 (1939).
(18) Pollack, M., *J. Chem. Phys.* **43**, 908 (1965).
(19) Scheraga, H. A., Edsall, J. T., Gadd, J. O., *J. Chem. Phys.* **19**, 1101 (1951).
(20) Schwan, H. P., *Advan. Biol. Med. Phys.* **5**, 147 (1957).
(21) Schwan, H. P., "Physical Techniques in Biological Research," Chap. 6, Vol. 6, Academic Press, New York, 1963.
(22) Schwan, H. P., Schwarz, Maczuk, J., Pauly, H., *J. Phys. Chem.* **66**, 2626 (1962).
(23) Schwarz, G., *J. Phys. Chem. 66*, 2636 (1962).
(24) Sillars, R. W., *J. Inst. Elec. Engrs. (London)* **80**, 378 (1937).
(25) Stellwagen, N. C., Shirai, M., O'Konski, C. T., Abstracts, Annual Biophysical Society Meeting, San Francisco, Calif., Feb. 24, 1965.
(26) Stratton, J. A., "Electromagnetic Theory," McGraw-Hill, New York, 1941
(27) Takashima, S., *J. Mol. Biol.* **7**, 455 (1963).
(28) Takashima, S., *J. Phys. Chem.* **70**, 1372 (1966).
(29) Wagner, K. W., *Arch. Elektrotech.* **3**, 83 (1914).

RECEIVED March 1, 1966, work supported by NIH Grants GM-12083-02 and HE-01253-14, and by NSF Institutional Grant IG-66-4.

Structure and Thermodynamic Properties of Single-Strand Helical Polynucleotides

J. BRAHMS and K. E. VAN HOLDE[7]

Centre de Recherches sur les Macromolécules, 6, rue Boussingault, Strasbourg, France

Publication Date: January 1, 1967 | doi: 10.1021/ba-1967-0063.ch018

Some polynucleotides exist in solution as ordered structures different from double-strand helical conformation. Two model compounds—oligomers of adenylic acid (oligo A) and poly-N^6-hydroxyethyladenylic acid—exhibit spectra similar to that of poly A at neutral pH and different from that of the double-strand helical poly A at acid pH. A single-chain helical structure, consistent with steric requirements, can explain the spectra. At neutral pH oligo A melting is uninfluenced by chain length; thus, the process is largely noncooperative. However at pH 4.5, the "melting" of double-stranded oligo A depends on chain length and thus is characteristic of a cooperative process.

Most consideration of the structures of polynucleotides has been based upon the concept of double or multichain helices, stabilized by hydrogen bonds. Such models are supported by x-ray diffraction studies of fibers of DNA (*29*), of fibers prepared from acidic solutions of poly A (*20*), and of a number of other polynucleotides in the solid state. In aqueous solution, the application of both light scattering (*21*) and low-angle x-ray scattering (*17*, *30*) indicates that the same kind of configuration is maintained. Such molecules behave hydrodynamically like rigid rods. The double-strand structures exhibit sharp "melting points" in their transition to disordered structures, for the disruption of such multihelices is apparently a highly cooperative process, exhibiting some resemblance to a phase transition.

Recently, it has become evident that hydrogen bonding alone may not account for the stability of DNA-like structures. Indications that forces other than hydrogen bonds might be important were obtained from the

[7] Present address, Department of Chemistry and Chemical Engineering, University of Illinois, Urbana, Ill.

In Ordered Fluids and Liquid Crystals; Porter, R., el al.;
Advances in Chemistry; American Chemical Society: Washington, DC, 1967.

studies of hypochromicity of small oligonucleotides (*18*), the destabilization of DNA by various organic solvents (*9*, *10*, *11*, *15*), and also by x-ray scattering of RNA (*24*).

Theoretical investigations by Zimm and Kallenbach (*32*) and by Devoe and Tinoco (*5*) suggest that "stacking interactions" between parallel bases may also contribute an appreciable fraction to the helix free energy. This has tended to reopen the neglected question as to whether other kinds of organized polynucleotide structures may be stable under appropriate conditions. In general, it has been assumed that polynucleotides which were not in double or multihelical conformation behaved as random coils—for example, poly A, poly C, or poly U at neutral pH, or even RNA. Results of conventional methods such as sedimentation, viscometry, and light scattering seemed to confirm this idea (*7*, *22*). However, a number of optical techniques, including circular dichroism (*2*, *3*), rotatory dispersion (*6*, *13*), and absorption spectroscopy (*16*, *18*, *26*), indicated that even in these circumstances these polymers gave indications of possessing an organized structure. For example, poly A, poly C, and poly U (at low temperature, ~0°C.) all exhibit intense circular dichroism bands in the spectral region of the base absorption, as well as corresponding Cotton effects in the ORD spectrum. Similarly, low-angle x-ray scattering data are consistent with a partially rodlike structure for poly A and poly U at neutral pH and low temperature. Some of these results are summarized in Table I, where they are compared with data for a typical two-strand helix, poly A, at low pH.

Table I. Properties of Polynucleotides

	1 H, %	*2* $R \times 10^{40}$	*3* μ, $A.^{-1}$
Poly A (pH 7)	40[a]	32[b]	51[c]
Poly C (pH 7)	30[a]	37[d]	—
Poly U (pH 7) (0°C.)	25[e]	30[d]	43[c]
Poly A (pH 4.8 to 5.0)	45[a]	65[d]	89[c]

1. % hypochromicity calculated as $H = 1 - \epsilon_{max\ p}/\epsilon_{max\ m}$.
2. R = rotational strength of longer wavelength band, in c.g.s. units.
3. μ = linear electron density in electrons / A.

[a] (*26*)
[b] (*3*)
[c] (*30*)
[d] (*2*)
[e] (*16*)

These data suggest that poly A, poly C, and poly U can exhibit some kind of an ordered configuration in neutral solutions. This structure can be reversibly "melted" by heating; however, the transition is not sharp like that of DNA but occurs over a wide temperature range. To account for

Publication Date: January 1, 1967 | doi: 10.1021/ba-1967-0063.ch018

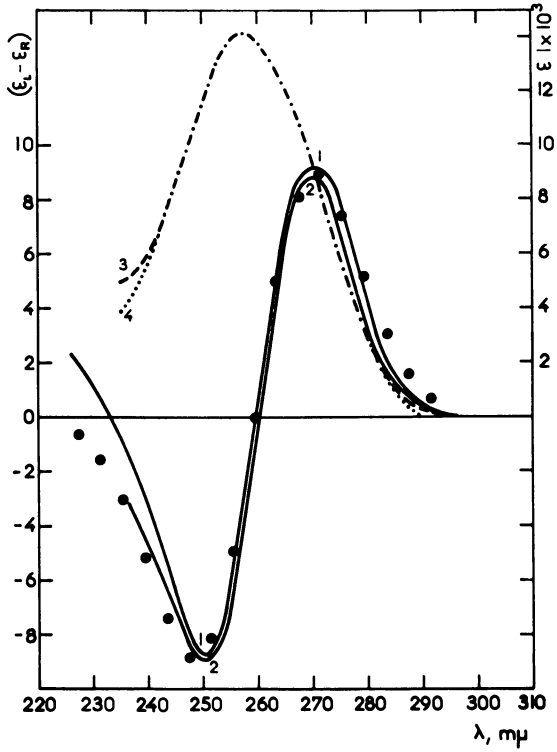

Figure 1. Circular dichroic spectra and absorption spectra of dimer ApA

1,2. Circular dichroism at pH 7.4 and 4.9, respectively (both at 5.5°C.)
3,4. Corresponding absorption spectra
● *Theoretical curve*

various properties of such structures, a number of models have been proposed:

Conformations involving both double-strand regions and random coil segments in the same molecule (*8*).

A double-strand helix with intercalated bases (*30*).

Single-strand helices, stabilized by base stacking (*6, 13, 25, 30*).

To eliminate some of the present ambiguity concerning these structures, we have examined the behavior of a number of oligomers and the polymer of adenylic acid, as well as the polymer of N^6-hydroxyethyladenylic acid (poly HEA). We have been concerned with both the explanation of their optical properties in terms of proposed models and the thermodynamics of the melting process. It is hoped that the information so obtained will help to clarify the importance of order-disorder phenomena in biology and questions concerning the structure of such biologically important polynucleotides as RNA.

Publication Date: January 1, 1967 | doi: 10.1021/ba-1967-0063.ch018

Structures of Adenylate Polymers in Neutral Solution

We have chosen to investigate, primarily by circular dichroism measurements, a series of oligomers of adenylic acid (including the high polymer) as well as the closely related poly-N^6-hydroxyethyladenylic acid. The latter is of interest because the blocking of the nitrogen should prevent the formation of hydrogen-bonded double-strand helices under all conditions.

A glance at the circular dichroic spectra shown in Figures 1, 2, and 3 demonstrates a fundamental point: starting from the dimer, all of these substances in neutral solution at low temperature exhibit the same kind of dichroic spectrum. While there are small differences in the positions and

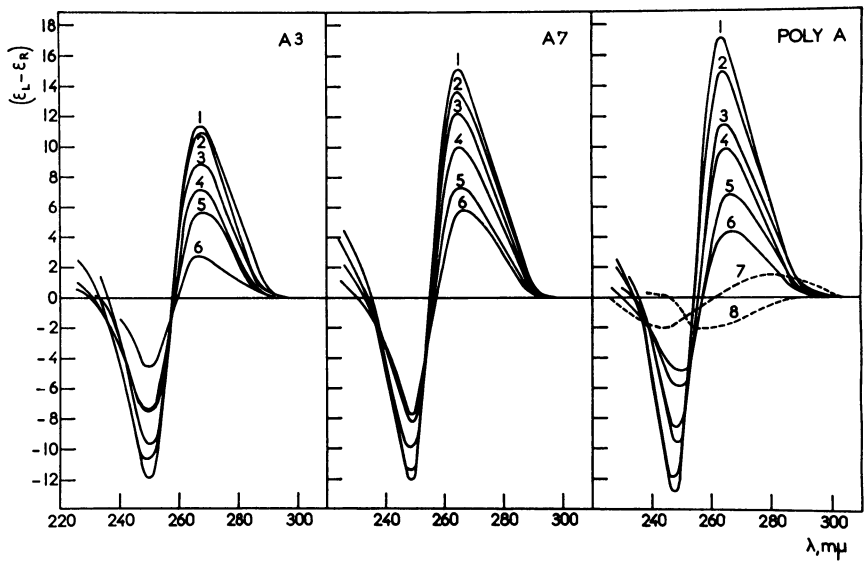

Figure 2. Circular dichroic spectra of adenylate oligonucleotides at pH 7.4 at various temperatures

Left. Trimer at:
1. *−2°C.*
2. *+0.5°C.*
3. *4.5°C.*
4. *18°C.*
5. *25°C.*
6. *47°C.*

Center. Heptamer at:
1. *−2°C.*
2. *+0.5°C.*
3. *8°C.*
4. *18.5°C.*
5. *32°C.*
6. *40°C.*

Right. Polymer at:
1. *−2° to +6°C.*
2. *17°C.*
3. *34°C.*
4. *42°C.*
5. *57°C.*
6. *74°C.*
7. *Poly A in 98% ethanol*
8. *AMP*

intensities of the bands (analyzed below), in every case a pair of bands of opposite sign are found in the region of the adenylate absorption band. This circular dichroism is entirely different from, and many times more in-

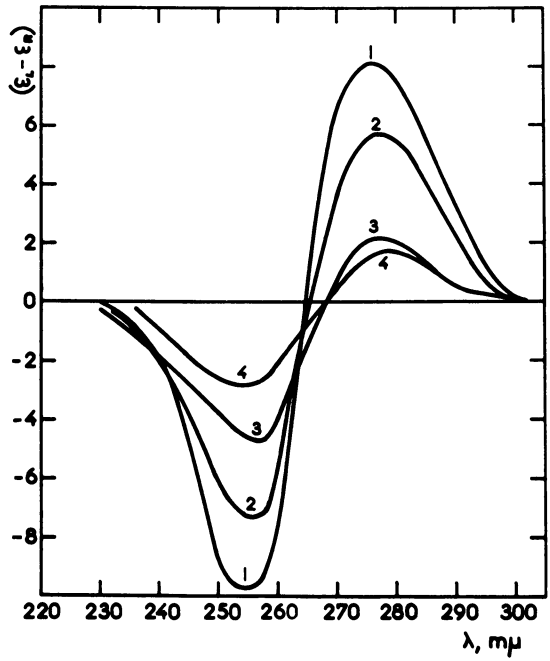

Figure 3. Circular dichroic spectra of poly HEA at various temperatures in 0.1M NaCl, 0.1M acetate, pH 4.9

Approximate temperature

1. *4°C.*
2. *22°C.*
3. *35°C.*
4. *50°C.*

tense than the weak dichroic spectrum of the monomer. We conclude that it must result from a specific kind of dissymmetric conformation common to all of these compounds under these conditions. This cannot be a hydrogen-bonded multichain structure for similar results are observed with poly HEA and even with the dimer, ApA; furthermore, it has been shown that even in the "melting" region the spectrum is insensitive to concentration of the samples and can be observed at very high dilution ($\sim 10^{-4}$ *M*). An extended configuration with the two bases tilted as proposed by Kuhn and Rometsch (*14*) for substituted diphenyls cannot be accepted as an explanation for the optical activity of ApA since the distance between two oscillators is too great (~20 A.) to allow an effective coupling.

A further indication of the nature of this "neutral pH structure" is provided by a contrast of Figures 2 and 4. In acidic solution, where poly A is known to form a two-strand helix, both poly A and the higher oligomers demonstrate a different circular dichroic spectrum, whereas the curves for poly HEA and the lower oligomers of A are unchanged (Figure 1) (*25*).

A key to the nature of the conformation in neutral solutions is provided by examining models of the dimer, ApA. A parallel "stacked base"

Publication Date: January 1, 1967 | doi: 10.1021/ba-1967-0063.ch018

configuration can be easily adopted by this molecule (*25*); furthermore, this configuration involves a rotation of one base with respect to the other by about 30°–45°. Thus, it can represent the start of a single-strand helix similar in dimensions to half of a double-strand polynucleotide helix. This concept is supported by the values of electron density given in Table I.

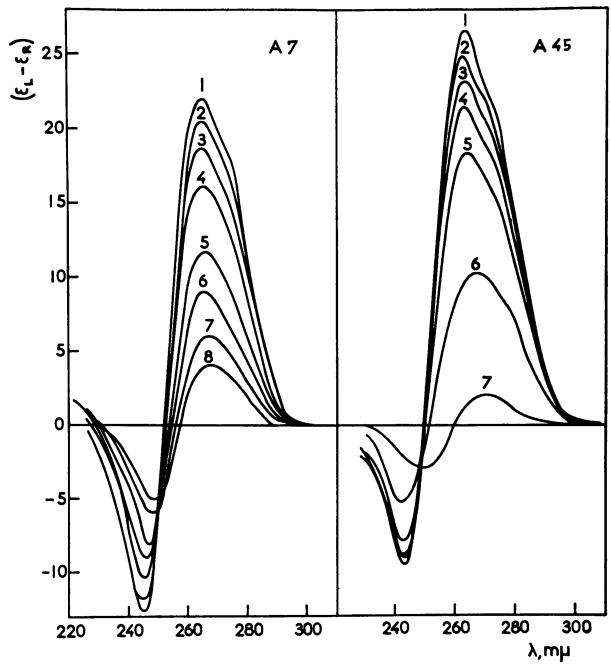

Figure 4. Circular dichoic spectra of adenylate oligomers at pH 4.5

Left. Heptamer at various temperatures between −2° and 45°C.
Right. Sample of N = 45, between 0° and 85°C.

Indeed, such a general model was proposed as one possibility by Witz and Luzzati (*30*) and again by Holcomb and Tinoco (*13*) on the basis of their ORD and viscosity studies. The idea of the stabilization of helical structures by interactions between stacked, parallel bases has been suggested by a number of authors.

Analysis of the Optical Activity of Adenylate Oligomers

The validity of a model, such as that suggested above, can be tested by such data as circular dichroic spectra only if an adequate theory of optical activity is available. While several such theories have been developed, those based upon the exciton theory seem particularly appropriate to the investigation of polymeric structures (*1*, *19*, *23*). As in a molecular crystal, such theories depict the interaction of the identical residues in an

Publication Date: January 1, 1967 | doi: 10.1021/ba-1967-0063.ch018

N-mer as producing an N-fold splitting of the excited state. Consequently, each absorption band of the monomer (of frequency ν_0) is split into N bands in the N-mer. In the simplest of these theories, which assumes only nearest-neighbor interactions (*1*), the frequencies of these bands are given by

$$\nu_K = \nu_o + \frac{2V}{h} \cos \frac{\pi K}{N+1} \qquad K = 1,2\cdots, N \tag{1}$$

where V is the interaction energy. If the polymeric structure is dissymmetric, these bands may be optically active. From the theory of Bradley (*1*), it is easy to show (*4*) that for a helical, single-strand N-mer the rotational strength of the Kth band will be given by

$$R_K = -\frac{2\pi Z {\mu_\perp}^2}{\lambda_o(N+1)} \sum_{\substack{i,j \\ j>i}}^{N} (j-i) \sin \frac{\pi K i}{N+1} \sin \frac{\pi K j}{N+1} \sin (j-i)\alpha \tag{2}$$

where Z is the spacing between residues in the direction of the helix axis, α is the angle or rotation of successive residues about that axis, and $\mu_\perp$ is the magnitude of the transition moment.

Figure 5 shows schematically the distributions of rotational strengths predicted by Equation 2 for adenylate oligomers as single-chain helices with eight residues per turn ($\alpha = 45°$). To estimate the band splittings, we have used the fact that the nearest-neighbor theory predicts that the absorption band of the infinite, stacked-base helix will be shifted from the monomer band by an amount $(2\ V \cos \alpha)/h$. Since this shift is experimentally known, V can be eliminated from Equation 1.

The predicted features of the dichroic spectra are in good agreement with observations for the adenylate oligomers in neutral solution. Taking the simplest case, the dimer, we see that there should be two bands of opposite sign, spaced above and below the position of the monomer band; their rotational strength should be given by

$$R_1 = -\frac{\pi Z}{2\lambda_o} {\mu_\perp}^2 \sin \alpha \qquad \text{and} \qquad R_2 = \frac{\pi Z}{2\lambda_o} {\mu_\perp}^2 \sin \alpha \tag{3}$$

Each of these bands will be of half-width comparable to that of the monomer band. Thus, while the difference in sign allows resolution in the circular dichroic spectrum, the bands cannot be resolved in the absorption spectrum. If we algebraically add two bands of appropriate width and intensity, the series of points shown in Figure 1 is obtained; this accurately represents the observed circular dichroic spectrum of the dimer. A calculation (*25*) of the rotational strength to be observed in either half of the curve leads to values in good agreement with experiment, if Z is assumed to be 3–4 A., and α is between 30° and 45°.

Publication Date: January 1, 1967 | doi: 10.1021/ba-1967-0063.ch018

In Ordered Fluids and Liquid Crystals; Porter, R., el al.;
Advances in Chemistry; American Chemical Society: Washington, DC, 1967.

Such calculations are more difficult for higher members of the oligomer series because of the larger number of overlapping bands to be taken into account. However, calculations for the trimer are also in good agreement with experiment (*4*). Since all of the distributions of rotational strength predicted for the various oligomers on the basis of the assumed model exhibit a negative band at low wavelength, followed by a series of positive bands, one may predict that the "crossing point" in the circular dichroic spectrum will move to lower λ as N increases. The comparison of predicted and observed crossing points shown in Figure 5 is satisfactory.

On the basis of all of the above results, we may describe the structure of poly A in neutral solutions at low temperature in terms of a single-chain, stacked-base helix. The similarity of the properties of poly HEA implies a similar conformation.

Publication Date: January 1, 1967 | doi: 10.1021/ba-1967-0063.ch018

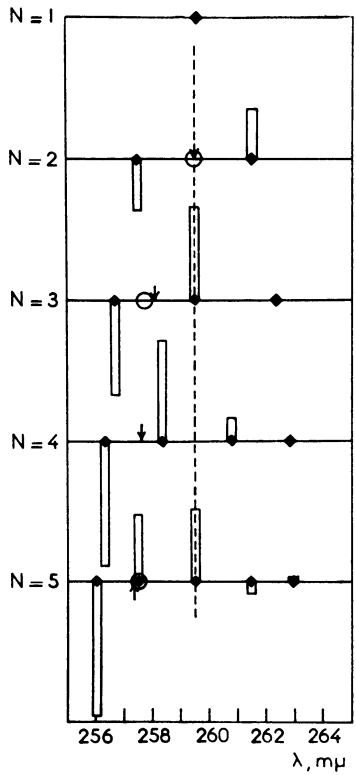

Figure 5. Schematic distributions of rotational strength as predicted by Equation 3 for first several adenylate oligomers

Band positions calculated as explained in text, α assumed to be 45°. Relative values of rotational strength given on basis of mole of oligomer

Some discussion should be devoted to the conditions under which two-strand helices can be formed. As has been shown, the configuration results in a circular dichroic spectrum differing markedly in intensity, form, and position on the wavelength scale from that of the single-chain helix.

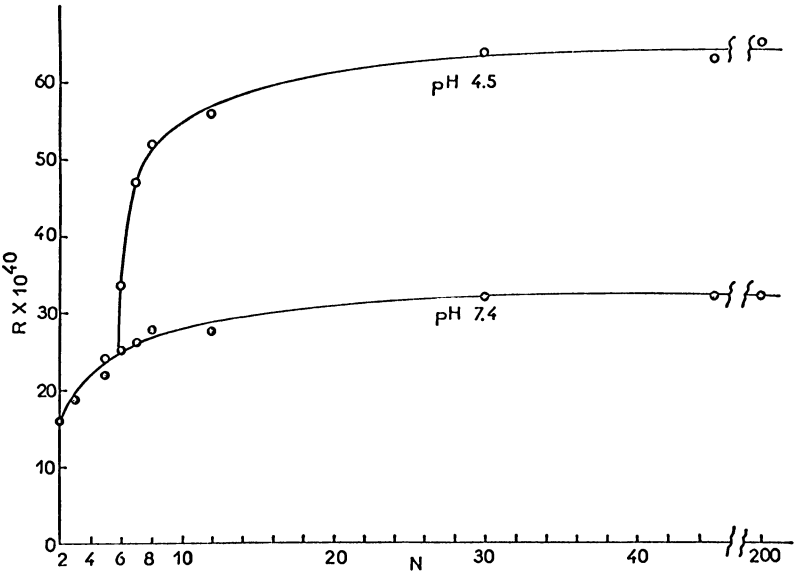

Figure 6. Rotational strength of positive dichroic band at 0°C. as a function of chain length N for adenylate oligomers

° *pH 4.5*
• *pH 7.4*

As expected, poly HEA cannot adopt this form under any conditions examined. It can be observed for poly A at pH values below 5 and at pH 4.5 all of the oligomers above the hexamer demonstrate circular dichroism characteristic of the two-chain helix. This is perhaps most clearly demonstrated in Figure 6, where the rotational strength increases suddenly at $N = 7$ in solutions at pH 4.5. On the other hand, at pH 7, the rotational strength increase smoothly with chain length from $N = 2$ to infinity.

Thermodynamics of Melting of Polynucleotide Structures

The circular dichroism which is typical of the ordered structures of adenylate oligomers, poly A, and poly HEA in neutral solutions disappears as the temperature is raised (Figures 2, 3, 7, and 8). This process is reversible, and presumably reflects the loss of the single-strand helical structure. Analogous to the behavior of DNA and other two-strand polynucleotides, we refer to this thermal transition as a "melting" process. However, a glance at Figures 7 and 8 will show that this transition is different in character from the sharp melting of DNA. The circular dichroism of

Publication Date: January 1, 1967 | doi: 10.1021/ba-1967-0063.ch018

these single-strand helices decreases gradually over the entire temperature range available to experimental measurement. Such a gradual change suggests a low value for the enthalpy of the process, a result which might be expected if the structure breaks down in a noncooperative fashion. The situation can be described more precisely by defining an apparent equilibrium constant, K, by

$$K = (R_o - R)/(R - R_n) \tag{4}$$

where R represents the rotational strength at a given temperature, and R_0 and R_n are the limiting values of R at low and high temperatures, respectively. We have chosen to use the integrated rotational strength of the

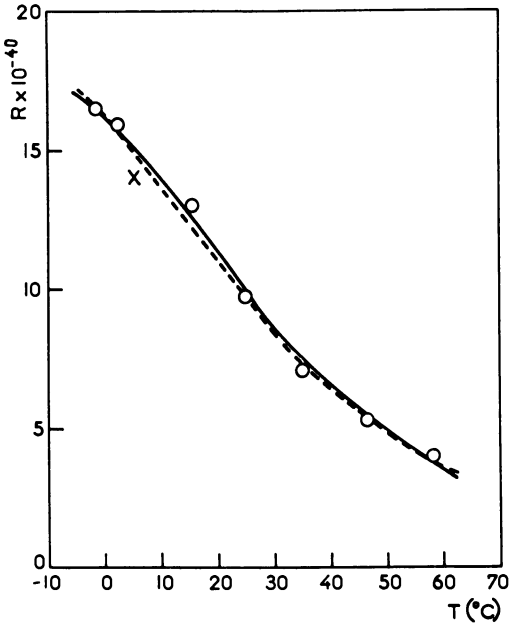

Figure 7. Rotational strength of positive dichroic band of ApA as a function of temperature
X Obtained by cooling previously heated solution
Curves calculated with various choices of parameters:
——— $R_o = 21 \times 10^{-40}$, *giving* $\Delta H° = 8.4$ *kcal.*, $\Delta S° = 28.5$ *e.u.*
– – – – $R_o = 23 \times 10^{-40}$, *giving* $\Delta H° = 7.8$ *kcal.*, $\Delta S° = 27.7$ *e.u.*

positive dichroic band for these calculations. Neither the lower nor the upper limits were reached in our experiments, and both must be estimated. At high temperature the values of R approach zero, the result expected for a completely disordered chain of optically inactive components. The low temperature limits have been estimated by extrapolating curves like those

Publication Date: January 1, 1967 | doi: 10.1021/ba-1967-0063.ch018

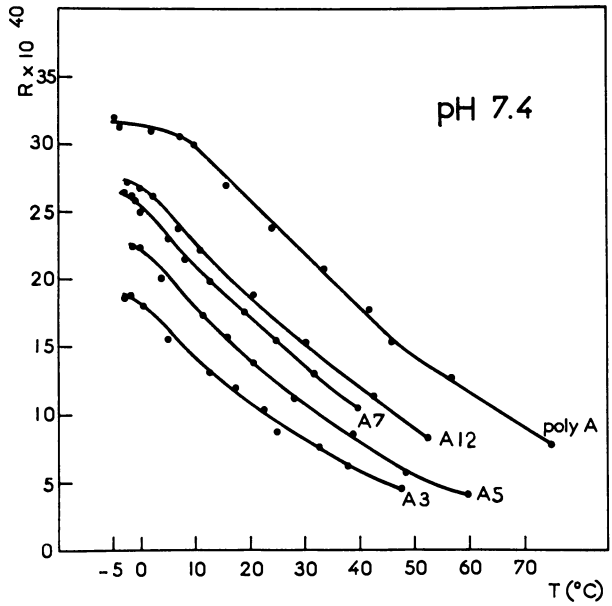

Figure 8. Change in rotational strength of positive dichroic band with temperature for some adenylate oligomers at pH 7.4 Chain length indicated by legend

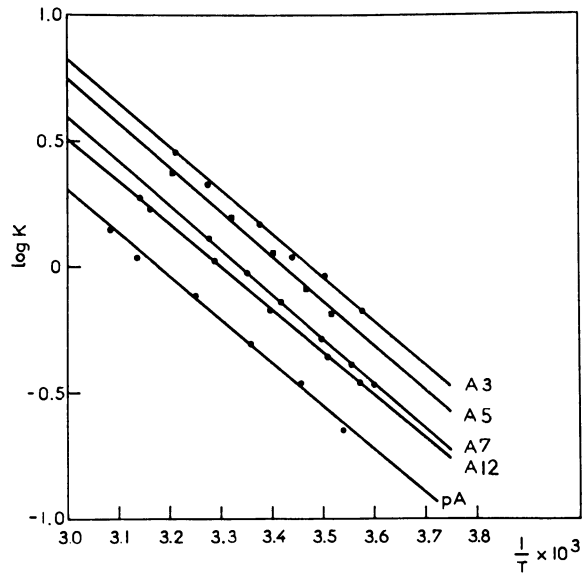

Figure 9. van't Hoff graphs corresponding to data shown in Figure 8

Equilibrium constants calculated according to Equation 4, with values of R_o and R_n estimated as described in text

shown in Figures 7 and 8 and by using the fact that $R = R_0/2$ at the inflection points of such curves.

With these values of equilibrium constants, it is possible to calculate $\Delta H°$ and $\Delta S°$ for the denaturation processes. As Figure 9 shows, straight van't Hoff graphs were invariably obtained. Furthermore, the lines are parallel, indicating that $\Delta H°$ must be the same for all of the adenylate oligomers and the high polymer; $\Delta S°$ is also nearly the same for all adenylates (Table II). This independence of thermodynamic properties upon chain length is typical of a noncooperative "melting" process (*4*). Essentially the same results are obtained for the high polymer as for the dimer because in both cases the elementary process is the independent unstacking of pairs of adjacent bases. While the slight dependence of the entropy change upon

Publication Date: January 1, 1967 | doi: 10.1021/ba-1967-0063.ch018

Table II. Thermodynamic Parameters for Thermal Denaturation of Adenylate Oligomers at Neutral pH (in 0.1M NaCl, 0.01 Mtris, pH 74).
(Data expressed per mole of nucleotide residue)

	$\Delta H°$, *Kcal/Mole*	$\Delta S°$, *E.U./Mole*	$\Delta F°$, *Kcal./Mole at 0°C.*	[a] $R_o \times 10^{40}$
Dimer	8.0	28	0.4	22
Trimer	8.0	28	0.4	25
Pentamer	8.1	28	0.5	29
Heptamer	8.0	27	0.6	30
Duodecamer	7.8	26	0.8	32
Poly A	7.9	25	1.1	37

[a] Values taken as low temperature limits for R.

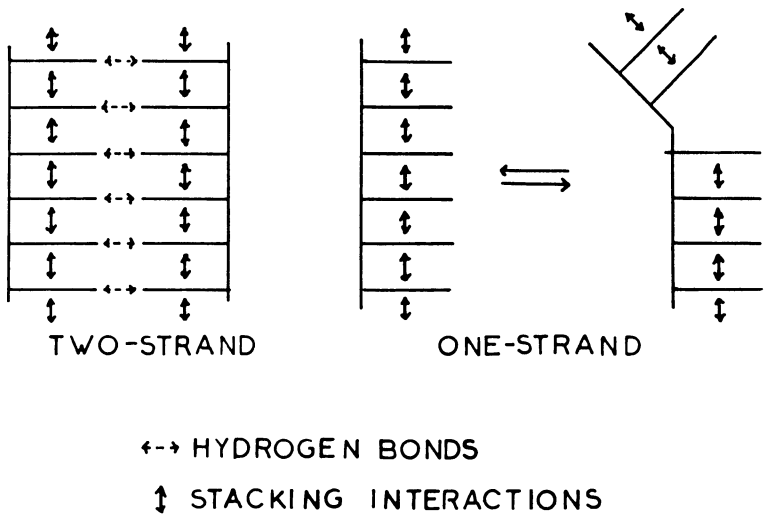

Figure 10. Highly schematic illustration of fundamental differences between one- and two-strand helices

Single-strand helix can melt noncooperatively because each "bond" is independent of all others

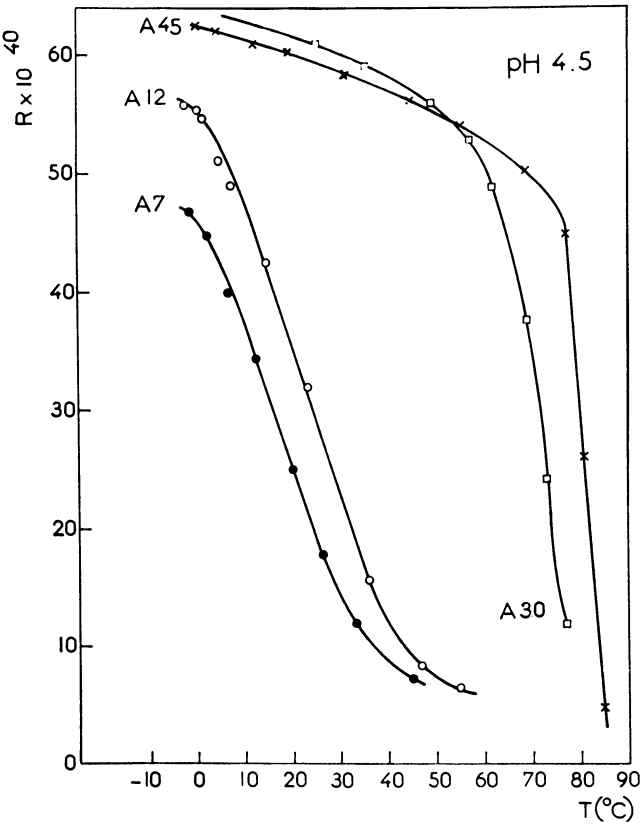

Figure 11. "Melting curves" for adenylate oligomers in acidic solution (pH 4.5)
As in Figure 8, rotational strength of positive band graphed vs. temperature

chain length indicates that the above statement is something of an oversimplification, the process viewed in this way is seen to be of an entirely different character from the cooperative melting of two-strand polynucleotides.

It is not surprising that single-strand and double-strand structures melt in a different way. Granted that stacking interactions between adjacent bases are of major importance (and the data obtained here indicate that each stacked pair contributes about 8 kcal. of enthalpy), we would expect a two-strand polynucleotide to be stabilized by a three-dimensional network of "stacking bonds" and hydrogen bonds. The deformation of any one bond is severely inhibited unless a group of adjacent bonds is simultaneously broken. Thus, the process must be cooperative. On the other hand, the single-strand structure can be visualized as a linear collection of "stacking bonds." Cooperative effects can arise only in a much

Publication Date: January 1, 1967 | doi: 10.1021/ba-1967-0063.ch018

more indirect way, and to a first approximation one would expect the state of any bond to be independent of that of its neighbors. The one- and two-strand structures are contrasted in Figure 10.

In confirmation of this point of view, adenylate oligomers and polymers, when in the two-strand conformation (at pH < 5), do melt in a cooperative manner. Figure 11 illustrates the change in circular dichroism with temperature for some of these oligomers at pH 4.5. We have not attempted thermodynamic analysis of these curves since they must represent a complex process of melting both double- and single-strand structures. However, it can be seen that the melting curves are markedly chain-length dependent and at least for the higher members of the series, become sharp. Thus, the same polymer poly A, depending upon its conformation, can exhibit either cooperative or noncooperative melting, indicating that the difference results from the kind of structure rather than the chemical nature of the polymer.

Publication Date: January 1, 1967 | doi: 10.1021/ba-1967-0063.ch018

Conclusions

The model proposed for poly A in neutral solutions as a result of these and other studies successfully resolves the ambiguities and contradictions which have been suggested by previous results. The single-chain, stacked-base structure can account adequately for the optical activity which has been observed. On the other hand, the melting studies indicate that even at 0°C. the helix will exhibit breaks at about 1 of 8 residues and that at room temperature only about two-thirds of the bases are stacked. The facts that the melting is noncooperative and that the free energy change is small ($\sim$1 kcal. at 0°C.) show that the molecule under these conditions can be in mobile equilibrium between a large number of configurations. By hydrodynamic and light-scattering measurements, such a molecule should indeed appear like a random coil.

Perhaps the most important consequence is the recognition that a second kind of organized structure (in addition to the Watson-Crick double helix) may be adopted by biologically important polynucleotides. In the case of RNA, both kinds of structure may be important since $\Delta F°$ for stacking is of the same order as that for hydrogen bonding. The behavior of a given kind of molecule will depend upon both the extent of base complementarity and the relative strengths of stacking interactions between various bases. The recognition of the noncooperative character of the "melting" of an ordered biopolymer may have important implication. It has generally been assumed in the major theoretical investigations that the helix-coil transition of a biopolymer is a cooperative process (*12*, *27*, *28*, *31*).

Acknowledgment

The authors thank C. Sadron and H. Benoit for their continued interest in and support of this research.

Literature Cited

(1) Bradley, D. F., Tinoco, J., Jr., Woody, R. W., *Biopolymers* **1**, 239 (1963).
(2) Brahms, J., *J. Am. Chem. Soc.* **79**, 3928 (1963).
(3) Brahms, J., *Nature* **202**, 797 (1964).
(4) Brahms, J., Michelson, A. M., Van Holde, K. E., *J. Molec. Biol.* **15**, 467 (1966).
(5) Devoe, H., Tinoco, J., Jr., *J. Mol. Biol.* **4**, 518 (1962).
(6) Fasman, G. D., Lindblow, C., Grossman, L., *Biochemistry* **3**, 1015 (1964).
(7) Fresco, J., Doty, P., *J. Am. Chem. Soc.* **79**, 3928 (1957).
(8) Fresco, J., Klemperer, E., *Ann. N. Y. Acad. Sci.* **81**, 730 (1959).
(9) Geiduschek, E. P., Herskovits, T. T., *Arch. Biochem. Biophys.* **95**, 114 (1961).
(10) Helmkamp, G. K., Ts'O, P. O. P., *Biochem. Biophys. Acta* **55**, 601 (1962).
(11) Herskovits, Y. T., *Biochemistry* **2**, 335 (1963).
(12) Hill, T. L., *J. Chem. Phys.* **30**, 383 (1959).
(13) Holcomb, D. N., Tinoco, J., Jr., *Biopolymers* **3**, 121 (1965).
(14) Kuhn, W., Rometsch, M., *Helv. Chim. Acta* **27**, 1090 (1944).
(15) Levine, L., Gordon, J. A., Jencks, W. P., *Biochemistry* **2**, 168 (1963).
(16) Lipsett, M. N., *Proc. Natl. Acad. Sci. U. S.* **46**, 445 (1960).
(17) Luzzati, V., Nicolaieff, A., Masson, F., *J. Mol. Biol.* **3**, 185 (1961).
(18) Michelson, A. M., *J. Chem. Soc.*, **1959**, 3655.
(19) Moffitt, W., *J. Chem. Phys.* **25**, 467 (1956).
(20) Rich, A., Davies, D. R., Crick, F. H. C., Watson, J. D., *J. Mol. Biol.* **3**, 71 (1961).
(21) Sadron, Ch., IIè Conseil de Chimie Solvay, Bruxelles, 1959.
(22) Steiner, R. F., Beers, R. F., Jr., *Biochem. Biophys. Acta* **26**, 336 (1957).
(23) Tinoco, J., Jr., Woody, R. W., Bradley, D. F., *J. Chem. Phys.* **38**, 1317 (1963).
(24) Timasheff, S. N., Witz, J., Luzzati, V., *Biophys. J.* **1**, 525 (1961).
(25) Van Holde, K. E., Brahms, J., Michelson, A. M., *J. Mol. Biol.* **12**, 726 (1965).
(26) Ts'O, P. O. P., Helmkamp, G. K., Sander, C. *Biochem. Biophys. Acta* **55**, 584 (1962).
(27) Volkenstein, M. V., *Biofizika* **6**, 257 (1961).
(28) Volkenstein, M. V., *Biophys. J.* **2**, 189 (1962).
(29) Watson, J. D., Crick, F. H. C., *Nature* **171**, 737 (1963).
(30) Witz, J., Luzzati, V., *J. Mol. Biol.* **11**, 620 (1965).
(31) Zimm, B. H., Bragg, J. K., *J. Chem. Phys.* **31**, 526 (1959).
(32) Zimm, B. H., Kallenbach, N. R., *Ann. Rev. Phys. Chem.* **13**, 171 (1962).

RECEIVED February 11, 1966.

19

Conformation of Pepsin and Pepsinogen

GERTRUDE E. PERLMANN

Rockefeller University, New York, N. Y.

Publication Date: January 1, 1967 | doi: 10.1021/ba-1967-0063.ch019

From the optical rotatory properties of pepsin and pepsinogen as functions of urea, temperature, and pH, it was shown that the macromolecular conformation of the zymogen differs markedly from that of the enzyme. Pepsin is essentially stabilized by hydrophobic interactions, and the fraction of amino acid residues present in a helical configuration is negligible. In contrast, the configuration of pepsinogen is stabilized by side chain interaction of an electrostatic nature between the basic amino acid residues of the peptide chain segment that are released during activation of pepsinogen to pepsin and some of the dicarboxylic acids of the pepsin moiety. Only a rough relation exists between the conformational changes observed and the susceptibility of the zymogen to activation.

One of the major aims of protein chemists is to understand the relation between the biological function of proteins and their structure and to define the type of forces which govern the specific folding of the polypeptide chain or chains of the molecule. In a current project of this laboratory directed toward establishing the conformational and functional determinants of the proteolytic enzyme, pepsin, and its zymogen, pepsinogen, chemical, physicochemical, and enzymic techniques are used to establish the function-structure relationship.

Before turning to the strategy adopted in our work, a few of the characteristics of the two proteins are reviewed. The physical and chemical properties of these proteins have been discussed in detail (*11*, *14*). As first shown by Langley, pepsin is present in its inactive form, pepsinogen, in the gastric mucosa. At acid pH, the zymogen is transformed by an autocatalytic reaction into pepsin, a proteolytic enzyme with an activity optimum at pH 2.0 and a wide specificity (*9*, *10*, *19*). Pepsin is rapidly inactivated above pH 6.0, whereas pepsinogen is stable at neutrality (*14*).

End group analyses of pepsinogen, a protein with a molecular weight of 40,000, revealed one *N*-terminal amino acid, leucine, and one *C*-terminal amino acid, alanine (*13*, *21*). In contrast, pepsin of 35,000 molecular weight

In Ordered Fluids and Liquid Crystals; Porter, R., el al.;
Advances in Chemistry; American Chemical Society: Washington, DC, 1967.

has isoleucine as the *N*-terminal and alanine as the *C*-terminal amino acid. These results support the concept that pepsinogen and pepsin are single-chain proteins which, as illustrated in Figure 1, are crosslinked by three disulfide bonds. The dashed line of Figure 1 indicates that most of the basic amino acid residues of pepsinogen are near the *N*-terminal end of the polypeptide chain, whereas the dicarboxylic acids, shown by the dotted line, are distributed over the major portion of the molecule. Below pH 6.0, pepsinogen is activated to pepsin with a concomitant release of several basic peptides from the *N*-terminal end of the polypeptide chain, thus leaving an acidic protein (*11*, *14*).

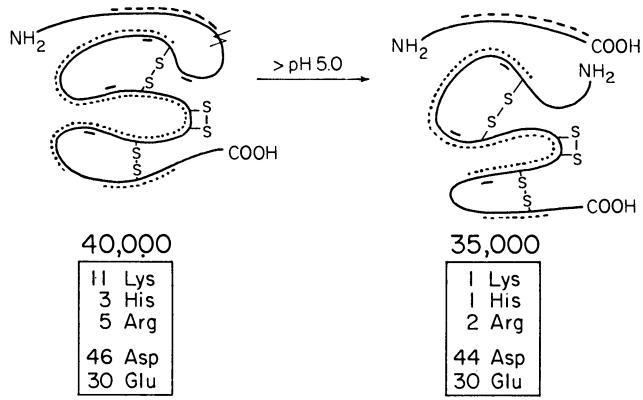

Figure 1. Conversion of pepsinogen to pepsin

Table I. Properties of Pepsinogen and Pepsin (1, 7)

	Pepsinogen	*Pepsin*
Molecular weight	40,000	35,000
Nitrogen content	15.0	14.8
Amino acid distribution	*No. Residues per Molecule*	
Acidic (Asp, Glu)	78	74
Basic (His, Lys, Arg)	19	4
Nonpolar (Gly, Val, Leu, Ileu, Ala, Met)	148	137
Hydroxy (Ser, Thr)	74	72
Aromatic (Tyr, Try, Phe)	39	38
Proline	19	15
½ Cys (-S-S)	6	6
Phosphorus	1	1

A closer examination of the amino acid distribution of the two proteins given in Table I reveals that during activation of the zymogen, ten lysines, two histidines, and three arginines are removed, in addition to 25 nonpolar amino acids, thereby reducing the number of basic residues in pepsin to four—one lysine, one histidine, and two arginines (*1*, *7*). It is,

Publication Date: January 1, 1967 | doi: 10.1021/ba-1967-0063.ch019

therefore, clear that this unusual amino acid distribution must influence the folding of the polypeptide chain. Hence, these two proteins must differ in their tertiary structure.

In 1958 we had reported that in contrast to most globular proteins, the specific optical rotation, $[\alpha]$, the hydrodynamic properties, and, most of all, the enzymic activity of pepsin remain unaltered if the protein is dissolved in concentrated urea solution or in guanidine hydrochloride, or if the solution is heated to 60°C. However, if the temperature is raised to 70°C., the rotatory dispersion constant, λ_c, increases from 216 to 236 mμ (*15*, *18*). Although hydrogen bonds of the type C = O . . . H − N and those involving the phenolic hydroxyls of tyrosine and the carboxylate ions of the acidic amino acid residues—i.e.,

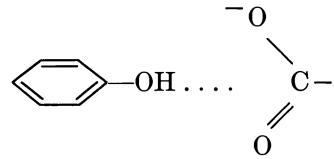

have been shown to exist in pepsin (*8*), they must be relatively unimportant in maintaining the conformation necessary for the enzymic activity of this protein. From these studies and from the fact that 70% of the molecule is made up of nonpolar amino acid residues which must be in van der Waals contact with their neighbors, we concluded that the fraction of residues present in α-helical configuration must be very low and almost negligible. Thus pepsin is essentially stabilized by hydrophobic interactions. This "apparent lack" of helicity in pepsin further follows from the fact that this protein has a high content of dicarboxylic amino acids which, in the pH range of greatest stability of the enzyme—i.e., pH 4.0 to 5.0—are ionized, and through electrostatic repulsion would prevent helix formation. The increase of the rotatory dispersion constant, λ_c, observed on heating of pepsin solutions above 60° reflects conformational transitions hitherto not yet described, which may be due in part to the presence of the hydroxy-amino acids—i.e., serine and threonine. Thus the presence of the hydroxy-amino acids in this protein may well favor a conformation such as a β-structure, and the conformational change observed on heating above 60°C. may be a β-sheet $\rightarrow$ coil transition.

In contrast, however, we have demonstrated that the macromolecular conformation of the zymogen differs markedly from that of the enzyme (*17*). Thus, if pepsinogen is transferred from an aqueous solution to concentrated urea, the specific rotation, $[\alpha]_{366}$, decreases from −200° to −320° in the concentration range of 1.5 to 4.0*M* urea, and the rotatory dispersion constant, λ_c, decreases from 236 to 216 mμ. As shown in Figure 2, which also includes the results obtained with pepsin, this change reflects a configurational transition, similar in sharpness to the transition from an α-

Publication Date: January 1, 1967 | doi: 10.1021/ba-1967-0063.ch019

helical conformation to random coil as observed for poly-α-amino acids on change of solvent composition.

Figure 3 shows that on heating of a pepsinogen solution to 70° or 75°C., the levorotation of pepsinogen increases within the narrow temperature range of 45° to 53°C. with a transition temperature $T_o = 49.5$°C. Between 55° and 60°C., $[\alpha]_{366}$ remains constant. Above 60°C., the levorotation further increases but never exceeds the 40% change of that observed when pepsinogen is dissolved in urea. In Figure 3 it is further indicated that a decrease of the rotatory dispersion constant from 236 to 216 mμ occurs in

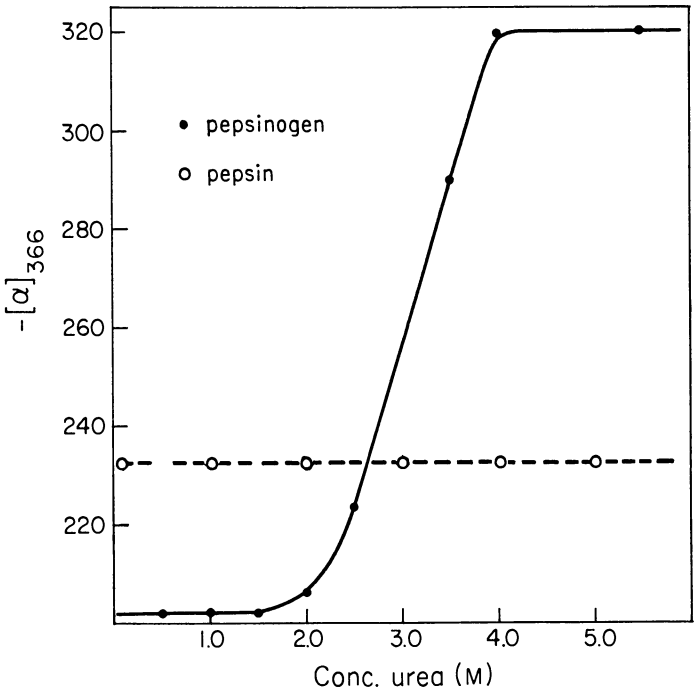

Figure 2. Dependence of specific optical rotation on urea concentration
——— Pepsinogen
------ Pepsin

the same narrow temperature range of 45° to 53°C. However, on raising the temperature from 60° to 75°C., λ_c increases to 226 mμ. This increase of 10 to 14 mμ is of exactly the same order of magnitude as has been observed with pepsin (*18*). Therefore, we feel that the changes of the optical rotatory properties observed during the first step of the transition reflect a conformational pattern reminiscent of a helix-coil transition—or, let me rather say, it is a transition from a "bonded" to an "unbonded" state. It is the polypeptide chain segment that is released during the activation of the zymogen to the enzyme which is responsible for establishing the struc-

Publication Date: January 1, 1967 | doi: 10.1021/ba-1967-0063.ch019

tural pattern in pepsinogen not present in pepsin. The second step, however, represents a conformational change in the pepsin moiety.

In view of the fact that the number of basic amino acid residues in pepsinogen exceeds that present in pepsin, and these residues may function as conformational determinants, the dependence of the specific optical rotation, $[\alpha]_{366}$, on the pH of the solution had to be considered. If the pH of the solution is altered from 6.5 to 11.5, the levorotation increases markedly in the pH range of 9.2 to 10.8 with the mid-point at pH 10.0. This value approximates the apparent pK of the ϵ-amino group of the lysyl residues if present in peptide linkage.

Recently, in collaboration with S. Beychok of Columbia University, an investigation of the optical properties of pepsin and pepsinogen in the far ultraviolet was initiated, using circular dichroism and optical rotatory dispersion. With both proteins a negative trough of the Cotton effect at 227 mμ was observed, which, in the case of pepsinogen but not with pepsin, is abolished in the presence of urea (Figure 4). As first shown by Pollock (*14*) and also reported by Blout *et al.* (*6*), on heating of the protein solutions or on altering of the pH, the minimum of the trough is shifted from 227 to 232 mμ and both the residue rotation and the molecular ellipticity become less negative. A notable observation, however, is the occurrence of small Cotton effects in the wave length range of 260 to 290 mμ. In Figure 4, these Cotton effects are set upon rather large and steeply changing back-

Publication Date: January 1, 1967 | doi: 10.1021/ba-1967-0063.ch019

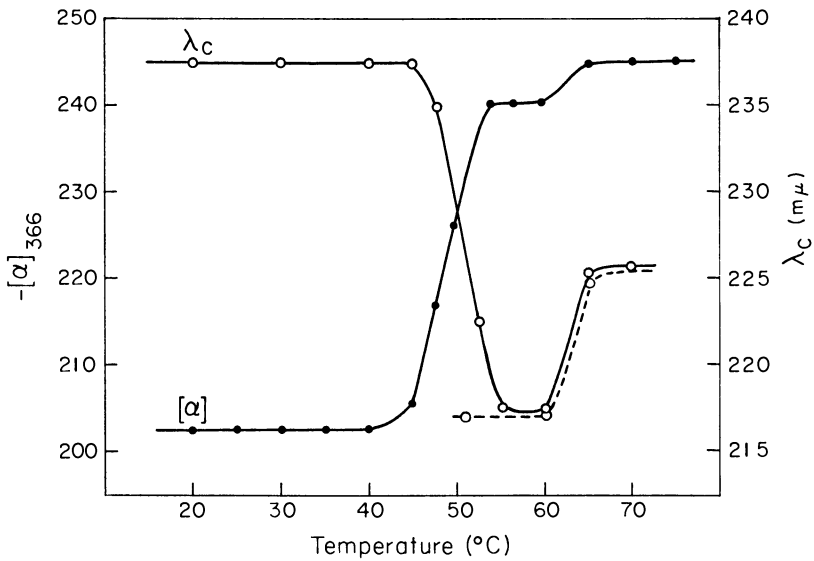

Figure 3. Dependence of specific optical rotation and rotatory dispersion constant on temperature

_____ Pepsinogen: In Na phosphate–NaCl, pH 7.7, Γ/2 = 0.15
------ Pepsin: In 0.1N Na acetate, pH 4.6

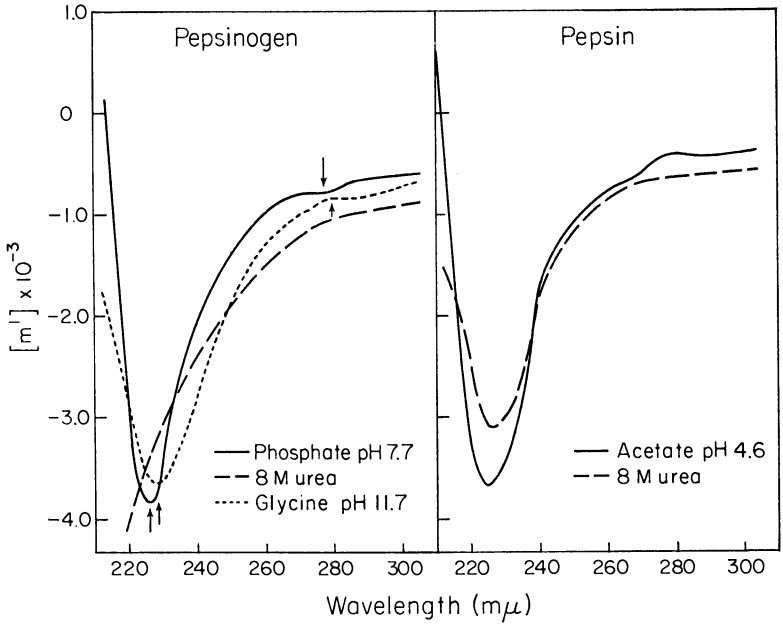

Figure 4. Dependence of optical rotatory dispersion of pepsinogen and pepsin in far-ultraviolet on pH and urea concentration

grounds. Thus it is difficult to specify exactly their location and signs from the optical rotatory dispersion measurements alone. These points are therefore more clearly illustrated with the aid of the dichroic spectra of pepsinogen at pH values between pH 7.7 and 11.6 and of pepsin at pH 4.6 in the wave length interval of 250 to 300 mμ (Figure 5). The ellipticity bands of pepsin at pH 4.6 and of pepsinogen between pH 7.7 and 9.5, while of opposite sign, have their maxima at essentially the same wave length—i.e., 280 mμ. The magnitude of the molecular ellipticities, on a mean residue weight basis, are approximately equal (cf. Figure 5).

The second noteworthy feature of the pepsinogen circular dichroism spectra is that as the pH of the protein solution is raised above pH 9.8, the wave length band at 280 mμ passes through zero and changes sign. Above pH 10.6 a broad wave length maximum between 265 and 275 mμ is observed, distinctly different from that of pepsin and of pepsinogen at pH values below pH 9.5.

It is of course tempting to speculate as to the nature of the residues responsible for these bands which, as evidenced by the smooth dispersion curves between 250 and 300 mμ in 8.0*M* urea, are clearly conformation-dependent. Both tyrosine and tryptophan are known to have ellipticity bands between pH 1.0 and 13.0 with a maximum near 265 mμ. For tyrosine above pH 11.0, the position of the band is shifted to 295 mμ (*3*, *4*, *5*, *20*). Since we have shown that at this pH all tyrosine residues of pep-

Publication Date: January 1, 1967 | doi: 10.1021/ba-1967-0063.ch019

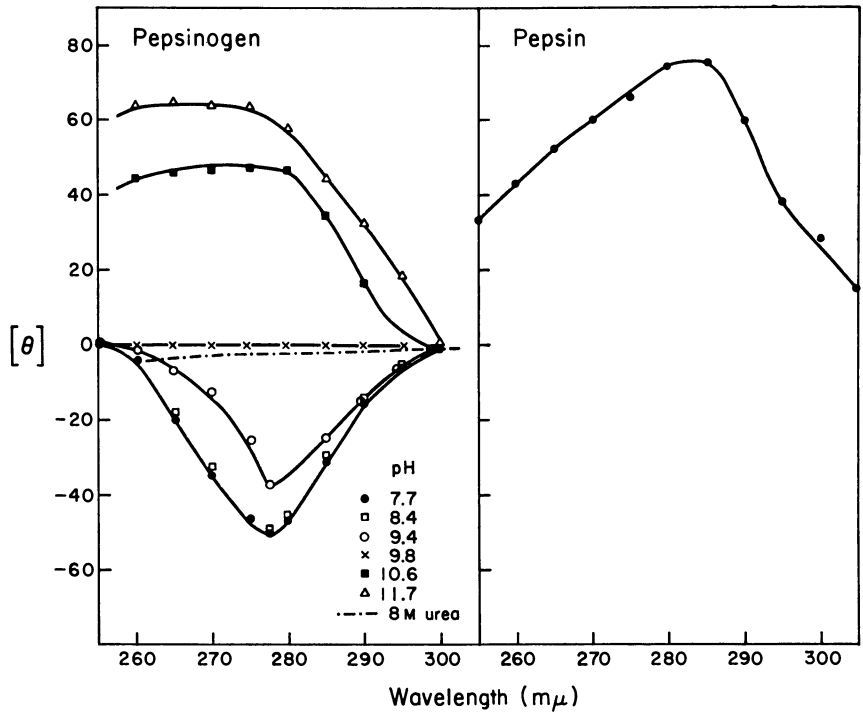

Figure 5. Circular dichroism of pepsinogen and pepsin
Buffers. Na phosphate–NaCl, pH 7.7, Γ/2 = 0.15
Na glycinate–NaCl in pH range 8.0 to 12.0
0.1N Na acetate, pH 4.6

sinogen are titratable and the absorption maximum of the protein is at 295 mμ (*16*), the location of the ellipticity maximum at 270 mμ (Figure 5), cannot be assigned to tyrosine. Tentatively, we should like to propose that in pepsinogen below pH 9.8 both types of residues are optically active. At higher pH values at which the protein is unfolded, tyrosine activity is abolished and the optical activity of the tryptophan residues is the major contributing factor. How this may be related to the conformational features in pepsin to give rise to a positive band at pH 4.6 is uncertain. It is clear, however, that in both proteins the rigidity of the molecule and the spatial arrangement of charges relative to the chromophores must play a major role.

What do these results indicate? As shown earlier, pepsinogen contains an appreciable number of basic amino acid residues all clustered within a relatively small part of the molecule, whereas the acidic groups are distributed over the pepsin moiety. At neutral pH a significant number of acidic side chains are neutralized by the proximity of the ε-amino groups. Thus these charged side chains participate in some mutual interaction,

Publication Date: January 1, 1967 | doi: 10.1021/ba-1967-0063.ch019

thereby stabilizing the protein molecule and locking it into its most stable conformation.

To sustain this view, two polypeptidyl pepsinogens were prepared by polymerization of the protein with the *N*-carboxy-α-amino acid anhydride of alanine and tyrosine, respectively (*2*). Here the ε-amino group with an apparent pK of 10.4 is replaced by an α-amino group of the amino acid attached, having the lower pK of 7.8. In another set of experiments pep-

Table II. Properties of Modified Pepsinogens

		Type of Modification		
	Pepsinogen	*Alanyl-pepsinogen*	*Tyrosyl-pepsinogen*	*Succinyl-pepsinogen*
Number of lysine residues reacted	none	3	2	10
Potential pepsin activity, %[a]	100	37	30	0
Optical rotatory dispersion constant, λ_c, mμ	236	219	224	218
Transition temperature, °C.	48.5	36.5	34.0	Not determined

[a] Potential pepsin activity of untreated pepsinogen taken as 100.

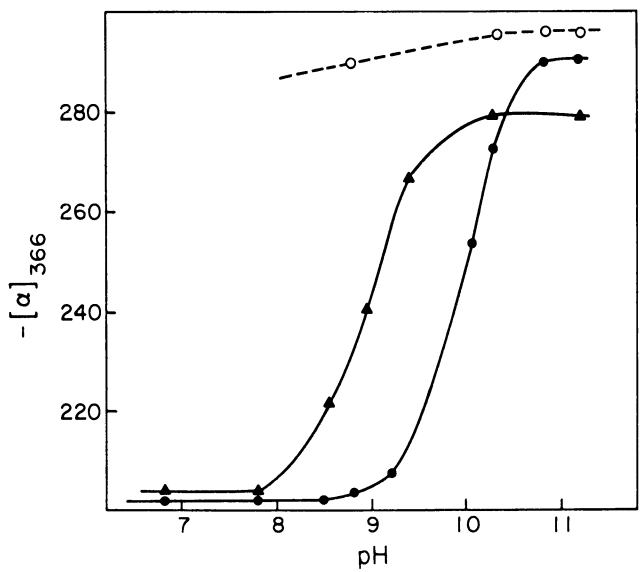

Figure 6. Dependence of specific optical rotation on pH

● *Pepsinogen*
▲ *Alanylpepsinogen*
○ *Pepsin*
Buffers. Na phosphate–NaCl, Γ/2 = 0.15, pH 6.5 to 8.0
Na glycinate–NaCl, pH 8.0 to 11.0

sinogen was made to react with succinic acid anhydride to form a succinyl derivative in which the ϵ-amino groups of the lysines are transformed into acidic side chains. As shown in Table II, the optical rotatory dispersion constant, λ_c, had decreased from 236 mμ to 219, 224, and 218 mμ for the polypeptidyl and succinyl derivatives, respectively. Furthermore, the transition temperature is lowered considerably, and as illustrated with the aid of Figure 6, the pH transition of the alanylpepsinogen has been shifted to a lower pH with a mid-point at pH 8.8. Although urea still has some effect on the optical rotatory properties of the polypeptidyl derivatives, the succinyl pepsinogen is not affected by this reagent. Therefore, these results corroborate the existence of side chain interactions as an important factor in maintaining the macromolecular conformation of pepsinogen.

To assess further the nature and the reactivity of the basic groups which contribute to the stabilization of pepsinogen, spectrophotometric

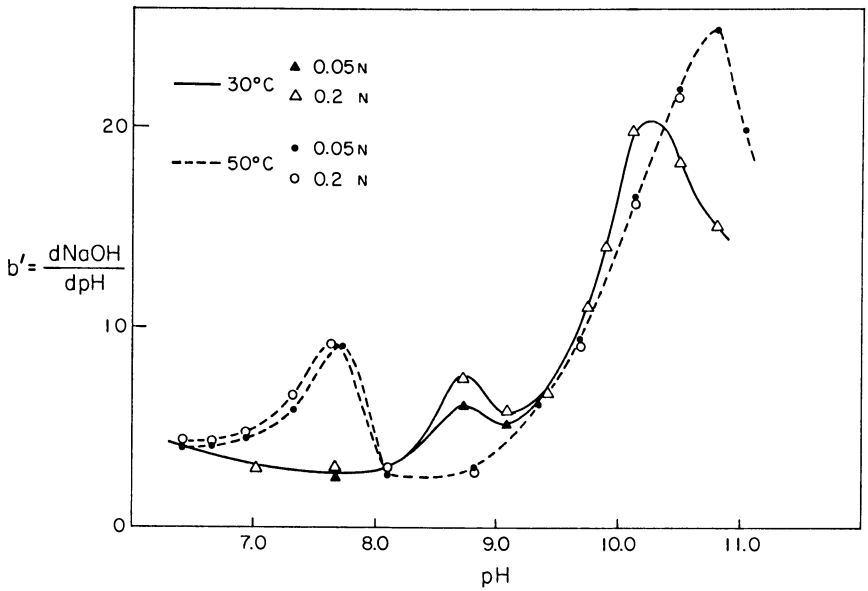

Figure 7. Dependence of potentiometric titration of pepsinogen in NaCl of various concentrations on temperature

and potentiometric titrations were performed in the pH range of 6.0 to 11.5 in 0.02 to 0.5*M* sodium chloride solutions and at various temperatures in the range of 20° to 60°C. where conformational changes occur. Above pH 11.0, where the protein is unfolded, all 17 tyrosines ionize normally with the standard heat of ionization, $\Delta H = 6.3$ kcal. per mole. In the pH range of 7.0 to 9.5, two residues will contribute to the absorbance only if the macromolecular conformation of the protein is altered by addition of 4.0*M*

Publication Date: January 1, 1967 | doi: 10.1021/ba-1967-0063.ch019

urea (*16*). These results suggest that two tyrosine residues are bonded to some other, as yet undefined, group within the molecule.

That, in the pH range of 6.0 to 9.0, not all of the histidines do titrate normally is illustrated with the aid of Figure 7, in which, instead of the conventional titration curve, the derivative $b' = d\text{NaOH}/d\text{pH}$ is plotted against pH. On assigning the pH range of 7.0 to 9.0 to histidine and that of pH 9.5 to 11.0 to lysine and tyrosine, respectively, and assuming that the pH of the maximum at which such a peak occurs corresponds to the pK of a given group, it becomes evident that at 30°C. the apparent pK of the histidines is shifted to a more alkaline pH—i.e., to pH 8.7. Thus the close vicinity of other charged groups—e.g., acidic groups—influences the ionization of the histidines, hence also their pK. Furthermore, as indicated in Figure 7, the lower peak in the pH range of 8.0 to 9.0 corresponds to the titration of the protein in 0.05*M* sodium chloride, whereas the higher one is a titration in 0.2*M*. Since the number of titratable residues can be derived from the height of the peak, it becomes apparent that more residues become accessible to titration if a conformational change is induced by an increase of the ionic strength of the medium. On raising the temperature to 45° and 50°C. where, as already shown with the optical rotation measurements, the conformation of pepsinogen changes, the histidine residues will become unmasked, and their pK normalized. From a comparison of the titration at 30° and 45°C., the standard heat of ionization, ΔH, of the histidines was calculated and a value appreciably higher than that for an unmasked imidazole group was obtained.

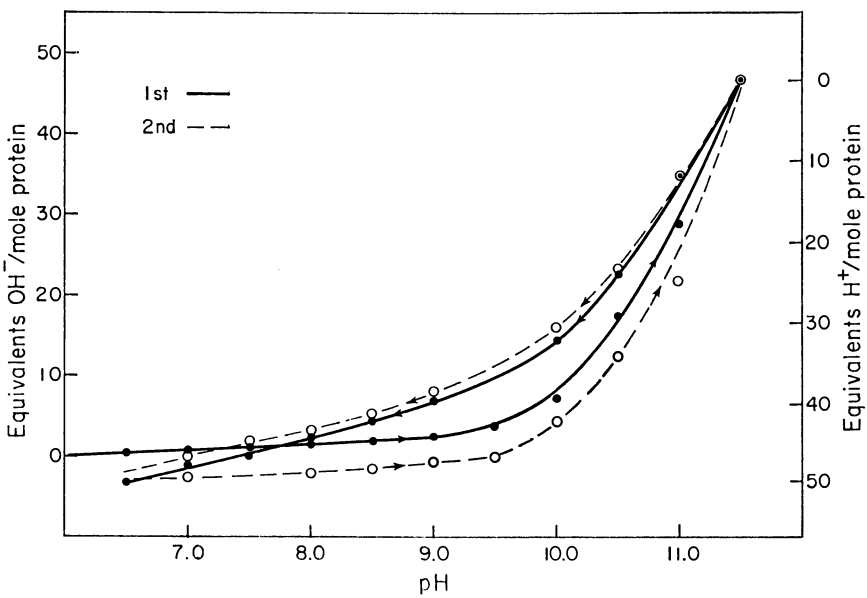

Figure 8. Forward and back titration of pepsinogen in 0.1N NaCl at 30°C.

In view of the anomalous behavior of these amino acid residues, the question arises whether these titrations are reversible. Figure 8 shows that reversibility could not be demonstrated on back titration from pH 11.5 with acid. The lower solid curve represents the forward titration, the upper one is the back titration, whereas the dashed curves are those of the second forward and back titration. It is clear that there is an increase in the number of titratable groups on back titration and the apparent pK of the imidazole residues has now been shifted to a lower value—e.g., to pH 6.9. Thus the irreversibility of these titrations can be taken as a reflection that an irreversible configurational change occurs on exposure of the protein to alkaline pH.

Turning now to a consideration of the activation of pepsinogen to pepsin and attempts to correlate the biological activity with the conformational characteristics, one sees immediately that only a rough correlation

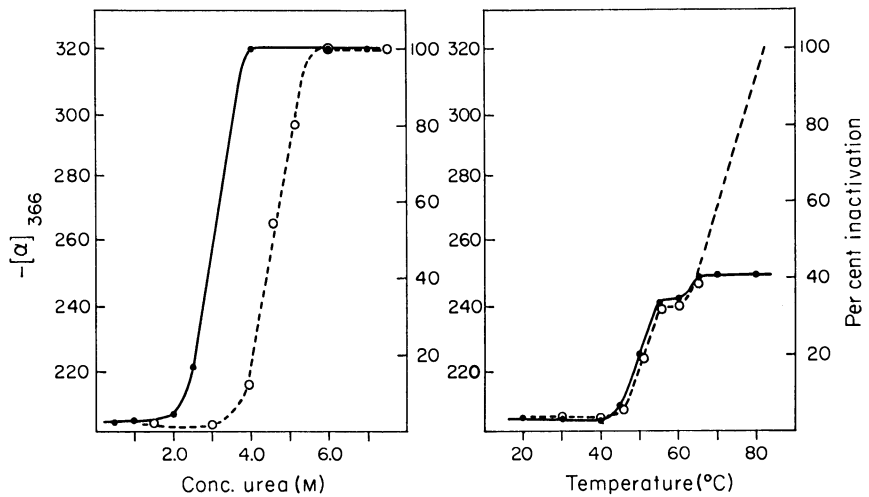

Figure 9. Dependence of specific optical rotation (——) and potential pepsin activity (- - - -) of pepsinogen on urea concentration and temperature

exists between the conformational changes observed and the susceptibility of the zymogen to activation. (Potential pepsin activity of pepsinogen refers to proteolysis of hemoglobin at pH 2.0 after activation with 0.1*N* hydrochloric acid at 37°C. for 10 minutes.) In some cases—i.e., in the heating experiments in the temperature range of 45° to 62°C. or on changing the pH of a pepsinogen solution from 7.0 to 12.0—the decrease of the potential pepsin activity and the configurational changes parallel each other closely. This is not the case in the urea experiments, where the onset of the conformational change precedes the loss of activity (Figure 9).

Similarly, the degree of reversal differs. If a pepsinogen solution maintained at 60° to 65°C. for 10 to 20 minutes is cooled to 25°C., the

Publication Date: January 1, 1967 | doi: 10.1021/ba-1967-0063.ch019

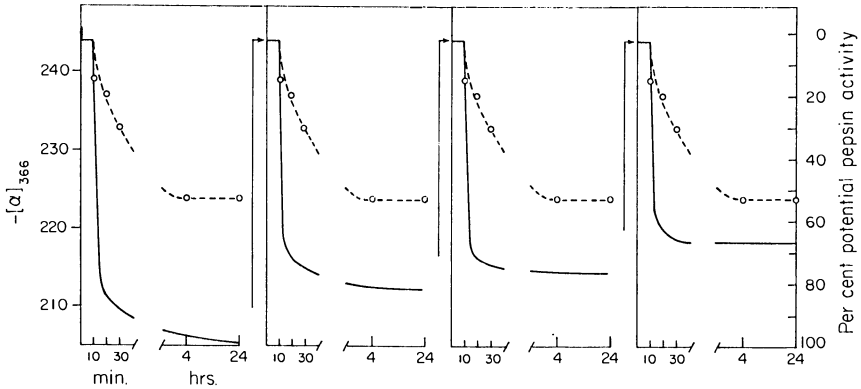

Figure 10. Reversal of specific optical rotation (- - - -) and potential pepsin activity (——) after repeated heating to 60°C. for 15 minutes, followed by rapid cooling to 25°C.

levorotation decreases slowly but never returns to its original value. However, the potential pepsin activity has been restored completely.

Figure 10 shows that if the cycle of heating and cooling is repeated several times, the levorotation on cooling always returns to the constant value—i.e., $[\alpha]_{366} = -220°$. However, the potential pepsin activity decreases progressively and after five times of heating and cooling is only 60% of its original value. Thus it appears that after each unfolding the protein molecule resumes a somewhat different macromolecular conformation. The molecule, however, has been refolded sufficiently to restore the active site and to permit activation of the zymogen to the enzyme. From this one must infer that although a "spectrum of configurations" is available to pepsinogen, a certain rigidity of the molecule is essential to ensure stability of the zymogen in the neutral pH range where pepsin is rapidly inactivated.

As already foreshadowed by the potentiometric titration and the hysteresis phenomenon observed on back-titration, the effect of pH and time on pepsinogen is more drastic. Inactivation occurs rapidly and is irreversible (Figure 11). All in all, one observes a process of aging. The protein molecule grows old rapidly and like all human beings, it loses its memory.

We may now ask, what is the structure which has emerged with progressively increasing clarity from these experiments? Both pepsinogen and pepsin are folded in a complex and unsymmetrical form, and their conformation is extremely compact. But what forces are responsible for maintaining the integrity of the whole structure? In pepsin the major contribution comes from the van der Waals forces between nonpolar residues which make up the bulk—i.e., 70%—of the protein. In pepsinogen there are a number of charge interactions between polar residues on the surface of the molecule. However, that does not exclude the fact that the peptide chain

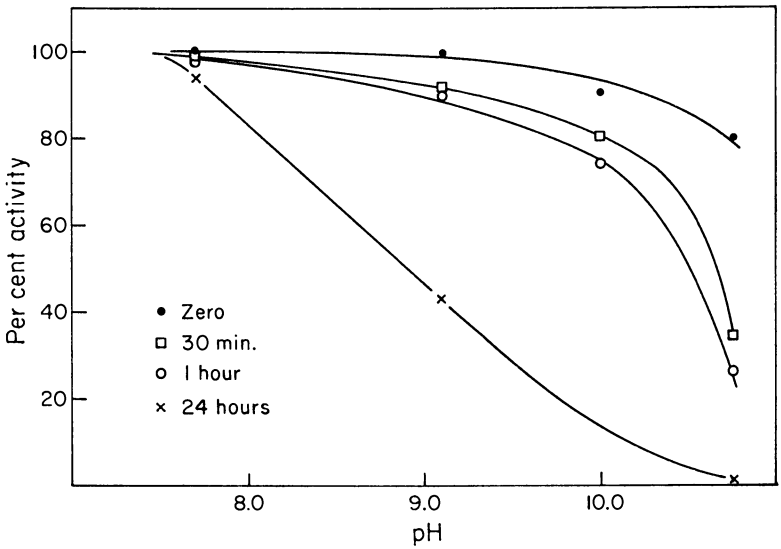

Figure 11. Dependence of potential pepsin activity of pepsinogen on pH and time

pH of each solution adjusted to 7.0 before activation at pH 2.0

segment, which is removed on activation of the zymogen, has a structure—for instance an α-helix—which is essentially different from, and independent of, the remainder of the pepsinogen molecule, thus directing on over-all structural pattern in the zymogen that is altered on activation to pepsin. The changes of the optical rotatory properties observed on heating and in urea resemble those of a helix-coil transition. However, the 40 residues at the *N*-terminal end of the polypeptide chain would at best represent ten helical turns; such a short helical segment should not yield as sharp transitions as those which we have observed. Even if the entire molecule had entered through some cooperative effects, the number of helical turns—i.e., $n = 100$—still would not explain the sharpness of the transition (*12*, *22*). However, when a pattern of a few crosslinkages is introduced by side chain interaction of electrostatic nature, it would contribute considerably toward strengthening the configuration as a whole. Thus the change from one conformation to another may be sharp and resemble a phase transition. Furthermore, such a structural pattern would also explain the changes of the optical rotatory properties observed if the pH of the solution is altered from pH 8.0 to 11.0. Therefore, we suggest that side chain interactions between the positively charged ϵ-amino groups of the lysines and the negatively charged carboxyls of the dicarboxylic amino acids are the essential features in stabilizing the conformation of pepsinogen and may be superimposed on a β-structure, prevalent in pepsin. This type of macromolecular conformation has hitherto not been described for proteins.

Publication Date: January 1, 1967 | doi: 10.1021/ba-1967-0063.ch019

Acknowledgment

The work carried out in our laboratory on the macromolecular conformation of pepsin and pepsinogen and its relation to the biological function would hardly have been possible without the active contribution of some of my collaborators. I acknowledge the help of S. Beychok in the dichroism experiments and my sincere thanks go to William F. Harrington and Aharon Katchalsky for many helpful discussions which made a vital contribution to this investigation. Most of all, I like to remember the friendship of the late K. Linderstrøm-Lang.

Literature Cited

(1) Arnon, R., Perlmann, G. E., *J. Biol. Chem.* **238**, 563 (1963).
(2) Becker, R. R., Stahmann, M. A., *J. Biol. Chem.* **204**, 745 (1956).
(3) Beychock, S., *Proc. Natl. Acad. Sci. U.S.* **53**, 999 (1965).
(4) Beychock, S., *Science*, in press.
(5) Beychock, S., Fasman, G. D., *Biochemistry* **3**, 1675 (1964).
(6) Blout, E. R., Pollock, E. J., Parrish, J. R., "Abstracts of Papers," 150th Meeting, ACS, September 1965, 23C.
(7) Blumenfeld, O. O., Perlmann, G. E., *J. Gen. Physiol.* **42**, 553 (1959).
(8) *Ibid.*, p. 563.
(9) Fruton, J. S., Bergmann, M., *J. Biol. Chem.* **127**, 627 (1939).
(10) Harington, C. R., Pitt-Rivers, R. V., *Biochem. J.* **38**, 417 (1944).
(11) Herriott, R. M., *J. Gen. Physiol.* **45**, 57 (1962).
(12) Lifson, S., Roig, A., *J. Chem. Phys.* **34**, 1963 (1961).
(13) Lokshina, L. A., Orekhovich, V. N., *Biokhimiya* **22**, 699 (1957).
(14) Northrop, J. H., Herriott, R. M., "Crystalline Enzymes," 2nd ed., pp. 28, 77, Columbia University Press, New York, 1948.
(15) Perlmann, G. E., Fourth International Congress on Biochemistry, Vol. VIII, p. 32, 1959.
(16) Perlmann, G. E., *J. Biol. Chem.* **239**, 3762 (1964).
(17) Perlmann, G. E., *J. Mol. Biol.* **6**, 452 (1963).
(18) Perlmann, G. E., *Proc. Natl. Acad. Sci. U.S.* **42**, 596 (1959).
(19) Sanger, F., Tuppy, H., *Biochem. J.* **49**, 481 (1951).
(20) Velluz, L., Legrand, M., *Angew. Chem.* (Intern. Ed.) **4**, 838 (1965).
(21) Van Vunakis, H., Herriott, R. M., *Biochim. Biophys. Acta* **23**, 600 (1957).
(22) Zimm, B. H., Bragg, J. K., *J. Chem. Phys.* **31**, 526 (1959).

RECEIVED March 1, 1966. Garvan Award Lecture. Work supported in part by the U. S. Public Health Service, Grant AM-02449, and by the National Science Foundation, Grant GB-2419.

20

Order and Structure in Concentrated Polymer Solutions and Gels

JAN HERMANS, JR.

Department of Biochemistry, University of North Carolina, Chapel Hill, N. C.

Publication Date: January 1, 1967 | doi: 10.1021/ba-1967-0063.ch020

Viscometric data demonstrate that concentrated solutions of poly-γ-benzyl-L-glutamate are ordered. The concentration limit above which ordering occurs is that predicted by Flory's theory. At high concentrations the elastic modulus of carboxy methylcellulose solutions varies as the square of the concentration. Further, G = 0 below the gel point. These results can be fitted with theoretical curves derived by assuming that the number of interparticle links per molecule is proportional to the concentration, and the network thus formed follows Flory's theory of gelation and is deformed as a rubber. Flow and elastic measurements and phase separation data on suspensions of cellulose microcrystals demonstrate that these particles have a strong tendency to side-by-side aggregation. A model is constructed in which this behavior gives rise to linear aggregates with few cross-links.

Several studies were done during the past few years at American Viscose Research and Development Co., Marcus Hook, Pa., to investigate the interactions between macromolecules in concentrated solutions and in gels. These were studied by measuring their mechanical properties—i.e., flow behavior and elasticity.

The results of experiments with different colloids demonstrate some of the ways in which macromolecules of various sizes, shapes, and surface properties may interact to form, in some cases, ordered solutions similar to liquid crystals and, in other cases, three-dimensional networks with the properties of a solid and how the order or the structure present determines the mechanical properties.

Order in Concentrated Polypeptide Solutions

The possibility of the occurrence of phase separation or ordering in solutions of rigid rodlike particles has been investigated theoretically by Onsager (*17*) and Flory (*15*). Flory showed that concentrated solutions of

In Ordered Fluids and Liquid Crystals; Porter, R., el al.;
Advances in Chemistry; American Chemical Society: Washington, DC, 1967.

rodlike particles should show phase separation even in the absence of interactions between rods. This result follows from an elegant application of the lattice model for polymer solutions. If the volume fraction, φ, of the rods in the solution is high enough, an ordered phase, with the molecules predominantly in parallel orientation, has a higher entropy than an isotropic solution of the same concentration, in which the molecules are randomly oriented. As a result, phase separation into a disordered solution of volume fraction φ^* and an ordered solution of volume fraction $\varphi^{*\prime}$ occurs when the over-all volume fraction is between φ^* and $\varphi^{*\prime}$. At higher volume fractions the solutions are again homogeneous but ordered. Values of φ^* and $\varphi^{*\prime}$ for solutions of noninteracting rods of axial ratio p are given in Table I. Furthermore, Flory has shown that φ^* may be approximated by the following closed expression for large values of p:

$$\varphi^* \backsim (8/p)(1 - 2/p) \tag{1}$$

Independently, Robinson and co-workers (*19*) showed that solutions of poly(benzyl glutamate) in organic solvents are birefringent at high concentrations and that at lower concentrations phase separation occurs. Flory later pointed out that the values of φ^* and $\varphi^{*\prime}$ obtained by Robinson *et al.* are in reasonable agreement with those of Table I.

Table I. Calculated Volume Fractions of Disordered and Ordered Phases in Equilibrium with Each Other, as a Function of Axial Ratio [Athermal Solutions, from Flory (*6*)]

Axial Ratio	φ^*	$\varphi^{*\prime}$
6.7	1.000	1.000
8	0.856	0.936
10	0.706	0.848
20	0.3790	0.5405
30	0.2599	0.3883
50	0.1597	0.2458
100	0.0806	0.1248
200	0.0404	0.0630

In a viscometric study of poly (benzyl glutamate) solutions in *m*-cresol we have been able to demonstrate that great changes in the flow properties are the result of the ordering of the molecules (*9*). The viscosity of the solutions depends, of course, on the shear stress since the individual rods are oriented by the shearing motion. However, in the range of shear stresses from 20 to 100 dynes per sq. cm., the viscosity of all solutions does not vary, and it must be concluded that this shear stress is too low to orient the molecules. Values of the viscosity, η, at low shear stress are shown in Figure 1 for solutions of three samples of different molecular weight. At low concentrations η increases rapidly with concentration, but the slope of the curves changes discontinuously to a negative value at concentrations

Publication Date: January 1, 1967 | doi: 10.1021/ba-1967-0063.ch020

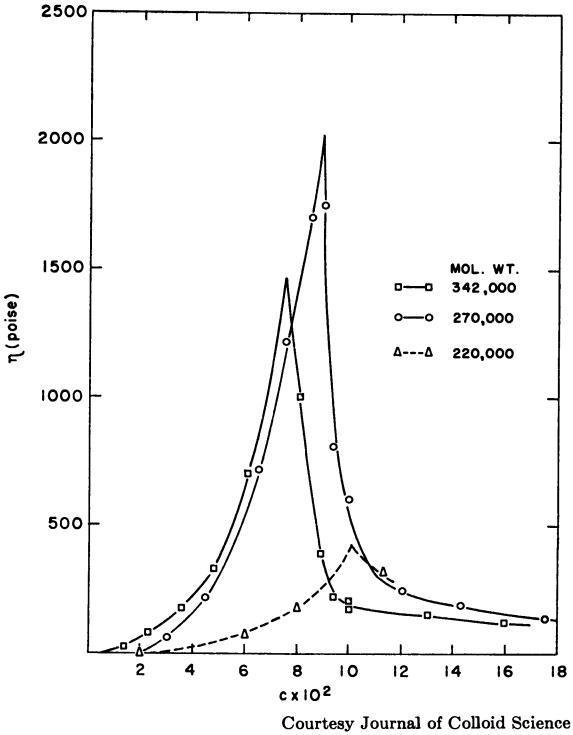

Courtesy Journal of Colloid Science

Figure 1. Viscosity at low shear stress as a function of concentration for solutions of three samples of poly-γ-benzyl-L-glutamate in m-cresol (9)

varying from 8–10%. At these concentrations phase separation takes place, and it is apparent that the ordered phase of volume fraction $\varphi^{*\prime}$ has a much lower viscosity than the random phase of volume fraction φ^* because the shear stress applied is more than sufficient to orient the ordered phase parallel to the flow lines (Figure 2) although the individual molecules are able to diffuse to random orientations.

Values of φ^* may be obtained from the data of Figure 1. These have been plotted as a function of the axial ratio in Figure 3, together with a curve according to Flory's theoretical results. The agreement is quite good.

Finally, a close analysis of the data shows that the molecules in the ordered solutions still possess considerable freedom of orientation, as predicted by theory (*15*). This follows in the first place from the complete data of viscosity as a function of shear stress and concentration (*9*), which show a large decrease of viscosity with the shear stress in the ordered solutions, in the same range where the viscosity of the random solutions decreases with the shear stress because of the ordering of the molecules paral-

Publication Date: January 1, 1967 | doi: 10.1021/ba-1967-0063.ch020

lel to the stream lines (Figure 2, *E* and *F*). In the second place, one has to explain the decrease of η with c for the fully ordered solutions ($c > c^{*\prime}$) by assuming that the disorder in these solutions decreases with increasing concentration; this effect tends to lower the viscosity apparently so strongly that the normal increase of the viscosity with the concentration is more than overcome.

Network Formation in Carboxymethylcellulose Solutions

In solutions of normally encountered randomly coiled macromolecules the formation of spontaneously birefringent phases is not expected. (Phase separation does occur when the interaction between solute molecules is strong.) Here, we have investigated solutions of the polyelectrolyte sodium carboxymethylcellulose in water, which are rubberlike at high concentrations (*12*). (Materials that form such solutions are commonly called gums.)

To explain the behavior of these rubbery solutions, it is assumed that the molecules are linked by noncovalent cross-links to a network which extends throughout the solution. Such a solution has the properties of a

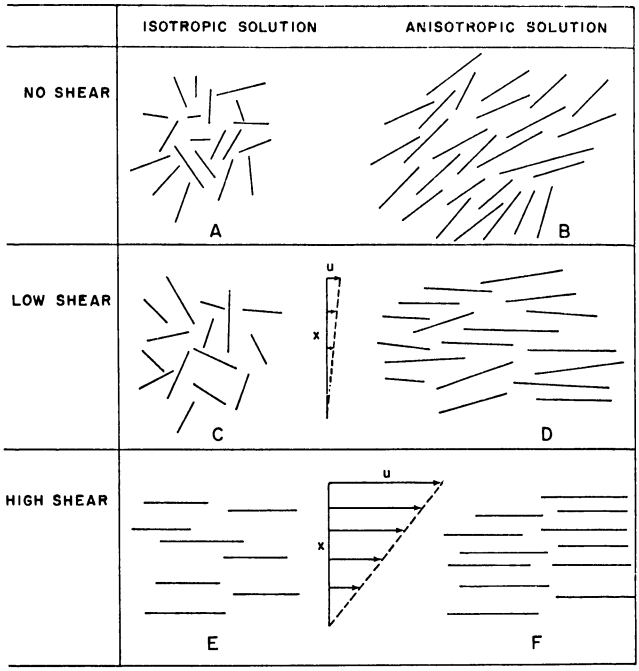

Courtesy Journal of Colloid Science

Figure 2. Schematic representation of solutions of poly(benzyl glutamate) at various values of shear rate, $D = du/dx$ (9)

solid although the shear stress necessary to induce a permanent deformation (the yield stress) is not high since the cross-links break (and reform) rather easily. Furthermore, because of the presence of so many interparticle links, the viscosity of these solutions is high (*3*, *7*, *13*, *20*, *21*). Unhappily, the flow behavior of this satisfactory model has not yet been investigated theoretically. However, it turned out that the elastic properties of these gelled solutions could be predicted easily after the introduction of a few minor assumptions. We here outline this theory and compare it with the experimental results obtained.

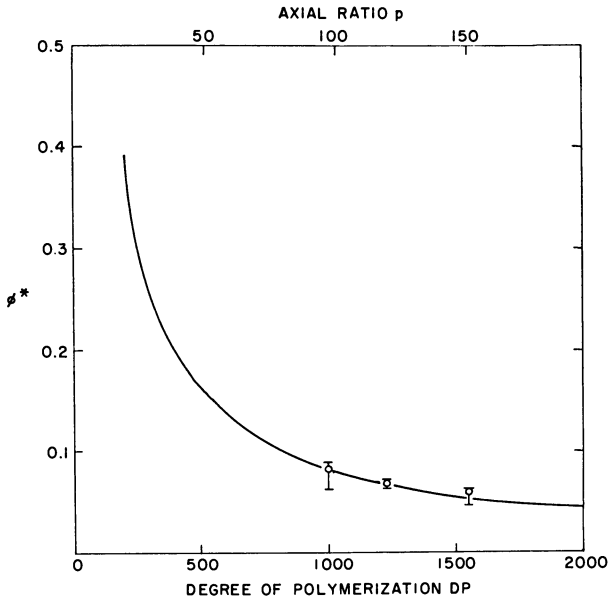

Courtesy Journal of Colloid Science

Figure 3. Volume fraction of φ^* at which phase separation first occurs

Obtained from data of Figure 1 (9). Curve according to theory (6)

In deriving the theory, three separate assumptions must be made. It must be asked: how many links between molecules are present in a solution of a given concentration, what will be the structure of the network formed, and what will be the elastic modulus of such a network? Three simple assumptions were made in this case.

1. Number of Links. The solution is assumed to contain per unit of volume N_0 identical molecules each carrying f identical groups, each of which is capable of reacting with one group on another molecule. A fraction, α, of these groups has reacted to form intermolecular links, and the reacted groups are supposed to be randomly distributed over the $N_0 f$ avail-

Publication Date: January 1, 1967 | doi: 10.1021/ba-1967-0063.ch020

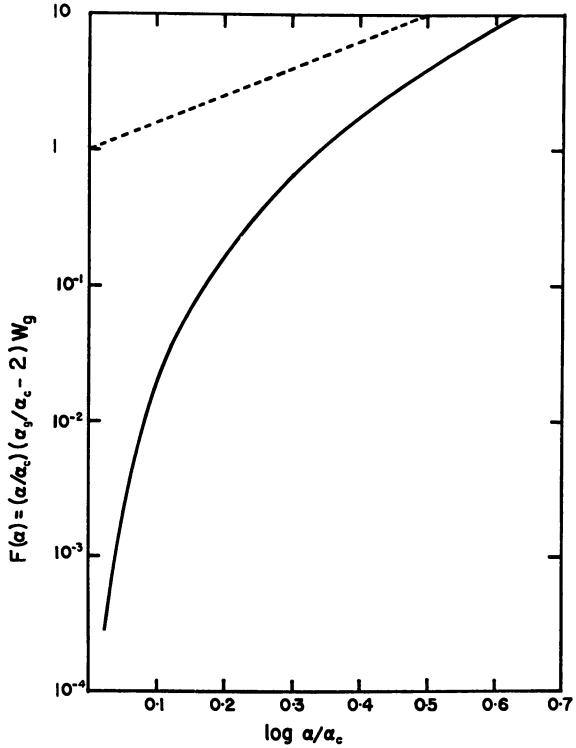

Courtesy Journal of Polymer Science

Figure 4. Graph of log $F(\alpha)$ as a function of log α/α_c, equivalent to a curve of log G as a function of log c for a monodisperse polymer

Log $F(\alpha)$ goes to $-\infty$ asymptotically for $\alpha/\alpha_c = 1$ (gel point). Dashed line with slope of 2 is asymptotic to curve at high α/α_c (high concentration) (12)

able groups. If these groups are assumed to be in a dimerization equilibrium, α will be proportional to the concentration, c, when c is small (as is usually the case in these gels).

$$\alpha = K' f N_o = Kc \tag{2}$$

2. Structure of Network. A theory of the structure of networks formed in cross-linked solutions of macromolecules has been worked out by Flory (*4*; *5*, Chap. 9). Since these results are well known, we mention only a few details. No infinite network is present when

$$\alpha < \alpha_c = 1/f \tag{3}$$

so that the gel point is inversely proportional to the molecular weight,

$$c_c = 1/Kf \tag{4}$$

Publication Date: January 1, 1967 | doi: 10.1021/ba-1967-0063.ch020

The fraction of the molecules in the gel, W_g, increases with α when $\alpha > \alpha_c$. At the same time, the number of links per molecule in the network increases from the minimum number of 1/2 at α_c. The links necessary to add the molecules to the network do not contribute to the elasticity. Rather, we must obtain an expression for the remaining number of links (called cross-links) which is given by

$$N_c = (1/2)(\alpha_g - 2\,\alpha_c) f\, W_g N_o \tag{5}$$

Expressions for α_g, the α of the gel fraction, and W_g as a function of α have been derived by Flory (*4*; *5*, Chap. 9).

3. Modulus of Elasticity. It is assumed that these gels are deformed according to the theory of rubber elasticity, which tells us that the shear modulus is given (*5*, Chap. 11) by

$$G = N_c kT \tag{6}$$

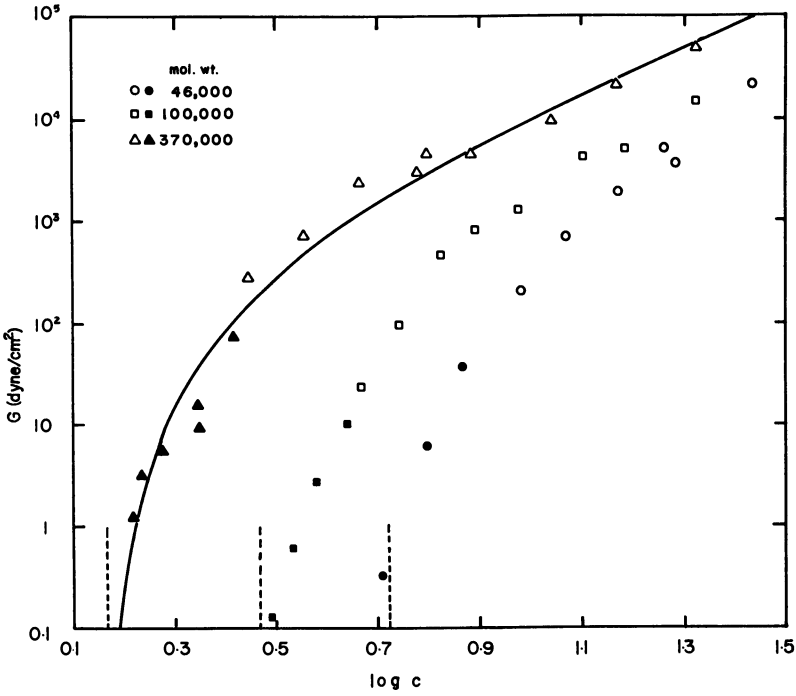

Courtesy Journal of Colloid Science

Figure 5. Values of shear modulus for three samples of carboxymethylcellulose as a function of concentration (grams per 100 ml.)
Open and filled symbols represent measurements with slightly different equipment
– – – – Gel points obtained by fitting curves of Figure 4 to these data
Best fitting curve drawn for experiments on sample of highest molecular weight (12)

Combining Equations 2, 5, and 6, we can write (*5*)

$$G = (RT/2fMK)\, F(\alpha) \tag{7}$$

where M is the molecular weight, and $F(\alpha)$ is a known function of α. Since α is proportional to c, the curve of log $F(\alpha)$ as a function of log α shown in Figure 4 is a theoretical curve of log G as a function of c, except for adjustable horizontal and vertical displacements.

Comparison with Experiment. We have measured the elasticity of three samples of carboxymethylcellulose of different molecular weight as a function of the concentration (*12*), by applying a shear stress to the gel and observing the shear. The shear reached a constant value in about 30 minutes and could be fully recovered by removing the stress at this or at considerably later times. Furthermore, the shear was found to be proportional to the stress (Figure 5). For the sample of highest molecular weight we have drawn the theoretical curve of Figure 4, which describes the data well. Further, gel points can be determined (dashed lines in Figure 5), and these change approximately with the molecular weight according to Equation 4.

The slope of the curves at high values of c becomes closely equal to 2, as is required by assumption 1 that the number of links per particle is proportional to the concentration. At high concentrations the number of links is much larger than the number of particles, and all links can be counted as cross-links. The number of cross-links and therefore the modulus will then vary as c^2. Thus our assumption 1 has been verified independently of assumption 2 regarding the structure of the network.

Phase Separation and Ordering in Suspensions of Cellulose Microcrystals

The third system investigated consisted of solutions of rigid rodlike particles capable of forming intermolecular links, so that at high enough concentrations infinite networks are present and the solutions are gels (*1*, *10*). Cellulose microcrystals have varying dimensions in the neighborhood of 0.4 micron long by 0.04 micron thick, as is evident from electron micrographs (*18*) (Figure 6). We present first the available information which suggests the way in which these particles tend to aggregate and secondly, the elastic and flow properties of the gels which are formed because of this aggregation.

Cellulose microcrystals can be suspended in dilute solution. Turbidity measurements suggest that the particles are not highly associated in the absence of added salt. In the presence of a low salt concentration, large aggregates are formed, as was shown by a study of light scattering by suspensions of ramie microcrystals (*15*). When the salt concentration is further increased, the microcrystals precipitate. Since the microcrystals

Publication Date: January 1, 1967 | doi: 10.1021/ba-1967-0063.ch020

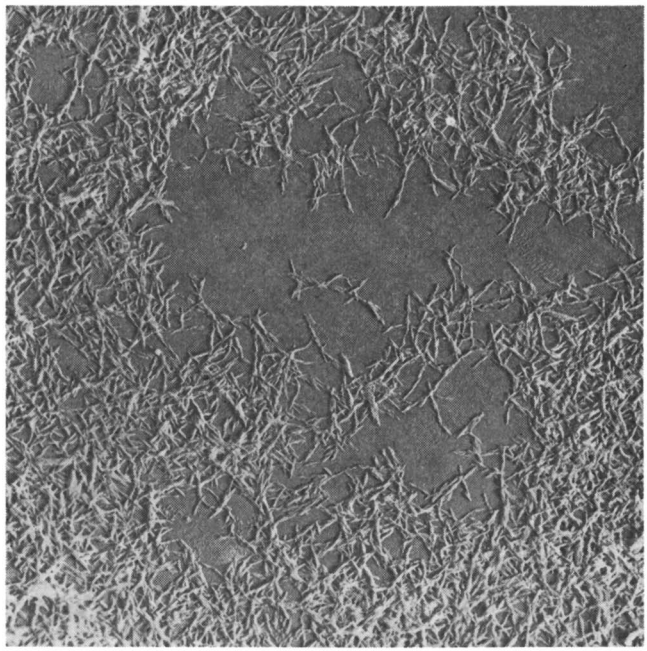

Courtesy Journal of Polymer Science

Figure 6. Electron micrograph of wood cellulose microcrystals 25,000 ×

carry a low negative charge (*2*), owing to the presence of ionized carboxyl groups, this behavior is typical of a lyophobic colloid (*21*).

E. G. Scalco and the author have studied the precipitation in detail. Some simple experiments were done, which consisted of bringing the salt concentration of microcrystal suspensions of different concentration to various values, centrifuging the solutions at approximately 2,000 *g* to separate the phases, and subsequently analyzing the volume and concentration of each of the phases. The results obtained were complex. Thus, the composition of the precipitate and the supernatant phases depends not only on the salt concentration but also on the concentration of microcrystals in the suspension or gel to which the salt was added. (The results given below represent selected data which illustrate the trends observed.) Furthermore, no fewer than three different kinds of precipitate were obtained.

To cause phase separation in a suspension or a gel of cellulose microcrystals, the salt concentration must exceed a certain value. This minimum value is shown in Figure 7 as a function of the concentration (solid curve). When this value of the salt concentration is exceeded, suspensions of 0.75% or higher separate into a more concentrated gel and a dilute suspension of concentrations approximately those expected if Figure 7 were

a phase diagram. However, in more dilute suspensions, two precipitates are noted, L_2 and L_3, which differ in cellulose concentration. Hence they settle at different rates and form layers of different opacity. Figure 8 shows the volumes of the precipitated phases as a function of NaCl molarity for a series of different initial cellulose concentrations. (The dense precipitate, L_3, is the one of smallest volume.) In Figure 7 are curves showing the trend of the variation of the concentration of phases L_2 and L_3 with the increase of the interaction between particles as the ionic strength is made larger. At high ionic strength the distinction between L_2 and L_3 disappears.

A test for birefringence of the various phases revealed that L_2 is not birefringent while L_3 is. Thus it would appear that in L_2 the rodlike par-

Publication Date: January 1, 1967 | doi: 10.1021/ba-1967-0063.ch020

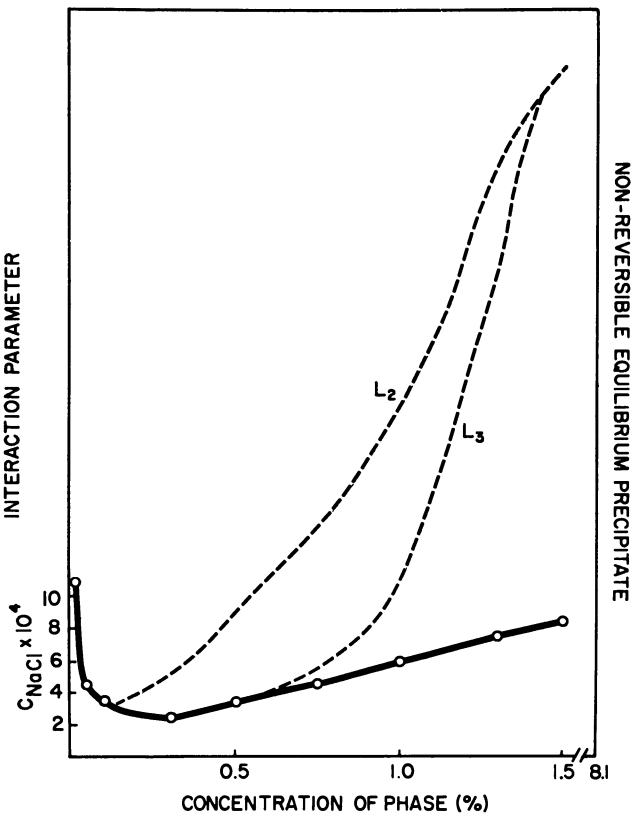

Figure 7. Minimum value of salt concentration needed to cause phase separation in suspensions of cellulose microcrystals of varying concentration

Also indicated are approximate concentrations of L_2 and L_3, obtained when salt is added to dilute suspensions. Concentration of precipitate obtainable by applying a high shear rate to a gel containing salt is indicated (8.1%)

ticles have aggregated in a random manner; in L_3 in a more nearly parallel manner. It is reasonable that the parallel arrangement produces a denser phase.

Finally, it was observed that phases L_2 and L_3 can be resuspended when the salt is removed by washing and diluting the precipitates with distilled water. However, in the presence of a high salt concentration the precipitates can be changed into yet another form which cannot be redissolved. When the gellike precipitates (L_2 or L_3) are subjected to high shear rates in a piston-type glass tissue grinder, a dense, grainy precipitate

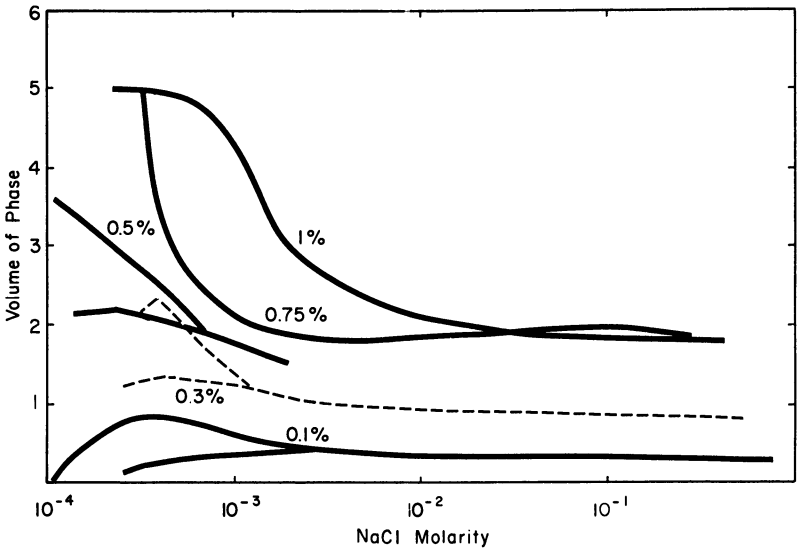

Figure 8. Volume of precipitate obtained on adding NaCl to 5 ml. of suspensions of microcrystals of different concentrations

For lowest concentrations there is a region in which the precipitate consists of two layers; lower curve is volume of lower layer (L_3), and upper curve is volume of total precipitate ($L_2 + L_3$)

is formed, which resembles cellulose powder. (Its concentration was determined to be 8.1%, indicating the continued presence of much solvent.) We believe that by the high shear stresses which are applied, the microcrystals are forced into positions where a great many additional bonds of the type responsible for the formation of the precipitates and gels can be formed. We suggest that the surfaces of the microcrystals manage to reform in part the stable cellulose crystal structure since this would also explain the tendency shown by the particles to assume parallel orientations.

Elasticity and Flow of Gels of Cellulose Microcrystals

The elasticity of a series of gels of different concentrations was investigated in an attempt to obtain information about the structure of the

Publication Date: January 1, 1967 | doi: 10.1021/ba-1967-0063.ch020

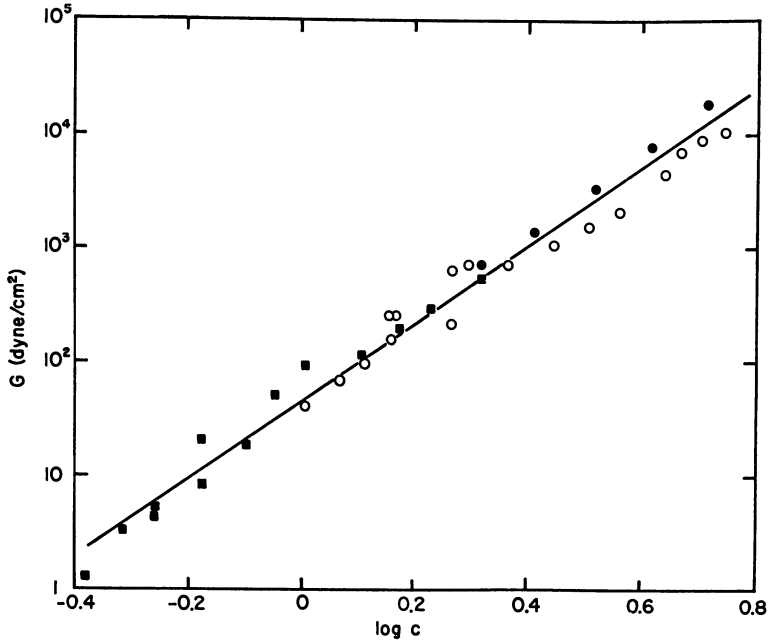

Figure 9. Values of shear modulus of gels of wood cellulose microcrystals Log-log plot. Line drawn to fit data, has slope of 3.5 (11)

particle network (*8*) (Figure 9). The data in this log-log plot can be fitted with a straight line of slope 3.5, and the existence of a gel point is not in evidence, much in contrast to what was found for carboxymethylcellulose (CMC) gels.

One must obviously ask which of the three assumptions with which the behavior of the CMC gels could be explained has to be altered. In the first place, the assumption about the elasticity of the network has to be somewhat modified since the individual microcrystals are much stiffer than the individual CMC molecules. The deformation of the former requires elastic energy while in deforming randomly coiled macromolecules the entropy changes. We have been able to show (*11*) that for a network of stiff rods,

$$G = (3 \pi E a^4/20 b) N_c \langle 1/n \rangle \quad (8)$$

where E is the elastic modulus of cellulose (3×10^{11}), a is the radius and b is the length of the segments of rod between links, N_c is the number of cross-links per unit of volume, and n is the number of rods between cross-links.

Publication Date: January 1, 1967 | doi: 10.1021/ba-1967-0063.ch020

On the other hand, when the number of links per rod is not small, the modulus should approach Ed, where d is the volume fraction of the cellulose (*14*):

$$G \backsim Ed \tag{9}$$

From the values of the moduli observed, it is evident that this limit is far from reached in the concentration range studied. Were it possible to describe the reaction linking the rods as a bimolecular equilibrium, N_c/N_0 should be proportional to c. Furthermore, $N_c/N_0 = 1/2$ at the gel point (*see above*). Since our measurements cover a 30-fold concentration range, N_c/N_o should be greater than 15 at the highest concentrations studied, and the modulus should be equal to the value given by Equation 9. It would therefore appear that the first of our three assumptions, the one regarding the variation of the number of cross-links with the concentration, must be modified.

Publication Date: January 1, 1967 | doi: 10.1021/ba-1967-0063.ch020

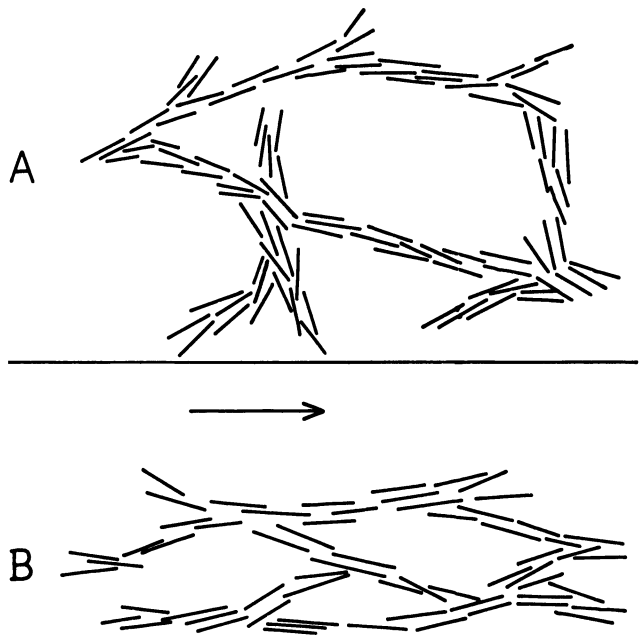

Courtesy Journa of Applied Polymer Science

Figure 10. Model for networks of cellulose microcrystals formed by almost parallel aggregation of rodlike particles

A. Gel in which aggregates are oriented at random
B. Gel in which aggregates have a nearly parallel orientation from a shearing motion applied before gel allowed to set (8)

We have been able to construct a model, partly based on the information obtained above, to explain the observed mechanical behavior. Since

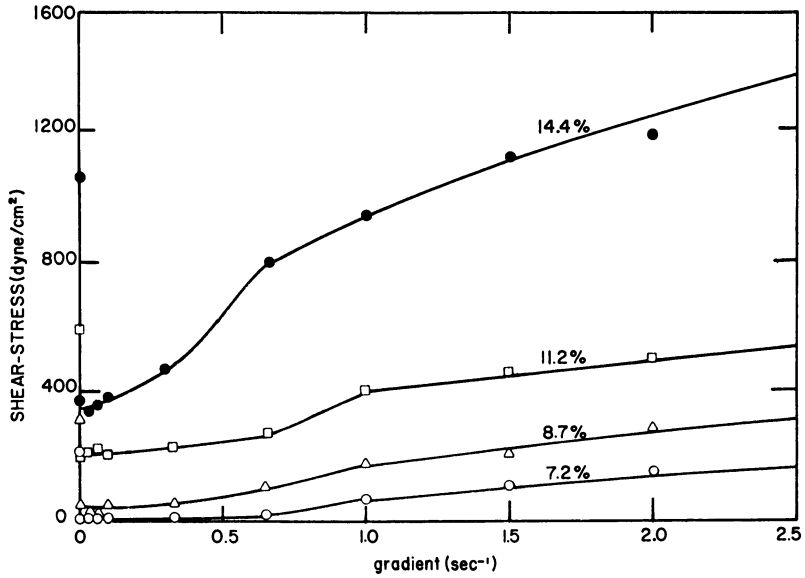

Courtesy Journal of Applied Polymer Science

Figure 11. Flow curves of gels of cotton cellulose microcrystals of different concentrations (10)

Note determination of two values of yield stress for each gel, low one after low shear rate applied, high one after gel sheared at shear rate of 80 sec.$^{-1}$, prior to measurement of yield stress

the tendency to parallel aggregation by the microcrystals is so strong, there is obviously a tendency for the formation of long strands containing many particles. For an infinite network to be formed, these strands must be cross-linked. We envision the formation of the cross-links as taking place by the branching and rejoining of different sheaflike aggregates throughout the solution (Figure 10, *A*). Because of the large size of the primary aggregates, the number of cross-links needed to form an infinite network is small and can increase a great many times before it becomes equal to the number of microcrystals. Also, almost every cross-link will be an "active" cross-link. It would be desirable to have the number of cross-links still proportional to c^2. In that case, $\langle 1/n \rangle \sim N_c/N_o$ will vary as c, and the modulus, which is proportional to both N_c and $\langle 1/n \rangle$ will vary as c^3 (cf. Equation 8). The predicted variation of G with c is close to that observed experimentally (G proportional to $c^{3.5}$).

Finally, the model shown in Figure 10 can explain an odd aspect of the flow behavior noted earlier (*8*). Figure 11 shows a series of flow curves of gels of cotton cellulose microcrystals. The peculiar feature of these data is the irregularity at a gradient (shear rate) of approximately 0.5 sec^{-1}. If

Publication Date: January 1, 1967 | doi: 10.1021/ba-1967-0063.ch020

one applies a shear rate below 0.5 sec.$^{-1}$ to the gel for some time and then increases it to a value greater than 0.5 sec.$^{-1}$, the shear stress measured increases with time to reach a steady value as shown. Conversely, after a shear rate greater than 0.5 sec.$^{-1}$ is applied, then lowered below this value, the shear stress gradually decreases to the values shown. However, if the critical value of 0.5 sec.$^{-1}$ is not passed upon going from one shear rate to another, the measured stresses instantaneously have their final value. Also, two values of the yield stress were obtained, as shown in Figure 11; the lower one, which lies at the extrapolation of the curve to zero shear rate, is found if the gel is brought to rest after application of a shear rate below 0.5 sec.$^{-1}$ while the higher one is found after application of a shear rate of 80 sec^{-1}.

Our explanation of these results is that under the influence of the shearing motion, the particles assume a parallel arrangement, which is retained when the shearing motion is stopped. [This is also suggested by the observation of birefringence in gels of microcrystals placed between microscope cover glasses (*16*).] In terms of our model, the resulting network may be depicted as shown in Figure 10, *B*. It is reasonable that more cross-links would be present and that the yield stress would consequently be higher when the rods are predominantly parallel.

Publication Date: January 1, 1967 | doi: 10.1021/ba-1967-0063.ch020

Conclusions

We felt it important to obtain data on the particle network in order to understand the flow of gels quantitatively. It is clear, however, that this is still impossible because an adequate theory going much beyond the ideas expressed by Goodeve (*7*) has not been developed. The flow properties of gels vary considerably; furthermore, some gels become temporarily liquid upon the application of shear, and others become thicker. Quantitatively explaining these various types of behavior on the basis of the particle network model does not appear easy. Nevertheless, the information obtained here should be of some aid, in that the model is now much more closely defined.

We have been able to collect considerable information about the interactions which cause the formation of infinite networks of particles in gels of cellulose microcrystals. Our findings about the manner of linking of the rods would appear to be peculiar to this material. The following argument suggests that this is perhaps not true. If colloidal particles interact weakly, they will not form a gel. However, if they interact strongly, they will precipitate. Thus, each gel-forming material must have peculiar properties, allowing it to escape either extreme. In many cases, this may mean that linear aggregation is easy, but that cross-linking of the linear aggregates is less probable.

In Ordered Fluids and Liquid Crystals; Porter, R., el al.;
Advances in Chemistry; American Chemical Society: Washington, DC, 1967.

Literature Cited

(1) Battista, O. A., Smith, P. A., *Ind Eng. Chem.* **54**, 20 (1962).
(2) Edelson, M. R., Hermans, J., *J. Polymer Sci.* **C2**, 145 (1963).
(3) Ferry, J. D., *Advan. Protein Chem.* **4**, 1 (1948).
(4) Flory, P. J., *J. Am. Chem. Soc.* **63**, 3083, 3091 (1941).
(5) Flory, P. J., "Principles of Polymer Chemistry," Cornell University Press, Ithaca, N. Y., 1953.
(6) Flory, P. J., *Proc. Roy. Soc.* (*London*) **A234**, 73 (1956).
(7) Goodeve, C. F., *Trans. Faraday Soc.* **35**, 342 (1939).
(8) Hermans, J., *J. Appl. Polymer Sci.* **9**, 1973 (1965).
(9) Hermans, J. *J. Colloid Sci.* **17**, 638 (1962).
(10) Hermans, J., *J. Polymer Sci.* **C2**, 129 (1963).
(11) *Ibid.*, **A2**, 4931 (1964).
(12) *Ibid.*, **A3**, 1859 (1965).
(13) Hermans, J. J., in "Flow Properties of Disperse Systems," p. 61, North Holland, Amsterdam, 1953.
(14) Litt, M., *J. Colloid Sci.* **16**, 297 (1961).
(15) Marchessault, R. H., Koch, M. J., Yang, J. T., *J. Colloid Sci.* **16**, 345 (1961).
(16) Marchessault, R. H., Morehead, F. F., Walters, N. M., *Nature* **184**, 632 (1959).
(17) Onsager, L., *Ann. N. Y. Acad. Sci.* **56**, 627 (1949).
(18) Ranby, B. G., *Discussions Faraday Soc.* **11**, 158 (1951).
(19) Robinson, C., Ward, J. C., Beevers, R. B., *Ibid.*, **25**, 29 (1958).
(20) Ward, A. G., Saunders, P. R., in "Rheology," F. R. Eirich, ed., Vol. II, p. 313, Academic Press, New York, 1958.
(21) Verwey, E. J. W., Overbeek, J. Th. C., "Theory of the Stability of Lyophobic Colloids," Elsevier, Amsterdam, 1948.

RECEIVED February 11, 1966.

21

Investigations of Motion in Crystalline Polymers and Related Substances

ARTHUR E. WOODWARD

Department of Chemistry, The City College of The City University of New York, New York, N. Y.

Publication Date: January 1, 1967 | doi: 10.1021/ba-1967-0063.ch021

Nuclear magnetic resonance line absorption, spin-lattice relaxation time, and dynamic mechanical methods have been used to investigate segmental motion at 1 to 10^8 c.p.s. in high polymers and related materials. Results on melt-formed specimens and their interpretation are summarized. More recent work has been done on solution-crystallized and other specially prepared samples, and past interpretations have been changed. The mechanisms favored to explain existing relaxation processes in order of increasing temperature include side-chain motion, motion in crystal defects, segmental movement in chains connecting lamellae and in chain folds, torsional oscillations in ordered regions, and motion of larger units comprising more than one chain such as lamellae.

As a result of numerous investigations carried out during the past decade, it is recognized that various physical properties of highly crystalline polymeric materials exhibit marked changes with temperature, some being detected many hundreds of degrees below the melting point. These alterations in properties can occur in more than one temperature region, the number, location on the temperature scale, and magnitude depending on the polymer composition and other factors. These phenomena are generally frequency-dependent, a given mechanism being found at higher temperatures, the higher the measuring frequency. Although the majority of studies have been made on melt-formed samples, work since 1964 has been concerned with samples of solution-crystallized and other specially prepared crystalline specimens. This has led to a number of revisions in and additions to earlier mechanisms suggested to explain these properties changes. The main purpose of this paper is to discuss these newer data and the alterations they have brought about in our understanding of these phenomena. Work up to 1964 is reviewed in a recent article (*90*).

In Ordered Fluids and Liquid Crystals; Porter, R., el al.;
Advances in Chemistry; American Chemical Society: Washington, DC, 1967.

Experimental methods frequently used to investigate relaxation phenomena include various dynamic mechanical techniques from which a storage modulus (stress and strain in phase) and a loss modulus (stress and strain 90° out of phase) are obtained for a sample vibrating sinusoidally at low amplitude (*72*), and steady-state and transient nuclear magnetic resonance (NMR) methods, the width (or second moment) of the NMR absorption being obtained from the former and the spin-lattice relaxation time from the latter (*49*). The frequency of such measurements, usually dictated by the particular method and apparatus, generally falls in the 0.1- to 10^8-c.p.s. region. Concerning the NMR experiments it is known from theory that the effects of motion of the magnetic nuclei, at a frequency of or greater than that corresponding to the absorption width, narrows the absorption; motion of the nuclei at a frequency near the resonance frequency leads to a shortening of the spin-lattice relaxation time (*49*). With respect to the mechanical measurements, the effect of a relaxation process on various combinations of elastic (springs) and viscous (dashpots) elements is to cause a peak in the loss modulus and a dispersion in the storage modulus, the latter decreasing with increasing temperature at constant frequency or decreasing frequency at constant temperature (*90*). The appearance of mechanical loss peaks and associated storage modulus changes has generally been attributed to the onset of motion of certain specific collections of units in the polymer chain at a frequency near that of the measurement (*72*, *90*). A more recent interpretation has been given (*1*, *2*) in terms of "the loosening of various types of intermolecular cohesive (secondary) bonding in the solid state" with changes in the state of motion being regarded as an associated effect (*1*). The validity of such an interpretation to explain any one process found for a given polymer has yet to be tested. For a polymer exhibiting multiple processes it is doubtful that enough different intermolecular associations exist to account for all of the property changes.

Publication Date: January 1, 1967 | doi: 10.1021/ba-1967-0063.ch021

Studies Using Melt-Formed Samples

In all studies to date in the region of the glass-to-rubber transformation for noncrystallizable polymers a mechanical loss maximum with an associated decrease in storage modulus (with increasing temperature), a narrowing of the NMR line width and second moment (with increasing temperature), and a T_1 minimum have been found. The NMR line ultimately narrows to values typical of viscous liquids, indicative of considerable segmental motion. Samples of crystallizable polymers formed from the melt at ordinary pressures in both quenched and annealed conditions show a similar process, but the corresponding changes in properties are less the greater the extent of order. The NMR line shape for a crystalline polymer above the temperature at which some main chain motion has commenced but below the melting region is usually composed of a broad component

indicative of rigid units and a narrow component owing to a mobile fraction while only a narrow component is found for a polymer of low crystalline order. This is apparent for the two polymers, poly(ethylene oxide) (PEO) and poly(*dl*-propylene oxide) (PdlPO), for which NMR data taken at 40 megacycles are given in Figure 1. The PEO specimen used for these measurements was Carbowax 20 M flakes; some characteristics of this highly crystalline material are (*81*) $\overline{Mn} = 10^4$; $\overline{Mv} = 10^5$. The PdlPO specimen supplied by the Dow Chemical Co. on the other hand has low crystallinity (density 1.048 grams per cc.) (*38*).

The temperature position for this process for a number of crystalline polymers is given in Table I. The apparent activation energies given were obtained from the slope of a plot of the log of the measuring frequency *vs.* the reciprocal of the temperature at which the loss maximum occurs. The motion responsible for these phenomena is believed to involve rotation about main-chain bonds in amorphous or disordered parts, leading to translation of chain segments from one position to another.

Publication Date: January 1, 1967 | doi: 10.1021/ba-1967-0063.ch021

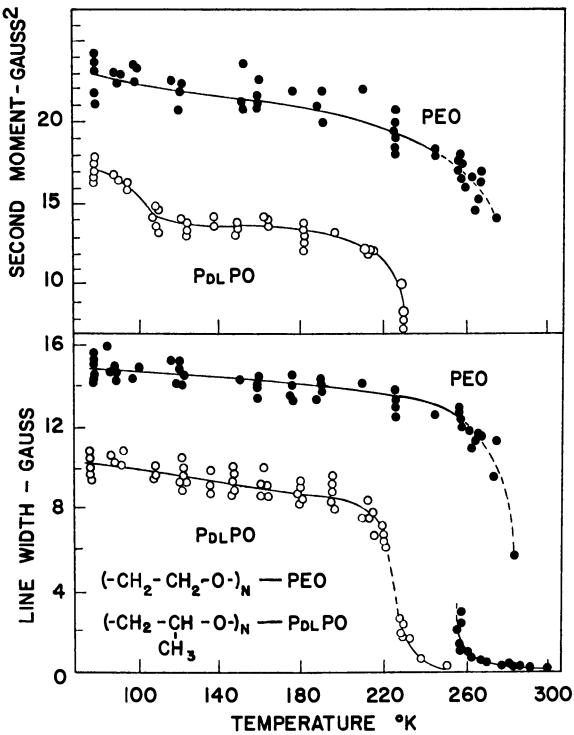

Figure 1. NMR line width and second moment vs. temperature

o *Poly (dl-propylene oxide) (38)*
• *Poly (ethylene oxide) (38)*

Table I. Temperature of Principal Amorphous Transformation for Various Crystalline Polymers

	Mechanical Tan δ_{max}			*"Apparent"* E_{act}		*NMR Process* ΔH *Narrow*		T_1 *Min.*	
Polymer	*Temp., °K.*	*Freq., c.p.s.*	*Ref.*	*Kcal./ mole*	*Ref.*	*~10⁴ to 10⁵ c.p.s.*	*Ref.*	*3 × 10⁷ c.p.s.*	*Ref.*
Poly(ethylene oxide)	220	1	(*56*)	—	—	250	Present work	330	(*7*)
66 nylon	370	600	(*87*)	60	(*84*)	350	(*88*)	430	(*35*)
6–10 nylon	350	600	(*87*)	—	—	320	(*88*)	420	(*35*)
Poly(ethylene terephthalate)	370	6	(*86*)	65	(*83*)	~380	(*34*)	—	—
Polypropylene	290	400	(*64*)	40	(*83*)	290	(*89*)	340	(*55*)
Poly(*dl*-propylene oxide)	210	0.4	(*59*)	—	—	220	Present work	270	(*6*)
Poly-1-butene	280[a]	900	(*91*)	~40	[b]	~300	(*89*)	—	—
Poly-1-pentene	260[a]	400	(*92*)	—	—	290	(*89*)	370	(*71*)
Poly(3-methyl-1-pentene)	390[a]	800	(*92*)	—	—	360	(*89*)	—	—
Poly(4-methyl-1-pentene)	330[a]	500	(*92*)	—	—	330	(*89*)	430	(*20*)
Polystyrene	380[a]	700	(*85*)	55	(*92*)	400	(*45*)	—	—
Polytrifluoro-monochloro-ethylene	380	3	(*67*)	50	(*83*)	410	(*43*)	—	—

[a] Dynamic loss modulus maximum.
[b] Calculated from data in Refs., *58*, *77*, *91*.

Other relaxation processes, at temperatures both above and below the glass transformation region, have been reported for a variety of crystalline high polymers. These particular processes do not affect all properties to the same extent. One of the best characterized of these, found principally by NMR techniques, is that ascribed to methyl group reorientations. That this occurs at temperatures below 200°K. (~10^4 c.p.s.) has been well established for polymers of various structure. Processes believed to be caused by methyl reorientation are listed in Table II for seven crystalline polymers. These assignments have been generally established by comparing observed and calculated second-moment values and in two cases, polypropylene (*55*, *89*) and poly(*dl*-propylene oxide) (*6*), by observations on deuterated polymers. As an example of using second-moment calculations for PdlPO, the rigid lattice value is calculated using the Van Vleck equation (*82*) as ~32 gauss² while that assuming methyl rotation is ~15 gauss². [The details of these particular calculations are given by Merrill (*38*).] Comparing these values with those on the second moment–temperature plot in Figure 1 indicates that the process taking place in the <77°–110°K. region (~10^4 c.p.s.) probably involves methyl reorientations. In contrast with PdlPO, comparison of the calculated rigid lattice second-moment value of ~24 gauss²

for PEO with the experimental values in Figure 1 indicates that little motion is taking place at $\leq$77°K.

For the poly α-olefins the methyl reorientation process does not appear to lead to a noticeable mechanical loss maximum. On the other hand a low-loss process is found (*9*) for P*dl*PO around ~90°K. (10^4 c.p.s.) which may include such reorientation.

There is a sizable loss maximum reported at 150°K. (~10^3 to 10^4 c.p.s.) for the poly-α-olefins (*92*) with ethyl, propyl, isopropyl, and isobutyl branches, at ~130°K. (~200 c.p.s.) for the poly(α-olefins) (*26*, *66*), poly-

Table II. Low Temperature Reorientation Processes for Various Polymers

	Temperature, °K.			
	NMR ΔH^2 decrease		*T_1 min.*	
Polymer	*($f \sim 10^4$ c.p.s.)*	*Ref.*	*($f \sim 3 \times 10^7$ c.p.s.)*	*Ref.*
Polypropylene	≲80	(*89*)	165	(*55*)
Poly(L-alanine)	≲80	(*30*)	—	—
Poly(*dl*-propylene oxide)	≲80	Present work	150	(*6*)
Poly-1-butene	<77	(*89*)	—	—
Poly-1-pentene	<77	(*89*)	150	(*71*)
Poly(3-methyl-1-butene)	90	(*89*)	—	—
Poly(4-methyl-1-pentene)	90	(*89*)	150	(*20*)
Poly (L-leucine)	80	(*30*)	170	(*20*)

1-hexene, poly-1-heptene, poly-1-octene, and poly-1-nonene, at ~180°K. (375 c.p.s.), for poly(4-iodo-1-butene) (*26*), at 185°K. (200 c.p.s.), for poly-(5-iodo-1-pentene) (*26*), and at 150°K. (400 c.p.s.) for poly(11-iodo-1-undecene) (*26*). Poly(vinyl stearate) (*5*, *38*) and poly(vinyl palmitate) (*5*), both highly crystalline substances, also show similar effects. These maxima have been attributed to motion of side-chain units larger than methyl. For poly(vinyl stearate) a decrease in the second moment of about 10 gauss^2 occurs in the 120°–200°K. range, also attributed (*39*) to side-chain reorientations (at ~10^4 c.p.s.). This reduction in second moment can be accounted for by assuming every chain as reorienting about the long axis for a planar zigzag hydrocarbon chain.

Polypropylene has a secondary loss maximum at 240°K. (10^3 c.p.s.) (*64*). If motion of polymer segments is responsible, portions of the main chain must be involved.

A variety of linear polymers—polyethylene (*86*), numerous polyamides with three or more CH_2 units between amide links (*30*, *86*) a polyurethane (*86*), a polyurea (*30*), and various polyesters of terephthalic acid (*10*, *21*)—exhibit a loss maximum at about 170°K. (~10^3 c.p.s.), the so-called γ process. T_1 minima, believed to correspond to the mechanical phenomenon, are found for linear polyethylene (*20*), 66 nylon (*35*), and 6–10 nylon

Publication Date: January 1, 1967 | doi: 10.1021/ba-1967-0063.ch021

(*35*). In addition, mechanical loss maxima are apparent for polytetrafluoroethylene at 200°K. ($\sim 10^3$ c.p.s.) (*62*) and for polyoxymethylene at 210°K. ($\sim 10^2$ c.p.s.) (*22*).

In the temperature region of the γ process a narrow component in the NMR spectra is first found for various linear polymers such as polyethylene (*65*), polyoxymethylene (*17*), 66 nylon (*13*), and polytetrafluoroethylene (*24*). This sharp component therefore appears at lower temperatures for linear than for branched polymers.

The motion responsible for the γ mechanism was originally believed to occur in the amorphous or disordered parts of the melt-formed structure and has been attributed to two distinct types of motion—oscillations within the energy minimum (local mode motion) (*60*) and conformational changes (*32*). As discussed below, experiments carried out using crystals from dilute solution have led to modifications of these suggestions. Motion of this type might also occur for branched polymers. In a number of cases secondary mechanical loss maxima have been so assigned, as follows: polypropylene (*64*) (245°K., 10^3 c.p.s.), PdlPO (*8*) (180°K., 10^4 c.p.s.), polytrifluoromonochloroethylene (*67*) (270°K., 10 c.p.s.), poly(vinyl chloride) (*67*) (240°K., 10 c.p.s.), and poly(vinyl fluoride) (*67*) (250°K., 1 c.p.s.). It is expected that the temperature of this process will shift to higher temperatures the larger the side chain, assuming the backbone chain is the same.

Studies on melt-formed samples showed that mechanical loss peaks (α processes) occur above the glass transformation but below the melting point for various crystalline polymers. Such mechanical loss processes have been reported for linear polyethylene (two processes) (*41*), polypropylene (*77*), poly(vinyl alcohol) (*77*), and polytrifluoromonochloroethylene (*37*). These have been attributed to motion in or of the crystalline regions. For linear polyethylene a NMR broad-line narrowing process (*65*) and a T_1 minimum (*20*) are also found in this temperature region.

As a crystalline polymer melts, a sharp reduction in NMR line width to values below 0.05 gauss occurs. There is also a decrease in the storage modulus of up to four decades ($\sim 10^{10}$ to $\sim 10^6$ dynes/sq. cm.). The sharp reduction in NMR line width is readily seen in low molecular weight substances such as the normal paraffins (*44*) and vinyl stearate (*5*).

For at least two polymers, polytetrafluoroethylene (*25*, *62*) and poly(*trans*-1,4-butadiene) (*4*, *25*), relaxation processes accompanying crystal-crystal phase transitions are found. Sharp NMR line narrowing has been observed at the transition temperature for various normal paraffins (*44*).

For polytetrafluoroethylene a mechanical loss maximum, initially attributed to motion accompanying the glass transformation, has been associated with motion in a paracrystalline phase (*80*).

Publication Date: January 1, 1967 | doi: 10.1021/ba-1967-0063.ch021

Solution-Grown Crystals and Related Samples

This section reviews and discusses results of dynamic mechanical and nuclear resonance measurements on polymer samples made up of dilute solution-grown crystals, samples prepared by uniaxial crystallization (*77*) or solid state polymerization, and samples formed from the melt under high pressures. Considerable evidence has led to the proposal that the dilute solution-grown crystals are composed of folded polymer chains (*11*), the chain length between folds depending on the crystallization conditions and the postcrystallization thermal history. For crystals not heated above the crystallization temperature this thickness is usually around 100 ± 50A. The uniaxially crystallized samples have the *b* axis oriented in a given direction with the *c* (chain axis) and the *a* axis changing orientation along the sample. Since crystallization is carried out from the melt, the lamellar thickness (chain length between folds) is several times greater than for solution-grown crystals. Samples crystallized from the melt under high pressure and those formed by solid-state polymerization are believed to consist mainly of extended chains (*12*, *93*).

The major number of these studies to date have been concerned with polyethylene. The first dynamic mechanical investigation was carried out using a vibrating wire (*79*) to which the crystals were cemented; by this method only a relative loss modulus is obtained. In this work the γ process was found to be greatly reduced if present at all; upon heating the crystals above 140°C. the magnitude of this process increased considerably. Subsequent work has all been carried out using pressed mats of crystals (*51*, *69*, *71*). Results have been obtained using a torsion pendulum at ~1 c.p.s. (*51*, *69*), a torsional resonator at 250, 1200, 12,000, and 36,000 c.p.s. (*51*), and a dynamic tensile stress apparatus at 3.5, 11, 35, and 110 c.p.s. (*76*). The crystals used were grown from dilute solution under various conditions: 0.1% Marlex 50 in xylene precipitated at 80°C. (*51*), 0.03% Marlex 9 in xylene precipitated at 70°C. (*76*), and 0.1% Grex 60–002 E in tetrachloroethylene precipitated under ambient conditions (*69*). In all three investigations a loss peak in the region of the γ process was found, but this maximum is smaller and occurs at lower temperatures than that for melt-formed samples.

Annealing a crystal mat for 30 minutes successively at temperatures of 100°, 110°, 120°, and 130°C. led to an increase in area of the γ maximum (log dec.) and a shift of this peak to higher temperatures, until the temperature found for the melt-formed specimen was reached (*69*).

A uniaxially oriented sample of linear polyethylene (*77*) also showed the γ maximum. In addition, a study (*48*) has been made on a rodlike sample of Marlex 50 prepared by heating at 175°C. for 119 hours under 40,000-p.s.i.g. pressure; it is presumed that this treatment leads to a sample containing principally extended chains. Using a transverse vibration

apparatus (*31*) at 10^3 c.p.s., a γ-loss maximum was exhibited by this specimen, which was essentially the same in height, position, and shape as that reported for Marlex 50 crystallized at $\leq$1-atm. pressure (*9*).

Neither the normal paraffin n-$C_{32}H_{66}$ (*61*) nor vinyl stearate (*63*), $CH_2 = C(H)OCO[CH_2]_{16}CH_3$, has a γ-loss maximum. Mixtures of n-$C_{16}H_{34}$, n-$C_{20}H_{42}$, and n-$C_{22}H_{46}$ with a few per cent of a normal paraffin of a chain length of 2 greater show (*50*) loss maxima at $-70°$ to $-80°$C. at $\sim 10^3$ c.p.s. It was suggested that this maximum was caused by double kink motion in the chain of the higher paraffin; this has been advanced (*51*) as an explanation of the γ process for polyethylene.

NMR line width studies have been obtained by various investigators on solution-crystallized samples of linear polyethylene (*61*, *24*, *28*, *44*, *52*, *53*, *54*, *62*, *69*, *70*). At all temperatures studied the mobile fraction of protons is less than that for samples melt-formed under 1-atm. pressure. The mobile fraction measured at room temperature depends on the crystal preparation; values reported by various investigators have ranged from <0.01 to 0.04. Since the exact value would depend on the method of separating the broad and narrow components, meaningful comparisons must be limited to different samples studied by the same investigator. For three different samples showing 112-, 120-, and 144-A.-fold periods the extent of narrow component above the background at 300°K. was essentially zero for the 112-A.-fold period sample, barely noticeable for the 144-A.-fold period specimen, and had a mobile fraction of 0.02 for the 120-A.-fold period sample (*28*, *44*). Applying $\sim 10^4$-p.s.i.g. pressure for 10 hours on the 112-A. sample led to the appearance of a narrow component at 300°K., yielding a mobile fraction of 0.02–0.03. [These samples were prepared by F. E. Karasz by precipitation from a 0.1% xylene solution at 80°C. (112-A.) and 90°C. (144-A.). The 144-A. sample was found by W. O. Statton of E. I. du Pont de Nemours & Co., Inc., to show four orders of low angle x-ray reflection. This indicates a high degree of regularity of the fold period, which in turn suggests a high degree of crystal perfection.] Measurements at lower temperatures (*24*) have shown a narrow component of <0.01 below $-40°$C. with no abrupt change in the mobile fraction-temperature plot. On the other hand an abrupt change in mobile fraction in the γ-process region ($-80°$ to $-100°$C.) is found for melt-formed sample (*24*).

A number of workers have shown that annealing of polyethylene crystals at temperatures above $\sim 100°$ to 110°C. leads to an increase in the mobile fraction at room temperature (*44*, *52*, *54*, *69*, *70*). Values as high as ~ 0.35 (annealing at $\sim 136°$C.) have been reported for this (*70*). Removal of the chain folds on polyethylene crystals (of unstated origin) with fuming nitric acid was reported (*53*) to lead to a reduction of the mobile fraction at 20°C. from a rather high value for crystals of 0.043 to a value of 0.014. This narrow component was not evident enough above the back-

Publication Date: January 1, 1967 | doi: 10.1021/ba-1967-0063.ch021

ground to enable a narrow fraction determination at temperatures below 20°C. Absence of the narrow line was recently reported for a sample crystallized from the melt at 5000 atm. and believed to contain principally extended chain lamellae (*46*). These latter results are direct evidence that the process responsible for the dynamic mechanical loss peak at ~170°K. (10^3 c.p.s.) in extended chain crystals is not the same as that leading to the NMR narrow component, the motional process responsible for the latter's taking place principally in the folds. It also appears to this author that disorder in the folds, introduced during the crystallization process or by heat treatment after crystallization, is necessary for this motion to be present. The absence of a narrow NMR component corresponding to the mechanical γ process suggests that the latter involves only very low amplitude motion and is therefore not expected to include conformational changes. This would rule out the motion of Reneker-type (*57*) or Peckhold-type (*51*) defects along the chain as causes of the mechanical γ process. However, torsional movement (local mode) motion within such a defect or in a disordered region would still be permissible.

Narrow NMR components have been reported (*44*) for melt-formed samples of the following normal paraffins: n-$C_{18}H_{38}$, n-$C_{19}H_{40}$, n-$C_{20}H_{42}$, n-$C_{21}H_{44}$, n-$C_{28}H_{58}$, n-$C_{35}H_{72}$, n-$C_{44}H_{90}$, and n-$C_{94}H_{190}$. The temperature at which they are first discernible above the background is higher the larger the number of carbon atoms, being ~190°K. for n-$C_{18}H_{38}$ and ~300°K. for n-$C_{44}H_{90}$. A narrow component was not found for recrystallized samples of n-$C_{21}H_{44}$ and n-$C_{35}H_{72}$. The mobile fraction was ~0.01 for n-$C_{20}H_{42}$ at 217°K. and for n-$C_{94}H_{190}$ at 300°K. This latter value is near that of 0.014 for nitric acid–treated polyethylene crystals (*53*). The narrow component for normal paraffins has been assumed to be caused by segmental motion either in grain boundaries or in disordered regions of the material (*44*).

A T_1 minimum for crystals of linear polyethylene grown isothermally has been reported at about 250°K. (3×10^7 c.p.s.) by two groups of investigators (*20*, *44*). It has been suggested that the motion responsible is the same as that causing the mechanical loss peak. The normal paraffin n-$C_{94}H_{190}$ does not show a T_1 minimum in this temperature region. As pointed out recently (*53*), crystals of n-$C_{94}H_{190}$ are nearly equivalent to polyethylene crystals with the folds removed, and therefore the absence of a minimum for this normal paraffin is further evidence that the low temperature NMR process is caused by motion in the folds. The number of folds in which this motion occurs could be small with respect to the total number, with the relaxation of other protons by spin diffusion largely contributing to the intensity of the T_1 minimum.

Single polyethylene crystals (*79*), mats of single crystals (*51*, *69*, *76*), and b axis–oriented melt-formed samples (*77*) all show an α mechanical loss process which is broader for the dilute solution-grown samples (~70° to

Publication Date: January 1, 1967 | doi: 10.1021/ba-1967-0063.ch021

110°C., 10^2 c.p.s.) (*76*) than for the *b* axis–oriented one (~80° to 100°C., 10^2 c.p.s.) (*77*) and which broadens as the frequency is lowered (*76*), indicating the presence of more than one mechanism. The area under the peak is found (*69*) to decrease with an increase in annealing temperature and to change upon high energy irradiation. This led to the hypothesis that segmental motion in crystal folds is responsible for this maximum (*69*). However, the work to date has not ruled out either chain torsion in the crystal or lamella movement as possible mechanisms.

The NMR broad line for polyethylene crystals undergoes narrowing in the ~60° to 120°C. region (*24*, *28*, *44*, *52*, *53*, *70*) for randomly oriented samples. For specimens with the chain direction oriented parallel to the magnetic field, this narrowing is not observed (*24*), as is also the case for highly drawn melt-formed specimens (*24*, *47*). The NMR process shifts to higher temperatures with a fold period increase (*24*, *44*). A polyethylene crystal sample with the folds removed (*53*) and a specimen of n-$C_{94}H_{190}$ (*44*) both showed a line narrowing similar to that for polyethylene crystals, further evidence that this process is caused by chain torsion. Therefore, regardless of the exact mechanism, if the α process (or any part of it) arises from the same cause as the broad line narrowing, motion in the folds cannot be responsible. Resolution of the exact mechanism or mechanisms awaits further work.

Finally for linear polyethylene T_1 minima have been reported at 400° and 420°K., respectively, for crystals grown at 80°C. (*20*), from xylene solution.

Dynamic mechanical and NMR investigations of crystals grown from dilute solutions for polymers other than linear polyethylene have been much less extensive. Studies have been reported for the linear polymers: polyoxymethylene (*3*, *40*, *94*), poly(ethylene oxide) (*3*, *78*), and nylon 6 (*42*), and the branched polymers: polypropylene (*40*), poly-1-butene (*19*, *95*), poly(4-methyl-1-pentene) (*33*), poly(vinyl alcohol) (*78*), and branched polyethylene (*78*). In addition, dielectric loss measurements have been made on crystal aggregates of poly(ethylene oxide) (*23*), poly(vinyl alcohol) (*68*), and polyoxymethylene (*3*) and mechanical loss measurements have been carried out on polyoxymethylene formed by solid state polymerization (*94*).

In one investigation, using a viscoelastometer, crystal mats of polyoxymethylene from cyclohexanol solution showed a γ-loss modulus peak at ~200°K. (~10^2 c.p.s.) (*40*), reduced in magnitude but at approximately the same temperature as that for melt-crystallized material. However, results obtained for crystals, grown at 97°C. from a 1% Delrin 500 solution in a 3:1 phenol-ethanol mixture (*3*), indicated that the attenuation peak for crystals suspended in methanol and the associated dielectric loss peak are at lower temperatures than that for the loss peak in melt-crystallized material, in agreement with results for polyethylene. A sample prepared by

Publication Date: January 1, 1967 | doi: 10.1021/ba-1967-0063.ch021

solid-state polymerization shows a much weaker mechanical loss maximum at lower temperatures (~170°K., 10^2 c.p.s.) (*94*) than that for crystal mats; a decrease in NMR second moment for this type of specimen from 24 to 19 gauss^2 at ~160° to 210°K. is also found (*94*).

Since the solid state–polymerized sample is believed to be well ordered as well as having extended chains, the lack of a maximum at 200°K. (10^2 c.p.s.) only indicates a dependence of this process on the presence of disordered regions in the bulk of the crystal or on the surface. The present results do not show whether or not the γ-loss maximum for polyoxymethylene is caused by the same mechanism as that for linear polyethylene.

It has been suggested (*94*) that the small peak at 170°K. (10^2 c.p.s.) for polyoxymethylene is caused by chain end motion. However, little proof has been put forward, and further investigations are needed.

Solution-grown crystals of polyoxymethylene have a mechanical loss modulus peak at 430°K. (10^2 c.p.s.) (*40*); for the solid state–polymerized sample this α maximum is reduced and appears as a shoulder on an E'' upswing with increasing temperature at or near the melting point. These results suggest that this process involves motion in the crystalline regions, but the details are not yet understood. The motion accompanying the increase in fold period with increasing annealing temperature has been cited as responsible for the α maximum (*94*). However, the results for the extended chain sample indicate that other mechanisms are active. Other possibilities include torsional chain movement and partial or complete lamella motion.

A mat of nylon 6 crystals from 0.05% glycerol solution exhibits (*42*) loss maxima at ~150°, ~230°, and ~410°K. (10^2 c.p.s.). The lower two maxima are similar to those found for melt-formed samples. The major maximum at ~410°K. is ~60° higher than the major loss peak for melt-formed samples and is therefore believed to be caused by a different mechanism. Other nylon 6 samples show (*42*) a loss modulus shoulder at ~470°K. (10^2 c.p.s.) near the melting point, and therefore the motion responsible is believed to take place in the crystalline regions, while the ~410°K. peak is ascribed to motion in a metastable crystalline phase made up of a mixture of the α and γ forms (*42*).

Two processes at 310°K. (10^2 c.p.s.) and ~350°K. (10^2 c.p.s.) have been found (*68*), using the dielectric technique, for atactic poly(vinyl alcohol) crystals, grown from 0.05% triethylene glycol solution while cooling from 180° to 165°C. These maxima have been previously attributed (*77*) to "local mode" and glass transformation motion, respectively.

Samples of poly(4-methyl-1-pentene) (P4MP1) prepared from mats of dilute solution–crystallized polymer have been investigated by NMR and dynamic mechanical techniques. Dynamic mechanical data for crystal mats of P4MP1 were obtained with a vibrating reed apparatus by J. A. E. Kail of Imperial Chemical Industries, Ltd., Plastics Division, on a

Publication Date: January 1, 1967 | doi: 10.1021/ba-1967-0063.ch021

specimen prepared by pressing together strips of a mat of material obtained by isothermal crystallization at 64°C. from 0.07% xylene solution. These samples were found by x-ray diffraction to be ≥70% crystalline. These results are given in Figure 2 along with T_1 measurements (*20*) on a P4MP1 crystal mat made up of material prepared by isothermal crystallization at 57°C. from a 0.07% xylene solution; this preparation was shown to contain square lamellae in addition to larger sheets of polymer.

At least two T_1 minima and two loss maxima are apparent in Figure 2, indicating the existence of at least three different mechanisms. Nonexpotential magnetization decay curves, decomposable into two parts each associated with a separate T_1 value, were observed for P4MP1 crystals from 77°–170°K. The occurrence of two spin-lattice relaxation mechanisms at

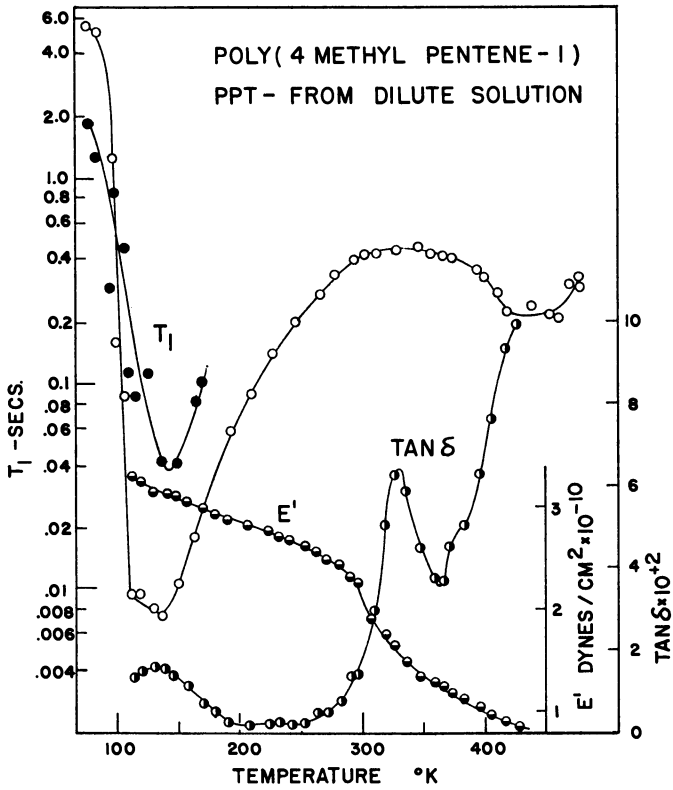

Figure 2. Mechanical loss tangent (tan δ) and elastic storage modulus at ~10² c.p.s. and spin-lattice relaxation time (20) vs. temperature for poly (4-methyl-1-pentene) crystallized from dilute solution

low temperature was observed for certain samples of polyethylene and for poly(L-leucine) (*20*). This behavior has not been satisfactorily explained. Melt-formed specimens of P4MP1 exhibit two T_1 minima (*20*) and two

Publication Date: January 1, 1967 | doi: 10.1021/ba-1967-0063.ch021

mechanical loss peaks (*92*) in about the same temperature regions as for the crystal specimens. In addition, broad-line NMR measurements on a crystal mat have been reported (*33*). The second moment decrease in the $\leq 77°$ to 120°K. region, believed to be associated with the ~130°K. (3.5×10^7 c.p.s.) T_1 minimum, has been attributed to methyl group reorientations (*89*).

The 130°K. (210 c.p.s.) loss maximum is believed to involve isobutyl motion. The tan δ maximum at 330°K. (150 c.p.s.) and the T_1 minimum at 450°K. (3.5×10^7 c.p.s.) for P4MP1 crystals are tentatively associated with motion in the disordered parts of the lamellae or of tie molecules between lamellae. This loss maximum is found to decrease in size with increasing crystallinity. Two maxima at 410° and 450°K. (~100 c.p.s.) (*14*), possibly involving chain motion in the crystalline regions, have been reported for melt-formed P4MP1 samples. There is some indication of one such mechanism in the mechanical loss data in Figure 2.

Dynamic mechanical results for polypropylene crystal aggregates (*40*) grown at 60°C. from 0.1% xylene and for poly(1-butene) crystals (*95*) from a 2% Decalin solution have been obtained at temperatures from ~210°K. For these specimens the peak caused by the principal amorphous transformation at ~300°K. (10^3 c.p.s.) (*64*, *91*) is greatly reduced while a loss maximum closer to the melting point is found at 390°K. (10^2 c.p.s.) for polypropylene and 340°–360°K. (10^2 c.p.s.) for poly(-1 butene); these maxima are attributed to motion in the crystalline regions.

Therefore, in all the polymer crystal specimens studied to date the principal loss tangent maximum found for melt-formed samples is greatly reduced in size if present at all, and a maximum at higher temperatures either appears or is more in evidence. The exact mechanism (or mechanisms) responsible for this "crystalline" loss process is still in doubt. The principal loss mechanism for melt-formed samples is believed to be associated with segmental motion in disordered regions which could possibly be those regions containing tie molecules between lamellae, the surface folds of the crystals, or both.

Numerous studies have been reported on various synthetic poly(α-amino acids). All of these samples were obtained by precipitation from the reaction solution during preparation of the polymer, by reprecipitation from a solvent-nonsolvent system, or by solvent evaporation. The majority of these investigations have involved the study of NMR spectra. Broad-line NMR studies have been carried out on poly(L-alanine) (*27*), poly(D, L-alanine) (*75*), poly(D, L-α-deuteroalanine) (*75*), poly(L-leucine) (*27*), poly(phenyl-L-alanine) (*27*), poly(γ-benzyl-L-glutamate) (*18*, *27*), poly(sodium-α-L-glutamate) (*27*), poly(γ-methyl-D-glutamate) (*73*), poly-(β-benzyl-L-aspartate) (*18*), poly(*S*-carbobenzoxyethyl-L-cysteine) (*29*), and poly(*S*-carbomethoxyethyl-L-cysteine) (*29*). The polymers with

Publication Date: January 1, 1967 | doi: 10.1021/ba-1967-0063.ch021

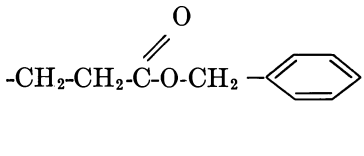
and
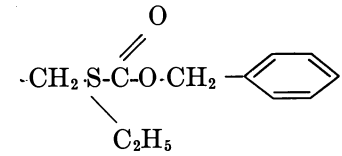

side chains show abrupt second-moment narrowing processes of ~10 gauss[2] around 300° and 260°K., respectively. Those with

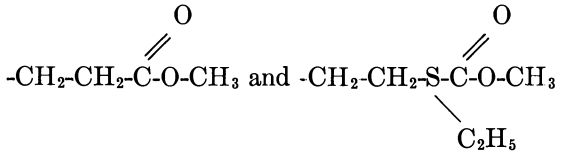
substituents have less

abrupt but large second-moment drops centered about 350° and 300°K., respectively. The polymers with

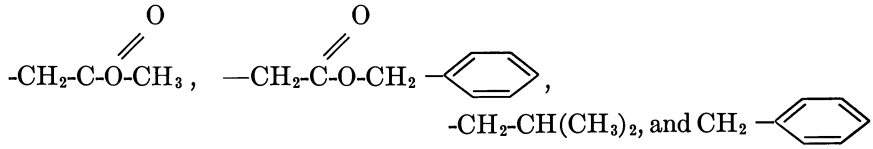

substituents show still more gradual second moment changes in the 100°–400°K. range. In all these cases the second moment after the transformation is 5 gauss[2] or less. These processes have been attributed principally to side-chain reorientations about the extended chain axis. The four polymers with methyl side side groups give abrupt changes at ≤77°–120°K., reducing the second moment from ~20 to ~11 gauss[2], attributed to methyl group reorientations. The deuterated polymer has a second abrupt narrowing region around 270°K., possibly involving main-chain motion. The


polymer with side chains was found to have a near constant line width and line shape from 77°–350°K., indicative of a near rigid network.

T_1 measurements on poly(L-leucine) yield a minimum at 175°K., (3×10^7 c.p.s.) attributed to methyl reorientations (*20*). A shallow minimum at 290°K. (3×10^7 c.p.s.) is believed caused by motion of side chain units larger than methyl (*20*). For poly(phenyl-L-alanine) a T_1 minimum at 200°K. has been assigned tentatively to phenyl motion and a very broad minimum at high temperatures to benzyl motion (*20*).

Dynamic mechanical results for poly(γ-benzyl-L-glutamate) have been reported by three groups of investigators (*15*, *59*, *74*) working in the 0.1- to 110-c.p.s. frequency region. In one study samples of the same polymer were cast from an α-helix-forming solvent (dioxane) and a random-coil

Publication Date: January 1, 1967 | doi: 10.1021/ba-1967-0063.ch021

forming solvent (trifluoroacetic acid). Specimens cast from dioxane and from trifluoroacetic acid show (*15*) different tan δ *vs.* temperature plots, the former yielding a shoulder at ~200°K. (10^2 c.p.s.), the latter being accompanied by a minimum in the storage modulus. The trifluoroacetic acid cast sample yields the low temperature shoulder plus a broad maximum at 330°K. (10^2 c.p.s.). The principal loss peak at 310°K. (10^2 c.p.s.) is associated with the NMR line-narrowing process at ~300°K. (~10^4 c.p.s.) (*27*). However, if these processes were caused by the same mechanism, the temperature positions of these two processes should be reversed. This apparent discrepancy could be caused by differences in sample preparation or by the fact that the motion for each is not exactly the same. Whether the dioxane cast sample shows an E'' maximum at ~380°K. (10^2 c.p.s.) corresponding to the tan δ maximum could not be ascertained from the data given. This tan δ maximum could be caused by the minimum in E', which is unexplained. The broad maximum at 330°K. for the random coiled form is presumably made up of side-chain and main-chain motion (*74*).

A dynamic mechanical investigation of poly(ethyl-L-glutamate) in the 250°–310°K. region has shown a maximum for this polymer at 280°K. (35 c.p.s.) (*74*). The results for the polypeptide samples composed of molecules which are believed to have large rigid (helical) sections can usually be explained in terms of side-chain reorientations; therefore, a distinct difference seems to exist between the polypeptides and other synthetic polymers, including the polyamides and the vinyl polymers.

Publication Date: January 1, 1967 | doi: 10.1021/ba-1967-0063.ch021

Literature Cited

(1) Andrews, R. D., *Polymer Preprints* **6**, 717 (1965).
(2) Andrews, R. D., Hammack, T. J., *J. Polymer Sci.* **B3**, 659 (1965).
(3) Arisawa, K., Tsuge, K., Wada, Y., *Japan. J. Appl. Phys.* **4**, 138 (1965).
(4) Baccaredda, M., Butta, E., *J. Polymer Sci.* **51**, S39 (1961).
(5) Butta, E., Magagnini, P. L., *Ann. Chim. (Italy)* **53**, 1034 (1963).
(6) Connor, T. M., Blears, D. J., Allen, G., *Trans. Faraday Soc.* **61**, 1097 (1965).
(7) Connor, T. M., Read, B. E., Williams, G., *J. Appl. Chem.* **14**, 74 (1964).
(8) Crissman, J. M., Sauer, J. A., Woodward, A. E., *J. Polymer Sci.* **A2**, 5075 (1964).
(9) Deeley, C. W., Sauer, J. A., Woodward, A. E., *J. Appl. Phys.* **29**, 1415 (1958).
(10) Farrow, G., McIntosh, J., Ward, I. M., *Makromol. Chem.* **38**, 147 (1960).
(11) Geil, P. H., "Polymer Single Crystals," Interscience, New York, 1963.
(12) Geil, P. H., Anderson, F. R., Wunderlich, B., Arakawa, T., *J. Polymer Sci.* **A2**, 3707 (1964).
(13) Glick, R. E., Phillips, R. C., *Ibid.*, **A3**, 1885 (1965).
(14) Griffith, J. H., Ranby, B. J., *Ibid.*, **44**, 369 (1960).
(15) Hashino, Y., Yoshino, M., Nagamatsu, K., *Rept. Progr. Polymer Phys. Japan* **8**, 221 (1965).
(16) Herring, M. J., Smith, J. A. S., *J. Chem. Soc.* **1960**, 273.
(17) Hikichi, K., Furuichi, J., *J. Polymer Sci.* **A3**, 3003 (1965).
(18) Hikichi, K., Tsutsumi, A., Furuichi, J., *Ann. Rept. Progr. Group Biophys. Japan* **3**, 19 (1963).
(19) Hukuda, K., Kusumoto, N., Kawano, I., Takayanagi, M., *Rept. Progr. Polymer Phys. Japan* **8**, 317 (1965).
(20) Hunt, B. I., Powles, J. G., Woodward, A. E., *Polymer* **5**, 323 (1964).

(21) Illers, K. H., Breuer, H., *J. Colloid Sci.* **18**, 1 (1963).
(22) Ishida, Y., Matsuo, M., Ito, H., Yoshimo, M., Irie, F., Takayanagi, M., *Kolloid Z.* **174**, 162 (1961).
(23) Ishida, Y., Matsuo, M., Takayanagi, M., J. *Polymer Sci.* **B3**, 321 (1965).
(24) Iwayanagi, S., Miura, I., *Japan. J. Appl. Phys.* **4**, 94 (1965).
(25) Iwayanagi, S., Miura, I., *J. Polymer Sci.*, in press.
(26) Kail, J. A. E., *Polymer* **6**, 535 (1965).
(27) Kail, J. A. E., Sauer, J. A., Woodward, A. E., *J. Phys. Chem.* **66**, 1292 (1962).
(28) Kail, J. A. E., Sauer, J. A., Woodward, A. E., *Polymer* **4**, 413 (1963).
(29) Kamashima, K., *Ann. Rept. Progr. Group Biophys. Japan* **3**, 23 (1963).
(30) Kawaguchi, T., *J. Appl. Polymer Sci.* **2**, 56 (1959).
(31) Kline, D. E., *J. Polymer Sci.* **22**, 449 (1956).
(32) Kline, D. E., Sauer, J. A., Woodward, A. E., *Ibid.*, **22**, 455 (1956).
(33) Kusumoto, N., Hukuda, K., Takayanagi, M., *Rept. Progr. Polymer Phys. Japan* **8**, 315 (1965).
(34) Land, R., Richards, R. E., Ward, I. M., *Trans. Faraday Soc.* **55**, 225 (1959).
(35) McCall, D. W., Anderson, E. W., *Polymer* **4**, 93 (1963).
(36) McCall, D. W., Douglass, D. C., *Ibid.*, **4**, 433 (1963).
(37) McCrum, N. G., *J. Polymer Sci.* **60**, S3 (1962).
(38) Merrill, L. J., Ph.D. dissertation, Pennsylvania State University, 1964.
(39) Merrill, L. J., Sauer, J. A., Woodward, A. E., *J. Polymer Sci.* **A3**, 4243 (1965).
(40) Minami, S., Takayanagi, M., *Rept. Progr. Polymer Phys. Japan* **7**, 241 (1964).
(41) Nakayasu, H., Markovitz, H., Plazek, D. J., *Trans. Soc. Rheol.* **5**, 261 (1961).
(42) Neki, K., Takayanagi, M., *Rept. Progr. Polymer Phys. Japan* **8**, 281 (1965).
(43) Nishioka, A., *J. Polymer Sci.* **37**, 163 (1959).
(44) Odajima, A., Sauer, J. A., Woodward, A. E., *J. Phys. Chem.* **66**, 718 (1962).
(45) Odajima, A., Sauer, J. A., Woodward, A. E., *J. Polymer Sci.* **57**, 107 (1962).
(46) Olf, H. G., Peterlin, A., *Bull. Am. Phys. Soc.* Ser. II, **11**, 213 (1966).
(47) Olf, H. G., Peterlin, A., *J. Appl. Phys.* **35**, 3108 (1964).
(48) Pae, K. D., Morrow, D. R., Lim, T., Sauer, J. A., Rutgers–The State University, unpublished results.
(49) Pake, G. E., "Solid State Physics," Vol. 2, pp. 1–92, Academic Press, New York, 1956.
(50) Peckhold, W., Blasenbrey, S., Woerner, S., *Kolloid Z.* **189**, 14 (1963).
(51) Peckhold, W., Eisile, U., Knauss, G., *Ibid.*, **196**, 27 (1964).
(52) Peterlin, A., Krasovec, F., Pirkmajer, E., Levstek, J., *Macromol. Chem.* **37**, 231 (1960).
(53) Peterlin, A., Meinel, G., Olf, H. G., *J. Polymer Sci.* **B4**, 399 (1966).
(54) Peterlin, A., Pirkmajer, E., *Ibid.*, **46**, 185 (1960).
(55) Powles, J. G., Mansfield, P., *Polymer* **3**, 340 (1962).
(56) Read, B. E., Williams, G., *Ibid.*, **2**, 239 (1961).
(57) Reneker, D. H., *J. Polymer Sci.* **59**, S39 (1962).
(58) Saba, R. G., M.S. thesis, Pennsylvania State University, 1962.
(59) Saba, R. G., Sauer, J. A., Woodward, A. E., *J. Polymer Sci.* **A1**, 1483 (1963).
(60) Saitô, N., Okano, K., Iwayanagi, S., Hideshima, T., "Solid State Physics," Vol. 14, p. 343, F. Seitz and D. Turnbull, eds., Academic Press, New York, 1963.
(61) Sandiford, W. D. H., private communication.
(62) Sauer, J. A., Kline, D. E., IXth International Congress on Applied Mechanics, University of Brussels, Vol. 5, p. 368, 1957.
(63) Sauer, J. A., Lim, T., *Bull. Am. Phys. Soc.*, Ser. II, **11**, 213 (1966).
(64) Sauer, J. A., Wall, R. A., Fuschillo, N., Woodward, A. E., *J. Appl. Phys.* **29**, 1385 (1958).
(65) Sauer, J. A., Woodward, A. E., *Rev. Mod. Phys.* **32**, 88 (1960).
(66) Schatski, T. F., *Polymer Preprints* **6**, 646 (1965).
(67) Schmieder, K., Wolf, K., *Kolloid Z.* **134**, 149 (1953).
(68) Shiba, K., Wada, Y., *Rept. Progr. Polymer Phys. Japan* **8**, 321 (1965).
(69) Sinnott, K. M., *J. Polymer Sci.* **B3**, 945 (1965).
(70) Slichter, W. P., *J. Appl. Phys.* **31**, 1865 (1960); *32*, 2339 (1961).

In Ordered Fluids and Liquid Crystals; Porter, R., el al.;
Advances in Chemistry; American Chemical Society: Washington, DC, 1967.

(71) Slichter, W. P., Davis, D. D., *Ibid.*, **35**, 10 (1964).
(72) Staverman, A. J., Schwartzl, F., "Die Physik der Hochpolymeren," Vol. 4, Chap. 1, Springer, Berlin, 1956.
(73) Sugai, S., Hikichi, K., *Oyo Butsuri* **32**, 705 (1963).
(74) Sugai, S., Kamashima, K., *Rept. Progr. Polymer Phys. Japan* **8**, 297 (1965).
(75) Sugai, S., Kamashima, K., Hikichi, K., *Japan. J. Appl. Phys.* **2**, 588 (1963).
(76) Takayanagi, M., *Kautschuk Gummi Kunststoffe* **17**, 164 (1964).
(77) Takayanagi, M., *Mem. Fac. Eng. Kyushu Univ.* **23**, 41 (1963).
(78) Takayanagi, M., Minami, S., Nagai, A., Neki, K., *Rept. Progr. Polymer Phys. Japan* **8**, 277 (1965).
(79) Thurn, H., *Kolloid Z.* **173**, 72 (1960).
(80) Tsuge, K., Enjoji, H., Terada, H., Ozawa, Y., Wada, Y., *Japan. J. Appl. Phys.* **1**, 270 (1962).
(81) Union Carbide Chemical Co., "Carbowax Polyethylene Glycols," 1958.
(82) Van Vleck, J. H., *Phys. Rev.* **74**, 1168 (1948).
(83) Wada, Y., *J. Phys. Soc. Japan.* **16**, 1226 (1961).
(84) Wada, Y., Hirose, H., Umebayashi, H., Otomo, M., *J. Phys. Soc. Japan* **15**, 2324 (1960).
(85) Wall, R. A., Sauer, J. A., Woodward, A. E., *J. Polymer Sci.* **35**, 281 (1959).
(86) Wolf, K., Schmieder, K., *Ric. Sci.* **25**, 732 (1955).
(87) Woodward, A. E., Crissman, J. M., Sauer, J. A., *J. Polymer Sci.* **44**, 23 (1960).
(88) Woodward, A. E., Glick, R. E., Sauer, J. A., Gupta, R. P., *Ibid.* **45**, 367 (1960).
(89) Woodward, A. E., Odajima, A., Sauer, J. A., *J. Phys. Chem.* **65**, 1384 (1961).
(90) Woodward, A. E., Sauer, J. A., "Physics and Chemistry of the Organic Solid State," Vol. II, Fox, D., Labes, M. M., and Weissberger, A., eds., pp. 637–723, 925–47, Interscience, New York, 1965.
(91) Woodward, A. E., Sauer, J. A., Wall, R. A., *J. Chem. Phys.* **30**, 854 (1959).
(92) Woodward, A. E., Sauer, J. A., Wall, R. A., *J. Polymer Sci.* **50**, 117 (1961).
(93) Wunderlich, B., Arakawa, T., *Ibid.*, **A2**, 3697 (1964).
(94) Yamada, N., Orito, Z., Minami, S., *Ibid.*, **A3**, 4173 (1965).
(95) Yasuda, H., Takayanagi, M., *Rept. Progr. Polymer Phys. Japan* **7**, 245 (1964).

RECEIVED February 11, 1966.

Analysis and Apparatus for Surface Rheological Measurements

R. A. BURTON and R. J. MANNHEIMER

Southwest Research Institute, San Antonio, Tex.

Publication Date: January 1, 1967 | doi: 10.1021/ba-1967-0063.ch022

The mathematical analysis presented here applies to the steady flow of a Newtonian fluid in an infinitely long channel having fixed side walls, a floor moving steadily in a direction parallel to the walls, and a flat, free surface which may exhibit the properties of surface viscosity and surface shear rigidity. In the corresponding experimental apparatus the infinitely long channel is simulated by an annulus. Using liquids with different viscosities as test fluids, the general predictions of the analysis are verified for the flow of simple fluids. The proposed apparatus configuration is adaptable to both insoluble and soluble surface films. This, coupled with the amenability of the configuration to direct analysis, gives promise of a potential for broad application.

In 1869, Plateau (*7*) inferred the existence of surface viscosity by observing the damping of the motion of a needle lying on the surface of a liquid. Since then numerous experimental approaches have been developed to permit more precise measurement of this and other surface-rheological properties; an increasingly coherent body of data has been accumulated in recent years. Such measurements are of broad interest since they shed light on the intermolecular forces at work in films and answer questions regarding the practical problems of foam formation, emulsion stability, and wave damping.

In effect, surface viscosity is directly equivalent to a significant increase of bulk viscosity in the vicinity of a liquid-gas or liquid-liquid interface. This region of enhanced viscosity may correspond to an insoluble monolayer floating on the surface of a substrate liquid. It may also be produced by soluble components in the bulk liquid, which tend to concentrate at an open surface or an interface.

In Ordered Fluids and Liquid Crystals; Porter, R., el al.;
Advances in Chemistry; American Chemical Society: Washington, DC, 1967.

The relation between surface viscosity and bulk viscosity is given by

$$\mu_s = \delta(\mu_b)_s$$

where $(\mu_b)_s$ is the equivalent bulk viscosity of the surface phase, and δ is the thickness of the surface region of enhanced viscosity. μ_s is called the surface viscosity and represents the combined effects of both viscosity and thickness of the surface layer. The units of μ_s are surface poises or dyne-seconds per centimeter rather than dyne-seconds per square centimeter of conventional bulk viscosity.

The task of measuring surface viscosity is twofold. First, geometry must be devised wherein some easily measured parameter of the flow is strongly influenced by the surface region of enhanced viscosity. Second, a mathematical analysis must be derived to relate the measurement observation to the desired quantity. Withal, the status of measurement techniques and apparatus has been such that the only arrangement suited for absolute property measurements is limited to insoluble surface films while the more broadly applicable arrangements have not successfully yielded to analytical treatment. The present work represents an approach toward bridging this gap. A modified configuration is introduced for a channel-type viscometer, offering both broad experimental applicability and amenability to mathematical analysis. This configuration is closely enough related to some of the earlier arrangements to permit its use with existing laboratory procedures, and it is applicable to both insoluble and soluble films.

Publication Date: January 1, 1967 | doi: 10.1021/ba-1967-0063.ch022

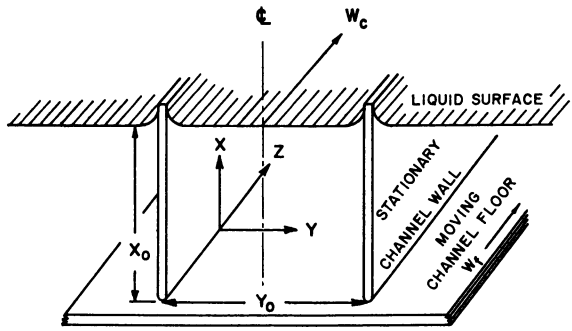

Figure 1. Sectional view of channel

The physical meaning of surface viscosity may best be illustrated in terms of the proposed measurement technique itself. Consider an annular channel with stationary walls and vertical axis of symmetry, that is partially filled with a liquid to a uniform depth, as illustrated in cross-section in Figure 1. The floor of the channel is capable of tangential sliding. When the floor is set in uniform motion, it gives rise to a corresponding motion in

the liquid, where the free-surface speed will be slower than the floor speed as a consequence of the influence of the channel walls. This speed can be observed in terms of the motion of particles of nonwetting material dusted onto the liquid surface.

If a film that shows surface viscosity is applied to the liquid, the surface speed will be further reduced. If the film shows surface rigidity (effectively, infinite surface viscosity), the surface motion will be brought to a complete halt, and the net effect of the moving floor will be to apply stress rather than motion to the film. Often a "rigid" film will break up at some limiting stress which can be termed surface yield strength. Following such a breakup, the film may exhibit surface viscosity in varying degrees.

With quantitative relationships among surface velocity, the geometric parameters, the substrate fluid viscosity, and the floor speed, this arrangement not only demonstrates surface viscosity effects but also provides a means for its measurement.

Publication Date: January 1, 1967 | doi: 10.1021/ba-1967-0063.ch022

Prior Developments

The reasons behind the specific choice of apparatus geometry can best be shown by a brief review of prior work. The earliest "canal type" surface viscometer was introduced by Dervician and Joly (*3*). In this apparatus, an insoluble monolayer is floated on a substrate fluid in a straight channel. The film is forced to flow through the channel by movement of a floating barrier. This motion is resisted principally by surface viscosity. Thus, the small force required to propel the film at a given speed may be measured and used to determine the surface viscosity of the film. A relatively complete theoretical treatment has been provided by Harkins and Kirkwood (*5*) for insoluble films with Newtonian surface viscosity in deep channels. Actual measurements are typically made in shallow channels, however, which are formed by floating the channel boundaries on the liquid surface. This method is not applicable to soluble surface films, which tend to diffuse through the substrate fluid and pass behind the barrier. Nevertheless, the most accurate values of surface viscosity available have been produced by this approach.

Ewers and Sack (*4*) have developed a related apparatus consisting of a vertical walled channel between two reservoirs, through which the substrate liquid moves as a consequence of a head difference between the reservoirs. Small nonwettable particles floated on the surface indicate the speed of surface elements of the fluid along the center line of the channel. This motion has been related to bulk-fluid movement by means of a thorough mathematical treatment, which is applicable to Newtonian surface films. Thus, the force measurement in the previous scheme is replaced here by a surface velocity and bulk-flow measurement. The only serious difficulty with this arrangement is that the transported surface material tends to accumulate in the lower reservoir. Thus, a surface pressure gra-

dient is created which affects the surface flow and limits the practical usefulness of the apparatus.

Davies (*2*) has improved on this design with his circular "viscous traction" instrument, which consists of an annular brass channel, formed by two concentric knife-edge rings. These are coated with wax and then lowered until they make contact with the surface of a liquid in a Petri dish. As the dish is rotated about its axis, the bulk motion of the fluid tends to provide a traction on the liquid surface between the two rings. As before, the speed of a suspended particle on the surface provides an indication of the surface viscosity. Although Davies was successful in eliminating the surface pressure effects that had plagued the previous channel viscometers, he has conceded that "the mathematical treatment of the retardation of the surface relative to the bulk of the liquid is rather complicated" (*2*). Davies, therefore, had to depend upon calibrating his system with insoluble films. The surface viscosities of these films had previously been determined by the canal method of Dervician and Joly. This approach has made it difficult to apply the apparatus to a broad variety of experimental conditions. Furthermore, the calibration data have been limited to insoluble films on aqueous substrates; therefore, substrate liquids with bulk viscosities appreciably different from water could not be investigated by this method.

The apparatus configuration proposed in this paper retains the annular flow features of Davies' apparatus while eliminating the hard-to-analyze ring configuration. Since it can be dealt with in terms of flow in a uniform channel, it may also be considered to retain the most favorable feature of the apparatus of Ewers and Sack without suffering from the problem of surface-pressure buildup.

In addition to those channel viscometers discussed here there is a separate type known as torsional viscometers, where surface viscosity is measured in terms of the traction on a wire, traversed lengthwise on the surface of a liquid. At this writing, none of these is known to have been subjected to a complete analysis. Joly (*6*) says, "furthermore, calculations based on the correct equation would depend upon the exact shape of the apparatus. As these calculations have so far not been carried out in any case, the values obtained by the rotation method are incorrect and certainly too high." Nevertheless, such approaches may offer special advantages and should be investigated fully. They must be considered as separate topics, however from the channel viscometers discussed here.

Theoretical Background

In an idealized version of the proposed configuration (Figure 1), an origin for Cartesian coordinates is placed at one wall and at the floor of the

Publication Date: January 1, 1967 | doi: 10.1021/ba-1967-0063.ch022

channel. The y-axis is directed across the channel, the x-axis is directed upward from the channel floor, and the z-axis is in a direction normal to the (x, y) plane. The following analysis is made under the assumptions that the free fluid-surface is flat, that the annular space between the concentric rings can be treated as a straight and infinitely long channel, that the flow in the channel is unaccelerated and laminar, and that both surface and bulk viscosities are Newtonian. The only velocity component will be w, which is directed along the z-axis; the magnitude of w will be a single-valued scalar function of x and y; and there will be no pressure gradients in the direction of flow. Under these conditions, the Navier-Stokes equation reduces to Laplace's equation in two dimensions for the substrate fluid, where μ is constant throughout:

$$\frac{\partial^2 w}{\partial x^2} + \frac{\partial^2 w}{\partial y^2} = 0 \tag{1}$$

The boundary conditions at the walls are such that

$$\begin{aligned} w &= 0 \text{ at } y = 0 \\ w &= 0 \text{ at } y = y_o \end{aligned} \tag{2}$$

At the floor, where w is constant, with magnitude w_f, the boundary condition is such that

$$w = w_f \text{ at } x = 0 \tag{3}$$

At the upper surface of the bulk or substrate flow the boundary condition is set by the effects of surface viscosity. Ewers and Sack (*4*) have shown this to be specified by Equation 4.

$$\mu_s \left.\frac{\partial^2 w}{\partial y^2}\right|_s = \mu_b \left.\frac{\partial w}{\partial x}\right|_s \tag{4}$$

Here $\mu_b \left.\frac{\partial w}{\partial x}\right|_s$ is recognized as the local shear stress, τ_{xz}, acting on a differential surface element. The term at the left results when it is assumed that the surface film is thin enough to share with the substrate the velocity w_s, which is a function of y only. The gradient of this velocity in the plane of the surface gives rise to a line stress in direct analogy to the viscous resistance of bulk flow. μ_b is the viscosity of the substrate flow and is assumed to have a constant magnitude throughout the bulk fluid. μ_s is surface viscosity and for the present analysis is assumed to have a constant magnitude at any point in the surface film.

Publication Date: January 1, 1967 | doi: 10.1021/ba-1967-0063.ch022

In Ordered Fluids and Liquid Crystals; Porter, R., el al.;
Advances in Chemistry; American Chemical Society: Washington, DC, 1967.

Derivation of Flow Equations

A general solution for Equation 1, that satisfies the boundary conditions of Equation 2, may be written as

$$w = \sum_{n=1}^{\infty} (a_n e^{n\pi x/y_o} + b_n e^{-n\pi x/y_o}) \sin n\pi y/y_o \tag{5}$$

where $n = 1, 2, 3, \ldots$.

The problem remaining is to apply the lower and upper surface boundary condition—i.e., at $x = 0$ and $x = x_0$—to evaluate coefficients a_n and b_n. It is helpful in this task to introduce the dimensionless coordinates:

$$X = \pi x/y_o \qquad Y = \pi y/y_o \tag{6}$$

from which Equation 5 becomes:

$$w = \sum_{n=1}^{\infty} (a_n e^{nX} + b_n e^{-nX}) \sin nY \tag{7}$$

At the channel floor, $X = 0$ and $w = w_f$, so that Equation 7 becomes:

$$w_f = \sum_{n=1}^{\infty} (a_n + b_n) \sin nY, \qquad 0 \leq Y \leq \pi \tag{8}$$

This is recognized to be in the form of a Fourier sine series over the interval $0 \leq Y \leq \pi$. Drawing upon the Dirichlet integral technique to evaluate the coefficient $(a_n + b_n)$

$$(a_n + b_n) = \frac{2}{\pi} \int_0^{\pi} w_f \sin n\, Y dY = \frac{4wf}{n\pi} \qquad (n, \text{odd})$$

$$(a_n + b_n) = 0 \qquad (n, \text{even}) \tag{9}$$

The requirement of symmetry about the channel center line can be satisfied only by odd values of n. From this, a_n may be derived and inserted into Equation 7, to obtain:

$$w = \sum_{n=1}^{\infty} \left[\left(\frac{4wf}{n\pi} - b_n \right) e^{nX} + b_n e^{-nX} \right] \sin nY \qquad (n, \text{odd}) \tag{10}$$

To evaluate b_n, the boundary conditions at the fluid surface may be used, as given in Equation 4, which, in the transformed coordinates, becomes:

$$\mu_s \left. \frac{\partial^2 w}{\partial Y^2} \right|_{X=\pi D} = \nu \left. \frac{\partial w}{\partial X} \right|_{X=\pi D} \tag{11}$$

where

$$\nu \equiv y_o \mu_b / \pi \text{ and } D \equiv x_o / y_o \tag{12}$$

Publication Date: January 1, 1967 | doi: 10.1021/ba-1967-0063.ch022

In Ordered Fluids and Liquid Crystals; Porter, R., el al.;
Advances in Chemistry; American Chemical Society: Washington, DC, 1967.

From Equations 10 and 11:

$$-\mu_s \sum_{n=1}^{\infty} \left[\frac{4w_f}{n\pi} e^{n\pi D} - 2b_n \sinh n\pi D \right] \sin nY \qquad (n, \text{odd})$$

$$= \nu \sum_{n=1}^{\infty} \left[\frac{4w_f}{n^2\pi} - \frac{2b_n \cosh n\pi D}{n} \right] \sin nY \qquad (n, \text{odd}) \qquad (13)$$

Again, equating coefficients of corresponding terms, this is reduced to

$$-\mu_s \left[\frac{4w_f e^{n\pi D}}{n\pi} - 2b_n \sinh n\pi D \right] = \nu \left[\frac{4w_f}{n^2\pi} e^{n\pi D} - \frac{2b_n \cosh n\pi D}{n} \right] \qquad (14)$$

Equation 14 is solved for b_n to yield:

$$b_n = \frac{(n\mu_s/\nu + 1)4w_f e^{n\pi D}}{2n\pi[(n\mu_s/\nu) \sinh n\pi D + \cosh n\pi D]} \qquad (n, \text{odd}) \qquad (15)$$

This result can be used in Equation 10 to give the fluid speed, w, at any point in the channel. Of particular interest is the surface speed, w_s, for which Equation 10 becomes:

$$w_s = \sum_{n=1}^{\infty} \left[\frac{4w_f e^{n\pi D}}{n\pi} - 2b_n \sinh n\pi D \right] \sin nY \qquad (n, \text{odd}) \qquad (16)$$

Eliminating b_n between Equation 15 and Equation 16 yields:

$$w_s = \frac{4w_f}{\pi} \sum_{n=1}^{\infty} \frac{\sin nY}{n[(n\mu_s/\nu) \sinh n\pi D + \cosh n\pi D]} \qquad (n, \text{odd}) \qquad (17)$$

Along the center line of the surface, $Y = \pi/2$ and $w_s = w_c$

$$w_c = \frac{4w_f}{\pi} \sum_{n=1}^{\infty} \frac{\sin n\pi/2}{n[(n\mu_s/\nu) \sinh n\pi D + \cosh n\pi D]} \qquad (n, \text{odd}) \qquad (18)$$

For deep channels—i.e., $D > 2/\pi$—the terms in this series for $n > 1$ are negligible. Thus Equation 18 may be simplified to

$$w_c \doteq \frac{4w_f}{\pi[(\mu_s/\nu) \sinh \pi D + \cosh \pi D]} \qquad D > \frac{2}{\pi} \qquad (19)$$

For example, at $D = 2/\pi$, the error incurred in using Equation 19 instead of Equation 18 is less than 0.5%. Since the experimental error will normally be greater than this, the use of Equation 19 can be justified in most instances. Stated differently, use of a deep channel is recommended for experimental measurements since it permits great simplification of the equation of flow.

If there is no film covering the surface, then $\mu_s = 0$, and the center line surface speed in a deep channel reduces to:

$$w_c^* \doteq \frac{4w_f}{\pi \cosh \pi D} \qquad D > 2/\pi \qquad (20)$$

where the asterisk denotes that $\mu_s = 0$.

Publication Date: January 1, 1967 | doi: 10.1021/ba-1967-0063.ch022

In Ordered Fluids and Liquid Crystals; Porter, R., el al.;
Advances in Chemistry; American Chemical Society: Washington, DC, 1967.

Furthermore, by taking the differences of Equations 19 and 20, the following relationships are obtained:

$$\frac{w_c^* - w_c}{w_c} \doteq \left(\frac{\mu_s}{\nu}\right) \tanh \pi D \qquad D > \frac{2}{\pi} \tag{21}$$

But since $\tanh \pi D \doteq 1$ for $D > 2/\pi$

$$\frac{w_c^* - w_c}{w_c} \doteq \frac{\mu_s}{\nu} \qquad D > \frac{2}{\pi} \tag{22}$$

This equation may be applied directly to compute surface viscosity from experimental measurements of w_c and w_c^*.

Derivation of Stress Equation for a Rigid Film

The quantity $\mu_s \dfrac{\partial w}{\partial y}$ may be dealt with as a line stress acting in the surface and given the symbol τ_s. It will be in units of dynes per cm. and will bear direct analogy to surface tension, except that it is a tangential rather than normal stress.

Returning to Equation 4 and inserting

$$\frac{d\tau_s}{dy} = \mu_b \left.\frac{\partial w}{\partial x}\right|_s \tag{23}$$

Or, in the transformed coordinates

$$\frac{d\tau_s}{dY} = \mu_b \left.\frac{\partial w}{\partial X}\right|_{X=\pi D} \tag{24}$$

From previous relations;—i.e., Equations 10 and 14,—it can be shown that

$$\left.\frac{\partial w}{\partial X}\right|_{X=\pi D} = \frac{-4wf}{\pi} \sum_{n=1}^{\infty} \frac{\sin nY}{[(\nu/n\mu_s) \cosh n\pi D + \sinh n\pi D]} \qquad (n, \text{odd}) \tag{25}$$

Furthermore, since the stress is zero at mid-channel and a maximum at either channel wall (i.e., $Y = 0$ or $Y = \pi$), integrating Equation 24 yields:

$$|\tau_s|_{\max} = \frac{4wf\mu_b}{\pi} \sum_{n=1}^{\infty} \frac{1}{[(\nu/\mu_s) \cosh n\pi D + n \sinh n\pi D]} \qquad (n, \text{odd}) \tag{26}$$

or for $D > \dfrac{2}{\pi}$

$$|\tau_s|\max \doteq \frac{4w_f\mu_b}{\pi[(\nu/\mu_s) \cosh \pi D + \sinh \pi D]} \qquad D > \frac{2}{\pi} \tag{27}$$

For a rigid film, $\mu_s \to \infty$, and $\nu/\mu_s \to 0$; therefore, the yield value is

$$T_s \doteq \frac{4w_f\mu_b}{\pi \sinh \pi D} = w_c^*\mu_b \qquad D > \frac{2}{\pi} \tag{28}$$

Publication Date: January 1, 1967 | doi: 10.1021/ba-1967-0063.ch022

Thus, the yield value can be obtained by measuring the minimum floor speed, w_f, required to initiate surface flow in a specified channel geometry. For systems in which the channel does not correspond to the exact theoretical model (discussed below), calibration of the apparatus with a simple liquid will provide the required value of w_c*.

Experimental Verification of Principal Assumptions

Questions may be raised as to the consequences of the basic assumptions used in the derivations since these neglect both the presence of a meniscus and the curvature of the channel. To answer these and provide experimental support for the derivations, an apparatus was constructed as shown in Figure 2 and the dimensioned, schematic cross-section (Figure 3).

Publication Date: January 1, 1967 | doi: 10.1021/ba-1967-0063.ch022

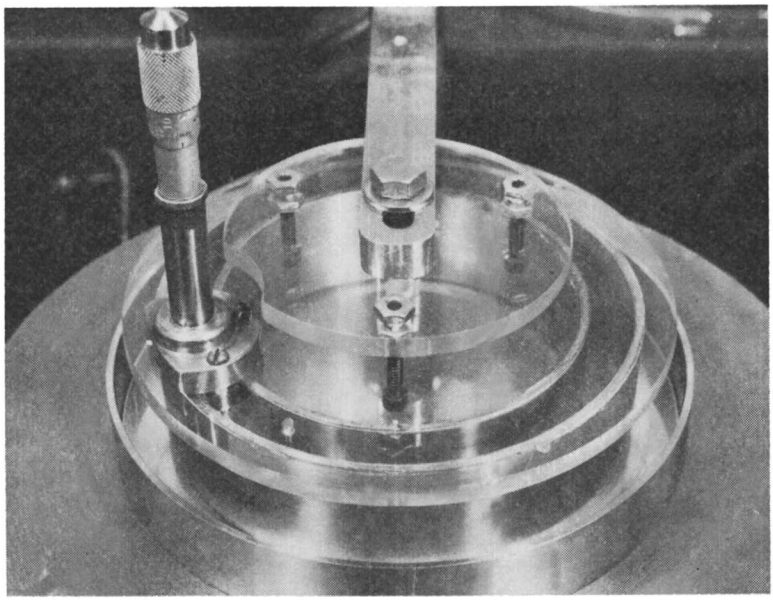

Figure 2. Deep-channel surface-viscosity apparatus

The channel is formed by two stainless steel cylinders, mounted on a transparent plastic support. A micrometer provides a means to measure the depth of the mid-channel surface of the liquid, and the entire channel can be raised and lowered or leveled relative to the floor of the liquid-containing dish. Using this arrangement, several types of tests were carried out to demonstrate different aspects of its operation. In each case, the rings were adjusted and leveled, the liquid was titrated into the dish to produce a preselected depth, the turntable was set in motion, and the progress of a floating Teflon particle was observed as it moved along in the liquid surface. Because of the concave-upward meniscus, the particle tended to remain at mid-channel and thus gave a measure of the center line surface velocity, w_c. The measurement taken was the particle time, the time required for one orbit of the particle around the channel.

In Ordered Fluids and Liquid Crystals; Porter, R., el al.;
Advances in Chemistry; American Chemical Society: Washington, DC, 1967.

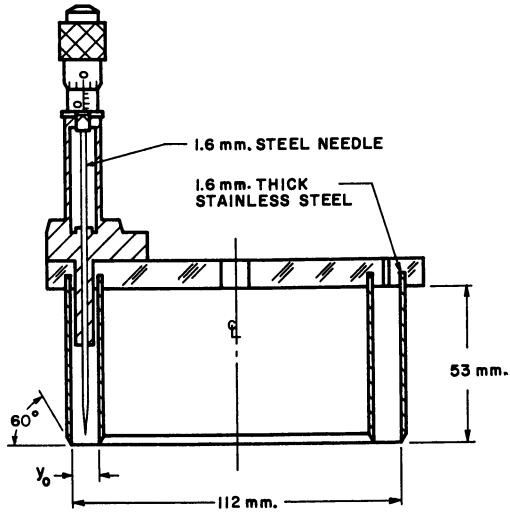

Figure 3. Schematic cross-section of deep-channel surface-viscosity apparatus

Table I. Typical Measurements[a] of Particle Time, (t_c*), for Pure Liquids

Material	*Surface Tension, Dynes/Cm.*	*Bulk Viscosity, Cp.*	t_c* *Seconds*
%Cetane	25	3	149
			149
			150
Mineral oil	30	150	149
			149
			150
Distilled water	73	1	149
			152
			153

[a] Representative of more than 100 determinations.

One question to be answered would concern the behavior of fluids of greatly differing viscosity and surface tension, which on the basis of other work would not be expected to exhibit surface viscosity. Table I shows the results for a particular set of runs for water, cetane, and a white mineral oil without additives. Although the surface tension ranged from 25 to 73 dynes per cm. and the bulk viscosity ranged from 1 to 150 cp., the particle time, t_c*, remained the same for each. Reference to Equation 20 for w_c*, indicates that this invariance should be expected since neither viscosity nor surface tension appears in the derived equation for particle velocity, w_c*. Also these data show that despite hypotheses of a surface structure for water, this fluid showed no significant departure from the behavior of the cetane, which is nonpolar and would be expected to have no such structure. Though no further reference is made to fluid type because of the observed

Publication Date: January 1, 1967 | doi: 10.1021/ba-1967-0063.ch022

similarities of behavior, the data in the remaining comparisons were also checked for more than one fluid.

Even though no surface-tension effect was apparent in Table I, runs with different channel widths indicate that the shape of the meniscus may have a measurable, though small, influence on the measured surface speed. For example, in Figure 4 a comparison is shown for operation with the lower edges of the channel in physical contact with the moving floor. Data for two channel widths are compared with the predictions of Equation 18. To nondimensionalize the plot, particle speed w_c^* is expressed in ratio to

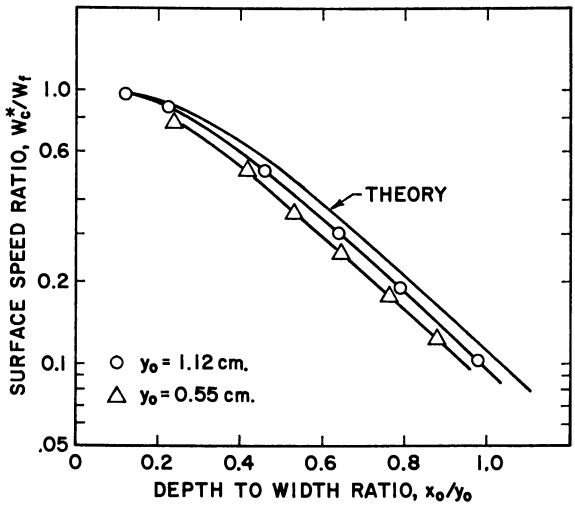

Figure 4. Effect of channel width on agreement between experimental and theoretical surface velocity measurements for fluids without surface viscosity

floor speed, and fluid depth is expressed as a fraction of channel width. Though close agreement with the theoretical prediction is indicated, it is clear that the wider channel gave the better results. Although yet unknown factors may ultimately account for this difference, the favored explanation is that the meniscus in the wide channel is the more nearly flat and thus in closer agreement with the assumed geometry. Attempts to produce a flat meniscus through control of contact angle at the wall have proved difficult and indecisive. Experiments with such a flat meniscus have proved fruitless since the particle tended to migrate to the channel walls. In any event, the effect appears to be small in its total influence on w_c. It would be expected to be even smaller in its influence on the calculation of surface viscosity from measurements since the pertinent velocities, w_c and w_c^*, appear in ratio to one another and both would be expected to be affected similarly by the meniscus.

Publication Date: January 1, 1967 | doi: 10.1021/ba-1967-0063.ch022

Figure 5 shows the effect of clearance between the lower lip of the channel and the moving floor. These measurements demonstrate that the general effect of clearance is to render the apparent depth-width ratio greater than the actual magnitude. These observations have two implications: that a small gap at the contact between channel and floor will not produce a disproportionate effect on the readings, and that the apparent flow behavior with a large gap is very much like that without a gap.

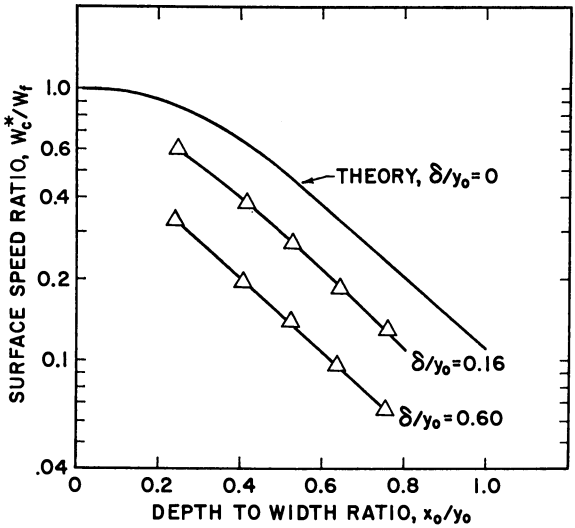

Figure 5. Effect of gap between channel and moving floor, on surface velocity for fluids without surface viscosity

From this latter observation the question immediately arises as to the possibility of applying Equation 22 to channels where there is a sizable gap between the channel and the floor. In addition one might ask to what degree the equation would be applicable to the apparatus of Davies (*1*), where the channel depth is extremely small since it is formed by the contact of rings with the liquid surface. Table II illustrates the application of Equation 22 to experimental data, where the reported surface viscosity was measured by the method of Dervician and Joly (*3*), and the particle times were measured by Davies. In terms of particle time Equation 22 becomes

$$\mu_s = \frac{\mu_b y_o}{\pi} \frac{(t_c - t_c^*)}{t_c^*} \tag{29}$$

The substrate was water in all cases, thus permitting μ_b to be estimated as 1 cp. The reported channel width was 3.5 mm., and the particle times for clean water provided t_c^*. Equation 29 has been applied to give the calculated surface viscosity. (For each film, surface concentration is indi-

Publication Date: January 1, 1967 | doi: 10.1021/ba-1967-0063.ch022

Table II. Application of Equation 29 to Calculation of Surface Viscosity from Davies' Measurements (*1*)

Material	*Reported Surface Viscosity, Surface Poises*	*Reported Particle Time, t_c Seconds*	*Calculated Surface Viscosity, Surface Poises*
Clean water	0	78	0
Stearic acid,			
A.² on 0.01*N* HCl	2.3×10^{-4}	105	3.8×10^{-4}
20.1 A.² on 0.01*N* HCl	6.3×10^{-4}	130	7.4×10^{-4}
20.1 A.² on 0.001*N* HCl	12×10^{-4}	161	12×10^{-4}
Octadecanol,			
20.8 A.² on 0.01*N* HCl	44×10^{-4}	300	32×10^{-4}

cated as A.² per molecule.) There was considerable scatter in the measured particle time, some uncertainty in the reported surface viscosity, and considerable question as to the applicability of Equation 29 to the zero depth channel. In view of all this, it is gratifying to see the agreement between calculated and reported surface viscosities. Since this apparatus geometry represents an extreme case, it should give rise to confidence in application of Equation 29 to channels more nearly like that upon which the derivation was based.

Publication Date: January 1, 1967 | doi: 10.1021/ba-1967-0063.ch022

Conclusions

An arrangement such as shown in Figures 2 and 3 can serve as a surface viscometer, and it is amenable to relatively precise analytical treatment. Its chief advantage is in the simplicity of the ultimate equations for surface viscosity (Equations 21, 22, and 29), and for surface stress in rigid film (Equation 28). Though it is demonstrated that Equation 29 applies also as an approximation in Davies' earlier configuration, this should not suggest abandonment of the advantages of the recommended deep-channel geometry. In the opinion of the writers the deep channel offers as basic, or absolute, an approach to the direct measurement of surface viscosity as does the configuration used by Joly and Dervician, and at the same time it is applicable to soluble films. Indeed, the "self correcting" nature of Equation 20 appears to make it the more accurate approach to obtaining absolute values of μ_s.

Work continues on developing equations for interfacial viscosity, where both fluids are liquids, and for non-Newtonian surface behavior, where μ_s varies with stress. In all such cases the deep channel geometry considerably simplifies these derivations. As these analyses are developed, the promise of this arrangement as a basic instrument should improve.

Nomenclature

$D =$ channel depth–width ratio
$w =$ velocity magnitude in z direction

In Ordered Fluids and Liquid Crystals; Porter, R., el al.;
Advances in Chemistry; American Chemical Society: Washington, DC, 1967.

w_c = mid-channel velocity magnitude in free surface of liquid
w_c^* = mid-channel velocity magnitude in free surface of liquid without surface viscosity
w_f = velocity magnitude of channel floor
x = coordinate measured upward from channel floor
x_0 = channel depth
X = dimensionless coordinate, $x\pi/y_0$
y = coordinate measured across channel
y_0 = channel width
Y = dimensionless coordinate, $y\pi/y_0$
z = coordinate measured along channel
μ_b = bulk viscosity of liquid
μ_s = surface viscosity of liquid
ν = modified bulk viscosity, $y_0\mu_b/\pi$
τ_s = shear stress on surface
T_s = yield value of shear stress for rigid films
s = subscript, refers to liquid surface
δ = thickness of surface region of enhanced viscosity

Literature Cited

(1) Davies, J. T., *Proc. Second Intern. Congr. Surface Activity* **1**, 220 (1957).
(2) Davies, J. T., Rideal, E. K., "Interfacial Phenomena," 2nd ed., p. 258, Academic Press, New York and London, 1963.
(3) Dervician, D. G., Joly, M., *Compt. Rend.* **204**, 1318 (1937).
(4) Ewers, W. E., Sack, R. A., *Australian J. Chem.* **17**, 40 (1954).
(5) Harkins, W. D., Kirkwood, J. Q., *J. Chem. Phys.* **6**, 53 (1938).
(6) Joly, M., "Recent Progress in Surface Science," p. 1, Academic Press, New York and London, 1964.
(7) Plateau, J. A. F., *Phil. Mag.*, Ser. 4, **38**, 445 (1869).

RECEIVED February 11, 1966. Preliminary findings of the U. S. Army Fuels and Lubricants Laboratory, Southwest Research Institute, San Antonio, Tex., currently conducting a program to determine the effect of surface rheology on oil foaming.

INDEX

Publication Date: January 1, 1967 | doi: 10.1021/ba-1967-0063.ix001

Publication Date: January 1, 1967 | doi: 10.1021/ba-1967-0063.ix001

Publication Date: January 1, 1967 | doi: 10.1021/ba-1967-0063.ix001